Age, Mineralogy and Geochemistry of the Mel and Dharma Kimberlites, Northern Canada

by

Nikita Kepezhinskas

A thesis submitted in partial fulfillment of the requirements for the degree of

Master of Sciences

Department of Earth and Atmospheric Sciences

University of Alberta

Abstract

This work presents new petrography, mineral major and trace element chemistry, whole rock major and trace element chemistry, whole rock Sr-Nd-Hf isotope composition, and phlogopite Rb-Sr isotope geochronology for the Mel kimberlite, Nunavut and Dharma kimberlite, Northwest Territories. This data provides an opportunity to confirm the classification of the Mel and Dharma bodies as true archetypal kimberlite, characterize the source region and intrusion/eruption history of the Mel and Dharma kimberlites, trace the magmatic evolution of the Mel and Dharma kimberlite, and provide thermal characteristics of the source mantle beneath the Mel and Dharma.

The diamondiferous Mel kimberlite is composed of north-south oriented hypabyssal and volcaniclastic kimberlite dikes exposed in float at the surface and intersected by diamond drilling at depth. Major element chemistry of phlogopite, ilmenite, and spinel from the Mel kimberlite indicate that the intrusion shares compositional characteristics with regional and world-wide kimberlites. This is further corroborated by whole rock major and trace element chemistry. Rb-Sr phlogopite geochronology of the kimberlite establishes a kimberlite emplacement age of 555.6 ± 2.7 Ma with an initial $^{87}Sr/^{86}Sr_{initial}$ ratio of 0.704414 ± 0.000012. Uncontaminated samples of the Mel kimberlite present $^{87}Sr/^{86}Sr_{initial}$ (0.70538 to 0.70686), $\varepsilon Nd_{initial}$ (2.35 to 3.04), and $\varepsilon Hf_{initial}$ (-15.44 to -1.05) ratios similar to that of Eoarchean to Cambrian primitive kimberlites in eastern Canada. Garnet mineral chemistry identified predominantly lherzolite and eclogite garnet groups. Chondrite-normalized REE patterns from lherzolite garnets record predominantly LREE-depleted patterns indicating melt-metasomatism. Ni-thermometry in most peridotite garnets from the Mel kimberlite records median mantle temperatures of 1250°C. Extrapolation of these temperatures to the West Central Rae Geotherm indicates that Mel kimberlite peridotite garnet was sampled from

a depth of 105 km to 185 km with 86% of mantle garnet sampled within the diamond stability field.

The diamondiferous Dharma kimberlite is part of a larger field of at least two discrete kimberlite bodies, Dharma and Dharma Uttar. Diamond drilling indicates that the Dharma kimberlite is composed of kimberlite tuff overlying kimberlite tuff-breccia that host at least two discrete domains of hypabyssal kimberlite. Major element chemistry of olivine, phlogopite, ilmenite, spinel, and rutile from the Dharma kimberlite indicate that the intrusion shares compositional characteristics with regional and world-wide kimberlites. Whole rock major and trace element chemistry of hypabyssal kimberlite further demonstrate evidence for the kimberlite classification. Rb-Sr phlogopite geochronology of the kimberlite establishes a kimberlite emplacement age of 225.3 ± 0.8 Ma with an initial $^{87}Sr/^{86}Sr_{initial}$ ratio of 0.707081 ± 0.00005. A single, high Rb/Sr, phlogopite macrocryst records an errorchron age of 222 ± 2 Ma regardless of its $^{87}Sr/^{86}Sr_{initial}$ ratio. Uncontaminated samples of the Dharma kimberlite present $^{87}Sr/^{86}Sr_{initial}$ (0.703902 to 0.704666), $\varepsilon Nd_{initial}$ (2.21 to 2.45), and $\varepsilon Hf_{initial}$ (1.4 to 6.8) ratios similar to that of Jurassic kimberlite from Jericho and perovskite from the Triassic to Jurassic Churchill kimberlite field. Garnet mineral chemistry identified lherzolite and harzburgite garnet groups in the Dharma kimberlite. LREE depleted chondrite-normalized REE patterns are found in most lherzolite and all G10B Ti harzburgite garnet indicating melt-metasomatism. Sinusoidal chondrite-normalized REE patterns typically associated with diamond-forming fluids are observed in a subset of lherzolite garnet and in all G10 harzburgite garnets. Ni-thermometry of peridotite garnet indicates sampling at mantle temperatures of 1100°C for lherzolite garnets, 1100°C for G10B Ti harzburgite garnet, and 1300°C for G10A harzburgite garnet. These temperatures are extrapolated to the Victoria Island geotherm

providing a depth sampling profile of 177 km to 182 km for lherzolite garnet and 176 km to 181 km for harzburgite garnet. These extrapolations are supported by the CaO and Cr_2O_3 content of G10A garnet which plot on the 47 kbar isobar (approx. 174 km). As a result, the Dharma kimberlite sampled 49% of mantle garnet from within the diamond stability field.

Dedication

Dr. Kazimir Bernardovich Kepezhinskas

And

Dr. Valentina Valentinovna Kepezhinskas

Acknowledgements

This study was funded through the NSERC CREATE grant for the Diamond Exploration and Research Training School. Santana Resources Inc. and North Arrow Minerals Inc. provided the necessary material for the Dharma and Mel kimberlites studied in this work. Michael MacMorran of North Arrow Minerals Inc. provided invaluable assistance and discussions in personnel communications.

I would like to thank Dr. Graham Pearson for providing the opportunity to complete two challenging and exciting projects as well as supporting my decisions to pursue full-time employment with APEX Geoscience Ltd. Dr. Bruce Kjarsgaard provided valuable insight and guidance throughout the completion of this work. To my examining committee: Dr. Graham Pearson, Dr. Bruce Kjarsgaard, and Dr. Thomas Stachel for reading this work and providing feedback. Dr. Andrew Dufrane, Dr. Andrew Locock, Dr. Yan Luo, Dr. Chiranjeeb Sarkar, and Dr. Sarah Woodland provided essential help in the analysis and processing of all data in this work. Additionally, Dr. Chiranjeeb Sarkar provided indispensable support in the development of laboratory methods used in this work. Mark Labbe delivered essential training and sample preparation. Anetta Banas' efforts to run the Diamond Exploration and Research Training School are commended.

A special thanks is given to Dr. David Foster and Dr. George Kamenov for their support at the University of Florida. Gratitude to my parents, Pavel and Irina Kepezhinskas, and to my sister, Svetlana Kepezhinskas, for fostering my love for rocks. And to Shelby Fuchs, who has challenged and built me to be the best person I can be.

Table of Contents

List of Tables

List of Figures

List of Abbreviations and Nomenclature

<LOD	below limit of detection
σ	sigma or one standard deviation unit from the mean
Ω	ohm
μm	micrometer
apfu	atoms per formula unit
BSE	backscattered Electron
ca.	circa
CCI	Clement's contamination index
CHR	chromium rich spinel (chromite)
dpi	dots per inch
EDS	energy dispersive spectroscopy
EPMA	electron probe microanalysis
g	gram
HFSE	high-field strength element
HR-ICP-MS	high resolution inductively coupled plasma mass spectrometry
HREE	heavy rare earth element
ICP-MS	inductively coupled plasma mass spectrometry
kbar	kilobar
kg	kilogram
km	kilometer
kV	kilovolt
l	liter

LA-ICP-MS	laser ablation inductively coupled plasma mass spectrometry
LOI	loss on ignition
LREE	light rare earth element
m	meter
MAG	iron rich spinel (magnetite)
ml	milliliter
MORB	Mid-Ocean Ridge Basalt
MREE	middle rare earth element
MUM	titanium rich spinel (magnesio-ulvöspinel-magnetite)
nA	nanoamp
N-MORB	“Normal” Mid-Ocean Ridge Basalt
NT	Northwest Territories
NU	Nunavut
OIB	Ocean Island Basalt
ppb	parts per billion
ppm	parts per million
REE	rare earth element
s	second
SEM	scanning electron microscopy
SRM	standard reference material
USGS	United States Geological Survey
volume %	modal/volume percent
XRF	X-ray fluorescence

Chapter 1: Introduction

1.1 Background

1.1.1 Overview

A wide variety of geologic settings host diamond bearing ultramafic and mafic rocks. The geochemistry, petrology, and genesis of these rocks is varied, resulting in the production of kimberlite, lamproite, melilite, and lamprophyre. Diamonds are overwhelmingly hosted in kimberlite (Faure, 2010) with olivine lamproite and carbonate-rich olivine lamproite (CROL) accommodating a minor percentage of host medium. This fact makes it a significant goal to properly identify and characterize new "kimberlite" intrusions the consequences of which influence academic and mineral industry applications. Identification provides regional context for kimberlite mapping and the evolution of kimberlite magmatism through time. This data is used to select robust diamond exploration targets and better understand an areas diamond potential.

Kimberlite identification depends on classification schemes. Petrographic classification produced the first groups of "basaltic kimberlite" and "lamprophyric/micaceous kimberlite" on the basis of mineralogy and texture (Wagner, 1914). Analytical developments in major element, trace element and isotope geochemistry refined kimberlite classification into "Group 1" and "Group 2/orangeite" kimberlites (Smith, 1983). Group 2 kimberlites contain higher SiO2 and Al2O3 and lower MgO, CaO, and CO2 contents than Group 1 kimberlites (Pearson et al., 2019). Group 2/orangeite are further renamed to "carbonate-rich olivine lamproites" (CROL) due to their major element similarities with lamproite (Pearson et al., 2019 and references therin).

1.1.2 Kimberlite

Kimberlite magmas are defined as volatile-rich (H_2O and CO_2), silica-undersaturated (19.9 to 37.9 wt.% SiO_2), Mg-rich (21.0 to 39.75 MgO wt.%) rocks, which are low in Al_2O_3 (<4 wt. %) and K_2O (<2.3 wt.%) contents (Mitchell, 1995; Kjarsgaard et al., 2009; Mitchell et al., 2019; Pearson et al., 2019). Kimberlites are enriched in incompatible trace elements, such as Sr, Zr, Hf, Nb and REE (Mitchell, 1986). These magmas are sourced at depths of over 150 km and are capable of erupting within 10 to 48 hours from their generation at source (Eggler, 1986; Russell et al., 2019). These eruptions create volcanoes composed of crater-, diatreme-, and root-zone kimberlite (Kjarsgaard, 2007, 2012; Giuliani and Pearson, 2019). More rarely, cinder cones, tuff rings and vents are observed. The kimberlite magma's rapid ascent results in a "hybrid" rock which hosts both primary magmatic and xenolith/xenocryst mineral assemblages (Mitchell et al., 2019). Olivine, Mg-Cr-Ti spinel, monticellite, phlogopite, apatite, perovskite, and calcite compose primary minerals in kimberlite.

Larger-sized "macrocrysts" of olivine, garnet, orthopyroxene, clinopyroxene, ilmenite, and Cr-Al spinel constitute mantle minerals foreign to the magma (Mitchell, 1986; Mitchell et al., 2019). Minerals larger than 1 cm compose the mantle-derived "megacryst" assemblage that display disequilibrium textures, a result of resorption delivered by the host kimberlite magma (Mitchell, 1986, 1995; Mitchell et al., 2019). Some melt pools and inclusions in megacrysts share radiogenic isotope signatures similar to their host kimberlites (Kamenetsky et al., 2014; Kargin et al., 2019). This association indicates that the megacryst suite is better refined to include xenocryst and "antecryst" phase minerals. Xenocryst phases correspond to disaggregated mantle peridotite and eclogite while antecryst phases share a genetic relationship with the host kimberlite and may

represent the failed generation of kimberlite melt production (Dongre and Tappe, 2019; Mitchell et al., 2019).

1.1.3 Lamproite

High Mg and ultra-potassic contents define lamproite magmas (Mitchell and Bergman, 1991). Lamproite magmas contain high SiO2 (29.5 to 57.4 wt.%), TiO2 (0.5 to 7.6 wt.%), P2O5 (0.3 to 4.0 wt.%) and Al2O3 (3.3 to 11.1 wt.%) and MgO (>5 wt.%), and CaO (1.52 to 17.2 wt.%) compared to kimberlite magmas (Mitchell and Bergman, 1991; Pearson et al., 2019). Although variable, lamproites are characteristically enriched in Ba (>2000 ppm), Zr (>500 ppm), Sr (>1000 ppm), and La (>200 pm), alongside incompatible elements like Nb and Rb (Mitchell and Bergman, 1991). Lamproite magmas are interpreted to form in anorogenic environments as products of MARID-type lithospheric mantle melting on the margins of mantle plumes (Mitchell and Bergman, 1991; Nowell et al., 2008). They are also observed in "subduction-like" settings, such as the Antarctic (Murphy et al., 2002) and the Mediterranean (Peccerillo and Martinotti, 2006; Prelević et al., 2008).

Unlike kimberlite, a lamproite eruption forms epizonal intrusions with surface expressions of diatremes, cinder cones or volcanic vents that include volcaniclastic deposits, lava flows, and lava lakes (Mitchell and Bergman, 1991; Stachel et al., 1991). Volcaniclastic rocks transition to hypabyssal sills and dikes connecting to small plutons at depth (Mitchell and Bergman, 1991).

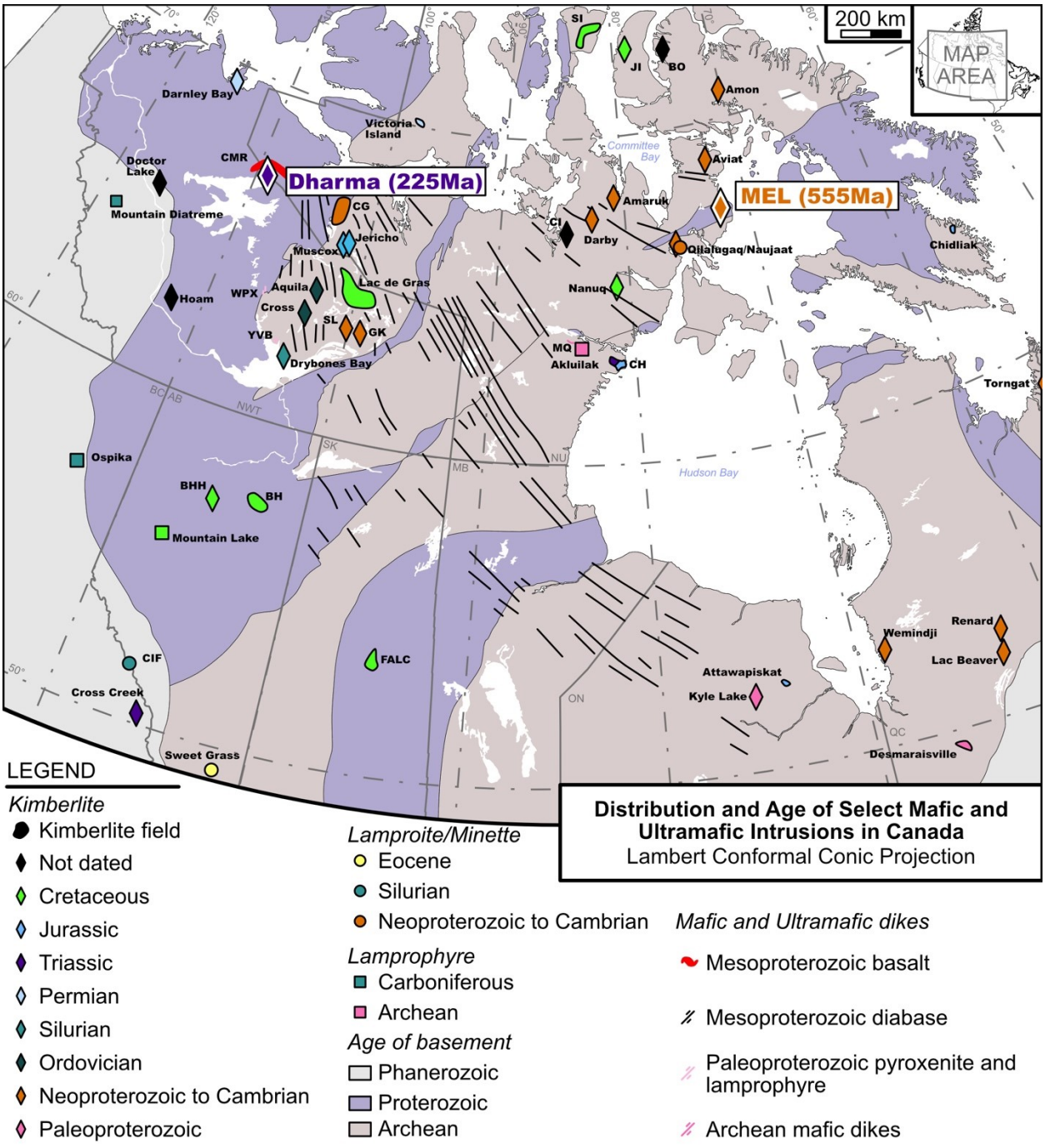

Figure 1.01: Map of ultramafic intrusions in Canada. Data on intrusions modified from LeCheminant (1996), Heaman et al. (2003), Heaman et al. (2004), Davis et al. (2006), Goff et al. (2008), Faure (2010), Gochnauer et al. (2010), Tappe et al. (2014), Ootes et al. (2015), Sarkar et al. (2018). BH – Birch Hills, BHH – Buffalo Head Hills , BO - Borden Peninsula , JI - Jackson Inlet, CG – Coronation Gulf , CH - Churchill , CI – Chesterfield Inlet , CIF – Columbia Ice Fields , CMR – Coppermine River basalts, FALC – Forte a la Corne, GK – Gahcho Kue, MQ – Macquoid Dike Swarm, SI – Somerset Island , SL – Snap Lake, WPX – Wopmay Pyroxenite, YVK – Yellowknife Volcanic Belt lamprophyre dikes.

Classification of lamproites is based on modal mineralogy (Mitchell and Bergman, 1991; Woolley et al., 1996). These rocks are mineralogically diverse but their mineral assemblage can be generalized to include diopside, Ti-rich Al-poor phlogopite, K-Ti richterite, leucite, sanidine, wadeite, priderite, and olivine with ilmenite, spinel, perovskite, and apatite constituting minor phases (Mitchell and Bergman, 1991; Woolley et al., 1996).

1.2 Kimberlite and Diamonds in Canada

Canada hosts kimberlites and related ultramafic intrusions of varying age (Figure 1.01). W.H. Hobbs (1899) was the first to suggest a Canadian origin for diamonds discovered in the glacial deposits of Wisconsin and Michigan between 1876 and 1897. Despite this, no kimberlite would be discovered until 1948. The first kimberlite was discovered by Satterly (1948) who catalogued a serpentinized, porphyritic, olivine bearing heavily weathered rock in two diamond drill core holes at the Michaud Gold Mine. Twenty years later, diamond exploration began in the country.

Exploration efforts would unearth kimberlites at Lake Timiskaming, ON, Somerset Island, NU, Cross Diatreme, BC, Otish Mountains, Quebec, Mountain diatreme, NT, and further kimberlites in Kirkland Lake, all containing sub-economic grades of diamonds (Kjarsgaard and Levinson, 2002). In 1991, drilling operations organized by Dia Met Minerals and BHP intersected kimberlite, with a diamond grade of 0.63 carat per tonne (cpt). The discovery spurred extensive claim staking and further work that produced Canada's first diamond mines at Ekati (1998) and Diavik (2003).

Diamond exploration efforts in the 21st century have, in part, shifted to the exploration of the Rae Craton in NU, to the Superior Craton in ON and QC, and to "off-craton" kimberlites in AB and

NT. As of 2021, Canada is the world's third largest producer of diamonds by value and volume, producing up to 23.2 million carats of diamonds (around 2.7 billion USD) annually (Government of Canada, 2021).

1.3 Rae Peninsula Regional Geology

1.3.1 Mel Area – Regional Geology and Rae Craton Tectonic History

The Rae Craton (Figure 1.02) is one of the largest cratonic blocks within the extensive Precambrian Churchill Province (Sanborn-Barrie et al., 2014; Liu et al., 2016). Exposed upper crust of the Rae Craton consists of Archean basement granite-gneiss, Archean komatiite-bearing greenstone belts, Paleoproterozoic metasedimentary rocks, and 2.62 to 2.58 Ga granitic plutons (Berman et al., 2005; Petts et al., 2014; Sanborn-Barrie et al., 2014; Liu et al., 2016). Kimberlite hosted lower crustal xenoliths record Mesoarchean to Neoarchean, granulite-facies metabasite and anorthosite (Petts et al., 2014). Peridotite xenoliths of 3.0 to 2.6 Ga suggest the presence of an Archean mantle root that aided the preservation of overlying Archean crust throughout the extensive collisional orogenesis that the Rae Craton would experience in the Precambrian (Liu et al., 2016).

Seven distinct orogenic events are identified in the Rae Craton. At 2.7 to 2.6 Ga, the Chesterfield Block accreted to the southern margin of the Rae Craton (Davis et al., 2006). Further collision reworked the rocks of the Chesterfield Block during the MacQuoid orogeny at 2.56 to 2.5 Ga (Berman et al., 2010; Pehrsson et al., 2013). At 2.5 to 2.3 Ga, the Arrowsmith orogeny accreted Andean-like arc volcanic and sedimentary rocks to the western margin of the craton (Berman et al., 2005, 2013). The Slave Craton was accreted to the Rae Craton at 2.02 to 1.90 Ga, coinciding with extensive plutonism along the Thelon tectonic zone and Taltson magmatic zone during the

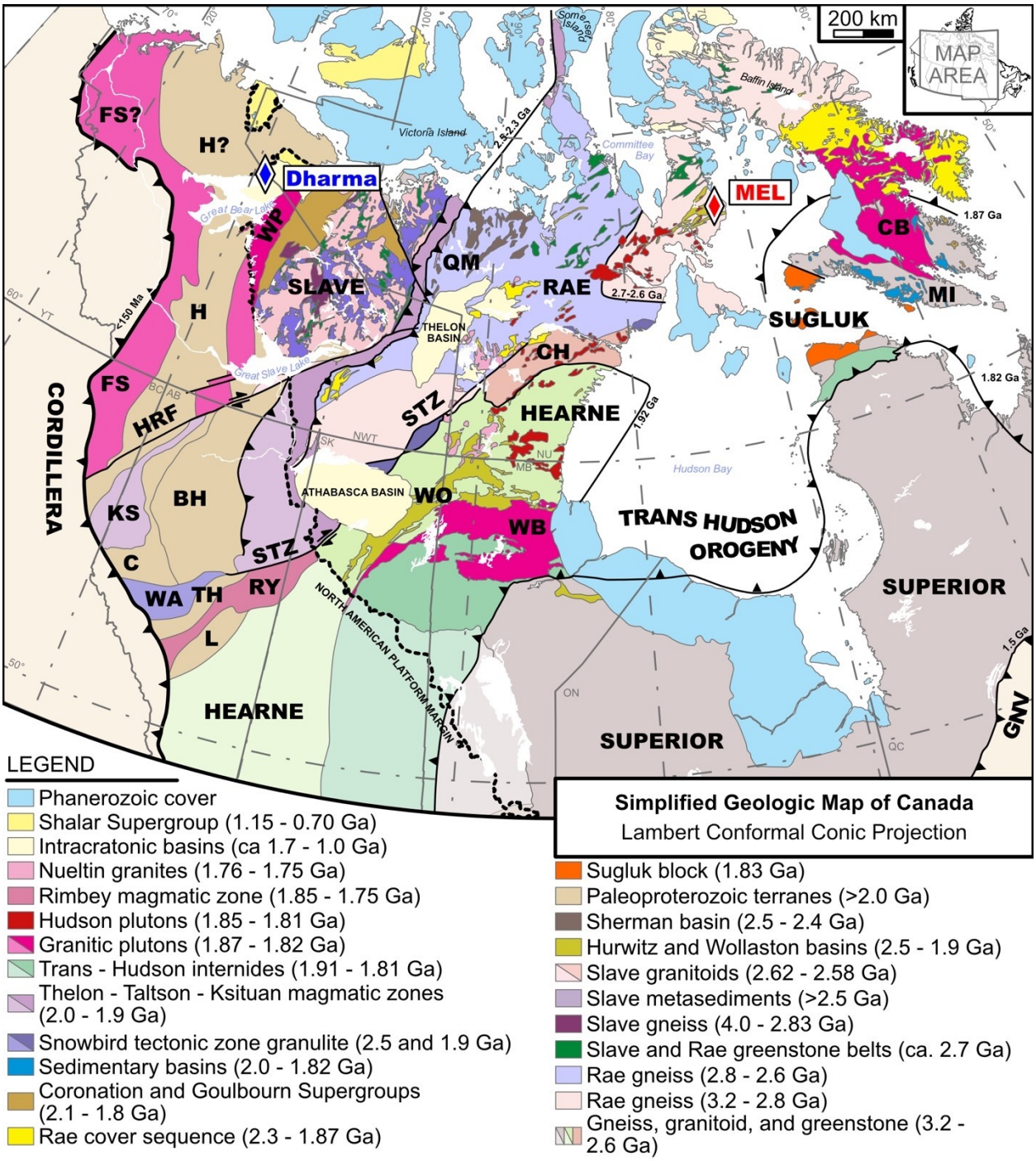

Figure 1.02: Simplified geologic map of Canada. Map modified after Ross et al. (1994), Wheeler et al. (1996), Smart et al. (2014), Liu et al. (2016). BH – Buffalo Head terrane, C – Chichaga terrane, CB – Cumberland batholith, CH – Chesterfield block, Complex, FS/FS? – Fort Simpson terrane, GNV – Grenville orogeny, H/H? – Hottah terrane, HRF – Hay River Fault, KS – Ksituan magmatic arc, L – Lacomb Domain, MI – Metaincognita terrane, QM – Queen Maud block, RY – Rimbey magmatic arc, STZ – Snowbird Tectonic Zone, TH – Thorsby terrane, WA – Wabamun domain, WB – Wathaman batholith, WO – Wollaston group, WP – Wopmay (Great Bear Arc) orogen.

Taltson and Thelon orogenies (Hanmer et al., 1992; Chacko et al., 2000; Card et al., 2010). The Hearne Craton accreted to the southern margin of the Rae Craton at 1.92 to 1.90 Ga during the Snowbird orogeny truncating the magmatic activity of the Taltson magmatic zone (Berman et al., 2007, 2013; Martel et al., 2008). The Meta Incognita-Sugluk-Hall Peninsula Block followed, thickening the Rae Craton along its southeastern flank at 1.87 Ga with the accretion of amphibolite-facies supracrustal rocks now exposed along the Committee Bay belt (Berman et al., 2010). Finally, the Superior Craton was accreted along the south-southeastern margin during the Trans Hudson orogeny at 1.9 to 1.8 Ga (Ansdell and Norman, 1995; Stern et al., 1995; St-Onge et al., 2006).

The orogenic events described above subjugated the Rae Craton to craton-altering magmatism. Potassium-rich granitic plutons exposed south of the Boothia Peninsula correspond to crustal thickening of the Rae Craton in the Neoarchean (Hinchey et al., 2011). Granitic plutons associated with the Trans Hudson orogeny intruded at 1.85 to 1.81 Ga (Liu et al., 2016) followed by post-orogenic bimodal magmatism at 1.77 to 1.70 Ga which underplated the Rae Craton with basalt (Peterson et al., 2002, 2015; Petts et al., 2014).

1.3.2 Regional Ultramafic and Mafic Intrusions of the Rae Craton

Ultramafic and mafic magmatism is present throughout the Rae Craton's history. The Prince Albert greenstone belt, located on the Melville Peninsula, hosts komatiitic lava flows and tuffs that are interpreted to be emplaced after adiabatic melting at 2.97 Ga (Skulski et al., 2003; Richan et al., 2015). The MacQuoid mafic dike swarm intruded along the southeastern boundary of the Rae Craton at 2.19 Ga in the Hearne subdomain (Tella et al., 2000; Hanmer et al., 2006; Davis et al.,

2006). These 2 to 20 m thick, east-trending mafic dikes correlate to the Tulemalu mafic dike swarm, together emplaced after Neoarchean deformation and prior to 1.90 Ga regional metamorphism (Hanmer et al., 2006). During the Trans Hudson orogeny, crust-mantle decoupling and extension produced ultrapotassic magmatism which lead to the emplacement of the Christopher Island Formation lamprophyre dikes (Peterson and LeCheminant, 1996). One of these dikes is the diamondiferous Akluilak lamprophyre dike which intruded at 1.832 ± 0.028 Ga (MacRae et al., 1996; Peterson and Pehrsson, 2010).

Kimberlite and related magmas are present in the Rae Craton. The Amon kimberlites intruded as a sill complex into the Rae Craton basement on Baffin Island at 673 Ma (Tappe et al., 2014). South of Amon, across the Fury and Hecla Strait, the Qilalugaq olivine lamproites and Aviat kimberlite dikes and sheets intruded between 545 and 530 Ma on the Melville peninsula (Sarkar et al., 2018). Similar aged kimberlites occur near Kugaaruk, NU, at Pelly Bay (540 to 535 Ma; Kienlen et al., 2008; Liu et al., 2016), and in the Darby Kimberlite field (542 Ma; Harris et al., 2018). Aviat CROL intruded at 507 to 503 Ma (Sarkar et al., 2018) on the northern Melville Peninsula. This latest Neoproterozoic to early Cambrian kimberlite and related magmatism corresponds to similar-aged kimberlites in the SE Slave Craton (Heaman et al., 2004), the northern Slave Craton (Armstrong et al., 2012), and lamprophyre and carbonatite intrusions from Labrador and west Greenland (Heaman et al., 2004; Tappe et al., 2011, 2014). The trend of low-volume ultramafic and ultrapotassic magmatism along the northern margin of Laurentia correlates to a rifted margin that opened the Iapetus Ocean, breaking apart the supercontinent of Rodinia (Sarkar et al., 2018). It is of note, that micro- and macro- diamonds have been recovered from Aviat (88 to 163 cpht; Armstrong et al., 2008) and Qilalugaq (14 to 39 cpht; Kupsch and Armstrong, 2012).

Discovered ultramafic and mafic magmatic centers of Phanerozoic age are limited to the Mesozoic, and Cenozoic (Figure 1.01). Upwelling asthenosphere and continental rifting produced the Chidliak kimberlite field on Baffin Island which intruded at 157.0 to 139.1 Ma (Heaman et al., 2015). Kimberlites from Somerset Island intruded at 103 to 95 Ma and are correlated to a Cretaceous kimberlite corridor which stretches from Somerset Island to Kansas (Heaman et al., 2004; Kjarsgaard et al., 2017). The Nanuq kimberlites intruded into Archean granite and gneiss in the Rae Craton near Ukkusiksalik Bay (Wager Bay) at 79.6 to 70.4 Ma (Pell et al., 2008; Webb et al., 2008). Finally, across from Baffin Island, Paleocene D-MORB like picritic lavas formed as a result of the initiation of Paleogene rifting between Greenland and North America (Clarke and Beutel, 2020).

1.4 Slave Craton and Mackenzie Platform Regional Geology

1.4.1 Dharma Kimberlite Area – Regional Geology and Tectonic History

The Slave Craton (Figure 1.02) is a relatively small craton in the northwestern portion of the Canadian Shield with an exposed surface extent of 190,000 sq. km. The craton consists of 4.0 to 2.9 Ga (east-dipping) Central Slave Basement Complex, 2.72 to 2.62 Ga Yellowknife Supergroup volcano-sedimentary rocks, and 2.65 to 2.58 Ga plutons (Bleeker et al., 1999; Davis et al., 2003; Iizuka et al., 2007). The eastern part of the craton is isotopically distinct and younger than the western Central Slave Basement Complex (Thorpe et al., 1992; Davis et al., 2003). Lower crustal xenoliths of the Slave Craton are predominantly composed of mafic and tonalitic granulites that record high-temperature and low-pressure regional metamorphism (Davis et al., 2003). Lithospheric mantle below the Slave Craton is thermally and compositionally zoned with mantle

xenoliths recording shallow, very Mg-rich, chemically depleted peridotite sitting on top of less-depleted peridotite and eclogite (Griffen et al., 1998; Kopylova and Russell, 2000; Menzies et al., 2004; Newton et al., 2016; Kopylova et al., 2016). Alongside this vertical stratification, three horizontal domains are interpreted from regional mantle garnet distributions from the Slave Craton. Simply put, the northern domain is richer in eclogitic garnet, the central domain is richer in depleted harzburgitic garnet, and the southern domain has less eclogitic and depleted harzburgite garnet (Grütter et al., 1999).

Following cratonic stabilization, the Slave Craton experienced a prolonged period of terrane accretion, magmatism, and orogenesis. The Rae Craton accreted to the Slave Craton at 2.02 to 1.9 Ga during the Taltson and Thelon orogeny (Hanmer et al., 1992; Card et al., 2010). Eastward-directed subduction evolved along the western margin of the Slave Craton, accreting rocks of the Wopmay Orogen at 1.9 Ga during the Calderian orogeny (Hoffman and Bowring, 1984; Hildebrand et al., 2010). This Wopmay Orogen's evolution began with the development of a rift margin of marine siliclastic and carbonate platform rocks now constituting the Corronation Supergroup (Hildebrand et al., 2010). The distal volcanic Hottah terrane, which developed around the same time as the Corronation Supergroup, accreted along the western margin of the slave, resulting in the mylonites of the Proterozoic Wopmay Fault Zone suture zone (Spratt et al., 2009; Hildebrand et al., 2010). Wopmay Orogen related calc-alkaline magmatism produced the volcanic and sedimentary rocks of the Great Bear magmatic zone at 1875 Ma (Hildebrand et al., 1987; Spratt et al., 2009).

1.4.2 Regional Ultramafic and Mafic Intrusions of the Slave Craton

Ultramafic and mafic magmatism in the Slave Craton constitutes greenstone belts, mafic dike swarms, and intrusions of carbonatite, lamprophyre, and kimberlite. The Archean Yellowknife Volcanic Belt includes flows, sills, and dikes of rift-associated tholeiitic N-MORB basalts (Cousens, 2000). Crustal-component rich, Archean lamprophyre is reported in the Lac de Gras field (Folinsbee, 1949). Archean carbonatite and minettes intruded alongside potassic-rich and silica undersaturated rocks of the Big Spruce Lake alkaline complex (Cavell and Baadsgaard, 1986). The Yellowknife Volcanic Belt hosts clinopyroxene-rich lamprophyre dikes with intrusion ages of 1.91 to 1.84 Ga, a result of subduction-related magmatism (LeCheminant, 1996). Similar aged pyroxenite plutonic pipes intruded along the Wopmay Fault Zone at 1.86 Ga with mineralogy and whole rock geochemistry comparable to calc-alkaline lamprophyre (Ootes et al., 2020). The Mackenzie diabase dike swarm intruded a significant portion of the Canadian shield, including the Slave Craton, at 1.27 Ga (LeCheminant and Heaman, 1989). These diabase dikes, and associated Muskcox intrusion and Coppermine River basalts, are believed to be the result of short-lived mantle plume magmatism (LeCheminant and Heaman, 1989).

On-craton kimberlite magmatism (Figure 1.01) is grouped into four domains with shared temporal and/or spatial characteristics (Heaman et al., 2003). Cambrian age kimberlite magmatism in the southeastern Slave domain is constrained by ages from AK5034, Kennady Lake, (542 Ma; Heaman et al., 2003) and Snap Lake dike (523 to 535Ma; Agashev et al., 2001). Neoproterozoic to Cambrian age kimberlite magmatism in the Northern Slave is constrained by ages from Anuri (613 Ma; Masun et al., 2004) and kimberlites of the Corronation Gulf (Artemisia, 616 Ma; Hydra, 601 Ma; Thrift, 538 Ma; Perseus, 534 Ma; Kikerk, 1,520 Ma; Armstrong et al., 2012). Ordovician to

Silurian kimberlite magmatism in the southwestern Slave domain is constrained by ages from Orion (435 Ma; Heaman et al., 2003), Drybones Bay (450 Ma; Heaman et al., 2003), Cross (450 Ma; Heaman et al., 2003), and Ursa (459 Ma; Heaman et al., 2003) of the Western Slave kimberlite field. To the north of the Slave Craton on Victoria Island, ages from Phalarope (256 Ma; Heaman et al., 2003), Snowy Owl (271 to 257 Ma; Heaman et al., 2003), Longspur (276 Ma; Heaman et al., 2003), Golden Plover (286 Ma; Heaman et al., 2003) define Permian kimberlite magmatism. In the Contwoyto field, the kimberlites of Jericho are of Jurassic age (173 Ma; Heaman and Kjarsgaard, 2002). The youngest kimberlite magmatism occurs in the central Slave domain and consists of Cretaceous to Eocene kimberlite magmatism based upon ages of the Lac de Gras and Hardy Lake fields (74 Ma to 48 Ma; Davis and Kjarsgaard, 1997; Berg and Carlson, 1998; Carlson et al., 1998; Graham et al., 1998; Armstrong and Moore, 1998; Scott Smith and McKinlay, 2002; Heaman et al., 2004).

Details regarding off-craton kimberlite magmatism on the Mackenzie Platform to the west of the Slave Craton are limited (Figure 1.01). Five kimberlite bodies were intersected by diamond drill coring on the HOAM diamond property south of Great Bear Lake (Goff et al., 2008; Mah, 2009; Gochnauer et al., 2010). West of Great Bear Lake and 60km North of Norman Wells, the Hillside Kimberlite was intersected by drill core on the Doctor Lake Property at the Sahtu project (Goff et al., 2008; Craigie, 2010). North of Great Bear Lake, The Horton River Project produced kimberlite-like geophysical anomalies and kimberlite indicator mineral showings but has, to date, failed to produce identifiable kimberlite specimens (Gochnauer et al., 2010; Davies and Davies, 2012). Nearby, work on the Greenhorn Diamond Property intersected two kimberlite pipes of the Dharma Kimberlite Complex and recovered 227 diamonds (Gochnauer et al., 2010; Gill, 2016).

South of Paulatuk, NT, exploration by Darnley Bay Resources intersected micro-brecciated and hypabyssal kimberlite at the Franklin Diamond Project on the Perry Peninsula (Reford, 2012).

1.4.3 Continental Crust Beneath the Mackenzie Platform

Traditional models of the genesis of diamondiferous kimberlites require source regions below stable Precambrian (>1.5 Ga) continental crust (Kennedy-Clifford Rule; Giuliani and Pearson, 2019). The presence of microdiamonds in the Darnley Bay kimberlites (Reford, 2012), Hillside Kimberlite (Goff et al., 2008), and the Dharma kimberlite (Gochnauer et al., 2010; Gill, 2016) has spurred interest in the further investigation of old, stable crust and lithospheric mantle beneath the Mackenzie Platform. Proponents of this theory indicate the presence of abundant kimberlite magmatism on the platform (extensive KIM including kelephyte rimmed on pyrope and leucoxene rims on ilmenite) alongside a large Bourger Gravity anomaly (Doyle and Bidwell, 2005). Furthermore, high seismic velocities (similar in magnitude to other North American cratons) have been reported between the Great Bear Magmatic Arc and the North American continental margin along the Beaufort Sea, supporting the existence of deeply buried stable cratonic crust and underlying thick mantle lithosphere (Schaeffer and Lebedev, 2014).

1.5 Project Objectives

This study presents the investigation of the on-craton Mel kimberlite and the off-craton Dharma kimberlite using petrography, mineral chemistry, and geochronology and tracer isotope geochemistry. This project focuses on the following objectives: 1) confirm the classification of the Mel and Dharma bodies as true archetypal kimberlite, 2) characterize the source region and intrusion/eruption history of the Mel and Dharma kimberlites, 3) trace the magmatic evolution of

the Mel and Dharma kimberlite, and 4) provide thermal characteristics of the source mantle beneath the Mel and Dharma. These objectives are accomplished through detailed descriptions of mineral textures and relationships, comparison of mineral chemistry and whole rock chemistry to regional kimberlites, and the assessment of garnet mineral chemistry with respect to regional mantle trends.

Chapter 2: Analytical Methods

2.1 Samples

Samples consist of cut Mel kimberlite core, core mineral separates (Table 2.01); float mineral separates were received from North Arrow Minerals Inc. Mel samples constitute three intersected bodies: ML8 Upper, ML8 Lower, and ML345. Cut Dharma core was sampled by D.G. Pearson with the permission and help of Dr. Troy Gill of Santana Resources Inc.; samples constitute volcaniclastic and hypabyssal rock from one drill hole (Table 2.01). Core samples were photographed, and zones of surface alteration and xenolith contamination demarcated. Billets were cut from core for thin sections and whole rock geochemistry.

Garnet and phlogopite grains were picked under binocular microscope from Mel kimberlite core mineral separates provided by North Arrow Minerals Inc. A minimum of 100 grains of garnet was picked from seven separate samples of 0.5 to 1 mm size. A minimum of 100 grains of phlogopite was picked from five separate samples of 0.25 to 0.5 mm size and three separate samples of 0.5 to 1 mm size. Additional phlogopite was picked from one Mel surface sample processed via electrical fragmentation with the SELFRAG Lab System.

Individual macrocryst phlogopite grains were picked directly from three samples of Dharma core. Selected Dharma core samples were processed via electrical fragmentation with the SELFRAG Lab System, to facilitate garnet and phlogopite picking. A minimum of 40 grains of garnet was picked from four separate samples of material sieved up to <1mm. A minimum of 50 grains of phlogopite was picked from two separate samples of material sieved to <1mm.

Table 2.01: Material description and analytical procedures for this study.

Hole ID	***Depth (m)***	***Sample ID***	***Material Description***	***Analytical Procedure***
Mel Kimberlite Material				
Surface float	0	M8SX	Rock Sample	Phlogopite Rb-Sr isotopes (ICP-MS, TIMS)
Surface float	0	47824	Mineral separate	Garnet major and trace elements (EPMA, LA-ICP-MS)
Surface float	0	49736	Mineral separate	Phlogopite Rb-Sr isotopes (ICP-MS, TIMS), garnet major/trace elements (EPMA, LA-ICP-MS)
18-ML-03	60.03-60.30	49725	Mineral separate	Garnet major and trace elements (EPMA, LA-ICP-MS)
18-ML-03	86.08-86.38	49741	Mineral separate	Garnet major and trace elements (EPMA, LA-ICP-MS)
18-ML-03	91.76-92.05	49742	Mineral separate	Garnet major and trace elements (EPMA, LA-ICP-MS)
18-ML-04	166.11-166.36	49746	Mineral separate	Phlogopite Rb-Sr isotopes (ICP-MS, TIMS), garnet major/trace elements (EPMA, LA-ICP-MS)
18-ML-06	25.78-25.96	49724	Mineral separate	Phlogopite Rb-Sr isotopes (ICP-MS, TIMS), garnet major/trace elements (EPMA, LA-ICP-MS)
18-ML-03	59.66-59.91	49716	Thin section	Thin section petrography
18-ML-03	59.66-59.91	49716.01	Cut core	Thin section petrography, EPMA
18-ML-03	59.66-59.91	49716.02	Cut core	WR major/trace elements (XRF), WR trace elements (HR-ICP-MS)
18-ML-03	59.66-59.91	49716.03	Cut core	Thin section petrography, EPMA
18-ML-03	59.66-59.91	49716.04	Cut core	WR major/trace elements (XRF), WR trace elements (HR-ICP-MS), WR Rb-Sr isotopes (ICP-MS, TIMS), WR Lu-Hf isotopes (ICP-MS), WR Sm-Nd isotopes (ICP-MS)
18-ML-03	59.66-59.91	49716.05	Cut core	Thin section petrography, EPMA
18-ML-03	109.23-109.49	49720	Thin section	Thin section petrography
18-ML-03	109.23-109.49	49720.01	Cut core	Thin section petrography, EPMA
18-ML-03	109.23-109.49	49720.03	Cut core	WR major/trace elements (XRF)
18-ML-03	113.63-113.86	49721	Thin section	Thin section petrography
18-ML-03	113.63-113.86	49721.01	Cut core	WR major/trace elements (XRF), WR trace elements (HR-ICP-MS), WR Rb-Sr isotopes (ICP-MS, TIMS), WR Lu-Hf isotopes (ICP-MS), WR Sm-Nd isotopes (ICP-MS)
18-ML-03	113.63-113.86	49721.02	Cut core	Thin section petrography, EPMA
18-ML-03	113.63-113.86	49721.04	Cut core	WR major/trace elements (XRF)
18-ML-02	42.87-43.20	49722	Thin section	Thin section petrography
18-ML-02	42.87-43.20	49722.01	Cut core	Thin section petrography, EPMA
18-ML-02	42.87-43.20	49722.02	Cut core	WR major/trace elements (XRF), WR trace elements (HR-ICP-MS), WR Rb-Sr isotopes (ICP-MS, TIMS), WR Lu-Hf isotopes (ICP-MS), WR Sm-Nd isotopes (ICP-MS)
18-ML-06	42.87-43.20	49722.03	Cut core	Thin section petrography, EPMA
18-ML-06	25.95-26.21	49723	Thin section	Thin section petrography

Table 2.01 (continued): Material description and analytical procedures for this study.

Hole ID	***Depth***	***Sample ID***	***Material Description***	***Analytical Procedure***
Mel Kimberlite Material (continued)				
18-ML-06	25.95-26.21	49723.01	Cut core	WR major/trace elements (XRF), WR trace elements (HR-ICP-MS), WR Rb-Sr isotopes (ICP-MS, TIMS), WR Lu-Hf isotopes (ICP-MS), WR Sm-Nd isotopes (ICP-MS)
18-ML-06	25.95-26.21	49723.02	Cut core	Thin section petrography, EPMA
18-ML-06	25.95-26.21	49723.04	Cut core	WR major/trace elements (XRF)
18-ML-06	25.95-26.21	49723.06	Cut core	WR major/trace elements (XRF)
Dharma Kimberlite Material				
DD007-GH001	58.89-58.96	D86	Cut core	Thin section petrography, EPMA, WR major/trace elements (XRF)
DD007-GH001	60.19-60.27	D89	Mineral separate	Phlogopite Rb-Sr isotopes (ICP-MS, TIMS), garnet major/trace elements (EPMA, LA-ICP-MS)
DD007-GH001	63.17-63.29	D91	Cut core, mineral separate	Thin section petrography, EPMA, WR major/trace elements (XRF), WR trace elements (HR-ICP-MS), garnet major/trace elements (EPMA, LA-ICP-MS)
DD007-GH001	63.73-63.80	D92	Cut core	Thin section petrography, EPMA, WR major/trace elements (XRF), WR trace elements (HR-ICP-MS), WR Rb-Sr isotopes (ICP-MS, TIMS), WR Lu-Hf isotopes (ICP-MS), WR Sm-Nd isotopes (ICP-MS)
DD007-GH001	65.41-65.48	D93	Mineral separate	Phlogopite Rb-Sr isotopes (ICP-MS, TIMS), garnet major/trace elements (EPMA, LA-ICP-MS)
DD007-GH001	66.10-66.29	D94	Cut core, macrocryst phlogopite	Thin section petrography, EPMA, WR major/trace elements (XRF), WR trace elements (HR-ICP-MS), phlogopite and WR Rb-Sr isotopes (ICP-MS, TIMS)
DD007-GH001	67.79-67.87	D95	Cut core	Thin section petrography, WR major/ trace elements (XRF), WR trace elements (HR-ICP-MS)
DD007-GH001	70.58-70.75	D98	Cut core	Thin section petrography, WR major/trace elements (XRF)
DD007-GH001	80.52-80.60	D101	Cut core	Thin section petrography, WR major/trace elements (XRF)
DD007-GH001	82.76-82.90	D104	Cut core, mineral separate	Thin section petrography, EPMA, WR major/ trace elements (XRF), WR trace elements (HR-ICP-MS), WR Rb-Sr isotopes (ICP-MS, TIMS), WR Lu-Hf isotopes (ICP-MS), WR Sm-Nd isotopes (ICP-MS), garnet major/trace elements (EPMA, LA-ICP-MS)
DD007-GH001	83.15-83.21	D105	Cut core	Thin section petrography
DD007-GH001	89.53-89.63	D108	Cut core	Thin section petrography, EPMA, WR major/trace elements (XRF), WR trace elements (HR-ICP-MS), WR Rb-Sr isotopes (ICP-MS, TIMS), WR Lu-Hf isotopes (ICP-MS), WR Sm-Nd isotopes (ICP-MS)
DD007-GH001	91.31-91.36	D109	Cut core, macrocryst phlogopite	Thin section petrography, EPMA, WR major/trace elements (XRF), phlogopite Rb-Sr isotopes (ICP-MS, TIMS)
DD007-GH001	33.92-34.03	D112	Cut core	Thin section petrography, WR major and trace elements (XRF)
DD007-GH001	34.20-34.26	D113	Macrocryst phlogopite	Phlogopite Rb-Sr isotopes (ICP-MS, TIMS)

Table 2.01 (continued): Material description and analytical procedures for this study.

Hole ID	***Depth***	***Sample ID***	***Material Description***	***Analytical Procedure***
Dharma Kimberlite Material (continued)				
DD007-GH001	37.41-37.45	D114	Cut core	Thin section petrography, WR major/trace elements (XRF)
DD007-GH001	43.11-43.21	D116	Cut core	Thin section petrography, WR major/trace elements (XRF)
DD007-GH001	45.03-45.16	D117	Cut core	Thin section petrography
DD007-GH001	48.42-48.51	D118	Cut core	Thin section petrography, WR major/trace elements (XRF)
DD007-GH001	54.78-54.84	D122	Cut core	Thin section petrography, WR major/trace elements (XRF)
DD007-GH001	17.42-17.50	D128	Cut core	Thin section petrography, WR major/trace elements (XRF)
DD007-GH001	21.09-21.18	D129	Cut core	Thin section petrography, WR major/trace elements (XRF)
DD007-GH001	29.97-30.03	D132	Cut core	Thin section petrography, WR major/trace elements (XRF)

2.2 Petrography

Preliminary optical petrography was performed on polished, 50µm-thick thin sections. Mineral phase identification was conducted cautiously as thicker thin sections alter interference colors and render difficult identification for groundmass phase minerals. Variable alteration rendered it important to select areas where matrix and mineral phases are the least altered, particularly in Mel samples. In practice, thin sections were cut from the core that had the least number of crustal xenoliths and secondary veins. A total of nine thin sections were produced from the Mel core with samples spanning three prospective kimberlitic bodies. A total of twenty thin sections were produced from the Dharma Core spanning the drill hole from 17.4 to 91.3 m.

To assist traditional optical petrography, high-resolution scans of thin sections were acquired with Nikon Coolscan 9000 at the Digital Imaging Facility, University of Alberta, at a resolution of 4000 dpi for digital point counting. Digital point counting was completed in the program Rock.Ar (Larrea et al., 2014). An area of 1500 pixels by 900 pixels (9514.20 by 5708.52 µm) areas were selected from these images with 1 pixel corresponding to a length of 6.4 µm or an area of 40.96µm^2. A 100 by 60 grid was used with a grid-cell equal to 15 by 15 pixels (95.14 by 95.14µm). This grid spacing was chosen in order to differentiate matrix (<100 µm), microphenocryst (100 to 500µm), and macrocryst (>500µm) phases.

Optical petrography was accompanied by petrographic analysis using SEM at the University of Alberta using a Zeiss Sigma 300 VP-FESEM. SEM backscatter electron images were collected alongside EDS point analysis to identify matrix phase minerals and capture microscopic textures.

Petrographic descriptions followed the textural classification scheme outlined in Mitchell (1989). Mineral petrographic grouping corresponds to mineral size measured on long axis. The main petrographic groups are groundmass (minerals <100μ), microphenocryst (minerals 100 to 500 μm), and phenocryst (minerals >500μm). Microphenocryst and/or phenocryst minerals that correspond to xenocrysts are assigned to separate mineral categories. If identified, xenoliths are assigned to separate "mantle xenolith" or "crustal xenolith" categories. Groundmass minerals are identified but do not influence final point counting percentages. The designations of groundmass, microphenocryst, and phenocryst phases are strictly used in this text as size designations with no underlying genetic connotation.

2.3 Electron Probe Microanalysis

Electron probe microanalysis (EPMA) was completed at the Canadian Center for Isotopic Microanalysis at the University of Alberta using a JEOL JXA-8900R. Samples consisted of polished thin sections of kimberlite core and garnet grain mounts. Silicate and oxide analyses was completed using an accelerating voltage of 20 kV, a beam current of 20 nA, a spot-sized beam diameter (<1 μm), and a total count time of 6 minutes with 20 to 60 s for both peak and background. Quantitative compositional data were acquired using wavelength-dispersive spectrometry and Probe for EPMA software (Donovan et al. 2012). EPMA analyses for individual target minerals were calibrated using natural and synthetic standard reference material (SRM; Tables 2.02 to 2.09; Figures 2.01 to 2.08). Matrix corrections were performed using ZAF or φ (ρZ) calculations (Armstrong, 1988). Peak interference corrections were applied for Ti (interference peak by Ba), and Na (interference by Zn).

Table 2.02: EPMA parameters for Mel mica in situ analysis.

Mica (Mel) EPMA Parameters					
Accelerating voltage:					20 kV
Beam current:					20 nA
Element	*Crystal*	*On Peak*	*Off Peak*	*01/30/20 Std.*	*01/31/20 Std.*
Si Ka	TAP	40	40	Frank Smith pyrope garnet	
Ca Ka	PETH	20	20	Plagioclase (labradorite) 115900	
Na Ka	TAP	60	60	NaAlSi3O8 albite VA 131705	
Fe Ka	LIFH	20	20	Fe2SiO4 fayalite Rockport	
Mn Ka	LIFH	20	20	(Mn,Fe)3Al2Si3O12 spessartine, Navegadora Mine	
K Ka	PETH	20	20	KAlSi3O8 sanidine Itrongay	
Ti Ka	PET	20	20	TiO2 Rutile MTI	
Al Ka	TAP	40	40	Plagioclase (labradorite) 115900	
Cr Ka	PET	20	20	Cr2O3 chromium oxide Alfa	
V Ka	PET	20	20	V vanadium Alfa	
Ni Ka	LIFH	20	20	Ni nickel Alfa	
Zn Ka	LIFH	20	20	Sphalerite ZnS	
Mg Ka	TAP	40	40	Frank Smith pyrope garnet	
Nb La	PETH	20	20	Niobium, Nb - ESPI	
Ba Lb	PET	20	20	BaSi2O5 Sanbornite, Fresno	
P Ka	PETH	20	20	Ca5(PO4)3F apatite, Wilberforce	

Table 2.03: EPMA parameters for Mel oxide in situ analysis.

Oxide (Mel) EPMA Parameters						
Accelerating voltage:						20 kV
Beam current:						20 nA
Element	*Crystal*	*On Peak*	*Off Peak*	*01/30/20 Std.*	*01/31/20 Std.*	*07/13/21 Std.*
Si Ka	TAP	40	40	Frank Smith pyrope garnet		CaMgSi2O6 diopside Wakefield
Ca Ka	PETH	20	20	Plagioclase (labradorite) 115900		CaMgSi2O6 diopside Wakefield
Na Ka	TAP	60/40*	60/40*	NaAlSi3O8 albite VA 131705		
Fe Ka	LIFH	20	20	FeTiO3 Ilmenite 96189		Fe2SiO4 fayalite Rockport
Mn Ka	LIFH	20	20	(Mn,Fe)3Al2Si3O12 spessartine, Navegadora Mine		
K Ka	PETH	20	20	KAlSi3O8 sanidine Itrongay		
Ti Ka	PET	20	20	FeTiO3 Ilmenite 96189		TiO2 Rutile MTI
Al Ka	TAP	40	40	Plagioclase (labradorite) 115900		Frank Smith pyrope garnet
Cr Ka	PET	20	20	Cr2O3 chromium oxide Alfa		
V Ka	PET	20	20	V vanadium Alfa		
Ni Ka	LIFH	20	20	Ni nickel Alfa		
Zn Ka	LIFH	20	20	Sphalerite ZnS		
Mg Ka	TAP	40	40	Frank Smith pyrope garnet		CaMgSi2O6 diopside Wakefield
Nb La	PETH	20	20	Niobium, Nb - ESPI		
Ba Lb	PET	20	20	BaSi2O5 Sanbornite, Fresno		
P La	PETH	20	20	Ca5(PO4)3F apatite, Wilberforce		not measured

**First value for 01/30/20 and 01/31/20 SRM. Second value for 07/13/21 SRM.*

Table 2.04: EPMA parameters for Mel garnet separate analysis.

Garnet Separate (Mel) EPMA Parameters					
Accelerating voltage:					20 kV
Beam current:					20 nA
Element	*Crystal*	*On Peak*	*Off Peak*	*12/15/20 Std.*	*12/18/20 Std.*
Si Ka	TAP	30	30	Frank Smith pyrope garnet	
Ca Ka	PETH	60	60	Plagioclase (labradorite) 115900	
Na Ka	TAP	30	30	NaAlSi3O8 albite VA 131705	
Fe Ka	LIFH	20	20	Fe2SiO4 fayalite Rockport	
Mn Ka	LIFH	20	20	(Mn,Fe)3Al2Si3O12 spessartine, Navegadora Mine	
Ti Ka	PET	20	20	TiO2 Rutile MTI	
Mg Ka	TAP	30	30	Frank Smith pyrope garnet	
Al Ka	TAP	30	30	Frank Smith pyrope garnet	
Cr Ka	PET	20	20	Cr2O3 chromium oxide Alfa	
Ni Ka	LIFH	20	20	Ni nickel Alfa	
V Ka	PET	20	20	V vanadium Alfa	

Table 2.05: EPMA parameters for Dharma olivine in situ analysis.

Olivine (Dharma) EPMA Parameters						
Accelerating voltage:						20 kV
Beam current:						20 nA
Element	*Crystal*	*On Peak*	*Off Peak*	*01/13/20 Std.*	*01/14/20 Std.*	*01/15/20 Std.*
Si Ka	TAP	40	40	Fo90.5		
Ca Ka	PETH	20	20	CaMgSi2O6 diopside Wakefield		
Na Ka	TAP	60	60	NaAlSi3O8 albite VA 131705		
Fe Ka	LIFH	20	20	Fe2SiO4 fayalite Rockport		
Mn Ka	LIFH	20	20	(Mn,Fe)3Al2Si3O12 spessartine, Navegadora Mine		
K Ka	PETH	20	20	KAlSi3O8 sanidine Itrongay		
Ti Ka	PET	20	20	TiO2 Rutile MTI		
Al Ka	TAP	40	40	Frank Smith pyrope garnet		
Cr Ka	PET	20	20	Cr2O3 chromium oxide Alfa		
V Ka	PET	20	20	V vanadium Alfa		
Ni Ka	LIFH	20	20	Ni nickel Alfa		
Zn Ka	LIFH	20	20	Sphalerite ZnS		
Mg Ka	TAP	40	40	Fo90.5		
Nb La	PETH	20	20	Niobium, Nb - ESPI		
Ba Lb	PET	20	20	BaSi2O5 Sanbornite, Fresno		
P Ka	PETH	20	20	Ca5(PO4)3F apatite, Wilberforce		

Table 2.06: EPMA parameters for Dharma pyroxene in situ analysis.

Pyroxene (Dharma) EPMA Parameters						
Accelerating voltage:						20 kV
Beam current:						20 nA
Element	*Crystal*	*On Peak*	*Off Peak*	*01/13/20 Std.*	*01/14/20 Std.*	*01/15/20 Std.*
Si Ka	TAP	40	40	CaMgSi2O6 diopside Wakefield		
Ca Ka	PETH	20	20	CaMgSi2O6 diopside Wakefield		
Na Ka	TAP	60	60	NaAlSi3O8 albite VA 131705		
Fe Ka	LIFH	20	20	Fe2SiO4 fayalite Rockport		
Mn Ka	LIFH	20	20	(Mn,Fe)3Al2Si3O12 spessartine, Navegadora Mine		
K Ka	PETH	20	20	KAlSi3O8 sanidine Itrongay		
Ti Ka	PET	20	20	TiO2 Rutile MTI		
Al Ka	TAP	40	40	Frank Smith pyrope garnet		
Cr Ka	PET	20	20	Cr2O3 chromium oxide Alfa		
V Ka	PET	20	20	V vanadium Alfa		
Ni Ka	LIFH	20	20	Ni nickel Alfa		
Zn Ka	LIFH	20	20	Sphalerite ZnS		
Mg Ka	TAP	40	40	CaMgSi2O6 diopside Wakefield		
Nb La	PETH	20	20	Niobium, Nb - ESPI		
Ba Lb	PET	20	20	BaSi2O5 Sanbornite, Fresno		
P Ka	PETH	20	20	Ca5(PO4)3F apatite, Wilberforce		

Table 2.07: EPMA parameters for Dharma mica in situ analysis.

Mica (Dharma) EPMA Parameters						
Accelerating voltage:						20 kV
Beam current:						20 nA
Element	*Crystal*	*On Peak*	*Off Peak*	*01/13/20 Std.*	*01/15/20 Std.*	*07/13/21 Std.*
Si Ka	TAP	40	40	Frank Smith pyrope garnet		CaMgSi2O6 diopside Wakefield
Ca Ka	PETH	20	20	Plagioclase (labradorite) 115900		CaMgSi2O6 diopside Wakefield
Na Ka	TAP	60/40*	60/40*	NaAlSi3O8 albite VA 131705		
Fe Ka	LIFH	20	20	Fe2SiO4 fayalite Rockport		
Mn Ka	LIFH	20	20	(Mn,Fe)3Al2Si3O12 spessartine, Navegadora Mine		
K Ka	PETH	20	20	KAlSi3O8 sanidine Itrongay		
Ti Ka	PET	20	20	TiO2 Rutile MTI		
Al Ka	TAP	40	40	Plagioclase (labradorite) 115900		Frank Smith pyrope garnet
Cr Ka	PET	20	20	Cr2O3 chromium oxide Alfa		
V Ka	PET	20	20	V vanadium Alfa		
Ni Ka	LIFH	20	20	Ni nickel Alfa		
Zn Ka	LIFH	20	20	Sphalerite ZnS		
Mg Ka	TAP	40	40	Frank Smith pyrope garnet		CaMgSi2O6 diopside Wakefield
Nb La	PETH	20	20	Niobium, Nb - ESPI		
Ba Lb	PET	20	20	BaSi2O5 Sanbornite, Fresno		
P Ka	PETH	20	20	Ca5(PO4)3F apatite, Wilberforce		Not Measured

**First value for 01/13/20 and 01/15/20 SRM. Second value for 07/13/21 SRM.*

Table 2.08: EPMA parameters for Dharma oxide in situ analysis.

Oxide (Dharma) EPMA Parameters					
Accelerating voltage:					20 kV
Beam current:					20 nA
Element	*Crystal*	*On Peak*	*Off Peak*	*01/14/20 Std.*	*01/15/20 Std.*
Si Ka	TAP	40	40	Fo90.5	
Ca Ka	PETH	20	20	CaMgSi2O6 diopside Wakefield	
Na Ka	TAP	60	60	NaAlSi3O8 albite VA 131705	
Fe Ka	LIFH	20	20	Fe2SiO4 fayalite Rockport	
Mn Ka	LIFH	20	20	(Mn,Fe)3Al2Si3O12 spessartine, Navegadora Mine	
K Ka	PETH	20	20	KAlSi3O8 sanidine Itrongay	
Ti Ka	PET	20	20	TiO2 Rutile MTI	
Al Ka	TAP	40	40	Frank Smith pyrope garnet	
Cr Ka	PET	20	20	Cr2O3 chromium oxide Alfa	
V Ka	PET	20	20	V vanadium Alfa	
Ni Ka	LIFH	20	20	Ni nickel Alfa	
Zn Ka	LIFH	20	20	Sphalerite ZnS	
Mg Ka	TAP	40	40	Fo90.5	
Nb La	PETH	20	20	Niobium, Nb - ESPI	
Ba Lb	PET	30	30	BaSi2O5 Sanbornite, Fresno	
P Ka	PETH	20	20	Ca5(PO4)3F apatite, Wilberforce	

Table 2.09: EPMA parameters for Dharma garnet separate analysis.

Garnet (Dharma) EPMA Parameters					
Accelerating voltage:					20 kV
Beam current:					20 nA
Element	*Crystal*	*On Peak*	*Off Peak*	*02/26/21 Std.*	*03/02/21 Std.*
Ti Ka	PET	20	20	TiO2 Rutile MTI	
Mg Ka	TAP	30	30	Frank Smith pyrope garnet	
Si Ka	TAP	30	30	Frank Smith pyrope garnet	
Fe Ka	LIFH	20	20	Fe2SiO4 fayalite Rockport	
Cr Ka	PET	20	20	Cr2O3 chromium oxide Alfa	
Na Ka	TAP	30	30	NaAlSi3O8 albite VA 131705	
Ca Ka	PETH	60	60	Plagioclase (labradorite) 115900	
Al Ka	TAP	30	30	Frank Smith pyrope garnet	
Ni Ka	LIFH	20	20	Ni nickel Alfa	
Mn Ka	LIFH	20	20	(Mn,Fe)3Al2Si3O12 spessartine, Navegadora Mine	
V Ka	PET	30	30	V vanadium Alfa	

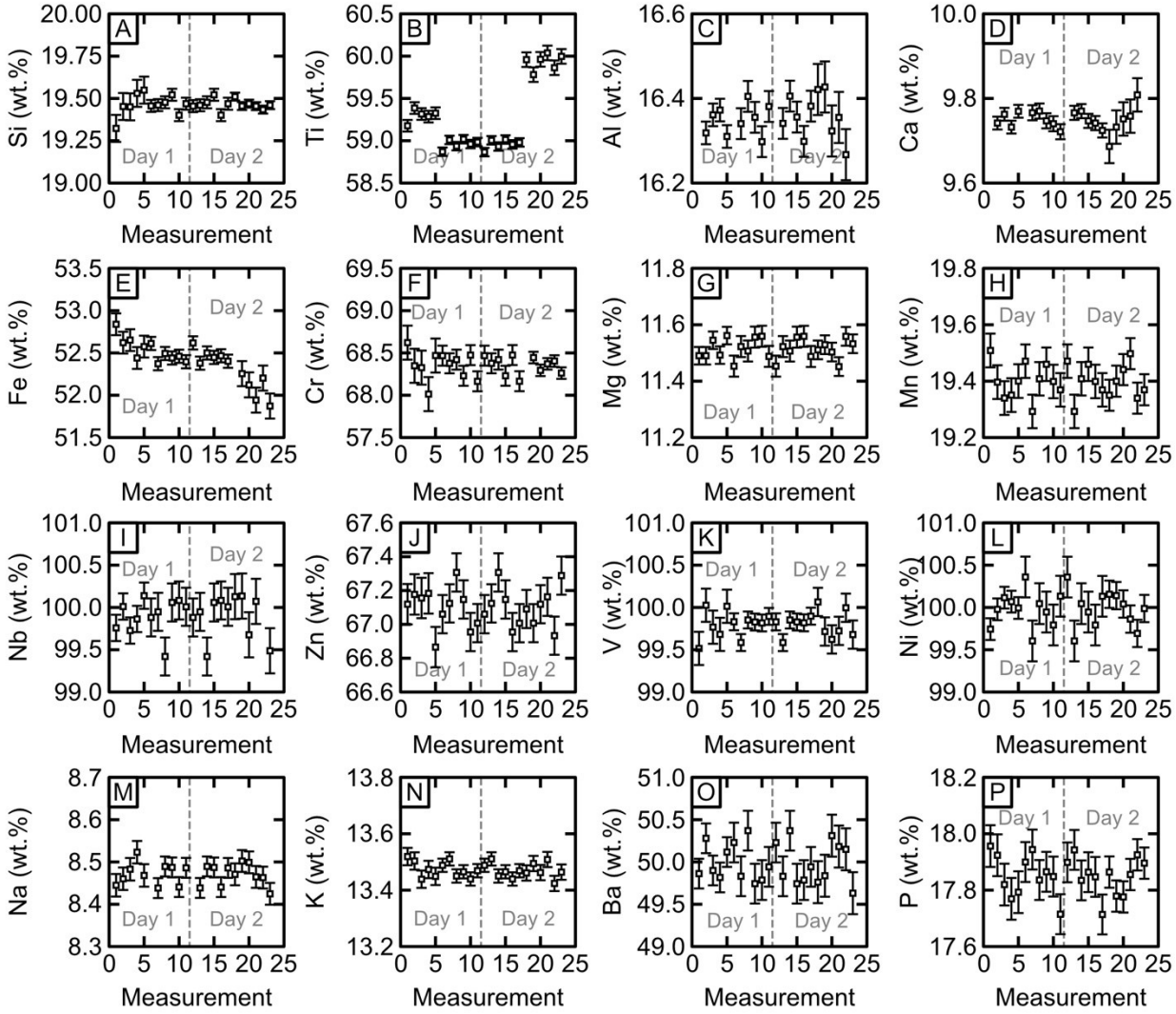

Figure 2.01: Plots of element variability in EPMA SRM used for Mel mica analysis. Natural and synthetic reference materials: A) Frank Smith pyrope garnet, B) TiO2 Rutile MTI, C) Plagioclase (labradorite) 115900, D) Plagioclase (labradorite) 115900, E) Fe2SiO4 fayalite Rockport, F) Cr2O3 chromium oxide Alfa, G) Frank Smith pyrope garnet, H) (Mn,Fe)3Al2Si3O12 spessartine - Navegadora Mine, I) Niobium - Nb - ESPI, J) Sphalerite ZnS, K) V vanadium Alfa, L) Ni nickel Alfa, M) NaAlSi3O8 albite VA 131705, N) KAlSi3O8 sanidine Itrongay, O) BaSi2O5 Sanbornite, Fresno, P) Ca5(PO4)3F apatite, Wilberforce. Day 1 and Day 2 correspond to reference material measurements on 01/30/2020 and 01/31/2020 respectively.

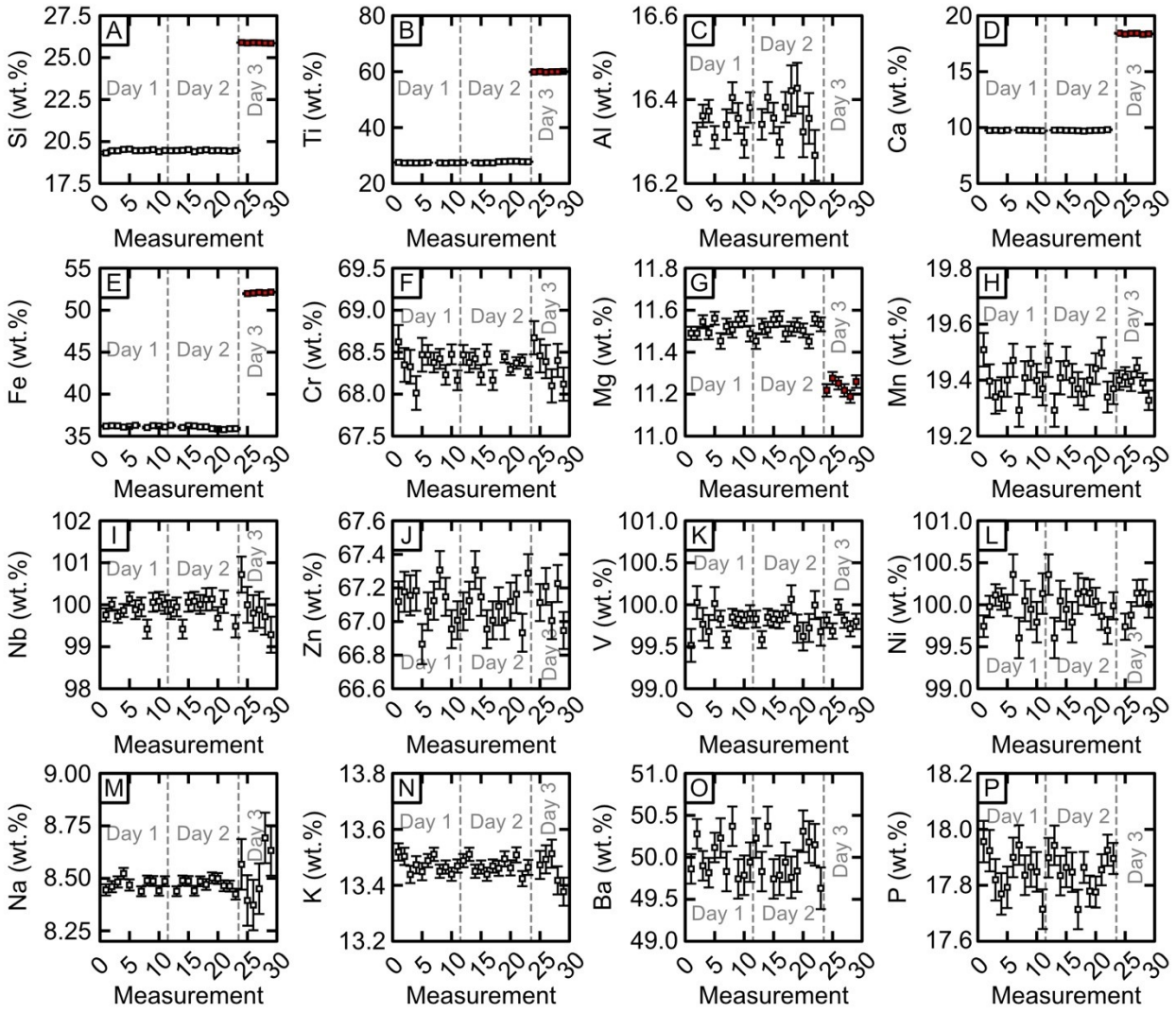

Figure 2.02: Plots of element variability in EPMA SRM used for Mel oxide analysis. Natural and synthetic reference materials: A) Frank Smith pyrope garnet (white square) and CaMgSi2O6 diopside Wakefield (red square), B) FeTiO3 Ilmenite 96189 (white square) and TiO2 Rutile MTI (red square), C) Plagioclase (labradorite) 115900, D) Plagioclase (labradorite) 115900 (white square) and CaMgSi2O6 diopside Wakefield (red square), E) FeTiO3 Ilmenite 96189 (white square) and Fe2SiO4 fayalite Rockport (red square), F) Cr2O3 chromium oxide Alfa, G) Frank Smith pyrope garnet (white square) and CaMgSi2O6 diopside Wakefield (red square), H) (Mn,Fe)3Al2Si3O12 spessartine - Navegadora Mine, I) Niobium – Nb-ESPI, J) Sphalerite ZnS, K) V vanadium Alfa, L) Ni nickel Alfa, M) NaAlSi3O8 albite VA 131705, N) KAlSi3O8 sanidine Itrongay, O) BaSi2O5 Sanbornite, Fresno, P) Ca5(PO4)3F apatite, Wilberforce. Day 1, Day 2, and Day 3 correspond to reference material measurements on 01/30/2020, 01/31/2020, and 07/13/2021 respectively.

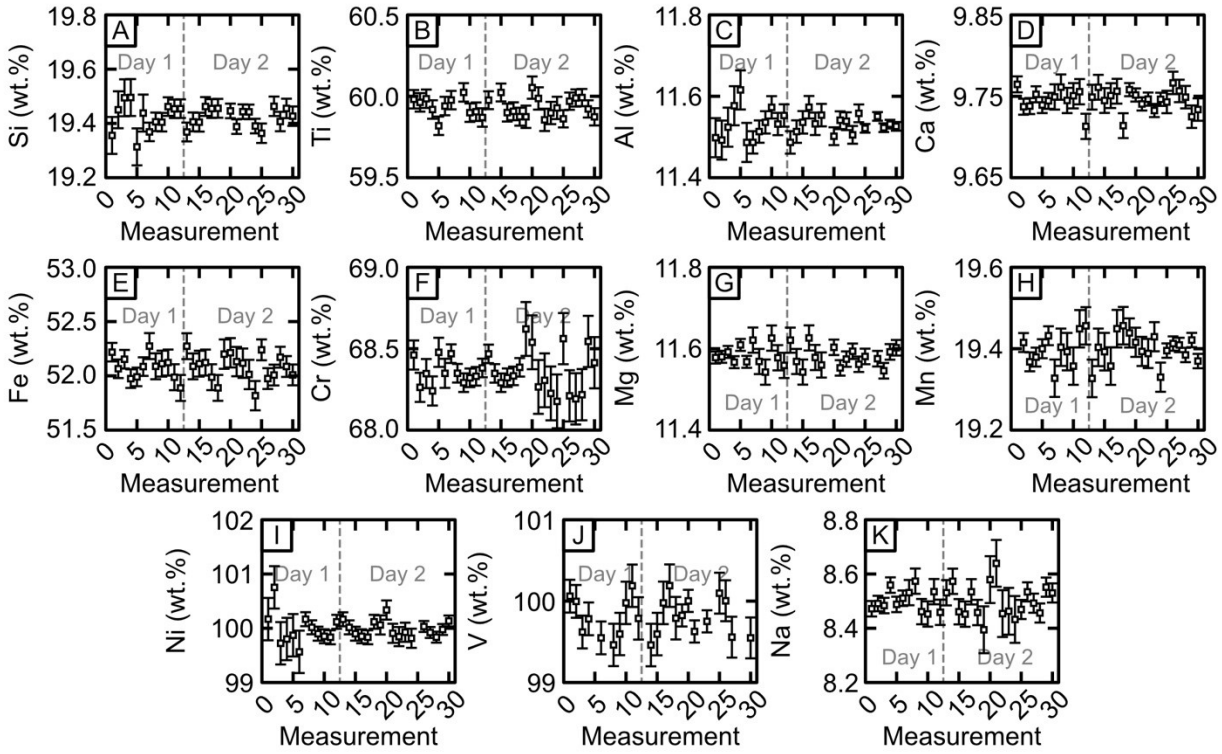

Figure 2.03: Plots of element variability in EPMA SRM used for Mel garnet analysis. Natural and synthetic reference materials: A) Frank Smith pyrope garnet, B) TiO2 Rutile MTI, C) Frank Smith pyrope garnet, D) Plagioclase (labradorite) 115900, E) Fe2SiO4 fayalite Rockport, F) Cr2O3 chromium oxide Alfa, G) Frank Smith pyrope garnet, H) (Mn,Fe)3Al2Si3O12 spessartine - Navegadora Mine, I) Ni nickel Alfa, J) V vanadium Alfa, K) NaAlSi3O8 albite VA 131705. Day 1 and Day 2 correspond to reference material measurements on 12/15/2020 and 12/18/2020 respectively.

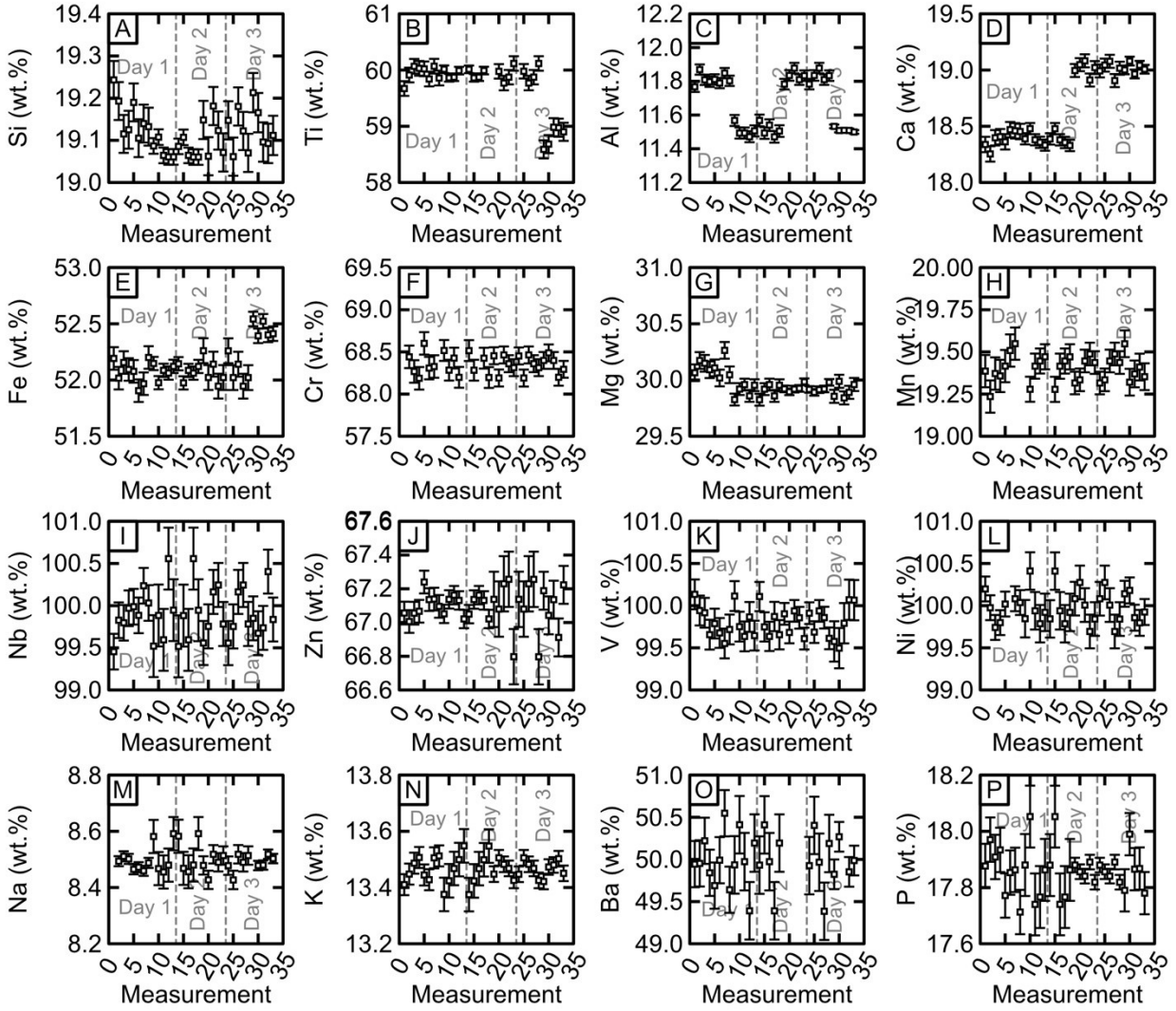

Figure 2.04: Plots of element variability in EPMA SRM used for Dharma olivine analysis. Natural and synthetic reference materials: A) Fo90.5, B) TiO2 Rutile MTI, C) Frank Smith pyrope garnet, D) CaMgSi2O6 diopside Wakefield, E) Fe2SiO4 fayalite Rockport, F) Cr2O3 chromium oxide Alfa, G) Fo90.5, H) (Mn,Fe)3Al2Si3O12 spessartin - Navegadora Mine, I) Niobium – Nb-ESPI, J) Sphalerite ZnS, K) V vanadium Alfa, L) Ni nickel Alfa, M) NaAlSi3O8 albite VA 131705, N) KAlSi3O8 sanidine Itrongay, O) BaSi2O5 Sanbornite, Fresno, P) Ca5(PO4)3F apatite. Day 1, Day 2, and Day 3 correspond to reference material measurements on 01/13/2020, 01/14/2020, and 01/15/2020 respectively.

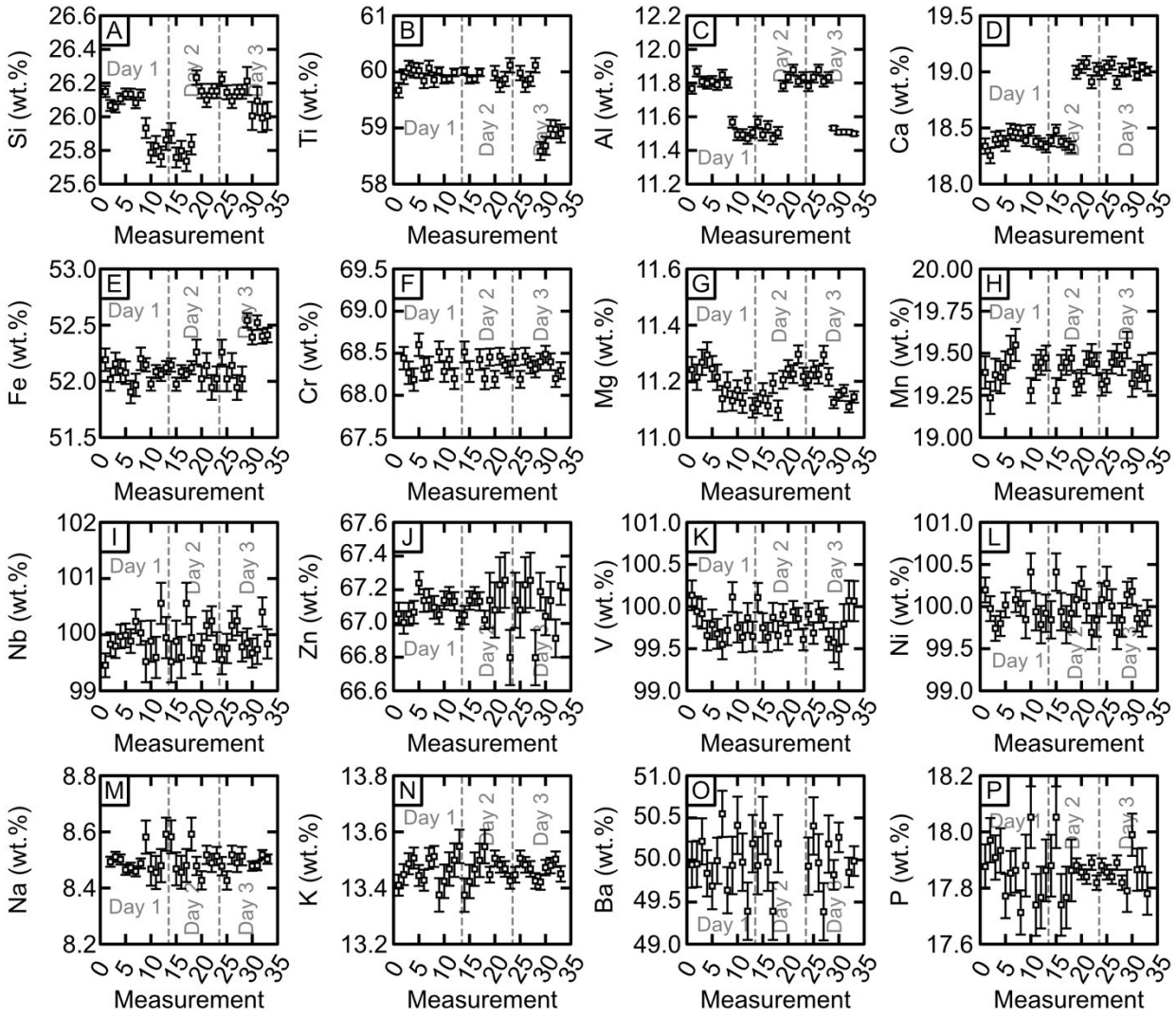

Figure 2.05: Plots of element variability in EPMA SRM used for Dharma pyroxene analysis. Natural and synthetic reference materials: A) CaMgSi2O6 diopside Wakefield, B) TiO2 Rutile MTI, C) Frank Smith pyrope garnet, D) CaMgSi2O6 diopside Wakefield, E) Fe2SiO4 fayalite Rockport, F) Cr2O3 chromium oxide Alfa, G) CaMgSi2O6 diopside Wakefield, H) (Mn,Fe)3Al2Si3O12 spessartine - Navegadora Mine, I) Niobium – Nb-ESPI, J) Sphalerite ZnS, K) V vanadium Alfa, L) Ni nickel Alfa, M) NaAlSi3O8 albite VA 131705, N) KAlSi3O8 sanidine Itrongay, O) BaSi2O5 Sanbornite, Fresno, P) Ca5(PO4)3F apatite. Day 1, Day 2, and Day 3 correspond to reference material measurements on 01/13/2020, 01/14/2020, and 01/15/2020 respectively.

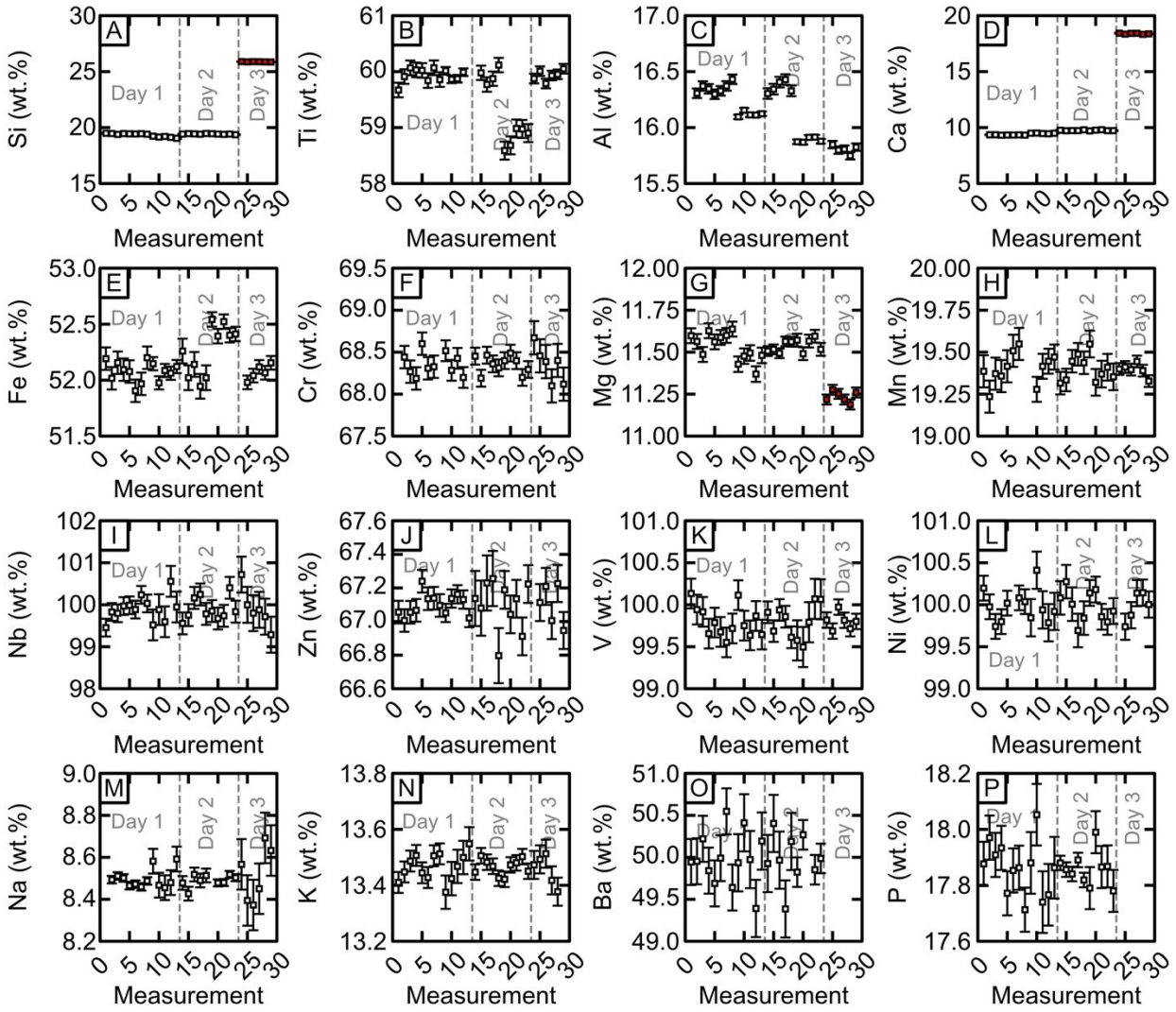

Figure 2.06: Plots of element variability in EPMA SRM used for Dharma mica analysis. Natural and synthetic reference materials: A) Frank Smith pyrope garnet (white square) and CaMgSi2O6 diopside Wakefield (red square), B) TiO2 Rutile MTI, C) Plagioclase (labradorite) 115900, D) Plagioclase (labradorite) 115900 (white square) and CaMgSi2O6 diopside Wakefield (red square), E) Fe2SiO4 fayalite Rockport, F) Cr2O3 chromium oxide Alfa, G) Frank Smith pyrope garnet (white square) and CaMgSi2O6 diopside Wakefield (red square), H) (Mn,Fe)3Al2Si3O12 spessartine - Navegadora Mine, I) Niobium – Nb-ESPI, J) Sphalerite ZnS, K) V vanadium Alfa, L) Ni nickel Alfa, M) NaAlSi3O8 albite VA 131705, N) KAlSi3O8 sanidine Itrongay, O) BaSi2O5 Sanbornite, Fresno, P) Ca5(PO4)3F apatite. Day 1, Day 2, and Day 3 correspond to reference material measurements on 01/13/2020, 01/1/2020, and 07/13/2021 respectively.

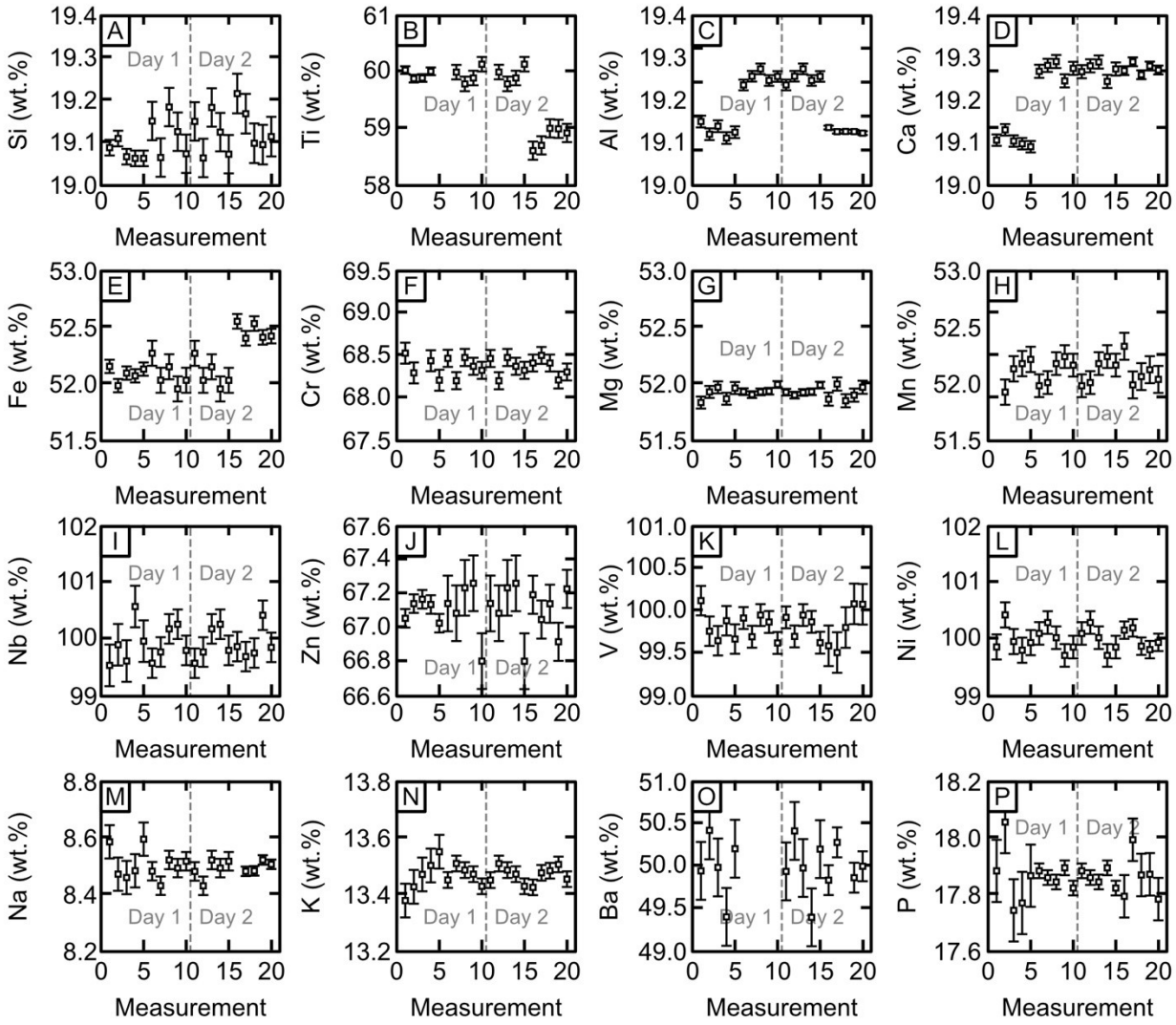

Figure 2.07: Plots of element variability in EPMA SRM used for Dharma oxide analysis. Natural and synthetic reference materials: A) Fo90.5, B) TiO2 Rutile MTI, C) Frank Smith pyrope garnet, D) CaMgSi2O6 diopside Wakefield, E) Fe2SiO4 fayalite Rockport, F) Cr2O3 chromium oxide Alfa, G) Fo90.5, H) (Mn,Fe)3Al2Si3O12 spessartine, Navegadora Mine, I) Niobium – Nb-ESPI, J) Sphalerite ZnS, K) V vanadium Alfa, L) Ni nickel Alfa, M) NaAlSi3O8 albite VA 131705, N) KAlSi3O8 sanidine Itrongay, O) BaSi2O5 Sanbornite, Fresno, P) Ca5(PO4)3F apatite. Day 1 and Day 2 correspond to reference material measurements on 01/14/2020 and 01/15/2020 respectively.

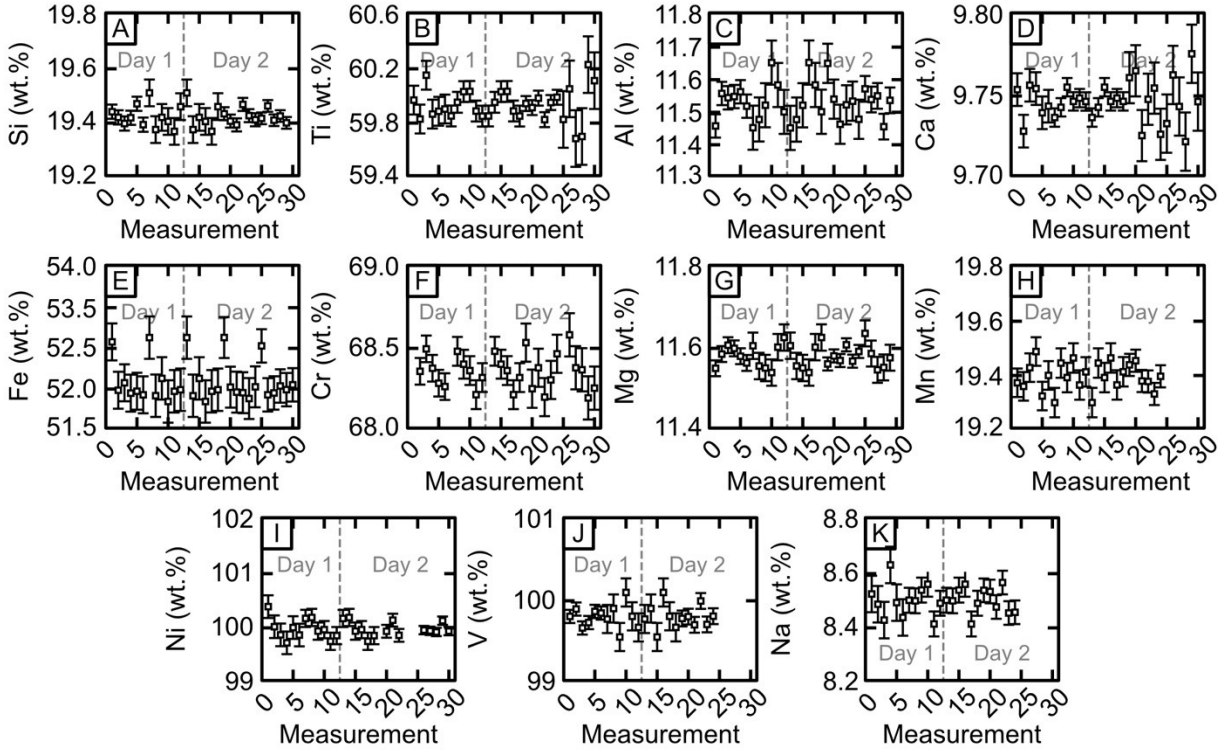

Figure 2.08: Plots of element variability in EPMA SRM used for Dharma garnet analysis. Natural and synthetic reference materials: A) Frank Smith pyrope garnet, B) TiO2 Rutile MTI, C) Frank Smith pyrope garnet, D) Plagioclase (labradorite) 115900, E) Fe2SiO4 fayalite Rockport, F) Cr2O3 chromium oxide Alfa, G) Frank Smith pyrope garnet, H) (Mn,Fe)3Al2Si3O12 spessartine - Navegadora Mine, I) Ni nickel Alfa, J) V vanadium Alfa, K) NaAlSi3O8 albite VA 131705. Day 1 and Day 2 correspond to reference material measurements on 02/26/2021 and 03/02/2021 respectively.

Sixteen oxides were analyzed in silicate and oxide phases (Nb_2O_5, SiO_2, TiO_2, ZnO, Al_2O_3, V_2O_3, Cr_2O_3, FeO, NiO, MgO, CaO, BaO, Na_2O, K_2O, P_2O_5) with H2O calculated for hydrous minerals (i.e. phlogopite and biotite). Iron was analyzed as FeOT for all phases. Final compositions for oxides were recalculated on the basis of 16 oxides using a 16-oxide charge-balance calculation spreadsheet available from Electron Microprobe Laboratory at the Department of Earth and Atmospheric Sciences at the University of Alberta (www.eas.ualberta.ca/eml, 2019). Final reported analysis for all mineral compositions include analysis with total oxide values greater than 97.9 wt.% and were checked for acceptable stoichiometry. Sizes of analyzed phases follow the convention outlined in section 2.2 of this chapter.

2.4 Laser Ablation ICPMS and Ni in Garnet Geothermometry

Trace element analysis of picked Mel and Dharma garnet grains in epoxy mounts was completed by laser ablation inductively coupled plasma mass spectrometry (LA-ICP-MS) using a RESOlution 193 nm ArF Excimer Laser Ablation system equipped with a Laurin-Technic S-155 dual cell and a Thermo Element II XR ICP-MS. Prior to analysis, garnets were analyzed by EPMA to identify target grains (see section 2.3.3). The size of the garnet grain dictated the use of three spot sizes of 285 µm, 130 µm, or 90 µm. Unknown samples were bracketed with trace elements in glass SRM NIST612 and internal garnet SRM PHN3511-C (Figure 2.09; Hardman, 2020). Data is reduced in Iolite 4 using the "Trace Element" data reduction scheme with detection limits calculated using Pettke et al. (2012). SiO2 is used as an internal element standard with silica values referenced to those determined by EPMA measurement. Ni from the garnet trace elements was used to calculate mantle temperatures using calculations from Ryan et al. (1996), Canil (1999),

Shu and Brey (2015), and Sudholz et al. (2021), as shown in Equations 2.1, 2.2 and 2.3 respectively.

Equation 2.01 (Ryan et al., 1996):

$$T_{Ni} = \frac{1000}{\left(1.506 - \left(0.189 \times ln\left(Ni_{ppm}^{grt}\right)\right)\right)} - 273$$

Equation 2.02 (Canil, 1999):

$$T_{Ni} = \frac{8772}{\left(2.53 - \left(0.189 \times ln\left({Ni_{ppm}^{grt}}/{2900}\right)\right)\right)} - 273$$

Equation 2.03 (Shu and Brey, 2015):

$$T_{Ni} = \frac{-8245.568}{\left(\left(3.023 \times \frac{Ca_{apfu}^{grt}}{\left(Ca_{apfu}^{grt} + Fe_{apfu}^{grt} + Mg_{apfu}^{grt}\right)}\right) + \left(2.307 \times \frac{Cr_{apfu}^{grt}}{\left(Cr_{apfu}^{grt} + Al_{apfu}^{grt}\right)}\right) + \ln\left({Ni_{ppm}^{grt}}/{3000}\right) - 2.639\right)} - 273 \pm 55$$

Equation 2.04 (Sudholz et al., 2021):

$$T_{Ni} = \frac{\left(\left(\frac{1000}{-0.435 \times log_{10}\left({Ni_{ppm}^{grt}}/{30}\right)}\right)\right) + \left(\frac{8772}{\left(2.53 - ln\left({Ni_{ppm}^{grt}}/{2900}\right)\right)}\right)}{2}$$

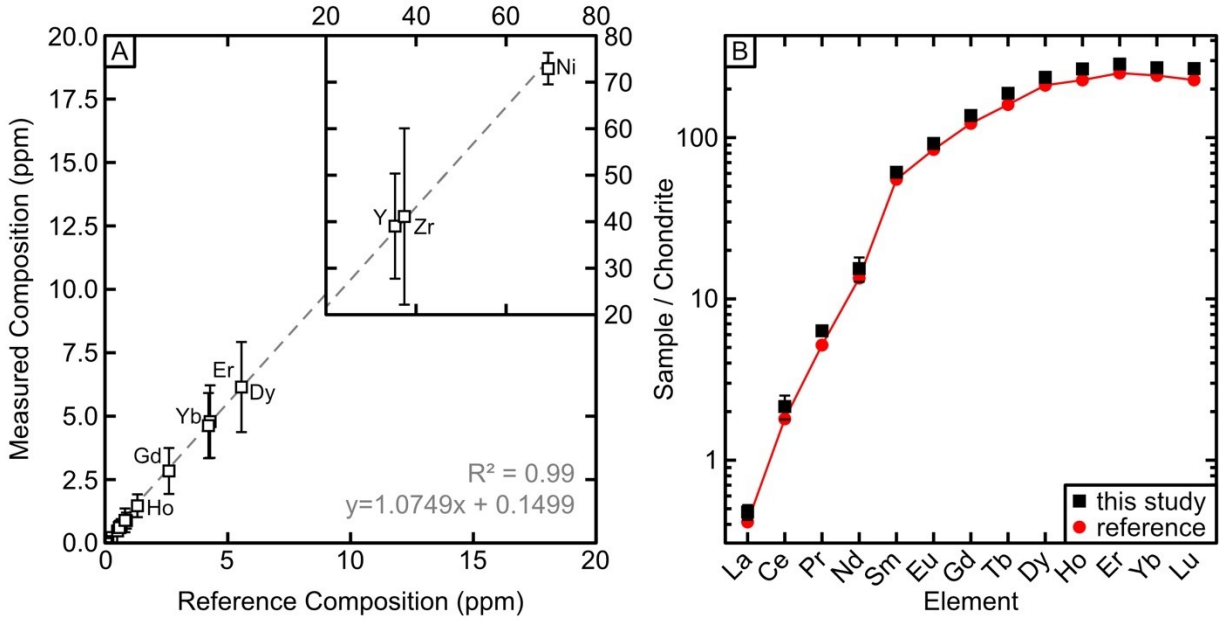

Figure 2.09: Trace element variability of PHN3511-C internal standard. A) PHN3511-C internal standard composition compared to reference composition (Hardman, 2020). B) Chondrite normalized (Palme and O'Neill, 2014) REE of PHN3511-C from this study and reference composition (Hardman, 2020).

2.5 Whole Rock Major Element and Trace Element Geochemistry by XRF

Sample preparation for major and trace element analyses were completed at the Arctic Resources Laboratory (University of Alberta). Samples of hypabyssal kimberlite with minimal surface alteration were cut in order to minimize the crustal and mantle contaminants (e.g. mantle xenocrysts, crustal xenoliths). Samples were manually crushed to 10 mesh and processed into a powder in an agate puck mill. This powder was split for major element and trace element analysis and stored in clean plastic containers.

Major element analyses were completed at Franklin and Marshall College following procedures outlined in Waterton et al (2020), which gives long-term performance data for SRM analyzed during the course of this study. Powdered samples were measured for loss on ignition (LOI) after 1.5 hours at 950 C in a muffle furnace. After LOI, 0.4000 ± 0.0001 g of anhydrous sample powder and 3.6000 ± 0.0002 g of lithium tetraborate was fused in a platinum crucible heated by a meeker burner and cast into glass beads. Sample glass beads were analyzed by X-Ray Fluorescence (XRF) using a Panalytical PW 2404 X-ray Fluorescence spectrometer and data are reported as SiO_2, TiO_2, Al_2O_3, Fe_2O_3 (total Fe), MnO, MgO, CaO, Na_2O, K_2O, and P_2O_5 oxides by weight percent.

Pressed pellet trace element analysis by XRF was completed at Franklin and Marshall College. 1.4000 ± 0.0002 of high purity copolywax powder is added to 7.0000 ± 0.0004 grams of whole rock powder and mixed for ten minutes. The mixed powder is pressed into a briquette at 50,000 psi. Data are reported as parts per million (ppm) for Rb, Sr, Y, Zr, V, Ni, Cr, Nb, Ga, Cu, Zn, Co, Ba, U, Th, La, Ce, Sc, and Pb. Waterton et al (2020) present long-term accuracy and precision data for SRM.

Unknown samples were analyzed alongside USGS SRM BHVO-2. The major element precision and accuracy of this SRM is reported on the Franklin and Marshall College XRF laboratory website (Waterton et al., 2020).

2.6 Whole Rock Trace Element Geochemistry by HR-ICP-MS

Pressed pellet XRF trace element analyses are supplemented by additional whole rock trace element geochemistry using a method modified from Ottley, et al. (2003) at the Arctic Resources Geochemistry Laboratory, University of Alberta. High-resolution magnetic sector inductively-coupled plasma mass spectrometry (HR-ICP-MS) was utilized to determine the trace element compositions of five Mel, six Dharma samples, and USGS international rock RSM's AGV-2, BCR2-2, and BHVO-2 (Table 2.10). The analyses were completed on a Thermo Scientific Element XR coupled with an ESI PC3 (a Peltier cooled spray chamber), using an ESI Teflon nebulizer with an uptake rate of approximately 50µL/min.

Approximately 100 mg were weighed into 15ml Savillex Teflon beakers, pre-cleaned using HCL/HNO_3. Samples dissolve in 2.5ml conc. HNO_3 and 4ml of conc. HF at 150 °C for 48 hrs. All acids used are Teflon distilled in-house. Insoluble fluorides were removed by addition of 1 mL conc. HNO_3 and evaporation to near dryness twice. The dried samples were diluted to 10ml by addition of a stock solution of 3% HNO_3, with trace HF, doped with 10ppb In as an internal standard.

Table 2.10: Trace element compositions (in mg/g) of USGS SRM. Analyses by HR-ICP-MS in this work compared to preferred values (Ref.) after Jochum et al. (2016).

SRM	BIR-1				BHVO-2				BCR-2						AGV-2					
Sample	1	2σ	Ref.	2σ	1	2σ	Ref.	2σ	1	2σ	2	2σ	Ref.	2σ	1	2σ	2	2σ	Ref	2σ
Co	57	3	52.22	0.57	48	2	44.9	0.3	39	2	40	2	37.33	0.37	16.4	0.6	16.6	0.6	15.46	0.5
Ni	179	8	168.9	1.9	128	4	120	1	12.9	0.5	12.3	0.6	12.57	0.3	18.8	0.7	18.8	0.7	18.87	0.41
Cu	123	5	120.7	1.6	136	4	129	1	19.9	0.8	17.9	0.9	19.66	0.72	52	2	53	2	51.51	0.65
Zn	78	3	70.4	1.1	113	16	104	1	142	6	137	21	129.5	1.8	91	3	92	13	86.7	1.2
Rb	0.20	0.02	0.21	0.0081	9.1	0.5	9.3	0.1	50	12	46	2	46.02	0.56	46	12	70	5	67.79	0.66
Sr	113	9	108.6	0.7	420	26	394	2	460	19	360	24	337.4	6.7	872	31	686	38	659.5	5.7
Y	13.3	0.5	15.6	0.17	24	1	25.9	0.3	38	2	34	2	36.07	0.37	14	0.5	18.7	0.9	19.14	0.84
Zr	14.3	0.6	14.8	0.22	177	3	171	1	195	9	191	5	186.5	1.5	244	11	239	4	232	2.3
Nb	0.52	0.03	0.553	0.014	18	1	18.1	0.2	12.2	0.5	12.1	0.7	12.44	0.2	13.8	0.5	13.5	0.7	14.12	0.22
Cs	0.005	0.002	0.0065	0.0007	0.096	0.007	0.1	0.002	1.19	0.08	1.16	0.07	1.16	0.023	1.1	0.05	1.15	0.05	1.173	0.018
Ba	6.7	0.5	6.75	0.13	135	9	131	1	929	61	706	37	683.9	4.7	1531	56	1158	58	1134	8
La	0.61	0.02	0.627	0.012	14.9	0.8	15.2	0.08	25	1	25	1	25.08	0.16	35	6	37	2	38.21	0.38
Ce	1.99	0.07	1.92	0.023	37	2	37.5	0.2	67	3	54	3	53.12	0.33	73	3	71	3	69.43	0.57
Pr	0.38	0.01	0.3723	0.0047	5.3	0.3	5.34	0.03	6.9	0.3	6.8	0.3	6.827	0.044	7.2	0.2	8.1	0.4	8.165	0.084
Nd	2.42	0.09	2.397	0.043	24	1	24.3	0.3	29	1	29	1	28.26	0.37	28	1	30	1	30.49	0.47
Sm	1.11	0.05	1.113	0.018	5.9	0.3	6.02	0.06	6.6	0.3	6.7	0.3	6.547	0.047	5.0	0.2	5.4	0.3	5.509	0.078
Eu	0.54	0.03	0.5201	0.0047	2	0.1	2.04	0.01	2	0.1	2	0.1	1.989	0.024	1.46	0.06	1.58	0.09	1.553	0.015
Gd	1.59	0.08	1.809	0.021	6.1	0.4	6.21	0.04	6.7	0.3	6.9	0.3	6.811	0.078	4.5	0.2	5.1	0.2	4.678	0.064
Tb	0.33	0.01	0.3623	0.005	0.93	0.06	0.939	0.006	1.01	0.04	1.07	0.07	1.077	0.026	0.56	0.02	0.65	0.03	0.651	0.0073
Dy	2.41	0.09	2.544	0.028	5.2	0.3	5.28	0.03	6.1	0.2	6.4	0.3	6.424	0.055	3.1	0.1	3.5	0.2	3.549	0.031
Ho	0.54	0.02	0.5718	0.0047	0.97	0.05	0.989	0.005	1.23	0.05	1.30	0.06	1.313	0.011	0.58	0.02	0.66	0.03	0.682	0.0081
Er	1.59	0.06	1.68	0.015	2.5	0.1	2.51	0.01	3.5	0.1	3.7	0.2	3.67	0.038	1.61	0.06	1.84	0.09	1.825	0.013
Yb	1.57	0.07	1.631	0.015	2	0.1	1.99	0.03	3.3	0.1	3.4	0.2	0.5341	0.006	1.44	0.06	1.65	0.08	1.653	0.013
Lu	0.232	0.009	0.2484	0.0032	0.27	0.01	0.275	0.002	0.47	0.02	0.5	0.04	0.5049	0.0078	0.211	0.007	0.25	0.01	0.251	0.0033
Hf	0.54	0.02	0.5822	0.0088	4.4	0.3	4.47	0.03	4.8	0.2	5	0.4	4.972	0.034	4.9	0.2	5.3	0.2	5.137	0.057
Ta	0.035	0.002	0.0414	0.002	1.07	0.06	1.15	0.02	0.72	0.03	0.74	0.04	0.785	0.018	0.76	0.03	0.8	0.04	0.865	0.019
Pb	3	0.1	3.037	0.049	1.47	0.07	1.65	0.04	9.7	0.4	9.5	0.5	10.59	0.17	11.8	0.4	12.6	0.6	13.14	0.15
Th	0.029	0.002	0.0328	0.0015	1.13	0.06	1.22	0.02	5.7	0.2	5.7	0.3	5.828	0.05	5.3	0.2	5.8	0.3	6.174	0.063
U	0.01	0.002	0.0105	0.0004	0.40	0.02	0.41	0.04	1.72	0.09	1.7	0.1	1.683	0.017	1.56	0.06	1.82	0.09	1.885	0.015

The samples were placed on a hotplate at 80 °C overnight to ensure dissolution. If undigested grains are not visible at this stage, each sample is diluted further to a final dissolution factor of x5000. Each step of dilution uses the same stock diluent with In internal standard in order to ensure consistency of the internal standard. This stock diluent is later used to correct samples for fluctuations in instrumental conditions through the sample run.

A calibration line was established daily on the Element XR using a standard solution with concentrations that mimic element dissolution in a basic silicate rock. The standard is made up to five different dilutions, for a five-point calibration line, using the same stock as the samples. This stock solution is used as the calibration blank and from there the rock standard forms a line of increasing concentrations up to at least 5000 times dilution so that it brackets the expected element concentrations in the samples.

The Element XR is tuned to give a signal sensitivity equivalent to 1.2 MCPS on 115 In (1ppb) and oxide formation rate of around 3% (UO^+/U^+). The Auxiliary gas ran at 0.78 mL/min and the sample gas at 1.012 L/min. Each measurement cycle lasts approx. 3 minutes and involves 6 runs and 4 passes, 50 samples per peak with 0.01 sec sampling times.

The accuracy of the three USGS secondary SRM relative to their accepted values is generally within 10% or better for most Elements.

The data were processed using an in-house data reduction spreadsheet (Waterton et al., 2017), which propagates uncertainties from the calibration lines for each element, corrections for isobaric

interferences (including uncertainties in oxide production), blank correction and internal standard normalization into the final uncertainty estimates.

2.7 Whole Rock Isotope Geochemistry by ICP-MS

Whole rock preparation for Lu-Hf, and Sm-Nd isotopes was completed at the Arctic Resources Laboratory (University of Alberta). Approximately 100 mg (0.1 g) of three Dharma samples, four Mel samples, and four USGS SRM BHVO-2 powders were loaded into 15ml Savillex Teflon beakers (precleaned with HCl/HNO_3). Samples were dissolved with 1.5 ml conc. HF and 0.5 ml conc. HNO_3 at 140 °C for 48 to 72 hours. Following first step dissolution, samples dry down on hot plate at 100°C for 1.5 hours or until gel. Samples were dissolved with 2 ml conc. HCl at 140°C for up to 168 hours. Following second step dissolution, samples dry down on hot plate at 100°C for 2 hours or until gel. Dry samples were dissolved into 1 ml of 3.00M HCl.

Dissolved rocks undergo a four-column chromatography procedure. The first column (Table 2.12) collects Lu and Hf aliquots and consists of 7.5 cm long column. The first column is stored in 1M TD HCL. The first column is preloaded with Ln Spec (100-150 μm) resin. The second column (Table 2.12) collects Sr and LREE aliquots and consists of a 7.5 cm long column. The second column is stored in Mili-Q-H_2O. The second column is preloaded with AG50W X8 20-50 mesh resin. The third column (Table 2.12) collects Sm, Nd, and remaining REE aliquots and consists of a 7.5 cm long column. The third column is stored in in 1M TD HCl. The third column is preloaded with Ln Spec (50-100 μm) resin. The fourth column collects the final Sr aliquot and is identical to the procedure outlined in Table 2.13.

Sm and Nd samples were analyzed at the Arctic Resources Laboratory (University of Alberta) using a Neptune Plus Inductively Coupled Plasma Mass Spectrometer (ICP-MS). Nd isotopes were measured in static mode, acquiring 60 ratios of 8 s integration per scan while 30 Sm ratios were measured with 4 s integrations. Mass fractionation of Nd isotopes was exponentially corrected by applying a $^{146}Nd/^{144}Nd$ ratio of 0.7219 outlined by Vance and Thirlwall (2002). The ^{149}Sm signal was monitored and the invariant ratio of $^{149}Sm/^{144}Sm$ was used to correct for any isobaric interference of Sm on ^{144}Nd. A 100 ppb solution of JNdi-1 was used as a primary SRM and it was measured repeatedly throughout the session. An average of 15 measurements of the JNdi-1 yielded a value of 0.512088 ± 0.000014 (2SD, n=15) which is slightly lower (33 ppm) than the accepted value (Jochum et al., 2005). All the secondary SRM and the samples were standard-corrected using a simple factor (Table 2.11). Initial $^{143}Nd/^{144}Nd$ isotope ratios were calculated using a ^{147}Sm decay constant of $6.539 \times 10^{-12} \pm 9.9 \times 10^{-14}$ (Lugmair and Marti 1978).

Whole rock Rb and Sr isotope preparation and analyses were completed at the Arctic Resources Laboratory (University of Alberta) following the procedure outlined in the following section (Table 2.13). Unlike in the procedure for phlogopite preparation, approximately 5 mg (0.005 g) of rock powder is weighed out and no ^{87}Rb-^{84}Sr spike is added.

εHf was calculated with the following constant values: $\lambda^{176Lu} = 1.867 \times 10^{-11} \pm 8.00 \times 10^{-14}$ (Soderlund et al., 2004), CHUR $(^{176}Hf/^{177}Hf)_{present} = 0.282785 \pm 0.000011$ (Bouvier et al., 2008), $^{176}Lu/^{177}Hf = 0.0336 \pm 0.0001$ (Bouvier et al., 2008). εNd was calculated with the following constant values: $\lambda^{147Sm} = 6.539 \times 10^{-12} \pm 6.1 \times 10^{-14}$ (Begemann et al., 2001), CHUR

($^{143}Nd/^{144}Nd)_{present}$ = 0.512638 ± 0.000025 (Jacobsen and Wasserburg, 1980; Hamilton et al., 1983), $^{147}Sm/^{144}Nd$ = 0.1967 ± 0.004 (Jacobsen and Wasserburg, 1980; Hamilton et al., 1983).

Table 2.11: Isotope compositions of USGS SRM BHVO-2. Analyses measured by ICP-MS and TIMS. Preferred values (Ref.) after mean values in the GeoReM database (Jochum et al., 2007).

SRM	***Method***	$^{87}Sr/^{86}Sr$	***2σ***	$^{143}Nd/^{144}Nd$	***2σ***	$^{176}Hf/^{177}Hf$	***2σ***
BHVO-2-1	ICP-MS	-	-	0.512982	0.000043	0.283077	0.000006
BHVO-2-2	ICP-MS	-	-	0.512992	0.000059	0.283070	0.000005
BHVO-2-3	ICP-MS	-	-	0.512994	0.000049	0.285272	0.000005
BHVO-2-4	ICP-MS	-	-	0.51299	0.00004	0.283074	0.000005
BHVO-2-1362*	TIMS	0.703488	0.000006	-	-	-	-
BHVO-2-1415*	TIMS	0.703473	0.000006	-	-	-	-
BHVO-2-1417	TIMS	0.703503	0.000006	-	-	-	-
BHVO-2-1442	TIMS	0.703484	0.000005	-	-	-	-
BHVO-2-1371	TIMS	0.703496	0.000005	-	-	-	-
BHVO-2-1395	TIMS	0.7035	0.00001	-	-	-	-
This Work	-	0.70349	-	0.512989	-	0.283623	-
Ref.	-	0.70348	0.00003	0.51297	0.00001	0.28308	0.00001

Table 2.12: Four column chromatography procedure for Lu-Hf and Sm-Nd separation.

Step	***Column Volume***	***Acid***
Column 1: Ln Spec resin 100-150 µm (0.1 cm diameter, 7.5 cm length)		
Preparation	6.00 ml	2.00 M HF
Preparation	6.00 ml	6.00 M HCl
Precondition	6.00 ml	3.00 M HCl
Precondition	1.00 ml	3.00 M HCl
Precondition	1.00 ml	3.00 M HCl
Load sample	1.00 ml	3.00 M HCl
Elution – collect matrix	1.00 ml	3.00 M HCl
Elution – collect matrix	1.00 ml	3.00 M HCl
Elution – collect matrix	5.00 ml	3.00 M HCl
Elution – collect matrix	5.00 ml	3.00 M HCl
Collect Lu	5.00 ml	6.00 M HCl
Collect Lu	5.00 ml	6.00 M HCl
Elution	5.00 ml	6.00 M HCl
Elution	5.00 ml	6.00 M HCl
Elution	1.00 ml	Mili-Q-H2O
Collect Ti	20.00 to 30.00 ml	0.30 HNO_3 + 0.09 M $C_6H_8O_7$ + 1% H_2O_2
Elution	3.00 ml	0.30 HNO_3 + 0.09 M $C_6H_8O_7$
Collect Hf	5.00 ml	2.00 M HF
Collect Hf	5.00 ml	2.00 M HF
Collect Hf	5.00 ml	2.00 M HF
Elution	4.00 ml	2.00 M HF
Elution	6.00 ml	6.00 M HCl
Elution	6.00 ml	2.00 M HF
Column 2: AG50W X8 20-50 mesh resin (0.1 cm diameter, 7.5 cm length)		
Preparation	6.00 ml	6.00 M HCl
Preparation	2.50 ml	Mili-Q-H2O
Precondition	1.20 ml	2.00 M HCl
Load sample	1.00 ml	2.00 M HCl
Elution	4.00 ml	2.00 M HCl
Collect Sr	6.00 ml	2.50 M HCl
Collect REE	5.00 ml	2.50 M HCl
Collect REE	5.00 ml	2.50 M HCl
Collect REE	3.00 ml	6.00 M HCl
Column 3: Ln Spec resin 50-100 µm (0.1 cm diameter, 7.5 cm length)		
Preparation	2.00 ml	6.00 M HCl
Preparation	2.00 ml	6.00 M HCl
Precondition	0.50 ml	0.25 M HCl
Precondition	0.50 ml	0.25 M HCl
Load sample	0.50 ml	0.25 M HCl
Elution	2.00 ml	0.25 M HCl
Collect Nd	3.50 ml	0.25 M HCl
Collect Nd	3.50 ml	0.25 M HCl
Elution	1.00 ml	0.50 M HCl
Collect Sm	5.00 ml	0.50 M HCl
Elution	2.00 ml	6.00 M HCl
Transfer to storage	0.50 ml	0.25 M HCl
Column 4: Sr Spec resin (0.1 cm diameter, 1.8 cm length)		
See procedure in Table 2.13		

2.8 Rb-Sr Phlogopite Geochronology

Sample preparation for Rb-Sr geochronology analysis was completed at the Arctic Resources Laboratory (University of Alberta). Phlogopite unknown samples were loaded into 15ml Savillex Teflon beakers (precleaned with HCl/HNO_3) and loaded with 2 ml of 0.75 M to 1.00 M HCL and left overnight. The next day, samples were ultrasonicated for 30 minutes to remove any carbonate alteration. 5 mg to 15 mg (0.005 to 0.015 g) of sample is weighed into new 15 ml Savillex Teflon beakers, precleaned with HCl/HNO_3. USGS SRM BHVO-2 and a procedural blank were prepared alongside unknown samples. All phlogopite samples were spiked with two drops (calibrated to 5mg) of ^{87}Rb-^{84}Sr isotope spike.

Samples undergo three-step dissolution. Samples were dissolved with 2 ml conc. HF and 0.5 ml conc. HNO_3 at 140 °C for 48 hours. Following first step dissolution, samples dry down on hot plate at 100°C for 2.5 hours or until gel. Samples were dissolved with 1 ml 6.00M HCL at 140°C for 24 to 48 hours. Following the second step dissolution, samples were dried down on a hot plate at 100°C for 1.5 hours or until gelatinous. The previous step is repeated for the third dissolution. Following final dry down, samples were loaded with 1.5 ml of 2.50M HCl.

Final Rb and Sr aliquots were collected using two column chromatography procedure. The first column (Table 2.13) is modeled after Yue-heng Yang et al. (2010) and consists of 15.5 cm long glass columns that isolate Rb and Sr from other cations. The first column is pre-loaded with AG50W-X12 200-400 mesh resin (stored in 10% TD HCl). The second column (Table 2.13) consists of 4 cm long column that is used to clean the Sr aliquot from the previous column. Second column is stored in low concentration 1.00M HNO_3. Sr fraction is dried down overnight at 90 °C.

Prior to chromatography, the second column is cleaned with Mili-Q-H_2O and optima acetone. After cleaning, Sr Spec resin (Eichrom 50–100 μm) is added to the neck of the second column. After completion of second column chromatography, the second column is cleaned with Mili-Q-H_2O and the resin is discarded.

Rb isotope analyses was completed at the Arctic Resources Laboratory (University of Alberta) using a Thermo ICAP-Q quadrupole Inductively Coupled Plasma Mass Spectrometer. Rb samples were dried down prior to analysis and loaded with 10.0% HNO_3 + 2.00% HF + 5 ppb Zr solution. Each sample measurement consists of 60 measurements. Unknown samples, a procedural blank, and USGS SRM BHVO-2 are bracketed with seven measurements of analytical blank solution (10.0% HNO_3 + 2.00% HF) and ten measurements of 10 ppm Rb standard solution. Prior to the final run, each sample is measured to test Rb concentration and further diluted if ^{87}Rb cps are greater than one million cps. Following the run, samples are reduced in an in-house program that subtracts the analytical blank from the samples, applies a mass bias correction on $^{87}Rb/^{85}Rb$ using $^{92}Zr/^{90}Zr$ (Nebel et al., 2005), and applies a mean absolute deviation filter to limit the influence of outlier measurements. Following corrections, 60 mass scans are averaged into six measurements for export into the final in-house Rb-Sr isotope program.

Sr isotope analysis was completed at the Arctic Resources Laboratory (University of Alberta) using a Thermo Triton Plus Multicollector Thermal Ionization Mass Spectrometer. Prior to analysis, samples are dried down and loaded with TaF_6 onto Re filaments. 100ppm SRM987 Sr SRM was loaded alongside unknown samples, procedural blank, and USGS SRM BHVO-2. Samples were run at approximately 3000 mA and 1400°C to 1500 °C depending on filament

Table 2.13: Two column chromatography procedure for separation of Rb and Sr.

Step	***Column Volume***	***Acid***
Column 1: AG50 X12 200-400 mesh resin (0.5 cm diameter, 10 cm length)		
Preparation	5.00 ml	6.00 M HCl
Preparation	5.00 ml	6.00 M HCl
Elution	5.00 ml	Mili-Q-H2O
Precondition	2.00 ml	2.50 M HCl
Precondition	2.00 ml	2.50 M HCl
Load sample	1.50 ml	2.50 M HCl
Elution	2.00 ml	2.50 M HCl
Elution	2.50 ml	5.00 M HCl
Collect Rb	2.50 ml	5.00 M HCl
Elution	2.00 ml	5.00 M HCl
Collect Sr	5.00 ml	5.00 M HCl
Collect REE	2.00 ml	6.00 M HCl
Elution	4.00 ml	6.00 M HCl
Transfer to storage	1.00 ml	2.50 M HCl
Column 2: Sr Spec resin (0.1cm diameter, 1.8 cm length)		
Preparation	0.60 ml	7.00 M HNO3
Elution	0.60 ml	Mili-Q-H2O
Elution	0.60 ml	Mili-Q-H2O
Precondition	0.15 ml	3.00 M HNO3
Load sample	0.15 ml	3.00 M HNO3
Collect REE	0.05 ml	3.00 M HNO3
Collect REE	0.10 ml	3.00 M HNO3
Collect REE	0.20 ml	3.00 M HNO3
Collect Ba	0.90 ml	7.00 M HNO3
Collect Sr	0.60 ml	0.05 M HNO3
Collect Sr	0.60 ml	0.05 M HNO3
Collect Sr	1.00 ml	0.05 M HNO3
H3PO4 addition to collected Sr	1 to 2 drops	0.10 M H3PO4

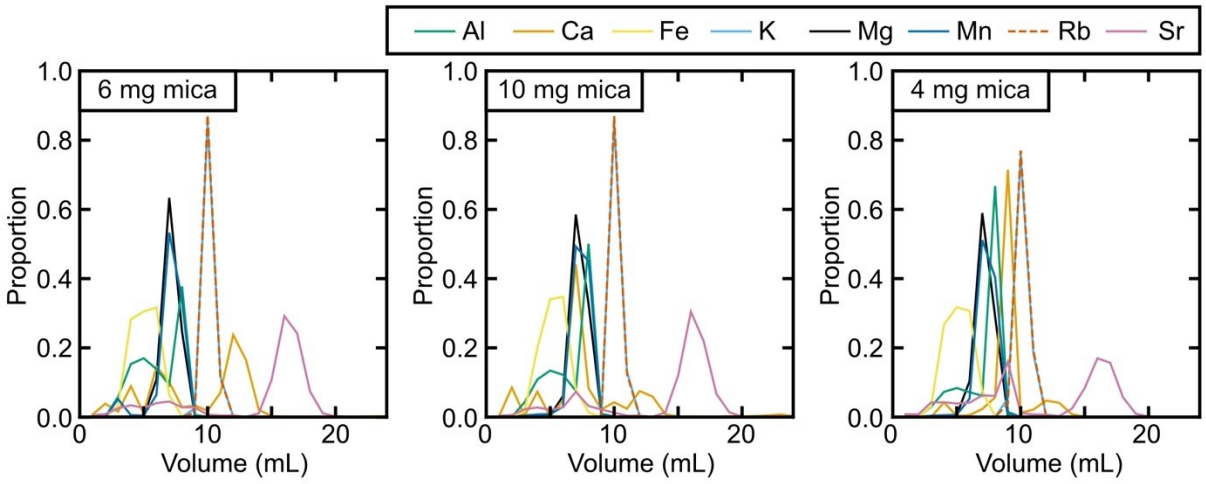

Figure 2.10: Elution curves of 6 mg, 10 mg, and 4mg phlogopite mica samples. Proportion corresponds to proportion of counts per second recorded on each cation out of one. Volume corresponds to total elution volume.

loading efficiency. ^{84}Sr, ^{85}Rb, ^{86}Sr, ^{87}Sr, and ^{88}Sr were collected on faraday cups configured to either 10^{11}, 10^{12}, or 10^{13} Ω amplifiers. Once the signal was stable, peak overlap and peak centering was performed prior to each measurement. Measurements are taken on 10 blocks of 10 cycles with one cycle corresponding to an integration time of 8.369 seconds. This results in a total of 100 raw measurements. Collected measurements were exported into an in-house Rb-Sr isotope program include ^{88}Sr/^{86}Sr, ^{87}Sr/^{86}Sr, and ^{84}Sr/^{86}Sr raw ratios and ^{88}Sr voltage.

The collected Sr data and previously exported Rb data is reduced in an in-house Rb-Sr isotope program. The program corrects for the contribution of the procedural blank, ^{87}Rb-^{84}Sr isotope spike, Rb interference, and mass bias by using the invariant ratio of ^{88}Sr/^{86}Sr of 8.379. A secondary check is performed by the invariant ratio of ^{84}Sr/^{86}Sr. The program then calculates a corrected ^{87}Sr/^{86}Sr and conducts outlier test to reject values outside two standard deviations. Corrected ^{87}Sr/^{86}Sr ($Sr_{corrected}$) is calculated following Equation 2.4. $\bar{X}_{IDfactor}$ corresponds to the mean of isotope dilution factor. g_{spike} corresponds to the mass of the ^{87}Rb-^{84}Sr isotope spike. $Sr_{filtered}$ corresponds to the uncorrected mean of unrejected ^{87}Sr/^{86}Sr ratios. $\bar{X}_{SRM987}$ corresponds to the mean of Rb corrected ^{87}Sr/^{86}Sr ratios of SRM SRM987. g_{blank} corresponds to the mass of blank which is 3 x 10^{-11}g. Sr_{blank} corresponds to the ^{87}Sr/^{86}Sr ratio of the blank which is 0.77028.

The total Rb uncertainty ($\Delta Rb_{propagated}$) is calculated from standard error of the sample measurement, the standard error on the refence material measurement, and an assumed ^{87}Rb-^{84}Sr isotope spike error of 0.75% (Equation 2.5). $2\sigma_{Rb\ sample}$ corresponds to the standard deviation of the six, ^{92}Zr/^{90}Zr corrected ^{87}Rb/^{85}Rb sample measurements. $N_{Rb\ sample}$ corresponds to the number of samples (six total). $\bar{X}_{Rb\ standard}$ corresponds to the mean of the six, ^{92}Zr/^{90}Zr corrected

$^{87}Rb/^{85}Rb$ sample measurements. $2\sigma_{Rb\ standard}$ corresponds to the standard deviation of ten, $^{92}Zr/^{90}Zr$ corrected $^{87}Rb/^{85}Rb$ SRM measurements. $\bar{X}_{Rb\ standard}$ corresponds to the mean of ten, $^{92}Zr/^{90}Zr$ corrected $^{87}Rb/^{85}Rb$ SRM measurements. All Rb measurements yielded a total $\Delta Rb_{propagated}$ less than 1%.

The total Sr uncertainty ($\Delta Sr_{propagated}$) is calculated from the standard error on of the calculated sample measurement and the standard error on the SRM987 SRM measurement. Note that the calculated sample measurement includes the blank correction and the ^{87}Rb-^{84}Sr isotope spike correction. $2\sigma_{Sr\ sample}$ corresponds to the standard deviation of unrejected $^{87}Sr/^{86}Sr$ sample ratios. $N_{Sr\ sample}$ corresponds to the number of unrejected $^{87}Sr/^{86}Sr$ sample ratios. $2\sigma_{Sr\ standard}$ corresponds to the standard deviation of ten, Rb corrected $^{87}Sr/^{86}Sr$ ratios of SRM987. $\bar{X}_{SRM987}$ corresponds to the mean of Rb corrected $^{87}Sr/^{86}Sr$ ratios of SRM987.

Model ages are calculated using initial $^{87}Sr/^{86}Sr$ of 0.7035, 0.705, and 0.710 to illustrate the effect of a varying initial Sr isotope ratio. Isochron plots and isochron calculated ages are produced using IsoplotR (Vermeesch, 2018). Constant ratios used in normal and inverse isochron plots are an $^{85}Rb/^{87}Rb$ ratio of 2.59265 ± 8.5 x 10^{-4}, $^{84}Sr/^{86}Sr$ ratio of 0.056549 ± 7.15 x 10^{-5}, $^{87}Sr/^{86}Sr$ ratio of 0.69938 ± 1.624 x 10^{-3}, $^{88}Sr/^{86}Sr$ ratio of 8.37861 ± 1.624 x 10^{-3}, and an ^{87}Rb decay constant of 1.3972 x 10^{-5} ± 4.5 x 10^{-7}. USGS SRM BHVO-2 ran within error of accepted value (Table 2.11).

Equation 2.05:

$$Sr_{corrected} = \frac{\left((\bar{X}_{IDfactor} \times g_{spike} \times 4.3705467 \times 10^{-11}) \times Sr_{filtered} \times \left(\frac{0.710245}{\bar{X}_{SRM987}}\right)\right) - \left(\left(\frac{g_{blank}}{87.62}\right) \times 0.0986\right) \times Sr_{blank}}{(\bar{X}_{IDfactor} \times g_{spike} \times 4.3705467 \times 10^{-11}) - \left(\left(\frac{g_{blank}}{87.62}\right) \times 0.0986\right)}$$

Equation 2.06:

$$\Delta Rb_{propagated} = \sqrt{\left(\frac{\left(2\sigma_{Rb\ sample} / N_{Rb\ sample}^{0.5}\right)}{\bar{X}_{Rb\ sample}}\right)^2 + \left(2\sigma_{Rb\ standard} / \bar{X}_{Rb\ standard}\right)^2 + 0.75^2}$$

Equation 2.07:

$$\Delta Sr_{propagated} = \sqrt{\left(\frac{\left(2\sigma_{Sr\ sample} / N_{Sr\ sample}^{0.5}\right)}{Sr_{corrected}}\right)^2 + \left(2\sigma_{Sr\ standard} / \bar{X}_{Sr\ standard}\right)^2}$$

2.9 Rb-Sr Phlogopite Geochronology Calibration

First, column chromatography was calibrated using test phlogopite of 6 mg (0.006g), 10 mg (0.01g), 4 mg (0.004g) material from Dharma. The results of the calibration detailed in the previous section were plotted in Figure 2.10. Following this calibration, five samples of phlogopite from Forte à la Corne was run following the procedure outlined in the previous section. The data were compared to previous unpublished data and the obtained ages were found to be within error of unpublished ages (Figure 2.11).

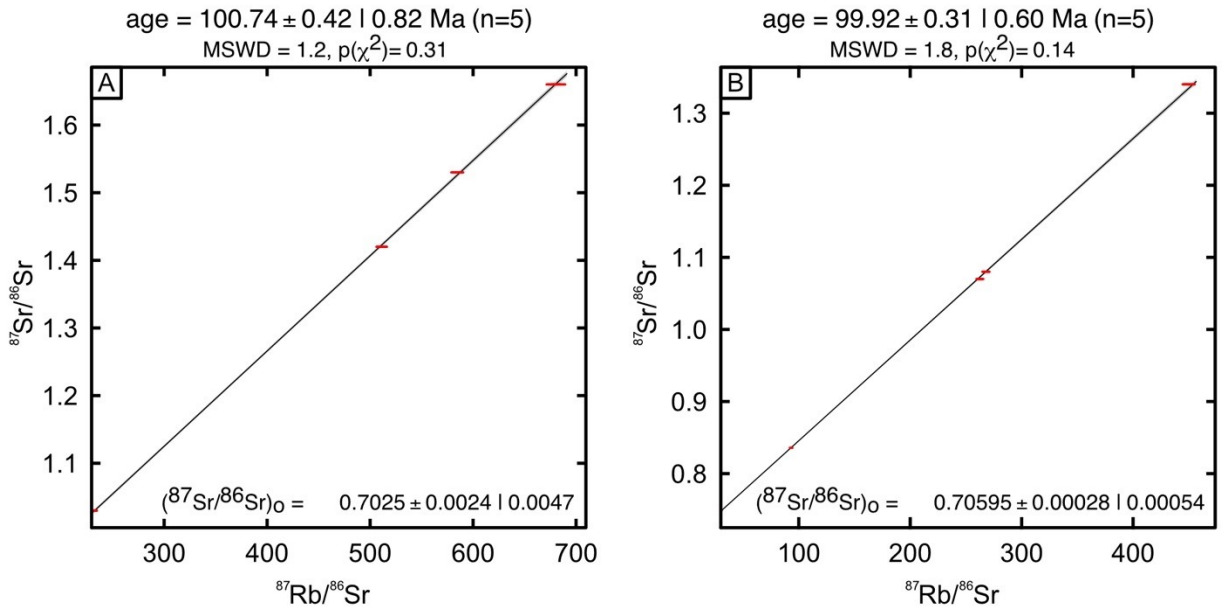

Figure 2.11: Rb-Sr isochron calibration results for Fort a la Corne phlogopite samples. A) Rb-Sr isochron for Fort a la Corne phlogopite samples from this study. B) Rb-Sr isochron for Fort a la Corne phlogopite samples from previous unpublished work. Age legend: isochron age ± estimated uncertainty of isochron age | 100(1-α)% confidence interval (n=population). MSWD legend: MSWD = Mean Square of the Weighted Deviates (MSWD) for the linear fit, p(χ2) =chi-squared p-value for the linear fit. (87Sr/86Sr)o legend: (87Sr/86Sr)o= initial 87Sr/86Sr isotope ratio obtained by linear regression ± estimated uncertainty of initial 87Sr/86Sr isotope ratio | 100(1-α)% confidence interval.

Chapter 3: Geochronology, Geochemistry, and Petrology of the Mel Kimberlite, NU, Canada.

3.1 Introduction

The northeastern portion of the Rae craton is exposed on the Melville Peninsula of Nunavut, Canada. Several diamondiferous ultramafic intrusions have been discovered in the area of the peninsula as a result of diamond exploration in recent years. These intrusions can be broadly grouped into the Aviat kimberlite cluster discovered by Stornoway Diamonds in 2002 and the Qilalugaq cluster discovered by BHP Billiton (as "Repulse Bay") in 2003 – both described briefly in Sarkar et al. (2018). In 2017, North Arrow Minerals Inc. discovered float samples of kimberlite-like material on Hall Beach Inuit Owned Land approximately 100 km southwest of Hall Beach, NU. In 2018, drilling on North Arrow's mineral exploration claims identified several intrusions logged as kimberlites (North Arrow Minerals Inc., 2019). The purpose of this study is to confirm the kimberlite classification assigned to the Mel intrusions, to date their emplacement, identify their igneous petrogenesis, and understand the nature of the mantle beneath these intrusions.

3.2 Mel Kimberlite Geology

The Mel kimberlite is located between the Qilalugaq olivine lamproites and Aviat kimberlites and CROL on the Melville Peninsula, NU (Figure 3.01). The geometry of the Mel kimberlite body was reconstructed from drill logs provided by North Arrow Minerals Inc. (Gainer and MacMorran, 2019; MacMorran, personal communication, 2019). It consists of at least three kimberlite bodies (ML8 Upper, ML8 Lower, and ML345) intersected by drilling at depth (Figure 3.02). The kimberlite bodies consist of hypabyssal (with flow-banding) and volcaniclastic kimberlite

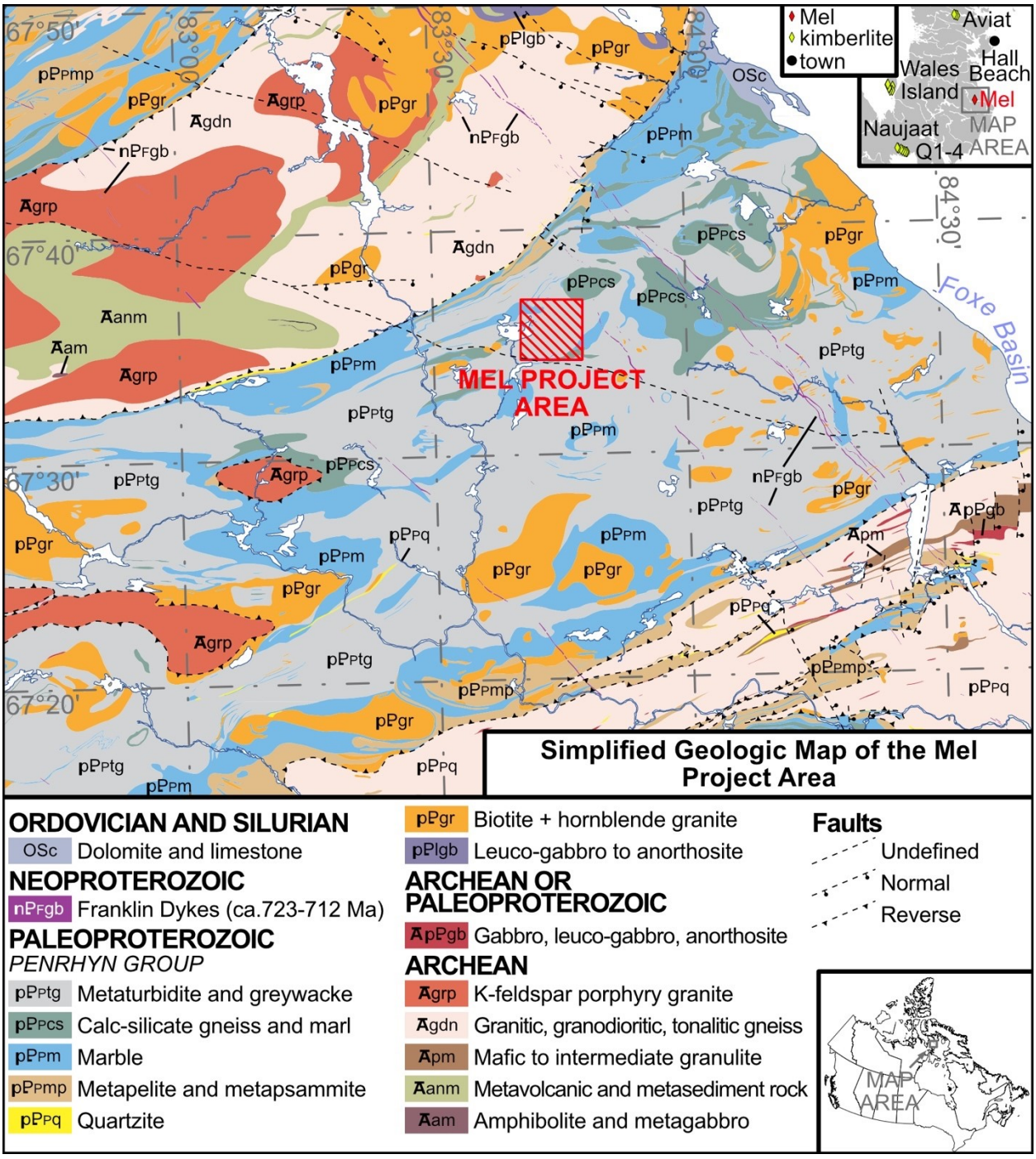

Figure 3.01: Simplified regional geologic map of the Mel kimberlite project area. Geologic map modified after Corrigan et al. (2020). Insert of Melville Peninsula map after North Arrow Minerals Inc. (2019). Labels: Aviat – Aviat kimberlite pipes and CROL sheets, Naujuaat – Naujaat kimberlite dikes, Q1-4 – Qilalugaq Q1-4 olivine lamproite pipe, Wales Island – W1, W2, and W3 kimberlites.

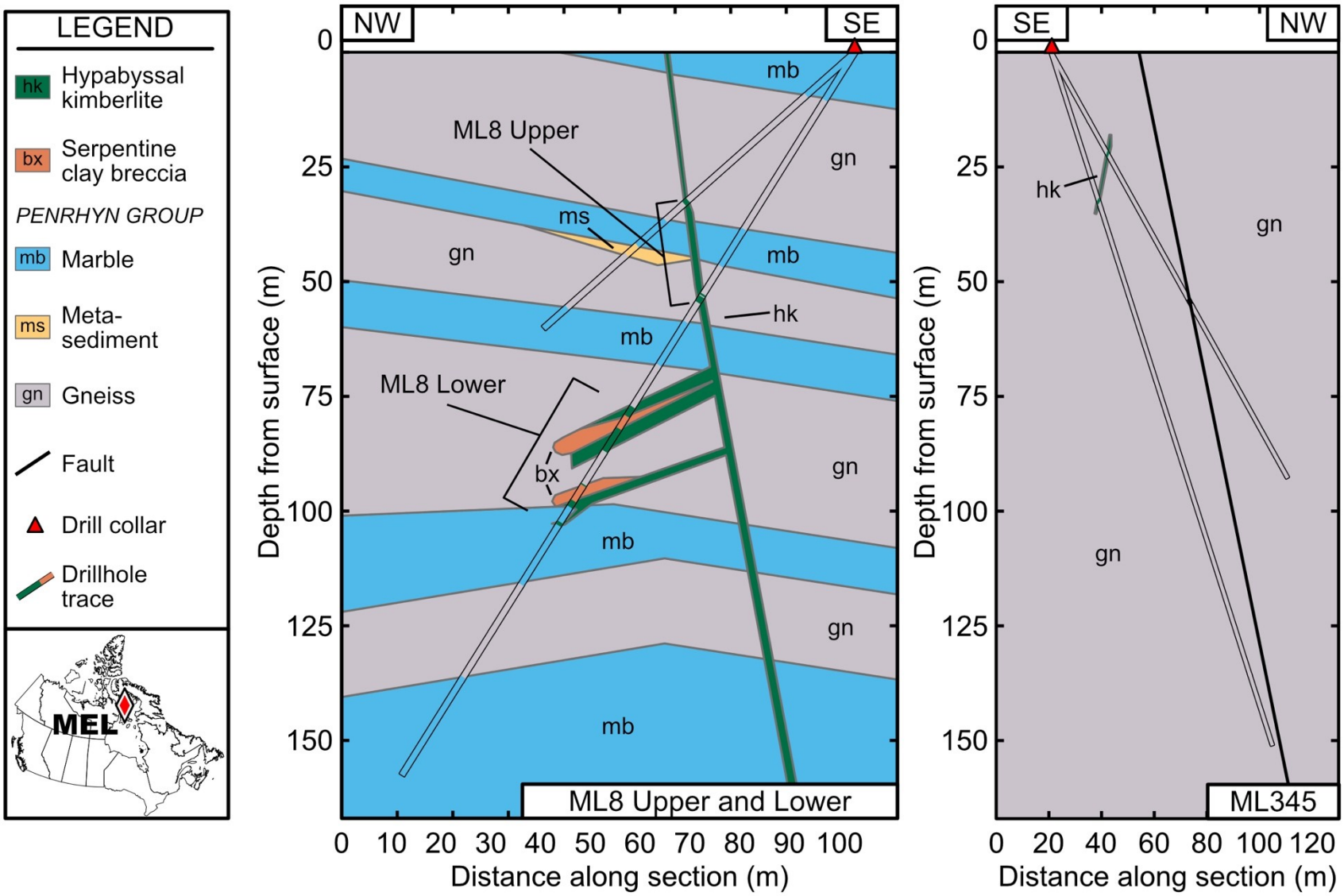

Figure 3.02: Simplified geologic cross-sections of Mel kimberlite. Mel kimberlite bodies include ML8 Upper, ML8 Lower, and ML345. Cross-sections constructed from drill logs provided by North Arrow Minerals Inc. Drill hole trace width exaggerated to show logging results.

dikes, oriented north to south, intruding interlayered calc-silicate gneiss and marble of the Paleoproterozoic Penrhyn Group (Partin et al., 2014; Gainer and MacMorran, 2019; North Arrow Minerals Inc., 2019). Hypabyssal kimberlite in drill core displays gray to green-gray coloration, clay and carbonate alteration, and several occurrences of crosscutting carbonate veins.

3.3 Results

3.3.1 Petrography

A petrographic study was conducted on eight thin sections from the three intersected Mel kimberlite bodies. Modal abundances of mineral phases and textural characteristics are variable between thin sections; however, the following description summarizes petrographic results and provides a general description of the kimberlite. Detailed petrography is presented in Table 3.01. Point count maps and thin section scans are listed in Appendix A.01 to Appendix A.13. It should be reiterated that groundmass (<100μm), microphenocryst (100 to 500μm), and phenocryst (>500μm) descriptors are strictly limited to describing sizes and not genetic interpretations.

The Mel kimberlite bodies are dominated by flow-banded coherent kimberlite. The groundmass is composed of serpentine + phlogopite + carbonate + spinel + apatite + ilmenite (in order of most to least abundant, Figure 3.03) and constitutes 56 volume % to 74 volume % in all three bodies. Groundmass serpentine and carbonate are predominantly anhedral (Figures 3.03F and 3.03G). Euhedral groundmass phlogopite is replaced by carbonate + chlorite where altered. Groundmass spinel is present as polycrystalline aggregates, euhedral atoll spinels with “lagoons” of carbonate ± serpentine (Figures 3.03F and 3.03G), and anhedral single unaltered crystals (Figure 3.03E). Anhedral to subhedral groundmass apatite is embayed and intergrown with phlogopite;

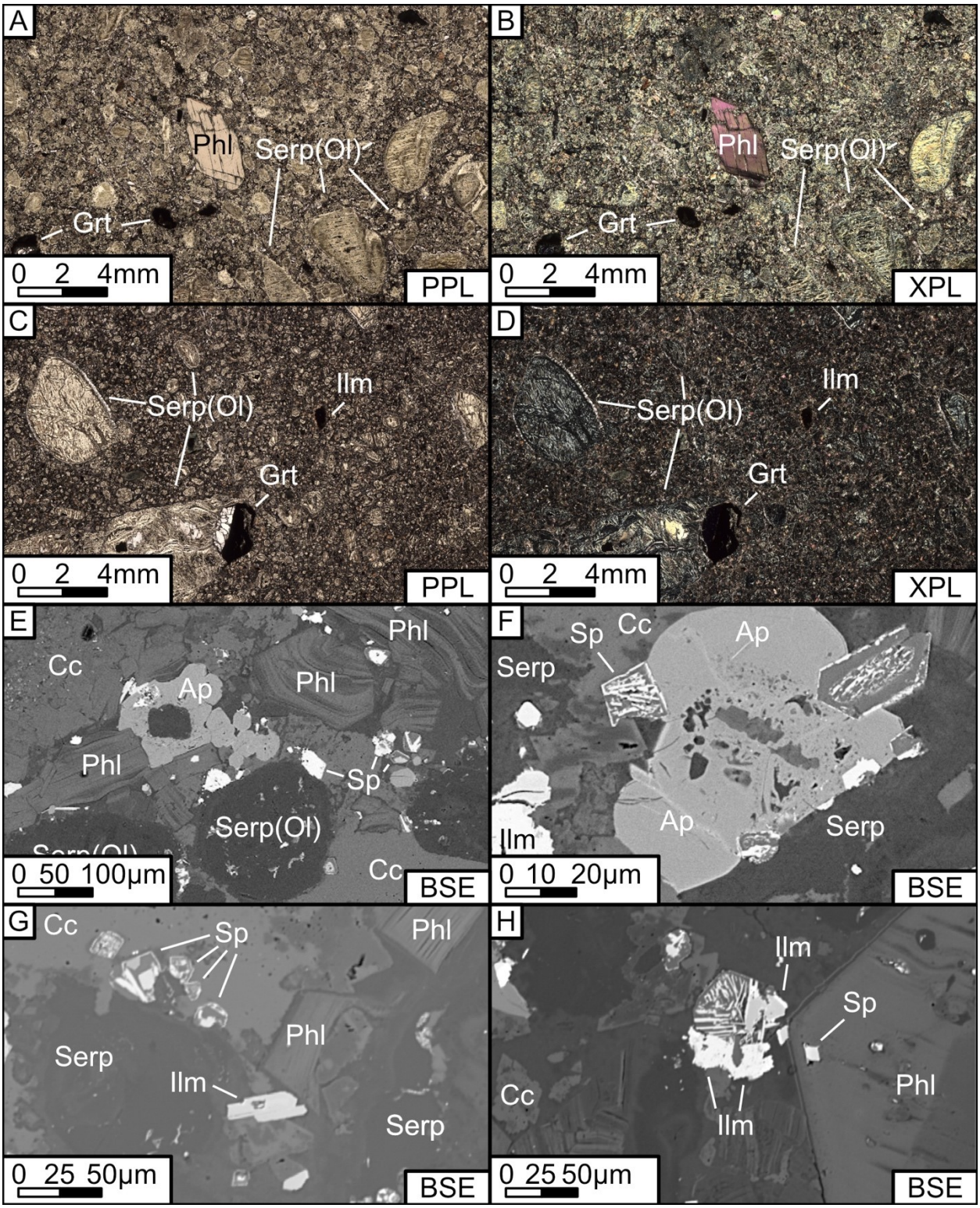

Figure 3.03: Petrography of the Mel kimberlite. A) Plain polarized and B) cross polarized photomicrographs of sample 49716.03. C) Plain polarized and D) cross polarized photomicrographs of sample 49723.02. BSE images of sample E) 49716.01, F) 49716.03, G) 49716.03, and H) 49716.01. Labels: Ap – apatite, Cc – carbonate, Grt – garnet, Ilm – ilmenite, Phl – phlogopite mica, Serp – serpentinite, Serp(ol) – serpentinite pseudomorph after olivine, Sp – spinel.

phlogopite contains inclusions of both atoll spinel and single unaltered spinel crystals (Figures 3.03E and 3.03F). Groundmass ilmenite is present as unzoned, euhedral to subhedral, tabular crystals (Figure 3.03G) and zoned, subhedral crystals (Figure 3.03H). Tabular ilmenite is partially intergrown with groundmass phlogopite. A small portion of the groundmass (up to 2 volume %) is composed of serpentine + carbonate segregations.

Anhedral to subhedral, phenocryst olivine altered to serpentine constitutes between 15 volume % to 27 volume % in ML8 Upper, 16 volume % to 21 volume % in ML8 Lower, and 14 volume % in ML345 (Figures 3.03A to 3.03D). Anhedral to subhedral oxide phenocrysts constitute up to 3 volume % in all kimberlite bodies and are predominantly ilmenite (chemically zoned) with rims of atoll spinel (Figures 3.03C and 3.03D). Oxide phenocrysts of spinel group minerals are rare. Subhedral to euhedral phenocryst phlogopite is variably altered to chlorite and constitutes up to 1 volume % in all kimberlite bodies. Phenocryst phlogopite is chemically zoned with a distinct core, intermediate zone, and rim/rind (Figure 3.03H). Anhedral to euhedral carbonate micro-phenocrysts constitute up to 1 volume % (Figure 3.03H). Euhedral microphenocrystic olivine altered to serpentine constitutes 8 volume % to 10 volume % in ML8 Upper, 6 volume % to 11 volume % in ML8 Lower, and 7 volume % to 10 volume % in ML345 (Figure 3.03E). Subhedral to euhedral microphenocrystic phlogopite constitutes between 2 volume % to 3 volume % in ML8 Upper, up to 4 volume % in ML8 Lower, and up to 5 volume % in ML345. Microphenocrystic phlogopite often includes subhedral magnetite and chromite (Figure 3.03E).

The xenocryst assemblage of the Mel kimberlite is dominated by mantle garnet (up to 6 volume %; Figures 3.03A to 3.03D). Garnet xenocrysts are anhedral to subhedral, with kelephyte rims of

Table 3.01: Distribution of mineral phases in hypabyssal Mel kimberlite bodies ML8 Upper, ML8 Lower, and ML345. Percentage in volume % analyzed by point-counting. Abbreviations: Cb – carbonate group mineral, Grt – garnet group mineral, Olv(alt) – serpentine group altered olivine, Ox – oxide mineral (i.e. ilmenite, spinel), Phl – phlogopite mica, Seg – segregated groundmass of predominantly serpentine group minerals and/or carbonate, Uni – uniform crystalline groundmass, X-cryst – xenocryst, X-lith – xenolith.

Petrographic Group:		***Phenocryst***			***Microphenocryst***			***Groundmass***		***X-cryst***	***X-lith***
Kimberlite	*Sample No.*	*Olv(alt)*	*Ox*	*Phl*	*Cb*	*Olv(alt)*	*Phl*	*Uni*	*Seg*	*Grt*	*Crustal*
ML8											
Upper	49716A	27%	3%	-	<1%	10%	3%	56%	<1%	-	2%
Upper	49716.01	18%	-	-	<1%	10%	3%	67%	<1%	1%	-
Upper	49716.03	18%	-	1%	<1%	9%	2%	65%	-	4%	-
Upper	49716.05	28%	<1%	<1%	<1%	8%	2%	59%	-	3%	-
Upper	49722A	15%	-		1%	9%	3%	65%	<1%	6%	1%
Upper	49722.01	23%	<1%	1%	<1%	8%	2%	62%	2%	-	-
Upper	49722.03	24%	2%	-	<1%	9%	3%	62%	-	-	-
Lower	49720A	21%	-	-	-	11%	4%	63%	-	1%	-
Lower	49720.01	18%	-	-	-	10%	2%	66%	-	5%	<1%
Lower	49721A	18%	-	<1%	-	6%	3%	69%	-	-	2%
Lower	49721.02	16%	-	1%	-	8%	<1%	74%	-	-	2%
ML345											
ML345	49723A	14%	-	<1%	-	7%	5%	70%	-	-	3%
ML345	49723.02	14%	-	-	-	10%	7%	69%	-	-	-

varying thicknesses (0.1 to 0.5 mm). Crustal xenoliths of marble and siliciclastic rock constitute up to 3 volume % of the Mel kimberlite.

3.3.2 Kimberlite Mineral Chemistry

A total of 185 EPMA analyses was performed on phlogopite, ilmenite, and spinel from the Mel kimberlite. Detailed mineral chemistry results are tabulated in Appendix B. Analytical methods are described in Chapter 2 section 2.3. As previously mentioned, the classifiers of groundmass, microphenocryst, and phenocryst are strictly used to denote size.

3.3.2.1 Phlogopite

EPMA analyses encompass one phenocryst (core n=1, intermediate zone n=1, rim n=1), 34 microphenocrysts (core n=32, intermediate zone n=20, rim n=17), and seven groundmass (core

n=6, rim n=1) phlogopites (Appendix B.01). 61 analyses were completed on ML8 Upper phlogopite, 10 analyses on ML8 Lower phlogopite, and 10 analyses on ML345 phlogopite

Mel kimberlite phlogopite falls on the edge of the kimberlite groundmass field and overlaps with phlogopite compositions most similar to Naujaat kimberlite dike phlogopite (Figures 3.04A and 3.04B). All phlogopite is eastonite to phlogopite in composition with one groundmass mica of biotite composition (Figure 3.04C). The analyzed biotite is assumed to be of crustal origin and is not discussed further.

Phenocryst and microphenocryst phlogopite display chemical zonation (visible in BSE imaging; Figure 3.03H). Al_2O_3 content generally increases from core to rim coupled with a decrease in TiO_2 and FeO_T content (Figures 3.04A and 3.04B). A few intermediate zone and rim compositions trend to a narrow range of 4 to 5 wt.% TiO_2 and 5 to 8 wt.% FeO with their cores lying outside of this range. The rim of the single phenocryst grain is enriched in BaO (1.04 wt.%) compared to its core (<LOD). BaO content increases from core (0.15 wt.% median, 1.14 wt.% maximum) to rim (0.33 wt.% median, 1.03 wt.% maximum) in microphenocryst phlogopite. Groundmass phlogopite contains little BaO compared to microphenocryst and phenocryst phlogopite (0.19 wt.% and 0.73 wt.% content in two analyses).

Zonation trends and compositions of microphenocrystic phlogopite differ across the three Mel kimberlite bodies (ML8 Upper n=52, ML8 Lower n=8, ML345 n=9). Phlogopite from ML8 Upper increases in FeO_T (5.76 wt.% median core, 6.29 wt.% median intermediate zone) and Al_2O_3 (14.56 wt.% median core, 15.36 wt.% median intermediate zone) content from core to intermediate zones

with rims decreasing in FeO_T (6.03 wt.% median rim) and Al_2O_3 (14 wt.% median rim) content compared to intermediate zones. BaO content increases from core (0.17 wt.% median core) to rim (0.44 wt.% median rim). TiO_2 content decreases from core (4.79 wt.% median core) to rim (4.42 wt.% median rim). Phlogopite from ML8 Lower increases in FeO_T (5.89 wt.% median core, 7.00 wt.% median intermediate zone) and TiO_2 (4.76 wt.% median core, 5.14 wt.% median intermediate zone) content from core to intermediate zones with rims decreasing in FeO_T (6.22 wt.% median rim) and TiO_2 (4.04 wt.% median rim) content compared to intermediate zones. ML8 Lower increase from core to rim in Al_2O_3 (14.4 wt.% median core, 15.2 wt.% median rim) and BaO (0.09 wt.% median core, 0.45 wt.% median rim) content. Phlogopite from ML345 increases from core to intermediate zones in Al_2O_3 (14.1 wt.% median core, 14.7 wt.% median intermediate zone) and BaO (0.03 wt.% median core, 0.4 wt.% median intermediate zone) content with rims decreasing in Al_2O_3 (13.94 wt.% median rim) and BaO (0.32 wt.% median rim) content compared to intermediate zones. FeO_T content in ML345 phlogopite increases from core (5.84 wt.% median core) to rim (6.87 wt.% median rim). TiO_2 content in ML345 phlogopite decreases from core (5.09 wt.% median core) to rim (4.81 wt.% median rim).

Phlogopite from ML8 Upper exhibits the highest FeO_T (3.04 to 12.5 wt.%, 6.00 wt.% median), Al_2O_3 (12.4 to 18 wt.%, 14 wt.% median), and BaO (<1.37 wt.%, 0.345 wt.% median) content as compared to median FeO_T, Al_2O_3, BaO values from ML8 Lower and ML345 phlogopite. TiO_2 is highest in phlogopite from ML345 (4.49 to 5.22 wt.%, 5 wt.% median) compared to median TiO_2 in phlogopite from ML8 Upper and ML8 Lower.

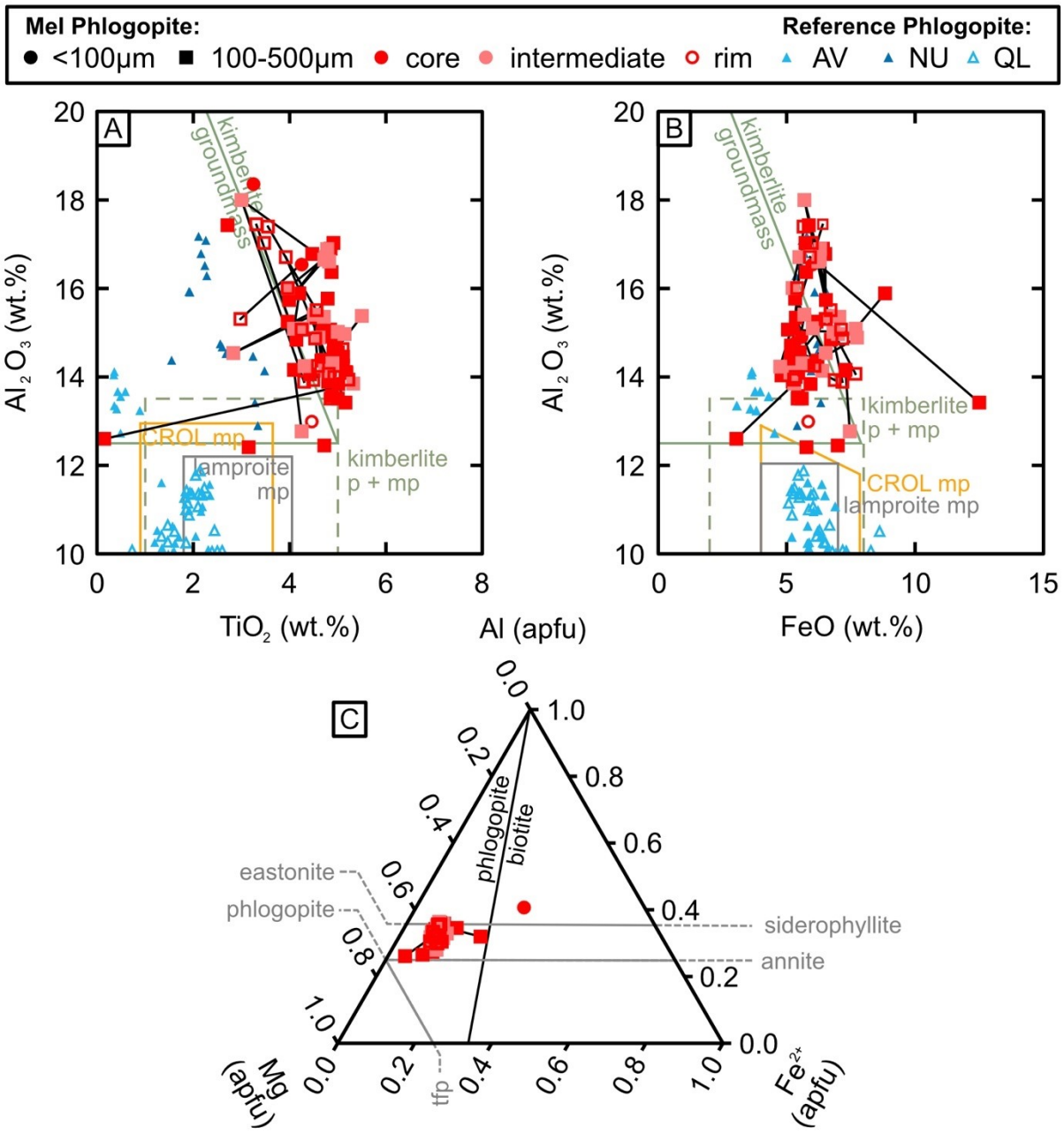

Figure 3.04: Composition of phlogopite mica from the Mel kimberlite. A) Al_2O_3 against TiO_2 phlogopite mica plot. B) Al_2O_3 against FeO phlogopite mica plot. C) Phlogopite Al apfu- Mg apfu-Fe^{2+}apfu ternary diagrams for phlogopite mica. Reference phlogopite compositions: AV – Aviat kimberlite pipes and CROL sheets (Sarkar et al., 2018), NU – Naujaat dikes (Sarkar et al., 2018), QL – Qilalugaq olivine lamproite pipes (Sarkar et al., 2018). Labels: bi – biotite, CROL mp – carbon – rich olivine lamproite microphenocryst phlogopite, kimberlite p + mp – kimberlite phenocryst and microphenocryst phlogopite, lamproite mp – lamproite microphenocryst phlotpite, phl – phlogopite, tfp – tetraferriphlogopite.

3.3.2.2 Ilmenite

EPMA analyses encompass five phenocryst (core n=8, intermediate zone n=5, rim n=4), nine microphenocrystic (core n=14, intermediate zone n=4, rim n=5), and 25 groundmass (core n=19, intermediate zone n=3, rim n=3) ilmenites (Appendix B.02). 49 analyses were completed on ML8 Upper ilmenite, 16 analyses on ML8 Lower ilmenite, and 25 analyses on ML345 ilmenite.

Mel kimberlite ilmenite is of dominant geikielite ($MgTiO_3$) to ilmenite ($FeTiO_3$) composition and falls within the field typical of kimberlite ilmenite compositions (Figure 3.05A). Mel ilmenite, particularly phenocryst ilmenite, is enriched in hematite (Fe_2O_3) component compared to the field of kimberlite ilmenite (Figure 3.05B). A small number of ilmenite rim analyses are of near "true" ilmenite composition and fall within the field of carbonate and CROL ilmenite (Figures 3.05A and 3.05B). The MgO and TiO_2 content of the majority of Mel ilmenite falls within the field of North American kimberlite and overlaps with ilmenite from the Aviat kimberlite in TiO_2 content (Figure 3.05C).

The ilmenite component of phenocryst ilmenite decreases from core (51% $FeTiO_3$ median core) to intermediate zones (43% $FeTiO_3$ median intermediate zone) and increases from intermediate zones to rim (46% $FeTiO_3$ median rim). One ilmenite phenocryst rim is 91% $FeTiO_3$. The geikielite component of phenocrysts increases from core (28% $MgTiO_3$ median core) to intermediate zones (40% $MgTiO_3$ median intermediate zone) and decreases from intermediate zones to rim (33% $MgTiO_3$). The hematite component of ilmenite phenocrysts decreases from core (39% Fe_2O_3 median core) to rim (23% Fe_2O_3 median rim). Ilmenite phenocrysts increase in MgO (7.72 wt.% median core, 11.44 wt.% median intermediate zone) and Cr_2O_3 (0.87 wt.% median core, 0.91 wt.%

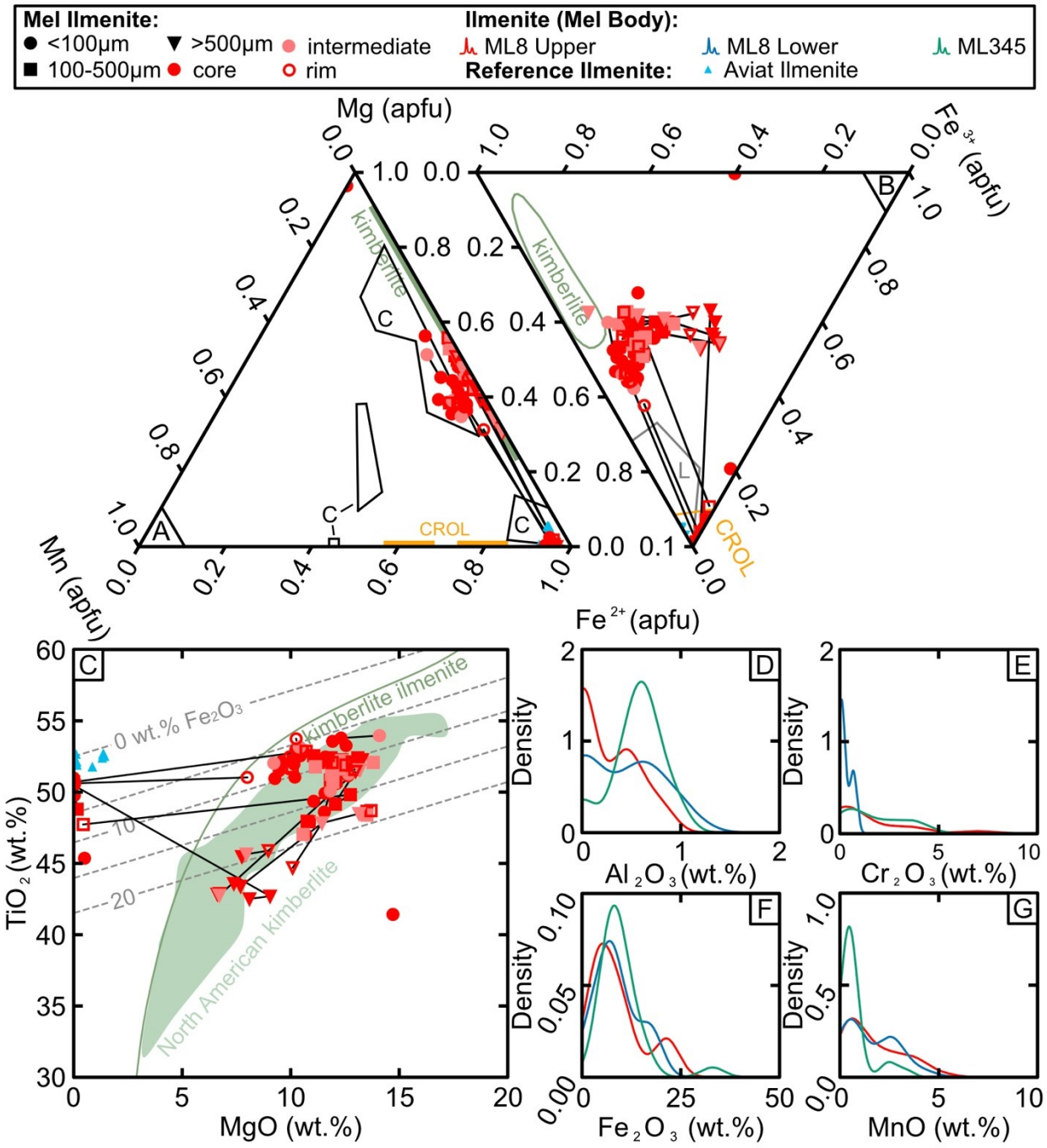

Figure 3.05: Composition of ilmenite from the Mel kimberlite. A) Geikielite ($MgTiO_3$, Mg apfu) – ilmenite ($FeTiO_3$, Fe^{2+} apfu) – pyrophanite ($MnTiO_3$ – Mn apfu) ternary discrimination plot after Mitchell (1995). B) Geikielite ($MgTiO_3$, Mg apfu) – ilmenite ($FeTiO_3$, Fe^{2+} apfu) – hematite ($Fe2O_3$, Fe^{3+} apfu) ternary discrimination plot after Mitchell (1995). C) Ilmenite composition on TiO_2 against MgO plot modified after Wyatt et al. (2004). Kernel density estimation plot for D) Al_2O_3 ,E) Cr_2O_3, F) Fe_2O_3, and G) MnO in Mel kimberlite bodies ML8 Upper, ML8 Lower, ML345. Density corresponds to density of analysis under the curve. Reference ilmenite compositions: Aviat Ilmenite – Aviat kimberlite pipes (Sarkar et al., 2018). Labels: C – carbonatites, CROL – carbon-rich olivine lamproite, kimberlite – kimberlite groundmass and megacryst, L – lamproite.

median intermediate zone) content from core to intermediate zones with rims decreasing in MgO (9.53 wt.% median rim) and Cr_2O_3 (0.89 wt.% median rim) content compared to intermediate zones. TiO_2 (32.14 wt.% median core, 48.19 wt.% median rim) and MnO (0.27 wt.% median core, 0.60 wt.% median rim) content increases from core to rim.

The ilmenite component in microphenocryst ilmenite decreases from core (45% $FeTiO_3$ median core) to intermediate zones (44% $FeTiO_3$ median intermediate zone) and increases from intermediate zones to rim (51% $FeTiO_3$ median rim). One microphenocrystic ilmenite decreases in ilmenite component from core (92% to 93% $FeTiO_3$ core) to rim (51% to 52% $FeTiO_3$ rim). The geikielite component of microphenocrysts slightly increases from core (42% $MgTiO_3$ median core) to intermediate zones (44% $MgTiO_3$ median intermediate zone) and decreases from intermediate zones to rim (36% $MgTiO_3$ median rim). The hematite component of microphenocrysts slightly increases from core (14.17% Fe_2O_3 median core) to intermediate zones (14.5% Fe_2O_3 median intermediate zone) and decreases from intermediate zones to rim (9.36% Fe_2O_3 median rim). Microphenocrysts increase from core to intermediate zones in MgO (11.96 wt.% median core, 12.70 wt.% median intermediate zone) and Cr_2O_3 (0.87 wt.% median core, 2.16 wt.% median intermediate zone) content and decrease from intermediate zones to rims in MgO (10.11 wt.% median rim) and Cr_2O_3 (0.13 wt.% median rim). A slight increase in TiO_2 (50.78 wt.% median core, 51.77 wt.% median rim) and a strong increase in MnO (0.66 wt.% median core, 2.71 wt.% median rim) is observed from core to rim.

A majority (n= 33) of groundmass ilmenite have compositions somewhat similar to ilmenite from other kimberlites, but are richer in Mn and Fe^{3+} end-members (Figures 3.05A and 3.05C). Three

groundmass ilmenites contain >89% $FeTiO_3$ component. One ilmenite rim on groundmass spinel is 43% $FeTiO_3$, 43% $MgTiO_3$, and 14% Fe_2O_3. Limited analyses indicate a decrease in ilmenite component from core to rim (94% to 60% $FeTiO_3$ in 16.03.012ox; 45% to 38% $FeTiO_3$ in 16.05.009ox). In these same ilmenites, core to rim increases are observed in MgO (0.05 to 8 wt.% in 16.03.012ox; 12.32 to 14.09 wt.% in 16.05.009ox), TiO_2 (50.61 to 51.03 wt.% in 16.03.012ox; 53.79 to 53.96 wt.% in 16.05.009ox), and MnO (1.96 to 2.09 wt.% in 16.03.012ox; 3.72 to 3.73 wt.% in 16.05.009ox) contents. Generally, MgO and MnO contents decrease with increasing TiO_2 contents. Groundmass ilmenite contains little Cr_2O_3 (<3.28 wt.%, 0.09 wt.% median).

Ilmenite from ML8 Upper and ML8 Lower shares a similar bimodal distribution of Al_2O_3 content (Figure 3.05D). The median Al_2O_3 content of ilmenite increases from ML8 Upper (0.15 wt.% median composition), to ML8 Lower (0.47 wt.%), to ML345 (0.6 wt.% median composition). Cr_2O_3 and Fe_2O_3 content have a similar distribution in ML8 Upper and ML345 (Figure 3.05E). A greater number of ilmenites from ML345 are low MnO (0.44 wt.% median composition) compared to ML8 Upper (1.02 wt.% median composition) and ML8 Lower (0.68 wt.% median composition).

3.3.2.3 Spinel

EPMA analyses encompass two spinel rims on phenocryst ilmenite (rim n=2), one spinel rim on microphenocrystic ilmenite (rim n=1), two atoll spinels on microphenocrystic ilmenite rim (rim n=2), six groundmass spinels (core n=6, intermediate zone n=1), one spinel rim on groundmass atoll ilmenite (rim n=1), and two spinel inclusions (core n=2) in microphenocrystic phlogopite (Appendix B.03). 11 analyses were completed on ML8 Upper spinel, one analysis on ML8 Lower groundmass spinel, and three analyses on ML345 groundmass spinel.

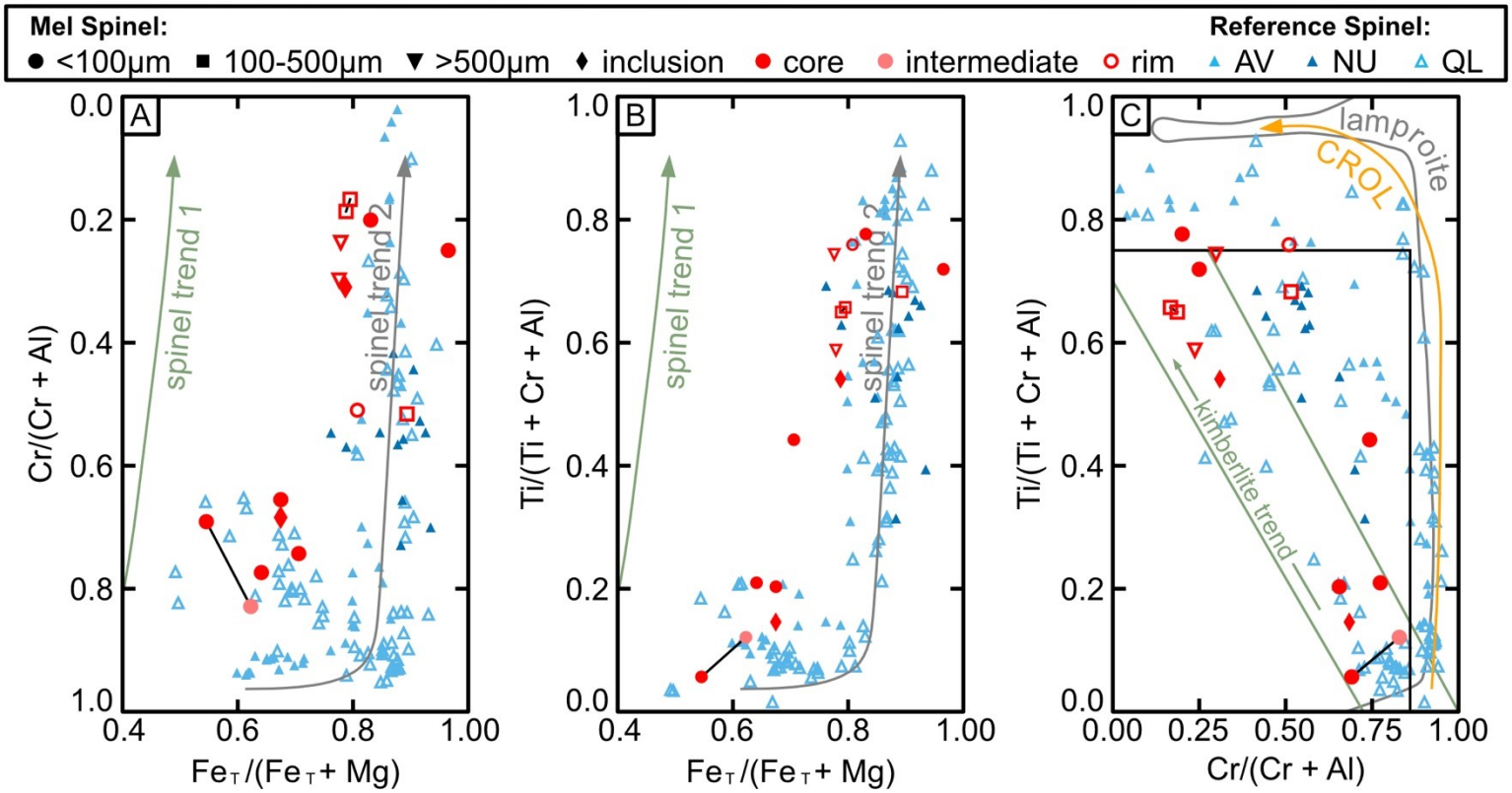

Figure 3.06: Composition of spinel from the Mel kimberlite. A) Spinel composition on Cr apfu/(Cr apfu + Al apfu) against Fe_T apfu/(Fe_T apfu + Mg apfu) plot after Mitchell (1986,1995) and Sarkar et al. (2018). B) Spinel composition on Ti apfu/(Ti apfu + Cr apfu + Al apfu) against Fe_T apfu/(Fe_T apfu + Mg apfu) plot after Mitchell (1986,1995) and Sarkar et al. (2018). C) Spinel composition on Ti apfu/(Ti apfu + Cr apfu + Al apfu) against Cr apfu/(Cr apfu + Al apfu) plot modified after Mitchell (1995). Labels: spinel trend 1 – trend of low Fe^{2+}apfu/(Fe^{2+}apfu + Mg apfu) spinel compositions unique to kimberlites, spinel trend 2 – trend of medium to high Fe^{2+}apfu/(Fe^{2+}apfu + Mg apfu) not unique to kimberlites (Mitchell, 1986). Reference compositions: AV – Aviat kimberlite pipes (Sarkar et al., 2018), NU – Naujaat dikes (Sarkar et al., 2018), QL – Qilalugaq olivine lamproite pipes (Sarkar et al., 2018).

Mel kimberlite spinel falls primarily on along Trend 2 (kimberlite, CROL, lamproite, and other ultramafic rocks; Mitchell, 1986) with Fe_T apfu/(Fe_T apfu + Mg apfu) higher (0.54 minimum, 0.96 maximum, 0.78 median) than typical kimberlite (Figures 3.06A and 3.06B). Mel kimberlite spinel Fe_T apfu/(Fe_T apfu + Mg apfu) is lower than spinel from Naujaat kimberlite dikes and similar to spinel from Aviat kimberlite pipes (Figures 3.06A and 3.06B). The Ti apfu/(Ti apfu + Cr apfu + Al apfu) and Cr apfu/(Cr apfu + Al apfu) systematics of Mel kimberlite spinel plot along the kimberlite trend of Mitchell (1986).

All spinel analyzed in Mel kimberlites belong to the oxyspinel (oxygen anion) group and can be divided into three main sets based on terminology from Roeder and Schulze (2008), major element chemistry, and end-member compositions.

The Cr-rich group (CHR) consists of groundmass spinel (n=2) and spinel inclusion (n=1) dominated by end members of magnesiochromite (26.02 to 34.84 mol% $MgCr_2O_4$) and chromite (7.21 to 29.13 mol% $FeCr_2O_4$) composition along with lesser magnesioferrite (4.13 to 22.42 mol% $MgFe_2O_4$) and Al - spinel (7.61 to 15.65 mol% $MgAl_2O_4$) end-member components. Minor Ti-spinel component is present as qandilite (3.03 to 10.95 mol% Mg_2TiO_4) and ulvöspinel (1.8 to 9.07 mol% Fe_2TiO_4) compositions. CHR spinel Fe_T apfu/(Fe_T apfu + Mg apfu) is constrained between 0.55 and 0.67 with the highest content of NiO (0.11 to 0.17 wt.%), Al_2O_3 (5.95 to 13.33 wt.%), and Cr_2O_3 (24.65 to 44.45 wt.%) content amongst all analyzed spinels. CHR spinel TiO_2 (4.06 to 12.21 wt.%, median 7.46 wt.%) content is lower than MUM spinel. CHR spinel FeO (19.40 to 26.43 wt.%) and Fe2O3 (5.53 to 19.69 wt.%) content is the lowest of all analyzed spinels.

The Ti-rich group (MUM) consists of atoll spinel rims on microphenocrystic ilmenite (n=2), groundmass spinel (n=1), and the only group to contain atoll spinel aggregated as rims on phenocryst ilmenite (n=2). MUM spinel is dominated by magnesioferrite (31.09 to 53.19 mol% $MgFe_2O_4$), qandilite (21.53 to 26.23 mol% Mg_2TiO_4), ulvöspinel (0.59 to 3.14 mol% Fe_2TiO_4), and magnetite (1.20 to 17.59 mol% $FeFe_2O_4$). Al - spinel component is higher in spinel rims found on phenocryst ilmenite (5.61 to 12.29 mol% $MgAl_2O_4$) and microphenocrystic ilmenite (9.45 to 11.13 mol% $MgAl_2O_4$) than in groundmass MUM spinel (4.07 mol% $MgAl_2O_4$). MUM spinel Fe_T apfu/(Fe_T apfu + Mg apfu) is constrained between 0.78 and 0.81 with the highest content of TiO_2 (16.66 to 20.72 wt.%) and FeO (31.47 to 34.7 wt.%) content of all analyzed spinels. Spinel rims on phenocryst ilmenite contain the highest content of MnO (0.81 to 0.90 wt.%) of all analyzed spinels. A single groundmass spinel (49723.02_008) from ML345 falls between MUM and CHR groups and is not included definitively in either grouping.

The Fe-rich group (MAG) consists of spinel rims on microphenocrystic ilmenite (n=1), groundmass spinel (core n=3, intermediate zone n=1), and spinel inclusion (n=1) dominated by magnetite (35.12 - 88.12 mol% $FeFe_2O_4$) and magnesioferrite (10.20 to 20.76 mol% $MgFe_2O_4$). MAG spinel contains lesser Ti-rich spinel components of ulvöspinel (0.55 to 16.67 mol% Fe_2TiO_4) and qandilite (0.06 to 8.43 mol% Mg_2TiO_4). MAG spinel Fe_T apfu/(Fe_T apfu + Mg apfu) is constrained between 0.79 and 0.97 with the highest Fe_2O_3 (34.05 to 68.83 wt.%). TiO_2 content in MAG spinel (0.43 to 14.86 wt.%, median 10.84 wt.%) is lower than MUM spinel but comparable to CHR spinel. NiO content is lowest in MAG spinel rim on microphenocrystic ilmenite (0.04 wt.%) and groundmass phase spinel (0.03 to 0.07 wt.%) compared to other spinel groups with MAG spinel inclusion sharing an identical NiO (0.11 wt.%) content to CHR spinel inclusion.

3.3.2.4 Rutile

EPMA analyses encompass four groundmass rutile analyses (Appendix B.04). All rutile analyzed is from Mel kimberlite body ML345. Analyzed rutile contains low Cr_2O_3 (<0.36 wt.%), medium Nb_2O_3 (0.93 to 1.6 wt.%), and high CaO (1.09 to 2.35 wt.%). TiO_2 contents of rutile range from 80 to 94.97 wt.%. All analyzed rutile is interpreted to be of crustal origin and is not discussed further in this work.

3.3.3 Garnet Xenocryst Mineral Chemistry and Ni Geothermometry

Garnet was the only mantle xenocrysts found in samples of the Mel kimberlite. A total of 426 garnet core and 424 garnet rim treace element analyses were completed on Mel kimberlite drill core heavy mineral separates (Appendix D.01). The data described in this section addresses only the garnet cores (n=423). Of the analyzed cores, four are crustal (CRST, Appendix D.01) garnet, 10 are G0 (unclassified) garnets, 179 are G1 (megacryst suite) garnets, three are G11 (Ti metasomatized peridotite) garnets of which two fall in the G9A field and one in the G10B field, four are G12 (wehrlite) garnets, four are G3 (eclogite) garnets, 21 are G3 Na (Na rich eclogite) garnets, 29 are G9A (low-Ca lherzolite) garnets, 155 are G9A Ti (Ti enriched low-Ca lherzolite) garnets, four are G9B (lherzolite) garnets, and 10 are G9B Ti (Ti enriched lherzolite) garnets after a modified classification of Snyder et al. (2021; Figure 3.07A). The classified G3 and G3-Na eclogite garnets fall within the mantle garnet field of Schulze (2003; Figure 3.07C) and within the decision boundary for mantle garnet (Hardman et al., 2018; Figure 3.07D).

Garnet types are distributed irregularly in the Mel kimberlite bodies (Table 3.02). Trench samples along with the upper and lower portions of ML8 are the only hosts of G11 garnet. G12 garnets are

Table 3.02: Distribution and classification of garnet xenocrysts in Mel kimberlite bodies.

Kimberlite	***CRST***	***G0***	***G1***	***G11***	***G12***	***G3***	***G3-Na***	***G9A***	***G9A Ti***	***G9B***	***G9B Ti***
ML8 Trench*	-	-	40	1	-	-	3	9	41	-	6
ML8 Upper	-	7	33	1	-	4	-	3	50	-	1
ML8 Lower	4	1	90	1	4	-	7	12	41	4	2
ML345	-	2	16	-	-	-	11	5	23	-	1
Total count:	4	10	179	3	4	4	21	29	155	4	10

only observed in the lower portions of ML8. G3 garnets are observed in all Mel bodies but the greatest amount of Na-rich G3 garnet is found in ML345. The greatest amounts of lherzolitic (G9A, G9A Ti, G9B, and G9B Ti) garnet are recorded in ML8 Upper and Lower.

Trace element patterns for mantle garnet from the Mel kimberlite are divided into two groups based on the pattern of their chondrite normalized REE (Figure 3.08). The majority of garnets (n=88) fall into the group of LREE depleted garnet (Figures 3.08A, 3.08B, and 3.08C). The LREE depleted garnet group includes G3, G3-Na, G9A, G9A Ti, G9B, G9B Ti, G11, and G12 garnets. The LREE depletion predominantly ends at Sm in most garnets (Figures 3.08A and 3.08C), however this is not the case for the Ti-enriched garnets (Figure 3.08B). The second group constitutes a diverse group of garnets with variably sinusoidal (G9A, G9A Ti, and G3-Na) to flat REE patterns (Figure 3.08D). Weakly sinusoidal garnets display Pr and Nd depletion in G9A garnet compared to the flattened G9A garnet and flat pattern LREE depletion in G3-Na garnet (Figure 3.08D). These garnets have generally negative LREE slopes from La to Ce ± Pr (Figure 3.08D). Flat pattern garnet displays both slight LREE enrichment (G9A, G9B Ti, and G3-Na) or LREE depletion (G9A) that is not as significant as the LREE depleted group of garnets (Figure 3.08D). The Mel kimberlite G9A garnets dominantly plot onto the depleted mantle trend of Woodland et al. (2021; Figure 3.09) and mainly fall between the depleted and high T geotherm fields of Griffin and Ryan (1995; Figure 3.07B). The Ti-rich G9A and G9B garnets form a high

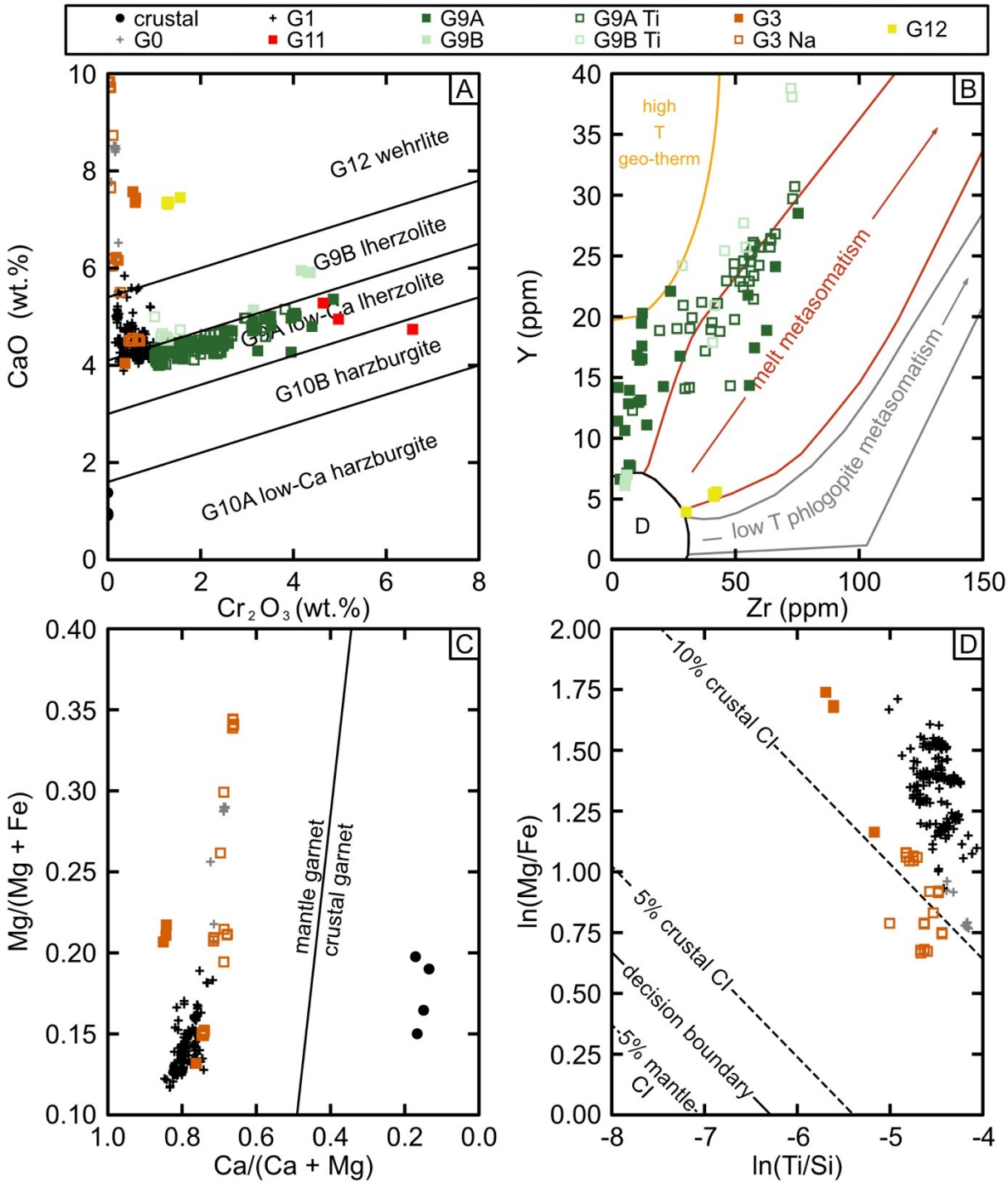

Figure 3.07: Composition of garnet xenocrysts from the Mel kimberlite. A) CaO against Cr2O3 discrimination plot modified after Sobolev et al. (1973), Gurney and Zweistra (1995), Grütter et al. (2004), and Preston et al. (2012) as per Snyder et al. (2021). B) Y ppm against Zr ppm trace element discrimination plot for mantle source environment after Griffin and Ryan (1995). C) Mg apfu/(Mg apfu + Fe apfu) against Ca apfu/(Ca apfu + Mg apfu) discrimination plot for mantle and crustal garnet after Schulze (2003). D) ln(Mg apfu / Fe apfu) against ln (Ti apfu / Si apfu) discrimination plot for mantle and crustal garnet after Hardman et al. (2018). Garnet groups: G0 – unclassified, G1 – megacryst, G11 – Ti metasomatized peridotite, G9A – low – Ca lherzolite, G9B – lherzolite, G9A Ti – Ti enriched low – Ca lherzolite, G9B Ti – Ti enriched lherzolite, G3 – eclogite, G3 Na – Na rich eclogite, G12 – wehrlite. Labels: D – depleted mantle.

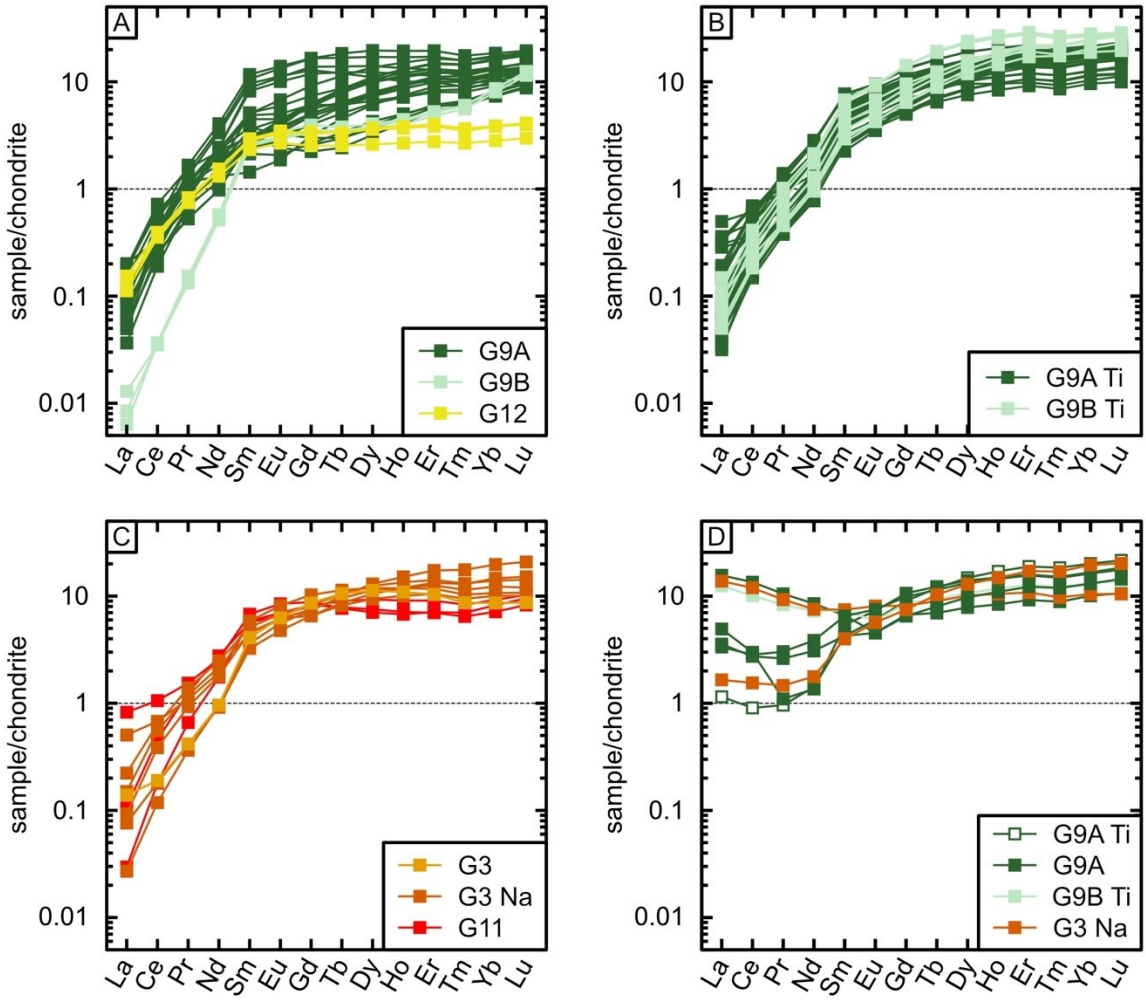

Figure 3.08: REE multi-element diagram of garnet xenocrysts from the Mel kimberlite. Garnet normalized to chondrite composition (Palme and O'Neil, 2014). A) LREE depleted group of low-Ca lherzolite garnet (G9A), lherzolite garnet (G9B), and wehrlite garnet (G12). B) LREE depleted and Ti enriched group of low-Ca lherzolite garnet (G9A Ti) and lherzolite garnet (G9B Ti). C) LREE depleted group of eclogitic (G3 and G3 Na) and Ti-metasomatized peridotite garnet (G11). D) Weakly sinusoidal to Irregular to flat REE group of low-Ca lherzolite garnet (G9A), Ti enriched lherzolite garnet (G9B), and eclogitic garnet (G3 Na).

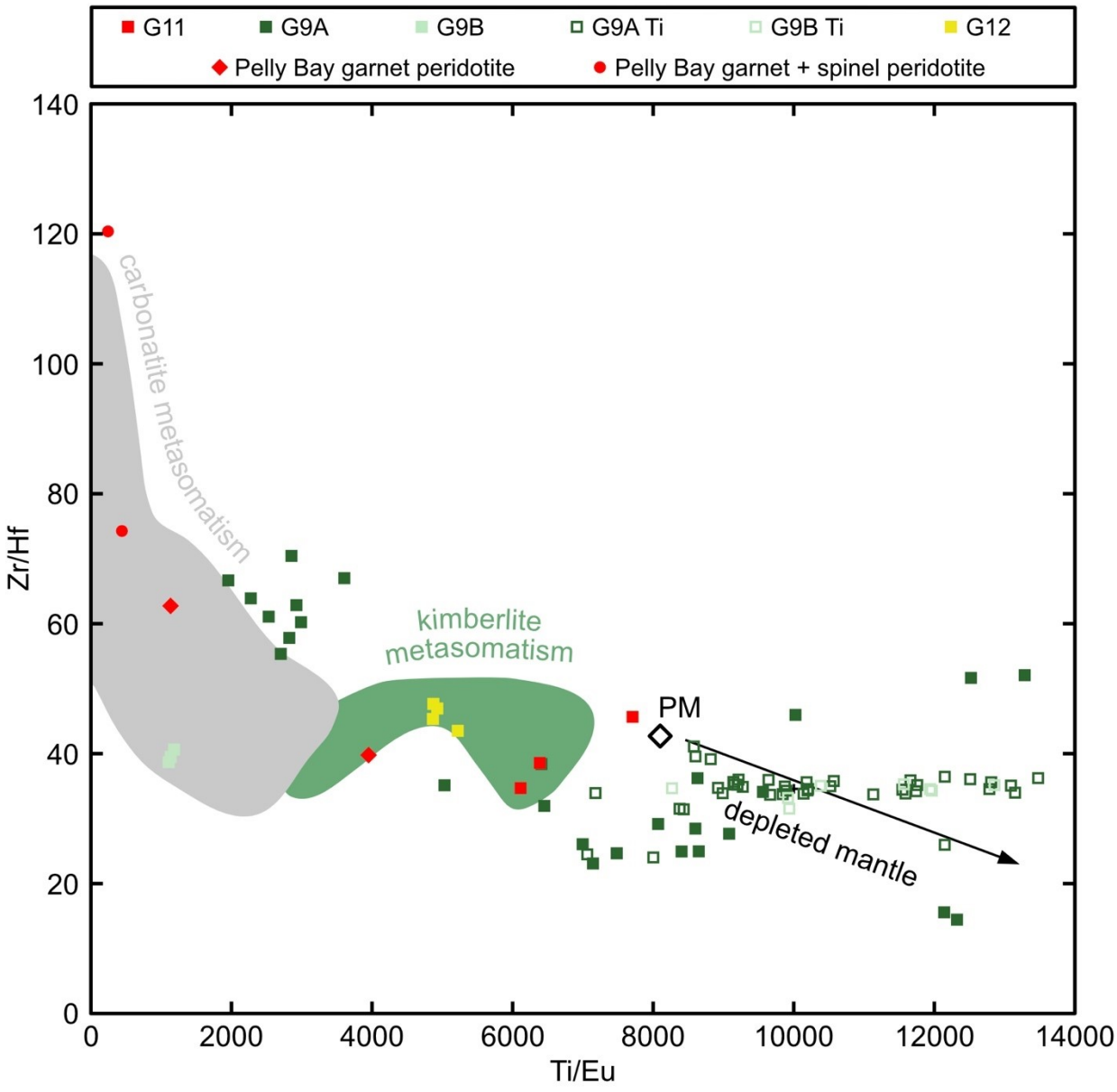

Figure 3.09: Composition of garnet xenocrysts from the Mel kimberlite on Zr/Hf against Ti/Eu discrimination plot. Plot modified from Woodland et al. (2021). Metasomatism fields after Shu and Brey (2015). Pelly Bay peridotite compositions after Woodland et al. (2021).

Ti/Eu extension of the kimberlite metasomatism field of Shu and Brey (2015; Figure 3.09) and the melt metasomatism trend of Griffin and Ryan (1995; Figure 3.07B).

Ni concentrations in garnet have been used to calculate equilibration temperatures using four garnet thermometers. These thermometers include Ryan et al. (1996; T_{Ryan}), Canil (1999; T_{Canil}), Shu and Brey (2015; $T_{ShuBrey}$), and Sudholz et al. (2021; $T_{Sudholz}$). G9B garnets recorded the lowest median Ni temperatures (T_{Ryan} = 675 °C, T_{Canill} = 808 °C, $T_{ShuBrey}$ = 757 °C, $T_{Sudholz}$ = 827 °C, Appendix F.01). The highest median Ni temperatures are recorded in G9A (T_{Ryan} = 1371 °C, T_{Canill} = 1252 °C, $T_{ShuBrey}$ = 1359 °C, $T_{Sudholz}$ = 1277 °C, n=27, Appendix F.01) and G9A Ti (T_{Ryan} = 1390 °C, T_{Canill} = 1262 °C, $T_{ShuBrey}$ = 1374 °C, $T_{Sudholz}$ = 1247 °C, n=40, Appendix F.01). G9A garnets share minimum Ni temperatures (T_{Ryan} = 660 °C, T_{Canill} = 796 °C, $T_{ShuBrey}$ = 743 °C, $T_{Sudholz}$ = 792 °C, n=27, Appendix F.01) similar to the median Ni temperatures of G9B. G9B Ti garnets record median Ni temperatures that are lower than G9A garnets and G9A Ti garnets (T_{Ryan} = 1349 °C, T_{Canill} = 1240 °C, $T_{ShuBrey}$ = 1341 °C, $T_{Sudholz}$ = 1230 °C, n=8, Appendix F.01). Median G12 garnet Ni temperatures fall below G9B Ti Ni temperatures and above G9B garnet temperatures (T_{Ryan} = 970 °C, T_{Canill} = 1019 °C, $T_{ShuBrey}$ = 1021 °C, $T_{Sudholz}$ = 1045 °C, n=4, Appendix F.01).

3.3.4 Whole Rock Major and Trace Element Geochemistry

Major and trace whole-rock geochemistry for Mel kimberlites is summarized in Table 3.03 and Table 3.04. Low SiO_2 contents (28.55 to 32.89 wt.%) and high MgO contents (21.86 to 28.05 wt.%) of the Mel intrusive units corresponds to ultrabasic compositions while TiO_2 (1.81 to 2.71 wt.%) and Fe_2O_3 (7.13 to 11.03 wt.%) contents place the compositions as similar to archetypal kimberlite (Mitchell, 1986; Pearson et al., 2019; Figure 3.10A to 3.10H). The Mel intrusions are characteristically potassium enriched with all samples enriched in K_2O (0.8 to 1.19 wt.%) in comparison to Na_2O (0.01 to 0.14 wt.%) with K_2O/Na_2O ratios ranging from 6.26 to 8.35.

The three bodies of the Mel kimberlite display systematic variations in major and trace elements (Figures 3.11 and 3.12). All samples of ML345 plot into the field of contaminated kimberlite (Figure 3.11A). All samples of ML8 Upper and Lower plot as uncontaminated kimberlite on the basis of Clement's Contamination Index (CCI <1.3; Clement, 1982). Two samples of ML8 Lower plot in the field of contaminated kimberlite with their ln(Si/Al) less than 2.3. All samples of ML8 Upper are classified as uncontaminated (Figure 3.11A). TiO_2 and SiO_2 increase while CaO and Al_2O_3 decrease with decreasing MgO contents (Figures 3.11B to 3.11E,). ML8 Upper displays the highest MgO (27.61 to 28.05 wt.%), highest SiO_2 (31.24 to 32.85 wt.%), lowest Al_2O_3 (2.32 to 2.41 wt.%), and lowest CaO (9.67 to 9.82 wt.%). ML345 displays the highest Al_2O_3 (3.31 wt.%), CaO (17.66 wt.%), and alkalis (1.19 wt.% K_2O, 0.14 wt.% Na_2O) in comparison to the ML8 Upper and ML8 Lower.

Mel kimberlites have trace element compositions similar to those of archetypal kimberlite (Figure 3.12). The Mel kimberlites have a lower range in Ni content (788 to 1168 ppm) than the kimberlite

/ CROL intrusions on the Melville Peninsula described by Sarkar et al. (2018; Figure 3.12) and have Ni contents spanning those of archetypal kimberlite (Figure 3.12A). All Mel kimberlites have low Nb contents (<100 ppm) compared to other kimberlites (Figures 3.12B and 3.12C) however Ba/Nb ratios fall within the kimberlite field (Figure 3.12D). Primitive mantle normalized trace elements have enriched LILE compared to HFSE (Figure 3.13A) and are LREE-rich REE (Figure 3.13B). All samples display prominent Nb and Ta enrichments while ML345 displays enrichment in Th, U, Zr, Hf, and REE (Dy, Y, Lu, Yb; Figure 3.13A). Chondrite normalized REE multi-element plots display clear LREE/HREE enrichment in all samples, with a subtle depletion in Eu (Figure 3.13B). As in the primitive mantle normalized multi-element plot, the REE trend for ML345 is enriched in REE compared to ML8 Lower and ML8 Upper (Figure 3.13B).

Table 3.03: Major element (in weight percent oxide) and trace element (in mg/g) compositions collected by XRF from fused bead and pressed pellet samples of the Mel kimberlite.

Kimberlite	ML8 Upper			ML8 Lower			ML345		
Sample	49716.02	49716.04	49722.02	49721.01	49720.03	49721.04	49723.01	49723.04	49723.06
SiO_2	31.24	31.90	32.85	28.55	32.03	29.82	29.49	32.93	26.83
TiO_2	2.71	2.22	1.81	2.10	1.80	2.23	2.29	2.04	1.86
Al_2O_3	2.41	2.32	2.32	2.64	2.46	2.90	3.31	2.73	2.43
Fe_2O_3T	10.49	10.20	9.91	11.03	8.66	11.96	7.13	6.97	6.39
MnO	0.15	0.15	0.11	0.15	0.13	0.13	0.11	0.08	0.11
MgO	27.80	27.61	28.05	24.83	26.84	26.59	21.86	23.83	19.73
CaO	9.79	9.67	9.82	13.21	11.93	10.25	17.66	14.75	22.56
Na_2O	0.13	0.13	0.09	0.11	0.09	0.15	0.14	0.10	0.12
K_2O	0.81	0.90	0.80	1.02	0.82	1.16	1.19	1.04	1.01
P_2O_5	0.32	0.29	0.36	0.18	0.16	0.51	0.40	0.06	0.71
LOI	16.41	17.03	16.05	19.27	17.65	16.65	19.52	18.28	22.23
Total	102.26	102.41	102.18	103.09	102.57	102.34	103.10	102.81	103.98
Rb	46.6	50.0	44.2	53.0	46.9	57.2	63.5	56.1	55.3
Sr	541	511	496	434	292	406	138	54	232
Y	9.8	9.5	6.7	9.2	8.9	9.8	35.1	30.3	44.1
Zr	143	133	138	110	90	91	323	319	349
V	163	161	160	149	154	132	189	186	182
Ni	1212	1173	1158	970	1091	1012	1398	1549	1224
Cr	1530	1647	1442	1313	1442	1477	1932	1758	1623
Nb	70.9	74.8	65.0	82.8	62.2	66.1	77.3	67.3	73.8
Ga	4.2	4.4	4.1	5.1	4.2	5.5	5.0	5.6	4.6
Cu	125	121	134	183	122	177	158	126	156
Zn	60	61	24	26	36	23	318	60	266
Co	99	98	102	97	88	87	122	122	105
Ba	493	502	448	622	420	669	488	413	440
La	43	44	34	42	44	30	37	22	49
Ce	72	68	45	66	70	51	62	43	77
U	1.1	0.5	1.2	0.5	0.5	0.5	6.9	2.3	8.8
Th	4.6	4.8	4.3	4.3	3.6	4.2	12.4	8.6	33.6
Sc	21	20	20	23	22	21	29	25	31

Table 3.04: Trace element composition (in mg/g) collected by HR-ICP-MS of the Mel kimberlite.

Kimberlite	ML8 Upper						ML8 Lower		ML345	
Sample	49716.02	2σ	49716.04	2σ	49722.02	2σ	49721.01	2σ	49723.01	2σ
Co	94	4	89	4	99	4	87	4	104	6
Ni	1066	41	1011	30	1066	54	788	28	1168	62
Cu	117	6	111	6	111	7	144	8	133	9
Zn	62	2	64	1	25	1	27	1	214	11
Rb	48	2	51	1	44	2	54	2	65	3
Sr	552	21	532	16	522	18	448	16	131	10
Y	9	0.4	8	0.2	6.4	0.3	8.2	0.3	28	2
Zr	123	5	113	2	116	4	88	3	290	4
Nb	67	3	71	2	64	2	81	3	75	4
Cs	1.49	0.06	1.51	0.04	1.61	0.06	1.37	0.05	1.8	0.1
Ba	561	26	566	27	525	22	687	30	541	32
La	44	2	44	2	35	2	39	1	36	2
Ce	74	3	75	2	56	2	74	3	68	4
Pr	7.8	0.3	7.9	0.2	6.1	0.2	8.1	0.3	7.8	0.4
Nd	28	1	28.3	0.6	21.8	0.7	30	1	30	2
Sm	4.4	0.2	4.55	0.09	3.4	0.1	5.1	0.2	5.8	0.3
Eu	1.09	0.04	1.11	0.02	0.9	0.03	1.41	0.05	1.35	0.07
Gd	4.1	0.2	4.1	0.1	3.0	0.1	4.6	0.2	5.8	0.3
Tb	0.47	0.02	0.46	0.01	0.32	0.01	0.52	0.02	0.85	0.05
Dy	2.25	0.09	2.10	0.06	1.49	0.05	2.29	0.08	4.8	0.3
Ho	0.39	0.01	0.35	0.01	0.257	0.009	0.36	0.01	0.92	0.05
Er	1	0.04	0.87	0.02	0.69	0.02	0.86	0.03	2.4	0.1
Yb	0.71	0.04	0.59	0.02	0.55	0.03	0.55	0.02	1.57	0.08
Lu	0.092	0.006	0.076	0.002	0.077	0.004	0.072	0.004	0.22	0.01
Hf	2.01	0.08	2.05	0.07	3.2	0.2	2.16	0.08	12.2	0.6
Ta	4.6	0.2	4.9	0.1	4.1	0.1	4.7	0.2	4.9	0.3
Pb	8.2	0.3	9.2	0.2	4.4	0.2	16.6	0.6	13.1	0.7
Th	5.3	0.2	5	0.1	5.7	0.3	4.7	0.2	11.9	0.9
U	1.1	0.04	1.02	0.02	2.13	0.07	0.92	0.03	6	0.3

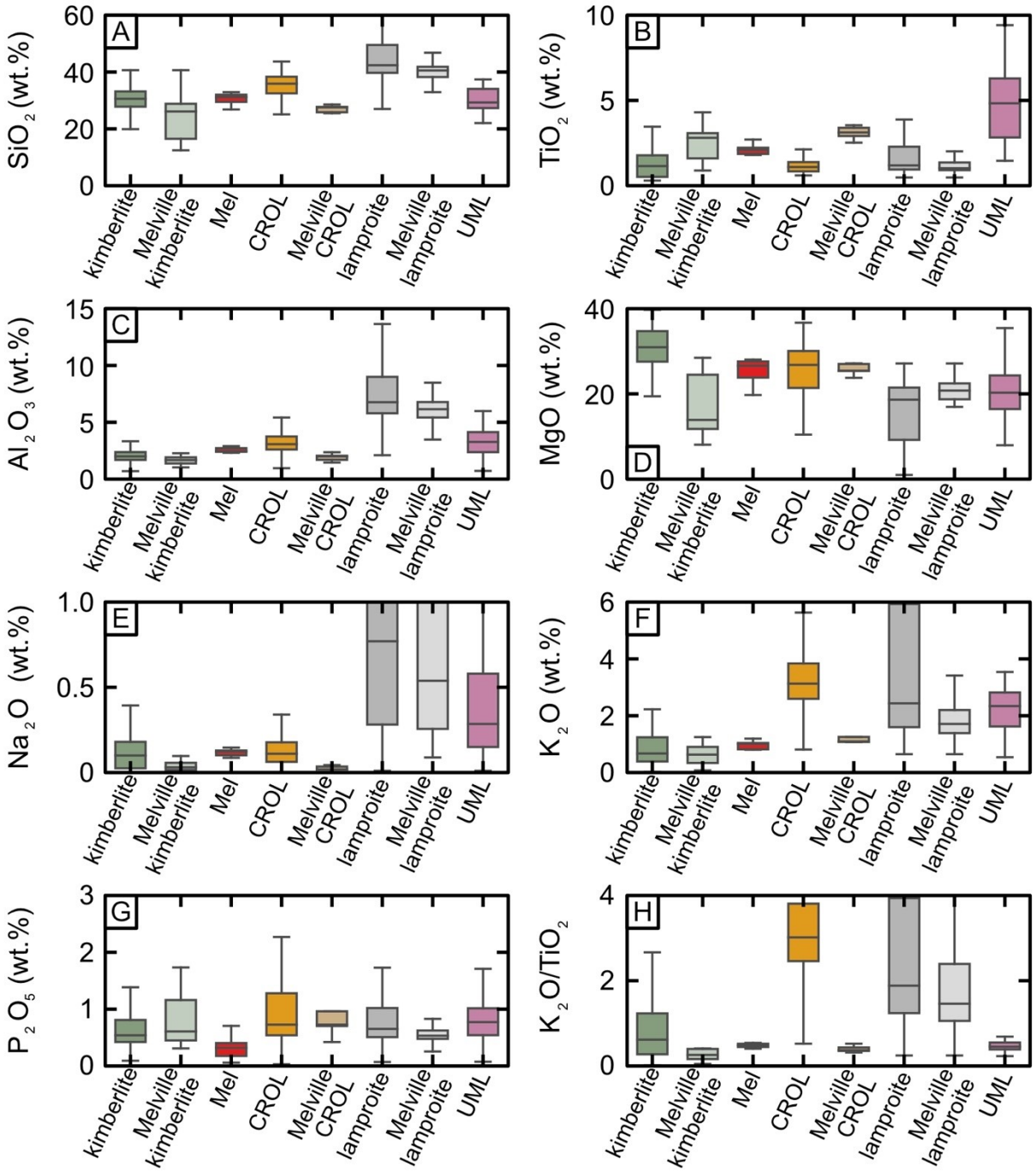

Figure 3.10: Box and whisker plots of whole rock major element compositions of the Mel kimberlite. Compared to regional kimberlites and lamproites, and global compilation of kimberlite and related rocks modified after Pearson et al. (2019). A) SiO_2. B) TiO_2. C) Al_2O_3. D) MgO. E) Na_2O. F) K_2O. G) P_2O_5. H) K_2O/TiO_2. Reference compositions: Melville kimberlite – Aviat kimberlite pipes and Naujaat dikes, Melville CROL – Aviat CROL sheets, Melville lamproite – Qilalugaq olivine lamproite pipes (Sarkar et al., 2018). Labels: CROL – carbon-rich olivine lamproite, UML – ultramafic lamprophyre.

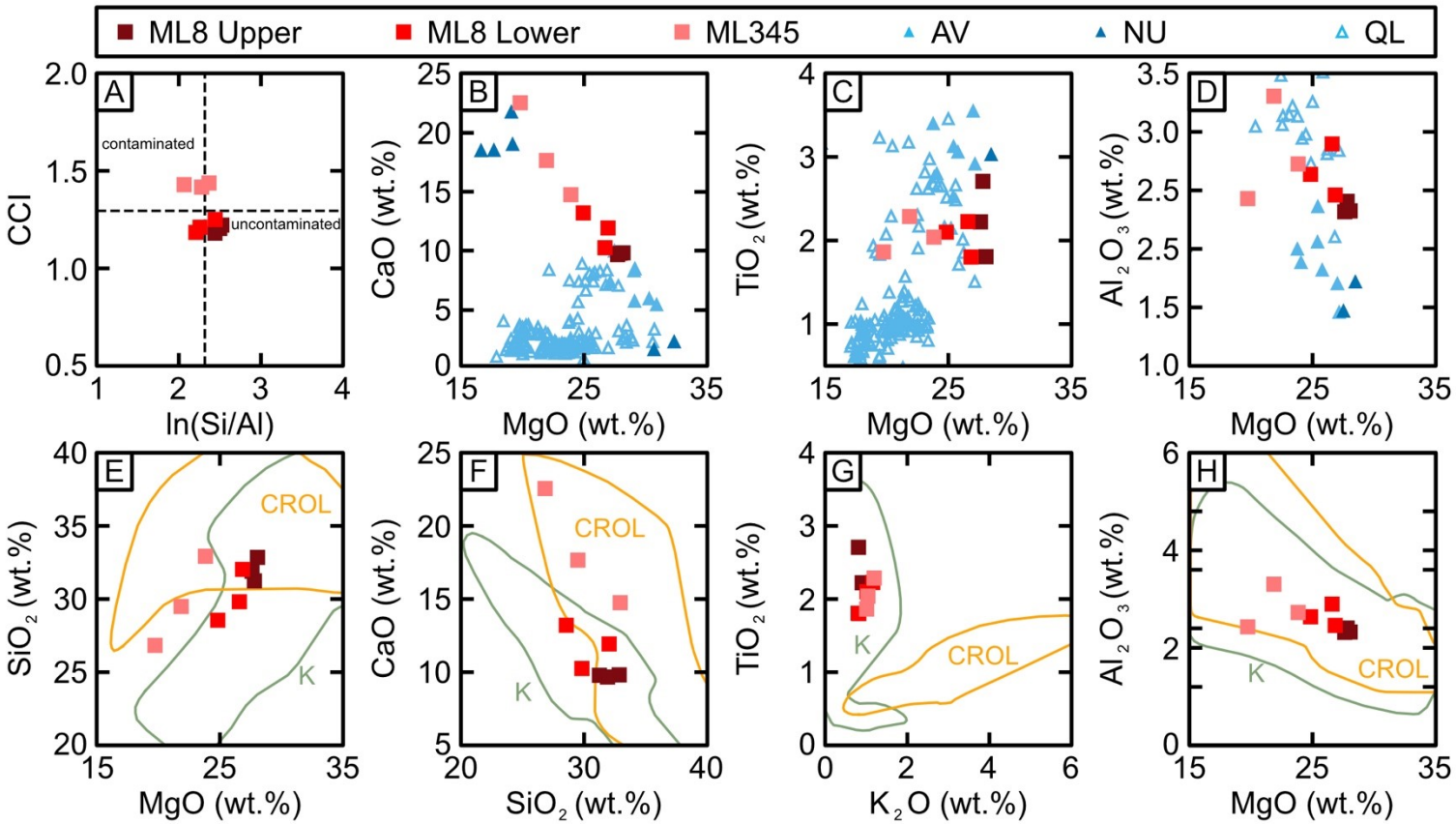

Figure 3.11: Whole rock major element variation of Mel kimberlite bodies ML8 Upper, ML8 Lower, and ML345. A) Clement (1982) CCI against ln(Si/Al) contamination index (Kjarsgaard et al., 2009) plot modified after Sarkar et al. (2018). B) CaO against MgO. C) TiO_2 against MgO. D) Al_2O_3 against MgO. E) SiO_2 against MgO plot modified after Sarkar et al. (2018). F) CaO against SiO_2 plot modified after Sarkar et al. (2018). G) TiO_2 against K_2O plot modified after Sarkar et al. (2018). H) Al_2O_3 against MgO plot modified after Sarkar et al. (2018). Reference whole rock compositions: AV – Aviat kimberlite pipes and CROL sheets, NU – Naujaat dikes, QL – Qilalugaq olivine lamproite pipes (Sarkar et al., 2018). Labels: CROL – carbon-rich olivine lamproite (Becker and Le Roex 2006; Coe et al. 2008), K – South Africa and North America kimberlite (Le Roex et al., 2003; Nowell et al., 2004; Becker and Le Roex, 2006; Kjarsgaard et al., 2009).

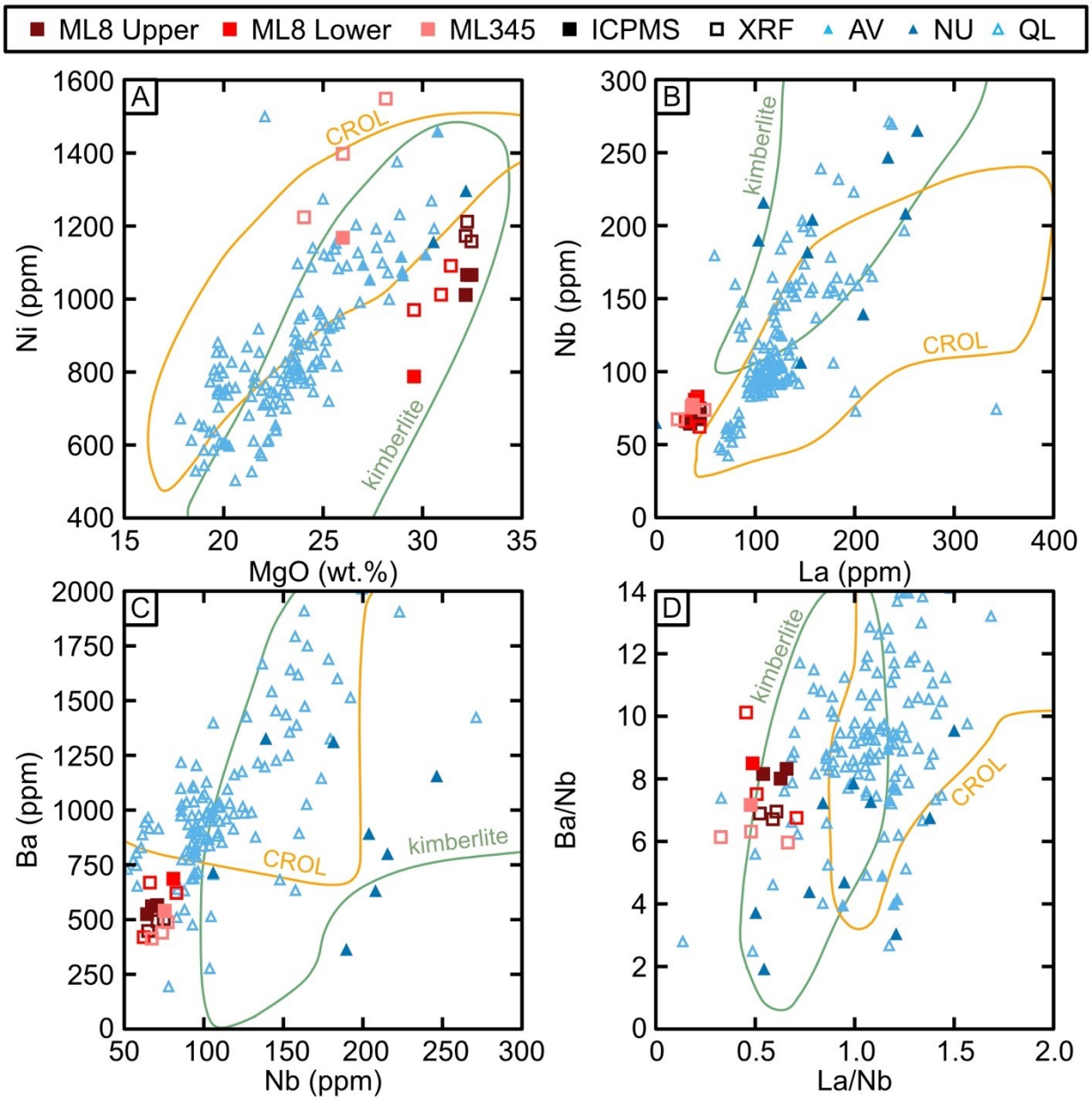

Figure 3.12: Whole rock trace element variation of Mel kimberlite bodies ML8 Upper, ML8 Lower, and ML345. A) Ni against MgO plot modified after Sarkar et al. (2018). B) Nb against La plot modified after Sarkar et al. (2018). C) Ba against Nb plot modified after Sarkar et al. (2018). D) Ba/Nb against La/Nb plot modified after Sarkar et al. (2018). Reference whole rock compositions: AV – Aviat kimberlite pipes and CROL sheets, NU – Naujaat dikes, QL – Qilalugaq olivine lamproite pipes (Sarkar et al., 2018). Labels: CROL – carbon-rich olivine lamproite (Becker and Le Roex 2006; Coe et al. 2008), K – South Africa and North America kimberlite (Le Roex et al., 2003; Nowell et al., 2004; Becker and Le Roex, 2006; Kjarsgaard et al., 2009).

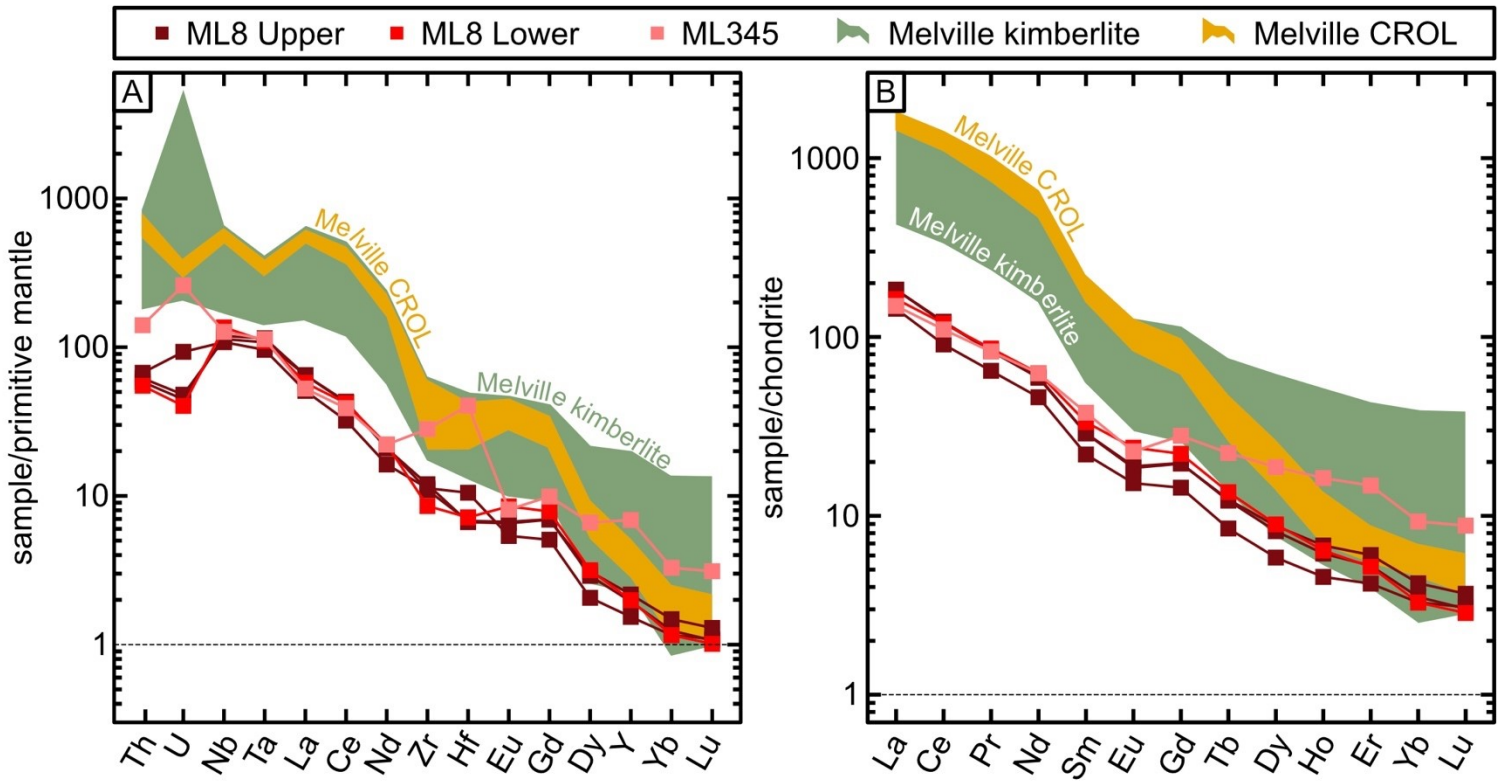

Figure 3.13: Whole rock trace element multi-element and REE diagrams of Mel kimberlite bodies ML8 Upper, ML8 Lower, and ML345. Whole rock normalized to primitive mantle and C1 chondrite compositions (Palme and O'Neill, 2014). A) Primitive mantle normalized multi-element plot. B) C1 chondrite normalized REE multi – element plot. Reference compositions: Melville kimberlite – Melville peninsula Aviat kimberlite pipes and Naujaat dikes, Melville CROL – Melville peninsula Aviat CROL sheets (Sarkar et al., 2018).

3.3.5 Phlogopite Rb-Sr Geochronology

A total of nine multi-grain (mixed) phlogopite phenocryst fractions (ML8 Trench n=1, ML8 Lower n=3, ML8 Float n=3, ML345 n=2) and one phlogopite phenocryst grain were analyzed from trench, drill core, and float samples of the Mel kimberlite. $^{87}Rb/^{86}Sr$ ranges from 60.3 to 277.5 across all samples, with Ediacaran to Cambrian model age samples having an $^{87}Rb/^{86}Sr$ range between 77.5 and 121.8 (Table 3.05). Mesoproterozoic to Paleoproterozoic age phlogopite (1472 Ma to 1689 Ma model age, $^{87}Sr/^{86}Sr_{initial} = 0.705$, n=6, Table 3.05) and Cambrian to Ediacaran age phlogopite (530 Ma to 548 Ma model age, $^{87}Sr/^{86}Sr_{initial} = 0.705$, n=4, Table 3.05) are the two age groups present in the Mel kimberlite. The phlogopites with Mesoproterozoic to Paleoproterozoic Rb/Sr model ages are interpreted to represent mica entrained in the kimberlite from the Paleoproterozoic Penrhyn group metasediments. These grains were avoided in further examination/interpretation of the kimberlite geochronology.

Three samples of Mel kimberlite float are considered for establishing a kimberlite emplacement isochron age of 555.6 ± 2.7 Ma (Figure 3.14A). The $^{87}Sr/^{86}Sr_{initial}$ ratio was constrained using an average of whole rock compositions, with an $^{87}Sr/^{86}Sr_{initial}$ ratio of 0.704414 ± 0.000012. This ratio is within the range of Canadian kimberlite $^{87}Sr/^{86}Sr_{initial}$ compositions (0.701 to 0.704 from Churchill Province phlogopite isochrons, Zurevinski et al., 2008; 0.704 to 0.7086 Slave Craton phlogopite, Heaman et al., 2003; Creaser et al., 2004; 0.7041 to 0.7095 Rae Craton whole rock and perovskite, Sarkar et al., 2018). The single analyzed phlogopite phenocryst has a younger, early Cambrian model age of 530Ma (assumed $87Sr/^{86}Sr_{initial} = 0.705$, Table 3.05). The single phenocryst model age generally agrees with the isochron age. The inverse isochron plot of Mel kimberlite

Table 3.05: Rb and Sr isotope composition of phlogopite from the Mel kimberlite. Row labels: Error – propagated two times standard error, T $Ma_{0.7035}$ – model age calculated with $^{87}Sr/^{86}Sr_{initial}$ (y-intercept) = 0.7035, T $Ma_{0.705}$ – model age with $^{87}Sr/^{86}Sr_{initial}$ (y-intercept) = 0.705, T $Ma_{0.710}$ – model age with $^{87}Sr/^{86}Sr_{initial}$ (y-intercept) = 0.710. Labels: mix – mixed multiple grain phlogopite sample, p – single phenocryst sample, average – average (whole rock) sample.

Kimberlite	ML8 Trench	ML8 Lower			ML8 Float				ML345		Whole Rock
Sample	736-1	746-1	746-2	746-3	M8SX-1	M8SX-2	M8SX-3	M8SX-4	724-1	724-2	-
Type	mix	mix	mix	mix	mix	mix	p	mix	mix	mix	average*
Mass (g)	0.00588	0.00995	0.00593	0.00579	0.00545	0.00661	0.00277	0.00836	0.0057	0.00508	-
Sr (ppm)	16.72	14.28	14.60	6.49	6.23	9.32	5.70	6.16	21.35	17.64	-
Rb (ppm)	586.77	263.85	331.97	376.45	240.00	292.27	144.49	198.40	395.66	404.76	-
$^{87}Rb/^{86}Sr$	128.5	61.2	77.9	277.5	121.8	97.4	77.5	100.2	60.3	77.4	0.283
Error	1.1	0.5	0.7	2.5	1.0	0.8	0.7	0.9	0.5	0.7	0.003
$^{87}Sr/^{86}Sr$	3.41995	2.18045	2.59682	7.39305	1.65617	1.46670	1.29044	1.47949	1.98306	2.39738	0.706596
Error	0.00008	0.00005	0.00006	0.00026	0.00004	0.00003	0.00004	0.00003	0.00004	0.00005	0.000005
T $Ma_{0.7035}$	1473	1680	1690	1677	549	549	531	543	1478	1525	-
TMa$_{0.705}$	1472	1678	1689	1677	548	548	530	542	1477	1524	-
T $Ma_{0.710}$	1470	1672	1685	1676	545	545	525	539	1471	1520	-

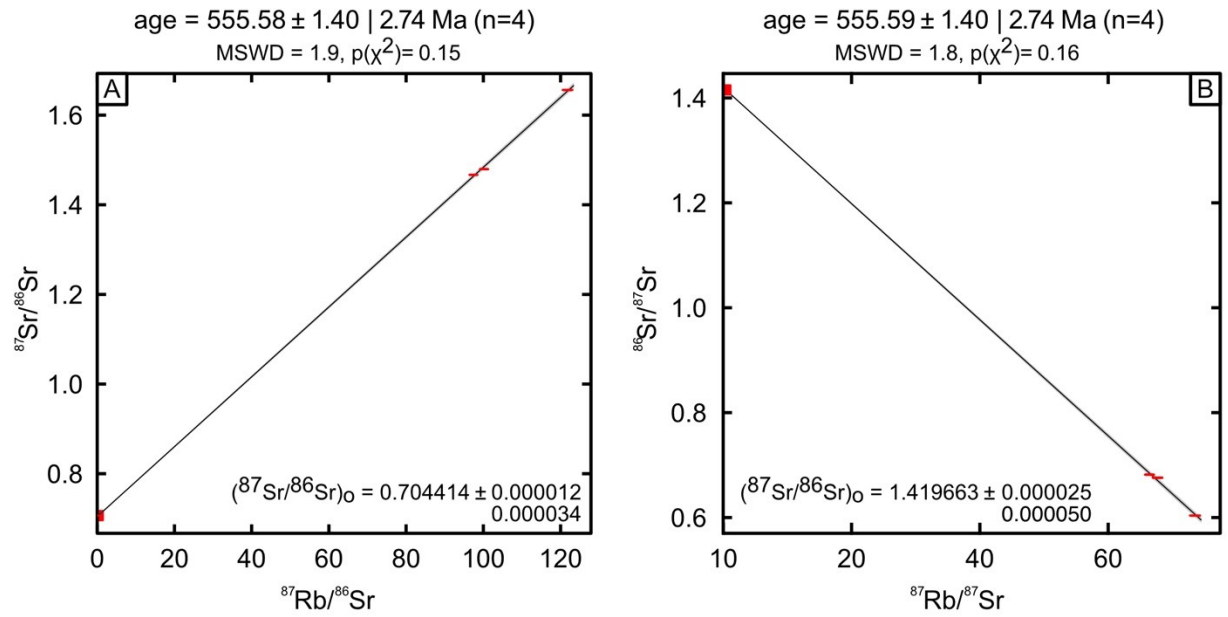

Figure 3.14: Mel kimberlite isochron plots. A) Phlogopite mica and average whole rock $^{87}Sr/^{86}Sr$ against $^{87}Rb/^{86}Sr$ isochron plot. B) Phlogopite mica and average whole rock $^{87}Sr/^{86}Sr$ against $^{87}Rb/^{86}Sr$ reverse isochron plot. Age legend: isochron age ± estimated uncertainty of isochron age | 100(1-α)% confidence interval (n=population). MSWD legend: MSWD = Mean Square of the Weighted Deviates (MSWD) for the linear fit, $p(\chi^2)$ =chi-squared p-value for the linear fit. $(^{87}Sr/^{86}Sr)_o$ legend: $(^{87}Sr/^{86}Sr)_o$= initial $^{87}Sr/^{86}Sr$ isotope ratio obtained by linear regression ± estimated uncertainty of initial $^{87}Sr/^{86}Sr$ isotope ratio | 100(1-α)% confidence interval.

phlogopite reveals little spread in the data with both isochrons agreeing in the isochron age (555.6 Ma) and error (± 2.7 Ma; Figures 3.14A and 3.14B).

3.3.6 Whole Rock Isotope Geochemistry

Whole-rock Hf-Nd-Sr isotopes were measured on two samples of ML8 Upper, one sample of ML8 Lower, and one sample of ML345 (Tables 3.06 to 3.08). Initial Hf, Nd and Sr isotope ratios are corrected to the isochron emplacement age of 555.6 Ma. Uncontaminated Mel kimberlite samples show a range of $^{87}Sr/^{86}Sr_{initial}$ from 0.70538 to 0.70686 and $\varepsilon Nd_{initial}$ from 2.35 to 3.04 (Figure 3.15A). Uncontaminated Mel kimberlite samples show a large spread of non-radiogenic $\varepsilon Hf_{initial}$ from -15.44 to -1.05 (Figure 3.15B). Sample 49723.01 (ML345) shares a much higher-$^{87}Sr/^{86}Sr_{initial}$ (0.71758 ± 0.000008) to other samples with significantly less radiogenic in $\varepsilon Nd_{initial}$ (-4.00), and

$\varepsilon Hf_{initial}$ (-30.95) than other Mel kimberlite samples (Figure 3.15B) and is interpreted as being contaminated. The two uncontaminated kimberlite compositions, ML8 Lower sample (49721.01) and ML8 Upper (49716.04) share an $\varepsilon Nd_{initial}$ and $\varepsilon Hf_{initial}$ composition similar to primitive and more depleted kimberlite compositions found in older kimberlites (Woodhead et al., 2019; Figure 3.15B). Although the $^{87}Sr/^{86}Sr_{initial}$ of all Mel kimberlites falls within the range of worldwide kimberlite, they are more radiogenic than those of Aviat kimberlites and fall outside of the mantle array, along a linear trend (Figure 3.15A).

Table 3.06: Mel kimberlite Sm and Nd isotope composition.

Kimberlite	ML8 Upper	ML8 Upper	ML8 Lower	ML345
Sample	49716.04	49722.02	49721.01	49723.01
Age	555.58 ± 2.74	555.58 ± 2.74	555.58 ± 2.74*	555.58 ± 2.74*
Sm (ppm)	4.8	3.4	5.3	6.1
Nd (ppm)	29.5	21.9	30.2	30.8
$^{147}Sm/^{144}Nd$	0.097819	0.095001	0.106090	0.119817
$^{143}Nd/^{144}Nd$	0.512434	0.512427	0.512429	0.512154
2SE	0.000005	0.000007	0.000006	0.000010
$^{145}Nd/^{144}Nd$	0.348417	0.348398	0.348417	0.348392
2SE	0.000004	0.000004	0.000004	0.000006
$\varepsilon Nd_{initial}$	3.04	3.10	2.35	-4.00
$\varepsilon Nd_{present}$	-3.99	-4.12	-4.09	-9.45

***** *Assumed same emplacement age as ML8 Upper sample.*

Table 3.07: Mel kimberlite Sr isotope composition.

Kimberlite	ML8 Upper	ML8 Upper	ML8 Lower	ML345
Sample	49716.04	49722.02	49721.01	49723.01
Age	555.58 ± 2.74	555.58 ± 2.74	555.58 ± 2.74*	555.58 ± 2.74*
Rb ppm	51.1	53.6	44.1	65.1
Sr ppm	531.9	448.0	521.5	130.5
$^{88}Sr/^{86}Sr$	8.355856	8.363094	8.311945	8.312226
$^{87}Sr/^{86}Sr_{present}$	0.706103	0.707411	0.706273	0.717758
$^{87}Sr/^{86}Sr_{initial}$	0.706313	0.706856	0.705379	0.707046
2SE	0.000006	0.000004	0.000006	0.000008
$^{84}Sr/^{86}Sr$	0.056494	0.056484	0.056489	0.056489
2SE	0.000002	0.000001	0.000002	0.000002

***** *Assumed same emplacement age as ML8 Upper sample.*

Table 3.08: Mel kimberlite Lu and Hf isotope composition.

Kimberlite	ML8 Upper	ML8 Upper	ML8 Lower	ML345
Sample	49716.04	49722.02	49721.01	49723.01
Age	555.58 ± 2.74	555.58 ± 2.74	555.58 ± 2.74*	555.58 ± 2.74*
Lu (ppm)	0.091	0.094	0.081	0.298
Hf (ppm)	1.933	2.982	2.005	11.438
$^{176}Hf/^{177}Hf$	0.282387	0.282045	0.282465	0.281599
2σ	0.000006	0.000007	0.000008	0.000005
$^{178}Hf/^{177}Hf$	1.467304	1.467292	1.467331	1.467386
2σ	0.208360	0.250361	0.293029	0.185432
$^{176}Lu/^{177}Hf$	0.00665	0.00448	0.00573	0.00370
2σ	0.00008	0.00004	0.00006	0.00021
$\varepsilon Hf_{initial}$	-4.16	-15.44	-1.05	-30.95
$\varepsilon Hf_{present}$	-14.09	-26.16	-11.32	-41.93

** Assumed same emplacement age as ML8 Upper sample.*

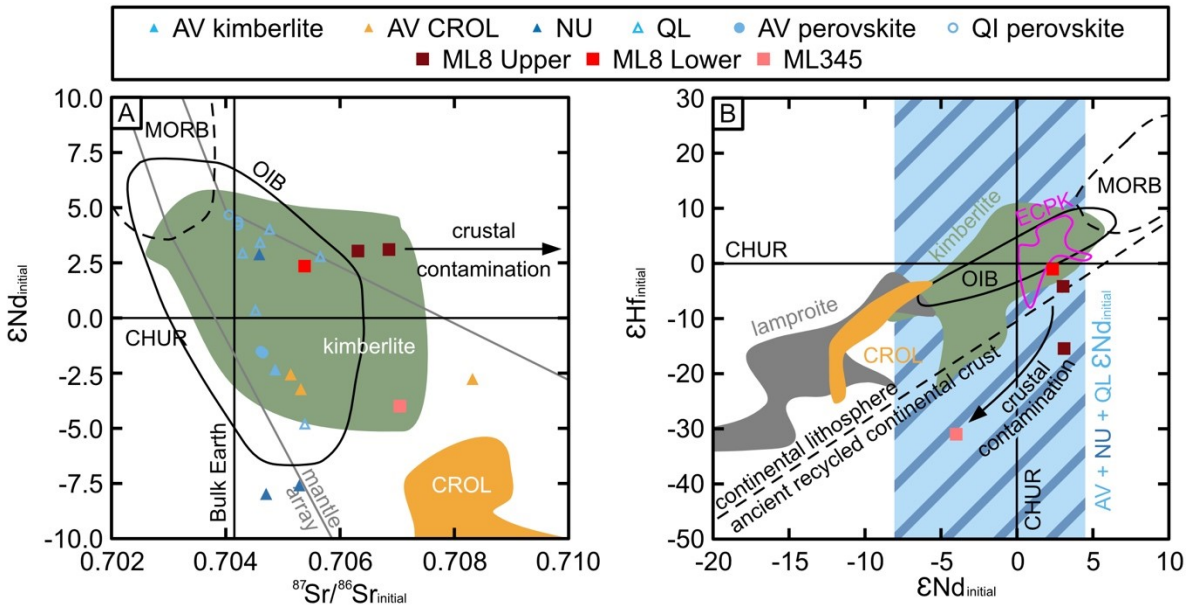

Figure 3.15: Whole rock radiogenic isotope plots of Mel kimberlite bodies ML8 Upper, ML8 Lower, and ML345. A) $\varepsilon Nd_{initial}$ against $^{87}Sr/^{86}Sr_{inital}$ isotope ratio modified after Sarkar et al. (2018). C) $\varepsilon Hf_{initial}$ against $\varepsilon Nd_{initial}$ discrimination plot modified after Pearson et al. (2019). Reference whole rock compositions: AV CROL = Aviat CROL sheets, AV kimberlite – Aviat kimberlite pipes, NU – Naujaat dikes, QL – Qilalugaq olivine lamproite pipes (Sarkar et al., 2018). Labels: Bulk Earth – Bulk Earth reservoir after Sarkar et al. (2018), CHUR – chondritic uniform reservoir model composition after Bouvier et al. (2008), CROL – worldwide carbon – rich olivine lamproite field, ECPK – eastern Canada primitive kimberlite after Woodhead et al. (2019), kimberlite – worldwide kimberlite field, lamproite – worldwide lamproite field, MORB – worldwide mid-ocean ridge basalt field, OIB – worldwide ocean island basalt field.

3.4 Discussion

3.4.1 Classification of Mel Magmatic Rocks

ML8 consists of a central sub-vertical dike (ML8 Upper) and at least two kimberlite sills (ML8 Lower) that branch off from the main dike (Figure 3.02, North Arrow Minerals Inc., 2019). ML345 constitutes a single, sub-vertical dike (Figure 3.02). The intrusions are structurally controlled by steeply dipping faults and are similar to root zone kimberlite feeder dikes (Mitchell, 1986). Fragmental crater and diatreme zone kimberlite, typical of other kimberlite intrusions (Hawthorne, 1975; Mitchell, 1986; Field and Scott Smith, 1999; Kjarsgaard, 2007), are currently undiscovered at the Mel kimberlite although country rock and serpentine-rich breccia is recorded along the margins of the ML8 Lower sills (Figure 3.02; Gainer and MacMorran, 2019; MacMorran, personal communication, 2019; North Arrow Minerals Inc., 2019).

The Mel kimberlite shares petrographic characteristics similar to other kimberlites worldwide. The main phase of the Mel kimberlite hosts two generations of olivine (serpentine pseudomorph after olivine) and phlogopite typical of kimberlite (Mitchell, 1986; Mitchell et al., 2019). The phenocryst/xenocryst olivine is anhedral to subhedral, a result of magmatic corrosion altering the morphology of the original olivine during kimberlite ascent and emplacement (Arndt et al., 2006; Brett et al., 2015). Groundmass and microphenocryst olivine are euhedral, indicating magmatic crystallization. The groundmass and microphenocrystic olivine contents is slightly lower (<11 volume %) than typical kimberlite (~25%; Mitchell et al., 2019). The first generation of rounded, subhedral macrocrystic phlogopite likely corresponds to early kimberlite formation. Euhedral groundmass and microphenocrystic phlogopite record later stage magmatic growth. Xenocrystic

rutile found in the Mel kimberlite is similar to rutile reported from the Naujaat kimberlite (Sarkar et al., 2018).

The major and minor element mineral chemistry of both phlogopite and ilmenite are consistent with kimberlite mineral compositions and evolution trends. For instance, Mel kimberlite phlogopite increases in Al_2O_3 with decreasing, TiO_2 and FeO, consistent with the kimberlite "trend 3" of Mitchell (1986). Core to rim enrichment in Ba and Al is also consistent with other kimberlitic phlogopite (Mitchell, 1986, 1995) and is analogous to phlogopite from the Naujaat kimberlite, Rae craton (Sarkar et al., 2018). As observed in worldwide kimberlites, Mel kimberlite ilmenite is Mg-rich in phenocryst, microphenocryst, and groundmass phases (Mitchell, 1986, 1995; Wyatt et al., 2004). Groundmass ilmenite contains the highest MnO and Fe_2O_3 content, consistent with substitution of Mg by Mn (Wyatt et al., 2004). Spinel compositions from the Mel kimberlite do not align perfectly with "trend 1" spinel typical of kimberlite (Figures 3.06A and 3.06B), instead scattering along "trend 2", a trend in common with Aviat and Naujaat kimberlites on the Melville Peninsula (Sarkar et al., 2018). Despite this, the Mel kimberlite spinel dominantly plot along the kimberlite trend in Ti/(Ti+Cr+Al) and Cr/(Cr+Al) systematics (Figure 3.06C). This result indicates that some revision is likely necessary to the definition and applicability of the spinel trends first developed by Mitchell (1986).

As with mineral chemistry, bulk whole-rock geochemical compositions of the Mel kimberlites share many characteristics in common with global and regional kimberlites (Figures 3.10, 3.11, and 3.12; Sarkar et al., 2018; Pearson et al., 2019). Mel kimberlite SiO_2, TiO_2, MgO, K_2O, and Ni contents are within the range of compositions present at the Aviat and Naujaat kimberlites on the

Melville Peninsula, to the north of Mel (Figures 3.11 and 3.12A; Sarkar et al., 2018). The Mel kimberlite has a lower median Nb, Ba, and La content compared to other kimberlites but retains the same Ba/Nb and La/Nb ratios (Figures 3.12B and 3.12D). Absolute concentrations of incompatible elements are a strong function of the amount of xenocrystic olivine present while the ratios should remain largely unaffected. $\varepsilon Hf_{initial}$ and $\varepsilon Nd_{initial}$ of two Mel kimberlite samples fall within the kimberlite field (Figure 3.15, Pearson et al., 2019).

3.4.2 Crystallization Sequence of the Mel Kimberlite

Assuming a magmatic origin, phenocryst olivine crystallized first followed by phenocryst phlogopite (Figure 3.16). A portion of olivine and phlogopite phenocrysts are likely xenocrysts in the kimberlite melt as is evidenced by their round and subhedral crystal habit, a consequence of magmatic corrosion. A portion of phlogopite phenocrysts are cognate to the kimberlite magma. These phlogopites retain euhedral crystal habits and display clear chemical zoning unlike the xenocrystal biotite and phlogopite. Ilmenite phenocrysts are interpreted as megacryst phases, corresponding to phases growing in the proto-kimberlite melt (discussed further in section 3.4.4). Microphenocryst ilmenite correspond to fragments of disaggregated ilmenite megacrysts.

CHR spinel growth commenced before the crystallization of microphenocryst phlogopite as is evidenced by CHR spinel inclusions in both phenocryst and microphenocryst phlogopite (Figures 3.03H and 3.16). Euhedral microphenocrystic olivine crystallized next followed by the growth of euhedral, Ti-rich microphenocryst phlogopite (Figure 3.16). Groundmass CHR, MUM, and MAG spinel crystallization began before groundmass phlogopite crystallization as is evidenced by spinel

inclusions in groundmass phlogopite. Apatite crystallized next and did not develop a well-defined crystal habit due to limited space (Figures 3.03E, 3.03F, and 3.16).

Following magmatic crystallization, the Mel kimberlite underwent at least two stages of fluid precipitation, and alteration. Serpentine and carbonate precipitated from fluids forming fine-grained serpentine and euhedral carbonate in the groundmass along with serpentine and carbonate segregations (Figures 3.03G, 3.16). At the same time and subsequently, olivine was altered to serpentine (Figures 3.03E, 3.16). Additionally, most macrocryst and phenocryst phlogopite and some microphenocryst phlogopite were altered to chlorite. The final alteration is punctuated by macroscopic and microscopic carbonate veins crosscutting the Mel kimberlite.

3.4.3 Crustal Contamination and Secondary Alteration of Mel Kimberlite

The geochemistry of the Mel kimberlite, as with most kimberlites, is influenced by crustal xenolith/xenocryst and mantle xenocryst contamination accompanied by significant secondary alteration. Crustal xenoliths constitute up to 2 volume % in ML8 Upper and ML8 Lower and up to 3 volume % in ML345. Garnet xenocrysts constitute up to 6 volume % in ML8 Upper and ML8 Lower. ML8 Upper and ML8 Lower have significantly more carbonate veining than ML345.

A CCI of less than 1.3 and a ln(Si/Al) greater than 2.3 both provide a potential measure of uncontaminated kimberlite (Clement, 1982; Sarkar et al., 2018), though with both indices, they can be levered by additional of mantle olivine which may mask crustal input in some circumstances (Kjarsgaard et al., 2009). Using these indices, ML8 Upper is the least contaminated Mel kimberlite, with CCI from 1.15 to 1.19 and a ln(Si/Al) from 2.44 to 2.55. ML345 is the most contaminated

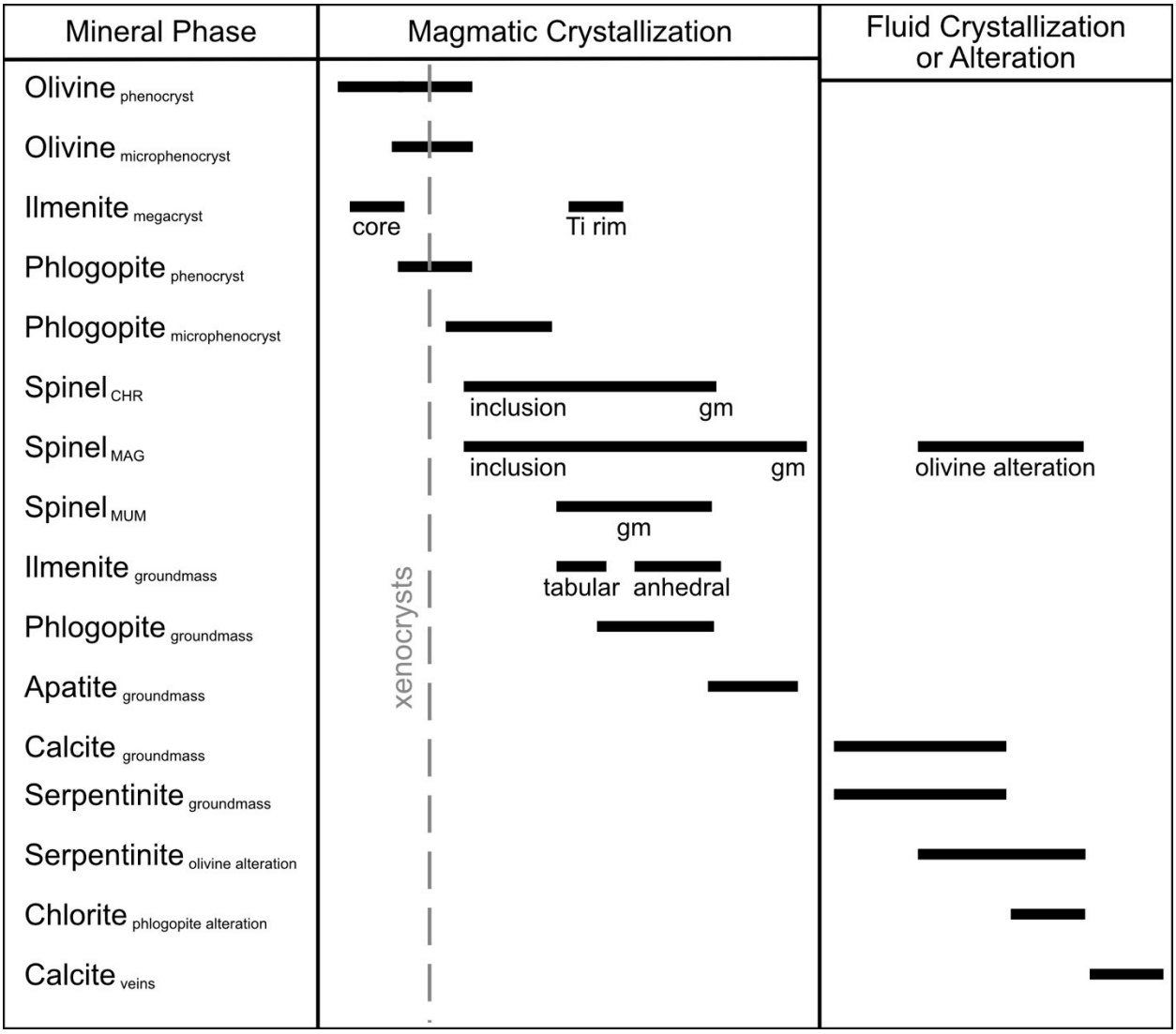

Figure 3.16: Generalized crystallization sequence of mineral phases in the Mel kimberlite. Sequence determined from mineral inclusions and textural relationships. Labels: CHR – Cr-rich spinel, MAG – Fe-rich spinel, MUM – Ti-rich spinel, gm – groundmass.

kimberlite with a CCI from 1.35 to 1.38 and a ln(Si/Al) from 2.06 to 2.38. ML345 also displays higher REE from Gd to Lu than other samples of the Mel kimberlite pointing to further evidence of crustal contamination. The contamination of ML345 is evident in its isotope composition which records the lowest $\varepsilon Hf_{initial}$ and $\varepsilon Nd_{initial}$ of the Mel suite analyzed here, consistent with the incorporation of continental crust (Figure 3.15B). $^{87}Sr/^{86}Sr_i$ falls outside the mantle array along a linear trend attributed to groundwater-driven alteration or crustal contamination (Afanasyev et al., 2014; Giuliani et al., 2017).

Although secondary alteration has spared the majority of microphenocryst phlogopite in the Mel kimberlite, multi-grain (mixed) phlogopite aliquots record Paleoproterozoic model ages, which seem to be the result of incorporating mica xenocrysts from the Penrhyn group metasediments (Partin et al., 2014).

3.4.4 Magmatic Evolution and Mantle Source of the Mel Kimberlite

As for any mafic or ultramafic intrusion, it is important to establish the mantle sources and magmatic evolution that may have contributed to the formation of the Mel kimberlite. The evolution of the Mel kimberlite magma can be evaluated based on the compositions of ilmenite megacrysts and magmatic spinel, whole-rock major and trace element systematics, and whole-rock isotope signatures.

Ilmenite phenocrysts from the Mel kimberlite record both initial mantle and subsequent magma conditions. All ilmenite phenocryst cores are Mg and Cr rich with a median content of 7.72 wt.% MgO and 0.87 wt.% Cr_2O_3. Ilmenite core Fe^{2+} contents are about 1.5 times greater than Fe^{3+}.

These compositional characteristics are found in most kimberlites and reflect a parental kimberlitic magma whose f_{O_2} increases with evolution (Mitchell, 1986; Wyatt et al., 2004; Golubkova et al., 2013; Mitchell et al., 2019). The parental kimberlitic melt results from a complex process that begins with the partial melting of carbon-bearing peridotite in the asthenosphere which produces a more Mg-rich melt than the melting of carbonate-free peridotite (Moore and Belousova, 2005; Tappe et al., 2014). This melt migrates to the base and lower part of the lithospheric mantle where it assimilates peridotite and generates a "pegmatite"-vein network of parental kimberlite magma from which ilmenite megacrysts precipitate (Golubkova et al., 2013; Mitchell et al., 2019).

In the above model, ilmenite megacrysts, formed in an initial stage of "proto-kimberlite" activity, are entrained in the parental kimberlite magma, their rims undergoing progressive magmatic corrosion and chemical reaction with the evolving kimberlite melt that entrains them. Mel ilmenite phenocrysts are interpreted as megacrysts with ilmenite microphenocrysts corresponding to fragments of disaggregated ilmenite megacrysts. Mel kimberlite ilmenite megacryst internal zones have a higher Mg and Cr (median MgO = 10.79 wt.%, median Cr_2O_3 = 0.99 wt.%). Most kimberlite ilmenites record an increase in Mg and Cr from cores to rims possibly indicative of magma mixing or the decomposition of magnesite during ascent (Schulze et al., 1995; O'Brien and Tyni, 1998; Wyatt et al., 2004). Some Mel kimberlite ilmenite megacrysts decrease in Fe^{3+} from core to rim indicating that the ilmenite rims equilibrated with a more reduced magma than the ilmenite cores (Schulze et al., 1995). Furthermore, ilmenite megacryst rims contain complex "rinds" of atoll Ti-rich spinels. These "rinds" are reaction zones that indicate a higher Ti content of the kimberlite magma than the parental kimberlite melt recorded in the ilmenite megacryst cores (Schulze et al., 1995; Kamenetsky et al., 2014).

Spinel compositions of Mel kimberlite are intermediate between “trend 1” (magnesian-ulvöspinel) and trend 2 (titanomagnetite) domains. This compositional trend is becoming increasingly common in kimberlites that occur outside southern Africa, being recorded in the Amon kimberlite sill on Baffin Island (Tappe et al., 2014), the Renard kimberlites of the Superior craton (Birkett et al., 2004), and some Pikoo kimberlites in the Sask craton (Smyth, 2019). This trend is also evident in the carbonate-rich ultramafic lamprophyres of Labrador and West Greenland (Tappe et al., 2006, 2009; Nielsen et al., 2009). As discussed above, both Cr-rich and Fe-rich spinels are the first group to crystalize in the kimberlite magma, documented by their inclusion in microphenocryst phlogopite. Ti-rich spinels become more abundant and dominate groundmass spinels and rinds on ilmenite megacrysts and microphenocrysts. These details indicate that the Cr- and Fe-rich magma evolved to become more Ti-rich. In the Amon kimberlite, the change in spinel composition from “trend 1” to “trend 2” is attributed to magma mixing between a kimberlite melt and an ultramafic lamprophyre melt (Tappe et al., 2014). Alternatively, a similar spinel compositional trend in the Renard kimberlite was attributed to the contamination of the original kimberlite magma by felsic country rock which increases the Al content of spinel (Birkett et al., 2004). The Mel kimberlite spinel trend is likely the result of a scenario similar to magma mixing in the Amon kimberlite. Spinel from the Aviat kimberlite and Qilalugaq olivine lamproite share similar trends to the Mel kimberlite while the Naujaat kimberlite hosts exclusively trend 2 type spinels (Sarkar et al., 2018). The source of the Mel kimberlite is likely similar to the source that produced the kimberlite magmatism on the Melville Peninsula.

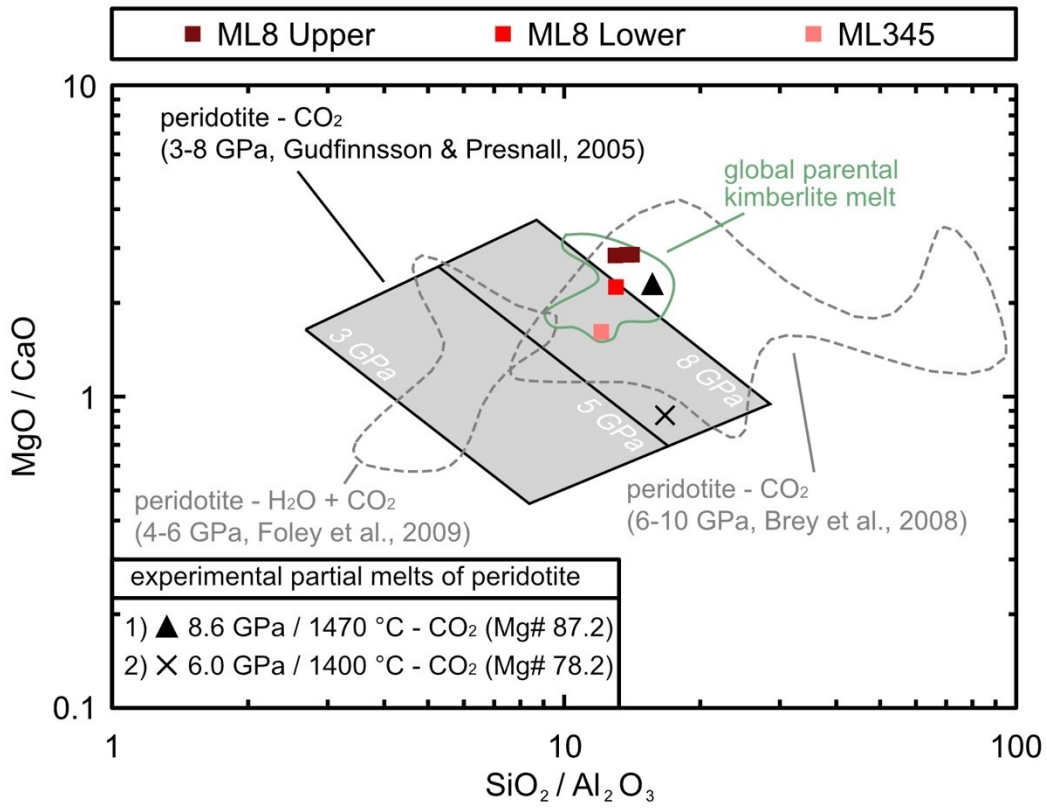

Figure 3.17: MgO/CaO against SiO_2/Al_2O_3 plot of the Mel kimberlite. Plot after Tappe et al. (2014). Note only ML345 is considered contaminated based on the samples contamination indices. Field of global parental kimberlite melt after Le Roex et al. (2003), Harris et al. (2004), Becker and Le Roex (2006), Kamenetsky et al. (2007), Kopylova et al. (2007), and Kjarsgaard et al. (2009). Experimentally produced melt compositions from synthetic carbonated peridotite with phlogopite between 4 and 6 GPa after Foley et al. (2009) and from synthetic peridotite with no phlogopite between 6 and 10 GPa after Brey et al (2008). Experimental partial melts of peridotite after 1) Dasgupta et al. (2009) and 2) Brey et al. (2008).

Additional constraints on the conditions of magma formation are derived based on MgO/CaO against SiO_2/Al_2O_3 systematics of uncontaminated (i.e. CCI <1.3 and ln(Si/Al) >2.3) hypabyssal Mel kimberlite (Figure 3.17; ML345 contaminated compositions plotted for comparison). Mel kimberlite whole-rock compositions fall within the field of compositions proposed for kimberlite melt from the Slave craton (e.g., Tappe et al., 2013). Mel kimberlite compositions resemble experimentally derived, near–solidus, partial melts of phlogopite–poor, carbonated peridotite at pressures between 6 GPa and >8 GPa or roughly 180km to >240km of depth. This indicates that the primary melt of the Mel kimberlite was produced in the convecting asthenospheric mantle from a partial melt of carbonated, volatile-enriched peridotite. Furthermore, high LREE/HREE ratios like those found in the Mel kimberlite are produced in modeling of low-degree partial melting of fertile peridotite in the presence of CO_2 in the asthenospheric mantle (Tappe et al., 2014). Since these conditions are outside the stability field of phlogopite (Frost, 2006), phlogopite growth began after melt migration to the base of the lithosphere where the kimberlite could interact with previously volatile enriched metasomes at the base of the lithosphere, promoting phlogopite growth and oxidation of the primary kimberlite magma (Le Roex et al., 2003; Paton et al., 2009; Foley et al., 2019).

Incompatible trace element concentrations of the Mel kimberlites (such as Nb, Ba, and La) are more depleted than other kimberlites on the Melville Peninsula. Nb contents of the Mel kimberlite are particularly depleted in comparison to worldwide kimberlite compositions while Ba/Nb and La/Nb ratios are within the range of kimberlite compositions. This characteristics may be the result of the kimberlite melt entraining a significant amount of mantle olivine, lowering the abundances of trace elements. Alternatively, the relative depletion of trace elements is a result of

higher degrees of partial melting than found in the other Melville kimberlites (Sarkar et al., 2018). ML8 Upper and ML8 Lower have Nb/U ratios (30 to 87) similar to plume-related intraplate oceanic magmas (Nb/U = 47 ± 10; Hofmann et al., 1986). ML345 has Nb/U ratios (8 to 29), likely the result of country rock contamination increasing the content of U.

The source region for melting of the Mel kimberlite is further constrained by Nd-Sr-Hf isotopes. ML8 Lower plots onto the mantle array and with $\varepsilon Nd_{initial}$ values similar to kimberlite and lamproite from depleted mantle reservoirs on the Melville Peninsula. Similarly, the $\varepsilon Hf_{initial}$ value of one ML8 Upper and one ML8 Lower sample fall close to the field of worldwide kimberlite and are likely the most reliable isotopic measure of source characteristics. Similar isotope systematics have been attributed to kimberlite magma sourced from the convecting upper mantle (Smith, 1983; le Roex, 1986; Nowell et al., 2004; Tappe et al., 2014). The very low $\varepsilon Hf_{initial}$ of one ML8 Upper sample may be the result of the contribution of MARID type melts to the parental Mel kimberlite melt at the base of the lithosphere (Choukroun et al., 2005) or, more likely, the result of crustal contamination. The very low $\varepsilon Nd_{initial}$ and $\varepsilon Hf_{initial}$ of ML345 are likely unrelated to principle mantle source characteristics and is instead the result of crustal contamination. Despite this contamination, Nd and Hf isotopic compositions of the least contaminated Mel kimberlite bodies are compatible with a source similar to that of typical kimberlite.

3.4.5 Emplacement Age and Regional Implications

Rb-Sr geochronology results show that the Mel kimberlite body, ML8 Upper, was emplaced during the Late Ediacaran (555 Ma). This age is assumed to be the same for ML8 Lower and ML345 due to the petrologic, geochemical, and spatial similarities between the three kimberlite bodies.

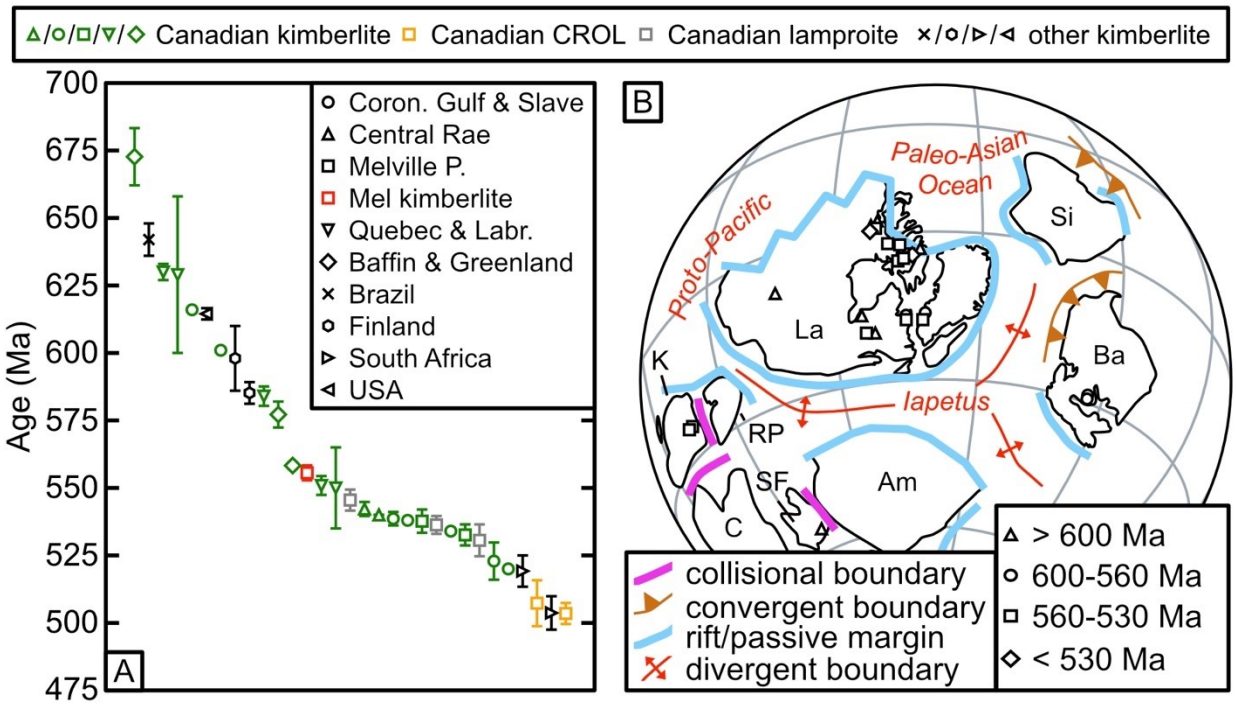

Figure 3.18: Age of the Mel kimberlite compared to Canadian and worldwide kimberlite and related intrusions. A) Age of Neoproterozoic to Cambrian kimberlite, CROL, and lamproite intrusions from Canada and select locations worldwide. Abbreviations: Coron. Gulf & Slave – kimberlites from Coronation Gulf and Slave craton, Melville P. – kimberlites, CROL, and lamproites from the Melville Peninsula, Quebec & Labr. – kimberlites from Quebec and Labrador, Baffin & Greenland, kimberlites from Baffin Island and Greenland, USA – kimberlites from the State Line District in the United States of America. Data references: Heaman et al. (2003), Hetman et al.(2004), Kienlen et al. (2008), Faure (2010), Tappe et al. (2011, 2014), Donatti-Filho et al. (2013), Harris et al. (2018), Sarkar et al. (2018), Dalton et al. (2020). Note legend at top and on Figure 3.17A pertain only to Figure 3.17A. B) Paleogeographic reconstruction of Earth at ca. 550 Ma (after Cawood et al., 2016) with ultramafic magmatism age groups. Abbreviations: Am – Amazonia, Ba – Baltica, C – congo, K – Kalahari, La – Laurentia, RP – Rio de la Plata, SF – Sao Francisco, Si – Siberia.

The Mel kimberlite age determined here (555.6 ± 2.74 Ma) is similar to the age of the Darby kimberlite field, Nunavut, central Rae craton (542.2 ± 2.6 Ma, Figure 3.18A, Harris et al., 2018), the Amaruk kimberlite from Pelly Bay (540 Ma, Figure 3.18A, Kienlen et al., 2008), hypabyssal kimberlite and UML intrusions from the Coronation Gulf and central Slave craton (616 to 520 Ma, Figure 3.18A Armstrong et al., 2012), and Neoproterozoic to Cambrian age ultramafic lamprophyres from Labrador and West Greenland (Heaman et al., 2004; Tappe et al., 2011, 2014). Additionally, kimberlite intrusions from Quebec and Labrador (including Renard – 630 ± 3 Ma, Wemendji – 629 ± 29 Ma, Torngat – 584 ± 3.6 Ma) span a similar time frame. In the immediate area of the Melville Peninsula, the late Ediacaran age of the Mel kimberlite extends kimberlite magmatism from 555.6 ± 2.74 Ma to 532.6 ± 3.9 Ma. The Aviat kimberlites to the North and the Qilalugaq olivine lamproites to the South (545.5 ± 3.9 to 530.6 ± 5.9 Ma, Sarkar et al., 2018) were emplaced after the Mel kimberlite. CROL magmatism followed kimberlite and lamproite magmatism with CROL sheets intruding at Aviat around 500 Ma (Sarkar et al., 2018). Since the Mel kimberlite is also petrographically and geochemically similar to other kimberlites on the Melville Peninsula, it is interpreted as an extension of the same type of magmatism that reflects deep lithospheric disturbances of thick cratonic lithosphere.

Sarkar et al. (2018) suggest that Neoproterozoic to Cambrian, low-volume ultramafic magmatism on the Melville Peninsula is potential evidence for the breakup of Rodinia and formation of the Iapetus ocean. Reconstructions of the northern margin of Laurentia during the formation of the Iapetus ocean indicate an extensive rift and passive margin around the whole continent at ca. 550 Ma (Cawood et al., 2016). Likewise, Neoproterozoic kimberlites and carbonatites of west Greenland are interpreted as magmatism caused by the extremities of a broad mantle plume driving

rifting along the present-day northern and eastern margin of North America (Secher et al., 2009). A majority of dated Neoproterozoic to Cambrian kimberlites in Canada are found along its eastern margin in the Rae and Superior cratons (Figure 3.18B, Heaman et al., 2004). Additionally, kimberlite intrusions from Quebec and Labrador as well as kimberlites from Brazil, Finland, South Africa, and the U.S.A. span a similar time frame and appear to be spatially concentrated along the margins of the opening Iapetus ocean (Figures 3.18A and 3.18B). Ultramafic and mafic magmatism along the eastern margin of North America was produced similarly during the rifting of Pangea and lasted from late Jurassic to Eocene time (Mazza et al., 2017; Tappe et al., 2018). As a result, the spatial and temporal distribution of Ediacaran to Cambrian kimberlite magmatism along the eastern margin of present-day North America is well correlated with Iapetus rifting (Figure 3.18B).

3.4.6 Mantle Lithosphere Characteristics and Diamond Potential of the Mel Kimberlite

As previously mentioned, garnet xenocrysts were the only clear mantle material collected from separates of the Mel kimberlite, with no fresh olivine observed. Rare clinopyroxene was noted by North Arrow Minerals Inc. (MacMorran, personal communication, 2019). Recovered garnet xenocrysts allow a preliminary view of the nature of the lithospheric mantle and the depth sampling profile of the Mel kimberlite. From the perspective offered by the garnet Ca and Cr systematics plot (Figure 3.07A), the Mel kimberlite sampled a heterogenous mantle composed of lherzolite, wehrlite, and eclogite, with no observed harzburgite. Of the peridotite garnets, 43% classify as G9A low-Ca lherzolite garnet, 3% classify as G9B lherzolite garnets, and less than 1% (n=4) classify as G12 wehrlite garnets. G3 eclogite garnets constitute 6% of garnet with 84% of these (n=21) classified as Na-rich (>0.07 wt.%) eclogite garnets.

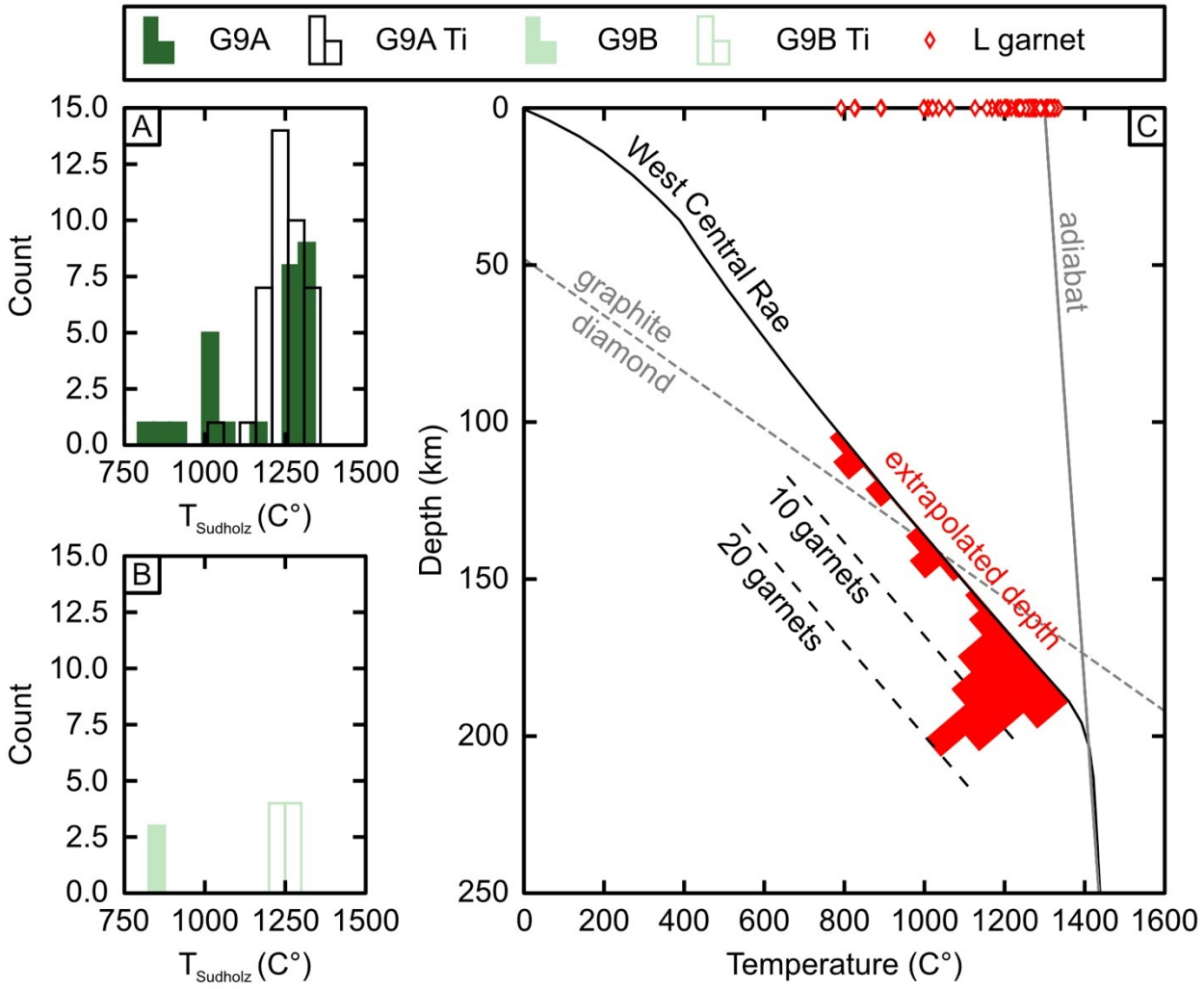

Figure 3.19: Mantle temperatures and derived depths of garnet xenocrysts sampled by the Mel kimberlite. A) and B) Histograms of the distribution of mantle temperatures (bin width = 50°C) beneath the Mel kimberlite calculated from Ni in garnet thermometry after Sudholz et al. (2021). C) Ni in garnet temperatures extrapolated onto the West Central Rae craton geotherm (Harris et al., 2018) with a histogram of peridotite (red) garnet by extrapolated depth (bin width = 5 garnets). Graphite to diamond transition line after Kennedy and Kennedy (1976). Labels: G9A – low – Ca lherzolite, G9B – lherzolite, G9A-Ti – Ti enriched low – Ca lherzolite, G9B-Ti – Ti enriched lherzolite, L garnet – lherzolite garnet Ni thermometry after Sudholz et al. (2021).

Trace elements from peridotitic garnet xenocrysts indicate that Rae craton mantle peridotite beneath the Mel kimberlite experienced depletion and re-enrichment by various metasomatic agents. Most lherzolite, Ti-rich lherzolite, and wehrlite garnet from beneath the Mel kimberlite display chondrite normalized, melt-metasomatized patterns of depleted, positively sloped LREE with flat MREE and HREE. This chondrite normalized trace element pattern is typical of lherzolite garnet from cratonic mantle (Lehtonen and O'Brien, 2009; Harris et al., 2018; Woodland et al., 2021). Alternatively, the LREE depletion in garnets can be the result of garnet equilibration with the kimberlite melt which, in turn, is enriched in LREE. Subparallel patterns are observed in four low-Ca lherzolite garnet, and one Ti-rich lherzolite garnet. The Ti-rich lherzolite garnet's flattened pattern and Ti/Eu are similar to primitive mantle garnet compositions (Stachel et al., 1998). However, the Ti-Zr systematics of this sample suggests that the chondrite normalized trace element pattern is a result of LREE re-enrichment during melt metasomatism. Sub parallel patterns in low-Ca lherzolite garnet and low-Ca, Ti-enriched garnet are likely the results of similar re-enrichment of originally LREE depleted low-Ca lherzolite. Weak sinusoidal patterns are observed in G9A, G9A Ti, and G3 Na garnet (Figure 3.08D). However, these patterns are not similar to those that are often typical of interaction with diamond-forming carbonatitic fluids that can occur in lherzolitic garnet (Klein-BenDavid and Pearson, 2009; Liu et al., 2018).

Na-rich and "normal" eclogite garnet display chondrite normalized trace element patterns that are similar to patterns observed in garnet xenocrysts from some lherzolites. Likewise, eclogite garnets with flattened REE patterns are also a result of LREE re-enrichment. LREE re-enrichment is likely the result of multiple episodes of carbonatitic and kimberlite melt percolation through the dominantly depleted mantle beneath the Mel kimberlite.

Zr-Y systematics indicates that most Ti-rich lherzolite garnets are enriched by melt metasomatism likely associated with a kimberlite melt. Additionally, all "low Ti" lherzolite (G9B) garnets analyzed from the Mel kimberlite record low Ti/Eu indicative of carbonatitic metasomatism (Woodland et al., 2021). Five low-Ca lherzolitic garnet xenocrysts display high Y (>20) at low Zr values reminiscent of MARID style metasomatism (Gregoire et al., 2003; Woodland et al., 2021). Zr-Y systematics of wehrlitic garnet have lower Y than all other garnet from the Mel kimberlite. Although these wehrlitic garnets scatter around the field of low-T phlogopite metasomatism in terms of their Zr-Y systematics, they have a stronger signature of kimberlitic melt metasomatism. Na- and K- rich carbonatite melts can increase the CaO content of garnet at a constant Cr_2O_3 content and convert orthopyroxene to clinopyroxene (Shatskiy et al., 2020). This process, dubbed "wehrlitization", produces wehrlite assemblages from peridotite protoliths such as lherzolite and harzburgite (Sokol et al., 2015; Shatskiy et al., 2020). In the absence of mantle xenoliths from the Mel kimberlite, it is reasonable to accept that the observed wehrlite garnets are the result of carbonate and/or proto-kimberlite melt metasomatism of lherzolite.

Harris et al. (2018) reconstructed a paleogeotherm from mantle xenoliths for the West-Central Rae craton brought to the surface by the Darby kimberlite at 542.2 ± 2.6 Ma. Without clear evidence of significant thermal disturbances from 550 Ma to 540 Ma, we can use Ni-thermometry in garnets, extrapolated to a West-Central Rae mantle geotherm (Harris et al., 2018) because this is the best constrained mantle geotherm for the Rae craton. 76% of lherzolite garnet xenocrysts record high temperatures (>1200° C) as recorded by 17 G9A, 34 G9A Ti, and 8 G9B Ti garnets (Figures 3.19A and 3.19B). This indicates a strong mantle sampling profile at the base of the lithosphere, close to, or within the diamond stability field. Garnets with low temperatures (<950C) and generally low

sampling depths, constitute less than 8% of the peridotite garnet population (Figures 3.19A and 3.19B) and are recorded only by 3 G9A and 3 G9B garnets. Assuming a similar geotherm to the western Rae craton constructed from xenoliths in the Darby kimberlite field (Figure 3.19C, Harris et al., 2018) the temperature range recorded by garnet xenocrysts from the Mel kimberlite indicate a mantle sample between 105 km and 185 km. The graphite diamond transition for the Darby mantle geotherm occurs at a temperature of 1030 °C and a depth of 141km. Thus, the Mel kimberlite sampled 86% of its garnet xenocrysts from below a depth greater than 141km indicating that the kimberlite would have sampled a significant portion of mantle in the diamond stability field during its ascent.

Using conventional peridotite garnet evaluation, the garnet record from the Mel kimberlite seemingly does not present strong indications for diamond potential. Peridotite diamond inclusions are overwhelmingly associated with harzburgitic compositions (Stachel and Harris, 2008). This association reflects the subsolidus diamond crystallization conditions that are more efficient than melt driven diamond crystallization in lherzolite and eclogite lithologies (Stachel and Luth, 2015). Additionally, the sinusoidal chondrite-normalized REE patterns of lherzolite garnet associated with diamond forming fluids are absent from Mel kimberlite garnets (Stachel et al., 2018). Despite this, several factors suggest a diamond potential in the mantle beneath the Mel kimberlite. The dominance of G9A garnets suggests a significant sampling of diamond-associated, depleted lherzolite (Stachel and Harris, 2008). Grütter et al. (2004) proposes that garnets derived from temperature conditions inside the diamond stability field have a MnO contents of less than 0.36 wt.%. Of the 184 G9A and Ti-rich G9A garnets from the Mel kimberlite, 95% pass the MnO criterion. Moreover, the Mel kimberlite records the presence of G3 eclogite garnets which

comprise 6% of its sampled garnet xenocrysts. Eclogite is the second principle source, after harzburgite, of diamond in the cratonic mantle (Stachel and Harris, 2008). Eclogitic garnet inclusions in diamonds are associated with a Na content of greater than 0.07 wt.% (Sobolev and Lavrent'ev, 1971; McCandless and Gurney, 1982). 84% (n=21) of G3 eclogite garnets from the Mel kimberlite classify as Na-rich eclogite garnets under this criterion with a NaO content ranging from 0.08 to 0.19 wt.% with a median NaO content of 0.12 wt.%.

Diamonds from the Victor Diamond Mine in the Attawapiskat kimberlite field of the Superior Craton are generally considered to be of lherzolite and eclogite paragenesis (Smit et al., 2014c, 2014a; Stachel et al., 2018). Furthermore, eclogite and lherzolite garnets from the Victor Diamond Mine share similar geochemistry to garnets from the Mel kimberlite, with eclogite garnet showing similar chondrite-normalized REE patterns in particular (Smit et al., 2014b, 2014a).

North Arrow Minerals reports that it recovered a total of 69 stones from a 270.6 kg sample of ML8 Upper and 8 stones from 24.1 kg sample of ML8 Lower, resulting in a concentration of 2.5 stones / 10 kg and 3.3 stones / 10 kg respectively (North Arrow Minerals Inc., 2019). For stones greater than 0.6 mm, five were recovered from ML8 Upper and two from ML8 Lower. This corresponds to 0.2 stones / 10 kg for ML8 Upper and 0.8 stones / 10 kg for ML8 Lower of larger size. Four macrodiamonds (>0.85mm) were recovered from both ML8 Upper and ML8 Lower (North Arrow Minerals Inc., 2019). With these characteristics in mind, the mantle sampling profile indicated by the garnets is consistent with the presence of diamonds in the mantle below the Mel kimberlites.

3.5 Conclusions

1. The Mel ultramafic intrusive dykes and sills discovered by North Arrow Resources Inc have petrographic, mineral chemical, geochemical, and isotopic characteristics that identify them as archetypal kimberlite magmas. Subtle variations in ilmenite mineral chemistry and whole-rock major and trace element geochemistry are observed in ML8 Upper, ML8 Lower, and ML345 kimberlite bodies. These variations provide an opportunity to distinguish ML345 from ML8Upper and ML8 Lower.

2. The Mel kimberlite shares petrographic, geochemical, and isotopic characteristics with other kimberlites on the Melville Peninsula including the Aviat kimberlites, Naujaat kimberlite.

3. The Rb/Sr mica isochron emplacement age of 555.58 ± 1.40 Ma for the Mel kimberlite increases the age of kimberlite magmatism on the Melville Peninsula to late Ediacaran time. The current understood timespan of kimberlite and lamproite magmatism on the Melville Peninsula begins at 555.58 ± 1.40 Ma and ends at 530.6 ± 5.9 Ma. CROL magmatism followed at around 505 Ma. This magmatism likely relates to the latter stages of the breakup of Rodinia and the opening of the Iapetus ocean.

4. Sr-Nd-Hf isotope systematics and whole-rock geochemistry indicate that the parental magma of the Mel kimberlite was sourced from in the asthenospheric mantle.

5. Assuming a similar geotherm to the West Central Rae craton and extrapolating garnet Ni-temperatures to this geotherm indicates that the Mel kimberlite magma sampled 86% of its mantle

load from the diamond stability field. A total of four macrodiamonds (>0.85 mm) and 73 microdiamonds have been discovered in the Mel kimberlite to date.

6. The preferred tectonic-magmatic model for the Mel kimberlite involves the initiation of low volume, kimberlite magmatism related to the breakup of Rodinia and the rifting of the Iapetus ocean. A thermal pulse from upwelling mantle-initiated magmatism along all of Laurentia. As such, the Mel kimberlite cluster forms one of the many late Ediacaran to early Cambrian kimberlite, CROL, lamproite, and ultramafic lamprophyre intrusions along the present-day eastern margin of North America relating to this wide-spread rifting episode.

Chapter 4: Geochronology, Geochemistry, and Petrology of the Dharma Kimberlite Complex, Great Bear Lake, NT, Canada.

4.1 Introduction

The Slave Craton, and surrounding area, are host to at least 326 documented kimberlite occurrences (Kjarsgaard and Levinson, 2002) including the historic and active diamond mines of Diavik, Ekati, Gahcho Kue, Jericho, and Snap Lake. Alongside these major kimberlite areas, located within the Archean nucleus (using the definitions given in Pearson et al., 2021), other diamond exploration projects have identified kimberlites within the broader Proterozoic areas of the craton, e.g., at the HOAM property near Fort Simpson, NT, Parry Peninsula property near Paulatuk, NT, and the Greenhorn property north of Great Bear Lake, NT (Goff et al., 2008; Falck et al., 2012). The Greenhorn property encompasses the Dharma kimberlite complex (i.e. Dharma kimberlite). Drilling programs by Sanatana Resources Inc and Kennecottt Canada Exploration Inc. intersected an "ultramafic breccia" of the Dharma kimberlite in 2007 and also intersected the Dharma Uttar kimberlite 50 m to the north of Dharma in 2008 (MacFarlane et al., 2007; Goff et al., 2008; Gochnauer et al., 2010). Although bulk samples (1457.36 kg total) of the kimberlite at Dharma and Dharma Uttar yielded a total of 764 diamonds, with 13 stones greater than 0.85 mesh, the project was considered to have insufficient tonnage to warrant further economic evaluation (Goff et al., 2008; Gochnauer et al., 2010).

This study presents the first published mineral and bulk rock chemistry plus geochronology or the kimberlites and associated mantle xenocrysts of the Dharma kimberlite. The study aims are to confirm the kimberlite classification assigned to the Dharma kimberlite and define its age. Further

goals were to evaluate the geochemical aspects of the kimberlite relative to kimberlites emplaced within the Archean nucleus, explore the implications for the evolution of the western margin of the Slave Craton, and help evaluate further the economic potential of kimberlites erupted in the Proterozoic cratonic regions that surround the Slave Archean nucleus in the context of diamond exploration in northern Canada.

4.2 Geology of the Dharma Kimberlite

The Dharma kimberlite is located to the west of the Archean nucleus that defines the Slave Craton, on the Northern Shore of Great Bear Lake in the Paleoproterozoic Hornby Bay Basin (Figure 4.01; Goff et al., 2008). Drilling in 2007 and 2008 intersected and delineated two kimberlite target bodies, Dharma and Dharma Uttar, with a total intersect of 717.9 m of volcaniclastic kimberlite and 77.1 m of hypabyssal kimberlite (Gill, 2016; Figure 4.02). The intersected proposed kimberlite bodies of the Dharma kimberlite are interpreted as a complex of diatreme blows connecting to sills and dykes at depth which intruded into laminated dolomite and mudstone of the Dismal Lakes and Hornby Bay Groups (Figure 4.01; Gill, 2016).

A reconstruction based on the drilling data provided in this report (Gill, 2016) indicates the presence of at least two volcanic diatremes (Figure 4.02C). The Dharma Kimberlite studied here focusses on the larger diatreme within this complex (Figure 4.02). Cross-sections constructed from five diamond core drill holes suggest that a central diatreme is volumetrically dominated by volcaniclastic kimberlite tuff (VK_t) and tuff-breccia (VK_b). Volcaniclastic kimberlite tuff overlies the volcaniclastic kimberlite tuff-breccia at depths of 82.8 m in hole DD07GH001 and 175.2 m in hole DD07GH004 (Figures 4.02A and 4.02B). At least two separate hypabyssal

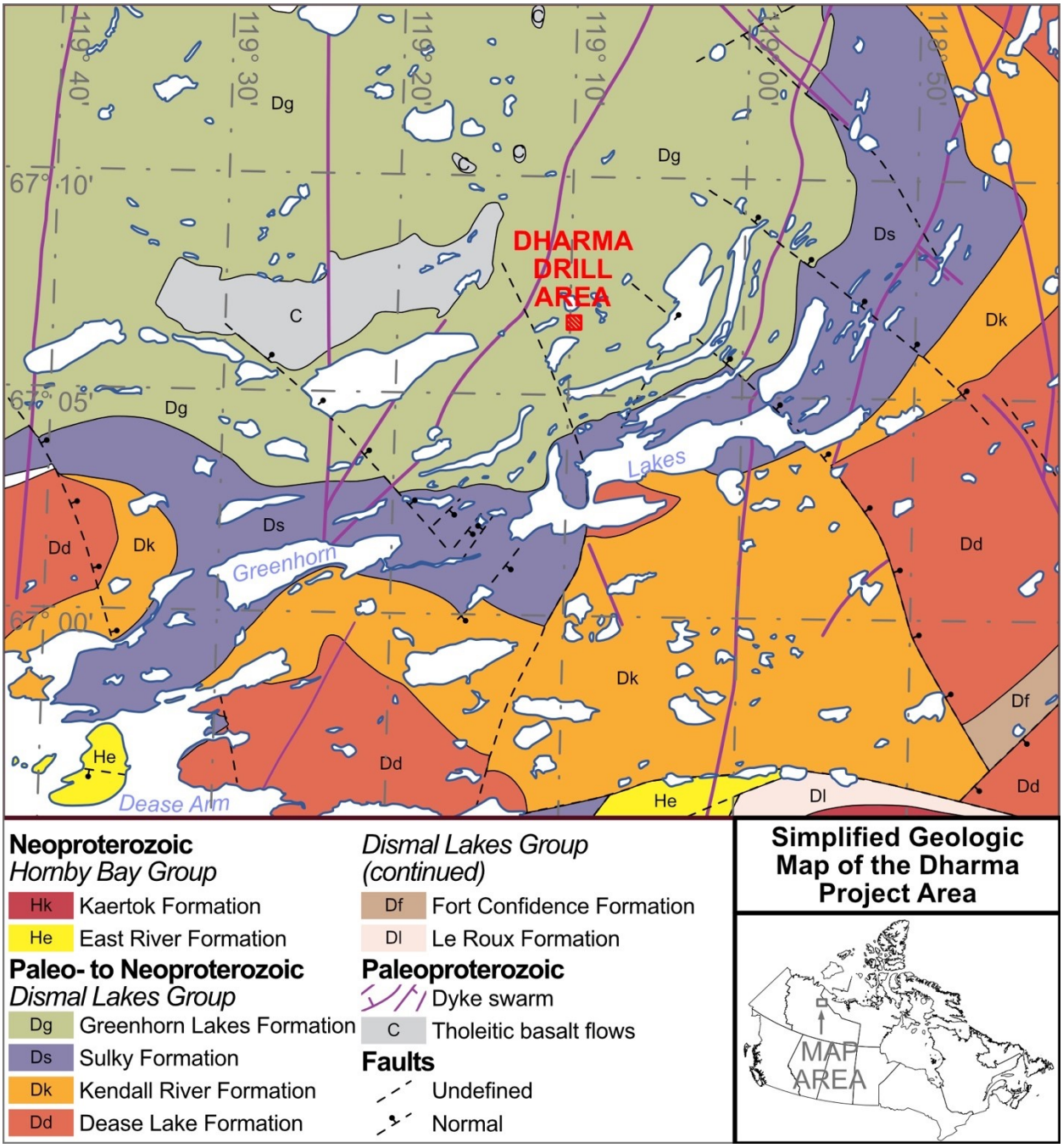

Figure 4.01: Simplified geologic map of the Dharma kimberlite project area. Geologic map after Ross and Kerans (1989).

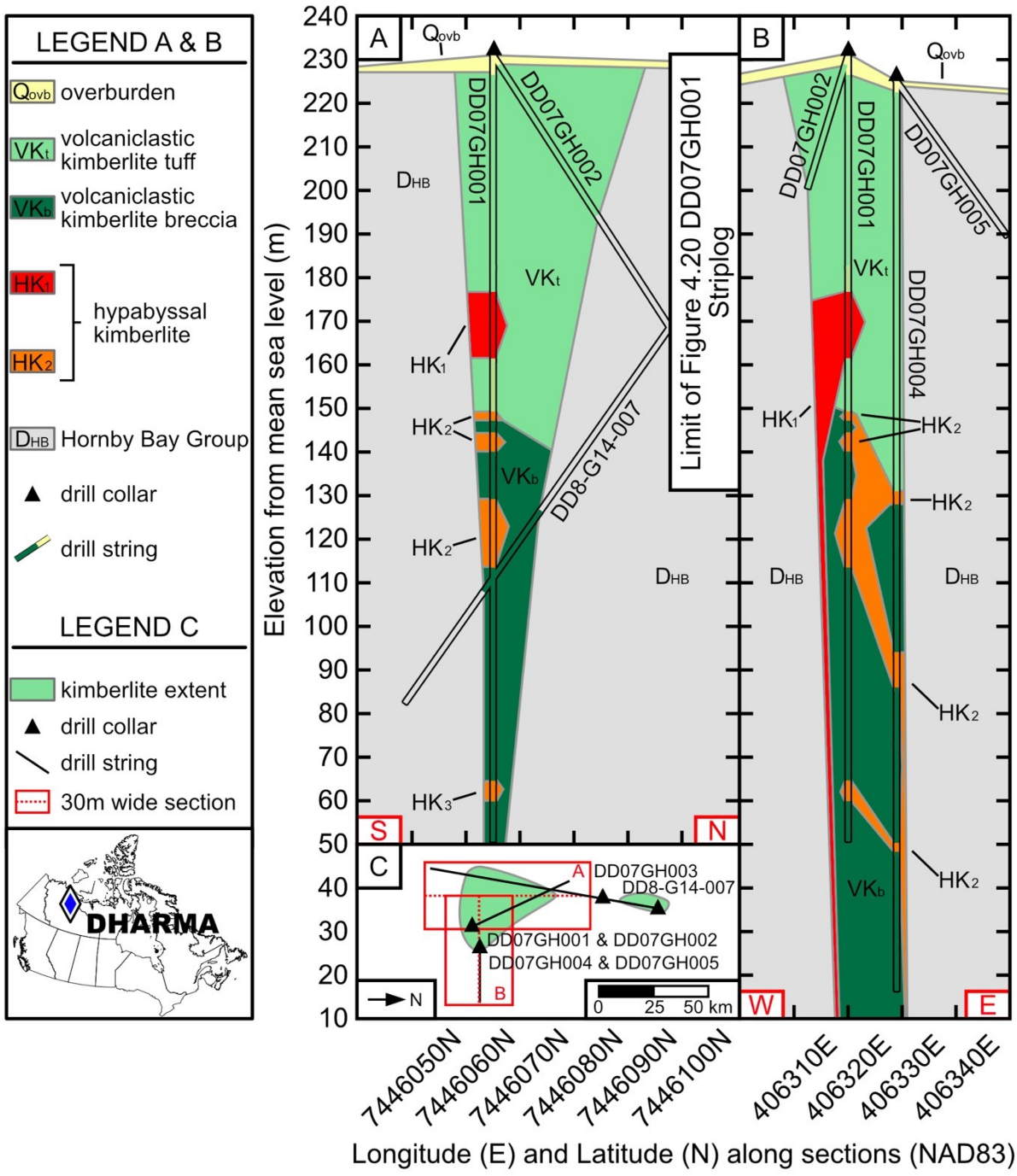

Figure 4.02: Simplified geologic cross-sections of the main Dharma kimberlite pipe. Cross sections along transects from A) South to North and B) West to East. Cross-section reconstructed from drill logs in Gill (2016). Drill hole trace width exaggerated to show logging results. C) Plan view map of the main Dharma kimberlite pipe and secondary pipe.

kimberlite bodies are intersected by diamond drilling. The first body (HK_1) consists of one interval from 54.78 m to 70 m in hole DD07GH001 of black to dark grey, hypabyssal kimberlite with dolomite and shale xenoliths. The second body (HK_2) consists of two intervals from 82.2 m to 84.3 m and 87 m to 91.4 m in hole DD07GH001 of black to dark grey, hypabyssal kimberlite with dolomite xenoliths. Although not sampled in this work, extensions of kimberlite bodies HK_1 and HK_2 are delineated in holes DD07GH001 and DD07GH004. In hole DD07GH001, two intervals from 102.3 m to 118 m and from 166.9 m to 171.6 m consist of massive black, hypabyssal macrocrystic ilmenite-phlogopite bearing kimberlite. In hole DD07GH004, three intervals from 94.5 m to 97.5 m, 131.4 m to 139.5 m, and 175.2 m to 177.2 m consist of dark grey to black, macrocrystic hypabyssal ilmenite kimberlite. Preserved fragments of coral and bivalve fossils indicate that the Dharma kimberlite age is younger than Devonian (Santana Resources Inc., 2008).

4.3 Results

4.3.1 Petrography

A petrographic study was conducted on ten hypabyssal kimberlite and ten volcaniclastic kimberlite samples. Modal abundances of mineral, clastic, and lithic phases are variable within the group of hypabyssal and volcaniclastic kimberlites respectively. Detailed petrography is presented in Table 4.01. Point count maps and thin section scans are presented in Appendix A.14 to A.33. It should be reiterated that groundmass (<100μm), microphenocryst (100 to 500μm), and phenocryst (>500μm) descriptors are strictly limited to describing sizes and not genetic interpretations.

Table 4.01: Distribution of mineral phases in hypabyssal Dharma kimberlite. Percentage in volume % analyzed by point-counting. Abbreviations: Cb – carbonate group mineral, Cpx – Clinopyroxene, Grt – garnet group mineral, Olv – olivine, Ox – oxide mineral (i.e. ilmenite, spinel), Phl – phlogopite mica, Seg – segregated matrix of predominantly serpentine group minerals and/or carbonate, Uni – uniform crystalline matrix.

Sample	***Depth (m)***		***Phenocryst***				***Microphenocryst***				***Groundmass***		***Xenocryst***		***Xenolith***	
Sample No.	*From*	*To*	*Olv*	*Ox*	*Phl*	*Cb*	*Olv*	*Ox*	*Phl*	*Cb*	*Uni*	*Seg*	*Cpx*	*Grt*	*Crustal*	*Mantle*
D86	58.89	58.96	28%	-	-	-	5%	-	-	-	56%	-	5%	-	6%	-
D91	63.17	63.29	16%	<1%	-	-	9%	<1%	-	-	66%	<1%	-	3%	5%	-
D92	63.73	63.80	18%	1%	-	-	5%	<1%	-	-	69%	2%	-	3%	2%	-
D94	66.10	66.29	22%	<1%	-	-	6%	<1%	-	<1%	63%	2%	3%	<1%	4%	-
D95	67.79	67.87	26%	-	3%	-	7%	<1%	<1%	<1%	62%	<1%	-	<1%	<1%	-
D104	82.76	82.90	21%	<1%	-	-	5%	<1%	-	<1%	66%	2%	-	5%	1%	-
D105	83.15	83.21	27%	-	-	-	6%	<1%	-	1%	62%	3%	-	1%	<1%	-
D108	89.53	89.63	21%	-	<1%	1%	5%	<1%	-	<1%	63%	1%	1%	4%	-	4%
D109	91.31	91.36	30%	-	1%	-	5%	-	-	-	60%	<1%	-	3%	-	-
D122	54.78	54.84	25%	-	-	-	12%	<1%	-	-	59%	1%	1%	-	1%	1%

Table 4.02: Distribution of mineral phases in volcaniclastic Dharma kimberlite. Percentage in volume % analyzed by point-counting. Abbreviations: Cb – carbonate group mineral, Cpx – Clinopyroxene, Crst Ash – crustal xenolith cored ash, Crst Lapilli – crustal xenolith cored lapilli, Grt – garnet group mineral, Mnt Ash – mantle xenolith cored ash, Mnt Lapilli – mantle xenolith cored lapilli, Olv – olivine, Ox – oxide mineral (i.e. ilmenite, spinel), Phl – phlogopite mica, Seg – segregated matrix of predominantly serpentine group minerals and/or carbonate, Uni – uniform crystalline matrix.

Sample	*Sample No.*	*D98*	*D101*	*D112*	*D114*	*D116*	*D117*	*D118*	*D128*	*D129*	*D132*
Depth (m)	*From*	70.58	80.52	33.92	37.41	43.11	45.03	48.42	17.42	21.09	29.97
	To	70.75	80.60	34.03	37.45	43.21	45.16	48.51	17.50	21.18	30.03
Phenocrysts	*Olv*	4%	1%	4%	2%	-	1%	12%	2%	5%	3%
	Ox	-	-	-	-	<1%	2	-	-	-	-
	Phl	-	-	-	5%	2%	1%	4%	1%	1%	1%
	Cb	<1%	-	-	-	-	-	-	-	-	-
Microphenocrysts	*Olv*	1%	1%	1%	<1%	1%	1%	1%	1%	2%	1%
	Ox	<1%	-	-	-	<1%	<1%	<1%	-	<1%	-
	Phl	<1%	<1%	<1%	<1%	-	<1%	1	<1%	<1%	<1%
	Cb	<1%	<1%	<1%	-	<1%	<1%	<1%	-	<1%	<1%
Ash (<2mm)	*Juvenile*	3%	<1%	9%	2%	4%	2%	6%	-	-	2%
	Olv core	4%	4%	1%	1%	-	-	2%	-	2%	6%
	Ox core	-	-	-	-	1%	-	-	-	-	-
	Phl core	2%	-	-	-	-	-	3%	2%	-	-
	Cpx core	-	-	<1%	-	-	-	-	-	-	-
	Gt core	-	-	-	<1%	-	-	-	-	-	-
Lapilli (>2mm)	*Juvenile*	2%	-	13%	-	-	-	17%	-	-	13%
	Olv core	14%	27%	16%	26%	5%	48%	5%	-	-	5%
	Phl core	-	-	-	-	2%	-	3%	-	-	-
	Cb core	-	-	-	-	10%	-	-	-	-	-
	Cpx core	-	-	-	19%	-	-	-	-	43%*	-
	Gt core	-	-	-	-	3%	-	-	-	-	-
Inter-Clast Matrix	*Uni*	50%	32%	24%	30%	37%	38%	31%	33%	19%	32%
	Seg	-	8%	<1%	1%	4%	1%	1%	1%	-	<1%
Crustal Components	*Crustal*	7%	18%	7%	6%	19%	6%	5%	16%	13%	2%
	Crst Ash	-	-	-	-	-	-	-	5%	-	1%
	Crst Lapilli	12%	8%	25%	8%	12%	1%	11%	23%	8%	24%
Mantle Components	*Mantle*	-	-	-	-	-	-	-	2%	6%	-
	Mnt Ash	-	-	-	-	-	-	-	1%	-	-
	Mnt Lapilli	-	-	-	-	-	-	-	13%	-	9%

**a majority of this thin section sample is a single clinopyroxene grain, which is not representative of typical xenocryst content*

4.3.1.1 Hypabyssal Coherent Kimberlite

Hypabyssal Dharma kimberlite is a flow-banded macrocrystic kimberlite. The uniform groundmass is composed of carbonate + spinel + serpentine + apatite + ilmenite ± olivine (in order of most to least abundant (Figure 4.03G and 4.03H) and constitutes 56 volume % to 69 volume %. Groundmass carbonate is present as anhedral carbonate and euhedral to subhedral, microcrystalline carbonate. Groundmass serpentine is present as both anhedral serpentine and serpentine polymorphed after subhedral olivine. Rare egions of the groundmass contain segregations of carbonate>serpentine (3 volume %), commonly forming around euhedral microphenocryst carbonate. Groundmass spinel is present predominantly as euhedral single crystals (Figure 4.03H), atoll spinel (Figure 4.03H), and one occurrence of spinel + ilmenite intergrowth. Groundmass apatite is present as isolated euhedral crystal laths (Figure 4.03H) and as multi-crystal "sprays" (Figure 4.03G). When not intergrown with spinel, groundmass ilmenite is subhedral. Where present, groundmass olivine is subhedral and often replaced by serpentine (Figures 4.03H and 4.04A). Rare carbonate veins crosscut several samples of hypabyssal kimberlite.

Olivine is the predominant crystal phase in the hypabyssal Dharma kimberlite, which is mostly unaltered (92 to 100 volume % unaltered olivine) in five of ten samples and commonly unaltered (41 to 77 volume %) in two of ten samples. Anhedral to subhedral phenocryst olivine constitutes 16 volume % to 30 volume % of hypabyssal kimberlite, found concentrated apart from smaller-sized olivine (Figure 4.03C), and can display undulated extinction (Appendix A.15). Anhedral to subhedral phlogopite phenocrysts constitute up to 3 volume % and display strong chlorite alteration. Many phlogopite phenocrysts are serpentinized (D094005), oxides (D104001), and

other phlogopite phenocrysts (D117_04). One phenocrystic phlogopite displays microscopic dislocations along its principal cleavage planes (D104001). Subhedral oxide phenocrysts constitute up to 1 volume % and are predominantly made up of ilmenite (Figures 4.03B and 4.04B). Phenocryst carbonate was only observed to constitute 1 volume % of sample D108 along segregated groundmass alongside microphenocryst carbonate.

Subhedral to euhedral olivine crystals constitute 5 volume % to 12 volume %. Subhedral oxide microphenocrysts constitute up to 1 volume %. Mica microphenocrysts constitute up to 1 volume % and are made up of more biotite than phlogopite. One microphenocrystic phlogopite analyzed by EPMA (D117_08) displays euhedral habit. Microphenocrystic carbonate constitutes up to 1 volume % and is found almost exclusively within groundmass segregations of carbonate and serpentine.

The xenocrystic assemblage of the Dharma kimberlite consists of mantle-derived clinopyroxene and garnet. Subhedral mantle clinopyroxene xenocrysts constitute up to 5 volume % and are fractured and broken (Figures 4.03E and 4.03F). Subhedral mantle garnet xenocrysts constitute up to 5 volume % and are fractured with 100μm-thick kelyphite rims (e.g. Appendix A.15, Appendix A.16).

Crustal xenoliths constitute up to 6 volume % and mainly consist of dolomite, sandstone, and one clast of biotite + magnetite + apatite lithology. Mantle xenoliths constitute up to 4 volume % with garnet harzburgite (Figures 4.03E and 4.03F) and garnet dunite present and are dominated by granoblastic textures. One serpentine + oxide xenolith is classified as an altered spinel peridotite.

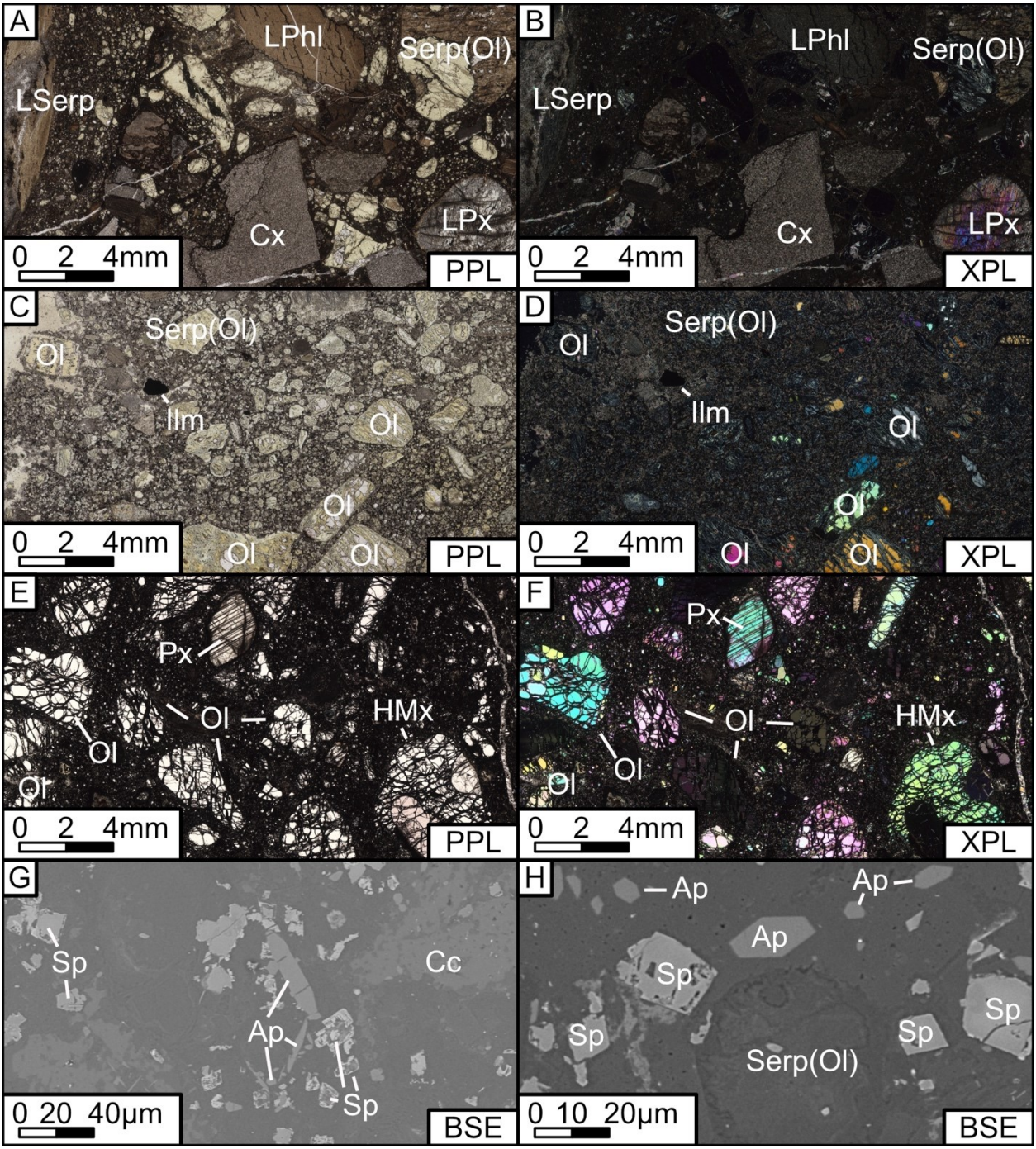

Figure 4.03: Petrography of the Dharma kimberlite. A) Plain polarized photomicrograph and B) cross polarized photomicrograph of volcaniclastic kimberlite (sample D129; 21 m depth). C) Plain polarized photomicrograph and D) cross polarized photomicrograph of transitional kimberlite (sample D122; 55 m depth). E) Plain polarized photomicrograph and F) cross polarized photomicrograph of hypabyssal kimberlite (sample D86; 59 m depth). Back scatter electron image of kimberlite sample G) D109 (depth 91 m) and H) D108 (depth 89.5 m). Abbreviations: Ap – apatite, Cc – carbonate, HMx – harzburgite mantle xenolith, Ilm – ilmenite, LPhl – phlogopite cored lapilli, LPx – pyroxene cored lapilli, LSerp – serpentinite cored lapilli, Phl – phlogopite mica, Serp(ol) – serpentinite pseudomorph after olivine, Sp – spinel.

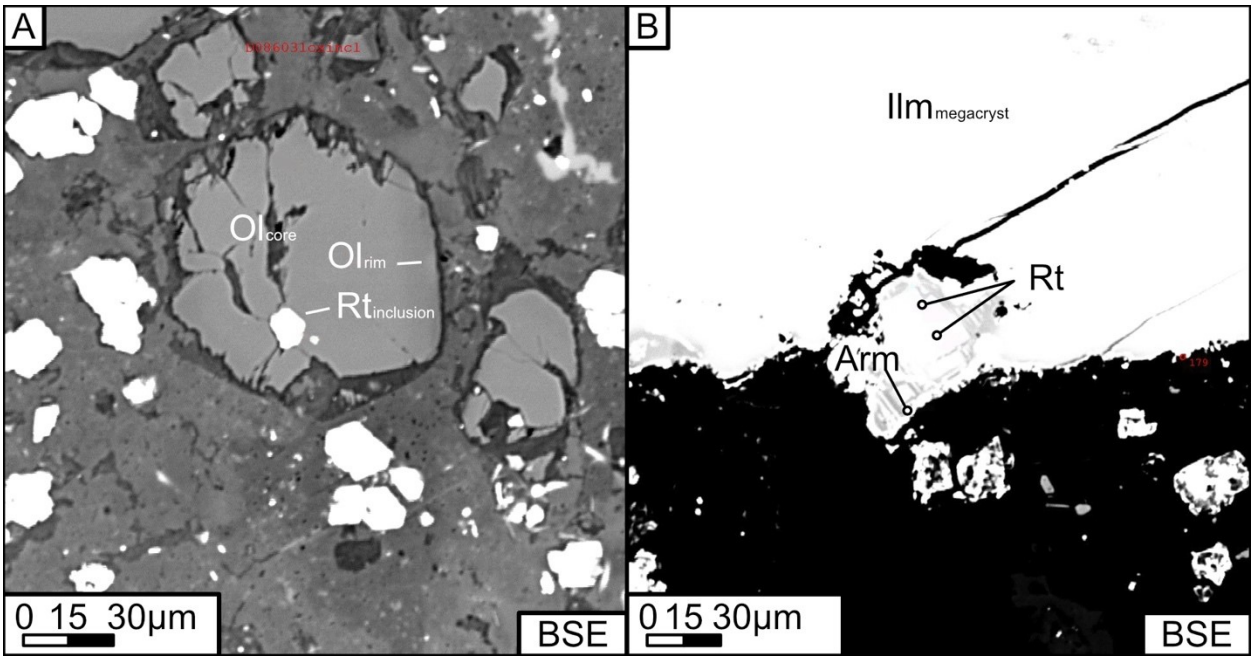

Figure 4.04: Rutile occurrences in Dharma hypabyssal kimberlite. A) Rutile inclusion in olivine. B) Rutile with armalcolite rim on ilmenite megacryst. Abbreviations: Arm – armalcolite, $Ilm_{megacryst}$ – ilmenite megacryst, Ol_{core} – olivine core, Ol_{rim} – olivine rim, Rt – rutile, $Rt_{inclusion}$ – rutile inclusion.

4.3.1.2 Volcaniclastic Kimberlite

The volcaniclastic facies kimberlite of the Dharma kimberlite is a poorly-sorted, crystal and clast–rich, clast-supported volcaniclastic kimberlite. The inter-clast matrix consists of serpentine ± olivine + carbonate + oxide minerals (in order of most to least abundant). Matrix serpentine is typically euhedral to subhedral in appearance. Subhedral to euhedral matrix olivine is variably altered to serpentine. Matrix carbonate is subhedral. Subhedral to euhedral oxide minerals predominantly belong to the spinel group. Two generations of carbonate veins are identified in volcaniclastic kimberlite. One generation of carbonate veins cross-cuts the matrix but does not intersect clasts, following the clast-matrix boundary instead. This generation of carbonate veins varies in thickness and some are large enough to accommodate the growth of subhedral to euhedral carbonate. The other generation of carbonate veins appears to be distributed within individual framework clasts.

Framework clasts consist of >500µm crystals, 100µm to 500µm crystals, ash, lapilli, xenocrysts, and xenoliths. The most dominant crystal phase (>500µm) is olivine, which constitutes up to 12 volume % and is mostly altered (e.g. Appendix A.26 and Appendix A.29). Olivine crystals (>500µm) are anhedral to subhedral and mesh textured. Subhedral phlogopite crystals constitute up to 5 volume %, can be optically concentrically zoned, and are variably altered to chlorite (e.g. Appendix A.29). Subhedral oxide crystals (>500µm) constitute up to 2 volume % and are predominantly composed of ilmenite. Subhedral crystalline carbonate (>500µm) has only been observed in sample D98 at a depth of 70.58 m to 70.75 m, where it constitutes less than 1 volume %. Microphenocrysts are rare in volcaniclastic kimberlite. Subhedral olivine crystals (100µm to 500µm) constitute up to 2 volume % and are predominantly altered to serpentine. Oxide,

phlogopite, and carbonate crystals (100µm to 500µm) all constitute at most 1 volume %. A single observed olivine-cored lapillus from sample D117 (45.03 m to 45.16 m depth) displays a distinct inner and outer zone (Appendix A.28). A heavily altered olivine core is rimmed by a light-colored inner to the dark-colored outer zone. These features are consistent with juvenile lapilli also known as magmaclasts (Scott Smith et al., 2012; Scott Smith et al., 2018).

Xenocrystic framework clasts include garnet and clinopyroxene cored ash and lapilli (Table 4.02). A single sample of D129 contains a large clinopyroxene cored lapilli with the clinopyroxene core up to 5 mm in size (Appendix A.32). Xenoliths in volcaniclastic kimberlite occur as individual lithic fragments and as cored lapilli and ash clasts. Several large (>5 mm) mantle and crustal microxenoliths are identified in samples of volcaniclastic kimberlite. Observed mantle xenoliths constitute up to 13% of all modal phases and are identified as lherzolite. Crustal xenoliths constitute up to 25% of all modal phases and are identified as siliciclastic and calcite-rich carbonate lithologies.

4.3.2 Kimberlite Mineral Chemistry

A total of 287 EPMA analyses was performed on phlogopite, ilmenite, and spinel from the Dharma kimberlite. Detailed mineral chemistry results are tabulated in Appendix C. Analytical methods are described in Chapter 2 section 2.3. As previously mentioned, the classifiers of groundmass, microphenocryst, and phenocryst are strictly used to denote size.

4.3.2.1 Olivine

EPMA analyses encompasses 27 phenocrysts (core n=27, intermediate zone n=23, rim n=26), 45 microphenocrysts (core n=20, intermediate zone n=5, rim n=20), nine groundmass (core n=4, intermediate zone n=1, rim n=4) olivine, and four olivine (core n=5, intermediate zone n=6, rim n=6) from mantle microxenoliths (Appendix C.01). All analyses were completed on hypabyssal kimberlite samples.

The Mg-number of Dharma kimberlite olivine ranges from 0.88 to 0.97. Ni content in all olivine ranges from 0.05 to 0.42 wt.% NiO. Mg-number ranges from 0.89 to 0.92 in phenocryst olivine with a median of 0.91. Microphenocrystic olivine has the highest range of Mg-number from 0.88 to 0.97 with a median value of 0.90. Mg-number in groundmass olivine ranges from 0.89 to 0.94 with a median value of 0.90. Mg-number of phenocrystic rims, microphenocryst, and groundmass olivine ranges from 0.89 to 0.92, 0.90 to 0.97, and 0.90 to 0.94 respectively. These values are similar to the range of Mg-number in olivine rims from typical kimberlite (Mitchell, 1986; Giuliani, 2018; Mitchell et al., 2019). Most core and intermediate zones of phenocryst, microphenocryst, and groundmass olivine overlap in NiO and Mg-number with olivine from dunite and garnet harzburgite microxenoliths (Figure 4.05). This indicates that 50% of groundmass olivine, 85% of microphenocryst olivine, and 85% of phenocryst olivine likely contains mantle xenocryst cores. Olivine from dunite and garnet harzburgite microxenoliths share similar NiO content with olivine from microxenoliths in the Darnley Bay and Victoria Island kimberlites but displays a lower Mg-number range (90 to 92; Figure 4.05).

Dharma kimberlite olivine displays two distinct NiO and Mg-number compositional trends. The first trend is characterized by a decrease in NiO content at a near-constant Mg-number from core to rim. This trend is observed in all olivine grains (Figure 4.05A to 4.05C). In phenocrysts, Ni

decreases from a median core NiO content of 0.41 wt.% to 0.12 wt.%. In microphenocrysts, Ni decreases from a median core NiO content of 0.33 wt.% to 0.15 wt.%. In groundmass olivine, Ni decreases from a median core NiO content of 0.30 wt.% to 0.12 wt.%.

The second trend is found in two microphenocrystic and two groundmass olivine and is characterized by an increase in Mg-number coupled with decreasing NiO content. In one microphenocrystic olivine, the core to intermediate zone decreases in NiO (0.37 to 0.18 wt.%) at a near-constant Mg-number (0.92 to 0.91). This grain then exhibits a sharp increase in Mg-number (0.91 to 0.97) and decrease in NiO content (0.18 to 0.05 wt.%). In the single analysis of groundmass olivine with an intermediate zone, the core is characterized by a sharp decrease of NiO content (0.37 to 0.11 wt.%) along with a slight decrease in Mg-number (0.92 to 0.84). The rim of this grain displays an increase in Mg-number from the intermediate zone (0.84 to 0.94) coupled with a slight decrease in NiO (0.11 to 0.08 wt.%).

Most olivine cores have near-zero TiO_2 contents at a variable CaO content, ranging from zero to 0.11 wt.%. These olivine cores correspond to typical mantle olivine compositions (Figure 4.05D). A few olivine cores record elevated TiO_2 content in comparison with a CaO content generally between 0.04 and 0.07 wt.%. Elevated TiO_2 content in phenocryst olivine cores is consistently between 0.03 to 0.04 wt.%. Intermediate zones and rims of phenocrysts generally display a similar range of TiO_2. One phenocrystic core plots into the field of kimberlite olivine (Figure 4.05D). Microphenocrystic olivine cores record the largest range in TiO_2 content from 0.05 wt.% to 0.09 wt.%. In groundmass olivine, TiO_2 content is similar to the lower end of TiO_2 in microphenocryst cores. Phenocryst and groundmass olivine cores display TiO_2 and CaO contents overlapping with olivine from the Muskox kimberlite (Figure 4.05D). The single high TiO_2 microphenocrystic core overlaps with olivine from till sediment sampling on Victoria Island (Figure 4.05D).

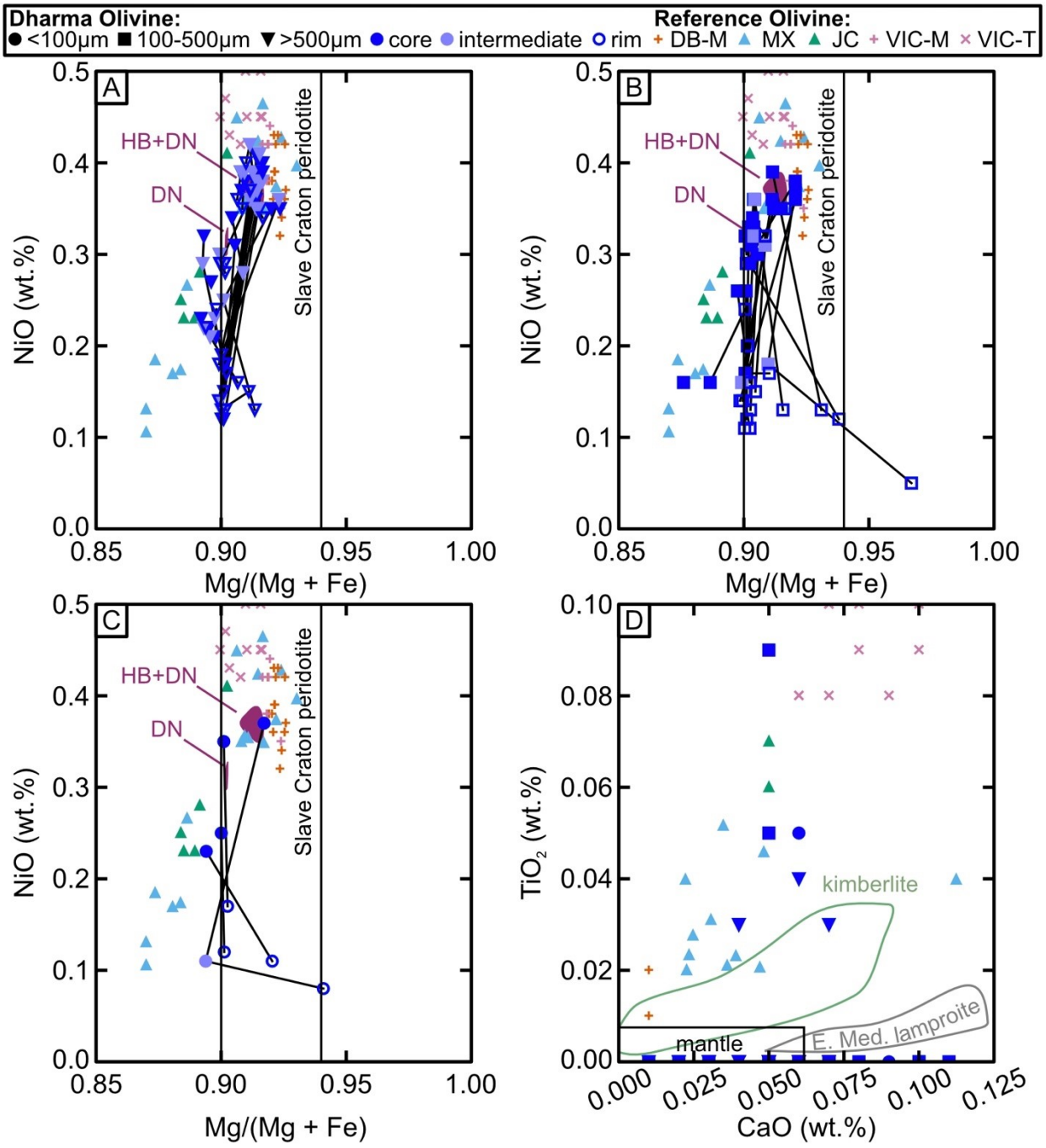

Figure 4.05: Composition of olivine from the Dharma kimberlite. NiO against Mg apfu / (Mg apfu + Fe apfu) of A) phenocryst (>500µm) olivine, B) microphenocryst (100µm to 500µm) olivine, and C) groundmass (<100 µm) olivine. D) TiO_2 against CaO discrimination plot for olivine cores after Foley et al. (2013). Abbreviations: E. Med. Lamproite – eastern Medeteranian lamproite, HB+DN – garnet harzburgite and dunite microxenoliths from sample D86, DN – dunite microxenolith from sample D91. Slave craton peridotite field after Moore and Costin (2016). Reference olivine compositions: DB-M – Darnley Bay olivine from mantle xenoliths (Brin, 2016), MX – Muscox macrocryst olivine (Hayman et al., 2009), JC – Jericho megacryst olivine (Kopylova and Hayman, 2008), VIC-M – Victoria Island olivine from mantle xenoliths (Brin, 2016), VIC-T – Victoria Island olivine from till sampling (LeCouteur, 2001).

4.3.2.2 Phlogopite and Biotite

EPMA analyses include both phlogopite and biotite mica. Phlogopite analyses consist of five phenocryst (core n=4, intermediate zone n=1, rim n=2) and two microphenocryst (intermediate zone n=2, rim n=1) analysis (Appendix C.03). Biotite analyses include four phenocryst (core n=4, intermediate zone n=2, rim n=4) and two microphenocryst (core n=2, intermediate zone n=2, rim n=2) biotite. Analyses of biotite mica are interpreted as crustal biotite and not discussed in further detail.

Phlogopite phenocrysts and microphenocrysts from the Dharma kimberlite fall into the field of kimberlite phlogopite phenocrysts and microphenocrysts (Figures 4.06A and 4.06B). Two phlogopite phenocrysts also straddle the edge of the field of kimberlite groundmass phlogopite (Figures 4.06A and 4.06B). Phlogopite compositions are broadly similar to compositions of phlogopite from the Muskox and Jericho kimberlites (Figures 4.06A and 4.06B). Phlogopite macrocrysts from the Churchill kimberlite field are also compositionally similar to the phlogopite population in Dharma kimberlite (Figures 4.06A and 4.06B). The majority of phlogopites from the Dharma kimberlite are eastonite to phlogopite in composition with one phenocryst core falling on the continuum between phlogopite and tetraferriphlogopite end-members (Figure 4.06C).

Phenocrystic phlogopite displays chemical zonation visible in the BSE imaging. Although not analyzed, phlogopites in volcaniclastic kimberlite are also optically zoned (Figures 4.03A and 4.03B). TiO_2 content generally decreases from core (median 2.88 wt.%) to rim (median 1.14 wt.%). Generally, Al_2O_3 content in phenocrystic phlogopite is relatively constant (11.6 and 12.8 wt.%.) A single phenocrystic phlogopite grain (D117_04) records substantial Al_2O_3 variations from 7.4 wt.% to 11.6 wt.% from intermediate zone to rim (Figure 4.06A). One grain of phenocrystic phlogopite displays the trend of decreasing TiO_2 at a constant Al_2O_3 from the core

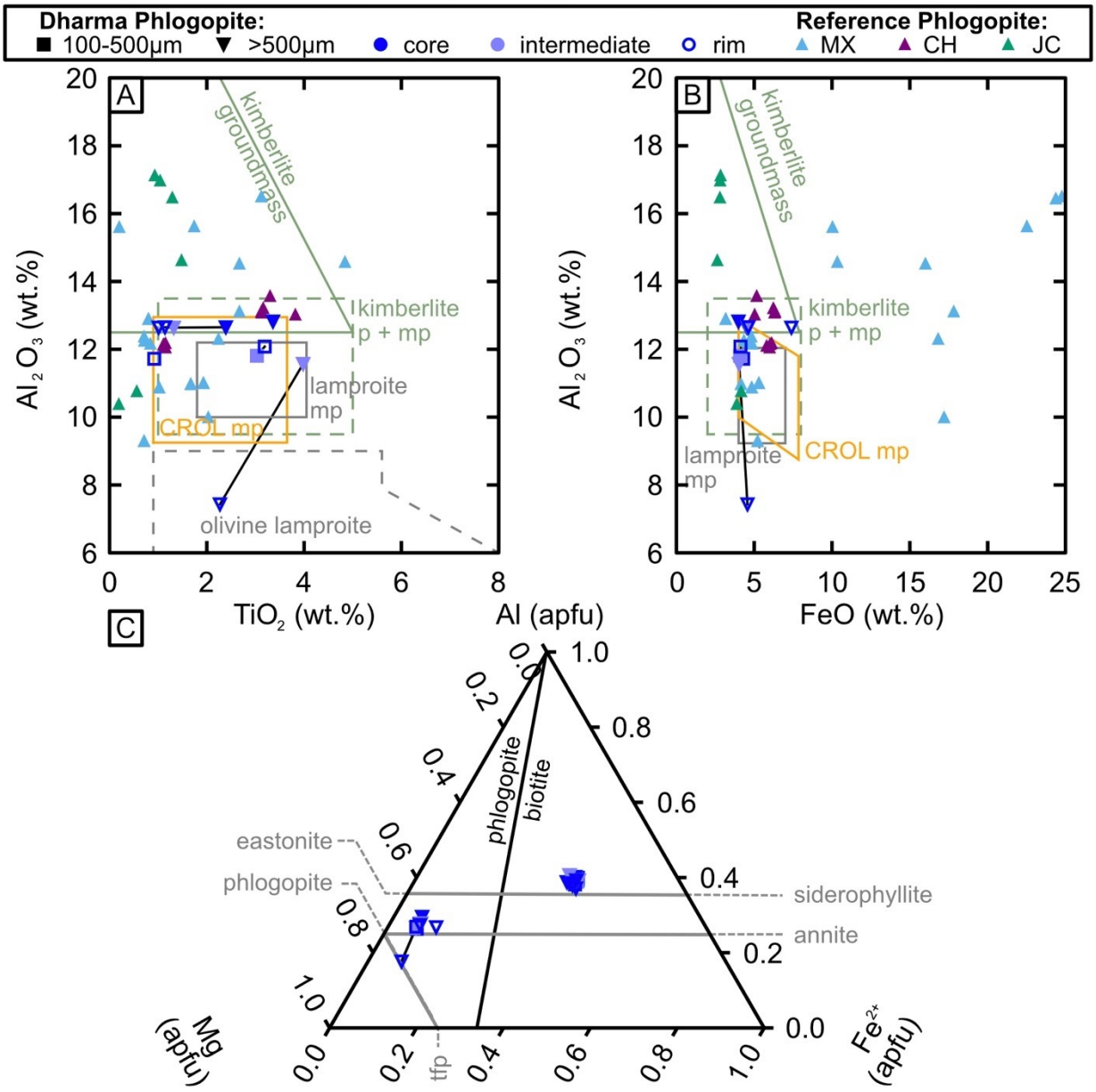

Figure 4.06: Composition of phlogopite mica from the Dharma kimberlite. A) Al_2O_3 against TiO_2 phlogopite mica plot. B) Al_2O_3 against FeO phlogopite mica plot. C) Al apfu-Mg apfu-Fe^{2+}apfu ternary diagrams for phlogopite and biotite mica. Reference phlogopite compositions: CH – phlogopite macrocrysts from the Churchill kimberlite field (Zurevinski et al., 2008), MX – Muskox phlogopite (Hayman et al., 2009), JC – Jericho phlogopite (Heaman et al., 2006; Kopylova et al., 2007). Labels: bi – biotite, CROL mp – carbon – rich olivine lamproite microphenocryst phlogopite, kimberlite p + mp – kimberlite phenocryst and microphenocryst phlogopite, lamproite mp – lamproite microphenocryst phlogopite, tfp – tetraferriphlogopite.

(2.39 wt.% TiO_2 and 12.7 wt.% Al_2O_3) to the rim (1.14 wt.% TiO_2 and 12.7 wt.% Al_2O_3). As with Al, phlogopite FeO contents generally fall between 3.99 wt.% and 4.62 wt.%. A single phenocrystic phlogopite (D094004phl) rim falls outside of this range with an FeO content of 7.39 wt.%. Although no significant Ba variability is observed within phlogopites, BaO is generally higher in two phenocrystic rims (0.09 wt.%) and in the single microphenocrystic rim (0.11 wt.%) compared to most phlogopite cores (<LOD to 0.04 wt.%). One phenocrystic phlogopite core has a BaO content of 0.12 wt.%, but no reliable rim analysis is available for this grain. A single microphenocrystic phlogopite (D117_08) records a slight increase in TiO_2 and Al_2O_3 content from its intermediate zone (3.03 wt.% median TiO_2, 11.8 wt.% median Al_2O_3) to its rim (3.19 wt.% median TiO_2, 12.1 wt.% median Al_2O_3).

4.3.2.3 Ilmenite

Ilmenite EPMA analyses encompass six crystals (core n=9, intermediate zone n=8, rim n=1), six groundmass grains (core n=4, intermediate zone n=1, rim n=1), and one inclusion in one olivine grain (Appendix C.04).

Ilmenite from the Dharma kimberlite can be divided into two compositional groups. The first group predominantly displays geikielite to ilmenite ($MgTiO_3$ equivalent to $FeTiO_3$) compositions. This group is exclusively composed of phenocrystic ilmenite (core n=9, intermediate zone n=5, rim n=1) and one groundmass intermediate zone. The second compositional group is dominated by geikielite (62% to 84% $MgTiO_3$) forming intermediate zones (n=3) in two phenocrysts, one inclusion in groundmass olivine, and five groundmass (core n=3, separate rim n=1) ilmenites. All ilmenite from the Dharma kimberlite falls within the field of ilmenite from typical kimberlites while being enriched in hematite (Figures 4.07A and 4.07B). TiO_2 and MgO systematics indicate that Dharma ilmenite falls within the field of kimberlitic ilmenite while being enriched in TiO_2

compared to the field of ilmenite from North American kimberlites (Figure 4.07C). The Cr_2O_3 and MgO systematics are generally similar to ilmenite trends found in kimberlites (Figure 4.07D; Mitchell, 1986). Ilmenite phenocrysts from the Dharma kimberlite are most similar to ilmenite compositions in the Muskox kimberlite (Hayman et al., 2009), and ilmenite recovered from till around the kimberlites of the Darnley Bay property (Reford, 2012).

In most ilmenite phenocrysts from the Dharma kimberlite, the geikielite component does not change from core to intermediate zones. Two ilmenite phenocrysts display chemical zonation from core to intermediate zones. The geikielite component increases from core (50% to 52% $MgTiO_3$ sample D091018ox, 48% $MgTiO_3$ D109003ox) to intermediate zones (62% to 67% $MgTiO_3$ sample D091018ox, 70% D109003ox). The increase in the geikielite component in these analyses does not correlate with an increase in the hematite component. In phenocrysts as a whole, MnO content slightly increases from the core (0.27 wt.% median) to intermediate zones (0.305 wt.% median) with a single rim analysis recording the highest MnO content (0.39 wt.% median). Generally, Cr_2O_3 content does not change in core and intermediate zones within grains.

Groundmass ilmenite from the Dharma kimberlite is rich in geikielite end-member (81% to 88% $MgTiO_3$) with one grain having near equal geikielite and ilmenite end-member proportions (54% $MgTiO_3$ and 45% $FeTiO_3$). The hematite component of groundmass ilmenite is generally higher (16.5% median Fe_2O_3) than phenocrystic ilmenite (Figure 4.07B). MgO and Cr_2O_3 content in groundmass ilmenite are generally higher than in phenocrystic ilmenite (Figures 4.07C and 4.07D). The MnO content of groundmass ilmenite cores is higher (0.525 wt.% median) than that of all individual zones in zoned phenocrysts.

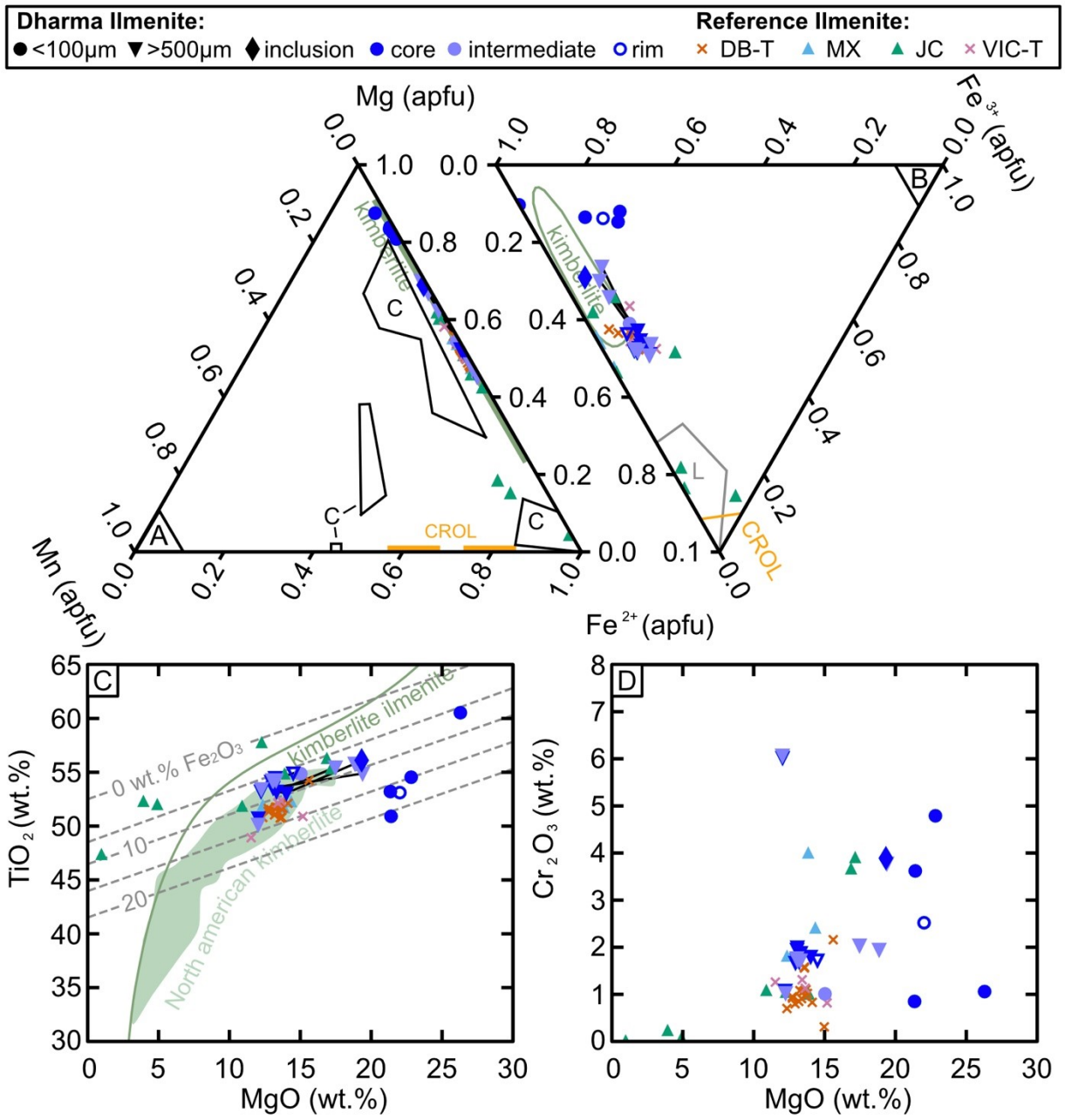

Figure 4.07: Composition of ilmenite from Dharma kimberlite. A) Geikielite ($MgTiO_3$, Mg apfu) – ilmenite ($FeTiO_3$, Fe^{2+} apfu) – pyrophanite ($MnTiO_3$ – Mn apfu) ternary discrimination plot after Mitchell (1995). B) Geikielite ($MgTiO_3$, Mg apfu) – ilmenite ($FeTiO_3$, Fe^{2+} apfu) – hematite (Fe_2O_3, Fe^{3+} apfu) ternary discrimination plot after Mitchell (1995). C) Ilmenite composition on TiO_2 against MgO plot modified after Wyatt et al. (2004). D) Cr_2O_3 against MgO plot modified after Wyatt et al. (2004). Reference ilmenite compositions: DB-T – Darnley Bay ilmenite from till (Reford, 2012), MX – Muscox ilmenite (Hayman et al., 2009), JC – Jericho ilmenite (Kopylova and Hayman, 2008), VIC-T – Victoria Island ilmenite from till sampling (LeCouteur, 2001). Labels: C – carbonatites, CROL – carbon-rich olivine lamproite, kimberlite – kimberlite groundmass and megacryst, L – lamproite.

The single analyzed ilmenite inclusion in groundmass olivine displays an intermediate composition between phenocrystic ilmenite cores and groundmass ilmenite while being most similar to the geikielite-dominant intermediate zones of phenocrystic ilmenite. The ilmenite inclusion is 69% geikielite which is similar to some intermediate zones of phenocrystic ilmenite (62% to 67% $MgTiO_3$ sample D091018ox, 70% D109003ox). Likewise, the MnO content of this inclusion (0.4 wt.%) is similar to that of one rim on an ilmenite phenocryst (0.39 wt.%). This inclusion contains the lowest hematite component of all analyzed ilmenite compositions within Dharma kimberlite (5% Fe_2O_3).

4.3.2.4 Spinel

EPMA analyses encompasses the spinel rims on six ilmenite phenocrysts (n=7), two spinel microphenocrysts (core n=2, intermediate zone n=2, rim n=2), and 29 groundmass spinel (core n=28, intermediate zones n=1, rim n=12). All EPMA microphenocryst analyses are part of a complex phlogopite + magnetite + apatite (xenolith) nodule and are not considered further in the text below. Detailed EPMA spinel analyses are tabulated in Appendix C.05.

Dharma kimberlite spinel predominantly falls along Trend 1 (kimberlite) in Cr apfu/(Cr apfu + Al apfu) vs. Fe^{2+} apfu/(Fe^{2+} apfu + Mg apfu) and Ti apfu/(Ti apfu + Cr apfu + Al apfu) vs. Fe_T apfu/(Fe_T apfu + Mg apfu) systematics (Figures 4.08A and 4.08B). One spinel groundmass core and rim along with all microphenocrystic spinel compositions fall at the highest end of Fe_T apfu/(Fe_T apfu + Mg apfu) along Trend 2 (i.e, the trend characteristic of lamproites and other ultramafic rocks; Mitchell, 1986). Generally, phenocryst and 25 groundmass spinels from the Dharma kimberlite share a Fe_T apfu/(Fe_T apfu + Mg apfu) range (0.41 to 0.64) similar to that of spinel recovered from till surrounding the Darnley Bay and Victoria Island kimberlite fields

(Figures 4.08A and 4.08B). However, Dharma spinels have lower Cr apfu/(Cr apfu + Al apfu) (0.03 to 0.31) and Ti apfu/(Ti apfu + Cr apfu + Al apfu) contents (0.26 to 0.88) compared with the spinels from Darnley Bay and Victoria Island till. Four groundmass spinel compositions from the Dharma kimberlite display consistent Fe_T apfu/(Fe_T apfu + Mg apfu) content (0.49) coupled with higher Cr apfu/(Cr apfu + Al apfu) contents (0.72 to 0.76) and fall within the compositional field of spinels from Darnley Bay and Victoria Island till (Figures 4.08A and 4.08B). Additionally, the Ti-rich and Cr-rich spinels from the Dharma kimberlite share similar Ti and Cr distributions with representative spinel compositions from the Churchill kimberlite field (Figures 4.08A and 4.08B).

All spinels from Dharma kimberlites belong to the oxyspinel (oxygen anion) group and can be divided into three main sub-groups based on terminology from Roeder and Schulze (2008), major element chemistry, and end-member compositions.

The Cr-rich group (CHR) consists of four groundmass spinels (n=4) dominated by magnesio-chromite (41 to 43 mol% $MgCr_2O_4$), chromite (21% $FeCr_2O_4$), and Al-spinel (14 to 16 mol% $MgAl_2O_4$) end-member compositions. One spinel is partially included in the rim of an olivine microphenocryst. This group of CHR spinels contains very minor hercynite (7 to 8 mol% $FeAl_2O4$, and magnetite (2 to 3 mol% $Fe^{2+}Fe^{3+}{}_2O_4$) components. The above molar compositions reflect the major element chemistry of spinel. The Fe_T apfu/(Fe_T apfu + Mg apfu) content (0.49), Cr_2O_3 (46.09 to 47.34 wt.%), TiO_2 (4.01 to 4.3 wt.%), MnO (0.2 to 0.25 wt.%) of CHR spinel show very limited compositional variation.

The Ti-rich group (MUM) consists of six spinel aggregate rinds on phenocrystic ilmenite (n=7) and 25 groundmass spinel (core n=23, intermediate zone n=1, rim n=11). All MUM spinel analyses on ilmenite phenocrysts are dominated by the qandilite (37 to 43 mol% Mg_2TiO_4) end-member.

Five of these spinel analyses contain a significant amount of magnesioferrite (27 to 33 mol% $MgFe_2O_4$) and Al-spinel (11 to 22 mol% $MgAl_2O_4$) components. Two spinel analyses contain a significant amount of ulvöspinel (23 to 24 mol% Fe_2TiO_4) and magnesioferrite (11 to 14 mol% $MgFe_2O_4$). One spinel rim displays two analyses that fall within the two trends described above (Figures 4.08A and 4.08B). The Fe_T apfu/(Fe_T apfu + Mg apfu) content of spinel rinds on ilmenite phenocrysts ranges from 0.41 to 0.52. TiO_2 content (23.19 to 33.64 wt.%) and MnO content (0.63 to 1.14 wt.%) in these spinels are higher than the TiO_2 and MnO content found in CHR spinel. Cr_2O_3 content in these spinels is significantly lower (0.75 to 3.57 wt.%) than CHR spinel.

Most groundmass MUM spinel analyses from the Dharma kimberlite (core n=22, intermediate zone n=1, rim n=11) are dominated by magnesioferrite (22 to 43 mol% $MgFe_2O_4$), Al-rich spinel (13 to 31 mol% $MgAl_2O_4$), and qandilite (12 to 41% Mg_2TiO_4). These groundmass spinels contain minor amounts of magnetite (up to 20 mol% $Fe^{2+}Fe^{3+}{}_2O_4$), ulvöspinel (up to 12 mol% Fe_2TiO_4), and hercynite (up to 11 mol% $FeAl_2O_4$) end-member components. One groundmass MUM spinel core is dominated by qandilite (41 mol% Mg_2TiO_4) and ulvöspinel (27 mol% Fe_2TiO_4) with minor components of Al-spinel (14 mol% $MgAl_2O_4$), hercynite (9 mol% $FeAl_2O_4$). All MUM groundmass spinel from the Dharma kimberlite contain small amounts of magnesiochromite (1 to 14 mol% $MgCr_2O_4$). The TiO_2 content (11.95 to 34.82 wt.%) and MnO content (0.39 to 0.9 wt.%) is similar to that of MUM spinel rinds on ilmenite phenocrysts. The Cr_2O_3 content (0.65 to 11.75 wt.%) recorded by groundmass MUM spinel is generally higher than the Cr_2O_3 content of MUM spinel rinds on ilmenite phenocrysts (0.75 to 3.57 wt.%).

One groundmass spinel core and one groundmass spinel rim are classified as Fe-rich (MAG) spinel. These two spinel analyses are associated with MUM spinel (Figures 4.08A and 4.08B). MAG spinel is dominated by magnetite (92 to 93 mol% $Fe^{2+}Fe^{3+}{}_2O_4$) end-member composition.

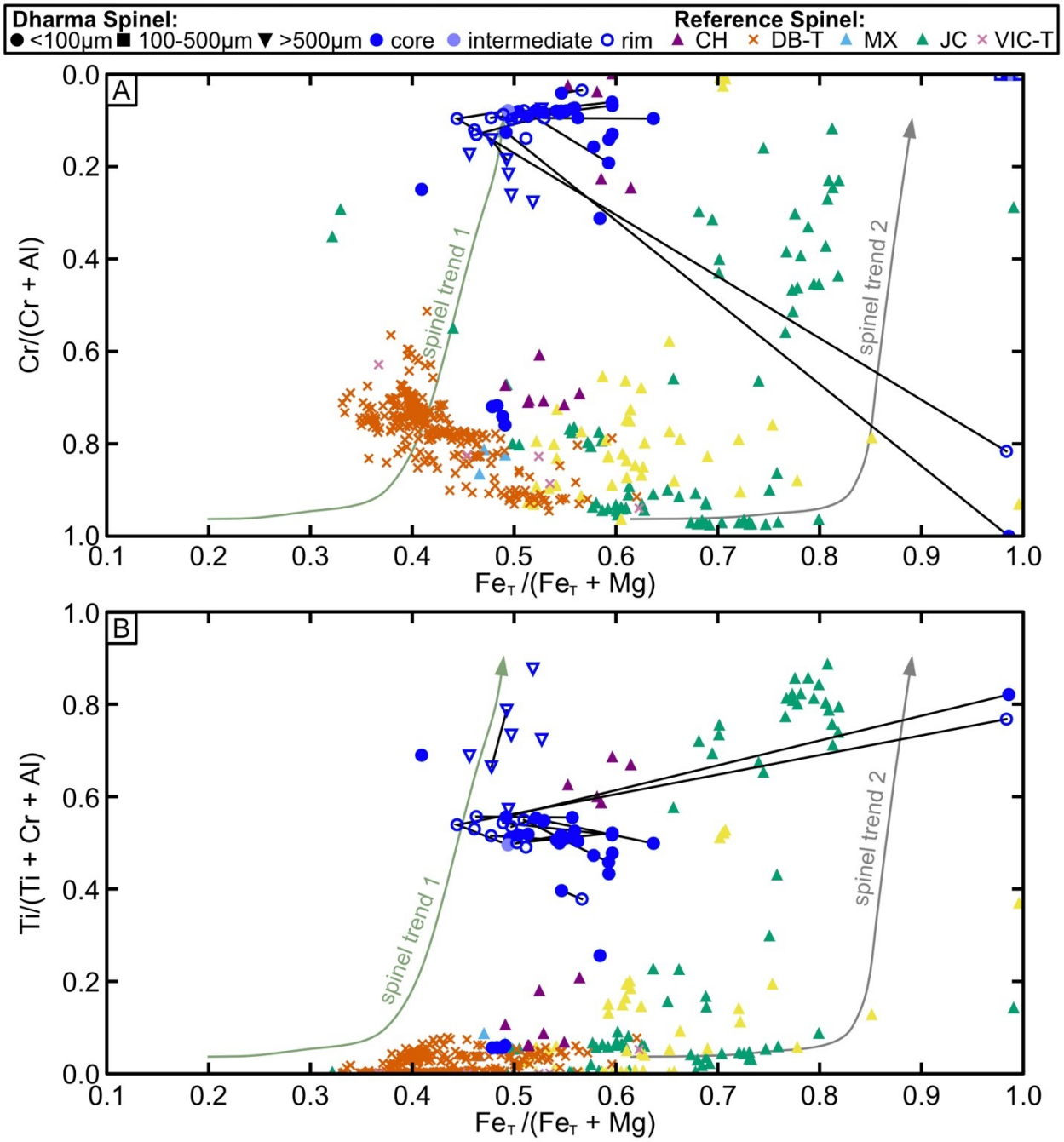

Figure 4.08: Composition of spinel from the Dharma kimberlite. A) Spinel composition on Cr apfu/(Cr apfu + Al apfu) against Fe_T apfu/(Fe_T apfu + Mg apfu) plot after Mitchell (1986,1995) and Sarkar et al. (2018). B) Spinel composition on Ti apfu/(Ti apfu + Cr apfu + Al apfu) against Fe_T apfu/(Fe_T apfu + Mg apfu) plot after Mitchell (1986,1995) and Sarkar et al. (2018). Reference compositions: CH – spinel from the Churchill kimberlite field (Zurevinski et al., 2008), DB-T – Darnley Bay spinel from till (Reford, 2012), MX – Muscox spinel (Hayman et al., 2009), JC – Jericho spinel (Kopylova and Hayman, 2008), VIC-T – Victoria Island spinel from till sampling (LeCouteur, 2001).

Very minor amounts of magnesioferrite (4 to 5 mol% $MgFe_2O_4$) end-member and jacobsite (2 mol% $MnFe_2O_4$) were also detected, of which the latter commonly forms a solid solution with magnetite. The TiO_2 content (0.38 to 0.56 wt.%) and Cr_2O_3 content (0.08 to 0.13 wt.%) are significantly lower in MAG spinels than in both CHR and MUM spinels. The MnO content (0.64 to 0.69 wt.%) of MAG spinel falls on the lower end of MUM spinel MnO compositions and is higher than MnO content in CHR spinel.

4.3.2.5 Rutile and Armalcolite

EPMA analysis of rutile encompasses two inclusions in microphenocryst olivine (Figure 4.04A), one inclusion in phenocryst olivine, and a zoned, multi-crystal rind on an ilmenite phenocryst (core n=2, intermediate zone n=1). A single armalcolite rim on the same zone, multi-crystal rind on ilmenite phenocryst was analyzed (Figure 4.04B). Detailed EPMA rutile analyses are tabulated in Appendix C.06.

Multi-crystal rutile rinds on phenocrystic ilmenite have Cr_2O_3 and TiO_2 compositions that plot into the field of rutile from the cratonic and off-craton mantle (Figure 4.09A). The Nb_2O_5 and Cr_2O_3 concentrations in these rutile rinds fall within the field of rutile + LIMA (lindsleyite and mathiasite) + YIHA (yimengite and hawthorneite) or armalcolite (Figure 4.09B). Multi-crystal rutile rinds show only minor variation in TiO_2 (97.88 to 98.12 wt.%), Cr_2O_3 (1.26 to 1.39wt.%), and Nb_2O_5 (0.49 to 0.58 wt.%). From core to rim, one analysis of zoned rutile on phenocryst ilmenite displays slight increases in FeO (0.28 wt.% core, 0.38 wt.% intermediate zone) coupled with a slight decrease in Nb_2O_5 (0.58 wt.% core, 0.51 wt.% intermediate zone) and TiO_2 (98.12 wt.% core, 97.67 wt.% intermediate zone). This same zoned rutile has a rim of armalcolite (Table 4.03).

Two rutile inclusions in microphenocrystic olivine plot into the field of rutile from the cratonic mantle and inside the field of deep-seated mantle rutile on the Cr_2O_3 vs. TiO_2 discrimination graph (Figure 4.09A). One inclusion plots within the field of groundmass rutile from kimberlite (Figure 4.09A). Both rutile inclusions fall within the field of vein and accessory rutile in a Nb_2O_5 vs. Cr_2O_3 discrimination graph (Figure 4.09B). Major element chemistry varies between these two inclusions. The TiO_2 content (91.42 to 93.43 wt.%), Nb_2O_5 content (2.67 to 2.96 wt.%), and CaO content (0.04 to 0.09 wt.%) show only minor variation. Cr_2O_3 content (2.52 to 2.79 wt.%) and Fe_2O_3 content (0.57 to 1.2 wt.%) varies slightly. MgO content has a wider range of variation (0.13 to 0.89 wt.%). The rutile inclusion that plots within the field of groundmass rutile from kimberlite has a measurable NiO content (0.03 wt.%) and Na_2O content (0.03 wt.%), unlike the other rutile inclusion.

Table 4.03: Composition of armalcolite rim on spinel rinds on ilmenite phenocrysts.

Sample	D109003oxzoned
Nb_2O_5	1.04
SiO_2	0.03
TiO_2	76.02
Cr_2O_3	1.12
FeO	2.14
Fe_2O_3	0.37
MnO	1.34
MgO	17.4
CaO	0.04
BaO	0.24
Total	99.5

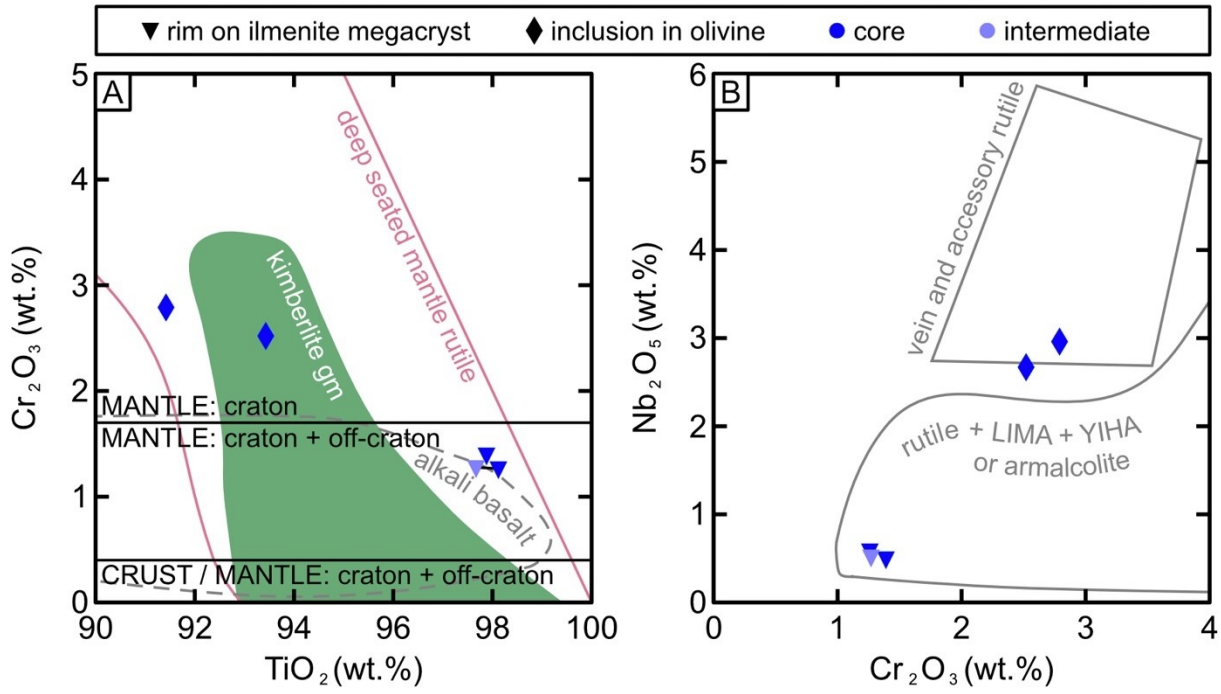

Figure 4.09: Composition of rutile from the Dharma kimberlite. A) Cr_2O_3 against TiO_2 plot after Malkovets et al. (2016). B) Nb_2O_5 against Cr_2O_3 plot after Haggerty (1995). Abbreviations: kimberlite gm – kimberlite groundmass rutile, LIMA – lindsleyite and mathiasite, YIHA – yimengite and hawthorneite.

4.3.3 Pyroxene and Garnet Xenocryst Mineral Chemistry and Garnet Ni Geothermometry

Orthopyroxene, clinopyroxene, and garnet are the only mantle xenocryst phases analyzed in samples of the Dharma kimberlite (Appendix C.02 and Appendix D.02). A total of 29 analyses were completed on pyroxene of which 23 analyses are clinopyroxene and six analyses are orthopyroxene. A total of 552 analyses were completed on garnet from the Dharma kimberlite.

4.3.3.1 Orthopyroxene

Orthopyroxene analyzed from the Dharma kimberlite includes one porphyroclast (core n=1, intermediate zone n=1, rim n=1) in a harzburgite microxenolith (Figures 4.03E and 4.03F), one xenocryst (core n=1, intermediate zone n=1), and one bimineralic grain intergrown with clinopyroxene (core n=1). The bimineralic grain is likely an example of orthopyroxene exsolving clinopyroxene.

Orthopyroxene in the Dharma kimberlite is enstatite, typical of cratonic peridotites (Pearson et al., 2003). (Figure 4.10A). The orthopyroxene microxenolith and xenocrystic orthopyroxene share similar major element compositions. The content of TiO_2 (0.04 wt.% core, 0.06 wt.% rim), Cr_2O_3 (0.33 wt.% core, 0.38 wt.% rim), MgO (34.7 wt.% core, 34.87 wt.% rim), CaO (0.93 wt.% core, 0.95 wt.% rim), and Na_2O (0.17 wt.% core, 0.18 wt.% rim) slightly increases from core to rim in orthopyroxene from the harzburgite microxenolith. The orthopyroxene xenocryst records lower Al_2O_3 (0.55 wt.% both core and intermediate zone), CaO (0.62 wt.% core, 0.61 wt.% rim), and Na_2O (0.15 wt.% core, 0.14 wt.% intermediate zone) than the orthopyroxene from the harzburgite microxenolith. The orthopyroxene xenocryst records a decrease in Cr_2O_3 (0.35 wt.% core, 0.27 wt.% intermediate zone) and MgO (35.12 wt.% core, 34.91 wt.% intermediate zone) from its core

to intermediate zone. The orthopyroxene intergrown with clinopyroxene records the highest content of TiO_2 (0.22 wt.%), Al_2O_3 (0.75 wt.%), Cr_2O_3 (0.8 wt.%), FeO (6.33 wt.%), MnO (0.2 wt.%), and CaO (1.24 wt.%) of the entire Dharma orthopyroxene population. This orthopyroxene xenocryst also records the lowest NiO (0.04 wt.%) and MgO (32.89 wt.%) contents of all analyzed orthopyroxene in Dharma kimberlite.

4.3.3.2 Clinopyroxene

Clinopyroxene analyzed from the Dharma kimberlite includes six xenocrysts (core n=7, intermediate zone n=6, rim n=8) and smaller, bimineralic orthopyroxene-clinopyroxene xenocryst (core n=1, rim n=1). Four xenocrysts (core n=4, intermediate zone n=3, rim n=4) and one xenocryst intergrown with clinopyroxene (core n=1, rim n=1) have augite compositions (Figure 4.10A). Two xenocrysts (core n=3, intermediate zone n=3, rim n=4) exhibit diopside to augite compositions (Figure 4.10A).

Compositions of clinopyroxene xenocrysts in the Dharma kimberlite are generally constrained between 0.08 wt.% to 0.31 wt.% TiO_2 and 0.9 to 0.92 Mg-number, overlapping with clinopyroxene xenocrysts and clinopyroxene from xenoliths from the Jericho kimberlite (Figure 4.10B). Most clinopyroxene xenocryst compositions from the Dharma kimberlite plot in the field of on-craton garnet peridotite and garnet pyroxenite in a Cr_2O_3 vs. Al_2O_3 classification graph (Figure 4.10C). Clinopyroxene from the Dharma kimberlite shares similar Cr_2O_3 and Al_2O_3 contents with clinopyroxene compositions from the Jericho kimberlite and with clinopyroxene recovered from till at Darnley Bay (Figure 4.10C).

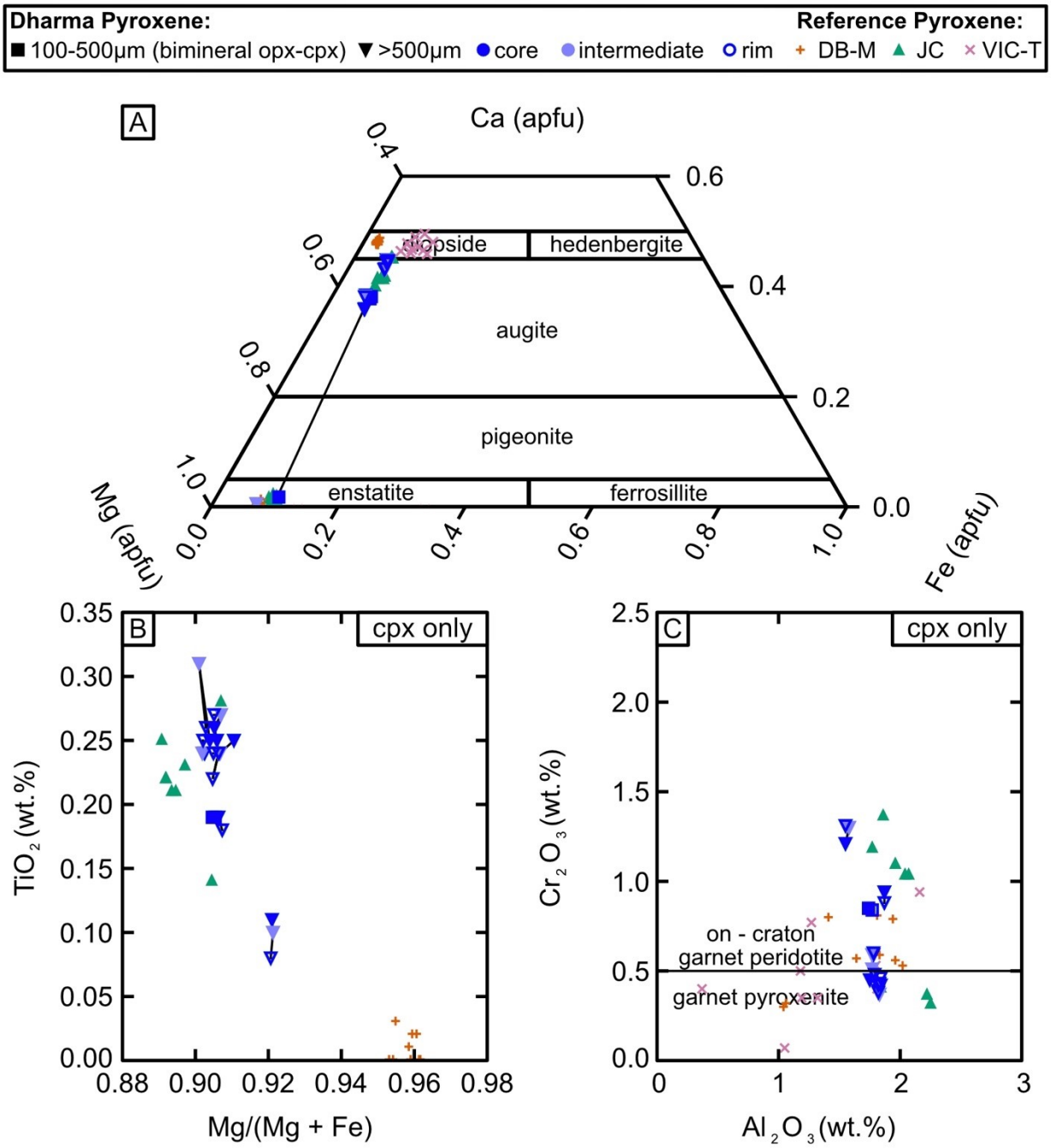

Figure 4.10: Composition of pyroxene from the Dharma kimberlite. A) Mg (apfu)-Ca (apfu)-Fe (apfu) pyroxene composition ternary. B) TiO_2 against Mg-number (Mg apfu / Mg apfu + Fe apfu) of clinopyroxene after (Aulbach et al., 2004), C) Cr_2O_3 against Al_2O_3 of clinopyroxene plot after Ramsay (1992). Reference pyroxene compositions: DB-M – Darnley Bay pyroxene from mantle xenoliths (Brin, 2016), JC – Jericho pyroxene (Kopylova and Hayman, 2008), VIC-T – Victoria Island pyroxene from till sampling (LeCouteur, 2001).

Clinopyroxene xenocrysts from Dharma are generally not chemically zoned. Most major element contents remain consistent between the core, intermediate, and rim zones. However, TiO_2 concentrations slightly decrease from core to rim in three analyses (Figure 4.10B). TiO_2 decreases from core to rim in sample D086011px (0.25 wt.% core, 0.24 wt.% rim), D086012px (0.19 wt.% core, 0.18 wt.% rim), D086013px (0.11 wt.% core, 0.1 wt.% intermediate zone, 0.08 wt.% rim).

4.3.3.3 Garnet

Garnet is the principal mantle xenocryst studied in from the Dharma kimberlite. A total of 276 garnet core and 276 garnet rim analyses were completed on Dharma kimberlite drill core heavy mineral separates (Appendix D.02). The data described in this subsection addresses only the garnet cores (n=276). Of the analyzed cores, 111 are G9A (low-Ca lherzolite) garnets, 122 are G9A Ti (Ti-enriched, low-Ca lherzolite) garnets, 23 are G9B (lherzolite) garnets, seven are G9B Ti (Ti-enriched lherzolite) garnets, five are G10A (low-Ca harzburgite) garnets, six are G10B Ti (Ti-enriched harzburgite) garnets, and two are G12 Ti (Ti-enriched wehrlite) garnets after a modified classification of Snyder et al. (2021; Figure 4.11A).

Table 4.04: Distribution and classification of garnet xenocrysts by relative depth of sample from the Dharma kimberlite drill core.

Sample	***Depth (m)***		***G9A***	***G9A Ti***	***G9B***	***G9B Ti***	***G10A***	***G10B Ti***	***G12 Ti***
	From	*To*							
D89	60.19	60.27	16	29	7	3	-	6	-
D91	63.17	63.29	21	18	14	1	-	-	-
D93	65.41	65.48	20	23	-	1	-	-	-
D104	82.76	82.90	54	52	2	2	5	-	2
Total:			*111*	*122*	*23*	*7*	*5*	*6*	*2*

Garnet types are distributed irregularly with depth in the Dharma kimberlite drill core sampled here (Table 4.04). Samples from 60.19 m to 65.48 m have a larger concentration of G9A Ti, G9B, and G9B Ti. G10B Ti garnets are only observed in kimberlite recovered from a depth of 60.19 m to 60.27 m. G10A and G12 Ti garnets are only observed in sample D104 (82.76 m to 82.90 m). G9A garnets are distributed equally between 60.19 m to 65.48 m and 82.76 m to 82.90m. G10A garnets fall onto the 47 kbar isobar above the 43 kbar graphite to diamond isobar (Figure 4.11A).

Trace element compositions (Appendix E.02) for peridotite garnet from the Dharma kimberlite can be divided into two groups based on their chondrite normalized REE patterns (Figure 4.12). Most garnet compositions (n=64) fall into the group of LREE depleted garnet (Figures 4.12A and 4.12B). The LREE-depleted garnet group includes G9A, G9A Ti, G9B, G9B Ti, G10B Ti, and G12 garnets. Significant LREE depletion predominantly ends at Sm with the REE following Sm recording weak negative sloped patterns (Figures 4.12A and 4.12B). The second group consists of G9A, G9B, and G10A garnets that display chondrite-normalized REE with sinusoidal patterns (Figures 4.12C and 4.12D). G9A garnet from this group displays a continuum of weakly sinusoidal to strongly sinusoidal patterns (Figure 4.12C). Weakly sinusoidal G9A garnets display positive-sloped La to Sm compositions, weakly negative sloped Sm to Ho compositions, and positively sloped Ho to Lu compositions. Strongly sinusoidal G9A garnets display positive sloped La to Nd compositions, negative sloped Nd to Gd compositions, and positive sloped Gd to Lu compositions. G9B and G10A garnet display strong sinusoidal patterns (Figures 4.12C and 4.12D). G9B garnet displays positive sloped La to Nd compositions, negatively sloped Nd to Gd ± Tb compositions, and positively sloped Gd ± Tb to Lu compositions. G10A garnet displays positively sloped La to Sm compositions, negative sloped Sm to Tm compositions, and weakly positive sloped Tm to Lu

compositions. All analyzed G10A, 18 analyzed G9B, and six analyzed G9A garnets fall within the field of depleted mantle garnet on the fields of Griffin and Ryan (1995; Figure 4.11B). Ten G9A and two G9B garnets fall between the depleted and high-temperature fields of Griffin and Ryan (1995) (Figure 4.11B). All other garnets (G9A, G9A Ti, G9B Ti, G10B Ti, G12) fall within the field of melt metasomatism (Figure 4.11B). Additionally, all G10A and a portion of G9A garnets fall within the field of carbonatite metasomatism (Figure 4.13) of Shu and Brey (2015). A significant portion of G9A and G9A Ti garnets fall within the field of kimberlite metasomatism of Woodland et al. (2021) (Figure 4.13). A portion of G9B garnets display Ti/Eu systematics similar to kimberlite metasomatized garnets but exhibit low Zr/Hf ratios (Figure 4.13). All other garnets fall within the primitive to depleted mantle compositional trend (Figure 4.13).

Ni concentrations in garnet have been used to calculate equilibration temperatures utilizing four Ni-in-garnet thermometers. These thermometers are detailed in Appendix F.02 and include Ryan et al. (1996), Canil (1999), Shu and Brey (2015), and Sudholz et al. (2021). Sudholz et al. (2021) are used for comparison below.

G12 Ti garnets record the lowest median Ni temperatures (1003 °C). The highest median Ni temperature are recorded in G9A Ti garnet (1215 °C). G10A garnets (1284 °C) and G10B Ti garnets (1111 °C) share similar median temperatures. Median temperatures from G9A garnets (1149 °C) are lower than G10A and G10B Ti garnets and slightly higher than G9B Ti garnets (1076 °C). Median temperatures derived from G9B garnets (1112 °C) are lower than G9B Ti garnets and higher than G12 Ti garnets.

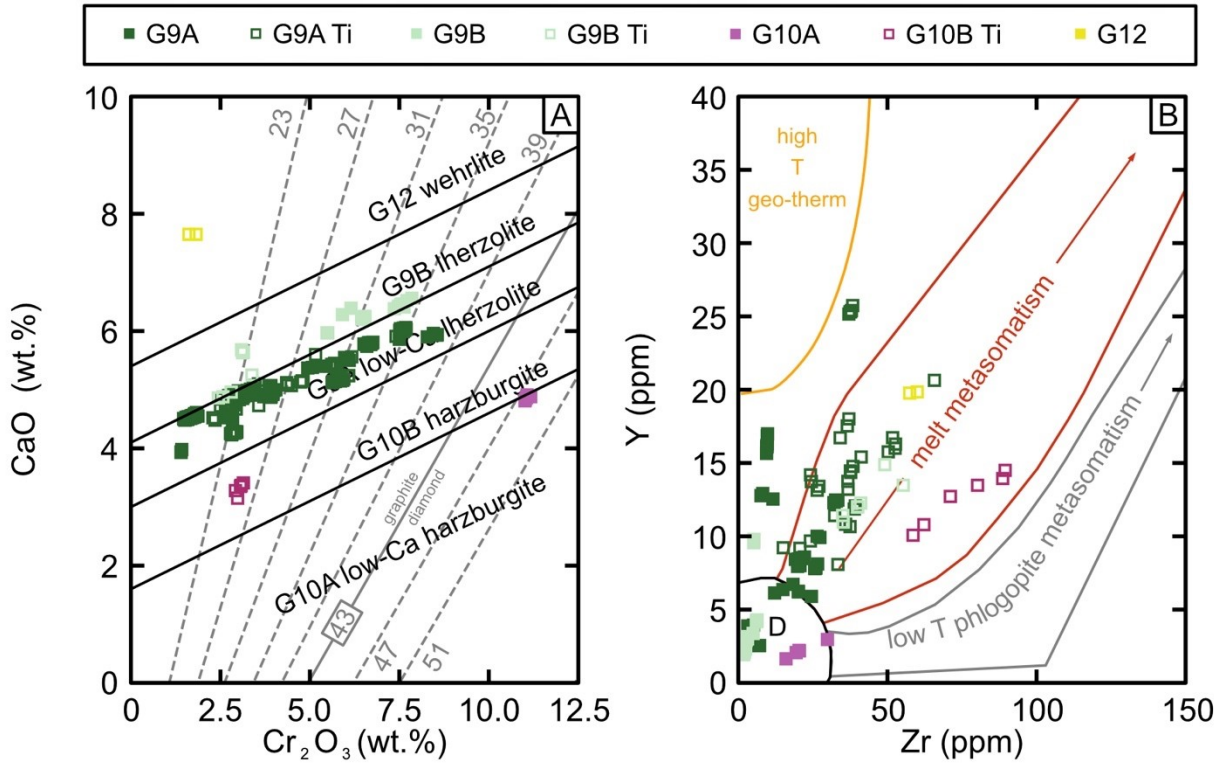

Figure 4.11: Composition of garnet xenocrysts from the Dharma kimberlite. A) CaO against Cr_2O_3 discrimination plot modified after Sobolev et al. (1973), Gurney and Zweistra (1995), Grütter et al. (2004), and Preston et al. (2012) as per Snyder et al. (2021). Grey dotted lines denote isobars after Grütter et al. (2006). B) Y ppm against Zr ppm trace element discrimination plot for mantle source environment after Griffin and Ryan (1995). Garnet groups: G9A – low-Ca lherzolite, G9B – lherzolite, G9A Ti – Ti enriched low-Ca lherzolite, G9B Ti – Ti enriched lherzolite, G10A – low-Ca harzburgite, G10B - Ti – Ti enriched harzburgite, G12 – wehrlite. Labels: D – depleted mantle.

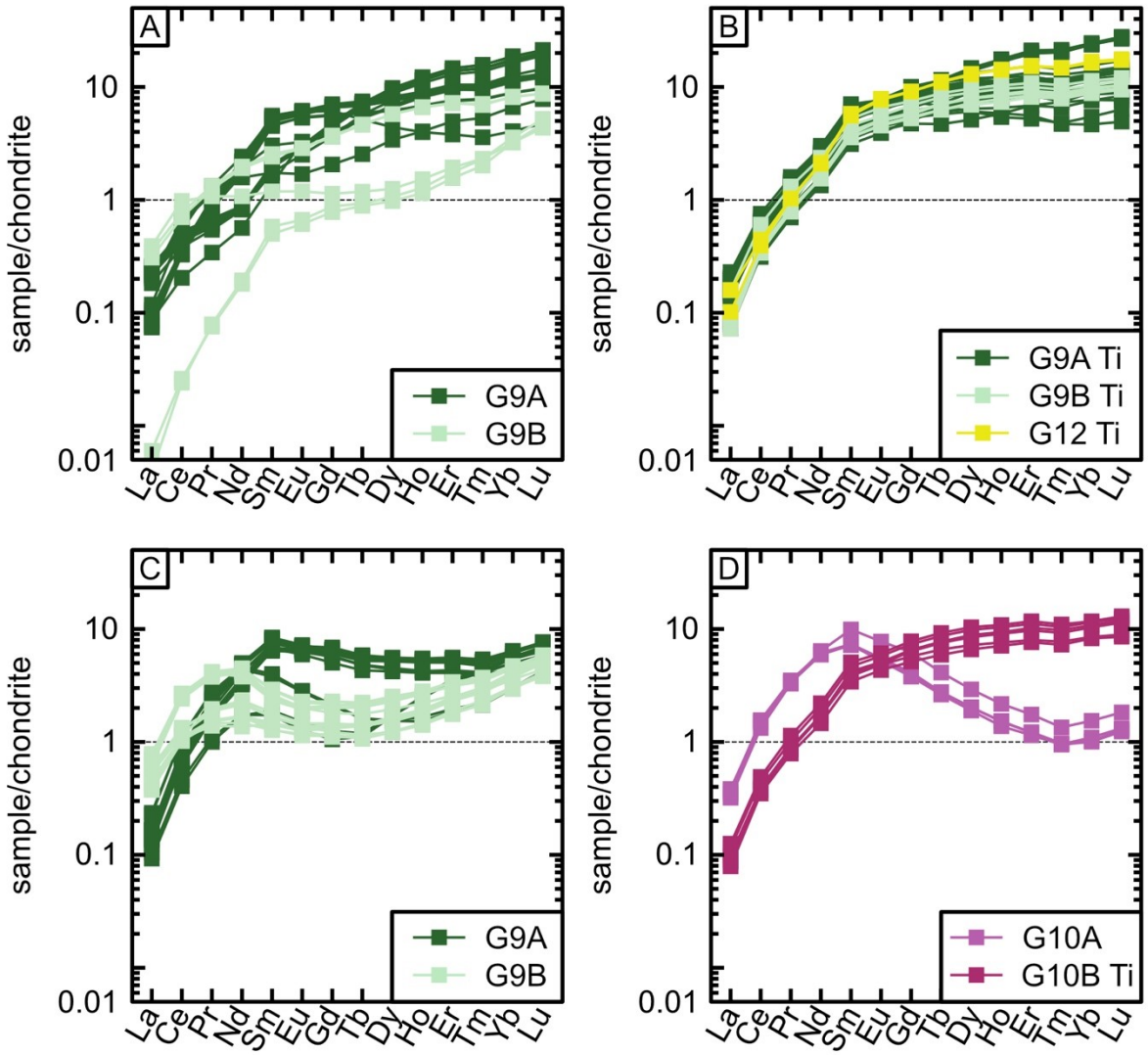

Figure 4.12: REE multi-element diagram of garnet xenocrysts from the Dharma kimberlite. Garnet normalized to chondrite composition (Palme and O'Neil, 2014). A) LREE depleted group of low-Ca lherzolite garnet (G9A), and lherzolite garnet (G9B. B) LREE depleted and Ti enriched group of low-Ca lherzolite garnet (G9A Ti), lherzolite garnet (G9B Ti), and wehrlite garnet (G12 Ti). C) Sinusoidal REE group of low-Ca lherzolite garnet (G9A), and lherzolite garnet (G9B). D) LREE depleted group of low-Ca harzburgite (G10A) and sinusoidal REE group of Ti enriched harzburgite (G10B Ti).

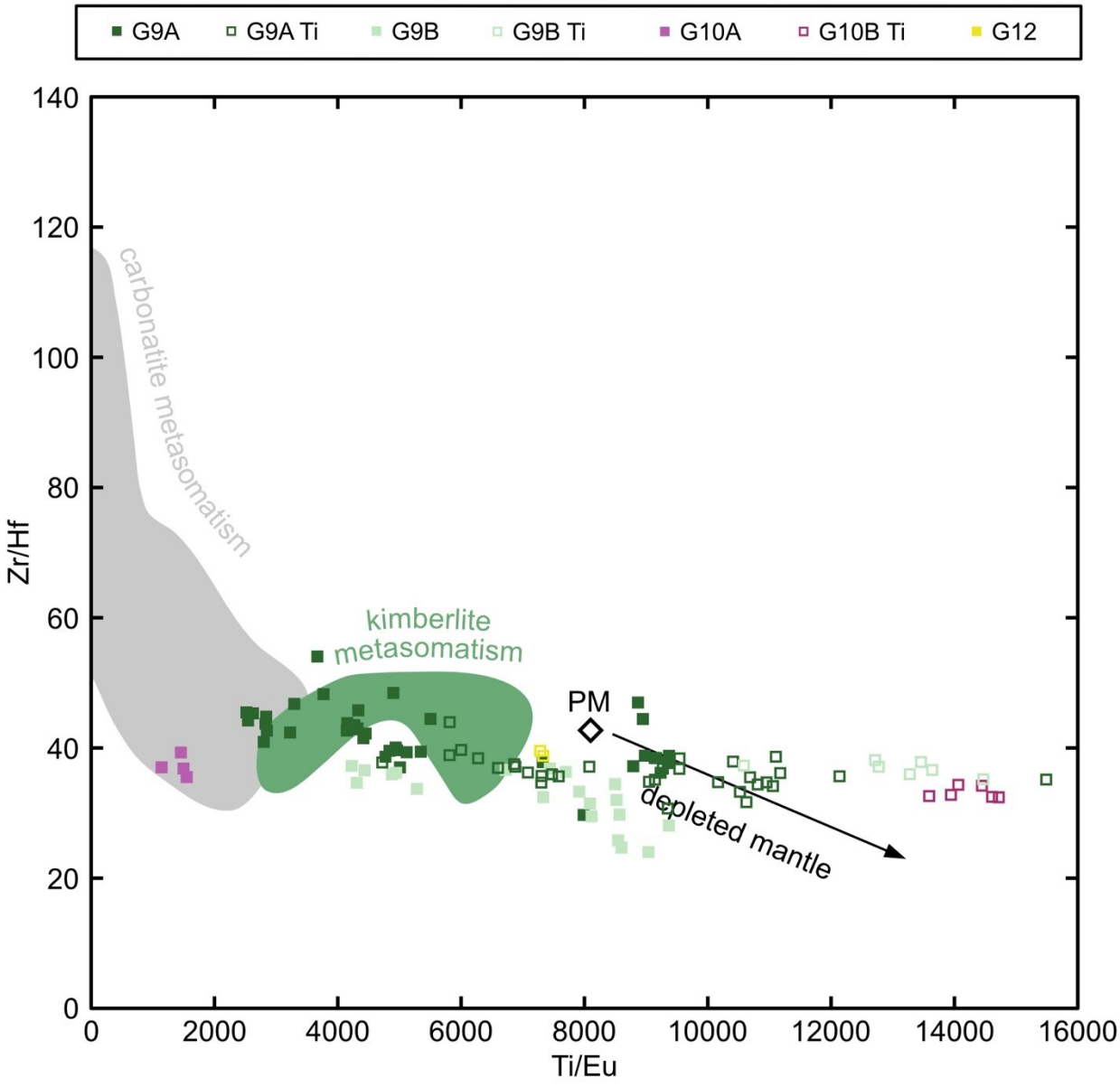

Figure 4.13: Composition of garnet xenocrysts from the Dharma kimberlite on Zr/Hf against Ti/Eu discrimination plot. Plot modified from Woodland et al. (2021). Carbonatite and kimberlite metasomatism fields after Shu and Brey (2015).

4.3.4 Whole Rock Major and Trace Element Geochemistry

Major and trace element whole-rock geochemistry for the Dharma kimberlite is summarized in Tables 4.05 to 4.07. Low SiO_2 contents (26 to 30.9 wt.%) and high MgO contents (22.7 to 35.5 wt.%) of the hypabyssal kimberlite samples correspond to ultrabasic compositions. TiO_2 (0.96 to 1.5 wt.%), Al_2O_3 (1.17 to 1.86 wt.%), Fe_2O_3T (7.41 to 10.68 wt.%), Na_2O (0.07 to 0.16 wt.%), and P_2O_5 (0.30 to 0.54 wt.%) contents of Dharma hypabyssal kimberlite is similar to archetypal kimberlite (Mitchell, 1986; Pearson et al., 2019; Figure 4.14. The Dharma kimberlite has a characteristically low K_2O content. The K_2O content (0.05 to 1.24 wt.%) of hypabyssal Dharma kimberlite falls in the lower range of archetypal kimberlite (Figure 4.14F). Despite this, Dharma hypabyssal kimberlite K_2O content is enriched in comparison to Na_2O (0.07 to 0.16 wt.%), with K_2O/Na_2O ratios displaying a wide range of 0.44 to 9.12, as is typical of kimberlites in general.

Volcaniclastic kimberlite has a higher content of Al_2O_3 (2.34 to 3.97 wt.%), and K_2O (0.72 to 1.25 wt.%) compared to hypabyssal kimberlite (Figures 4.14C, 4.14F, 4.15E to 4.15H). The CaO content of volcaniclastic kimberlite (18.5 to 25.1 wt.%) is higher than the CaO content of hypabyssal kimberlite (6.9 to 19.2 wt.%). Although the range of SiO_2 (24.6 to 31.1 wt.%) and TiO_2 (0.47 to 4.93 wt.%) in volcaniclastic kimberlite is wider than in hypabyssal kimberlite, the mean SiO_2 and TiO_2 contents in volcaniclastic kimberlite are lower than in hypabyssal kimberlite (Figure 4.14A and 4.14B). Volcaniclastic Dharma kimberlite has lower contents of Fe_2O_3T (4.67 to 6.87 wt.%), MgO (18.8 to 23 wt.%), Na_2O (0.06 to 0.1 wt.%), and P_2O_5 (0.15 to 0.22 wt.%) than hypabyssal kimberlite (Figure 4.14). Despite these variations that are likely due to a combination of higher concentration of dolostone and limestone crustal xenoliths and fluid-alteration processes,

volcaniclastic kimberlite major element compositions generally fall into the range of the archetypal kimberlite (Mitchell, 1986; Pearson et al., 2019: Figure 4.14).

All major element systematics of both hypabyssal and volcaniclastic kimberlite from Dharma fall within the range of major element compositions from the Jericho kimberlite (Price et al., 2000; Hayman and Cas, 2011; Figure 4.14). The TiO_2 and K_2O contents of Dharma volcaniclastic kimberlite resemble the high end of the K_2O / TiO_2 range reported from the Jericho kimberlite (Figure 4.14H). The MgO, Na_2O, and P_2O_5 contents of Dharma hypabyssal kimberlite are similar to the Muskox kimberlite (Hayman et al., 2009; Figure 4.14). The K_2O / TiO_2 of the Dharma hypabyssal kimberlite fall along the lower end of the K_2O / TiO_2 range in kimberlite from Muskox (Figure 4.14H). Volcaniclastic Dharma kimberlite shares similar Al_2O_3, Na_2O, K_2O contents and K_2O / TiO_2 ratios with the Muskox kimberlite (Figure 4.14).

Hypabyssal and volcaniclastic kimberlite from Dharma display systematic intra-sample variations in major and trace elements (Figure 4.15 and 4.16). All hypabyssal kimberlite samples classify as uncontaminated kimberlite (Figure 4.15A) on the basis of Clement's Contamination Index (CCI <1.3; Clement, 1982) and ln(Si/Al) systematics (>2.3) using the approach of Kjarsgaard et al. (2009). Volcaniclastic kimberlite from Dharma falls into the contaminated fields, an understandable result due to the incorporation of significant crustal xenoliths in these samples. One sample of volcaniclastic kimberlite records a very high TiO_2 content (4.93 wt.%) compared to all other samples (Figure 4.15C) and is likely the result of ilmenite megacryst over-sampling.

Table 4.05: Major element (in weight percent oxide) and trace element (in mg/g) compositions collected by XRF from fused bead and pressed pellet samples of hypabyssal kimberlite samples of the Dharma kimberlite.

Sample	D122	D86	D91	D92	D94	D95	D104	D108	D109
Depth From (m)	54.78	58.89	63.17	63.73	66.1	67.79	82.76	89.53	91.31
Depth To (m)	54.84	58.96	63.29	63.8	66.29	67.87	82.9	89.63	91.36
SiO_2	28.73	28.25	30.01	29.76	26.03	30.85	27.84	28.77	30.73
TiO_2	0.97	1.12	1.04	1.18	0.96	1.49	1.30	1.20	1.50
Al_2O_3	1.86	1.37	1.63	1.57	1.56	1.60	1.24	1.17	1.51
Fe_2O_3T	7.54	8.40	8.16	8.70	7.41	9.03	9.69	9.42	10.68
MnO	0.12	0.16	0.15	0.17	0.14	0.15	0.20	0.14	0.13
MgO	29.28	34.76	34.17	33.82	22.65	31.78	35.49	33.05	33.27
CaO	13.48	11.30	11.50	10.01	19.22	9.81	8.60	8.43	6.94
Na_2O	0.13	0.16	0.08	0.08	0.14	0.09	0.09	0.09	0.07
K_2O	0.46	0.07	0.12	0.09	1.24	0.15	0.08	0.05	0.05
P_2O_5	0.39	0.35	0.31	0.41	0.30	0.38	0.43	0.54	0.52
LOI	20.46	16.28	14.68	16.43	25.36	17.14	17.55	20.57	17.05
Total	103.43	102.20	101.86	102.21	105.02	102.48	102.49	103.43	102.45
Rb	55.5	9.7	17.6	10.6	104.9	19.9	12.3	6	4.5
Sr	636	591	454	431	871	443	427	575	292
Y	4.4	4.9	5.6	5.2	2.2	5.2	6.4	5.2	4.9
Zr	78	77	76	77	70	82	73	75	78
V	105	111	111	105	84	113	118	101	120
Ni	1251	1327	1364	1434	1208	1469	1521	1607	1606
Cr	1926	2252	2099	2244	1596	2241	2350	1946	2224
Nb	148.7	144.4	193.9	162.9	148.6	172.0	219.3	163.1	214.0
Ga	0.8	0.5	1.3	0.5	0.5	0.9	0.8	0.8	0.7
Cu	95	101	99	107	77	113	82	74	85
Zn	62	60	56	57	67	58	56	57	66
Co	79	87	89	90	77	98	97	109	105
Ba	1849	1261	1457	3040	1377	1002	1944	307	313
La	103	86	98	101	77	96	111	94	114
Ce	48	71	83	2	42	111	90	145	189
U	3.5	2.0	2.3	2.2	1.7	2.5	3.0	2.5	3.5
Th	14.7	20.2	14.9	20.0	9.9	21.0	20.9	19.3	22.5
Sc	19	19	18	19	21	17	18	15	17
Pb	11	7	9	7	7	7	7	7	6

Table 4.06: Trace element composition (in mg/g) collected by HR-ICP-MS for hypabyssal kimberlite samples of the Dharma kimberlite.

Sample	D91	2σ	D92	2σ	D94	2σ	D95	2σ	D104	2σ	D108	2σ
Depth From (m)	63.17		63.73		66.1		67.79		82.76		89.53	
Depth To (m)	63.29		63.8		66.29		67.87		82.9		89.63	
Co	86	3	84	3	68	3	87	4	91	4	91	4
Ni	1287	43	1149	27	1002	41	1181	41	1362	64	1207	43
Cu	75	3	84	4	63	3	89	4	67	3	64	3
Zn	52	2	55	1	77	3	56	2	52	2	54	2
Rb	11.1	0.6	6.4	0.2	110	7	16.9	0.5	9.8	0.6	5.3	0.2
Sr	484	25	427	10	980	62	441	16	354	21	630	22
Y	5	0.2	4.5	0.1	4.4	0.2	4.4	0.1	5.3	0.2	4.6	0.2
Zr	57	3	54	1	37	2	57	2	48	3	50	2
Nb	204	7	156	4	155	6	161	5	246	11	161	6
Cs	0.34	0.02	0.176	0.006	1.31	0.09	0.67	0.02	0.137	0.007	0.087	0.004
Ba	1677	65	2836	98	1787	97	1147	43	2321	110	374	16
La	96	4	89	2	91	4	89	3	126	6	97	3
Ce	153	5	135	3	144	6	136	4	187	9	150	5
Pr	11.5	0.4	12.5	0.3	10.6	0.4	12.7	0.4	14.6	0.7	14	0.5
Nd	36	1	39.6	0.9	33	1	40	1	46	2	44	2
Sm	4.2	0.2	4.5	0.1	3.7	0.2	4.6	0.1	5.3	0.2	4.9	0.2
Eu	1.06	0.04	1.24	0.03	0.96	0.04	1.19	0.03	1.34	0.07	1.22	0.04
Gd	3.1	0.2	4.5	0.2	2.75	0.1	4.48	0.2	3.79	0.2	4.8	0.2
Tb	0.285	0.009	0.324	0.008	0.24	0.01	0.33	0.02	0.34	0.02	0.35	0.01
Dy	1.19	0.05	1.14	0.03	1.02	0.04	1.14	0.04	1.39	0.07	1.22	0.04
Ho	0.189	0.008	0.179	0.004	0.164	0.007	0.177	0.005	0.21	0.01	0.184	0.007
Er	0.48	0.02	0.5	0.02	0.42	0.02	0.49	0.01	0.52	0.02	0.52	0.02
Yb	0.32	0.02	0.3	0.02	0.29	0.01	0.31	0.01	0.3	0.01	0.29	0.01
Lu	0.045	0.004	0.041	0.002	0.042	0.003	0.043	0.002	0.039	0.003	0.04	0.002
Hf	1.37	0.05	1.4	0.03	1.03	0.04	1.46	0.04	1.14	0.06	1.26	0.06
Ta	9.6	0.4	12.7	0.3	8.6	0.4	12.5	0.4	12.4	0.6	12.2	0.4
Pb	5.8	0.2	5.1	0.2	4.1	0.2	5.4	0.2	6.1	0.3	5.2	0.2
Th	13.3	0.5	16.9	0.9	8.7	0.3	17.8	0.8	17.4	0.8	17.5	0.7
U	1.7	0.07	2.6	0.1	1.5	0.07	2.7	0.08	3	0.2	2.6	0.09

Table 4.07: Major element (in weight percent oxide) and trace element (in mg/g) compositions collected by XRF from fused bead and pressed pellet samples of volcaniclastic kimberlite samples of the Dharma kimberlite. No trace elements collected by HR-ICP-MS for these samples.

Sample	D128	D129	D132	D112	D114	D116	D118	D98	D101
Depth From (m)	17.42	21.09	29.97	33.92	37.41	43.11	48.42	70.58	80.52
Depth To (m)	17.50	21.18	30.03	34.03	37.45	43.21	48.51	70.75	80.60
SiO_2	31.06	28.22	29.46	26.73	30.48	25.34	29.94	24.63	25.94
TiO_2	0.77	0.69	0.67	0.47	0.72	0.80	0.65	0.58	4.93
Al_2O_3	3.97	2.57	2.44	3.05	2.69	2.34	2.38	2.48	2.49
Fe_2O_3T	5.41	5.24	5.57	4.67	5.88	4.86	5.26	4.87	6.87
MnO	0.09	0.06	0.17	0.09	0.08	0.10	0.09	0.12	0.10
MgO	19.86	22.19	22.13	23.04	20.95	18.80	22.13	20.82	19.59
CaO	18.60	19.41	18.77	19.76	18.46	25.08	18.99	24.18	20.98
Na_2O	0.08	0.07	0.07	0.07	0.10	0.06	0.06	0.06	0.06
K_2O	1.22	1.07	0.81	1.11	1.25	1.11	1.21	0.97	0.72
P_2O_5	0.18	0.19	0.19	0.17	0.21	0.20	0.22	0.21	0.15
LOI	23.00	25.29	24.39	26.20	23.59	26.98	23.51	26.64	22.15
Total	104.23	105.01	104.67	105.36	104.42	105.68	104.44	105.55	103.97
Rb	83.7	84.7	69.3	73.2	99.2	89.3	87.9	82.9	52.4
Sr	549	384	466	393	501	487	494	636	531
Y	9.7	7.2	7.0	5.6	9.1	6.8	8.7	6.0	9.9
Zr	87	70	80	67	80	75	116	79	108
V	82	73	66	61	69	74	66	69	159
Ni	877	868	859	724	909	857	895	728	845
Cr	819	1081	964	865	1126	1081	1075	1252	1194
Nb	68.2	79.7	80.0	65.1	82.8	83.3	84.0	82.6	182.3
Ga	3.9	2.3	1.8	3.3	2.2	1.4	1.9	2.0	2.1
Cu	36	41	38	34	41	39	44	44	31
Zn	61	43	65	53	38	33	43	43	46
Co	63	60	61	49	61	59	60	50	62
Ba	1475	1321	1956	1166	1126	1161	864	777	623
La	49	53	48	42	52	50	53	58	53
Ce	20	22	3	2	35	36	61	59	65
U	2.0	2.2	2.0	2.1	1.6	1.1	1.7	2.2	0.6
Th	9.4	9.7	10.3	12.1	8.3	8.6	11.0	12.0	6.6
Sc	19	22	20	22	21	27	21	27	24
Pb	12	8	7	5	5	7	13	6	6

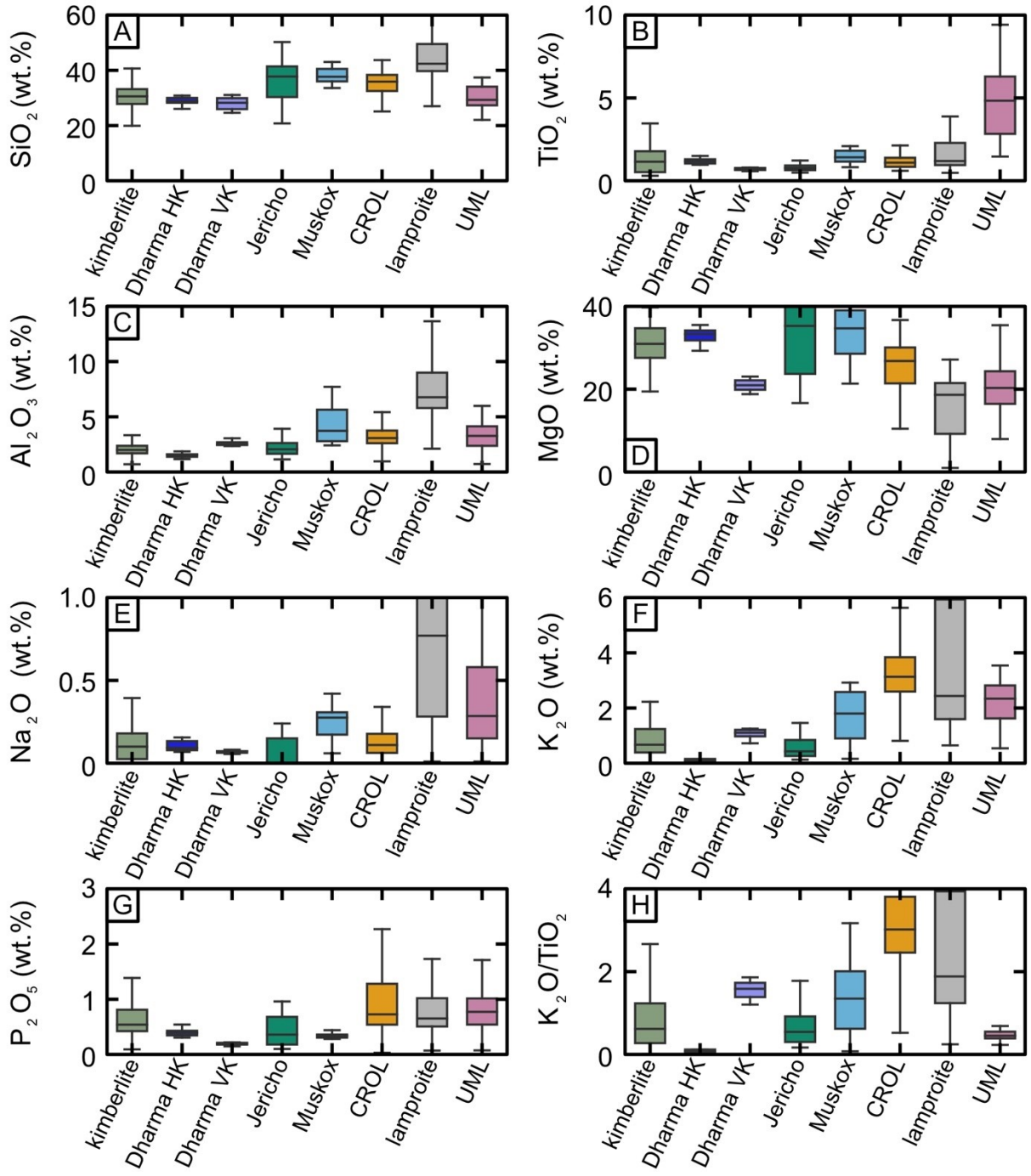

Figure 4.14: Box and whisker plots of whole rock major element compositions of hypabyssal (Dharma HK) and volcaniclastic (Dharma VK) Dharma kimberlite. Compared to regional kimberlites and lamproites, and global compilation of kimberlite and related rocks modified after Pearson et al. (2019). A) SiO_2. B) TiO_2. C) Al_2O_3. D) MgO. E) Na_2O. F) K_2O. G) P_2O_5. H) K_2O/TiO_2. Reference compositions: Jericho kimberlite (Price et al., 2000; Hayman and Cas, 2011), Muskox kimberlite (Hayman et al., 2009). Labels: CROL – carbon-rich olivine lamproite, UML – ultramafic lamprophyre.

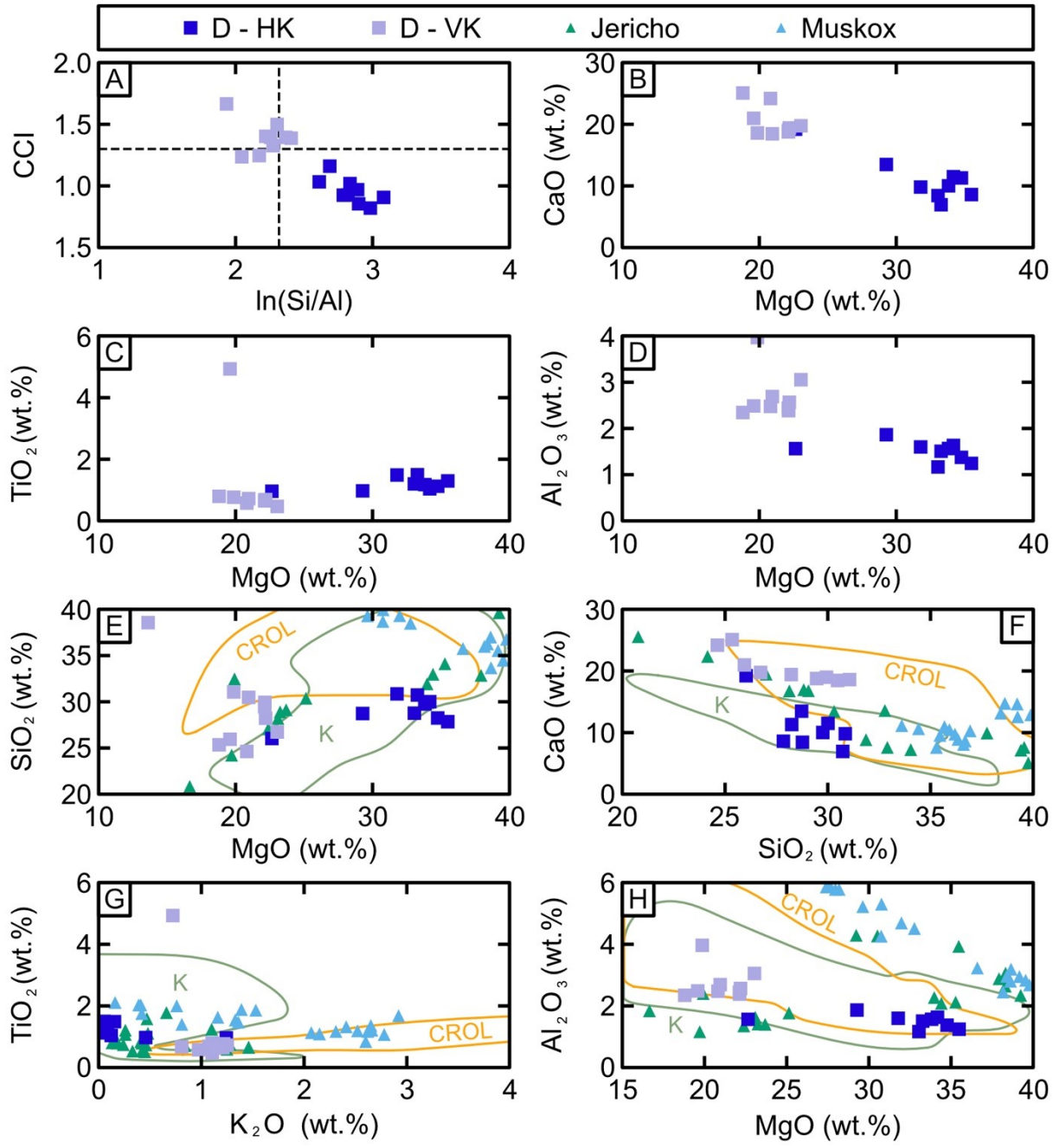

Figure 4.15: Whole rock major element variations in Dharma hypabyssal (D-HK) and volcaniclastic (D-VK) kimberlite. A) Clement (1982) CCI against ln(Si/Al) contamination index (Kjarsgaard et al., 2009) plot modified after Sarkar et al. (2018). B) CaO against MgO. C) TiO_2 against MgO. D) Al_2O_3 against MgO. E) SiO_2 against MgO plot modified after Sarkar et al. (2018). F) CaO against SiO_2 plot modified after Sarkar et al. (2018). G) TiO_2 against K_2O plot modified after Sarkar et al. (2018). H) Al_2O_3 against MgO plot modified after Sarkar et al. (2018). Reference whole rock compositions: Jericho kimberlite (Price et al., 2000; Hayman and Cas, 2011), Muskox kimberlite (Hayman et al., 2009). Abbreviations: CROL – carbon-rich olivine lamproite (Becker and Le Roex 2006; Coe et al. 2008), K – South Africa and North America kimberlite (Le Roex et al., 2003; Nowell et al., 2004; Becker and Le Roex, 2006; Kjarsgaard et al., 2009).

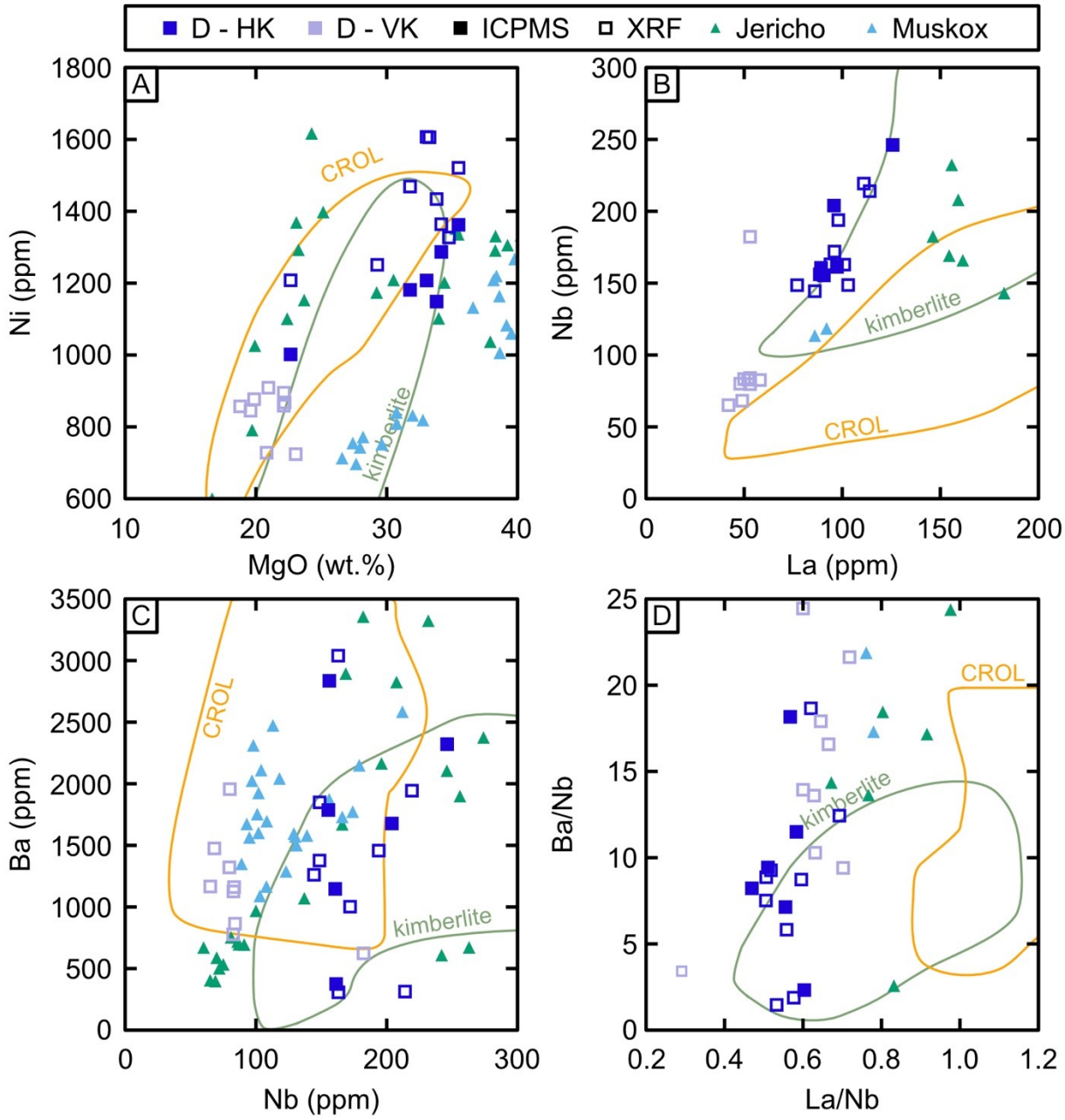

Figure 4.16: Whole rock trace element variations in Dharma hypabyssal (D-HK) and volcaniclastic (D-VK) kimberlite. A) Ni against MgO plot modified after Sarkar et al. (2018). B) Nb against La plot modified after Sarkar et al. (2018). C) Ba against Nb plot modified after Sarkar et al. (2018). D) Ba/Nb against La/Nb plot modified after Sarkar et al. (2018). Reference whole rock compositions: Jericho kimberlite (Price et al., 2000; Hayman and Cas, 2011), Muskox kimberlite (Hayman et al., 2009, Cone and Kopylova, 2020). Labels: CROL – carbon-rich olivine lamproite (Becker and Le Roex 2006; Coe et al. 2008), kimberlite – South Africa and North America kimberlite (Le Roex et al., 2003; Nowell et al., 2004; Becker and Le Roex, 2006; Kjarsgaard et al., 2009).

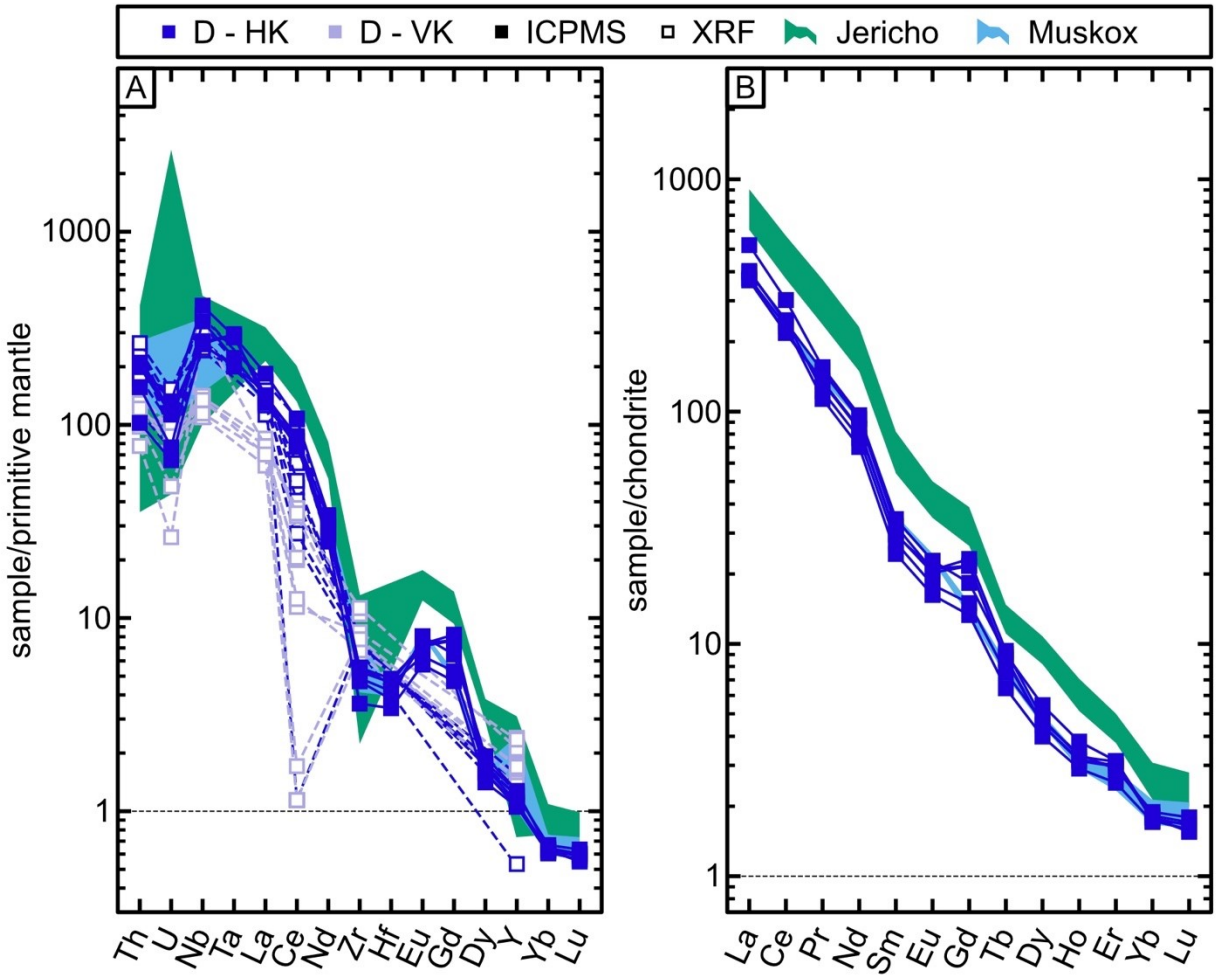

Figure 4.17: Whole rock trace element multi-element and REE diagrams of Dharma hypabyssal (D-HK) and volcaniclastic (D-VK) kimberlite. Whole rock normalized to primitive mantle and C1 chondrite compositions (Palme and O'Neill, 2014). A) Primitive mantle normalized multi element plot. B) C1 chondrite normalized REE plot. Reference compositions: Jericho kimberlite (Price et al., 2000; Hayman and Cas, 2011), Muskox kimberlite (Hayman et al., 2009, Cone and Kopylova, 2020).

The SiO_2, MgO, CaO, and TiO_2 systematics of Dharma hypabyssal kimberlite indicate its general affinity with archetypal kimberlite over CROL (Figures 4.15E to 4.15G). Dharma hypabyssal kimberlites plot primarily in the field of archetypal kimberlite on the Al_2O_3-MgO graph. Though they also overlap with Al_2O_3 and MgO concentrations of CROL they have much lower K and P than CROL (Figure 4.15H).

The trace element compositions of hypabyssal Dharma kimberlite are similar to those of archetypal kimberlite in elevated HFSE and high LREE/HREE ratios (Figure 4.16). Dharma hypabyssal kimberlite Ni contents are similar to the range of Ni found in both the Jericho and Muskox kimberlite (Price et al., 2000; Hayman et al., 2009; Hayman and Cas, 2011; Figure 4.16A). The Nb content of Dharma hypabyssal kimberlite (144 to 219 ppm by XRF, 155 to 246 ppm by HR-ICP-MS) falls within the field of archetypal kimberlite, while the La content (77 to 114 ppm by XRF, 88 to 126 ppm by HR-ICPM-MS) falls slightly below the range of La in archetypal kimberlite (Figure 4.16B). Most Ba contents of Dharma hypabyssal kimberlite (307 to 1944 ppm by XRF, 375 to 2321 ppm by HR-ICP-MS) are comparable to those of archetypal kimberlite (Figure 4.16C). Two duplicate analyses of sample D92 have a higher BaO content (3040 ppm by XRF, 2836 ppm by HR-ICP-MS), which exclusively plots into the field of CROL (Figure 4.16C). The Ba, Nb, and La concentrations and Ba/Nb and La/Nb ratios in Dharma hypabyssal kimberlite exhibit wider variations in comparison with the archetypal kimberlite (Figure 4.16D).

All Dharma hypabyssal kimberlite samples share near identical mantle-normalized trace element patterns. Primitive mantle normalized trace elements of Dharma hypabyssal kimberlite are enriched in large ion-lithophile elements (LILE) compared to high-field strength elements (HFSE)

(Figure 4.17A) and LREE-rich chondrite normalized REE patterns (Figure 4.17B). Hypabyssal kimberlite patterns display prominent Nb and Ta enrichments compared to U and La as well as a pronounced depletion in Zr and Hf compared to Nd and Eu (Figure 4.17A), similar to patterns for global hypabyssal kimberlites (Pearson et al., 2019; Giuliani et al., 2020). Hypabyssal samples, from the Dharma kimberlite have generally similar primitive mantle normalized trace element values apart from Ce which displays a wide range of values (Figure 4.17A). Additionally, one XRF analysis has a primitive mantle normalized Y concentration, which falls below other analyses of hypabyssal kimberlite.

Both primitive mantle normalized trace elements and chondrite normalized REE patterns of Dharma hypabyssal kimberlite are slightly depleted in comparison to Jericho kimberlite (Price et al., 2000; Hayman and Cas, 2011; Figures 4.17A and 4.17B). The primitive mantle normalized trace elements of the Dharma kimberlite are nearly identical to trace element compositions in the Muskox kimberlite with the following exceptions: Muskox kimberlite has higher maximum U, lower minimum Nb, and higher maximum Y (Hayman et al., 2009) (Figure 4.17A).

4.3.5 Phlogopite Rb-Sr Geochronology

A total of five multi-grain (mixed) phlogopite fractions and two phlogopite phenocryst grains from four hypabyssal kimberlite samples and one volcaniclastic kimberlite sample were analyzed for Rb-Sr isotopes (Table 4.08). $^{87}Rb/^{86}Sr$ ratios in mixed phlogopite fractions vary from 257 to 923, while individual phlogopite grains display $^{87}Rb/^{86}Sr$ ratios of 595 to 1209. Three separate model age calculations using different initial $^{87}Sr/^{86}Sr$ yield nearly identical model ages for most samples (Table 4.08). All samples record Late Triassic model ages of 219 ± 2 Ma to 225 ± 2 Ma, depending

on the assumed initial Sr isotope ration (Table 4.08). A single phlogopite macrocryst from a sample of hypabyssal kimberlite (D109B1; Table 4.08) contains a very high $^{87}Rb/^{86}Sr$ ratio of 1209 and yields an errochron age of 222 ± 2 Ma for any of these 3 initial Sr isotope compositions.

One average whole rock (Table 4.08) sample and all seven phlogopite samples define a kimberlite emplacement isochron age of 225.3 ± 0.8 Ma (Figure 4.18A). The $^{87}Sr/^{86}Sr_{initial}$ ratio was constrained using an average of whole rock compositions (n= 3; D92, D94, D104, D108), with an $^{87}Sr/^{86}Sr_{initial}$ ratio of 0.707081 ± 0.00005. This ratio falls on the higher end of $^{87}Sr/^{86}Sr_{initial}$ compositions for the Slave craton kimberlites (0.7053 for the Jericho kimberlite, Heaman et al., 2006; 0.7043 to 0.706 for the Ekati cluster, Davis and Kjarsgaard, 1997; Creaser et al., 2004; 0.7044 for the Snap Lake kimberlite dike, Agashev et al., 2008). However, the $^{87}Sr/^{86}Sr_{initial}$ of the Dharma kimberlite falls within the range of kimberlites from the Buffalo Head Hills (0.7036 to 0.710, Eccles et al., 2008). The isochron age is interpreted to represent the age of Dharma kimberlite emplacement, at 225.3 ± 0.8 Ma, though the single high Rb/Sr phlogopite "model age" of 222 ± 2 Ma is also within uncertainty.

4.3.6 Whole Rock Isotope Geochemistry

Whole rock Nd-Sr-Hf isotopes were measured on three samples of uncontaminated Dharma hypabyssal kimberlite (Table 4.09 to Table 4.11). One additional sample of Dharma kimberlite (D94) was measured only for Sr isotopes and will not be referenced in this section (Table 4.10). Initial Nd, Sr, and Hf isotope ratios are corrected to the isochron emplacement age of 225.4 Ma.

Table 4.08: Rb and Sr isotope composition of phlogopite from the Dharma kimberlite. Row labels: Error – propagated two times standard error, T $Ma_{0.7035}$ – model age calculated with $^{87}Sr/^{86}Sr_{initial}$ (y-intercept) = 0.7035, T $Ma_{0.705}$ – model age with $^{87}Sr/^{86}Sr_{initial}$ (y-intercept) = 0.705, T $Ma_{0.710}$ – model age with $^{87}Sr/^{86}Sr_{initial}$ (y-intercept) = 0.710. Labels: mix – mixed multiple grain phlogopite sample, p – single macrocryst sample, average – average (whole rock) sample.

Kimberlite	HK	HK	HK	HK	HK	HK	VK	HK
Sample	D89-1	D89-2	D93-1	D93-2	D94-1	D109B1	D113-1	WR
From (m)	60.19	60.19	65.41	65.41	66.10	91.31	34.20	
To (m)	60.27	60.27	65.48	65.48	66.29	91.36	34.26	
Type	mix	mix	mix	mix	mix	p	p	average*
Mass (g)	0.00906	0.00813	0.00955	0.00628	0.00854	0.00869	0.00973	-
Sr (ppm)	6.62	7.93	3.46	3.24	2.74	2.87	2.48	-
Rb (ppm)	651.30	652.92	305.13	285.91	681.45	871.98	431.39	-
$^{87}Rb/^{86}Sr$	312	257	277	277	923	1209	595	0.115
Error	3	2	2	2	8	10	5	0.001
$^{87}Sr/^{86}Sr$	1.703935	1.508459	1.586510	1.569991	3.611342	4.542566	2.566957	0.707081
Error	0.00009	0.00008	0.00008	0.00009	0.00048	0.00024	0.00013	0.000005
$TMa_{0.7035}$	225	220	224	220	222	223	220	-
$TMa_{0.705}$	225	220	224	220	221	223	220	-
$TMa_{0.710}$	224	219	223	218	221	223	219	-

** average whole-rock consists of samples D92, D94, D104, and D108 (Table 4.10)*

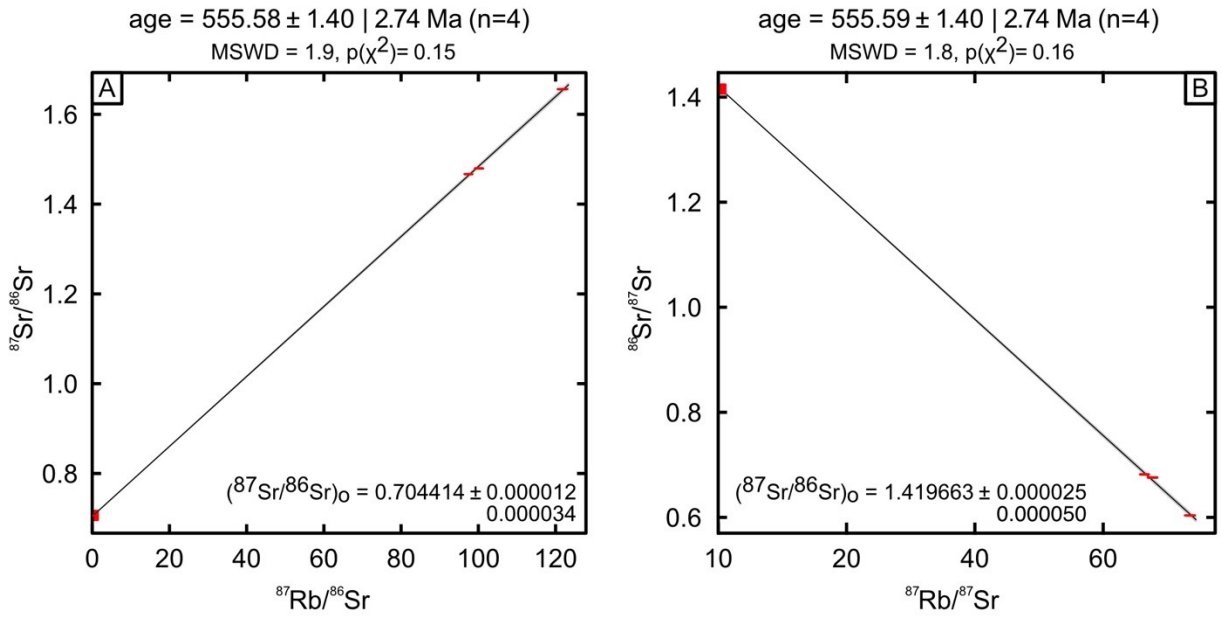

Figure 4.18: Dharma kimberlite isochron plots. A) Phlogopite mica and average whole rock $^{87}Sr/^{86}Sr$ against $^{87}Rb/^{86}Sr$ isochron plot. B) Phlogopite mica and average whole rock $^{87}Sr/^{86}Sr$ against $^{87}Rb/^{86}Sr$ reverse isochron plot. Age legend: isochron age ± estimated uncertainty of isochron age | 100(1-α)% confidence interval (n=population). MSWD legend: MSWD = Mean Square of the Weighted Deviates (MSWD) for the linear fit, $p(\chi^2)$ =chi-squared p-value for the linear fit. $(^{87}Sr/^{86}Sr)_o$ legend: $(^{87}Sr/^{86}Sr)_o$= initial $^{87}Sr/^{86}Sr$ isotope ratio obtained by linear regression ± estimated uncertainty of initial $^{87}Sr/^{86}Sr$ isotope ratio | 100(1-α)% confidence interval.

Dharma kimberlite samples show a range of $^{87}Sr/^{86}Sr_{initial}$ from 0.703902 to 0.704666 and $\varepsilon Nd_{initial}$ from 2.21 to 2.45 (Figure 4.19A). Dharma kimberlites shows a minimal spread in $\varepsilon Hf_{initial}$ from 1.4 to 6.8 (Figure 4.19B). The Nd and Hf isotope systematics suggest that Dharma kimberlite is slightly depleted in comparison to CHUR, consistent with most pre-Cretaceous uncontaminated kimberlites (Woodhead et al., 2019).

Dharma kimberlite samples fall within the field of ocean island basalts (OIB) and worldwide kimberlite on Sr-Nd-Hf isotope diagrams (Figures 4.19A and 4.19B). The Nd isotope composition of the Dharma kimberlite is similar to perovskite from kimberlite of the Late Triassic-Early Jurassic Churchill kimberlite field (Zurevinski et al., 2011). Additionally, the Nd and Hf isotope systematics of Dharma kimberlite are very similar to Jericho kimberlite (Figures 4.19A and 4.19B). Sr isotope compositions of the Dharma kimberlite fall within the lower range of $^{87}Sr/^{86}Sr$ values for kimberlites from the Jericho pipe (Figure 4.19A).

Table 4.09: Dharma kimberlite Sm and Nd isotope compositions.

Sample	D92	D104	D108
From (m)	63.73	82.76	89.53
To (m)	63.80	82.90	89.63
Age	225.3 ± 0.8	225.3 ± 0.8	225.3 ± 0.8
Sm (ppm)	4.5	5.6	5.0
Nd (ppm)	36.4	46.1	44.0
$^{147}Sm/^{144}Nd$	0.074539	0.072893	0.069166
$^{143}Nd/^{144}Nd$	0.512584	0.512569	0.512564
2SE	0.000005	0.000007	0.000007
$^{145}Nd/^{144}Nd$	0.348406	0.348414	0.348417
2SE	0.000004	0.000003	0.000004
$\varepsilon Nd_{initial}$	2.45	2.21	2.23
$\varepsilon Nd_{present}$	-1.06	-1.36	-1.43

Table 4.10: Dharma kimberlite Sr isotope composition.

Sample	D92	D94	D104	D108
From (m)	63.73	66.10	82.76	89.53
To (m)	63.80	66.29	82.90	89.63
Age	225.3 ± 0.8	225.3 ± 0.8	225.3 ± 0.8	225.3 ± 0.8
Rb ppm	6	110	10	5
Sr ppm	427	980	354	630
$^{88}Sr/^{86}Sr$	8.320435	8.345821	8.354070	8.341287
$^{87}Sr/^{86}Sr_{present}$	0.705517	0.707113	0.707113	0.707124
$^{87}Sr/^{86}Sr_{initial}$	0.703902	0.707528	0.704666	0.704337
2SE	0.000004	0.000006	0.000005	0.000006
$^{84}Sr/^{86}Sr$	0.056485	0.056499	0.056498	0.056490
2SE	0.000001	0.000002	0.000002	0.000002

Table 4.11: Dharma kimberlite Lu and Hf isotope composition.

Sample	D92	D104	D108
Form (m)	63.73	82.76	89.53
To (m)	63.80	82.90	89.63
Age	225.3 ± 0.8	225.3 ± 0.8	225.3 ± 0.8
Lu (ppm)	0.076	0.042	0.043
Hf (ppm)	1.231	1.157	1.154
$^{176}Hf/^{177}Hf$	0.282721	0.28286	0.28282
2σ	0.000009	0.00001	0.00001
$^{178}Hf/^{177}Hf$	1.47	1.47	1.47
2σ	0.33	0.35	0.38
$^{176}Lu/^{177}Hf$	0.0087	0.00521	0.00523
2σ	0.0002	0.00005	0.00007
$\varepsilon Hf_{initial}$	1.43	6.81	5.64
$\varepsilon Hf_{present}$	-2.28	2.57	1.41

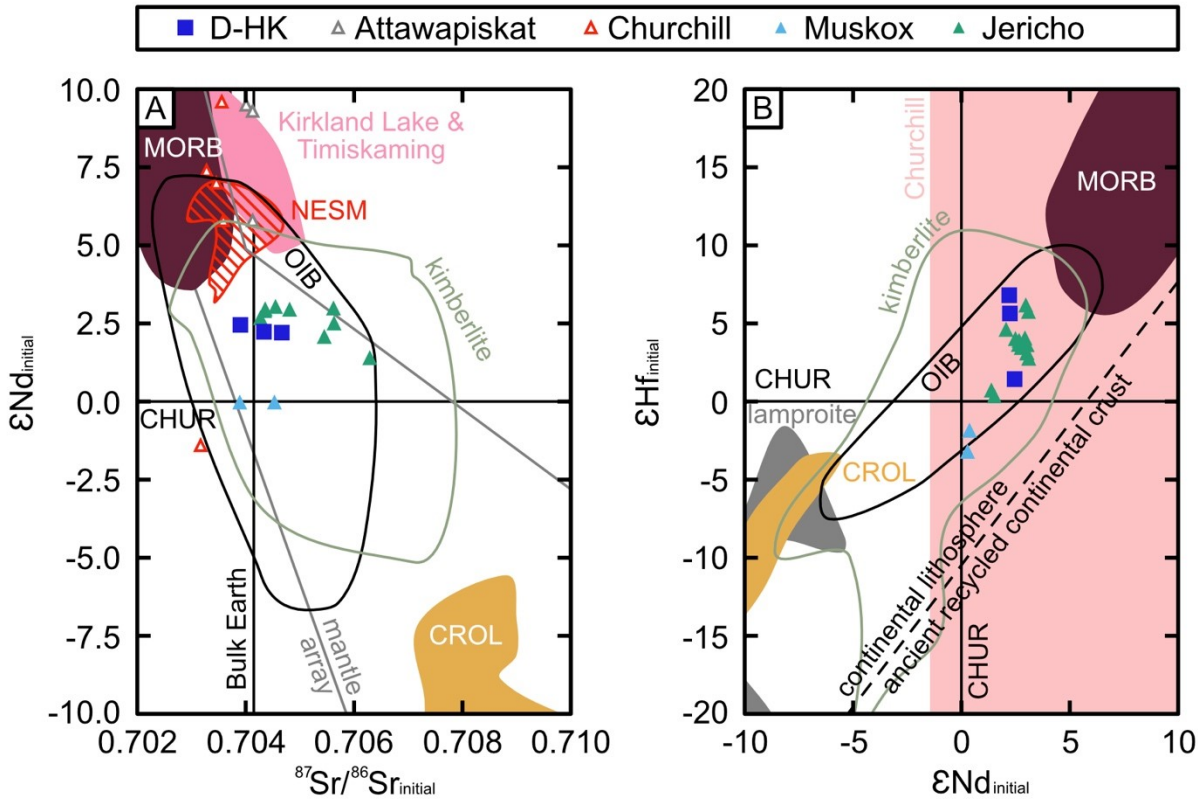

Figure 4.19: Whole-rock radiogenic isotope plots for hypabyssal Dharma kimberlite. A) $\varepsilon Nd_{initial}$ against $^{87}Sr/^{86}Sr_{initial}$ isotope ratio plot modified after Sarkar et al. (2018). B) $\varepsilon Hf_{initial}$ against $\varepsilon Nd_{initial}$ discrimination plot modified after Pearson et al. (2019). Reference whole rock compositions: perovskite from Attawapiskat kimberlite field (Zurevinski et al., 2011), perovskite from Churchill kimberlite field (Zurivenski et al., 2011), perovskite from Kirkland lake and Timiskaming kimberlite fields (Zurevinski et al., 2011), New England Sea Mounts (NESM) whole-rock compositions (Taras and Hart, 1987; Merle et al., 2019), Muskox kimberlite (Woodhead et al., 2019; Cone and Kopylova, 2020), Jericho kimberlite (Kopylova and Hayman, 2008; Woodhead et al., 2019; Cone and Kopylova, 2020) Labels (Pearson et al., 2019): Bulk Earth – Bulk Earth reservoir composition after Sarkar et al. (2018), CHUR – chondritic uniform reservoir model composition after Bouvier et al. (2008), CROL – worldwide carbon-rich olivine lamproite field, kimberlite – worldwide kimberlite field, lamproite – worldwide lamproite field, MORB – worldwide mid-ocean ridge basalt field, NESM – New England Seamounts, OIB – worldwide ocean island basalt field.

4.4 Dharma Kimberlite Domains and Diamond Sampling

All samples in this study originate from a diamond core drill hole DD07GH001 in the Dharma kimberlite (Final depth 179.8 m). This drill hole is interpreted to be drilled near the center of the main Dharma kimberlite pipe (Figure 4.02) and is sampled to a depth of 100 m in this work. This section builds upon the petrologic and geochemical results outlined in the previous sections as well as magnetic susceptibility and diamond sampling results procured by Sanatana Resources Inc. Four compositional domains corresponding to logged volcaniclastic and hypabyssal kimberlite intervals are identified on the basis of petrological, geochemical, and magnetic susceptibility properties in the diamond core drill hole DD07GH001 (Figure 4.20).

4.4.1 Kimberlite Domain Characteristics

The first domain consists of volcaniclastic kimberlite tuff (VK_t; Figure 4.20) intersected at two intervals from 5.00 m to 51.74 m (samples n=7) and from 70.00 m to 82.20 m (samples n=2). This domain records the lowest median magnetic susceptibility of 177 $X^{SI}x10^{-3}$ (Figure 4.20). Total olivine content (OLV %, black line) ranges from 3 volume % to 33 volume % with a median concentration of 19%. Crustal xenolith content (CRST %) ranges from 14 volume % to 44 volume % with a median concentration of 26%. Xenocryst and xenoliths that constitute total mantle phase content (MNTL %) ranges up to 49 volume % with a median concentration of 3 volume %. Olivine phenocrysts are between up to four times more abundant than olivine microphenocrysts in most sampled intervals with a total phenocryst olivine content (OLV%, grey line) up to 12%. This domain contains the highest TiO_2, Al_2O_3, and CaO content, likely the result of Ilmenite megacryst oversampling (for Ti) and high percentage of crustal xenoliths (Figure 4.20). Likewise, the low

fraction of olivine and other kimberlite mineral phases in this domain results in its low abundance of Nb, La, and Cr (Figure 4.20).

The second domain consists of hypabyssal kimberlite (HK_1; Figure 4.20) from a depth of 51.74 m to 70.00 m (samples n=6; Figure 4.20). This domain records the second highest median magnetic susceptibility of 444 $X^{SI}x10^{-3}$ (Figure 4.20). Total olivine content (OLV %, black line) ranges from 23 volume % to 37 volume % with a median concentration of 30 volume %. Crustal xenolith content (CRST %) ranges up to 6 volume % with a median concentration of 3 volume %. Total mantle phase content (MNTL %) ranges up to 5 volume % with a median concentration of 3 volume %. Olivine phenocrysts are generally 2 to 6 times more abundant than microphenocrysts with a total phenocryst olivine content (OLV%, grey line) between 16 volume % and 28 volume %. This domain contains the highest MgO content of all sampled domains alongside a higher median TiO_2 (1.08 wt.%) than in VK_t, reflecting the higher olivine and oxide concentration. This is further reflected in the Nb, La, and Cr concentrations of HK_1 which are higher than the trace element compositions found in VK_t (Figure 4.20).

The third domain consists of hypabyssal kimberlite (HK_2; Figure 4.20) intersected at two intervals from 82.20 m to 84.3 m (samples n=1; Figure 4.20) and from 87.00 m to 91.40 m (samples n=2; Figure 4.20). This domain records the highest median magnetic susceptibility of 1170 $X^{SI}x10^{-3}$ (Figure 4.20). Total olivine content (OLV %, black line) ranges from 26% to 36% with a median concentration of 26%. Crustal xenolith content (CRST %) ranges up to 1%. Total mantle phase content (MNTL %) ranges from 3% to 8% with a median concentration of 5%. Olivine phenocrysts are found in concentrations of 5 to 6 times greater than microphenocryst olivine with a total olivine

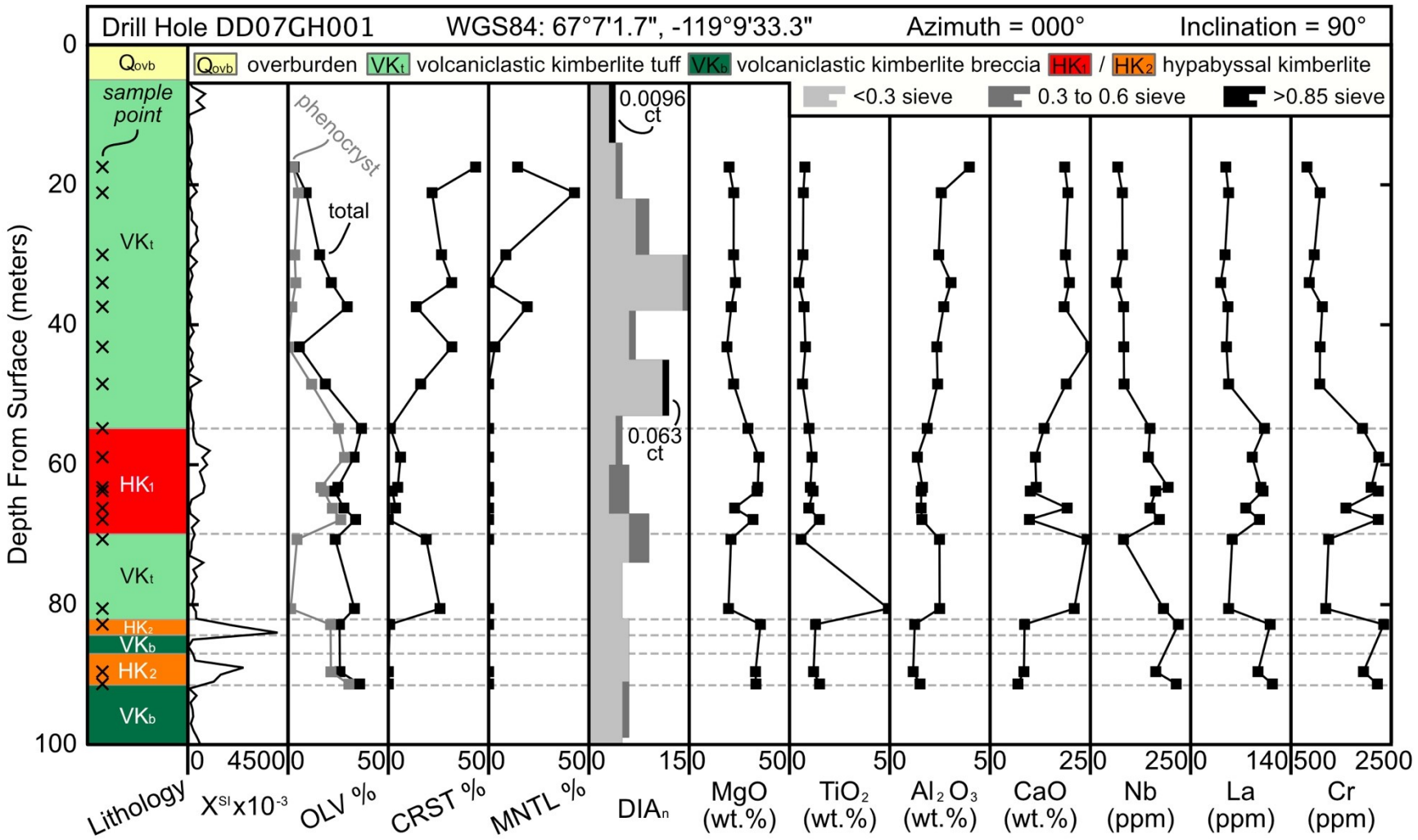

Figure 4.20: Down-hole strip log for a portion (0 m to 100 m) drill hole DD01GH001 in the Dharma kimberlite. Labels: $X^{SI}x10^{-3}$ – magnetic susceptibility in SI units, OLV % - modal percent (altered and unaltered) of phenocryst olivine (grey) and all olivine phases (black) including microphenocryst, phenocryst, olivine-cored ash, and olivine-cored lapilli, CRST % - modal percent of crustal xenolith, MNTL % - model percent of mantle xenolith + garnet xenocrysts (ash and lapilli) + pyroxene xenocrysts (ash and lapilli), DIA_n – stacked count of diamonds by sieve size (see legend for color). Note modal percent estimated from thin-sections.

phenocryst content (OLV%, grey line) between 21 volume % and 3o volume %. The MgO content of this domain is similar to HK_1 while the median TiO_2 (1.3 wt.%) content is the highest among all sampled domains. The Al_2O_3 and CaO content of HK_2 is the lowest among all domains, reflecting the low crustal xenolith content. This domain also records the highest concentration of Nb, La, and Cr.

No petrographic or geochemical samples were collected from the fourth domain of volcaniclastic kimberlite breccia (VK_b; Figure 4.20). However, this domain is clearly distinct from HK_1 and HK_2 with a lower median magnetic susceptibility of 229 $X^{SI}x10^{-3}$ (Figure 4.20).

4.4.2 Kimberlite Domain Diamond Sampling

Diamond sampling was conducted by Kennecott Canada Exploration Inc on behalf of Sanatana Resources Inc (Gill, 2016). Caustic fusion analysis reports provided in the supplementary material of the original property assessment report (Gill, 2016). Samples for caustic fusion analysis were collected in eight- to nine-meter intervals on average. A total of 106 diamonds were recovered in 13 sample intervals from 4.6 m to 103 m. Per sample interval, diamond concentrations range from 2.42 stones per 10 kg to 8.18 stones per 10 kg with a median concentration of 3.33 stones per 10 kg. Diamonds are dominated by fragmented stones with irregular morphologies (n=53). White, brown, and grey stones are recovered from the first 100m of drill hole DD07GH001. The most common stone color is white (n=60) with the majority of white stones (n=49) being transparent. It should be noted that the domain of HK_2 is combined with a portion of VK_b (Figures 4.20 and 4.21) in the following text due to the limitations of sampling. Details of sampling discussed below are located in Table 4.12.

*Table 4.12: Microdiamond and macrodiamond distribution and mean carat size in the domains of the Dharma kimberlite in drill hole DD07GH001. *Note sampling data only for DD07GH001 from 4.6m to 103m.*

Domain	***Total Mass of Unit (kg)***				***Total Length of Unit (m)***			
VK_t	122.04				56.4			
HK_1	53.85				21			
HK_2 & VK_b	38.72				17			
VK_b	29.8				12			
DD07GH001*	244.41				106.4			
	Count of Stones per Sieve Size (mm)							
	0.106	*0.15*	*0.212*	*0.3*	*0.425*	*0.6*	*0.85*	*1.7*
VK_t	27	12	11	2	2	1	1	1
HK_1	8	4	1	5	2	0	0	0
HK_2 & VK_b	4	3	4	1	0	0	0	0
VK_b	8	5	4	0	0	0	0	0
DD07GH001*	47	24	20	8	4	1	1	1
	Mean Carat Size							
VK_t	0.000081	0.00014	0.00047	0.00064	0.0018	0.005	0.0096	0.06315
HK_1	0.000047	0.00012	0.00032	0.00055	0.0043	0	0	0
HK_2 & VK_b	0.000055	0.000088	0.0005	0.00071	0	0	0	0
VK_b	0.000066	0.00016	0.00056	0	0	0	0	0
DD07GH001*	0.00007	0.00013	0.00049	0.00059	0.0031	0.005	0.0096	0.06315

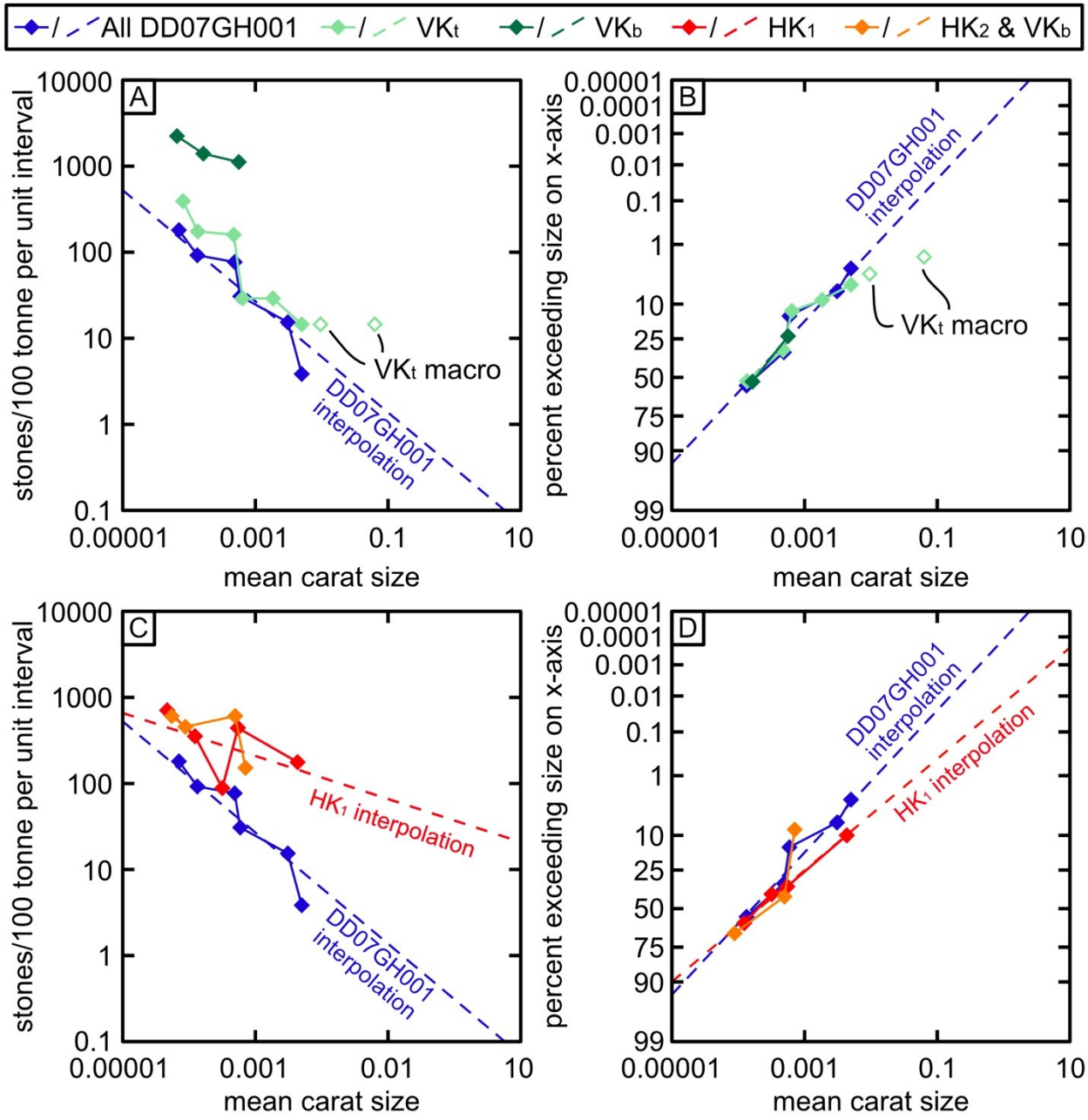

Figure 4.21: Diamond distribution in a portion (0 m to 100 m) of drill hole DD07GH001. A) Grade (in stones per 100 tonne per unit interval) against size (in mean carats) distribution for microdiamonds from VK_t and VK_b domains and macrodiamonds from VK_t domain. B) Log-probability distribution for microdiamonds from VK_t and VK_b domains and macrodiamonds from VK_t domain. C) Grade against size distribution for microdiamonds from HK_1 and combined HK_2 and VK_b domains. D) Log-probability distribution for microdiamonds from HK_1 and combined HK_2 and VK_b domains. Plots modified after Kjarsgaard et al. (2019). All DD07GH001 microdiamond samples and interpolation plotted for comparison. Dotted lines correspond to interpolated values. Note – All DD07GH001 microdiamond samples include only samples from 4.6m to 103m.

In the sampling interval studied in detail in this work, the overall grade-size distribution in DD07GH001 (4.6m to 103m) indicates a higher proportion of smaller stones to larger stones (Figure 4.21A and 4.21C). However, the grade-size distribution between domains differs. Although the VK_t domain includes macrodiamonds, samples of VK_t reflect a small-stone distribution similar to that of all samples of DD07GH001 (Figure 4.21A). In contrast, the domains of HK_1 and VK_b and the combined HK_2 and VK_b domain have flatter grade-size curves indicating a higher proportion of larger stones (Figure 4.21A and 4.21C). Due to the limited sampling of the VK_b domain and combination of the HK_2 and VK_b domains, HK_1 is the sole domain that demonstrates a high-grade potential with an interpolated grade of 20 stones per 100 tonne at a mean carat size of 11.5 carats. Although, this interpolation is likely poorly anchored.

The log-distribution of microdiamonds in all domains is generally similar with all domains falling closely to the interpolation constructed from all samples of DD07GH001 (Figure 4.21B and 4.21C). The interpolation from microdiamonds of all samples of DD07GH001 indicates that diamonds larger than 1 carat constitute 0.0001 % of all stones. As with the grade-size curves, the HK_1 domain interpolation implies a more favorable distribution with diamonds larger than 1 carat constituting 0.0164 % of all stones in the domain. Coupled with phenocryst olivine data, the HK_1 is a compelling target for further investigation.

4.5 Discussion

4.5.1 Classification of Magmatic Rocks from the Dharma Kimberlite

The Dharma intrusive rocks have been proposed to comprise “a complex of coherent textured sills and dykes with associated blows of volcaniclastic kimberlite of limited size” (Gill, 2016). A

reconstruction (Figure 4.02C) from the drilling data provided by Gill (2016) indicates the presence of at least two volcanic diatremes. The Dharma kimberlite samples studied in this chapter derive from the one larger diatreme in this complex (Figure 4.02). Cross sections constructed from five diamond core drill holes define a central diatreme volumetrically dominated by volcaniclastic kimberlite tuff (VK_t) and tuff-breccia (VK_b). Volcaniclastic kimberlite tuff overlies the volcaniclastic kimberlite tuff-breccia. One hypabyssal kimberlite body (HK_2) appears to intrude the volcaniclastic kimberlite tuff-breccia as evidenced by the sharp contacts between the hypabyssal kimberlite bodies and volcaniclastic kimberlite tuff-breccia. Only one hypabyssal kimberlite (HK_1) is observed in the volcaniclastic kimberlite tuff overlying the tuff breccia. These two hypabyssal kimberlite bodies are interpreted as later-stage intrusions. HK_2 intruded after or contemporaneously with the eruption of VK_b, while HK_1 was emplaced either after or contemporaneously with the eruption of VK_t. The complex intrusions at Dharma are similar to diatreme zones typical of other kimberlite intrusions worldwide (Hawthorne, 1975; Mitchell, 1986; Field and Scott Smith, 1999; Kjarsgaard, 2007). The absence of resedimented volcaniclastic kimberlite at Dharma indicates that the fragmental crater zone is eroded. Additionally, the absence of major intervals of massive hypabyssal kimberlite and the presence of volcaniclastic kimberlite at depth suggest that drilling did not penetrate the root zone of the Dharma diatreme.

The Dharma kimberlite shares petrographic characteristics similar to other kimberlites worldwide. Hypabyssal kimberlite from Dharma hosts at multiple generations of olivine and two generations of phlogopite, similar to most other kimberlites (Mitchell, 1986; Mitchell et al., 2019). Olivine macrocrysts makes up between 16% and vol. 30% and is dominantly anhedral to subhedral, a result of magmatic corrosion altering the morphology of the original olivine during kimberlite ascent and

emplacement (Arndt et al., 2006; Brett et al., 2015). Some olivine display undulose extinction which makes them distinct from other olivine phenocrysts. Undulose extinction has been found in archetypal kimberlite where these grains are characterized as xenocrysts produced from the deformation and metasomatism of the lithospheric mantle (Moore, 1988; Arndt et al., 2010; Cordier et al., 2015, 2017). Alternatively, undulose extinction has been interpreted to be associated with emplacement-related stresses in the crust (Moore et al., 2020). The second broad generation of olivine consists of subhedral-euhedral and groundmass olivine and constitutes between 5 to 12 volume % which is slightly lower than archetypal kimberlite (~25%; Mitchell et al., 2019). The first generation of phlogopite consists of rounded, subhedral phlogopite phenocrysts and corresponds to early kimberlite formation. Following crystal growth, these phlogopite experienced rounding through magmatic corrosion similar to that of olivine. A single euhedral phlogopite microphenocryst is interpreted as evidence for limited second stage magmatic growth.

The major and minor element mineral chemistry of olivine, phlogopite, and ilmenite from Dharma kimberlites are consistent with other kimberlite mineral compositions and evolutionary trends. Olivine rims display characteristic Ni variation at consistent Mg-number values associated with the fractionation of olivine and chromite during early stages of kimberlite crystallization (Arndt et al., 2010; Giuliani, 2018). Olivine rims display depletion in Ni content with increasing Mg-number, which is similar to the chemical trends observed in olivine rinds (rinds or rims) from typical kimberlites (Mitchell et al., 2019). Although phlogopite is found only sparingly in the Dharma kimberlite, some phlogopite grains record increases in Al_2O_3 with decreasing TiO_2 and FeO contents, consistent with the kimberlite phlogopite-eastonite zoning trend of Mitchell (1986). Furthermore, a single phlogopite records the kimberlite tetraferriphlogopite kimberlite trend from

high to low Al content (Figure 4.06A and 4.06B). Additionally, core to rim enrichment in BaO found in Dharma phlogopite is consistent with chemical variations observed in the other kimberlitic phlogopites (Mitchell, 1986, 1995). The Al_2O_3, TiO_2, and FeO systematics of Dharma phlogopite are also similar to phlogopite from Muskox and Jericho pipes (Heaman et al., 2006; Kopylova et al., 2007; Hayman et al., 2009).

As typical of the worldwide kimberlite population, Dharma kimberlite ilmenite is exclusively composed of Mg-rich megacryst and groundmass phases (Mitchell, 1986, 1995; Wyatt et al., 2004). Furthermore, almost all spinel compositions align or are adjacent to spinel "Trend 1" of Mitchell (1986) indicating spinel evolution from chromite to magnesio-ulvöspinel + magnetite, characteristic of kimberlite, (Mitchell, 1986, 1995) and some carbonatites and lamprophyres (Roeder and Schulze, 2008). The zonation of Dharma spinels to higher Mg-numbers is similar to spinel compositions in the Majuagaa kimberlite which grew in a volatile-rich, high-Mg silicate melt (Nielsen and Sand, 2008). A single inclusion of rutile in olivine plots within the field of groundmass rutile from kimberlite (Figure 4.09A; Malkovets et al., 2016).

As with mineral chemistry, the bulk whole-rock geochemical compositions of the Dharma kimberlite samples share many characteristics in common with global and regional, on-craton kimberlites (Figures 4.14 to 4.17;). Hypabyssal kimberlite from Dharma has TiO_2, Al_2O_3, P_2O_5, K_2O, and Na_2O contents that are most consistent with a kimberlite bulk composition (Figure 4.14; Pearson et al., 2019). Additionally, kimberlite from Dharma displays SiO_2, TiO_2, MgO, Na_2O, and P_2O_5 contents within the ranges characteristic of Jericho and Muskox kimberlites (Figures 4.14 and 4.15; Price et al., 2000; Hayman et al., 2009; Hayman and Cas, 2011). The Ni content of

hypabyssal kimberlite from Dharma almost completely overlaps with kimberlite from Jericho while Ba content overlaps with kimberlite from both Jericho and Muskox locations (Figures 4.16A and 4.16C; Price et al., 2000; Hayman et al., 2009; Hayman and Cas, 2011). Primitive mantle normalized trace element patterns for Dharma hypabyssal kimberlite display U, Zr, and Hf depletions analogous to primitive mantle normalized trace element patterns from both Jericho and Muskox pipes (Figure 4.17A; Price et al., 2000; Hayman et al., 2009; Hayman and Cas, 2011). Likewise, chondrite normalized REE patterns from Dharma hypabyssal kimberlite display LREE enriched, negative sloping REE patterns matching chondrite normalized REE patterns from Jericho and Muskox kimberlites (Figure 4.17B; Price et al., 2000; Hayman et al., 2009; Hayman and Cas, 2011). Dharma hypabyssal kimberlite REE patterns closely match REE patterns from Muskox kimberlite and are slightly depleted in comparison to Jericho kimberlite, which may reflect more dilution by olivine as MgO content is higher in the Dharma samples than in the Jericho samples (Figure 4.17; Price et al., 2000; Hayman et al., 2009; Hayman and Cas, 2011).

4.5.2 Crystallization Sequence of the Dharma Kimberlite

Like most kimberlites, the Dharma kimberlite involves the complex growth and incorporation of mineral phases at various stages of its crystallization history (Figure 4.22). As discussed in section 4.5.1, olivine phenocrysts with rounded morphologies likely belong to either xenocryst or antecryst populations. Several olivine phenocrysts display undulose extinction indicating that these phenocrysts were exposed to crystallographic strain in the mantle or during kimberlite emplacement (Moore, 1988; Arndt et al., 2010; Cordier et al., 2015, 2017; Moore et al., 2020). It is possible that a portion of olivine phenocrysts represent olivine that grew in the proto-kimberlite melt or was exposed to previous kimberlite metasomatism prior to entrainment in the Dharma

kimberlite (Howarth and Taylor, 2016). A few olivine phenocrysts are chemically zoned in BSE images (Figure 4.23 – D092*).

Subhedral to anhedral spinel is often included in these rim zones indicating that the lighter colored zone may reflect re-equilibration with the kimberlite magma. In either case, phenocrystic olivine is the first mineral phase to crystallize from the parental Dharma kimberlite melt. Ilmenite phenocrysts are interpreted as megacryst phases, corresponding to ilmenite growing in the proto-kimberlite melt (discussed further in section 4.5.4). These ilmenite megacrysts are characterized by cores with nearly equal geikielite and ilmenite end-member compositions. Similarly, phlogopite phenocrysts are interpreted as either antecryst or early cognate phenocryst phases in the proto-kimberlite melt. Straining and deformation of phlogopite cleavage provides strong evidence for the antecryst classification of phlogopite. Deformation features such as kink-banding and undulose extinction likely result from the entrainment of early magmatic phlogopite in the ascending kimberlite magma (Clement, 1982; Giuliani et al., 2016). A portion of olivine microphenocrysts are classified as olivine xenocrysts on the basis of similar core to rim compositions and generally anhedral to subhedral morphology (Figure 4.23 – D092010olv, D092012olv, and D092014olv). These microphenocrysts most likely represent portions of disaggregated olivine phenocrysts entrained by the kimberlite melt.

A single crystal of Cr-rich rutile began to grow prior to the crystallization of olivine microphenocrysts along with two rutile inclusions identified in the cores of olivine microphenocrysts (Figure 4.04A). A portion of olivine microphenocrysts includes Cr-rich spinel and hosts fluid-inclusion trails (Figure 4.23 – D086024olv and D086026px). Additionally, this

group of microphenocryst olivine displays a decrease in Ni content at constant Mg-number (Figure 4.23 – D086024olv and D086026px). Such features are associated with olivine growth during magmatic crystallization in the kimberlite melt (Howarth and Taylor, 2016). Therefore, olivine microphenocrysts of magmatic origin began to crystalize next in the kimberlite melt. Around the same time, a small amount of microphenocryst phlogopite began to crystalize alongside magmatic phlogopite phenocrysts creating semi-poikilitic assemblages. After the inception of olivine microphenocryst crystallization, the internal zones of ilmenite phenocrysts became enriched in geikielite. Ilmenite of similar end-member composition began to crystalize prior to growth of groundmass olivine as is evidenced by one inclusion analysis (D091013oxincl). The partial inclusion of CHR spinel in the rim of one olivine microphenocryst indicates that CHR spinel crystallization began before the end of microphenocryst olivine crystallization and prior to the growth of MUM and MAG spinel. However, the low abundance of CHR spinel in the Dharma kimberlite indicates that groundmass CHR spinel growth was at some point superseded by MUM and MAG spinel growth. Prior to the initiation of MUM and MAG spinel growth, groundmass ilmenite of geikielite composition began to crystalize as zoned, subhedral individual crystals (up to 90 μm in size) with irregular rims. MUM and MAG spinel growth began thereafter, with MUM spinel soon overtaking MAG spinel as the dominant compositional group. At this point, MUM spinel and olivine became the dominant groundmass phases with MAG spinel crystallizing in low abundance. Groundmass atoll spinels likely indicate episodes of no spinel crystallization due to the lack of spinel-forming constituents (Roeder and Schulze, 2008). Rinds of MUM spinel + Cr-poor rutile + armalcolite on ilmenite phenocrysts likely began to grow at the same time as groundmass MUM spinel (Figure 4.04B).

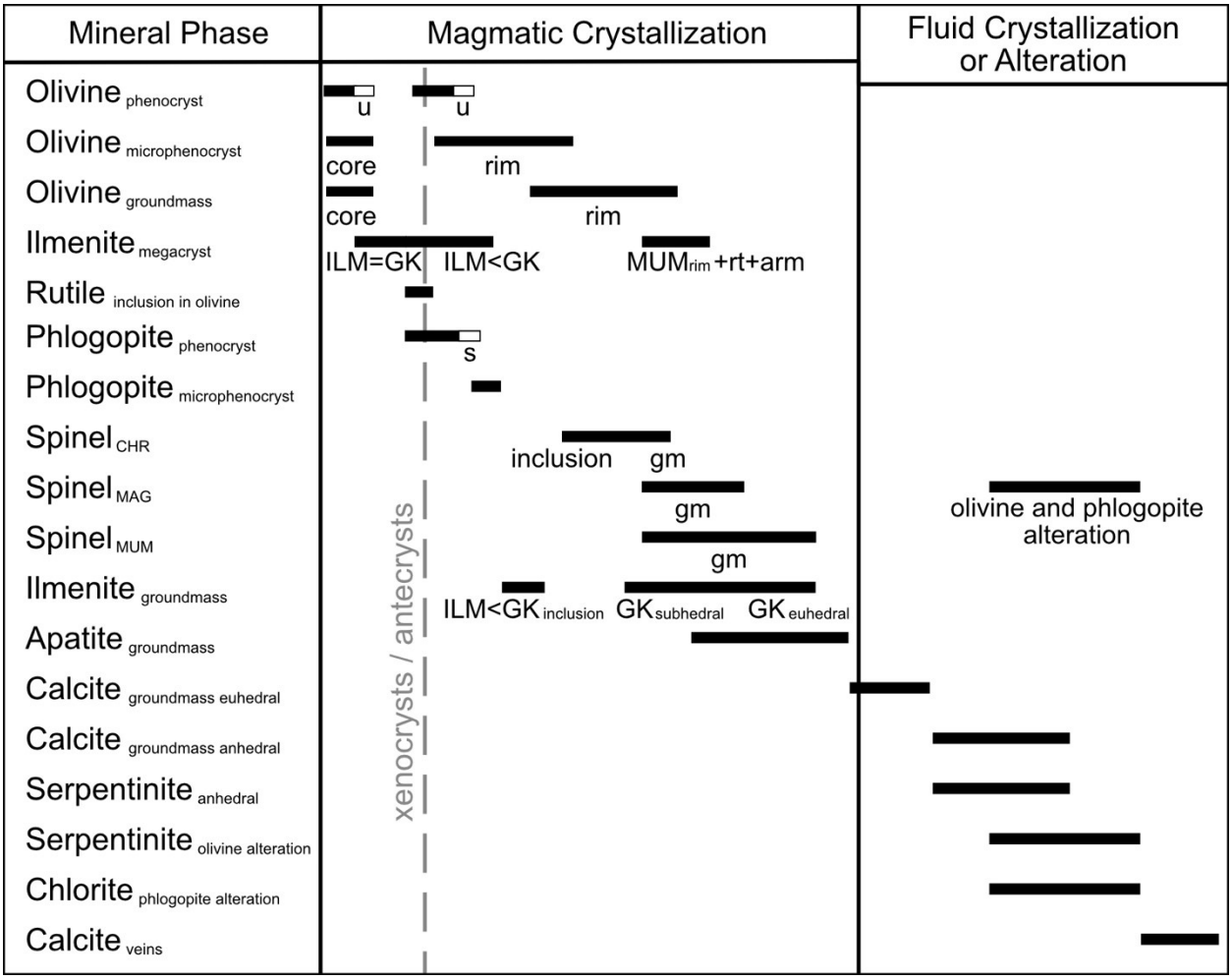

Figure 4.22: Generalized crystallization sequence of mineral phases in the Dharma kimberlite. Sequence determined from mineral inclusions and textural relationships. Labels: CHR – Cr-rich spinel, $GK_{inclusion}$ – geikielite inclusion with ilmenite less than geikielite composition, $GK_{subhedral}$ – subhedral geikielite, $GK_{euhedral}$ – euhedral geikielite, ILM=GK – ilmenite equal to geikielite composition, ILM<GK – ilmenite less than geikielite composition MAG – Fe-rich spinel, MUM – Ti-rich spinel, MUM_{rim}+rt+arm – Ti-rich spinel rim on ilmenite with rutile and armalcolite, gm – groundmass, u – olivine with undulose extinction, s – phlogopite with strain deformation on cleavage plane.

The growth of armalcolite in the Dharma kimberlite is likely the result of rutile interacting with Fe^{2+}-bearing silicate or melt and/or the decomposition of ilmenite and rutile at higher temperatures (Haggerty, 1995). The composition of rutile on ilmenite megacryst rims supports this hypothesis as they plot into the compositional field of rutile + lindsleyite-mathiasite (LIMA) + yimengite and hawthorneite (YIHA) or armalcolite (Figure 4.09B). Groundmass ilmenite morphology eventually changed with the crystallization of smaller (<30μm), variably zoned, subhedral to euhedral crystals. Apatite is interpreted as the final stage of magmatic growth with apatite sprays filling the remaining available space without the inclusion of any previously mentioned mineral phases.

Following magmatic crystallization, the Dharma kimberlite underwent at least two stages of both fluid precipitation and alteration. Euhedral, prismatic calcite precipitated from fluids forming groundmass calcite which then was enveloped in anhedral, microcrystalline carbonate and serpentine segregations (Figure 4.03G details segregation textures). At the same time and subsequently, olivine was variably altered to magnetite and serpentine (Figure 4.03H) while phlogopite phenocrysts variably replaced with magnetite and chlorite. Final alteration episodes are marked by macroscopic and microscopic carbonate veins crosscutting both hypabyssal and volcaniclastic kimberlite. Two stages of carbonate alterations are observed in the volcaniclastic kimberlite. One stage composed of larger veins with euhedral calcite is found exclusively in framework clasts. This alteration is likely similar to the carbonate alteration found in Dharma hypabyssal kimberlite. One stage of carbonate veins does not cross cut framework clasts indicating that carbonate alteration continued after the emplacement of the Dharma kimberlite diatreme in the upper crust.

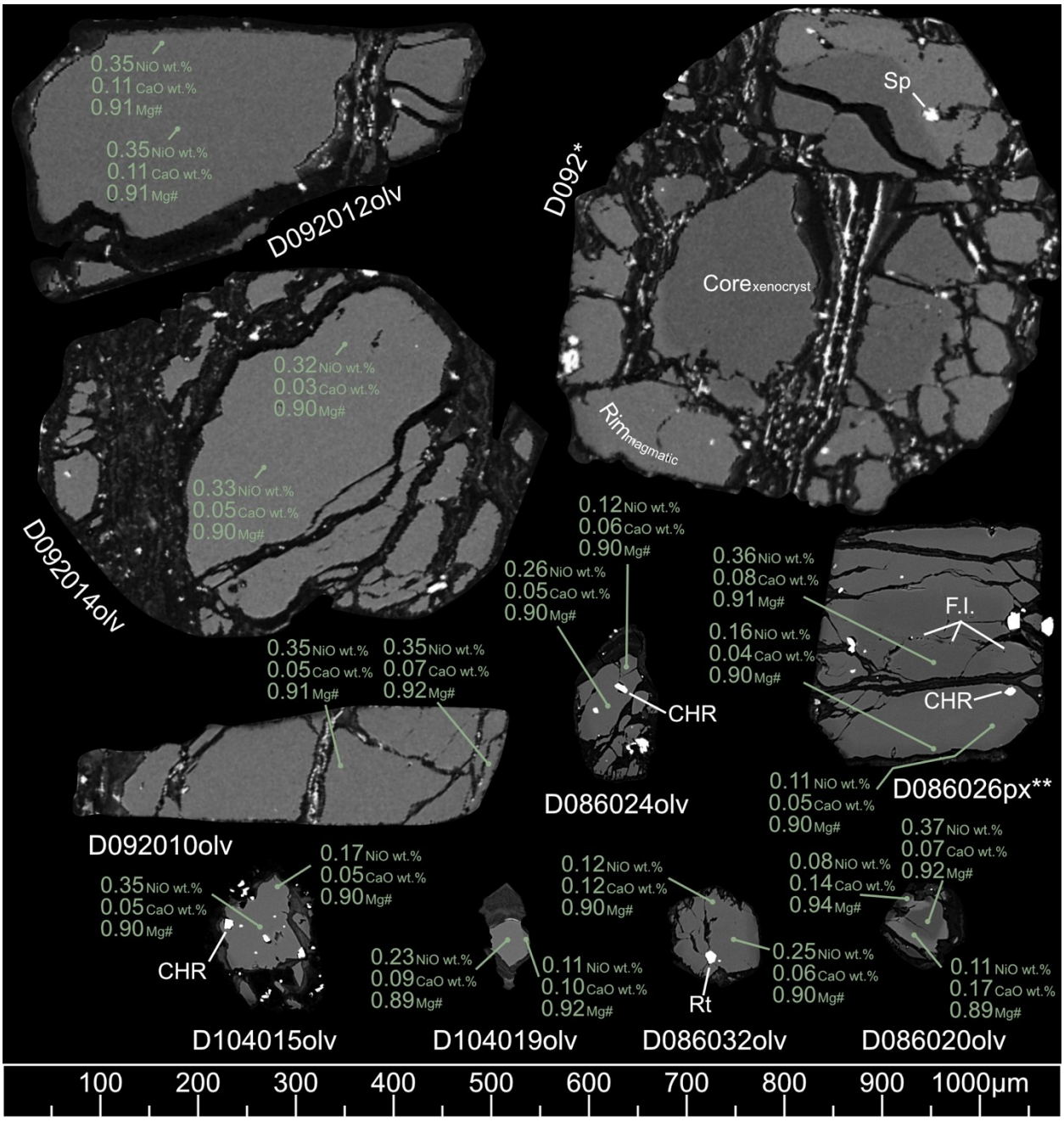

*Figure 4.23: Phenocryst, microphenocryst, and groundmass olivine morphology from hypabyssal Dharma kimberlite. Plotted with CaO, NiO, and Mg-number (Mg#) compositions. *olivine not analyzed. **olivine labeled as px (pyroxene) during EPMA analysis. Abbreviations: CHR – Cr-rich spinel, $Core_{xenocryst}$ – xenocryst olivine core, F.I. – fluid inclusion with a linear trend, $Rim_{magmatic}$ – early magmatic olivine rim with inclusions of spinel, Rt – rutile, Sp – spinel (not analyzed).*

4.5.3 Crustal Contamination and Secondary Alteration of the Dharma Kimberlite

The geochemistry of the Dharma kimberlite, as with most kimberlites, is influenced by crustal xenolith/xenocryst and mantle xenolith/xenocryst contamination accompanied by significant secondary alteration. Although geochemical samples were picked on the basis of least observable contamination, xenoliths and xenocrysts are still detectable in most of the samples analyzed. Crustal xenoliths constitute up to 6 volume % and mantle xenoliths constitute up to 4 volume % in the Dharma kimberlite while garnet xenocrysts constitute up to 5 volume % and clinopyroxene xenocrysts constitute up to 5 volume %. Additionally, carbonate veins associated with alteration are present in most volcaniclastic samples and one sample of hypabyssal kimberlite (D94, Appendix A.17).

A CCI of less than 1.3 and a ln (Si/Al) of greater than 2.3 both provide a potential measure of uncontaminated kimberlite (Clement, 1982; Sarkar et al., 2018). As was mentioned in Chapter 3, mantle olivine may mask crustal input in some circumstances (Kjarsgaard et al., 2009). Using these indices, all analyzed samples of hypabyssal kimberlite from Dharma classify as uncontaminated kimberlite. On the other hand, most volcaniclastic kimberlite samples from Dharma record ln(Si/Al) lower than 2.3 indicating that these samples are most likely contaminated. This result is expected as volcaniclastic kimberlite is produced in a more explosive environment than hypabyssal kimberlite. The relatively uncontaminated nature of the hypabyssal Dharma kimberlite samples is further constrained by their trace element and isotope compositions. REE patterns in the uncontaminated kimberlite generally preserve a linear distribution (Mitchell, 1986). All hypabyssal kimberlite samples from Dharam record near linear REE trace element distributions from LREE to HREE with the exception of small enrichment in Gd compared to Eu. This apparent

enrichment may be the result a higher concentration of garnet in some samples of hypabyssal kimberlite although this is typically coupled with enrichments in Sm and Eu (Shimizu, 1975).

Unlike hypabyssal kimberlite samples, volcaniclastic kimberlite samples of the Dharma kimberlite record elevated Zr, Y, and HREE. Assuming a linear distribution of REE in the volcaniclastic kimberlite, the elevated HREE are likely the result of greater degrees of crustal xenolith contamination. $\varepsilon Nd_{initial}$ and $\varepsilon Hf_{initial}$ compositions of the Dharma kimberlite are similar to the $\varepsilon Nd_{initial}$ and $\varepsilon Hf_{initial}$ compositions of the least contaminated sample of the Mel kimberlite (Chapter 3 section 3.4.3) and of other pre-Cretaceous kimberlites, being slightly supra-chondritic (Woodhead et al., 2019). Additionally, $^{87}Sr/^{86}Sr_i$ ratios of hypabyssal Dharma kimberlite samples fall within the mantle array with a small spread (0.7039 to 0.7046). Crustal contamination would affect the Dharma kimberlite samples by driving isotopic compositions towards negative εNd values, negative εHf, and higher $^{87}Sr/^{86}Sr$ ratios. Such effects of contamination on the isotope systematics of kimberlite are observed in samples from the Mel kimberlite (Chapter 3 section 3.4.3). In the absence of these characteristics, the isotope systematics of the Dharma kimberlite indicate low degrees of contamination and dominantly reflect their mantle source.

4.5.4 Magmatic Evolution and Mantle Source of the Dharma Kimberlite

As with any igneous rocks, it is important to establish the mantle sources and magmatic evolution that may have contributed to the formation of the Dharma kimberlite. The evolution of the kimberlite magma can be evaluated through the compositions of ilmenite megacrysts, olivine, and spinel as well as whole-rock major and trace element systematics, and whole-rock isotope signatures.

Ilmenite megacrysts record the early evolution of magma conditions. Ilmenite phenocrysts from the Dharma kimberlite are chemically classified as ilmenite megacrysts based on their Mg and Cr content. All ilmenite phenocryst cores are Mg and Cr rich with a median content of 13.06 wt.% MgO and 1.8 wt.% Cr_2O_3. The Fe^{2+} contents of ilmenite cores are about five to six time greater than Fe^{3+}. These compositional characteristics are found in most kimberlites and reflect a parental kimberlitic magma whose f_{O_2} increases with evolution (Mitchell, 1986; Wyatt et al., 2004; Golubkova et al., 2013; Mitchell et al., 2019). Once the partial melting of carbonated peridotite produces an Mg-rich proto-kimberlite melt, this melt will migrate to the base and lower part of the lithospheric mantle and precipitate ilmenite megacrysts (Mitchell, 1986; Moore and Belousova, 2005; Golubkova et al., 2013; Tappe et al., 2014). Once formed during the initial stage of "proto-kimberlite" activity and entrained in the parental kimberlite magma, Dharma ilmenite megacryst internal zones and rims record an increase in Mg (13.2 wt.% MgO median internal zone, 14.5 wt.% max rim). Most kimberlite ilmenites record an increase in Mg and Cr from cores to rims possibly indicative of magma mixing or the decomposition of magnesite during ascent (Schulze et al., 1995; O'Brien and Tyni, 1998; Wyatt et al., 2004). However, Mg appears to be the only component increasing in Dharma ilmenite megacrysts, with Cr_2O_3 content increasing from cores (1.8 wt.% median core) to intermediate zones (1.87 wt.% median intermediate zone) then decreasing to rims (1.72 wt.% max rim). A similar trend is observed in ilmenite megacrysts from the Monastery mine in South Africa where the crystallization of ilmenite megacrysts drives the depletion of Cr in the kimberlite magma, which, in turn, promotes the crystallization of the Cr-poor megacryst suite of minerals (Gurney et al., 1979; Moore et al., 1992). The Fe^{2+}/Fe^{3+} ratios generally decrease from

ilmenite megacryst cores to rims indicating that kimberlite magma became progressively more oxidized throughout the crystallization of ilmenite megacrysts.

The crystallization of MUM spinel + rutile + armalcolite as "rinds" on ilmenite megacrysts indicates that the ilmenite megacrysts are in disequilibrium with the host kimberlite magma. Such reaction zones indicate an enrichment in Ti content of the evolved kimberlite magma compared to the more primitive, parental kimberlite melt recorded in the ilmenite megacryst cores (Schulze et al., 1995; Kamenetsky et al., 2014).

Olivine in the Dharma kimberlite also records the evolution of the kimberlite magma. Olivine from harzburgite and dunite microxenoliths indicates that the Dharma kimberlite was sourced in a mantle with tightly constrained major and minor element composition. Microxenoliths record Mg-numbers between 0.90 and 0.91, a median NiO contents of 0.36 wt.%, and a median CaO contents of 0.05 wt.% (Appendix C.01). These Mg-numbers are not as depleted as those of typical Slave craton peridotites, or surrounding areas (Liu et al., 2021). The cores of all olivine phenocrysts record nearly identical compositions (0.89 to 0.92 Mg-number, 0.91 median Mg-number, 0.36 wt.% median NiO, 0.04 wt.% median CaO). Correspondingly, all phenocryst olivine cores are likely xenocrysts sourced from the same mantle wall-rocks in the form of microxenoliths.

The incorporation of olivine xenocrysts into a kimberlite melt will result in rims with decreasing NiO and TiO_2 coupled with increasing CaO and MnO contents at a similar Mg-number from core to rims (Giuliani, 2018; Mitchell et al., 2019). The decoupling of minor elements from Mg reflects the fractionation of olivine and chromite alongside the enrichment of Ca and Mn in residual melt

(Howarth and Taylor, 2016; Giuliani, 2018). This effect can be observed in one Dharma olivine rim analysis from the contact between an olivine from a dunite microxenolith and the host kimberlite. Most olivine analyses from this microxenolith record tightly constrained NiO (0.3 to 0.33 wt.%), TiO_2 (up to 0.04 wt.%), MnO (0.1 to 0.11 wt.%), and CaO (0.05 wt.%) contents. However, the rim of one olivine that is in contact with the groundmass of the Dharma kimberlite displays lower NiO (0.16 wt.%) and TiO_2 (<LOD) along with higher MnO (0.13 wt.%) and CaO (0.08 wt.%) concentrations. This compositional change reflects a depletion of Ni and Ti in the kimberlite melt coupled with an enrichment in Mn and Ca. Similar trends are observed in the intermediate zones of olivine phenocrysts (n=9) and microphenocrysts (n=2) with NiO content less than 0.3 wt.%. These intermediate zones display a decrease in NiO and increase in CaO from mantle compositions towards equilibration with the low-Ni, higher-Ca kimberlite magma within the Mg-number range of 0.89 to 0.91. These internal zones often include CHR (Cr-rich) spinel, providing further evidence for simultaneous olivine and chromite fractionation in the Dharma kimberlite. A portion of rims in phenocryst (n=20, <0.3 wt.% NiO), microphenocryst (n=15, <0.3 wt.% NiO), and groundmass olivine (n=3) reflects similar decreases in NiO and increases in CaO at constrained Mg-numbers (0.89 to 0.91 in phenocrysts, 0.90 to 0.92 in microphenocrysts and groundmass olivine). It should be noted that whole-rock Ni concentrations also decrease at a nearly constant Mg content (Figure 4.16A), similar to the trend outlined above. A few analyses of microphenocryst (n=3) and groundmass (n=1) olivine record an increase in Mg-number (up to 0.97) and CaO (up to 0.16 wt.%) with decreasing NiO. This trend is characteristic of olivine "rinds", which are interpreted to reflect increasing oxidation in the host kimberlite magma which, in turn, increases the forsterite content of olivine (Howarth and Taylor, 2016; Giuliani, 2018; Mitchell et al., 2019).

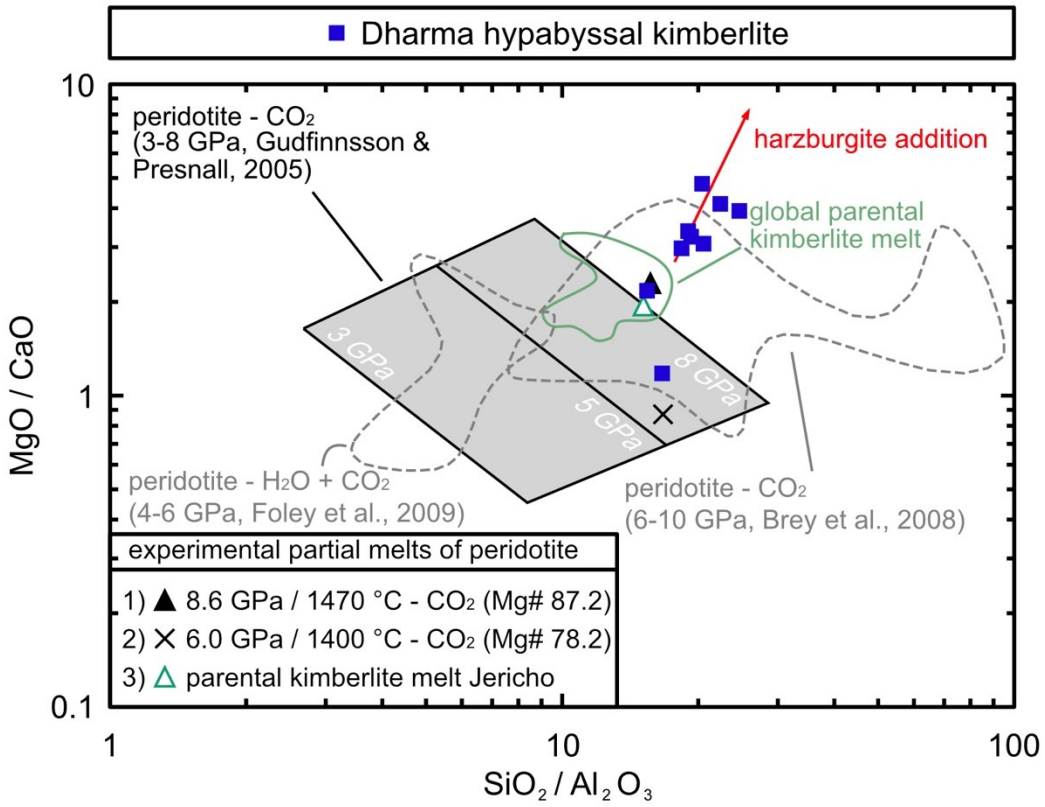

Figure 4.24: MgO/CaO against SiO_2/Al_2O_3 plot of the Dharma kimberlite. Plot after Tappe et al. (2014). With non-contaminated contamination indices plotted. Field of global parental kimberlite melt after Le Roex et al. (2003), Harris et al. (2004), Becker & Le Roex (2006), Kamenetsky et al. (2007), Kopylova et al. (2007), and Kjarsgaard et al. (2009). Harzburgite addition vector towards average slave craton harzburgite with composition after Kopylova and Russell (2000), Kopylova and Caro (2004), Wittig et al. (2008), and Liu et al. (2018). Experimentally produced melt compositions from synthetic carbonated peridotite with phlogopite between 4 and 6 GPa after Foley et al. (2009) and from synthetic peridotite with no phlogopite between 6 and 10 GPa after Brey et al (2008). Experimental partial melts of peridotite after 1) Dasgupta et al. (2009) and 2) Brey et al. (2008). Value for 3) parental kimberlite melt Jericho after Tappe et al. (2013).

Spinel compositions of the Dharma kimberlite fall into the “Trend 1” (magnesian-ulvöspinel) domain. This compositional trend is well established in most archetypal kimberlites and details significant compositional changes in the evolving kimberlite melt (Mitchell, 1986; Mitchell et al., 2019). The few Cr-rich spinels (CHR) from the Dharma kimberlite reflect early crystallization products that occurred while a considerable amount of Cr was still abundant in the kimberlite melt. Typically, these spinel crystalize in a carbonate rich melt (Roeder and Schulze, 2008). During ascent, Ti-rich spinels became more abundant resulting in the domination of MUM spinel compositions in kimberlite groundmass spinels. These compositional trends indicate that the Cr and Mg rich magma evolved to become more Ti-rich. Notably, representative spinel compositions from the Churchill kimberlite field share a very similar distribution in Ti-rich and Cr-rich spinel further supporting a similar magma source between the two kimberlite fields (Figures 4.08A and 4.08B; Zurevinski et al., 2008). Additionally, the zonation of spinels to higher Mg-numbers indicates that the Dharma kimberlite may have developed from a high-Mg silicate melt similar to the Majuagaa kimberlite (Nielsen and Sand, 2008).

Additional constrains on the conditions of magma formation are derived from the MgO/CaO against SiO_2/Al_2O_3 systematics of bulk hypabyssal kimberlite compositions (Figure 4.24. All samples of hypabyssal kimberlite from Dharma are included in this consideration as they are all classified as uncontaminated kimberlite (i.e. CCI <1.3 and ln(Si/Al)>2.3). Dharma kimberlite whole-rock compositions fall within the field of compositions proposed for kimberlite melt from the Slave craton (Tappe et al., 2013). Additionally, Dharma kimberlite compositions trend to harzburgite compositions demonstrating that a portion of kimberlite is being contaminated by harzburgite material (Figure 4.24). Dharma kimberlite compositions resemble experimentally

derived, near-solidus partial melts of phlogopite-poor, carbonated peridotite at pressures between 6 GPa and 10 GPa. This indicates that the primary melt of the Dharma kimberlite was likely produced in the convecting asthenospheric mantle from a partial melt of carbonated, volatile enriched peridotite. Likewise, the low abundance of phlogopite in the Dharma kimberlite serves as further evidence of a melt derived from a phlogopite-poor mantle source (Frost, 2006).

Furthermore, the trace element characteristics of Zr-Hf depletion coupled with high LREE/HREE ratios have been reproduced in trace element modeling of kimberlite melts derived from a low-degree partial melting of CO_2-rich, fertile peridotite in the convecting upper mantle beneath thick lithosphere (Tappe et al., 2014). Additionally, high Zr-Hf compositions are found in highly micaceous kimberlites, suggesting that the Zr-Hf depletion is a normal occurrence for mica-poor kimberlite such as Dharma (Mitchell, 1986).

The Dharma kimberlite shares the above trace element characteristics with the Jericho and Muskox kimberlites (Figures 4.17A and 4.17B). Assuming these trace element characteristics could be the result of similar processes, the Dharma kimberlite magma was likely similarly produced through the 0.7 to 0.9 % partial melting of carbonate-rich peridotite at depths of 200 to 300 km (Price et al., 2000). One key difference is the overall lower concentration of trace elements in hypabyssal kimberlite samples of the Dharma kimberlite as compared with the range of trace elements in the Jericho kimberlite. This is most likely due to the greater concentration of olivine in Dharma (18% to 30% phenocryst, 5% to 12% microphenocryst) than in Jericho (<15%, Price et al., 2000; 20% to 25%, Kopylova et al., 2007). However, this may not fully describe the lower trace element content of Dharma as there is no clear inverse correlation between La and MgO contents in samples

of hypabyssal kimberlite. On the other hand, the Muskox kimberlite shares nearly identical trace element concentration and a slightly lower concentration of olivine (15% to 20%; Hayman et al., 2009). If a similar source produced the Dharma kimberlite, an even lower bulk-rock trace element concentration would be observed in Dharma than in Muskox. Therefore, it is likely that the source of the Dharma kimberlite is compositionally closer to the Jericho kimberlite than to the Muskox kimberlite and that the lower bulk trace element concentration is the result of olivine dilution in the Dharma kimberlite.

The source region for the parental Dharma kimberlite melt is further constrained by Nd-Sr-Hf isotopes. Samples of the Dharma kimberlite plot onto the Nd-Sr isotope mantle array (Figure 4.19A) and have slightly super-chondritic Hf isotopes (Figure 4.19B). Kimberlites with similar Nd-Sr-Hf isotope compositions are interpreted to be sourced from a convecting mantle source that is broadly chondritic to super chondritic (slightly depleted in Sm/Nd, Lu/Hf and Rb/Sr relative to chondrite; Woodhead et al., 2019; Pearson et al., 2019). Although the Dharma kimberlite's $^{87}Sr/^{86}Sr_{initial}$ composition is within the range of $^{87}Sr/^{86}Sr_{initial}$ from Muskox the $\varepsilon Nd_{initial}$ of Dharma is considerably higher. However, the Muskox isotopic compositions may reflect the incorporation of garnet xenocrysts. The Nd-Sr-Hf isotope systematics of Dharma most similar to the Jericho kimberlite indicating that their sources experienced similar time-integrated isotopic evolution.

The Sr-Nd-Hf isotope systematics of the Dharma kimberlite suggest the similarity of its mantle source region to that which produces Ocean Island Basalt (OIB). Many Mid-Mesozoic to Eocene kimberlites share OIB isotope affinities that are interpreted to be the result of the incorporation of ancient subducted lithosphere in the mantle or by mixing with OIB-like melts in the lithosphere

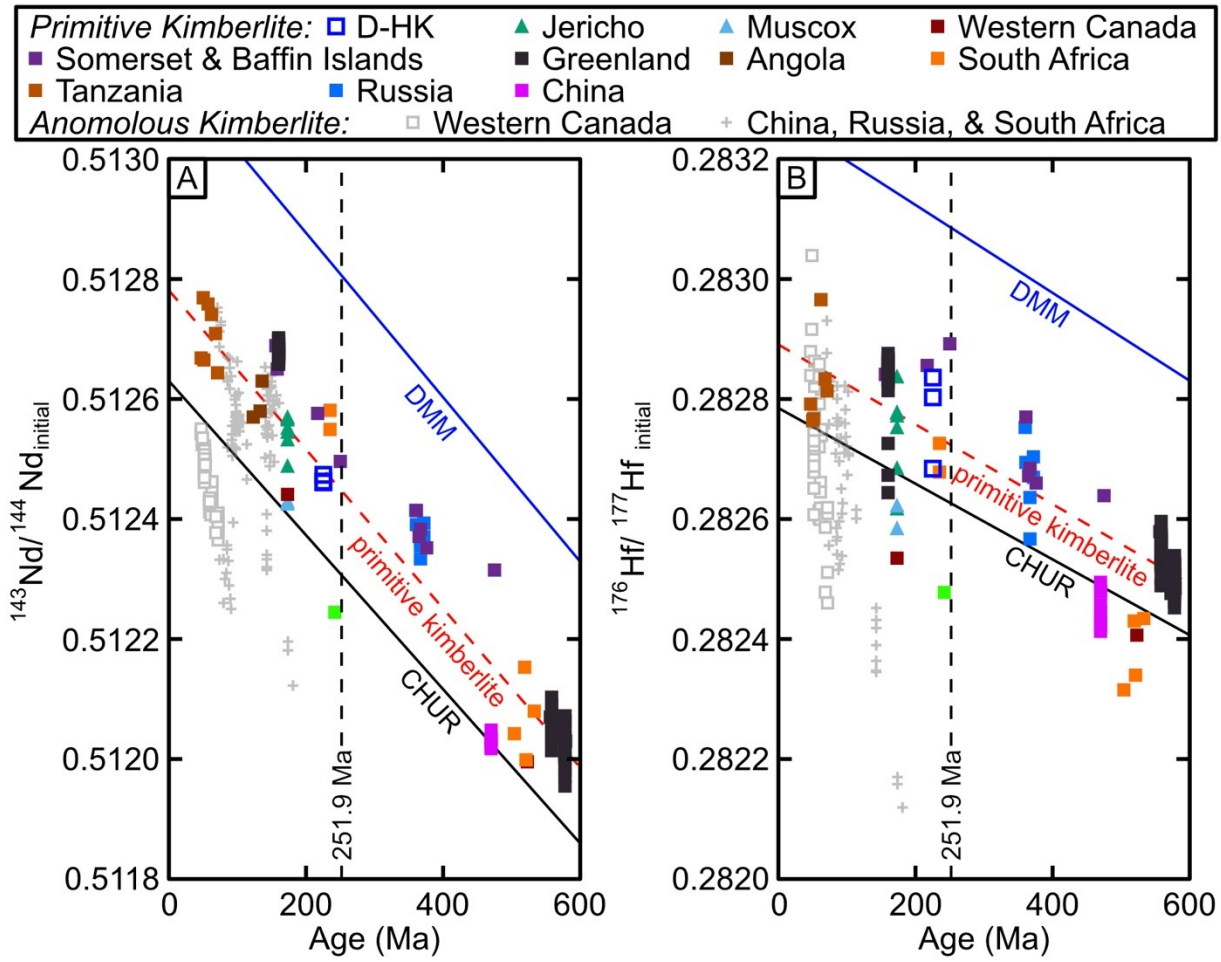

Figure 4.25: Hypabyssal Dharma kimberlite compared to the isotope evolution of global primitive kimberlite. Isotope evolution of the global kimberlite dataset for primitive (solid color symbols) and anomalous (light grey color symbols) kimberlites after Woodhead et al. (2019). A) $^{143}Nd/^{144}Nd_{initial}$ against Age plot. B) $^{176}Hf/^{177}Hf_{initial}$ against Age plot. Black dotted line (251.9 Ma) refers to Paleozoic – Mesozoic time boundary. Labels: D-HK – Dharma hypabyssal kimberlite, CHUR – Chondrite uniform reservoir model composition after Bouvier et al. (2008), DMM – Depleted mantle for Nd after Blichert-Toft and Puchtel (2010) and Hf after Dhuime et al. (2011), primitive kimberlite – regression line of primitive kimberlite compositions after Woodhead et al. (2019). Dotted line "251.9 Ma" corresponds to Paleozoic to Mesozoic boundary.

(Woodhead et al., 2019; Pearson et al., 2019). In contrast, the early Mesozoic Dharma kimberlite has Nd isotopic characteristics that are more similar to the consistently slightly super-chondritic values that characterize kimberlites older than the Mesozoic, such as the Churchill kimberlite field, Nunavut (Figure 4.19A; Zurevinski et al., 2011). Furthermore, the Dharma kimberlite plots onto the evolution line of primitive kimberlite in both Nd and Hf isotope systematics (Figures 4.25A and 4.25B) indicating that the Dharma kimberlite may be the result of CHUR and DMM reservoir mixing found in other primitive kimberlites despite it being surrounded by Mesozoic to Cenozoic kimberlites with anomalous isotope compositions (Woodhead et al., 2019). The kimberlite magmatism at Kirkland Lake, Timiskaming, and the Churchill field along with the New England and Great Meteor oceanic seamount magmatism is interpreted as the progression of the Great Meteor hotspot beneath North America and the northeast Atlantic Ocean (Heaman et al., 2004, 2019; Zurevinski et al., 2011). Following this reasoning, it is possible that the earliest stages of this hotspot (ca. 225 Ma) promoted melting of this primitive kimberlite mantle reservoir producing the Dharma kimberlite.

4.5.5 Emplacement Age and Regional Implications

Rb-Sr geochronology results detailed in section 4.3.5 indicate that the Dharma kimberlite was emplaced in the Late Triassic (approx. 225 Ma). This isochron age is calculated using samples from both hypabyssal and volcaniclastic lithofacies of the Dharma kimberlite. Model ages show little variation between six samples of hypabyssal kimberlite (218 Ma to 225 Ma; Table 4.08) and one sample of phlogopite from volcaniclastic kimberlite (219 Ma to 220 Ma; Table 4.08). As such, this age is assumed to be an accurate estimate of emplacement for all intrusive and extrusive phases of the Dharma kimberlite.

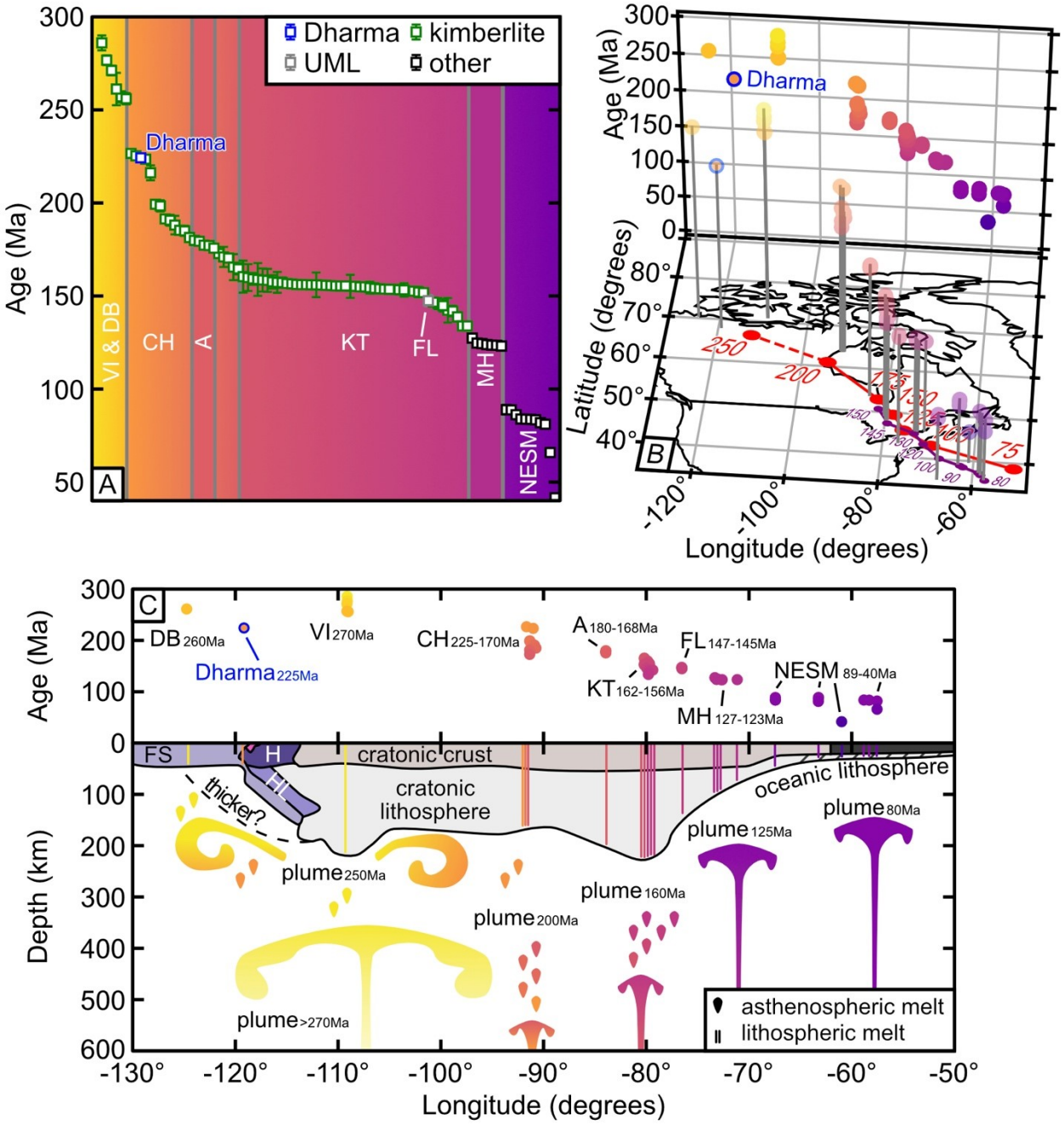

Figure 4.26: Age of the Dharma kimberlite compared to Great Meteor hotspot related magmatism and hypothesized Great Meteor hotspot track. A) Ages of Paleozoic to Cenozoic Great Meteor hotspot magmatism. Legend note: "other" for MH refers to gabbro, diorite, pyroxenite; for NESM refers to basalt. B) Age against geographic location for select Paleozoic to Cenozoic ultramafic to mafic volcanism and the modeled (purple – Kinney et al., 2021) and interpreted paths of the Great Meteor Hotspot from Heaman et al. (solid red; 2019) and this study (dashed red). C) Cross-section depicting age progression of the Great Meteor Hotspot and associated magmatism. Labels: A – Attawapiskat (Heaman and Kjarsgaard, 2000), CH – Churchill kimberlite field (Zurevinski et al., 2008), DB – Darnley Bay kimberlite field (Brin and Pearson, 2014), FL – Finger Lakes UML and kimberlite (Heaman and Kjarsgaard, 2000), KT – Kirkland Lake and Timiskaming kimberlite fields (Heaman and Kjarsgaard, 2000), MH -Monteregian Hills (Foland et al, 1986), NESM – New England Sea Mounts (Duncan, 1984), VI – Victoria Island kimberlite fields (Heaman et al., 2003). Cross section references: Spratt et al. (2009), Zurevinski et al. (2011), and Snyder et al. (2014).

The Dharma kimberlite isochron age determined here (225.3 ± 0.4 Ma; Figure 4.18A) is somewhat unique in respect to other kimberlite intrusions in Canada. Dated kimberlites with Triassic ages are limited to the Cross Creek (British Columbia) kimberlite (241 ± 5 Ma; Figure 4.26A; Smith et al., 1988) and the Churchill kimberlite field (226.6 ± 2.2 Ma to 216.2 ± 4.0 Ma; Figure 4.26A; Zurevinski et al., 2008). In the immediate vicinity of the Dharma kimberlite, kimberlites with Permian emplacement ages are reported from the Darnley Bay kimberlite field (261.2 ± 8.7 Ma; Figure 4.26A; Brin and Pearson, 2014; Brin, 2016) and kimberlites from Victoria Island (286.0 ± 4.0 Ma to 256.0 ± 3.0 Ma; Figure 4.26A; Heaman et al., 2003). As was noted in section 4.5.4, the Dharma kimberlite shares very similar phlogopite and spinel compositions with phlogopite macrocrysts and representative spinels from the Churchill kimberlite field. Additionally, the oldest recorded ages from the Churchill kimberlite field are nearly identical to the Triassic isochron age of the Dharma kimberlite.

Plate reconstructions and modelling of low-shear-wave-velocity provinces (LLSVP) have yielded instances of their correlation with kimberlite magmatism. The origins of LLSVP are complex with interpretations ranging from recycled oceanic crust to fertilized primitive mantle domains (Deschamps et al., 2012; Jackson et al., 2018). Kimberlite magmatism in certain instances is tied to hotspots forming at the margins of LLSVP (Torsvik et al., 2010; Tappe et al., 2018). However, plate reconstructions variably include (Torsvik and Cocks, 2013; Tappe et al., 2018) or exclude (Torsvik et al., 2010; Torsvik, 2019) the location of the Dharma kimberlite in the zone of the TUZO/Africa LLSVP. As a result, this work will focus on a strict single plume hypothesis for the origin of kimberlite magmatism at Dharma.

Modelling of plate motions and hotspot tracks have identified hotspots as a potential source of kimberlite magmatism (Crough et al., 1980; Heaman et al., 2004). Additionally, kimberlite and CROL (previously Group 2 kimberlite) magmatism in South Africa is tied to the tracks of Atlantic hotspots (Le Roex, 1986; Roberts and Skinner, 1998). In the case of North America, several kimberlite fields are identified as possible surface expressions of the Great Meteor hotspot track starting near the location of the Churchill kimberlite field at ca. 225 Ma and terminating at the ca. 80 Ma near the terminus of the New England Seamounts (Heaman and Kjarsgaard, 2000; Heaman et al., 2004; Zurevinski et al., 2008, 2011; Kinney et al., 2021) before terminating at the present day location of Seewarte Seamounts (a.k.a. the Atlantis-Great Meteor Seamounts) just south of the Azores (Wendt et al., 1976). Evidence for the southeast trending movement of the Great Meteor hot spot is observed in certain kimberlite fields of Canada. Zurevinski et al. (2008, 2011) indicated that the 40 Ma span of kimberlite magmatism in the Churchill kimberlite field trends to younger age from the northwest to the southeast. Furthermore, alkaline plutonic complexes in the Monteregian Hills of Quebec display progressively younger ages from the west to the east over a span of ca. 4 Ma (Figure 4.26A; Foland et al., 1986). Likewise, the age of the New England Seamounts decreases from the Bear Seamount in the northwest to the Nashville Seamount in the southeast over a span of 20 to 30 Ma (Figure 4.26A; Duncan, 1984). All these magmatic centers build strong evidence for hotspot-driven, mantle-derived magmatism from Nunavut to the North Atlantic (Figure 4.26B).

The nearly identical ages between the Dharma kimberlite and the Churchill kimberlite field solicits the question of extending Great Meteor hotspot related magmatism further west in the Late Triassic. However, one key issue arises from this consideration. The distance between the

Churchill kimberlite field at Rankin Inlet and the Dharma kimberlite field at Great Bear Lake (1400 km) presents a potential issue. If the magmatism of both kimberlite fields was stimulated by mantle plumes, then it is problematic to tie each kimberlite to an actual epicenter of a mantle plume. Alternatively, the mantle hotspot at ca. 225 Ma likely fell somewhere between the Dharma kimberlite field and the Churchill kimberlite field which resulted in kimberlite magmatism produced at the margins of the expanding, very large diameter plume head (Figure 4.26C). The size of mantle plume-heads is assumed to be a function of depth (Campbell, 2001). For example, mantle plumes that originate in the deep mantle are capable of producing plume-heads with a radius of 1000 km (Ernst and Buchan, 2002). If a similarly sized mantle plume formed between the Dharma kimberlite field and the Churchill kimberlite field in the Triassic, the heat flow at the margins of the plume may have promoted melting in the asthenospheric mantle after the plume head reached the lithosphere, eventually producing kimberlite magmatism at both Dharma and Churchill locations (Figure 4.26C).

If a mantle plume impacted continental North America at the location and time suggested in the previous paragraph, then one would expect evidence of Late Paleozoic to Mesozoic magmatism near the center of the plume head. Most plumes are associated with large igneous provinces and extensive (giant) dyke swarms (Campbell, 2005; Ernst and Bleeker, 2010; Sobolev et al., 2011). However, no such magmatism is present in Canada possibly due to the well-established, thick, lithospheric keel of the Slave craton (Figure 4.26C). In the absence of such magmatism, the Permian kimberlite magmatism on Victoria Island and Darnley Bay provides a possible measure of the center of plume impaction of the Great Meteor hotspot in Arctic Canada. As previously mentioned, kimberlites from Victoria Island yield ages from 286.0 ± 4.0 Ma at Golden Plover to

256.0 ± 3.0 at Phalarope (Heaman et al., 2003). The Victoria Island kimberlites are then believed to be the result of initial Great Meteor hotspot related magmatism that began at ca. 282 Ma in the Permian time (Figure 4.26C – $plume_{>250Ma}$). The kimberlites at Darnley Bay are located approximately 600 km to the west of the Victoria Island kimberlites and record an emplacement age of 261.2 ± 8.7 Ma (Brin and Pearson, 2014; Brin, 2016). It is possible, that after the impact of the initial wide plume head, the extremities of the plume progressed around the epicenter of the plume (i.e. up and around the Slave mantle keel; Figure 4.26C – $plume_{250Ma}$). Due to a thinner lithosphere at Darnley Bay (Brin, 2016; Liu et al., 2018), kimberlite magmatism was able to make it to the surface in the west, while any kimberlite melts in the east failed to break through the thicker lithosphere (Figure 4.26C) until Eocene time.

If the Dharma kimberlite represents an extension of Late Triassic magmatism related to the Great Meteor hotspot track, then the new ages of from the Dharma kimberlite extend the extent of the Great Meteor hotspot further west than was previously modeled (Heaman and Kjarsgaard, 2000; Heaman et al., 2003; Zurevinski et al., 2011). Additionally, the dating of the Triassic Dharma kimberlite provides geodynamic context for Permian kimberlite magmatism at Victoria Island and at Darnley Bay. New kimberlite discoveries and associated geochronology may clarify how applicable this general model is.

4.5.6 Mantle Lithosphere Characteristics and Diamond Potential of the Dharma Kimberlite

Pyroxene and garnet xenocrysts were the predominant mantle material collected from separates of the Dharma kimberlite. Additionally, microxenoliths found within thin sections provide direct evidence for mantle domains and sampling depths of this kimberlite. Based on the mineralogy of

microxenoliths, the Dharma kimberlite sampled a layered mantle composed of dunite, garnet dunite, and garnet harzburgite, typical of cratonic mantle in general (e.g., Pearson et al., 2021). From the perspective offered by garnet Ca and Cr systematics (Figure 3.06A), the Dharma kimberlite additionally sampled lherzolite and wehrlite. As discussed in section 4.3.3.3, the Dharma kimberlite primarily sampled low-Ca lherzolite garnet (84% of all garnets analyzed). Furthermore, microxenolith olivine Mg-numbers from Dharma are only slightly lower than xenoliths from Victoria Island (0.92 Mg-number; Liu et al., 2018) and Darnley Bay (0.92 to 0.93; (Liu et al., 2018). These similarities indicate that the mantle beneath the Dharma kimberlite is compositionally similar to the cratonic peridotite xenoliths recovered from kimberlite at Darnley Bay and Victoria Island.

Clinopyroxene from the Dharma kimberlite records Cr_2O_3 and Al_2O_3 systematics similar to clinopyroxene from garnet peridotites from Archean nuclei to cratons (Figure 4.10C). Although the Dharma kimberlite lies in a Proterozoic region of the greater cratonic structure of the Laurentia super-craton (see Pearson et al., 2021 for definition), the lithospheric structure was thick enough in the Late Triassic to stabilize diamond and host kimberlites. Most probably, this was due to the thickening of the lithosphere during the Wopmay Orogeny (Figure 4.26C; Spratt et al., 2009; Snyder et al., 2014).

Trace elements from peridotite-derived garnet xenocrysts indicate that the mantle peridotite beneath the Dharma kimberlite experienced depletion and re-enrichment by various metasomatic agents. Garnets from all wehrlite, Ti-enriched lherzolite, Ti-enriched harzburgite, and some lherzolites display chondrite normalized positively sloped, depleted LREE with flat MREE and

HREE (Figure 4.12). This chondrite normalized trace element pattern is typical of lherzolite garnet from cratonic mantle and off-craton mantle (e.g., Lehtonen and O'Brien, 2009; Harris et al., 2018; Woodland et al., 2021). It is important to note, that LREE depletion and comparable HREE enrichment in garnets can be the result of equilibration with the Dharma kimberlite melt (Doucet et al., 2013). Some of the G10 garnets have HREE depleted patterns indicating a likely origin from residues depleted in the spinel stability field (e.g., Stachel et al., 1998).

Wehrlitic garnets scatter in the field of kimberlite metasomatism in terms of their Zr against Y systematics and Zr/Hf against Ti/Eu systematics. As mentioned in section 3.4.6, Na- and K-rich carbonatite melts are capable of increasing the CaO content of garnet at constant Cr_2O_3 content while dissolving orthopyroxene or converting it to clinopyroxene (Shatskiy et al., 2020). This process, dubbed "Wehrlitization", produces wehrlite assemblages from original (pre-metasomatic) lherzolite and harzburgite protoliths (Sokol et al., 2015; Shatskiy et al., 2020). The absence of wehrlite microxenoliths in the Dharma kimberlite indicates that the observed wehrlite garnets may be the result of proto-kimberlite melt metasomatism of lherzolite or harzburgite lithologies and the subsequent disruption of these products during eruption.

Chondrite normalized sinusoidal REE patterns are observed in low-Ca lherzolite garnets, lherzolite garnets, and harzburgite garnets (Figure 4.12). The lack of Ti in these garnets coupled with their Y and Zr systematics of relatively depleted peridotite compositions indicate that these garnets reflect mantle lithologies not significantly metasomatized by the kimberlite melt. As mentioned in section 4.3.3.3, garnet grains with sinusoidal REE patterns are characterized by positively-sloped LREE, a maximum REE concentration around the LREE-MREE transition (i.e. Nd to Sm),

negatively-sloped MREE and HREE, and a tail of positively-sloped HREE. The tail of positively-sloped HREE occurs after the MREE in G9B lherzolite garnet and some G9A low-Ca lherzolite garnet while in most G9A low-Ca lherzolite and all G10A harzburgite garnet the inflection point is at Tm (Figure 4.12C and Figure 4.12D). It should be noted that garnet grains with these characteristics represent a well-known geochemical signature of garnet from cratonic harzburgite (Shimizu, 1975; Shimizu and Richardson, 1987; Shatskiy et al., 2020).

Sinusoidal REE patterns in harzburgite garnet are interpreted as the result of a two-stage process: an initial depletion of LREE and HREE as a result of extracting large volumes of melt such as komatiite (Shimizu and Richardson, 1987; Stachel et al., 1998; Lehtonen, 2005; McLean et al., 2007), followed by an enrichment of LREE and/or MREE by fluid- (Stachel et al., 1998) or melt- (Burgess and Hart, 2004) related metasomatism. In the case of G10A harzburgite garnet, the enrichment likely did not occur by way of carbonatite-influenced melt metasomatism as is indicated by the Zr/Hf and Ti/Eu systematics of this garnet group (Figure 4.13; Burgess and Hart, 2004). HREE enrichment found in all chondrite normalized REE sinusoidal-pattern garnets from Dharma kimberlite is likely a reflection of low-pressure melting residues (Stachel et al., 2004).

Brin (2016) and Liu et al. (2018) reconstructed a geotherm for Northwest Arctic Canada from mantle xenoliths recovered from the Victoria Island and Darnley Bay kimberlite fields. These mantle xenoliths record a paleogeotherm at 286.0 ± 4.0 Ma to 256.0 ± 3.0 Ma for the mantle beneath Victoria Island (Heaman et al., 2003; Brin, 2016; Liu et al., 2018) and 261.2 ± 8.7 Ma for the mantle beneath Darnley Bay (Brin and Pearson, 2014; Brin, 2016; Liu et al., 2018). Assuming plume activity was the only source of disturbances from ca. 250 Ma to 225 Ma, we can extrapolate

Ni-thermometry in garnet to the Victoria Island and Darnley Bay geotherms to constrain the depth of mantle-sampling by the Dharma kimberlite.

The Victoria Island and Darnley Bay (Parry Peninsula) geotherms indicate the presence of a thick lithospheric keel west of the Slave craton, in the Proterozoic region of cratonic material, during Permian to Early Triassic times. Lherzolite garnet from the Dharma kimberlite generally records a unimodal distribution with the greatest concentration of G9A garnet sampled from mantle temperatures of 1150 °C to 1200 °C (Figure 4.27A) and the greatest concentration of G9B garnet sampled from 1100 °C to 1150°C (Figure 4.27B). This indicates that both normal lherzolite and low-Ca lherzolite mantle domains are derived from similar lithospheric depths. In contrast, harzburgite garnet portrays a bimodal temperature distribution with Ti-enriched harzburgite sampled from temperatures similar to lherzolite garnet (1100 °C to 1150°C, Figure 4.27C) but lower temperature, therefore shallower, than low-Ca harzburgite garnet (1300 °C to 1350°C, Figure 4.27C). The temperature range recorded by garnet xenocrysts from the Dharma kimberlite indicates a mantle sample derived from depths between 141 km and 202 km based on the Victoria Island geotherm, or between 119 km and 170 km based on the Darnley Bay geotherm. Lherzolite garnet was sampled across this range with the greatest concentration sampled at a depth of 177 km to 182 km based on the Victoria Island geotherm, or 149 km to 154km based on the Darnley Bay geotherm (Figure 4.27D). Harzburgite garnet was sampled across approximately the deeper half of this range with the greatest concentration sampled at a depth of 176 km to 181 km based on the Victoria Island geotherm, or 148 km to 153 km based on the Darnley Bay geotherm (Figure 4.27D). Due to the proximity of the Dharma kimberlite to the Darnley Bay kimberlite field, it is more likely that the geotherm from Darnley Bay is a more accurate measure of the mantle geotherm

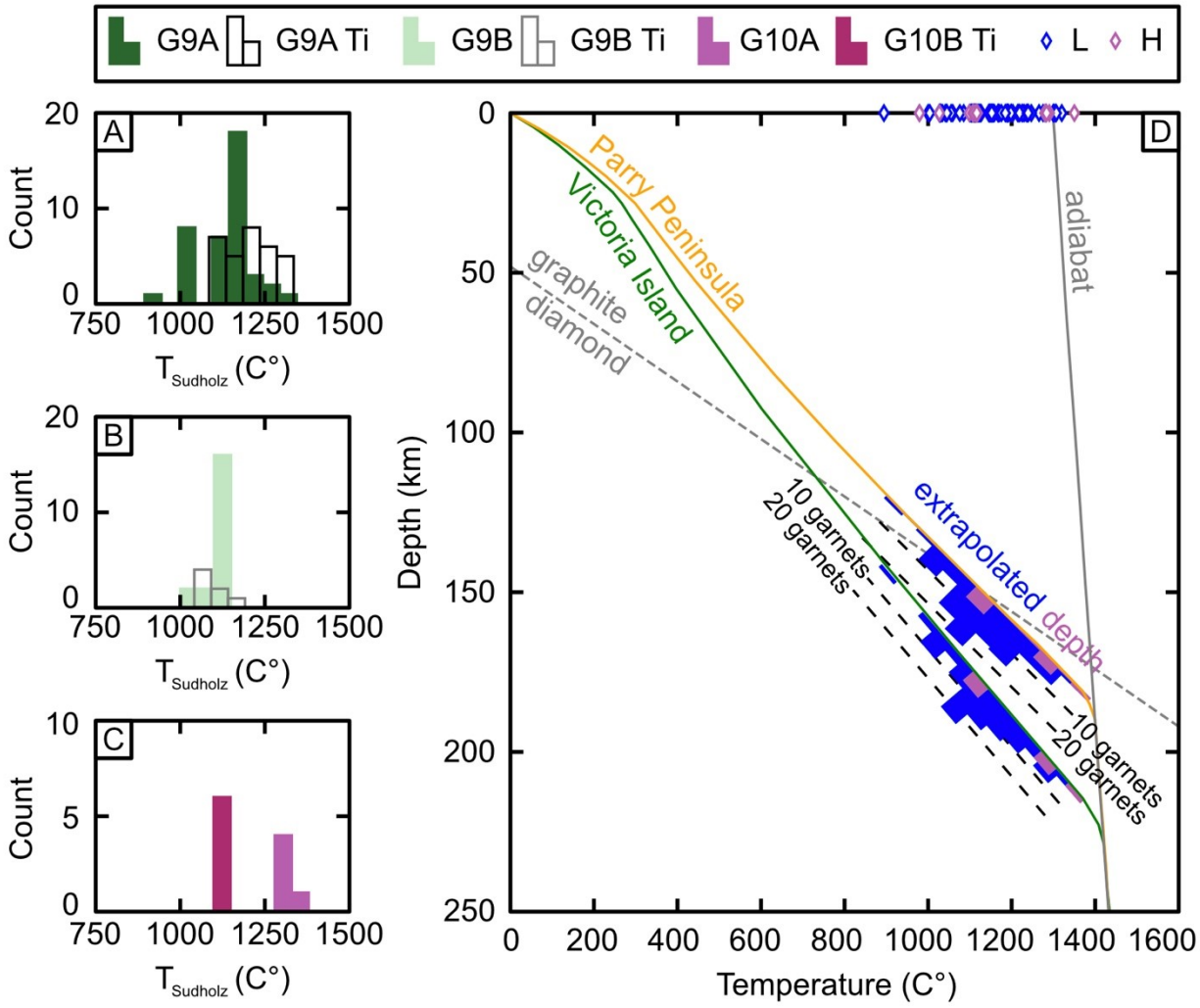

Figure 4.27: Mantle temperatures and derived depths of garnet xenocrysts sampled by the Dharma kimberlite. A), B), and C) Histograms of the distribution of mantle temperatures (bin width = 50°C) beneath the Dharma kimberlite calculated from Ni in garnet thermometry after Sudholz et al. (2021). D) Ni in garnet temperatures extrapolated onto the Parry Peninsula and Victoria Island geotherms (Liu et al., 2018) with histograms of peridotite (blue) and harzburgite (pink) garnet by extrapolated depth (bin width = 5 garnets). Graphite to diamond transition line after Kennedy and Kennedy (1976). Abbreviations: G9A – low-Ca lherzolite, G9B – lherzolite, G9A Ti – Ti enriched low-Ca lherzolite, G9B Ti – Ti enriched lherzolite, G10A – low-Ca harzburgite, G10B-Ti – Ti enriched harzburgite, L – lherzolite garnet, H – harzburgite garnet.

beneath Dharma. This is further supported by the chemistry of G10A harzburgite garnet which plots onto the 47 kbar isobar (Figure 4.11A) indicating a sampling depth of 174km (assuming 3.7 kbar = 37 km). In that case, the Dharma kimberlite sampled 49% of its garnet xenocrysts from below a depth of 150km indicating that half of the kimberlite's mantle load was acquired from within the diamond stability field during ascent.

Using conventional peridotite garnet evaluation, the garnet record from the Dharma kimberlite presents strong evidence for diamond potential. 46% of harzburgite garnet (5% of total analyzed garnets) fall within the diamond stability field on the Darnley Bay geotherm despite the lithosphere not extending far into the diamond stability field (Figure 4.27D). Peridotite diamond inclusions are overwhelmingly associated with harzburgite compositions (Stachel and Harris, 2008). This association reflects the subsolidus diamond crystallization conditions that are more efficient than melt-driven diamond crystallization in lherzolite and eclogite lithologies (Stachel and Luth, 2015). Additionally, the sinusoidal REE patterns recorded by lherzolite and harzburgite garnet from the Dharma kimberlite are typically associated with diamond-forming fluids (Stachel et al., 2018). Furthermore, a total of 106 diamonds are recovered from diamond drill core hole DD07GH001 in the Dharma kimberlite with a median concentration of 3.33 stones per 10 kg (Gill, 2016). Of the 106 diamonds, two macrodiamonds greater than 0.85 mm were recovered from the upper volcaniclastic kimberlite. Both of these macrodiamonds range from 0.0096 to 0.06315 carats, have transparent-brown color, and have fragmented octahedral morphologies, indicating that there is a potential for larger stones.

4.6 Conclusions

1. The Dharma ultramafic intrusive diatreme discovered in Diamond Drill Hole DD07GH001 by Sanatana Resources Inc. has petrographic, mineral chemical, geochemical, and isotopic characteristics that identify them as archetypal kimberlites. Subtle variations in modal mineralogy, whole-rock major and trace element chemistry, and diamond content are observed in volcaniclastic and hypabyssal kimberlite domains down-hole. This indicates that the Dharma diatreme is composed of tuffisitic and brecciated kimberlite intruded by at least two separate phases of hypabyssal kimberlite.

2. The Dharma kimberlite shares petrographic, geochemical, and isotopic characteristics with other kimberlites in Arctic Canada including the Jericho and Muskox kimberlite, kimberlites from the Darnley Bay kimberlite field, and kimberlites from the Churchill kimberlite field.

3. The Rb/Sr mica isochron emplacement age of 225.3 ± 0.4 Ma for the Dharma kimberlite indicates emplacement in the Triassic, with only some of the Churchill kimberlite field bodies being close to this age. If considered in the context of the Great Meteor hotspot hypothesis of Heaman et al., (2004), the Dharma eruption would place this hotspot track further to the northwest, potentially providing a context for kimberlite magmatism at Victoria Island, Darnley Bay, and Rankin Inlet (Churchill kimberlite field). The Dharma kimberlite and kimberlites of the Churchill kimberlite field could reflect kimberlite magmatism produced during the initial stages of a large-scale mantle plume that initially impacted the lithosphere in northern Canada and formed kimberlites in Victoria Island and Darnley Bay.

4. Sr-Nd-Hf isotope systematics and whole-rock geochemistry indicate that the parental magma of the Dharma kimberlite was sourced from the asthenospheric mantle, with similar isotope systematics to pre-Mesozoic kimberlites.

5. Assuming a similar paleo geotherm beneath Dharma to that established by xenoliths from the kimberlites of Darnley Bay (Parry Peninsula) and extrapolating garnet Ni-temperatures to this geotherm indicates that the Dharma kimberlite sampled approximately 50% of its mantle load from the diamond stability field. Furthermore, The Dharma kimberlite hosts a significant amount of G10 harzburgite garnet (49% of harzburgite garnet) that is interpreted to be recovered from within the diamond stability field. A total of two fragmented macrodiamonds (0.0096 to 0.06315 carats) and 104 microdiamonds have been recovered from diamond drill core hole DD07GH001.

Chapter 5: Conclusions and Recommendations for Further Work

5.1 Mel Kimberlite Conclusions

Based on geochemical and petrographic characteristics, the intrusive bodies at the Mel property are characterized as archetypal kimberlites. Samples available from diamond core drilling at the Mel property indicate that the intrusions are hypabyssal and identify three principal kimberlite bodies: ML8 Upper, ML8 Lower, and ML345. Most likely, the three bodies of the Mel kimberlite compose a dike system characteristic of kimberlite root zones worldwide. All bodies of the Mel kimberlite are classified as serpentine + phlogopite + carbonate + spinel + apatite + ilmenite kimberlites that have succumbed to various levels of weathering and surficial alteration. Subtle variations in ilmenite mineral chemistry and whole-rock major and trace elements are observed between ML8 Upper, ML8 Lower, and ML345. Generally, ML8 Upper and ML8 Lower share a bimodal ilmenite distribution in Al_2O_3 and lower Fe_2O_3 than ML345, while ilmenite from ML345 has a higher MnO content. Additionally, the major and trace element signature and whole-rock isotope signature of ML345 suggests a higher degree of alteration and contamination than recorded by ML8 Upper and ML8 Lower bodies.

The Mel kimberlite shares its petrographic features, along with geochemical characteristics, with other kimberlites on the Melville Peninsula, including Aviat and Naujaat. Likewise, the Mel kimberlite shares an Rb-Sr phlogopite isochron age (555.58 ± 1.40 Ma) with other expressions of kimberlite magmatism on the Melville Peninsula. The primitive proto-kimberlite magma was formed in the asthenospheric mantle and later evolved like an archetypal kimberlite before erupting at the Mel property. The span of Late Proterozoic to Early Cambrian magmatism in the Melville

peninsula is interpreted as the result of initial stages of rifting preceding the formation of the Iapetus ocean. Mantle garnet xenocrysts brought up to the surface by the Mel kimberlite indicate a heterogeneous mantle composed of lherzolite (including "wehrlitized" lherzolite) and eclogite. Although no strong sinusoidal REE signatures are detected in the garnets, the Mel kimberlite sampled 86% of its mantle load from within the diamond stability field assuming a paleo-geotherm similar to the western Rae craton. Four macrodiamonds were recovered from the Mel kimberlite to date proving that the kimberlite is diamond-bearing.

5.2 Dharma Kimberlite Conclusions

Based on geochemical and petrographic characteristics, the intrusive and extrusive bodies at the Greenhorn property are classified as the archetypal kimberlite. Samples available from diamond drilling at the Greenhorn property indicate that the Dharma kimberlites consist of a layered volcaniclastic tuff and breccia with at least two separate intrusive pulses of hypabyssal kimberlite. Generally, the hypabyssal Dharma kimberlite is classified as an ilmenite + apatite + serpentine + spinel + carbonate + olivine kimberlite. Kimberlite tuff, which occurs from surface to a depth of ca. 82 m is poorly-sorted, crystal and clast–rich, clast-supported volcaniclastic kimberlite. The two separate domains of hypabyssal kimberlite are HK_1 and HK_2. HK_1 is characterized by higher Al_2O_3 and CaO than HK_2 while HK_2 has the highest content of MgO, Nb, La, and Cr. Amongst all investigated samples, diamond concentration is highest in the volcaniclastic kimberlite tuff with a median value of 4.09 stones / 10 kg, with HK_1 being second highest with 3.24 stones / 10kg, and HK_2 being the lowest with 3.11 stones /10kg. Two fragmented macrodiamonds (0.0096 to 0.06315 carats) were recovered from the volcaniclastic kimberlite tuff samples with a concentration of

2.42 stones / 10kg and 6.73 stones /10 kg, respectively. The presence of fragmented macrodiamonds in the Dharma kimberlite indicates a potential for larger intact stones.

Rb-Sr phlogopite geochronology established an isochron age of 225.3 ± 0.4 Ma for the Dharma kimberlite. The Dharma kimberlite shares some petrographic and geochemical characteristics with other Late Triassic and Permian kimberlites from Victoria Island, Churchill, and Darnley Bay kimberlite fields. The age and geographic location of the Dharma kimberlite provide an additional geodynamic context for the Permian kimberlite magmatism on Victoria Island and at Darnley Bay, expanding the track of the Great Meteor hotspot to Western Canada in the Late Permian to Early Triassic. In principle, the Dharma kimberlite likely represents the waning stages of the impaction of a large-scale mantle plume that initially produced kimberlite magmatism at Victoria Island.

Mantle microxenoliths from the Dharma kimberlite provide evidence for the heterogeneous mantle composed primarily of garnet lherzolite, garnet harzburgite, and dunite. Clinopyroxene mineral chemistry further classifies a portion of the mantle beneath the Dharma kimberlite as “on-craton garnet peridotite”. Furthermore, mantle garnet xenocrysts brought up to the surface by the Dharma kimberlite indicate that the mantle is composed of lherzolite (including “wehrlitized” lherzolite) and harzburgite. Several lherzolite and harzburgite garnets record chondrite normalized, sinusoidal REE patterns indicating a signature associated with a mantle that has been metasomatized by diamond-forming fluids. Assuming a paleo-geotherm similar to that of the mantle beneath Darnley Bay, 49% of the mantle load sampled by the Dharma kimberlite was sourced from the diamond stability field. As mentioned previously in this section, the presence of a considerable number of

microdiamonds and two macrodiamonds in diamond drill core hole DD07GH001 indicates that the Dharma kimberlite is diamond-bearing.

5.3 Recommended Further Work

A significant amount of new research on both the Mel kimberlite and Dharma kimberlite is presented in this work. However, certain unresolved questions and untapped opportunities still exist for further work.

5.3.1 Further Work on the Mel Kimberlite

Two key opportunities for further work on the Mel kimberlite are identified below. These recommendations are likely to contribute to further understanding of kimberlite magmatism on the Melville Peninsula.

Perovskite was not the main target for the geochronological component of this study. However, perovskite is present in other kimberlites on the Melville peninsula. It may be a worthy enterprise to extract perovskite from samples of the Mel kimberlite for two reasons. Firstly, perovskite ages will provide additional context for Mel kimberlite magmatism and possibly refine the emplacement ages of ML8 Upper, ML8 Lower, and ML345. Secondly, perovskite Sr and Nd isotopes will provide a better measure of $^{87}Sr/^{86}Sr_{initial}$ and $\varepsilon Nd_{initial}$ than whole-rock measurements which are variably altered, weathered, and contaminated by crustal and mantle xenoliths/xenocrysts.

A significant limitation of the mantle interpretations in this work stems from the reliance on the Western Rae craton paleo-geotherm constructed from xenoliths recovered from the Darby kimberlite field. No clinopyroxene was recovered from samples of the Mel kimberlite. However, groundmass-sized clinopyroxene xenocrysts are reported from Qilalugaq CROL on the Melville peninsula (Sarkar et al., 2018). These clinopyroxenes could be utilized in geothermobarometric considerations that may better constrain the paleo-geotherm beneath the Melville Peninsula. In turn, constraining a paleogetherm for the Melville Peninsula will provide greater accuracy for interpreting garnet Ni-thermometry temperatures derived from the Mel kimberlite.

5.3.2 Further Work on the Dharma Kimberlite

A few key opportunities for further work exist in the case of the Dharma kimberlite. These contributions are capable of providing key information for the assessment of kimberlite magmatism in Western Canada.

Several prospective kimberlites have been drilled in Western Canada that do not have published ages. Publicly available property assessment reports indicate that both volcaniclastic and hypabyssal kimberlite were intersected at the HOAM property by Olivut Resources Ltd. in 2008 (Mah, 2009). Drill logs from this report indicate the presence of phlogopite in diamond core drill holes DH302-B01, DH303-01, DH1309-01, and DH1309-02 (Mah, 2009). At the Sahtu project, 104.4 m of kimberlite breccia superficially barren of macrocryst phases was intersected in diamond core drill hole DL08-4 (Craigie, 2010). Both of these kimberlites present an opportunity for a geochronologic, petrographic, and geochemical study that can provide meaningful context for kimberlite magmatism in Western Canada alongside the Dharma kimberlite. Additionally, whole-

rock measurements from kimberlites at Victoria Island and Darnley Bay would significantly contribute to the understanding of similarities between the Dharma kimberlite and these kimberlites. Furthermore, exploration for Mesozoic kimberlites and related rocks between Dharma and the Churchill kimberlite is of key importance. All of these factors will provide an opportunity to assess the validity of Great Meteor hotspot-related magmatism in Western Canada.

Although whole-rock from the Dharma kimberlite is capable of reasonably constraining the isotope systematics of the Dharma kimberlite, any recovered perovskite would further restrict the $^{87}Sr/^{86}Sr_{initial}$ and $\varepsilon Nd_{initial}$ signature. Furthermore, perovskite geochronology would be able to provide an additional measure for emplacement ages at Dharma. Finally, perovskite geochronology of all the identified kimberlite domains in the Dharma kimberlite would lead to a better understanding of emplacement ages between these domains.

As in the case of the Dharma kimberlite, the mantle interpretations of this work rely heavily on a paleo-geotherm from mantle xenoliths recovered at Darnley Bay and Victoria Island. Although clinopyroxene xenocrysts were identified alongside one harzburgite microxenolith in the Dharma kimberlite, time constraints limited the study of these mantle materials. The analysis of clinopyroxene and microxenoliths from the Dharma kimberlite could be conducted using traditional geothermobarometric techniques. A paleo geotherm fully constructed from mantle material recovered from the Dharma kimberlite would likely provide a much more accurate context for mantle conditions beneath Dharma in the Late Triassic.

References

Afanasyev, A. A., Melnik, O., Porritt, L., Schumacher, J. C., and Sparks, R. S. J. (2014). Hydrothermal alteration of kimberlite by convective flows of external water. *Contributions to Mineralogy and Petrology, 168*(1), 1-17.

Agashev, A. M., Pokhilenko, N. P., McDonald, J. A., Takazawa, E., Vavilov, M. A., Sobolev, N. V., and Watanabe, T. (2001). A unique kimberlite–carbonatite primary association in the Snap Lake dyke system, Slave Craton: evidence from geochemical and isotopic studies. *In The Slave Kaapvaal Workshop, Ext. Abstr. Vol. Merrickville*, Canada, unpaged.

Ansdell, K. M., and Norman, A. R. (1995). U-Pb geochronology and tectonic development of the southern flank of the Kisseynew Domain, Trans-Hudson Orogen, Canada. *Precambrian Research, 72* (1-2), 147-167.

Armstrong, J. T. (1988). Quantitative analysis of silicate and oxide minerals: Comparison of Monte Carlo, ZAF and φ (ρZ) procedures: in Newbury, DE, ed., Analysis microbeam: San Francisco, California.

Armstrong, R. A., and Moore, R. O. (1998). Rb-Sr ages on kimberlites from the Lac de Gras area, Northwest Territories, Canada. *South African Journal of Geology, 101* (2), 155-158.

Armstrong, J., Stubley, M., and Chang, F. (2008). Geology and exploration history of the Aviat kimberlite cluster, northern Rae Craton, Melville Peninsula, Nunavut Canada. In *International Kimberlite Conference: Extended Abstracts 9*, 3.

Armstrong, J. P., Fitzgerald, C. E., Kjarsgaard, B. A., Heaman, L., and Tappe, S. (2012). Kimberlites of the Coronation Gulf Field, Northern Slave Craton, Nunavut Canada. In *International Kimberlite Conference: Extended Abstracts*, *10*, 5.

Arndt, N. T., Boullier, A. M., Clément, J. P., Dubois, M., and Schissel, D. (2006). What olivine, the neglected mineral, tells us about kimberlite petrogenesis. *eEarth Discussions*, *1*(1), 37-50.

Arndt, N. T., Guitreau, M., Boullier, A. M., Le Roex, A., Tommasi, A., Cordier, P., and Sobolev, A. (2010). Olivine, and the origin of kimberlite. *Journal of Petrology*, *51*(3), 573-602.

Aulbach, S., Griffin, W. L., O'Reilly, S. Y., and McCandless, T. E. (2004). Genesis and evolution of the lithospheric mantle beneath the Buffalo Head Terrane, Alberta (Canada). *Lithos*, *77*(1-4), 413-451.

Begemann, F., Ludwig, K. R., Lugmair, G. W., Min, K., Nyquist, L. E., Patchett, P. J., Renne, P. R., Shih, C. Y., Villa, I. M., and Walker, R. J. (2001). Call for an improved set of decay constants for geochronological use. *Geochimica et Cosmochimica Acta*, *65*(1), 111-121.

Becker, M., and Le Roex, A. P. (2006). Geochemistry of South African on-and off-craton, Group I and Group II kimberlites: petrogenesis and source region evolution. *Journal of Petrology*, *47*(4), 673-703.

Berg, G. W., and Carlson, J. A. (1998, April). The Leslie kimberlite pipe of Lac de Gras, Northwest Territories, Canada: evidence for near surface hypabyssal emplacement. In *International Kimberlite Conference: Extended Abstracts*, *7*, 81-83.

Berman, R. G., Sanborn-Barrie, M., Stern, R. A., and Carson, C. J. (2005). Tectonometamorphism at ca. 2.35 and 1.85 Ga in the Rae Domain, western Churchill Province, Nunavut, Canada: Insights from structural, metamorphic and in situ geochronological analysis of the southwestern Committee Bay Belt. *The Canadian Mineralogist*, *43*(1), 409-442.

Berman, R. G., Davis, W. J., and Pehrsson, S. (2007). Collisional Snowbird tectonic zone resurrected: Growth of Laurentia during the 1.9 Ga accretionary phase of the Hudsonian orogeny. *Geology*, *35*(10), 911-914.

Berman, R. G., Sanborn-Barrie, M., Rayner, N., Carson, C., Sandeman, H. A., and Skulski, T. (2010). Petrological and in situ SHRIMP geochronological constraints on the tectonometamorphic evolution of the Committee Bay belt, Rae Province, Nunavut. *Precambrian Research*, *181*(1-4), 1-20.

Berman, R. G., Pehrsson, S., Davis, W. J., Ryan, J. J., Qui, H., and Ashton, K. E. (2013). The Arrowsmith orogeny: Geochronological and thermobarometric constraints on its extent and tectonic setting in the Rae craton, with implications for pre-Nuna supercontinent reconstruction. *Precambrian Research*, *232*, 44-69.

Birkett, T. C., McCandless, T. E., and Hood, C. T. (2004). Petrology of the Renard igneous bodies: host rocks for diamond in the northern Otish Mountains region, Quebec. *Lithos*, *76*(1-4), 475-490.

Bleeker, W., Ketchum, J. W., Jackson, V. A., and Villeneuve, M. E. (1999). The Central Slave Basement Complex, Part I: its structural topology and autochthonous cover. *Canadian Journal of Earth Sciences*, *36*(7), 1083-1109.

Blichert-Toft, J., and Puchtel, I. S. (2010). Depleted mantle sources through time: evidence from Lu–Hf and Sm–Nd isotope systematics of Archean komatiites. *Earth and Planetary Science Letters*, *297*(3-4), 598-606.

Bouvier, A., Vervoort, J. D., and Patchett, P. J. (2008). The Lu–Hf and Sm–Nd isotopic composition of CHUR: constraints from unequilibrated chondrites and implications for the bulk composition of terrestrial planets. *Earth and Planetary Science Letters*, *273*(1-2), 48-57.

Brett, R. C., Russell, J. K., Andrews, G. D. M., and Jones, T. J. (2015). The ascent of kimberlite: Insights from olivine. *Earth and Planetary Science Letters*, *424*, 119-131.

Brey, G. P., Bulatov, V. K., Girnis, A. V., and Lahaye, Y. (2008). Experimental melting of carbonated peridotite at 6–10 GPa. *Journal of Petrology*, *49*(4), 797-821.

Brin, L. E., and Pearson, G.D.P. (2014). The age and origin of lithospheric mantle beneath central Victoria Island and Parry Peninsula, in Program and Abstract Volume, 2014 ATLAS Research Symposium: Edmonton, University of Alberta, Alberta, Canada.

Brin, L. E. (2016). The Age and Origin of Lithospheric Mantle Beneath Central Victoria Island and Parry Peninsula, Northern Canada [M.Sc. Thesis]: Edmonton, University of Alberta.

Burgess, S. R., and Harte, B. E. N. (2004). Tracing lithosphere evolution through the analysis of heterogeneous G9–G10 garnets in peridotite xenoliths, II: REE chemistry. Journal of Petrology, 45(3), 609-633.

Campbell, I. H. (2001). Identification of ancient mantle plumes. *Special Papers-Geological Society of America*, 5-22.

Campbell, I. H. (2005). Large igneous provinces and the mantle plume hypothesis. *Elements*, *1*(5), 265-269.

Canil, D. (1999). The Ni-in-garnet geothermometer: calibration at natural abundances. *Contributions to Mineralogy and Petrology*, *136*(3), 240-246.

Card, C. D., Ashton, K. E., and Bethune, K. M. (2010). The case for separate Taltson and Thelon orogenies: Evidence from the Shield in western Saskatchewan. *Extended Abstracts. GeoCanada*, 10-14.

Carlson, J. A., Kirkley, M. B., Thomas, E. M., and Hillier, W. D. (1998, April). Recent major kimberlite discoveries in Canada. In *International Kimberlite Conference: Extended Abstracts*, *7*, 127-131.

Cavell, P. A., and Baadsgaard, H. (1986). Geochronology of the Big Spruce Lake alkaline intrusion. *Canadian Journal of Earth Sciences*, *23*(1), 1-10.

Cawood, P. A., Strachan, R. A., Pisarevsky, S. A., Gladkochub, D. P., and Murphy, J. B. (2016). Linking collisional and accretionary orogens during Rodinia assembly and breakup: Implications for models of supercontinent cycles. *Earth and Planetary Science Letters*, *449*, 118-126.

Chacko, T., De, S. K., Creaser, R. A., and Muehlenbachs, K. (2000). Tectonic setting of the Taltson magmatic zone at 1.9 2.0 Ga: A granitoid-based perspective. *Canadian Journal of Earth Sciences*, *37*(11), 1597-1609.

Choukroun, M., O'Reilly, S. Y., Griffin, W. L., Pearson, N. J., and Dawson, J. B. (2005). Hf isotopes of MARID (mica-amphibole-rutile-ilmenite-diopside) rutile trace metasomatic processes in the lithospheric mantle. *Geology*, *33*(1), 45-48.

Clarke, D. B., and Beutel, E. K. (2020). Davis Strait Paleocene picrites: Products of a plume or plates?. *Earth-Science Reviews*, *206*, 102770.

Clement, C. R. (1982). A comparative geological study of some major kimberlite pipes in the Northern Cape and Orange Free State [Ph.D. Thesis]: Cape Town, University of Cape Town.

Coe, N., Le Roex, A., Gurney, J., Pearson, D. G., and Nowell, G. (2008). Petrogenesis of the Swartruggens and Star Group II kimberlite dyke swarms, South Africa: constraints from whole rock geochemistry. *Contributions to Mineralogy and Petrology*, *156*(5), 627-652.

Cone, D., and Kopylova, M. (2021). Origin of megacrysts by carbonate-bearing metasomatism: a case study for the Muskox kimberlite, Slave craton, Canada. *Journal of the Geological Society*, *178*(3).

Cordier, C., Sauzeat, L., Arndt, N. T., Boullier, A. M., Batanova, V., and Barou, F. (2015). Metasomatism of the lithospheric mantle immediately precedes kimberlite eruption: new evidence from olivine composition and microstructures. *Journal of Petrology*, *56*(9), 1775-1796.

Cordier, C., Sauzeat, L., Arndt, N. T., Boullier, A. M., Batanova, V., and Barou, F. (2017). Quantitative modelling of the apparent decoupling of Mg# and Ni in kimberlitic olivine margins: a Reply to the comment on Cordier et al.(2015) by A. Moore. *Journal of Petrology*, *58*(2), 391-393.

Corrigan, D., Nadeau, L., Brouillette, P., Wodicka, N., Berman, R.G., and Houlé, M.G. (2020). Bedrock geology, Barrow River, Melville Peninsula, Nunavut, NTS 46-O and 46-P; Geological Survey of Canada, Canadian Geoscience Map 236, scale 1:150000.

Cousens, B. L. (2000). Geochemistry of the archean Kam group, Yellowknife greenstone belt, slave province, Canada. *The Journal of Geology*, *108*(2), 181-197.

Gainer, D., and MacMorran, M. (2019). Report on Exploration Activities (Diamond Drilling, Ground Geophysics, Heavy Mineral Sampling). Nunavut Geoscience Assessment Report.

Graham, I., Burgess, J. L., Bryan, D., Ravenscroft, P. J., Thomas, E., Doyle, B. J., Hopkins, R., and Armstrong, K. A. (1998, April). The Diavik kimberlites-Lac de Gras, Northwest Territories, Canada. In *International Kimberlite Conference: Extended Abstracts*, *7*, 259-261.

Cragie, E. R. (2010). Report of a Drilling Program: Sahtu Project. Northwest Territories Geoscience Office Assessment Report Repository, Report 085543, 21.

Creaser, R. A., Grütter, H., Carlson, J., and Crawford, B. (2004). Macrocrystal phlogopite Rb–Sr dates for the Ekati property kimberlites, Slave Province, Canada: evidence for multiple intrusive episodes in the Paleocene and Eocene. *Lithos*, *76*(1-4), 399-414.

Crough, S. T., Morgan, W. J., and Hargraves, R. B. (1980). Kimberlites: their relation to mantle hotspots. *Earth and Planetary Science Letters*, *50*(1), 260-274.

Dalton, H., Giuliani, A., Phillips, D., Hergt, J., Maas, R., Matchan, E., Woodhead, J., and O'Brien, H. (2020). A comparison of geochronological methods commonly applied to kimberlites and related rocks: Three case studies from Finland. *Chemical Geology*, *558*, 119899.

Dasgupta, R., Hirschmann, M. M., McDonough, W. F., Spiegelman, M., and Withers, A. C. (2009). Trace element partitioning between garnet lherzolite and carbonatite at 6.6 and 8.6 GPa with applications to the geochemistry of the mantle and of mantle-derived melts. *Chemical Geology*, *262*(1-2), 57-77.

Davies, R., and Davies, A. W. (2012, February). Kimberlite indicator minerals and "laterite", Canadian arctic. In *International Kimberlite Conference: Extended Abstracts 10*.

Davis, W. J., and Kjarsgaard, B. A. (1997). A Rb-Sr isochron age for a kimberlite from the recently discovered Lac de Gras Field, Slave Province, Northwest Canada. *The Journal of Geology*, *105*(4), 503-510.

Davis, W. J., Canil, D., MacKenzie, J. M., and Carbno, G. B. (2003). Petrology and U–Pb geochronology of lower crustal xenoliths and the development of a craton, Slave Province, Canada. *Lithos*, *71*(2-4), 541-573.

Davis, W. J., Hanmer, S., Tella, S., Sandeman, H. A., and Ryan, J. J. (2006). U–Pb geochronology of the MacQuoid supracrustal belt and Cross Bay plutonic complex: key components of the northwestern Hearne subdomain, western Churchill Province, Nunavut, Canada. *Precambrian Research*, *145*(1-2), 53-80.

Deschamps, F., Cobden, L., and Tackley, P. J. (2012). The primitive nature of large low shear-wave velocity provinces. *Earth and Planetary Science Letters*, *349*, 198-208.

Dhuime, B., Hawkesworth, C., and Cawood, P. (2011). When continents formed. *Science*, *331*(6014), 154-155.

Donatti-Filho, J. P., Tappe, S., Oliveira, E. P., and Heaman, L. M. (2013). Age and origin of the Neoproterozoic Brauna kimberlites: Melt generation within the metasomatized base of the São Francisco craton, Brazil. *Chemical Geology*, *353*, 19-35.

Dongre, A., and Tappe, S. (2019). Kimberlite and carbonatite dykes within the Premier diatreme root (Cullinan Diamond Mine, South Africa): New insights to mineralogical-genetic classifications and magma CO2 degassing. *Lithos*, *338*, 155-173.

Donovan, J. J., Kremser, D., Fournelle, J., and Goemann, K. (2012). Probe for EPMA: acquisition, automation and analysis. *Probe Software, Inc., Eugene, Oregon*, *http://www.probesoftware.com*.

Doucet, L. S., Ionov, D. A., and Golovin, A. V. (2013). The origin of coarse garnet peridotites in cratonic lithosphere: new data on xenoliths from the Udachnaya kimberlite, central Siberia. *Contributions to Mineralogy and Petrology*, *165*(6), 1225-1242.

Doyle, B. J., and Bidwell, G. (2005). MacKenzie Diamond Project - 2004 Report of Work Areas: Heavy Mineral Sampling Surveys. Northwest Territories Geoscience Office Assessment Report Repository, Report 084839, 96.

Duncan, R. A. (1984). Age progressive volcanism in the New England seamounts and the opening of the central Atlantic Ocean. *Journal of Geophysical Research: Solid Earth*, *89*(B12), 9980-9990.

Eggler, D. H. (1986). Kimberlites: how do they form? In *International Kimberlite Conference: Extended Abstracts 4*, 155-159.

Ernst, R., and Bleeker, W. (2010). Large igneous provinces (LIPs), giant dyke swarms, and mantle plumes: significance for breakup events within Canada and adjacent regions from 2.5 Ga to the Present. *Canadian Journal of Earth Sciences*, *47*(5), 695-739.

Ernst, R. E., and Buchan, K. L. (2002). Maximum size and distribution in time and space of mantle plumes: evidence from large igneous provinces. *Journal of Geodynamics*, *34*(2), 309-342.

Falck, H., and Gochnauer, K. (2012). 2011 Northwest Territories Mineral Exploration Overview, March 2012. Northwest Territories Geoscience Office, 35.

Faure, S. (2010). World kimberlites CONSOREM database (version 3). *Consortium de Recherche en Exploration Minérale CONSOREM, Université du Québec à Montréal*.

Field, M., and Scott Smith, B. H. (1999). Contrasting geology and near-surface emplacement of kimberlite pipes in southern Africa and Canada. In *Proceedings of the 7th international kimberlite conference*, *1*, 214-237.

Foland, K. A., Jiang-Feng, C., Gilbert, L. A., and Hofmann, A. W. (1988). Nd and Sr isotopic signatures of Mesozoic plutons in northeastern North America. *Geology*, *16*(8), 684-687.

Foley, S. F., Yaxley, G. M., Rosenthal, A., Buhre, S., Kiseeva, E. S., Rapp, R. P., and Jacob, D. E. (2009). The composition of near-solidus melts of peridotite in the presence of CO2 and H2O between 40 and 60ákbar. *Lithos*, *112*, 274-283.

Foley, S. F., Prelevic, D., Rehfeldt, T., and Jacob, D. E. (2013). Minor and trace elements in olivines as probes into early igneous and mantle melting processes. *Earth and Planetary Science Letters*, *363*, 181-191.

Foley, S. F., Yaxley, G. M., and Kjarsgaard, B. A. (2019). Kimberlites from source to surface: insights from experiments. *Elements: An International Magazine of Mineralogy, Geochemistry, and Petrology*, *15*(6), 393-398.

Folinsbee, R. E. (1949). Lac De Gras, District of Mackenzie, Northwest Territories. Geological Survey of Canada "A" Series Map 977A, scale 1:253,440.

Frost, D. J. (2006). The stability of hydrous mantle phases. *Reviews in Mineralogy and Geochemistry*, *62*(1), 243-271.

Gill, T. (2016). MacKenzie J.V. Diamonds Project - Greenhon Prospect: Till Sampling, Ground Geophysics, Diamond Drilling and RC Drilling for Diamond Exploration. Northwest Territories Geoscience Office Assessment Report Repository, Report 085557, 43.

Giuliani, A. (2018). Insights into kimberlite petrogenesis and mantle metasomatism from a review of the compositional zoning of olivine in kimberlites worldwide. *Lithos*, *312*, 322-342.

Giuliani, A., and Pearson, D. G. (2019). Kimberlites: from deep Earth to diamond mines. *Elements: An International Magazine of Mineralogy, Geochemistry, and Petrology*, *15*(6), 377-380.

Giuliani, A., Phillips, D., Kamenetsky, V. S., and Goemann, K. (2016). Constraints on kimberlite ascent mechanisms revealed by phlogopite compositions in kimberlites and mantle xenoliths. *Lithos*, *240*, 189-201.

Giuliani, A., Soltys, A., Phillips, D., Kamenetsky, V. S., Maas, R., Goemann, K., Woodhead, J. D., Drysdale, R. N., and Griffin, W. L. (2017). The final stages of kimberlite petrogenesis: petrography, mineral chemistry, melt inclusions and Sr-CO isotope geochemistry of the Bultfontein kimberlite (Kimberley, South Africa). *Chemical Geology*, *455*, 342-356.

Giuliani, A., Pearson, D. G., Soltys, A., Dalton, H., Phillips, D., Foley, S. F., Lim, E., Goemann, K., Griffin, W. L., and Mitchell, R. H. (2020). Kimberlite genesis from a common carbonate-rich primary melt modified by lithospheric mantle assimilation. *Science Advances*, *6*(17), eaaz0424.

Gochnauer, K., Falck, H., and Irwin, D. (2010). 2009 Northwest Territories Mineral Exploration Overview, March 2010. Northwest Territories Geoscience Office, 22.

Goff, S.P., Falck, H., and Irwin, D. (2008). 2008 Northwest Territories Mineral Exploration Overview, February 2009. Northwest Territories Geoscience Office, 21.

Golubkova, A. B., Nosova, A. A., and Larionova, Y. O. (2013). Mg-ilmenite megacrysts from the Arkhangelsk kimberlites, Russia: genesis and interaction with kimberlite melt and postkimberlite fluid. *Geochemistry International*, *51*(5), 353-381.

Government of Canada (2021). Diamond facts: https://www.nrcan.gc.ca/our-natural-resources/minerals-mining/minerals-metals-facts/diamond-facts/20513 (accessed February 2021).

Grégoire, M., Bell, D. R., and Le Roex, A. P. (2003). Garnet lherzolites from the Kaapvaal Craton (South Africa): trace element evidence for a metasomatic history. *Journal of Petrology*, *44*(4), 629-657.

Griffin, W. L., and Ryan, C. G. (1995). Trace elements in indicator minerals: area selection and target evaluation in diamond exploration. *Journal of geochemical Exploration*, *53*(1-3), 311-337.

Griffin, W.L., Doyle, B.J., Ryan, C.G., Pearson, N.J., O'Reilly, S.Y., Natapov, L., Kivi, K., Kretschmar, U. and Ward, J. (1998). Lithosphere structure and mantle terranes: Slave Craton, Canada. *International Kimberlite Conference: Extended Abstracts, 7*, 271-273.

Grütter, H. S., Apter, D. B., and Kong, J. (1999). Crust–mantle coupling: evidence from mantle-derived xenocrystic garnets. In *Proceedings of the 7th International Kimberlite Conference 1*, 307-313.

Grütter, H. S., Gurney, J. J., Menzies, A. H., and Winter, F. (2004). An updated classification scheme for mantle-derived garnet, for use by diamond explorers. *Lithos*, *77*(1-4), 841-857.

Grütter, H., Latti, D., & Menzies, A. (2006). Cr-saturation arrays in concentrate garnet compositions from kimberlite and their use in mantle barometry. *Journal of Petrology*, *47*(4), 801-820.

Gurney, J. J., and Zweistra, P. (1995). The interpretation of the major element compositions of mantle minerals in diamond exploration. *Journal of Geochemical Exploration*, *53*(1-3), 293-309.

Gurney, J. J., Jakob, W. R. O., and Dawson, J. B. (1979). Megacrysts from the Monastery kimberlite pipe, South Africa. *The mantle sample: inclusion in kimberlites and other volcanics*, *16*, 227-243.

Haggerty, S. E. (1995). Upper mantle mineralogy. *Journal of Geodynamics*, *20*(4), 331-364.

Hamilton, P. J., O'nions, R. K., Bridgwater, D., and Nutman, A. (1983). Sm-Nd studies of Archaean metasediments and metavolcanics from West Greenland and their implications for the Earth's early history. *Earth and Planetary Science Letters*, *62*(2), 263-272.

Hanmer, S., Bowring, S., van Breemen, O., and Parrish, R. (1992). Great Slave Lake shear zone, NW Canada: mylonitic record of Early Proterozoic continental convergence, collision and indentation. *Journal of Structural Geology*, *14*(7), 757-773.

Hanmer, S., Tella, S., Ryan, J. J., Sandeman, H. A., and Berman, R. G. (2006). Late Neoarchean thick-skinned thrusting and Paleoproterozoic reworking in the MacQuoid supracrustal belt and Cross Bay plutonic complex, western Churchill Province, Nunavut, Canada. *Precambrian Research*, *144*(1-2), 126-139.

Hardman, M. F., Pearson, D. G., Stachel, T., and Sweeney, R. J. (2018). Statistical approaches to the discrimination of crust-and mantle-derived low-Cr garnet–major-element-based methods and their application in diamond exploration. *Journal of Geochemical Exploration*, *186*, 24-35.

Hardman, M. (2020). Improving the use of eclogitic garnet as a diamond indicator mineral, and constraining the origin of eclogites in the subcontinental lithospheric mantle [Ph.D. Thesis]. Edmonton, University of Alberta.

Harris, M., le Roex, A., and Class, C. (2004). Geochemistry of the Uintjiesberg kimberlite, South Africa: petrogenesis of an off-craton, group I, kimberlite. *Lithos*, *74*(3-4), 149-165.
Harris, G. A., Pearson, D. G., Liu, J., Hardman, M. F., Snyder, D. B., and Kelsch, D. (2018). Mantle composition, age and geotherm beneath the Darby kimberlite field, west central Rae Craton. *Mineralogy and Petrology*, *112*(1), 57-70.

Hawthorne, J. B. (1975). Model of a kimberlite pipe. *Physics and Chemistry of the Earth*, *9*, 1-15.

Hayman, P. C., Cas, R. A. F., and Johnson, M. (2009). Characteristics and alteration origins of matrix minerals in volcaniclastic kimberlite of the Muskox pipe (Nunavut, Canada). *Lithos*, *112*, 473-487.

Hayman, P. C., and Cas, R. A. F. (2011). Reconstruction of a multi-vent kimberlite eruption from deposit and host rock characteristics: Jericho kimberlite, Nunavut, Canada. *Journal of volcanology and geothermal research*, *200*(3-4), 201-222.

Heaman, L. M., and Kjarsgaard, B. A. (2000). Timing of eastern North American kimberlite magmatism: continental extension of the Great Meteor hotspot track?. *Earth and Planetary Science Letters*, *178*(3-4), 253-268.

Heaman, L. M., and Kjarsgaard, B. A. (2002). A Cretaceous corridor of kimberlite magmatism: U–Pb results from the Fort à la Corne Field, central Saskatchewan. In *Geological Association of Canada/Mineralogical Association of Canada Meeting in Saskatoon, Saskatchewan*, *47*.

Heaman, L. M., Kjarsgaard, B. A., and Creaser, R. A. (2003). The timing of kimberlite magmatism in North America: implications for global kimberlite genesis and diamond exploration. *Lithos*, *71*(2-4), 153-184.

Heaman, L. M., Kjarsgaard, B. A., and Creaser, R. A. (2004). The temporal evolution of North American kimberlites. *Lithos*, *76*(1-4), 377-397.

Heaman, L. M., Creaser, R. A., Cookenboo, H. O., and Chacko, T. O. M. (2006). Multi-stage modification of the Northern Slave mantle lithosphere: evidence from zircon-and diamond-bearing eclogite xenoliths entrained in Jericho kimberlite, Canada. *Journal of Petrology*, *47*(4), 821-858.

Heaman, L. M., Pell, J., Grütter, H. S., and Creaser, R. A. (2015). U–Pb geochronology and Sr/Nd isotope compositions of groundmass perovskite from the newly discovered Jurassic Chidliak kimberlite field, Baffin Island, Canada. *Earth and Planetary Science Letters*, *415*, 183-199.

Heaman, L. M., Phillips, D., and Pearson, G. (2019). Dating kimberlites: Methods and emplacement patterns through time. *Elements: An International Magazine of Mineralogy, Geochemistry, and Petrology*, *15*(6), 399-404.

Hetman, C. M., Smith, B. S., Paul, J. L., and Winter, F. (2004). Geology of the Gahcho Kue kimberlite pipes, NWT, Canada: root to diatreme magmatic transition zones. *Lithos*, *76*(1-4), 51-74.

Hildebrand, R. S., Hoffman, P. F., and Bowring, S. A. (1987). Tectono-magmatic evolution of the 1.9-Ga Great Bear magmatic zone, Wopmay Orogen, northwestern Canada. *Journal of Volcanology and Geothermal Research*, *32*(1-3), 99-118.

Hildebrand, R. S., Hoffman, P. F., and Bowring, S. A. (2010). The Calderian orogeny in Wopmay orogen (1.9 Ga), northwestern Canadian shield. *Bulletin*, *122*(5-6), 794-814.

Hinchey, A. M., Davis, W. J., Ryan, J. J., and Nadeau, L. (2011). Neoarchean high-potassium granites of the Boothia mainland area, Rae domain, Churchill Province: U–Pb zircon and Sm–Nd whole rock isotopic constraints. *Canadian Journal of Earth Sciences*, *48*(2), 247-279.

Hoffman, P. F., and Bowring, S. A. (1984). Short-lived 1.9 Ga continental margin and its destruction, Wopmay orogen, northwest Canada. *Geology*, *12*(2), 68-72.

Hofmann, A. W., Jochum, K. P., Seufert, M., and White, W. M. (1986). Nb and Pb in oceanic basalts: new constraints on mantle evolution. *Earth and Planetary science letters*, *79*(1-2), 33-45.

Howarth, G. H., and Taylor, L. A. (2016). Multi-stage kimberlite evolution tracked in zoned olivine from the Benfontein sill, South Africa. *Lithos*, *262*, 384-397.

Iizuka, T., Komiya, T., Ueno, Y., Katayama, I., Uehara, Y., Maruyama, S., Hirata, T., Johnson, S. P., and Dunkley, D. J. (2007). Geology and zircon geochronology of the Acasta Gneiss Complex, northwestern Canada: new constraints on its tectonothermal history. *Precambrian Research*, *153*(3-4), 179-208.

Jackson, M. G., Becker, T. W., and Konter, J. G. (2018). Geochemistry and distribution of recycled domains in the mantle inferred from Nd and Pb isotopes in oceanic hot spots: Implications for storage in the large low shear wave velocity provinces. *Geochemistry, Geophysics, Geosystems*, *19*(9), 3496-3519.

Jacobsen, S. B., and Wasserburg, G. J. (1980). Sm-Nd isotopic evolution of chondrites. *Earth and Planetary Science Letters*, *50*(1), 139-155.

Jochum, K. P., Nohl, U., Herwig, K., Lammel, E., Stoll, B., and Hofmann, A. W. (2005). GeoReM: a new geochemical database for reference materials and isotopic standards. *Geostandards and Geoanalytical Research*, *29*(3), 333-338.

Jochum, K. P., Weis, U., Schwager, B., Stoll, B., Wilson, S. A., Haug, G. H., Andreae, M. O., and Enzweiler, J. (2016). Reference values following ISO guidelines for frequently requested rock reference materials. *Geostandards and Geoanalytical Research*, *40*(3), 333-350.

Kamenetsky, V. S., Kamenetsky, M. B., Sharygin, V. V., Faure, K., and Golovin, A. V. (2007). Chloride and carbonate immiscible liquids at the closure of the kimberlite magma evolution (Udachnaya-East kimberlite, Siberia). *Chemical Geology*, *237*(3-4), 384-400.

Kamenetsky, V. S., Golovin, A. V., Maas, R., Giuliani, A., Kamenetsky, M. B., and Weiss, Y. (2014). Towards a new model for kimberlite petrogenesis: Evidence from unaltered kimberlites and mantle minerals. *Earth-Science Reviews*, *139*, 145-167.

Kargin, A. V., Sazonova, L. V., Nosova, A. A., Lebedeva, N. M., Kostitsyn, Y. A., Kovalchuk, E. V., Tretyachenko, V. V., and Tikhomirova, Y. S. (2019). Phlogopite in mantle xenoliths and kimberlite from the Grib pipe, Arkhangelsk province, Russia: Evidence for multi-stage mantle metasomatism and origin of phlogopite in kimberlite. *Geoscience Frontiers*, *10*(5), 1941-1959.

Kennedy, C. S., and Kennedy, G. C. (1976). The equilibrium boundary between graphite and diamond. *Journal of Geophysical Research*, *81*(14), 2467-2470.

Kienlen, B., Blackmore, E., Curry, N., Gill, G., Kolebaba, M., Lyon, R., Ozyer, C., Pratt, Z., Vanderspiegel, R. (2008). The Amaruk project in Canada's new Pelly Bay diamond district. In *International Kimberlite Conference: Extended Abstracts*, *9*, 3.

Kinney, S. T., MacLennan, S. A., Keller, C. B., Schoene, B., Setera, J. B., VanTongeren, J. A., and Olsen, P. E. (2021). Zircon U-Pb Geochronology Constrains Continental Expression of Great Meteor Hotspot Magmatism. *Geophysical Research Letters*, *48*(11), e2020GL091390.

Kjarsgaard, B. A., and Levinson, A. A. (2002). Diamonds in Canada. *Gems and Gemology*, *38*(3), 208-238.

Kjarsgaard, B. A. (2007). Kimberlite pipe models: significance for exploration. In *Proceedings of exploration* 7, 667-677.

Kjarsgaard, B. A., Pearson, D. G., Tappe, S., Nowell, G. M., and Dowall, D. P. (2009). Geochemistry of hypabyssal kimberlites from Lac de Gras, Canada: comparisons to a global database and applications to the parent magma problem. *Lithos*, *112*, 236-248.

Kjarsgaard, B. A. (2012). Kimberlite pipe models: significance for exploration. In *International Kimberlite Conference: Extended Abstracts*, *10*, 1.

Kjarsgaard, B. A., Heaman, L. M., Sarkar, C., and Pearson, D. G. (2017). The N orth A merica mid-C retaceous kimberlite corridor: Wet, edge-driven decompression melting of an OIB-type deep mantle source. *Geochemistry, Geophysics, Geosystems*, *18*(7), 2727-2747.

Kjarsgaard, B. A., Januszczak, N., and Stiefenhofer, J. (2019). Diamond exploration and resource evaluation of kimberlites. *Elements: An International Magazine of Mineralogy, Geochemistry, and Petrology*, *15*(6), 411-416.

Klein-BenDavid, O., and Pearson, D. G. (2009). Origins of subcalcic garnets and their relation to diamond forming fluids—case studies from Ekati (NWT-Canada) and Murowa (Zimbabwe). *Geochimica et Cosmochimica Acta*, *73*(3), 837-855.

Kopylova, M. G., and Caro, G. (2004). Mantle xenoliths from the southeastern Slave craton: evidence for chemical zonation in a thick, cold lithosphere. *Journal of Petrology*, *45*(5), 1045-1067.

Kopylova, M. G., and Russell, J. K. (2000). Chemical stratification of cratonic lithosphere: constraints from the Northern Slave craton, Canada. *Earth and Planetary Science Letters*, *181*(1-2), 71-87.

Kopylova, M. G., Matveev, S., and Raudsepp, M. (2007). Searching for parental kimberlite melt. *Geochimica et Cosmochimica Acta*, *71*(14), 3616-3629.

Kopylova, M. G., and Hayman, P. (2008). Petrology and textural classification of the Jericho kimberlite, northern Slave Province, Nunavut, Canada. *Canadian Journal of Earth Sciences*, *45*(6), 701-723.

Kopylova, M. G., Beausoleil, Y., Goncharov, A., Burgess, J., and Strand, P. (2016). Spatial distribution of eclogite in the Slave cratonic mantle: The role of subduction. *Tectonophysics*, *672*, 87-103.

Kupsch, B., and Armstrong, J. P. (2013). Exploration and geology of the Qilalugaq kimberlites, Rae isthmus, Nunavut, Canada. In *Proceedings of 10th International Kimberlite Conference*, 67-78. Springer, New Delhi.

Larrea, M. L., Castro, S. M., and Bjerg, E. A. (2014). A software solution for point counting. Petrographic thin section analysis as a case study. *Arabian Journal of Geosciences*, *7*(8), 2981-2989.

Le Roex, A. P. (1986). Geochemical correlation between southern African kimberlites and South Atlantic hotspots. *Nature*, *324*(6094), 243-245.

Le Roex, A. P., Bell, D. R., and Davis, P. (2003). Petrogenesis of group I kimberlites from Kimberley, South Africa: evidence from bulk-rock geochemistry. *Journal of Petrology*, *44*(12), 2261-2286.

LeCheminant, A. N., and Heaman, L. M. (1989). Mackenzie igneous events, Canada: Middle Proterozoic hotspot magmatism associated with ocean opening. *Earth and Planetary Science Letters*, *96*(1-2), 38-48.

LeCheminant, A. N. (1996). Lamprophyre dykes in the Awry plutonic suite, North Arm, Great Slave Lake, Northwest Territories. *Geological Survey of Canada, Current Research*, 11-18.

LeCouter, P.C. (2001). Till Sampling. In *Report on Kimberlite Exploration, Victoria Island Properties, 1*. Northwest Territories Geoscience Office Assessment Report Repository, Report 084362, 221.

Lehtonen, M. (2005). Rare earth element characteristics of pyrope garnets from the Kaavi-Kuopio kimberlites-implications for mantle metasomatism. *Bulletin-Geological Society of Finland*, *77*(1), 31.

Lehtonen, M., and O'Brien, H. (2009). Mantle transect of the Karelian Craton from margin to core based on PT data from garnet and clinopyroxene xenocrysts in kimberlites. *Bulletin of the Geological Society of Finland*, *81*(2), 79-102.

Liu, J., Riches, A. J., Pearson, D. G., Luo, Y., Kienlen, B., Kjarsgaard, B. A., Stachel, T., and Armstrong, J. P. (2016). Age and evolution of the deep continental root beneath the central Rae craton, northern Canada. *Precambrian Research*, *272*, 168-184.

Liu, J., Brin, L. E., Pearson, D. G., Bretschneider, L., Luguet, A., van Acken, D., Kjarsgaard, B., Riches, A., and Mišković, A. (2018). Diamondiferous Paleoproterozoic mantle roots beneath Arctic Canada: A study of mantle xenoliths from Parry Peninsula and Central Victoria Island. *Geochimica et Cosmochimica Acta*, *239*, 284-311.

Liu, J., Pearson, D. G., Wang, L. H., Mather, K. A., Kjarsgaard, B. A., Schaeffer, A. J., Irvine, G. J., Kopylova, M. G., and Armstrong, J. P. (2021). Plume-driven recratonization of deep continental lithospheric mantle. *Nature*, *592*(7856), 732-736.

Lugmair, G. W., and Marti, K. (1978). Lunar initial 143Nd/144Nd: differential evolution of the lunar crust and mantle. *Earth and Planetary Science Letters*, *39*(3), 349-357.

MacFarlane, K. E., Goff, S. P., and Irwin, D. (2007). 2007 Northwest Territories Mineral Exploration Overview, November 2007. Northwest Territories Geoscience Office, 20.

MacRae, N. D., Armitage, A. E., Miller, A. R., Roddick, J. C., Jones, A. L., and Mudry, M. P. (1996). The diamondiferous Akluilak lamprophyre dyke, Gibson Lake area, NWT. *Searching for diamonds in Canada*, *3228*, 101-107.

Mah, D. (2009). HOAM Property: Diamond Drilling, Helicopter and Fixed Wing Aeormagnetic Geophysical Surveys. Northwest Territories Geoscience Office Assessment Report Repository, Report 085526, 76.

Malkovets, V. G., Rezvukhin, D. I., Belousova, E. A., Griffin, W. L., Sharygin, I. S., Tretiakova, I. G., Gibsher, A. A., O'Reilly, S. Y., Kuzmin, D. V., Litasov, K. D., Logvinova, A. M., Pokhilenko, N. P., and Sobolev, N. V. (2016). Cr-rich rutile: A powerful tool for diamond exploration. *Lithos*, *265*, 304-311.

Martel, E., van Breemen, O., Berman, R. G., and Pehrsson, S. (2008). Geochronology and tectonometamorphic history of the Snowbird Lake area, Northwest Territories, Canada: New insights into the architecture and significance of the Snowbird tectonic zone. *Precambrian Research*, *161*(3-4), 201-230.

Masun, K. M., Doyle, B. J., Ball, S., and Walker, S. (2004). The geology and mineralogy of the Anuri kimberlite, Nunavut, Canada. *Lithos*, *76*(1-4), 75-97.

Mazza, S. E., Gazel, E., Johnson, E. A., Bizimis, M., McAleer, R., and Biryol, C. B. (2017). Post-rift magmatic evolution of the eastern N orth A merican "passive-aggressive" margin. *Geochemistry, Geophysics, Geosystems*, *18*(1), 3-22.

McCandless, T. E., Gurney, J. J., Ross, J., Jaques, A. L., and Ferguson, J. (1989). Sodium in garnet and potassium in clinopyroxene: criteria for classifying mantle eclogites. *GROUP*, *2*, 30.
McLean, H., Banas, A., Creighton, S., Whiteford, S., Luth, R. W., and Stachel, T. (2007). Garnet xenocrysts from the Diavik mine, NWT, Canada: Composition, color, and paragenesis. *The Canadian Mineralogist*, *45*(5), 1131-1145.

Menzies, A., Westerlund, K., Grütter, H., Gurney, J., Carlson, J., Fung, A., and Nowicki, T. (2004). Peridotitic mantle xenoliths from kimberlites on the Ekati Diamond Mine property, NWT, Canada: major element compositions and implications for the lithosphere beneath the central Slave craton. *Lithos*, *77*(1-4), 395-412.

Merle, R. E., Jourdan, F., Chiaradia, M., Olierook, H. K., and Manatschal, G. (2019). Origin of widespread Cretaceous alkaline magmatism in the Central Atlantic: A single melting anomaly?. *Lithos*, *342*, 480-498.

Mitchell, R. H. (1986). Kimberlites: petrology, mineralogy and geochemistry. Plenum Press, New York.

Mitchell, R. H. (2012). Kimberlites, orangeites, and related rocks. Plenum Press, New York.

Mitchell, R. H., and Bergman, S. C. (1991). Petrology of lamproites. Springer Science and Business Media.

Mitchell, R. H., Giuliani, A., and O'Brien, H. (2019). What is a kimberlite? Petrology and mineralogy of hypabyssal kimberlites. *Elements: An International Magazine of Mineralogy, Geochemistry, and Petrology*, *15*(6), 381-386.

Moore, A. E. (1988). Olivine: a monitor of magma evolutionary paths in kimberlites and olivine melilitites. *Contributions to Mineralogy and Petrology*, *99*(2), 238-248.

Moore, A., and Belousova, E. (2005). Crystallization of Cr-poor and Cr-rich megacryst suites from the host kimberlite magma: implications for mantle structure and the generation of kimberlite magmas. *Contributions to Mineralogy and Petrology*, *149*(4), 462-481.

Moore, A., Yudovskaya, M., Proyer, A., and Blenkinsop, T. (2020). Evidence for olivine deformation in kimberlites and other mantle-derived magmas during crustal emplacement. *Contributions to Mineralogy and Petrology*, *175*(2), 1-9.

Moore, R. O., Griffin, W. L., Gurney, J. J., Ryan, C. G., Cousens, D. R., Sie, S. H., and Suter, G. F. (1992). Trace element geochemistry of ilmenite megacrysts from the Monastery kimberlite, South Africa. *Lithos*, *29*(1-2), 1-18.

Murphy, D. T., Collerson, K. D., and Kamber, B. S. (2002). Lamproites from Gaussberg, Antarctica: possible transition zone melts of Archaean subducted sediments. *Journal of Petrology*, *43*(6), 981-1001.

Nebel, O., Mezger, K., Scherer, E. E., and Münker, C. (2005). High precision determinations of 87Rb/85Rb in geologic materials by MC-ICP-MS. *International Journal of Mass Spectrometry*, *246*(1-3), 10-18.

Newton, D. E., Kopylova, M. G., Burgess, J., and Strand, P. (2016). Peridotite and pyroxenite xenoliths from the Muskox kimberlite, northern Slave craton, Canada. *Canadian Journal of Earth Sciences*, *53*(1), 41-58.

Nielsen, T. F., and Sand, K. K. (2008). The Majuagaa kimberlite dike, Maniitsoq region, West Greenland: constraints on an Mg-rich silicocarbonatitic melt composition from groundmass mineralogy and bulk compositions. *The Canadian Mineralogist*, *46*(4), 1043-1061.

Nielsen, T. F., Jensen, S. M., Secher, K., and Sand, K. K. (2009). Distribution of kimberlite and aillikite in the Diamond Province of southern West Greenland: a regional perspective based on groundmass mineral chemistry and bulk compositions. *Lithos*, *112*, 358-371.

North Arrow Minerals Inc. (2019). Mel project, Nunavut Canada's newest kimberlite field. Annual Mineral Exploration Roundup 2019, Vancouver.

Nowell, G. M., Pearson, D. G., Bell, D. R., Carlson, R. W., Smith, C. B., Kempton, P. D., and Noble, S. R. (2004). Hf isotope systematics of kimberlites and their megacrysts: new constraints on their source regions. *Journal of Petrology*, *45*(8), 1583-1612.

Nowell, G. M., Pearson, D. G., and Irving, A. J. (2008, October). Lu-Hf and Re-Os isotopic studies of lamproite genesis. In *International Kimberlite Conference: Extended Abstracts*, *9*, 3.

O'Brien, H. E., and Tyni, M. (1998, April). Mineralogy and geochemistry of kimberlites and related rocks from Finland. In *International Kimberlite Conference: Extended Abstracts*, *7*, 643-645.

Ootes, L., Sandeman, H., Cousens, B. L., Luo, Y., Pearson, D. G., and Jackson, V. A. (2020). Pyroxenitic magma conduits (ca. 1.86 Ga) in Wopmay orogen and slave craton: Petrogenetic constraints from whole rock and mineral chemistry. *Lithos*, *354*, 105220.

Ootes, L., Davis, W. J., Jackson, V. A., and van Breemen, O. (2015). Chronostratigraphy of the Hottah terrane and Great Bear magmatic zone of Wopmay Orogen, Canada, and exploration of a terrane translation model. *Canadian Journal of Earth Sciences*, *52*(12), 1062-1092.

Ottley, C. J., Pearson, G., and Irvine, G. J. (2003). A routine method for the dissolution of geological samples for the analysis of REE and trace elements via ICP-MS. *Plasma source mass spectrometry: Applications and emerging technologies*, (288), 221.

Palme, H., and O'Neill, H. St. C. (2014). 3.1 - Cosmochemical Estimates of Mantle Composition. In *Treatise on Geochemistry (Second Edition)*, 3, 1-39.

Partin, C. A., Bekker, A., Corrigan, D., Modeland, S., Francis, D., and Davis, D. W. (2014). Sedimentological and geochemical basin analysis of the Paleoproterozoic Penrhyn and Piling groups of Arctic Canada. *Precambrian Research*, *251*, 80-101.

Paton, C., Hergt, J. M., Woodhead, J. D., Phillips, D., and Shee, S. R. (2009). Identifying the asthenospheric component of kimberlite magmas from the Dharwar Craton, India. *Lithos*, *112*, 296-310.

Pearson, D. G., Woodhead, J., and Janney, P. E. (2019). Kimberlites as geochemical probes of Earth's mantle. *Elements: An International Magazine of Mineralogy, Geochemistry, and Petrology*, *15*(6), 387-392.

Peccerillo, A., and Martinotti, G. (2006). The Western Mediterranean lamproitic magmatism: origin and geodynamic significance. *Terra Nova*, *18*(2), 109-117.

Pehrsson, S. J., Berman, R. G., and Davis, W. J. (2013). Paleoproterozoic orogenesis during Nuna aggregation: a case study of reworking of the Rae craton, Woodburn Lake, Nunavut. *Precambrian research*, *232*, 167-188.

Pell, J., Holmes, P. K., Grenon, H., Sell, M. V., and Tam, L. (2008, October). Exploration and discovery of a new kimberlite cluster on the Nanuq Property, Western Churchill Province, Kivalliq area, Nunavut. In *International Kimberlite Conference: Extended Abstracts, 9*, 3.

Peterson, T. D., LeCheminant, A. N., Richardson, D. G., DiLabio, R. N. W., and Richardson, K. A. (1996). Ultrapotassic rocks of the Dubawnt Supergroup, District of Keewatin, NWT. *Searching for diamonds in Canada. Edited by AN LeCheminant, DG Richardson, RNW Dilabio, and KA Richardson. Geological Survey of Canada, Open File*, *3228*, 97-100.

Peterson, T. D., Van Breemen, O., Sandeman, H., and Cousens, B. (2002). Proterozoic (1.85–1.75 Ga) igneous suites of the Western Churchill Province: granitoid and ultrapotassic magmatism in a reworked Archean hinterland. *Precambrian Research*, *119*(1-4), 73-100.

Peterson, T. D., and Pehrsson, S. (2010). Proterozoic (1.85-1.7 Ga) igneous suites of the Western Churchill Province: constraints on tectonic assembly and crust-mantle dynamics. *GeoCanada 2010 Abstracts (on-line publication)*.

Pettke, T., Oberli, F., Audétat, A., Guillong, M., Simon, A. C., Hanley, J. J., and Klemm, L. M. (2012). Recent developments in element concentration and isotope ratio analysis of individual fluid inclusions by laser ablation single and multiple collector ICP-MS. *Ore Geology Reviews*, *44*, 10-38.

Petts, D. C., Davis, W. J., Moser, D. E., and Longstaffe, F. J. (2014). Age and evolution of the lower crust beneath the western Churchill Province: U–Pb zircon geochronology of kimberlite-hosted granulite xenoliths, Nunavut, Canada. *Precambrian Research*, *241*, 129-145.

Prelević, D., Foley, S. F., Romer, R., and Conticelli, S. (2008). Mediterranean Tertiary lamproites derived from multiple source components in postcollisional geodynamics. *Geochimica et Cosmochimica Acta*, *72*(8), 2125-2156.

Preston, R. F., Perritt, S. H., Seller, M. H., and Wyatt, B. A. (2012, February). Lithospheric structure beneath the Cretaceous Orapa kimberlite field, Botswana: 4D lithosphere imaging using garnet indicator mineral chemistry. In *International Kimberlite Conference: Extended Abstracts*, *10*, 5.

Price, S. E., Russell, J. K., and Kopylova, M. G. (2000). Primitive magma from the Jericho Pipe, NWT, Canada: constraints on primary kimberlite melt chemistry. *Journal of Petrology*, *41*(6), 789-808.

Ramsay, R. R. (1992). Geochemistry of diamond indicator minerals [Ph.D. Thesis]: Perth, University of Western Australia.

Reford, S. (2012). 2010 Diamond Drill Report on the Franklin Diamond Project. Northwest Territories Geoscience Office Assessment Report Repository, Report 33475, 66.

Richan, L., Gibson, H. L., Houlé, M. G., and Lesher, C. M. (2015). Mode of emplacement of Archean komatiitic tuffs and flows in the Selkirk Bay area, Melville Peninsula, Nunavut, Canada. *Precambrian Research*, *263*, 174-196.

Phillips, D., Machin, K. J., Kiviets, G. B., Fourie, L. F., Roberts, M. A., and Skinner, E. M. W. (1998). A petrographic and 40Ar/39Ar geochronological study of the Voorspoed kimberlite, South Africa: Implications for the origin of Group II kimberlite magmatism. *South African Journal of Geology*, *101*(4), 299-306.

Roeder, P. L., and Schulze, D. J. (2008). Crystallization of groundmass spinel in kimberlite. *Journal of Petrology*, *49*(8), 1473-1495.

Ross, G. M., Kerans, C., and Narraway, J. D. (1989). Hornby Bay and Dismal Lakes Groups, Coppermine Homocline, District of Mackenzie, Northwest Territories. Geological Survey of Canada Map 1663A, scale 1:250000.

Ross, G. M., Broome, J., and Miles, W. (1994). Potential fields and basement structure—Western Canada Sedimentary Basin, in geological atlas of the Western Canada Sedimentary Basin. *Canadian society of petroleum geologists and Alberta research council, special report*, *4*.

Russell, J. K., Sparks, R. S. J., and Kavanagh, J. L. (2019). Kimberlite volcanology: transport, ascent, and eruption. *Elements: An International Magazine of Mineralogy, Geochemistry, and Petrology*, *15*(6), 405-410.

Ryan, C. G., Griffin, W. L., Pearson, N. J., & Win, T. T. (1995). Garnet Geotherms: Derivation of PT data from Cr-pyrope garnets. *International Kimberlite Conference: Extended, 6*, 476-478.

Ryan, C. G., Griffin, W. L., and Pearson, N. J. (1996). Garnet geotherms: Pressure-temperature data from Cr-pyrope garnet xenocrysts in volcanic rocks. *Journal of Geophysical Research: Solid Earth*, *101*(B3), 5611-5625.

Sanborn-Barrie, M., Davis, W. J., Berman, R. G., Rayner, N., Skulski, T., and Sandeman, H. (2014). Neoarchean continental crust formation and Paleoproterozoic deformation of the central Rae craton, Committee Bay belt, Nunavut. *Canadian Journal of Earth Sciences*, *51*(6), 635-667.

Santana Resources Inc. (2008). Sanatana Finds New Kimberlite, Greenhorn Project NWT: http://sanatanaresources.com/s/news.asp?ReportID=519677 (accessed September, 2019).

Sarkar, C., Kjarsgaard, B. A., Pearson, D. G., Heaman, L. M., Locock, A. J., and Armstrong, J. P. (2018). Geochronology, classification and mantle source characteristics of kimberlites and related rocks from the Rae Craton, Melville Peninsula, Nunavut, Canada. *Mineralogy and Petrology*, *112*(2), 653-672.

Satterly, J. (1948). Geology of Michaud township. *Ontario Department of Mines Annual report*, *57*(4), 33.

Schaeffer, A. J., and Lebedev, S. (2014). Imaging the North American continent using waveform inversion of global and USArray data. *Earth and Planetary Science Letters*, *402*, 26-41.

Schulze, D. J., Anderson, P. F., Hearn Jr, B. C., and Hetman, C. M. (1995). Origin and significance of ilmenite megacrysts and macrocrysts from kimberlite. *International Geology Review*, *37*(9), 780-812.

Schulze, D. J. (2003). A classification scheme for mantle-derived garnets in kimberlite: a tool for investigating the mantle and exploring for diamonds. *Lithos*, *71*(2-4), 195-213.

Scott Smith, B. H., and McKinlay, T. (2002). Emplacement of the Hardy Lake kimberlites, NWT, Canada. In *Geological Association of Canada/Mineralogical Association of Canada Meeting in Saskatoon, Saskatchewan*, *106*.

Scott Smith, B. H., Nowicki, T. E., Russell, J. K., Webb, K. J., Mitchell, R. H., Hetman, C. M., Harder, M., Skinner, E. M. W., and Robey, J. A. (2012). Kimberlite terminology and classification. In *Proceedings of 10th international kimberlite conference*, *1*, 1-17

Scott Smith, B. H., Nowicki, T. E., Russell, J. K., Webb, K. J., Mitchell, R. H., Hetman, C. M., and Robey, J. V. (2018). A glossary of kimberlite and related terms. North Vancouver, Scott-Smith Petrology Inc., North Vancouver, 144.

Secher, K., Heaman, L. M., Nielsen, T. F. D., Jensen, S. M., Schjøth, F., and Creaser, R. A. (2009). Timing of kimberlite, carbonatite, and ultramafic lamprophyre emplacement in the alkaline province located 64–67 N in southern West Greenland. *Lithos*, *112*, 400-406.

Shatskiy, A., Bekhtenova, A., Podborodnikov, I. V., Arefiev, A. V., and Litasov, K. D. (2020). Metasomatic interaction of the eutectic Na-and K-bearing carbonate melts with natural garnet lherzolite at 6 GPa and 1100–1200° C: toward carbonatite melt composition in SCLM. *Lithos*, *374*, 105725.

Shimizu, N. (1975). Rare earth elements in garnets and clinopyroxenes from garnet lherzolite nodules in kimberlites. *Earth and Planetary Science Letters*, *25*(1), 26-32.

Shimizu, N., and Richardson, S. H. (1987). Trace element abundance patterns of garnet inclusions in peridotite-suite diamonds. *Geochimica et Cosmochimica Acta*, *51*(3), 755-758.

Shu, Q., and Brey, G. P. (2015). Ancient mantle metasomatism recorded in subcalcic garnet xenocrysts: Temporal links between mantle metasomatism, diamond growth and crustal tectonomagmatism. *Earth and Planetary Science Letters*, *418*, 27-39.

Skulski, T., Sandeman, H., Sanborn-Barrie, M., MacHattie, T., Young, M., Carson, C., Berman, R., Brown, J., Rayner, N., Panagapko, D., Byrne, D., and Deyell, C. (2003). Bedrock geology of the Ellice Hills map area and new constraints on the regional geology of the Committee Bay area, Nunavut. Geological Survey of Canada, Current Research, 2003-C22, 1-11.

Smart, K. A., Chacko, T., Simonetti, A., Sharp, Z. D., and Heaman, L. M. (2014). A record of Paleoproterozoic subduction preserved in the Northern Slave cratonic mantle: Sr–Pb–O isotope and trace-element investigations of eclogite xenoliths from the Jericho and Muskox kimberlites. *Journal of Petrology*, *55*(3), 549-583.

Smit, K. V., Pearson, D. G., Stachel, T., and Seller, M. (2014a). Peridotites from Attawapiskat, Canada: Mesoproterozoic reworking of Palaeoarchaean lithospheric mantle beneath the Northern Superior superterrane. *Journal of Petrology*, *55*(9), 1829-1863.

Smit, K. V., Stachel, T., Creaser, R. A., Ickert, R. B., DuFrane, S. A., Stern, R. A., and Seller, M. (2014b). Origin of eclogite and pyroxenite xenoliths from the Victor kimberlite, Canada, and implications for Superior craton formation. *Geochimica et Cosmochimica Acta*, *125*, 308-337.

Smit, K. V., Stachel, T., and Stern, R. A. (2014c). Diamonds in the Attawapiskat area of the Superior craton (Canada): evidence for a major diamond-forming event younger than 1.1 Ga. *Contributions to Mineralogy and Petrology*, *167*(1), 1-16.

Smith, C. B. (1983). Pb, Sr and Nd isotopic evidence for sources of southern African Cretaceous kimberlites. *Nature*, *304*(5921), 51-54.

Smith, C. B., Colgan, E. A., Hawthorne, J. B., and Hutchinson, G. (1988). Emplacement age of the Cross kimberlite, southeastern British Columbia, by the Rb–Sr phlogopite method. *Canadian Journal of Earth Sciences*, *25*(5), 790-792.

Smyth, D. (2020). Petrology, Geochemistry, and Geochronology of the Pikoo Kimberlites, Saskatchewan [M.Sc. Thesis]: Edmonton, University of Alberta.

Snyder, D. B., Hillier, M. J., Kjarsgaard, B. A., De Kemp, E. A., and Craven, J. A. (2014). Lithospheric architecture of the Slave craton, northwest Canada, as determined from an interdisciplinary 3-D model. *Geochemistry, Geophysics, Geosystems*, *15*(5), 1895-1910.

Snyder, D. B., Savard, G., Kjarsgaard, B. A., Vaillancourt, A., Thurston, P. C., Ayer, J. A., Roots, E. (2021). Multidisciplinary Modeling of Mantle Lithosphere Structure Within the Superior Craton, North America. *Geochemistry, Geophysics, Geosystems, 22*, 20.

Sobolev, N. V., and Lavrent'ev, J. G. (1971). Isomorphic sodium admixture in garnets formed at high pressures. *Contributions to Mineralogy and Petrology*, *31*(1), 1-12.

Sobolev, N. V., Lavrent'Ev, Y. G., Pokhilenko, N. P., and Usova, L. V. (1973). Chrome-rich garnets from the kimberlites of Yakutia and their parageneses. *Contributions to Mineralogy and Petrology*, *40*(1), 39-52.

Sobolev, S. V., Sobolev, A. V., Kuzmin, D. V., Krivolutskaya, N. A., Petrunin, A. G., Arndt, N. T., Radko, V. A., and Vasiliev, Y. R. (2011). Linking mantle plumes, large igneous provinces and environmental catastrophes. *Nature*, *477*(7364), 312-316.

Söderlund, U., Patchett, P. J., Vervoort, J. D., and Isachsen, C. E. (2004). The 176Lu decay constant determined by Lu–Hf and U–Pb isotope systematics of Precambrian mafic intrusions. *Earth and Planetary Science Letters*, *219*(3-4), 311-324.

Sokol, A. G., Kruk, A. N., Chebotarev, D. A., Palyanov, Y. N., and Sobolev, N. V. (2015). Conditions of carbonation and wehrlitization of lithospheric peridotite upon interaction with carbonatitic melts. In *Doklady Earth Sciences*, *465*(2), 1262-1267.

Spratt, J. E., Jones, A. G., Jackson, V. A., Collins, L., and Avdeeva, A. (2009). Lithospheric geometry of the Wopmay orogen from a Slave craton to Bear Province magnetotelluric transect. *Journal of Geophysical Research: Solid Earth*, *114*(B1).

St-Onge, M. R., Searle, M. P., and Wodicka, N. (2006). Trans-Hudson Orogen of North America and Himalaya-Karakoram-Tibetan Orogen of Asia: Structural and thermal characteristics of the lower and upper plates. *Tectonics*, *25*(4).

Stachel, T., and Harris, J. W. (2008). The origin of cratonic diamonds—constraints from mineral inclusions. *Ore Geology Reviews*, *34*(1-2), 5-32.

Stachel, T., and Luth, R. W. (2015). Diamond formation—Where, when and how?. *Lithos*, *220*, 200-220.

Stachel, T., Lorenz, V., Smith, C. B., and Jaques, A. L. (1991). Evolution of four individual lamproite pipes, Ellendale volcanic field (Western Australia). In *Proceedings of the 5th International Kimberlite Conference*, *1*, 177-194.

Stachel, T., Viljoen, K. S., Brey, G., and Harris, J. W. (1998). Metasomatic processes in lherzolitic and harzburgitic domains of diamondiferous lithospheric mantle: REE in garnets from xenoliths and inclusions in diamonds. *Earth and Planetary Science Letters*, *159*(1-2), 1-12.

Stachel, T., Aulbach, S., Brey, G. P., Harris, J. W., Leost, I., Tappert, R., and Viljoen, K. F. (2004). The trace element composition of silicate inclusions in diamonds: a review. *Lithos*, *77*(1-4), 1-19.

Stachel, T., Banas, A., Aulbach, S., Smit, K. V., Wescott, P., Chinn, I. L., and Kong, J. (2018). The Victor Mine (Superior Craton, Canada): Neoproterozoic lherzolitic diamonds from a thermally-modified cratonic root. *Mineralogy and Petrology*, *112*(1), 325-336.

Stern, R. A., Syme, E. C., Bailes, A. H., and Lucas, S. B. (1995). Paleoproterozoic (1.90–1.86 Ga) arc volcanism in the Flin Flon Belt, Trans-Hudson Orogen, Canada. *Contributions to Mineralogy and Petrology*, *119*(2), 117-141.

Sudholz, Z. J., Yaxley, G. M., Jaques, A. L., and Chen, J. (2021). Ni-in-garnet geothermometry in mantle rocks: a high pressure experimental recalibration between 1100 and 1325° C. *Contributions to Mineralogy and Petrology*, *176*(5), 1-16.

Tappe, S., Foley, S. F., Jenner, G. A., Heaman, L. M., Kjarsgaard, B. A., Romer, R. L., Stracke, A., Joyce, N., and Hoefs, J. (2006). Genesis of ultramafic lamprophyres and carbonatites at Aillik Bay, Labrador: a consequence of incipient lithospheric thinning beneath the North Atlantic craton. *Journal of Petrology*, *47*(7), 1261-1315.

Tappe, S., Steenfelt, A., Heaman, L. M., and Simonetti, A. (2009). The newly discovered Jurassic Tikiusaaq carbonatite-aillikite occurrence, West Greenland, and some remarks on carbonatite–kimberlite relationships. *Lithos*, *112*, 385-399.

Tappe, S., Pearson, D. G., Nowell, G., Nielsen, T., Milstead, P., and Muehlenbachs, K. (2011). A fresh isotopic look at Greenland kimberlites: cratonic mantle lithosphere imprint on deep source signal. *Earth and Planetary Science Letters*, *305*(1-2), 235-248.

Tappe, S., Pearson, D. G., Kjarsgaard, B. A., Nowell, G., and Dowall, D. (2013). Mantle transition zone input to kimberlite magmatism near a subduction zone: origin of anomalous Nd–Hf isotope systematics at Lac de Gras, Canada. *Earth and Planetary Science Letters*, *371*, 235-251.

Tappe, S., Kjarsgaard, B. A., Kurszlaukis, S., Nowell, G. M., and Phillips, D. (2014). Petrology and Nd–Hf isotope geochemistry of the Neoproterozoic Amon kimberlite sills, Baffin Island (Canada): evidence for deep mantle magmatic activity linked to supercontinent cycles. *Journal of Petrology*, *55*(10), 2003-2042.

Tappe, S., Smart, K., Torsvik, T., Massuyeau, M., and de Wit, M. (2018). Geodynamics of kimberlites on a cooling Earth: clues to plate tectonic evolution and deep volatile cycles. *Earth and Planetary Science Letters*, *484*, 1-14.

Taras, B. D., and Hart, S. R. (1987). Geochemical evolution of the New England seamount chain: Isotopic and trace-element constraints. *Chemical Geology*, *64*(1-2), 35-54.

Tella, S., Hanmer, S., Ryan, J. J., Sandeman, H. A., Davis, W. J., Berman, R., and Mills, A. (2000). 1: 100000 scale bedrock geology compilation map of the MacQuoid Lake-Gibson Lake-Cross Bay-Akunak Bay region, western Churchill province, Nunavut, Canada. In *Geological Association of Canada Mineral Association of Canada Program Abstracts*, *25*, 676.

Thorpe, R. I., Cumming, G. L., and Mortensen, J. K. (1992). A significant Pb isotope boundary in the Slave Province and its probable relation to ancient basement in the western Slave Province. *Geological Survey of Canada Open File*, *2484*, 179-184.

Torsvik, T. H. (2019). Earth history: A journey in time and space from base to top. *Tectonophysics*, *760*, 297-313.

Torsvik, T. H., Burke, K., Steinberger, B., Webb, S. J., and Ashwal, L. D. (2010). Diamonds sampled by plumes from the core–mantle boundary. *Nature*, *466*(7304), 352-355.

Torsvik, T. H., and Cocks, L. R. M. (2013). Gondwana from top to base in space and time. *Gondwana Research*, *24*(3-4), 999-1030.

Vance, D., and Thirlwall, M. (2002). An assessment of mass discrimination in MC-ICPMS using Nd isotopes. *Chemical Geology*, *185*(3-4), 227-240.

Vermeesch, P. (2018). IsoplotR: A free and open toolbox for geochronology. *Geoscience Frontiers*, *9*(5), 1479-1493.

Hobbs, W. H. (1899). The diamond field of the Great Lakes. *The Journal of Geology*, *7*(4), 375-388.

Wagner, P. A. (1914). *The diamond fields of southern Africa*. Transvaal leader.

Waterton, P., Pearson, D. G., Mertzman, S. A., Mertzman, K. R., and Kjarsgaard, B. A. (2020). A fractional crystallization link between komatiites, basalts, and dunites of the Palaeoproterozoic Winnipegosis Komatiite Belt, Manitoba, Canada. *Journal of Petrology*, *61*(5), egaa052.

Waterton, P., Pearson, D. G., Kjarsgaard, B., Hulbert, L., Locock, A., Parman, S., and Davis, B. (2017). Age, origin, and thermal evolution of the ultra-fresh~ 1.9 Ga Winnipegosis Komatiites, Manitoba, Canada. *Lithos*, *268*, 114-130.

Webb, K. J., Smith, B. H. S., Paul, J. L., and Hetman, C. M. (2004). Geology of the Victor Kimberlite, Attawapiskat, Northern Ontario, Canada: cross-cutting and nested craters. *Lithos*, *76*(1-4), 29-50.

Wendt, I., Kreuzer, H., Müller, P., Von Rad, U., and Raschka, H. (1976). K–Ar age of basalts from Great Meteor and Josephine seamounts (eastern North Atlantic). In *Deep Sea Research and Oceanographic Abstracts*, *23*(9), 849-862.

Wheeler, J. O., Hoffman, P. F., Card, K. D., Davidson, A., Sanford, B. V., Okulitch, A. V., and Roest, W. R. (1996). Geologic Map of Canada. Geological Survey of CanadaMap 1860A, scale 1:5000000.

Wittig, N., Pearson, D. G., Webb, M., Ottley, C. J., Irvine, G. J., Kopylova, M., Jensen, S. M., and Nowell, G. M. (2008). Origin of cratonic lithospheric mantle roots: A geochemical study of peridotites from the North Atlantic Craton, West Greenland. *Earth and Planetary Science Letters*, *274*(1-2), 24-33.

Woolley, A. R., Bergman, S. C., Edgar, A. D., Le Bas, M. J., Mitchell, R. H., Rock, N. M., and Scott Smith, B. H. (1996). Classification of lamprophyres, lamproites, kimberlites, and the kalsilitic, melilitic, and leucitic rocks. *The Canadian Mineralogist*, *34*(2), 175-186.

Woodhead, J., Hergt, J., Giuliani, A., Maas, R., Phillips, D., Pearson, D. G., and Nowell, G. (2019). Kimberlites reveal 2.5-billion-year evolution of a deep, isolated mantle reservoir. *Nature*, *573*(7775), 578-581.

Woodland, A. B., Gräf, C., Sandner, T., Höfer, H. E., Seitz, H. M., Pearson, D. G., and Kjarsgaard, B. A. (2021). Oxidation state and metasomatism of the lithospheric mantle beneath the Rae Craton, Canada: strong gradients reflect craton formation and evolution. *Scientific reports*, *11*(1), 1-10.

Wyatt, B. A., Baumgartner, M., Anckar, E., and Grütter, H. (2004). Compositional classification of "kimberlitic" and "non-kimberlitic" ilmenite. *Lithos*, *77*(1-4), 819-840.

Yang, Y. H., Zhang, H. F., Chu, Z. Y., Xie, L. W., and Wu, F. Y. (2010). Combined chemical separation of Lu, Hf, Rb, Sr, Sm and Nd from a single rock digest and precise and accurate isotope determinations of Lu–Hf, Rb–Sr and Sm–Nd isotope systems using Multi-Collector ICP-MS and TIMS. *International Journal of Mass Spectrometry*, *290*(2-3), 120-126.

Zurevinski, S. E., Heaman, L. M., Creaser, R. A., and Strand, P. (2008). The Churchill kimberlite field, Nunavut, Canada: petrography, mineral chemistry, and geochronology. *Canadian Journal of Earth Sciences*, *45*(9), 1039-1059.

Zurevinski, S. E., Heaman, L. M., and Creaser, R. A. (2011). The origin of Triassic/Jurassic kimberlite magmatism, Canada: Two mantle sources revealed from the Sr-Nd isotopic composition of groundmass perovskite. *Geochemistry, Geophysics, Geosystems*, *12*(9).

APPENDICES

Appendix A: Rock.AR Point Count Figures

Appendix A.01: Rock.AR Point Count of Mel kimberlite sample 49716A.

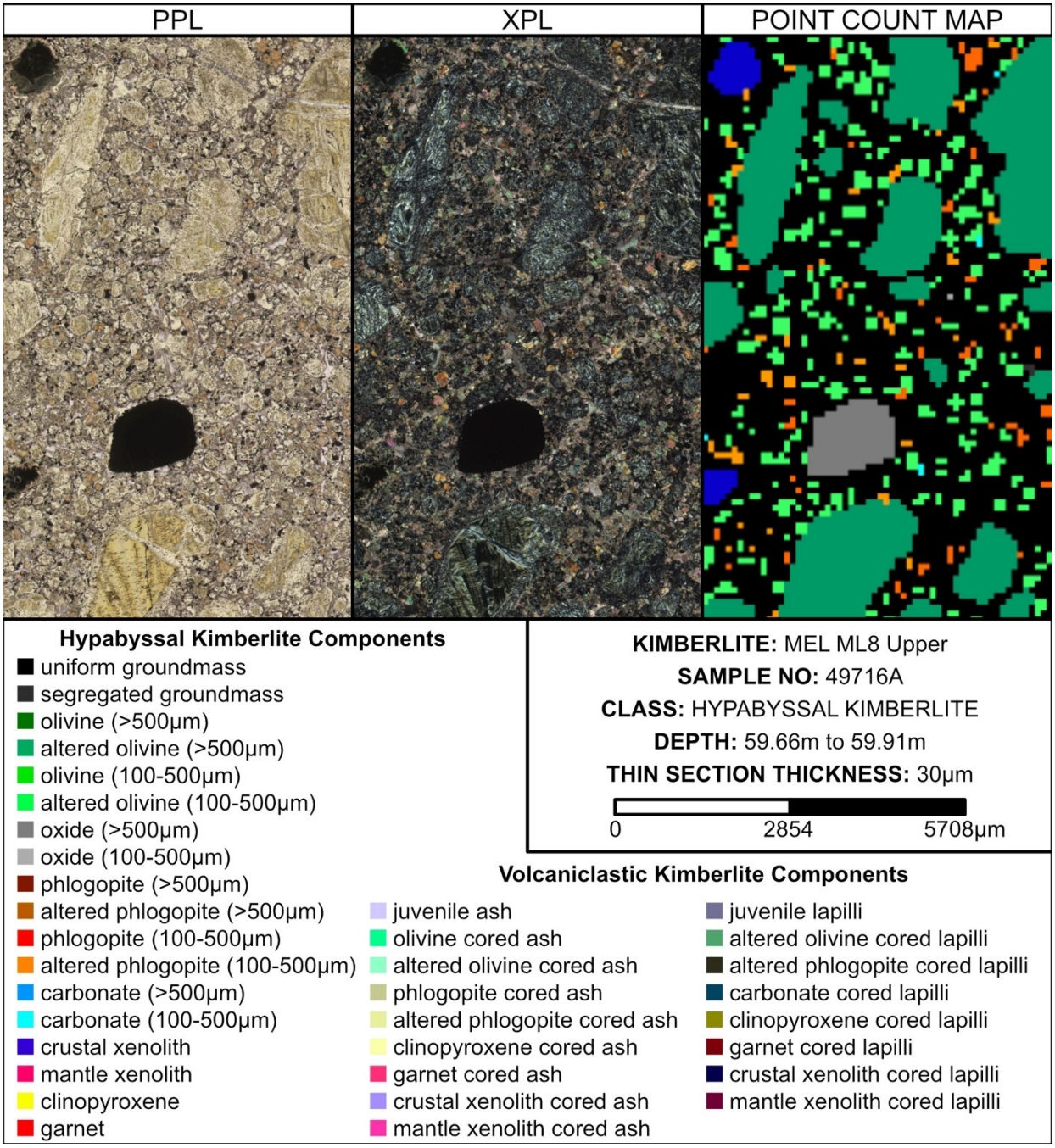

Appendix A: Rock.AR Point Count Figures

Appendix A.02: Rock.AR Point Count of Mel kimberlite sample 49716.01.

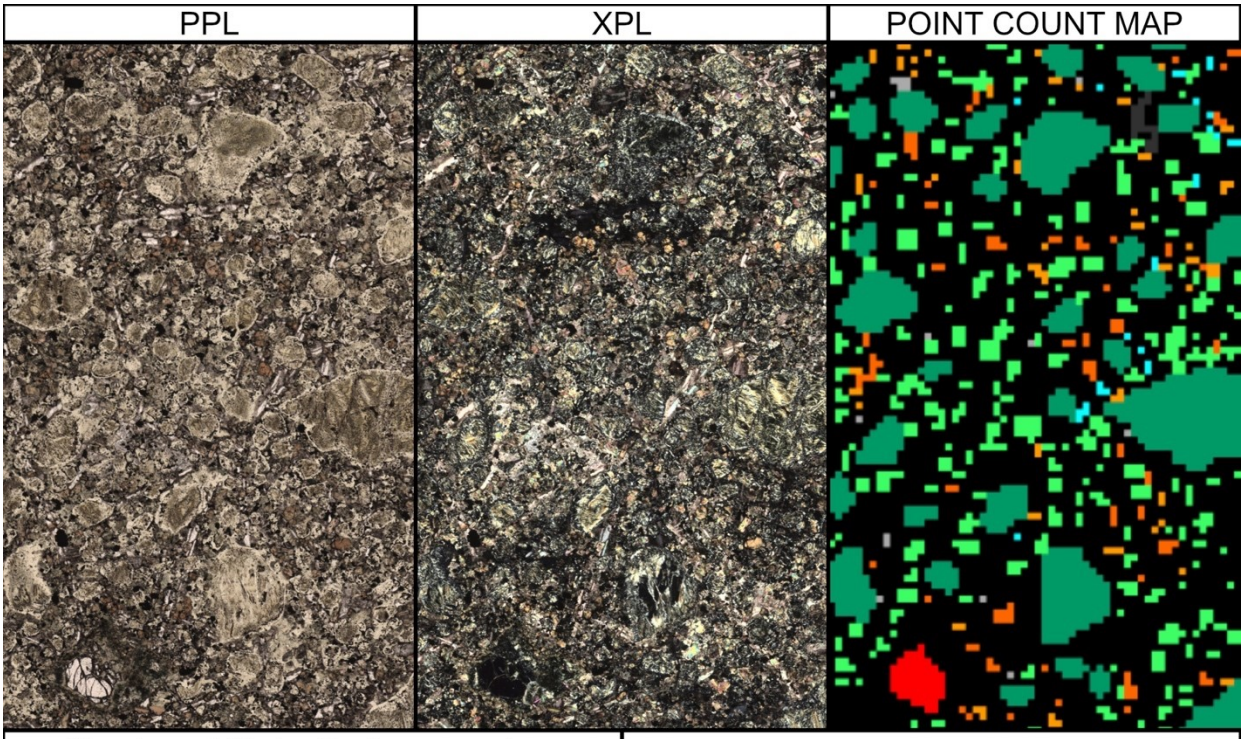

Hypabyssal Kimberlite Components

- uniform groundmass
- segregated groundmass
- olivine (>500µm)
- altered olivine (>500µm)
- olivine (100-500µm)
- altered olivine (100-500µm)
- oxide (>500µm)
- oxide (100-500µm)
- phlogopite (>500µm)
- altered phlogopite (>500µm)
- phlogopite (100-500µm)
- altered phlogopite (100-500µm)
- carbonate (>500µm)
- carbonate (100-500µm)
- crustal xenolith
- mantle xenolith
- clinopyroxene
- garnet

KIMBERLITE: MEL ML8 Upper
SAMPLE NO: 49716.01
CLASS: HYPABYSSAL KIMBERLITE
DEPTH: 59.66m to 59.91m
THIN SECTION THICKNESS: 50µm

0 2854 5708µm

Volcaniclastic Kimberlite Components

- juvenile ash
- olivine cored ash
- altered olivine cored ash
- phlogopite cored ash
- altered phlogopite cored ash
- clinopyroxene cored ash
- garnet cored ash
- crustal xenolith cored ash
- mantle xenolith cored ash
- juvenile lapilli
- altered olivine cored lapilli
- altered phlogopite cored lapilli
- carbonate cored lapilli
- clinopyroxene cored lapilli
- garnet cored lapilli
- crustal xenolith cored lapilli
- mantle xenolith cored lapilli

Appendix A: Rock.AR Point Count Figures

Appendix A.03: Rock.AR Point Count of Mel kimberlite sample 49716.03.

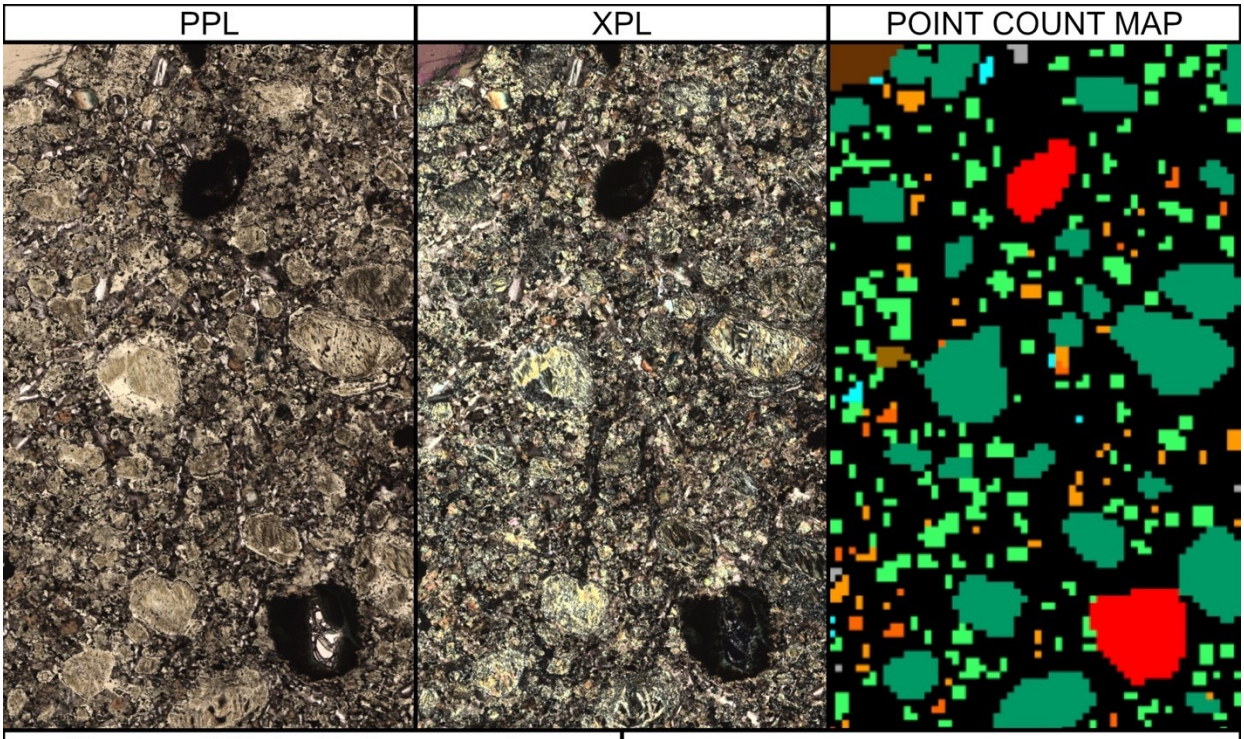

Hypabyssal Kimberlite Components

- uniform groundmass
- segregated groundmass
- olivine (>500µm)
- altered olivine (>500µm)
- olivine (100-500µm)
- altered olivine (100-500µm)
- oxide (>500µm)
- oxide (100-500µm)
- phlogopite (>500µm)
- altered phlogopite (>500µm)
- phlogopite (100-500µm)
- altered phlogopite (100-500µm)
- carbonate (>500µm)
- carbonate (100-500µm)
- crustal xenolith
- mantle xenolith
- clinopyroxene
- garnet

KIMBERLITE: MEL ML8 Upper
SAMPLE NO: 49716.03
CLASS: HYPABYSSAL KIMBERLITE
DEPTH: 59.66m to 59.91m
THIN SECTION THICKNESS: 50µm

0 2854 5708µm

Volcaniclastic Kimberlite Components

- juvenile ash
- olivine cored ash
- altered olivine cored ash
- phlogopite cored ash
- altered phlogopite cored ash
- clinopyroxene cored ash
- garnet cored ash
- crustal xenolith cored ash
- mantle xenolith cored ash
- juvenile lapilli
- altered olivine cored lapilli
- altered phlogopite cored lapilli
- carbonate cored lapilli
- clinopyroxene cored lapilli
- garnet cored lapilli
- crustal xenolith cored lapilli
- mantle xenolith cored lapilli

Appendix A: Rock.AR Point Count Figures

Appendix A.04: Rock.AR Point Count of Mel kimberlite sample 49716.05.

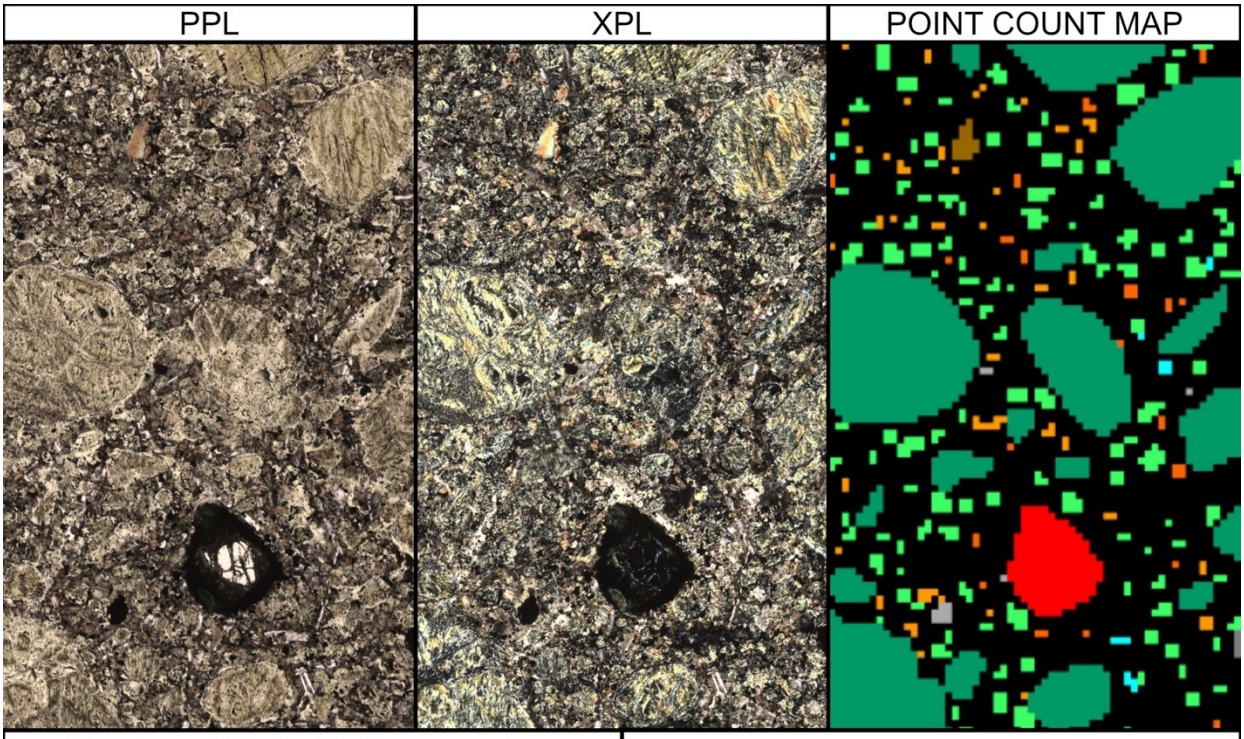

Hypabyssal Kimberlite Components

- uniform groundmass
- segregated groundmass
- olivine (>500µm)
- altered olivine (>500µm)
- olivine (100-500µm)
- altered olivine (100-500µm)
- oxide (>500µm)
- oxide (100-500µm)
- phlogopite (>500µm)
- altered phlogopite (>500µm)
- phlogopite (100-500µm)
- altered phlogopite (100-500µm)
- carbonate (>500µm)
- carbonate (100-500µm)
- crustal xenolith
- mantle xenolith
- clinopyroxene
- garnet

KIMBERLITE: MEL ML8 Upper
SAMPLE NO: 49716.05
CLASS: HYPABYSSAL KIMBERLITE
DEPTH: 59.66m to 59.91m
THIN SECTION THICKNESS: 50µm

0 2854 5708µm

Volcaniclastic Kimberlite Components

- juvenile ash
- olivine cored ash
- altered olivine cored ash
- phlogopite cored ash
- altered phlogopite cored ash
- clinopyroxene cored ash
- garnet cored ash
- crustal xenolith cored ash
- mantle xenolith cored ash
- juvenile lapilli
- altered olivine cored lapilli
- altered phlogopite cored lapilli
- carbonate cored lapilli
- clinopyroxene cored lapilli
- garnet cored lapilli
- crustal xenolith cored lapilli
- mantle xenolith cored lapilli

Appendix A: Rock.AR Point Count Figures

Appendix A.05: Rock.AR Point Count of Mel kimberlite sample 49720A.

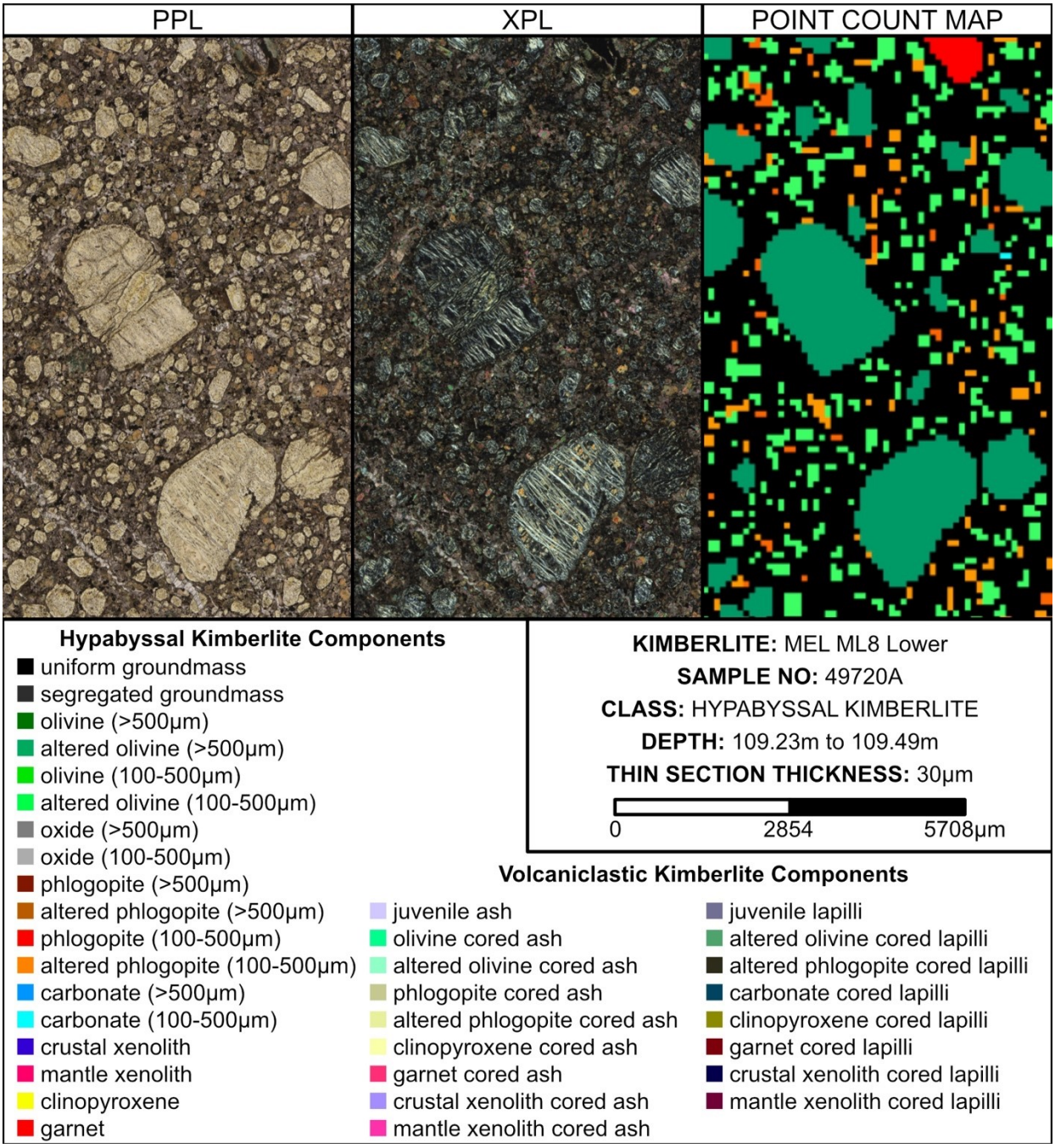

Appendix A: Rock.AR Point Count Figures

Appendix A.06: Rock.AR Point Count of Mel kimberlite sample 49720.01.

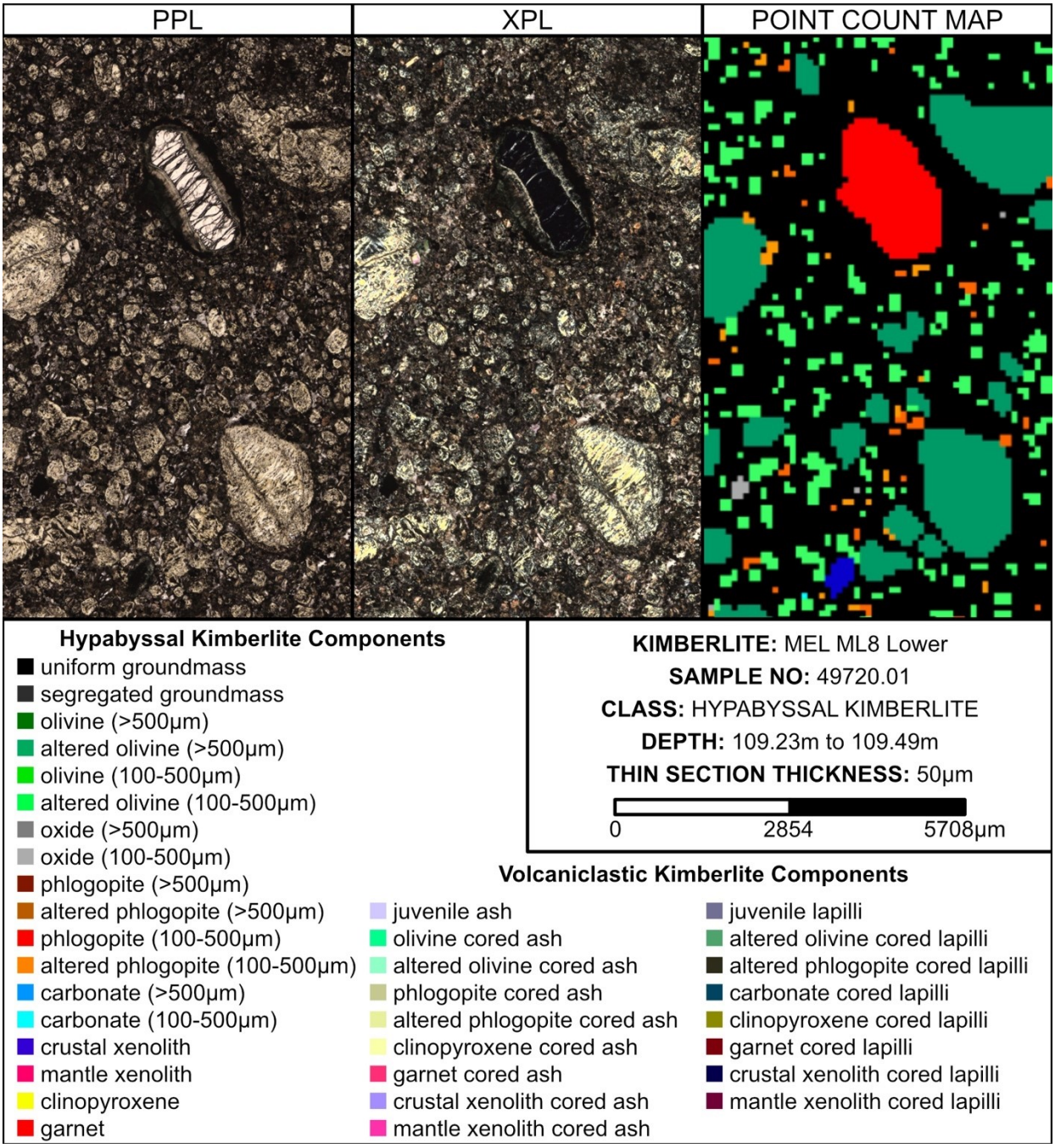

Appendix A: Rock.AR Point Count Figures

Appendix A.07: Rock.AR Point Count of Mel kimberlite sample 49721A.

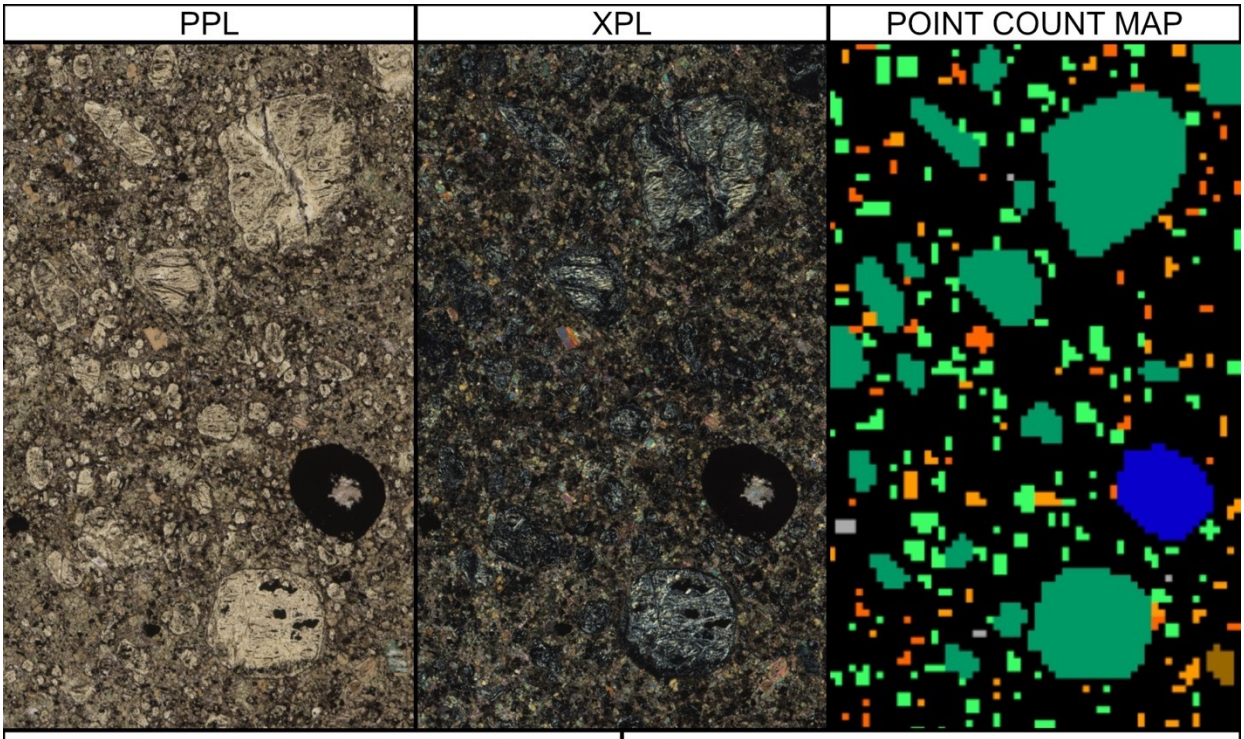

Hypabyssal Kimberlite Components

- uniform groundmass
- segregated groundmass
- olivine (>500µm)
- altered olivine (>500µm)
- olivine (100-500µm)
- altered olivine (100-500µm)
- oxide (>500µm)
- oxide (100-500µm)
- phlogopite (>500µm)
- altered phlogopite (>500µm)
- phlogopite (100-500µm)
- altered phlogopite (100-500µm)
- carbonate (>500µm)
- carbonate (100-500µm)
- crustal xenolith
- mantle xenolith
- clinopyroxene
- garnet

KIMBERLITE: MEL ML8 Lower
SAMPLE NO: 49721A
CLASS: HYPABYSSAL KIMBERLITE
DEPTH: 113.63m to 113.86m
THIN SECTION THICKNESS: 30µm

0 2854 5708µm

Volcaniclastic Kimberlite Components

- juvenile ash
- olivine cored ash
- altered olivine cored ash
- phlogopite cored ash
- altered phlogopite cored ash
- clinopyroxene cored ash
- garnet cored ash
- crustal xenolith cored ash
- mantle xenolith cored ash
- juvenile lapilli
- altered olivine cored lapilli
- altered phlogopite cored lapilli
- carbonate cored lapilli
- clinopyroxene cored lapilli
- garnet cored lapilli
- crustal xenolith cored lapilli
- mantle xenolith cored lapilli

Appendix A: Rock.AR Point Count Figures

Appendix A.08: Rock.AR Point Count of Mel kimberlite sample 49721.02.

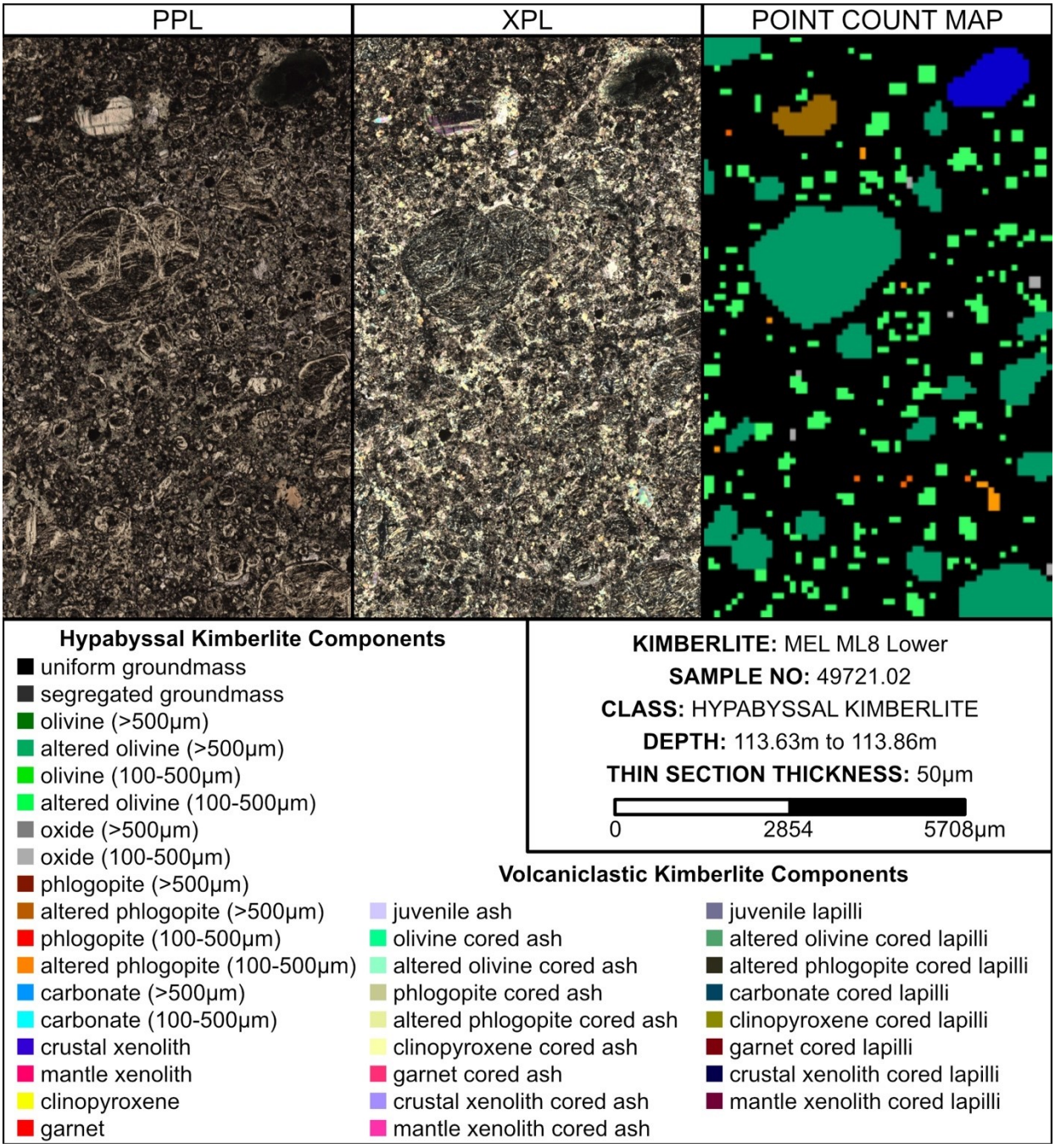

Appendix A: Rock.AR Point Count Figures

Appendix A.09: Rock.AR Point Count of Mel kimberlite sample 49722A.

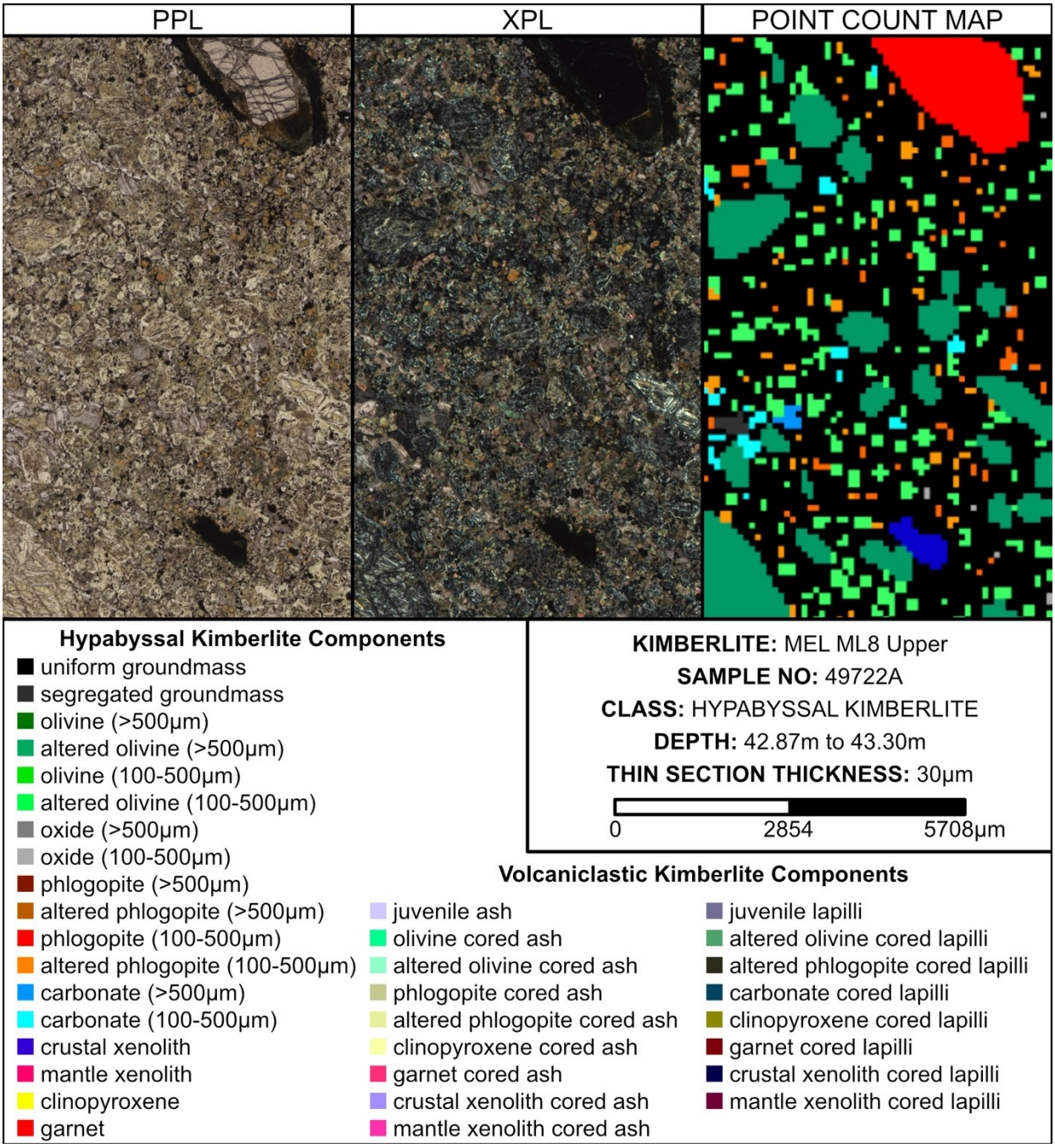

Appendix A: Rock.AR Point Count Figures

Appendix A.10: Rock.AR Point Count of Mel kimberlite sample 49722.01.

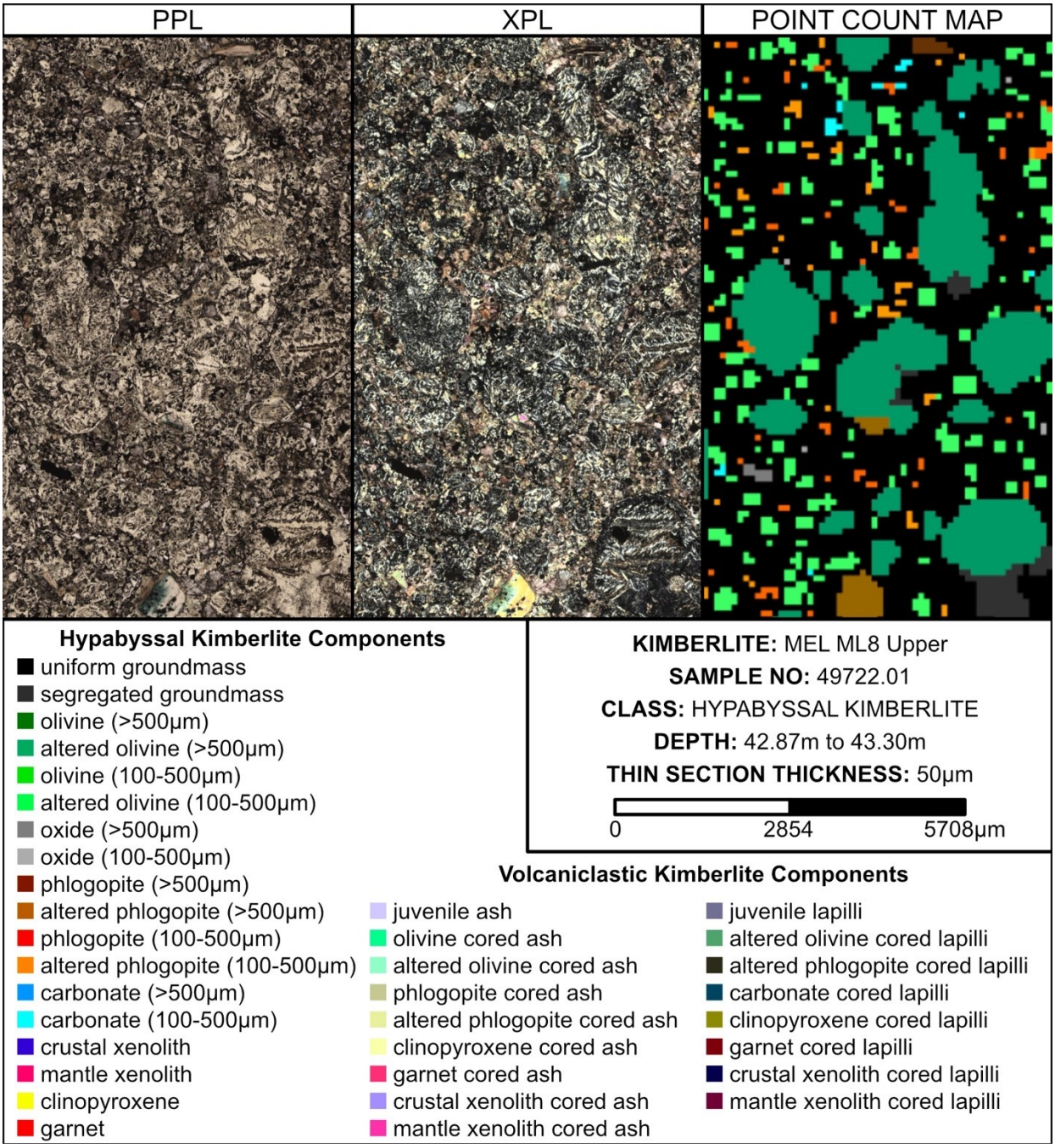

Appendix A: Rock.AR Point Count Figures

Appendix A.11: Rock.AR Point Count of Mel kimberlite sample 49722.03.

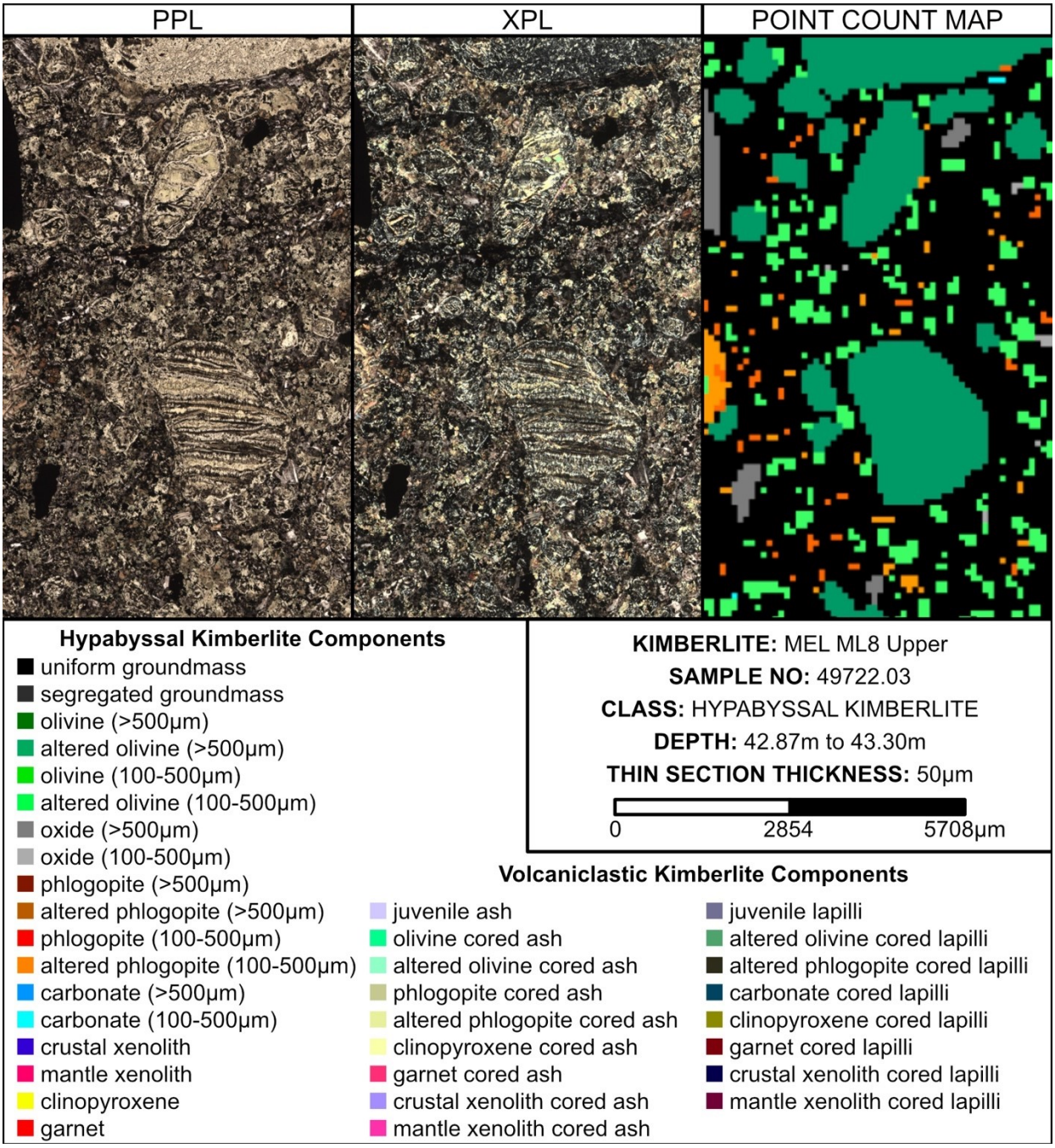

Appendix A: Rock.AR Point Count Figures

Appendix A.12: Rock.AR Point Count of Mel kimberlite sample 49723A.

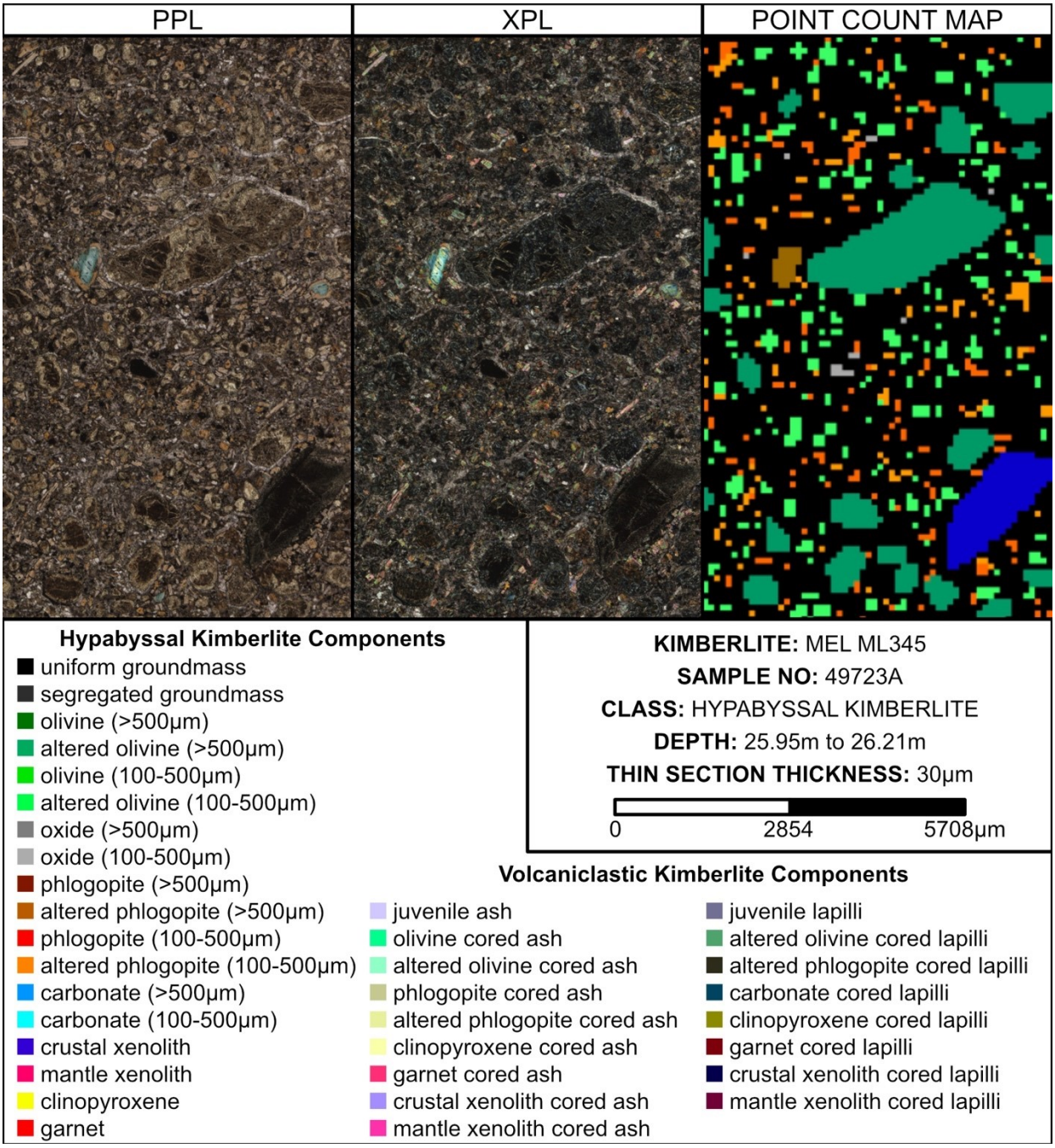

Appendix A: Rock.AR Point Count Figures

Appendix A.13: Rock.AR Point Count of Mel kimberlite sample 49723.02.

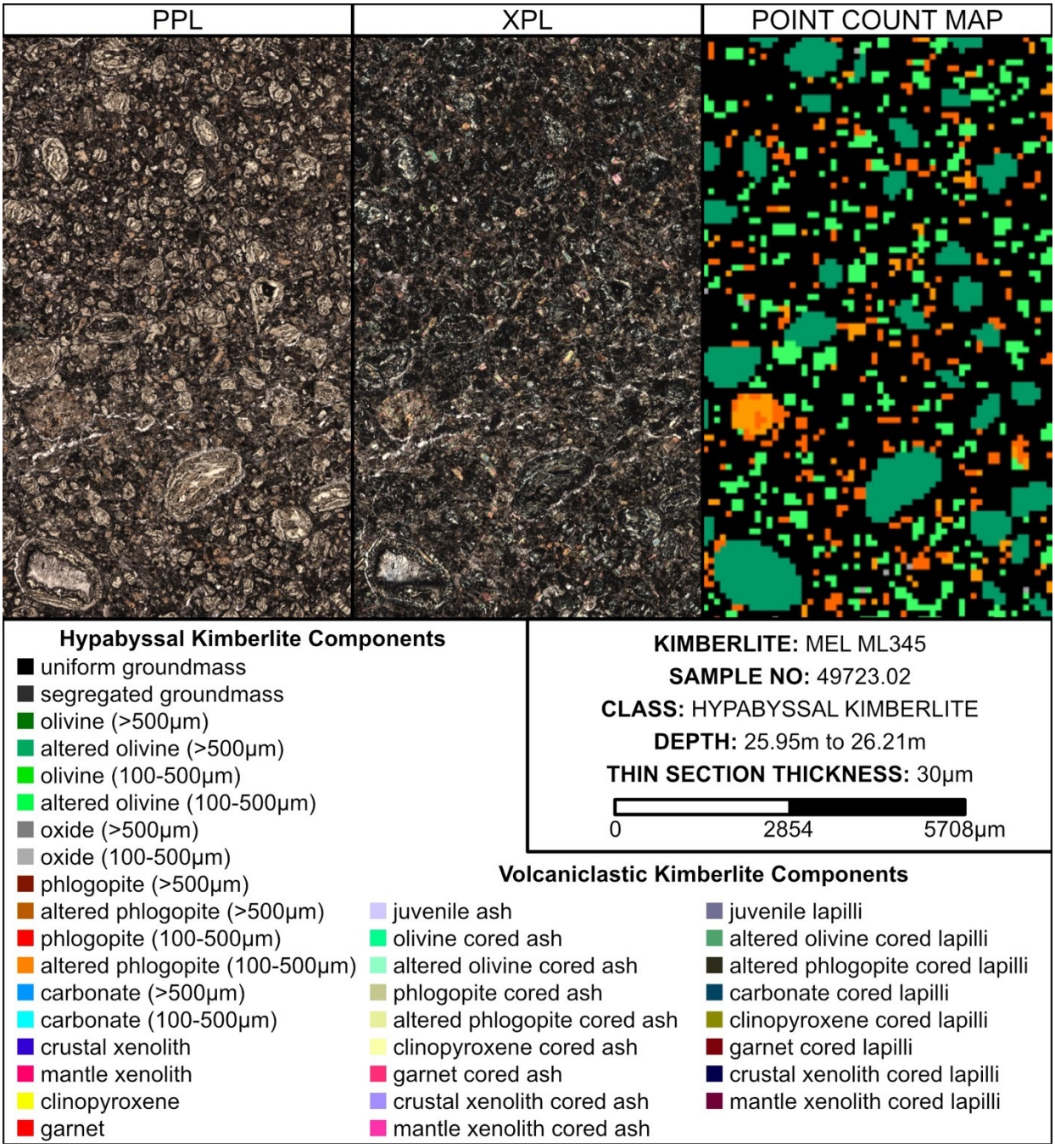

Appendix A.14: Rock.AR Point Count of Dharma kimberlite sample D86.

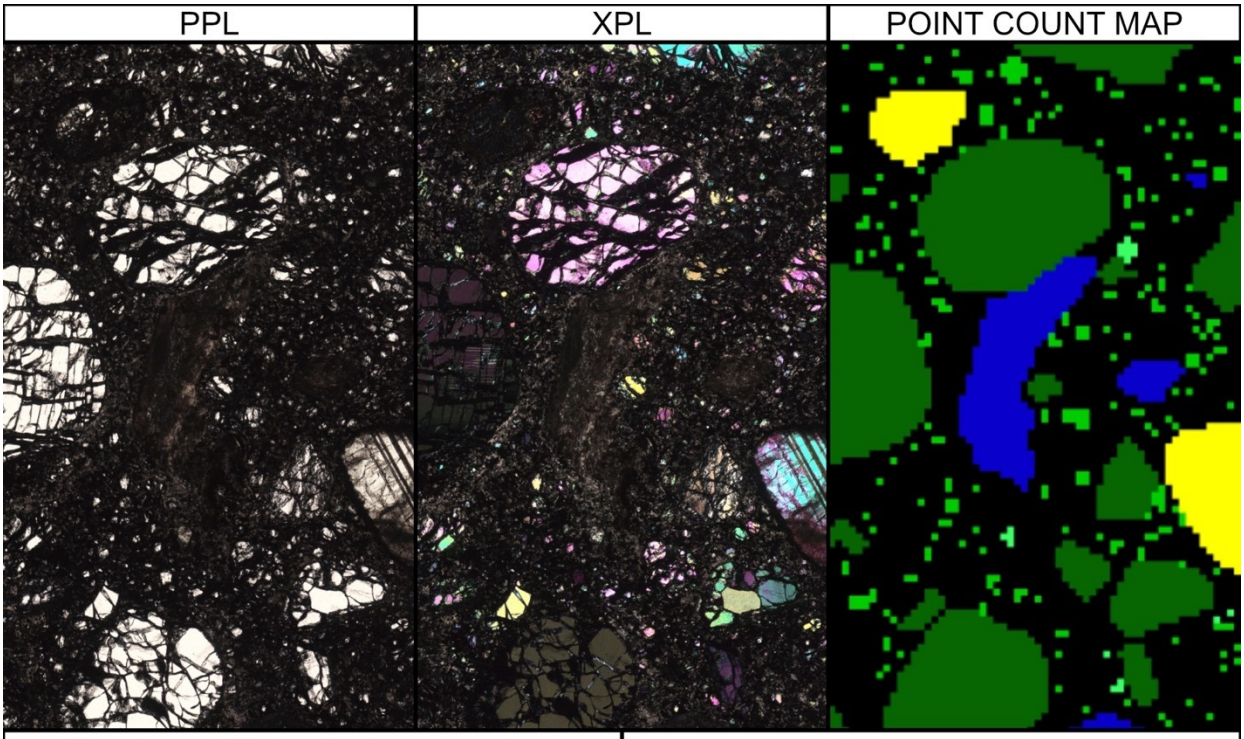

Hypabyssal Kimberlite Components

- uniform groundmass
- segregated groundmass
- olivine (>500µm)
- altered olivine (>500µm)
- olivine (100-500µm)
- altered olivine (100-500µm)
- oxide (>500µm)
- oxide (100-500µm)
- phlogopite (>500µm)
- altered phlogopite (>500µm)
- phlogopite (100-500µm)
- altered phlogopite (100-500µm)
- carbonate (>500µm)
- carbonate (100-500µm)
- crustal xenolith
- mantle xenolith
- clinopyroxene
- garnet

KIMBERLITE: DHARMA
SAMPLE NO: D86
CLASS: HYPABYSSAL KIMBERLITE
DEPTH: 58.89m to 58.96m
THIN SECTION THICKNESS: 50µm

0 2854 5708µm

Volcaniclastic Kimberlite Components

- juvenile ash
- olivine cored ash
- altered olivine cored ash
- phlogopite cored ash
- altered phlogopite cored ash
- clinopyroxene cored ash
- garnet cored ash
- crustal xenolith cored ash
- mantle xenolith cored ash
- juvenile lapilli
- altered olivine cored lapilli
- altered phlogopite cored lapilli
- carbonate cored lapilli
- clinopyroxene cored lapilli
- garnet cored lapilli
- crustal xenolith cored lapilli
- mantle xenolith cored lapilli

Appendix A.15: Rock.AR Point Count of Dharma kimberlite sample D91.

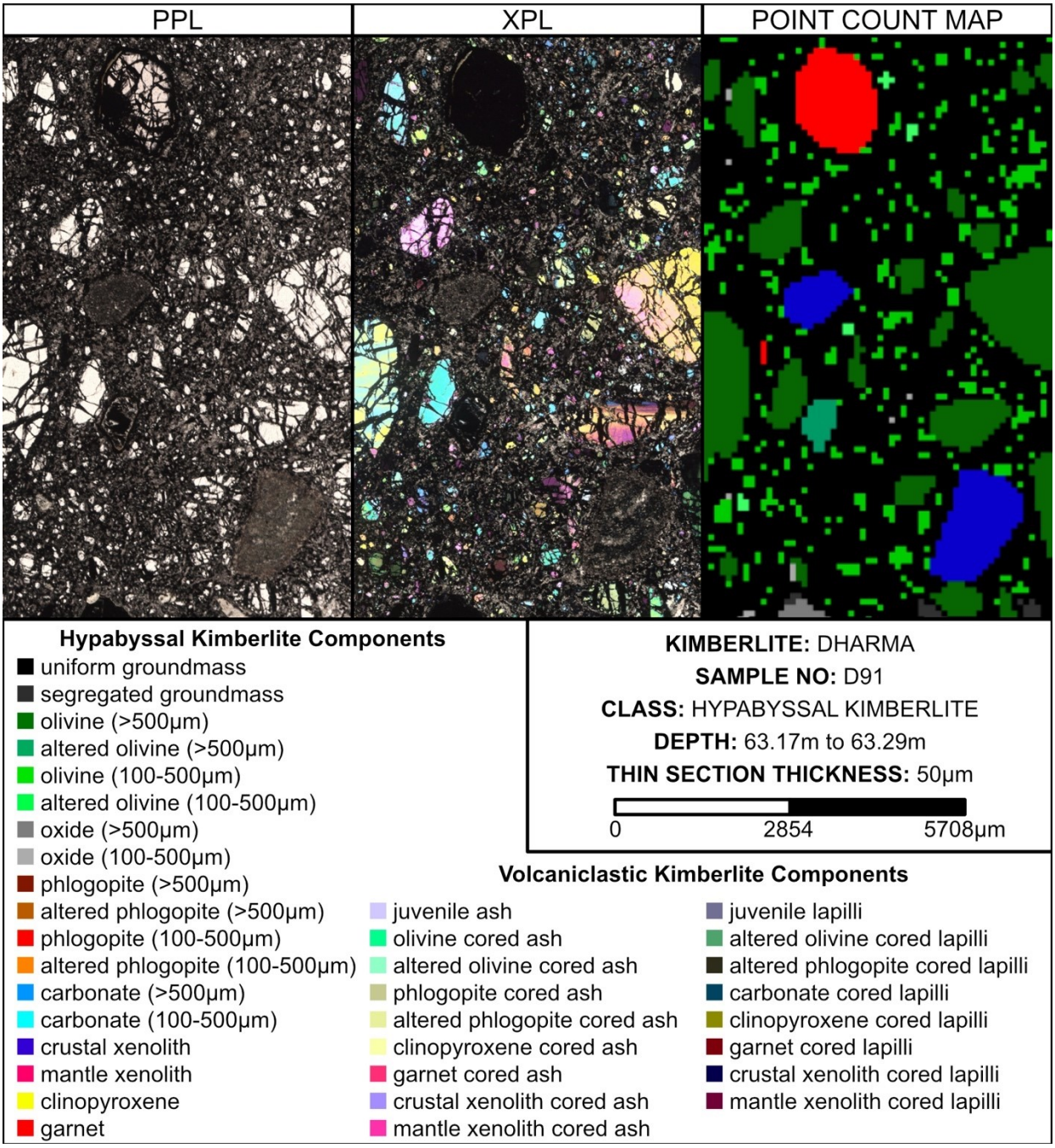

Appendix A: Rock.AR Point Count Figures

Appendix A.16: Rock.AR Point Count of Dharma kimberlite sample D92.

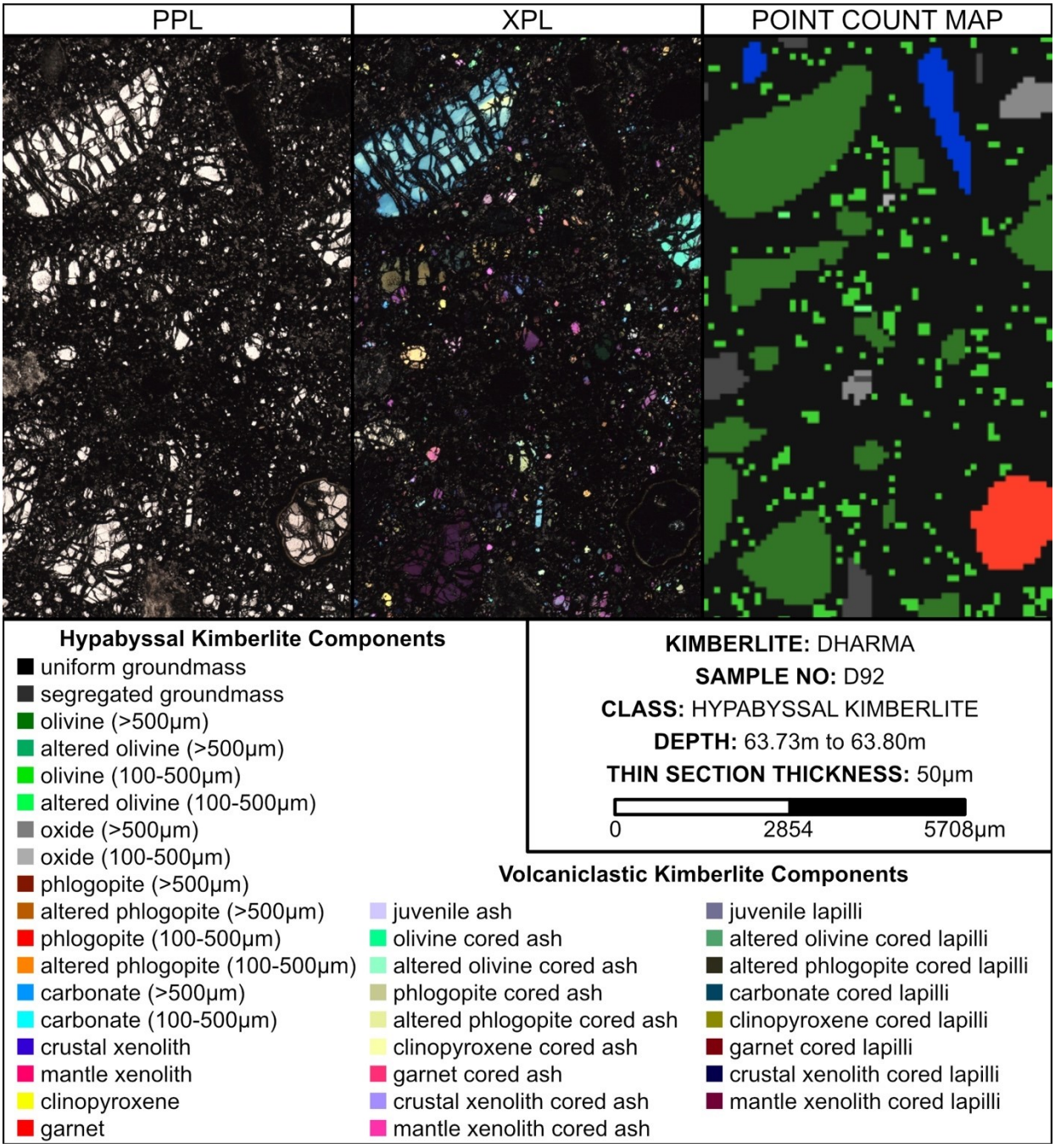

Appendix A.17: Rock.AR Point Count of Dharma kimberlite sample D94.

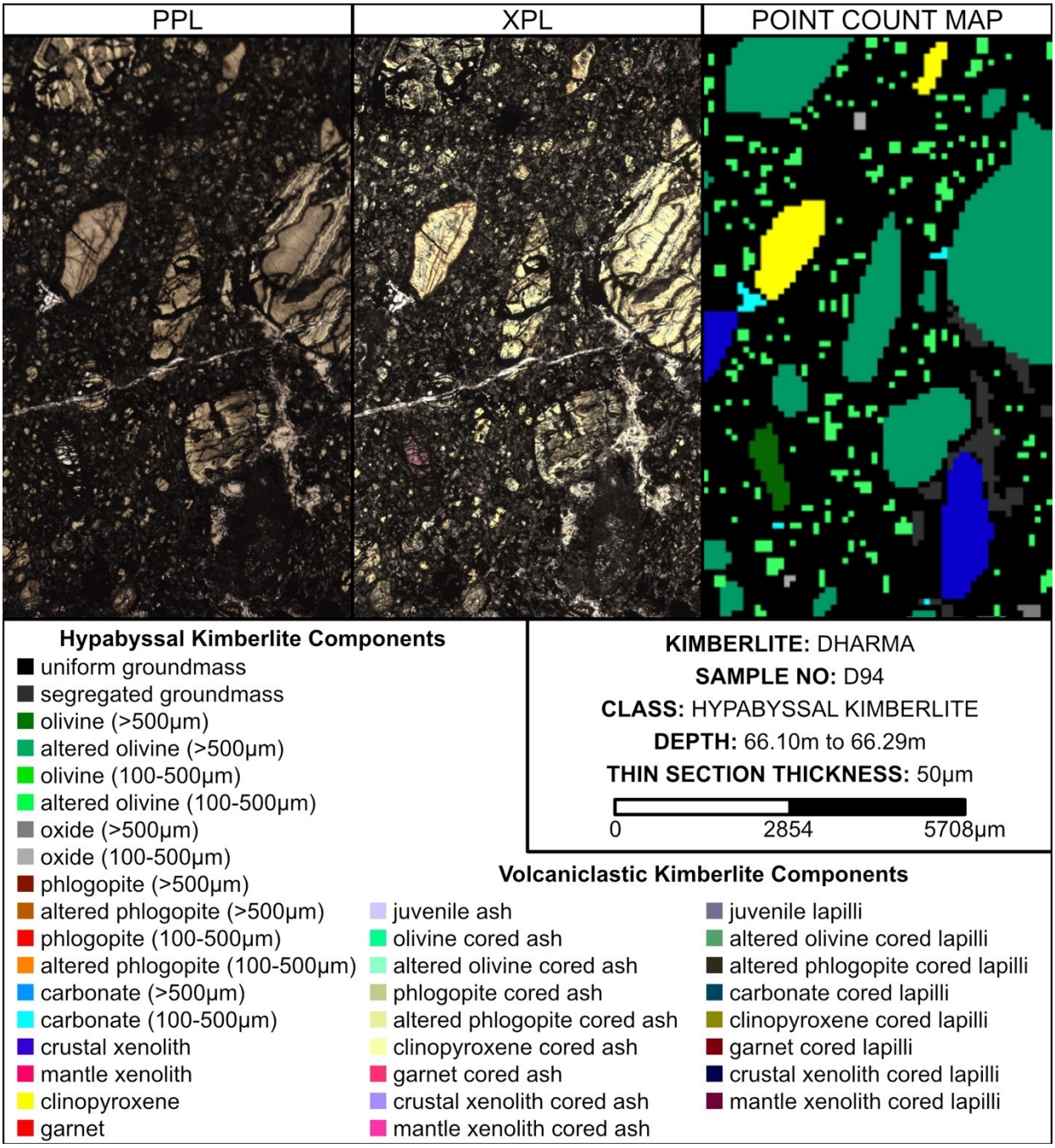

Appendix A.18: Rock.AR Point Count of Dharma kimberlite sample D95.

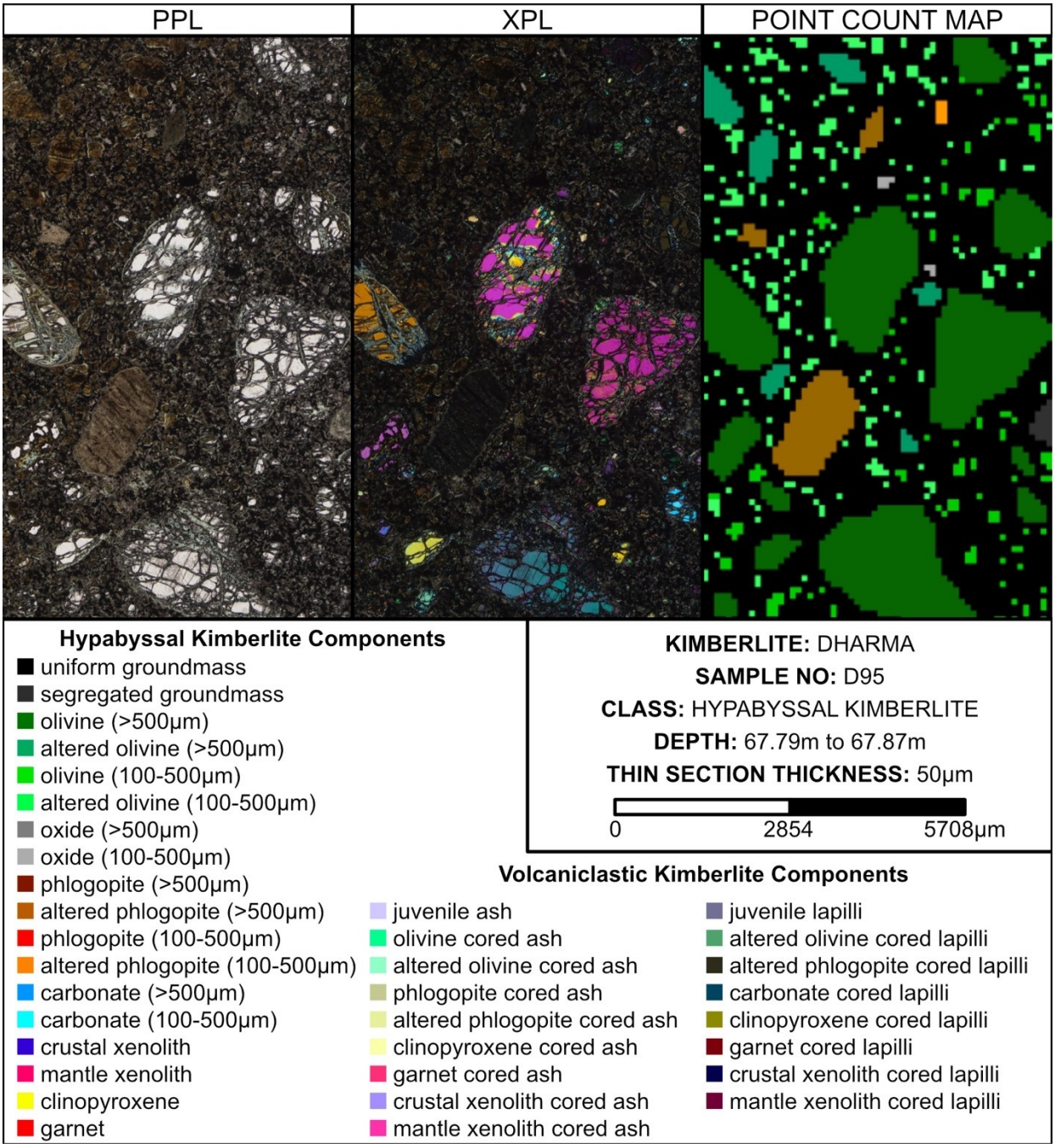

Appendix A.19: Rock.AR Point Count of Dharma kimberlite sample D98.

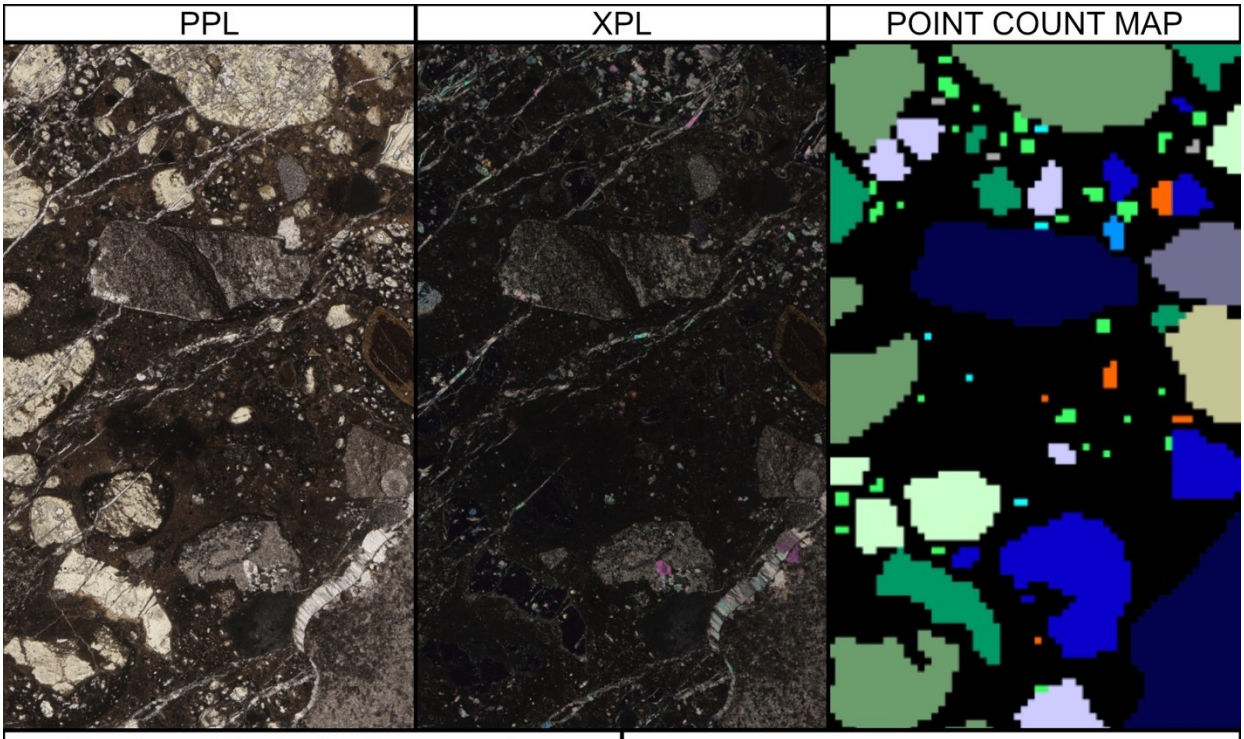

Hypabyssal Kimberlite Components

- uniform groundmass
- segregated groundmass
- olivine (>500µm)
- altered olivine (>500µm)
- olivine (100-500µm)
- altered olivine (100-500µm)
- oxide (>500µm)
- oxide (100-500µm)
- phlogopite (>500µm)
- altered phlogopite (>500µm)
- phlogopite (100-500µm)
- altered phlogopite (100-500µm)
- carbonate (>500µm)
- carbonate (100-500µm)
- crustal xenolith
- mantle xenolith
- clinopyroxene
- garnet

KIMBERLITE: DHARMA
SAMPLE NO: D98
CLASS: VOLCANICLASTIC KIMBERLITE
DEPTH: 70.58m to 70.75m
THIN SECTION THICKNESS: 50µm

0 2854 5708µm

Volcaniclastic Kimberlite Components

- juvenile ash
- olivine cored ash
- altered olivine cored ash
- phlogopite cored ash
- altered phlogopite cored ash
- clinopyroxene cored ash
- garnet cored ash
- crustal xenolith cored ash
- mantle xenolith cored ash
- juvenile lapilli
- altered olivine cored lapilli
- altered phlogopite cored lapilli
- carbonate cored lapilli
- clinopyroxene cored lapilli
- garnet cored lapilli
- crustal xenolith cored lapilli
- mantle xenolith cored lapilli

Appendix A: Rock.AR Point Count Figures

Appendix A.20: Rock.AR Point Count of Dharma kimberlite sample D101.

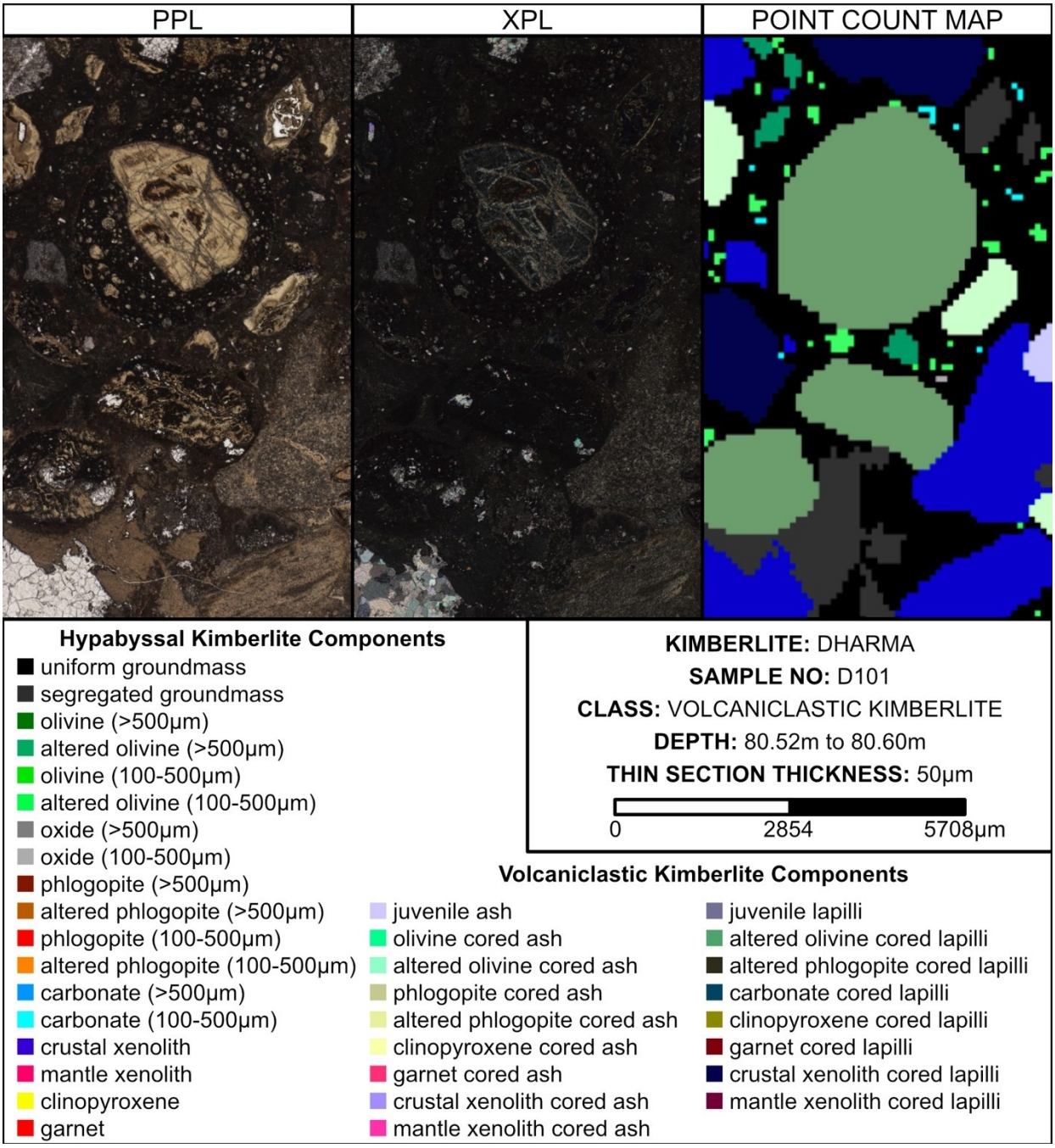

Appendix A: Rock.AR Point Count Figures

Appendix A.21: Rock.AR Point Count of Dharma kimberlite sample D104.

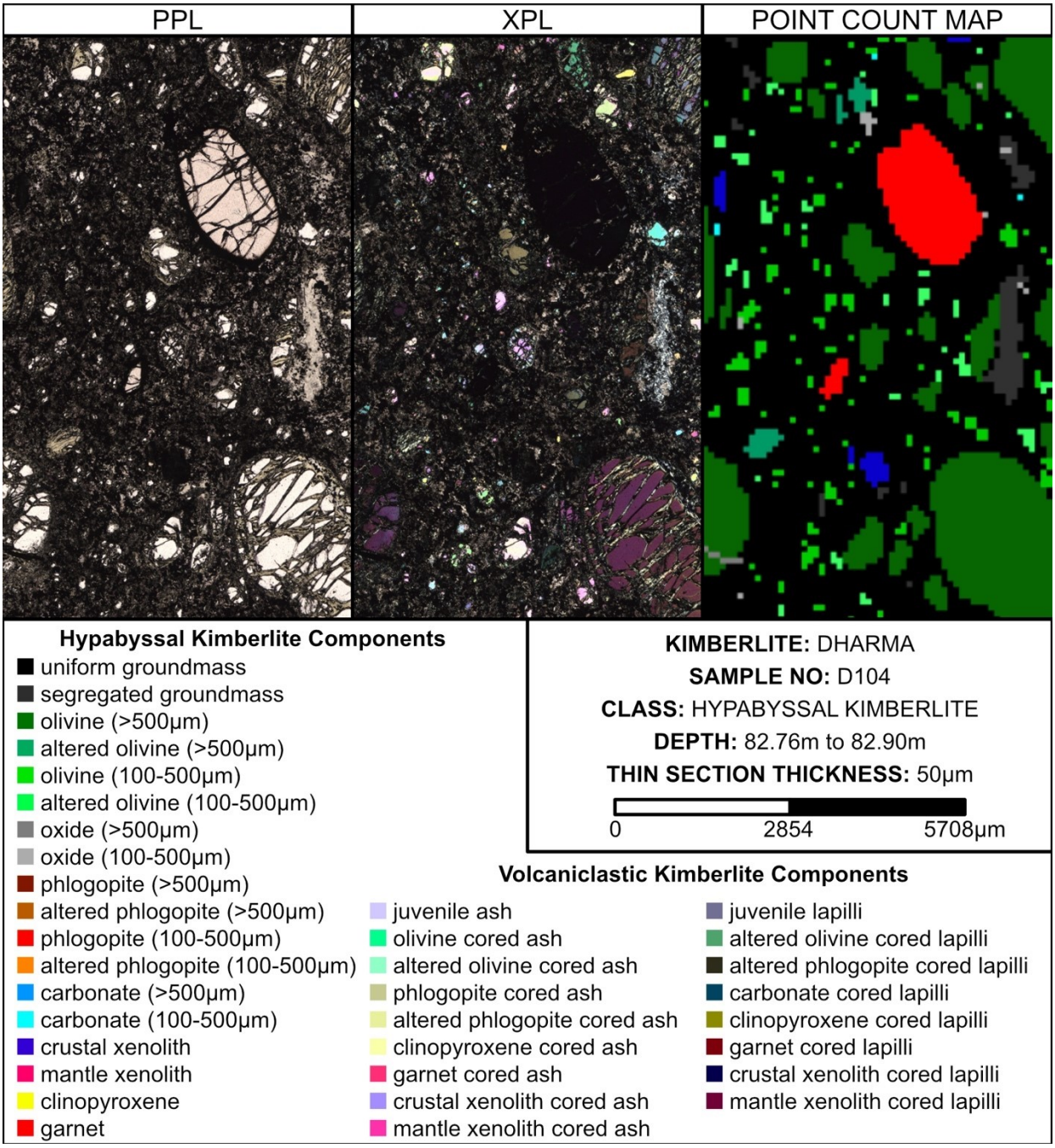

Appendix A: Rock.AR Point Count Figures

Appendix A.22: Rock.AR Point Count of Dharma kimberlite sample D105.

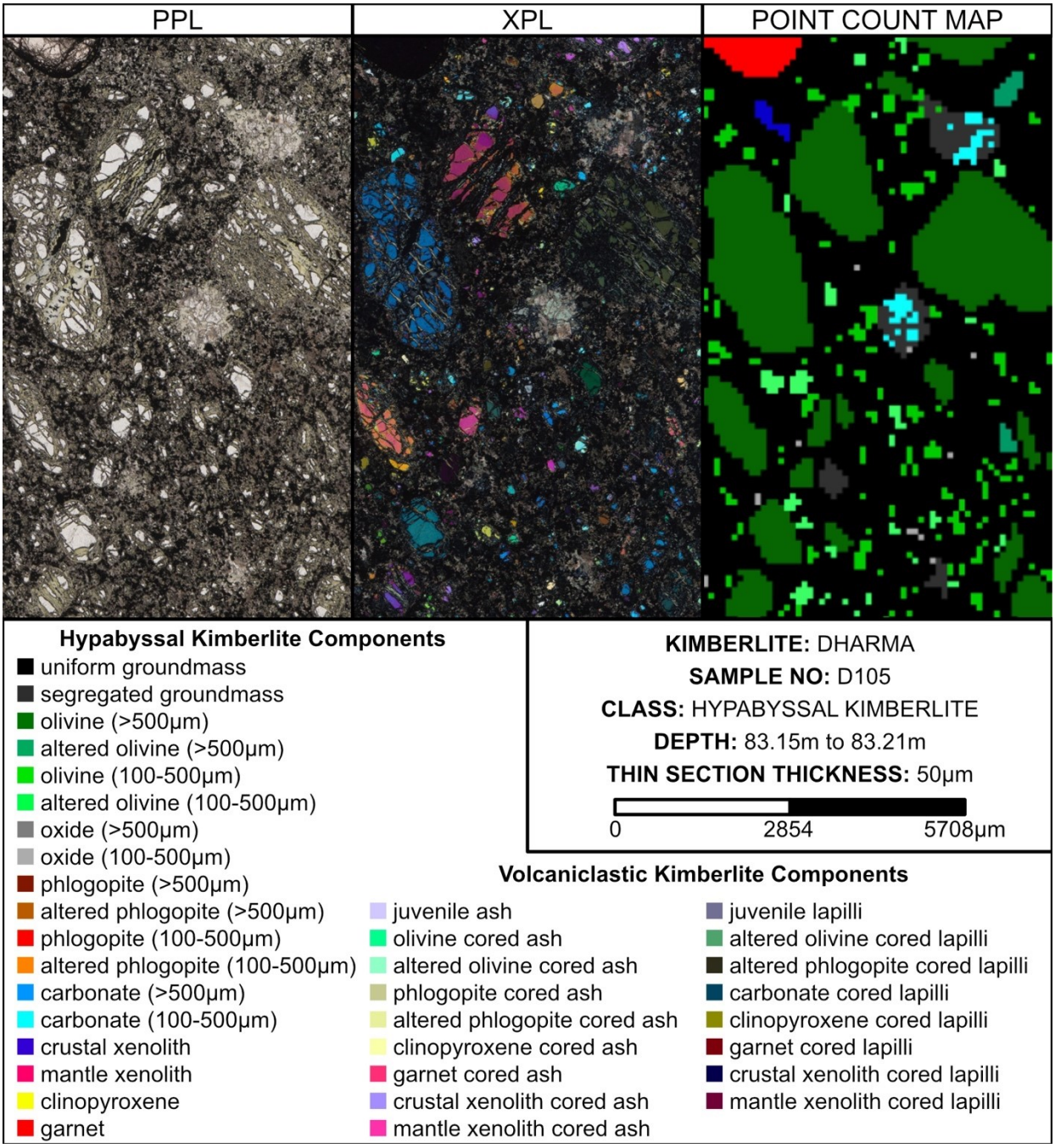

Appendix A: Rock.AR Point Count Figures

Appendix A.23: Rock.AR Point Count of Dharma kimberlite sample D108.

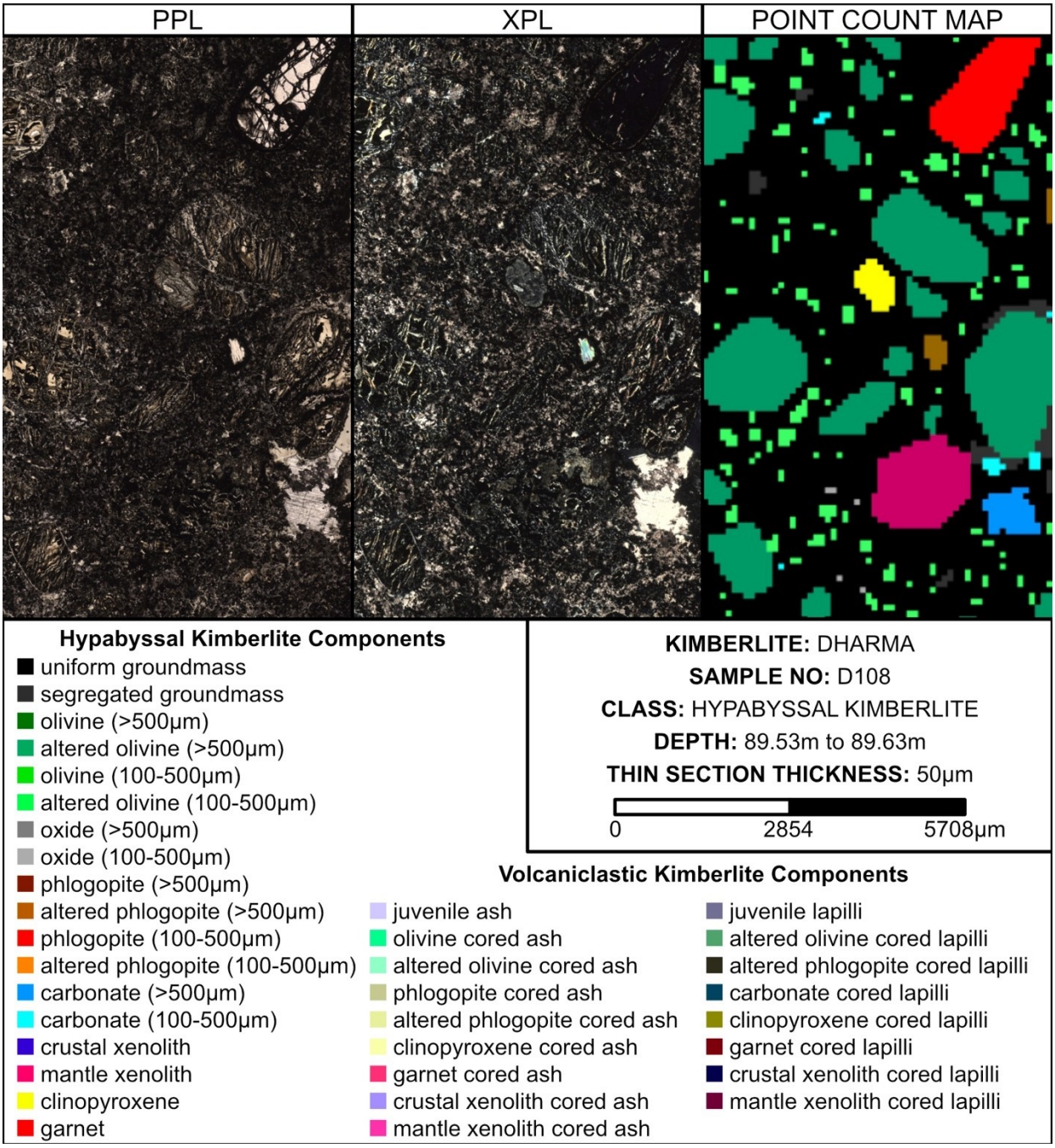

Appendix A.24: Rock.AR Point Count of Dharma kimberlite sample D109.

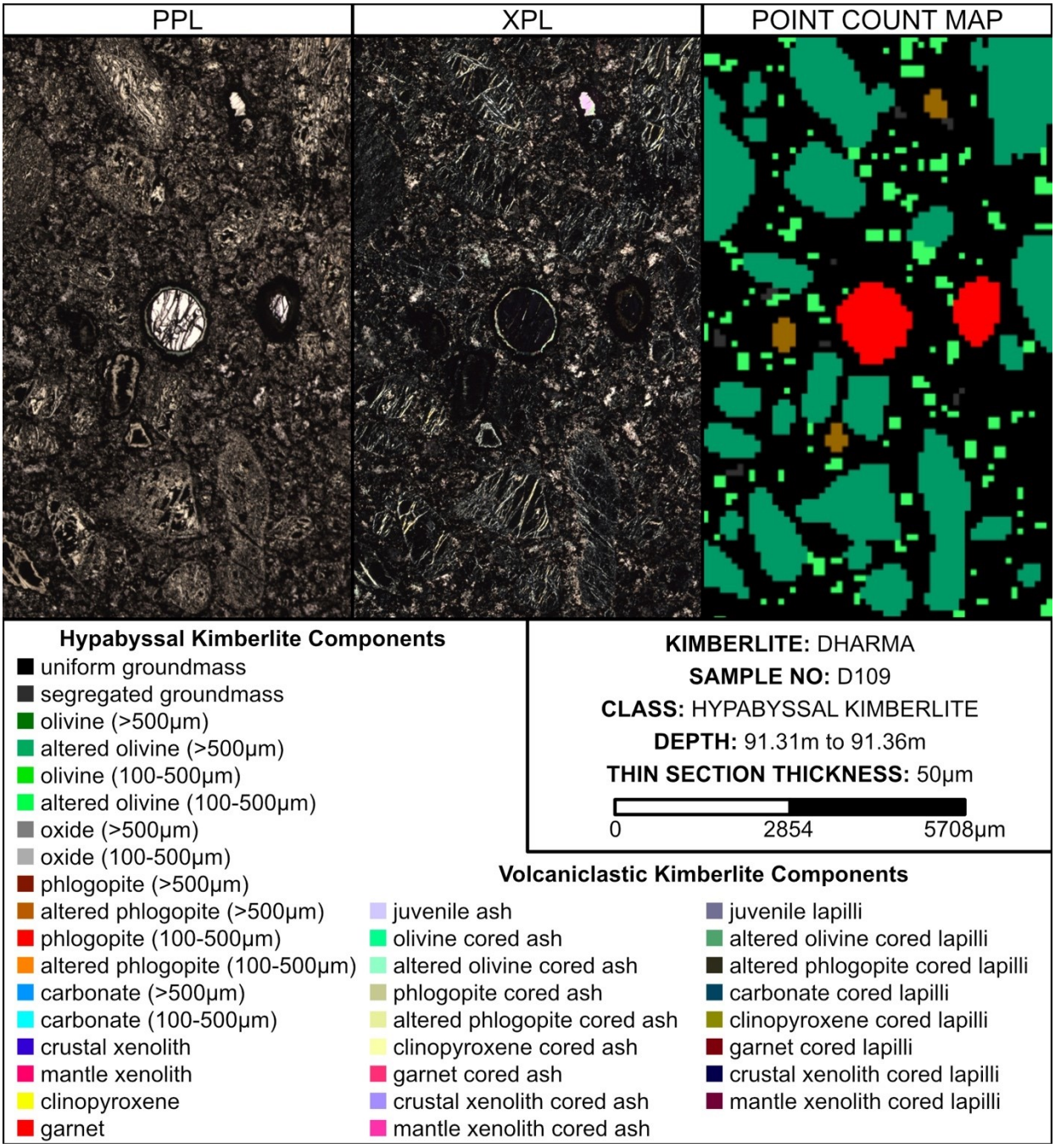

Appendix A.25: Rock.AR Point Count of Dharma kimberlite sample D112.

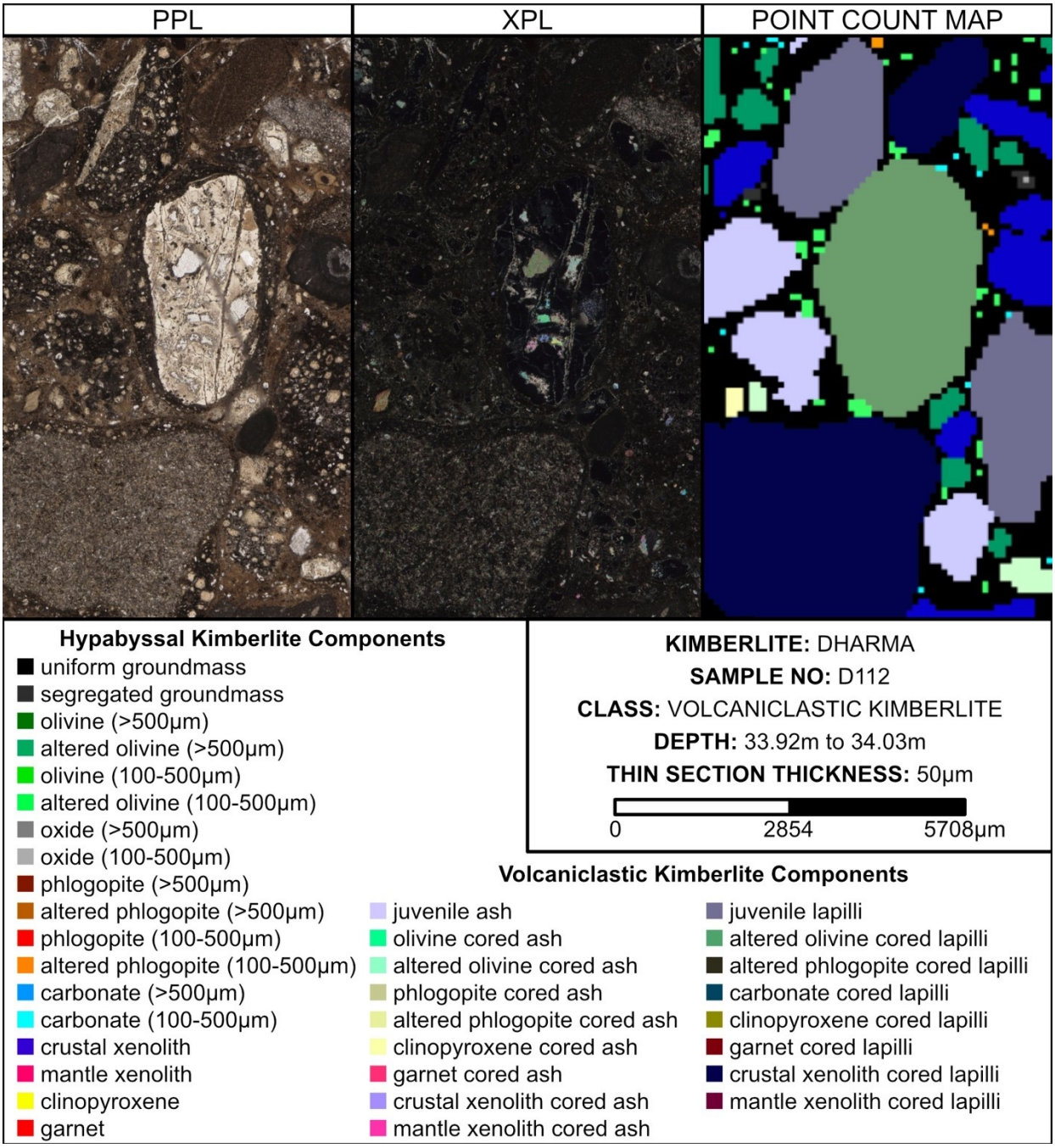

Appendix A: Rock.AR Point Count Figures

Appendix A.26: Rock.AR Point Count of Dharma kimberlite sample D114.

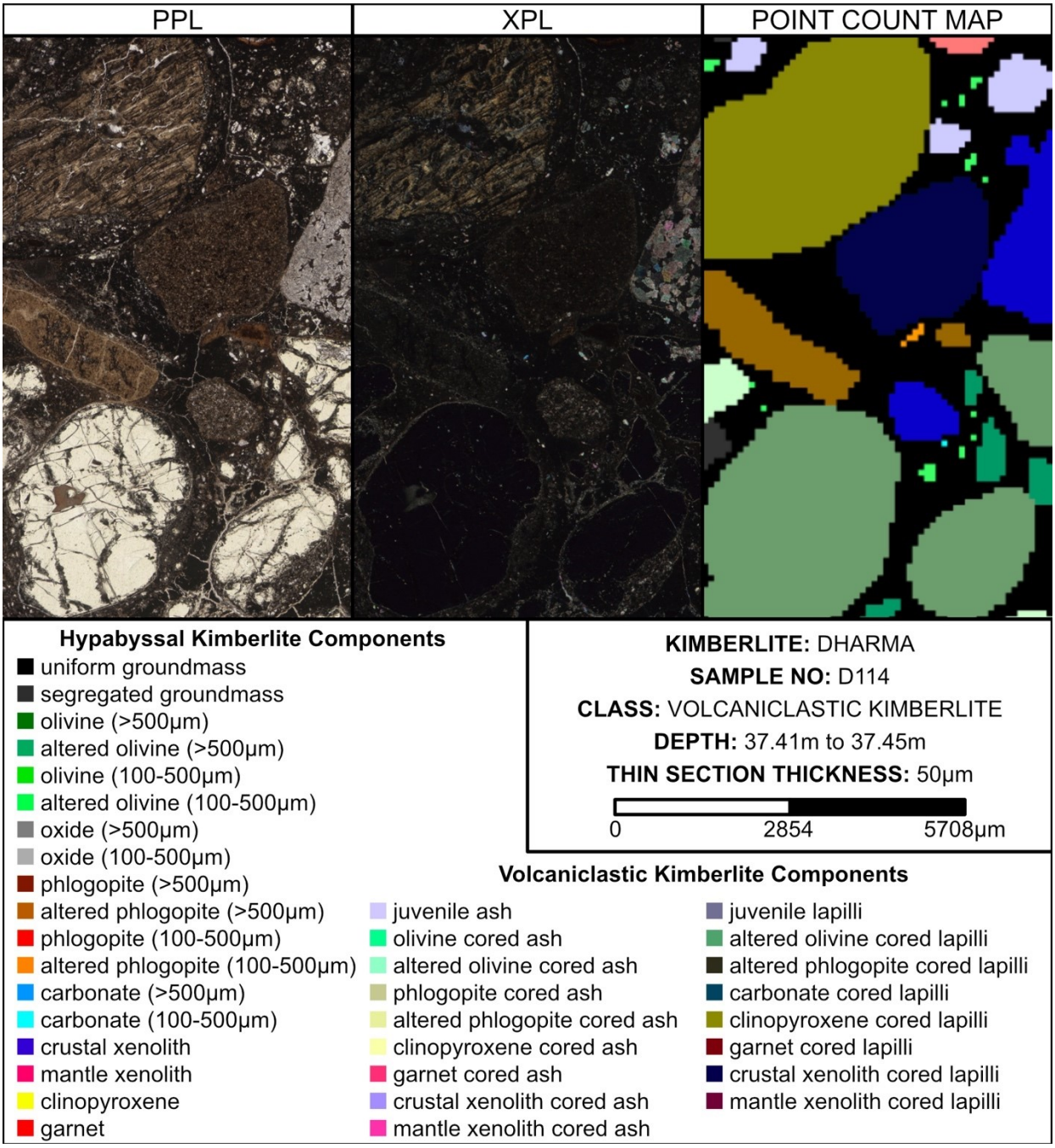

Appendix A.27: Rock.AR Point Count of Dharma kimberlite sample D116.

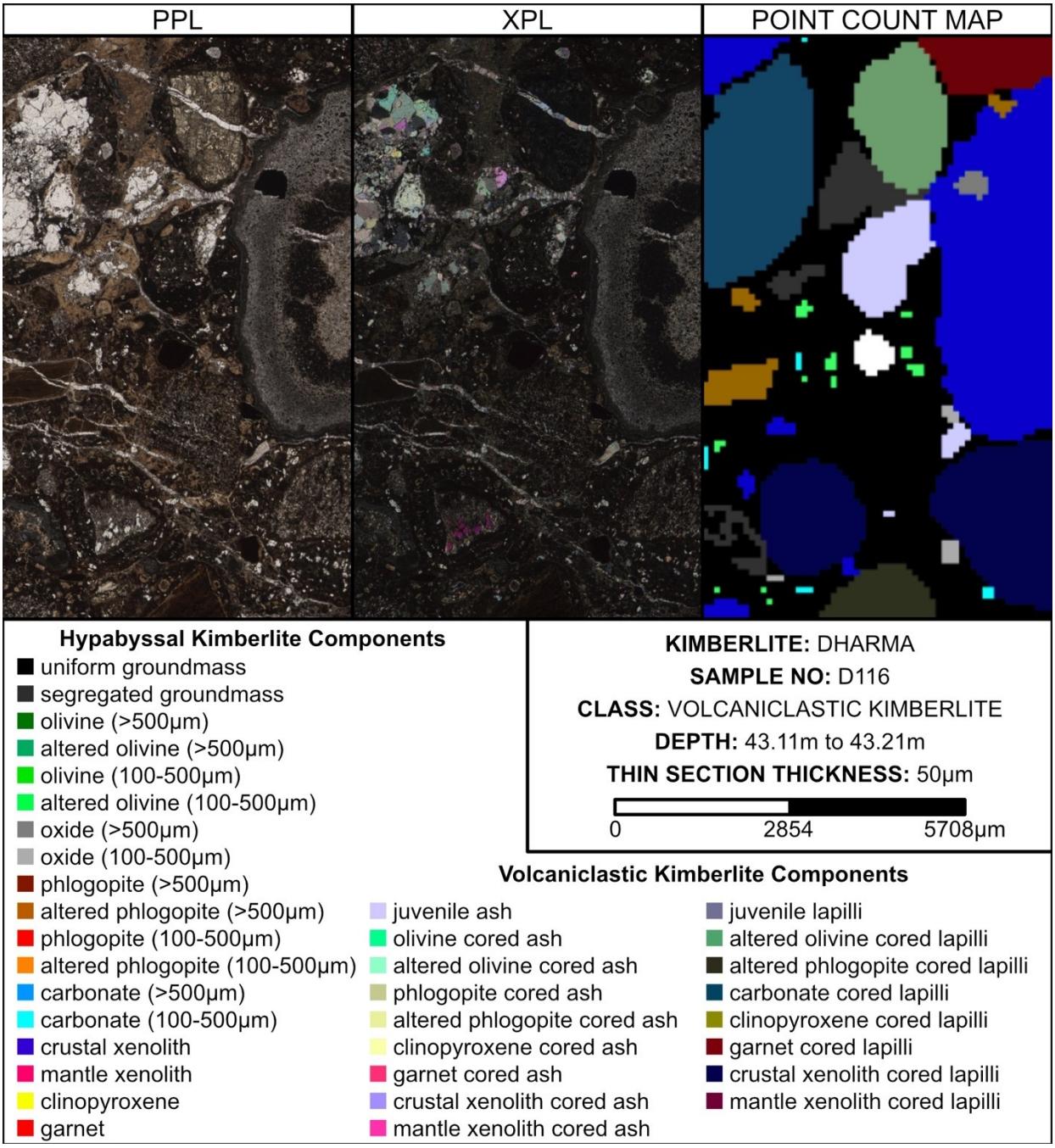

Appendix A.28: Rock.AR Point Count of Dharma kimberlite sample D117.

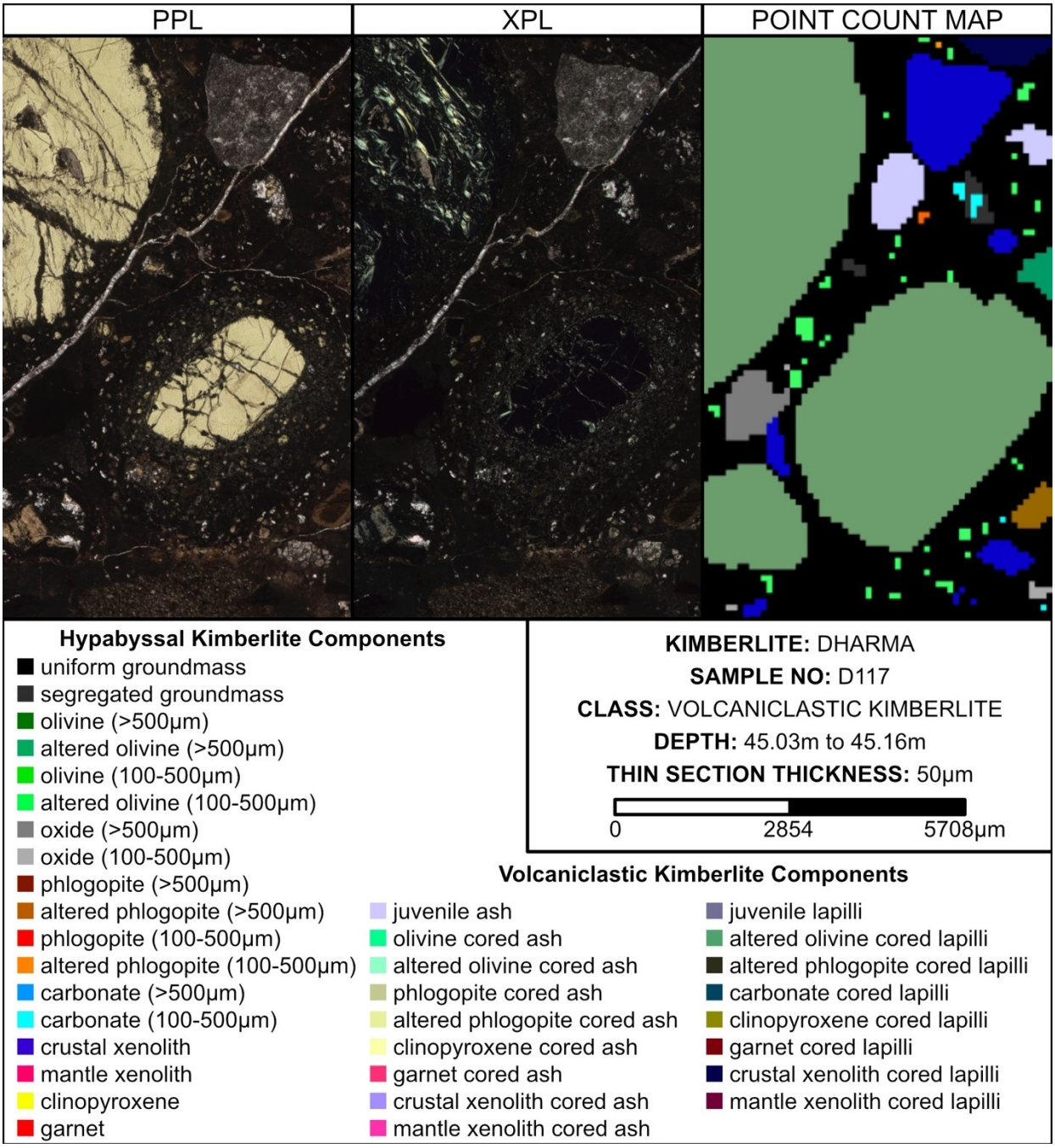

Appendix A: Rock.AR Point Count Figures

Appendix A.29: Rock.AR Point Count of Dharma kimberlite sample D118.

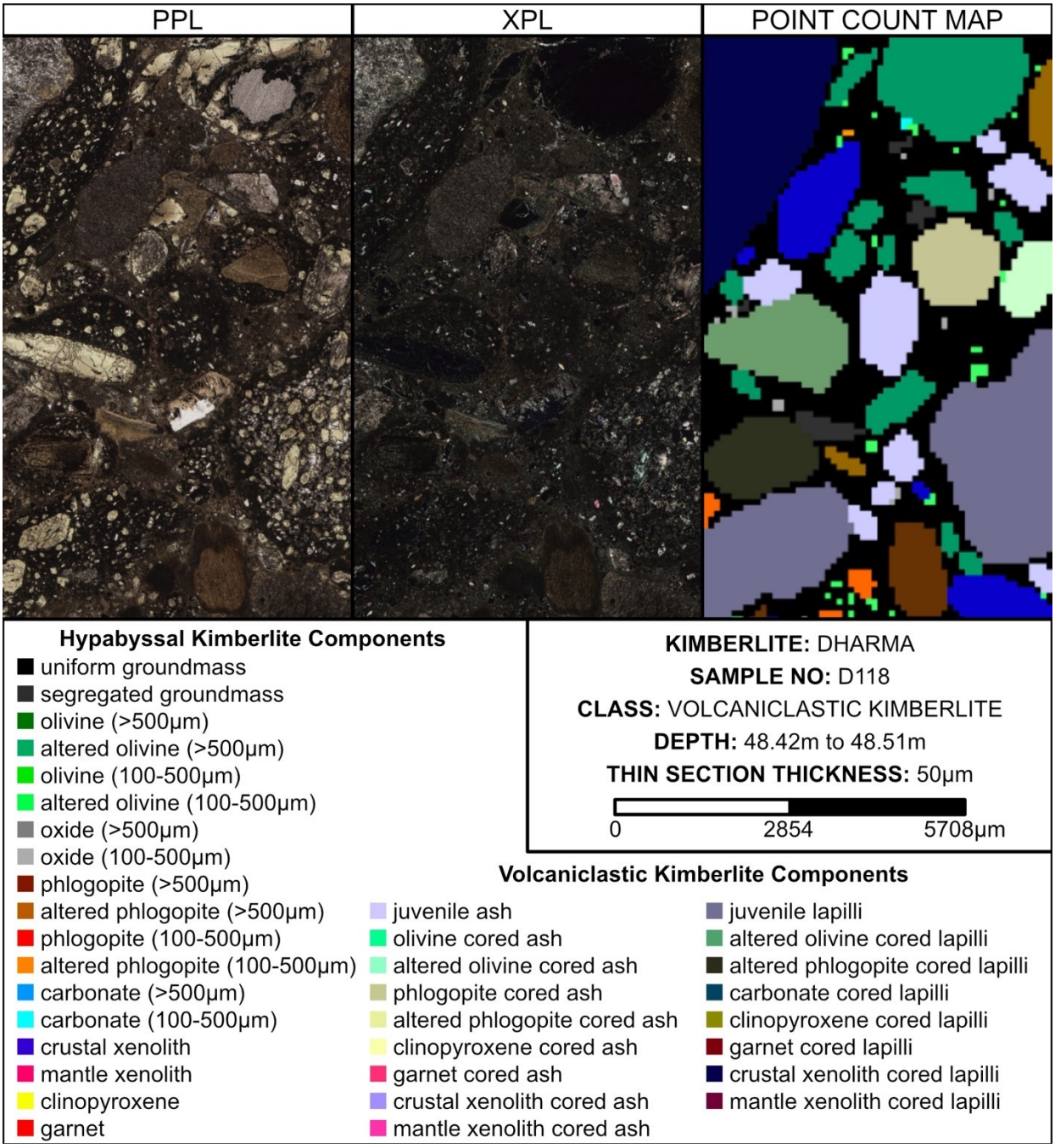

Appendix A.30: Rock.AR Point Count of Dharma kimberlite sample D122.

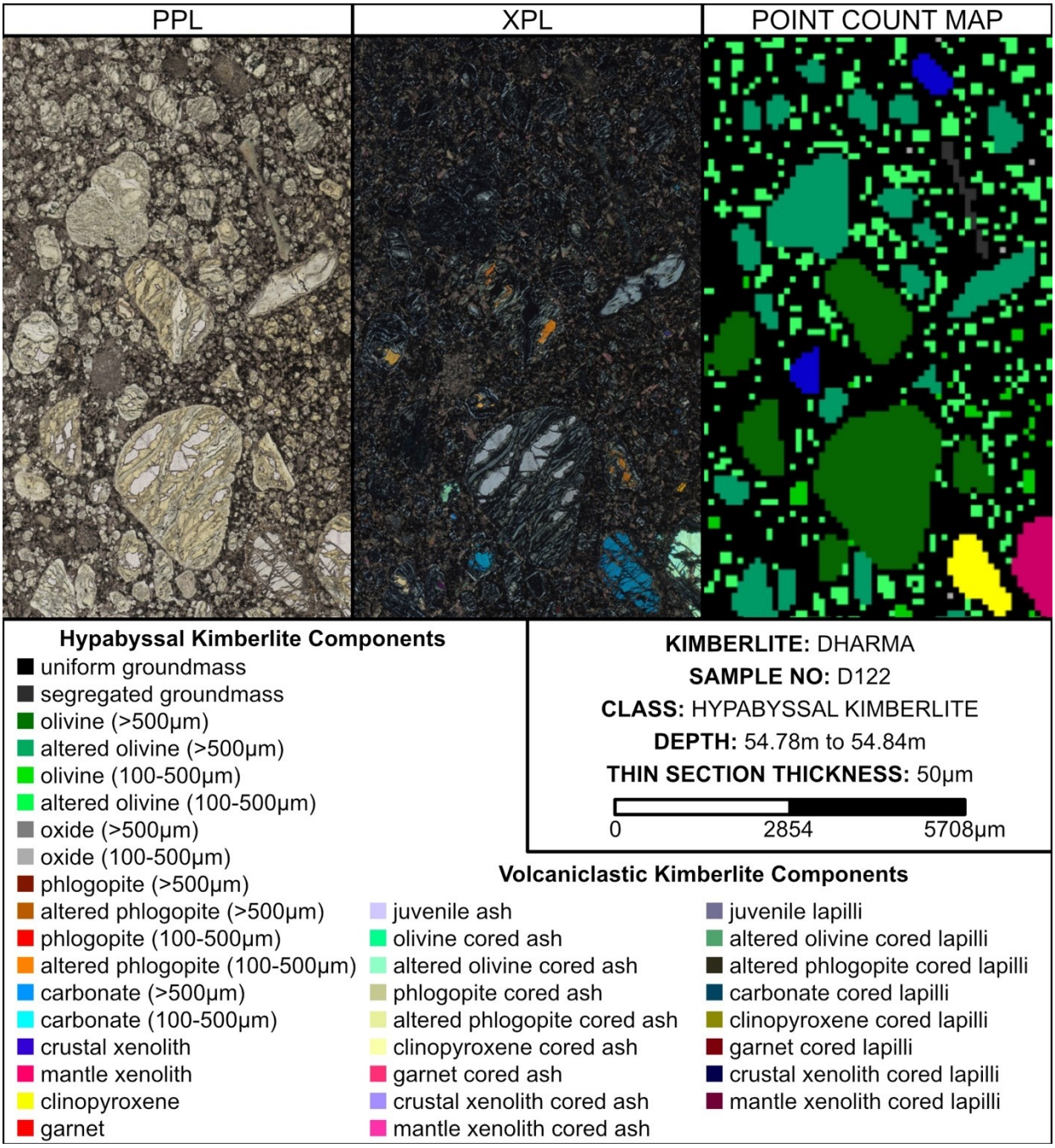

Appendix A: Rock.AR Point Count Figures

Appendix A.31: Rock.AR Point Count of Dharma kimberlite sample D128.

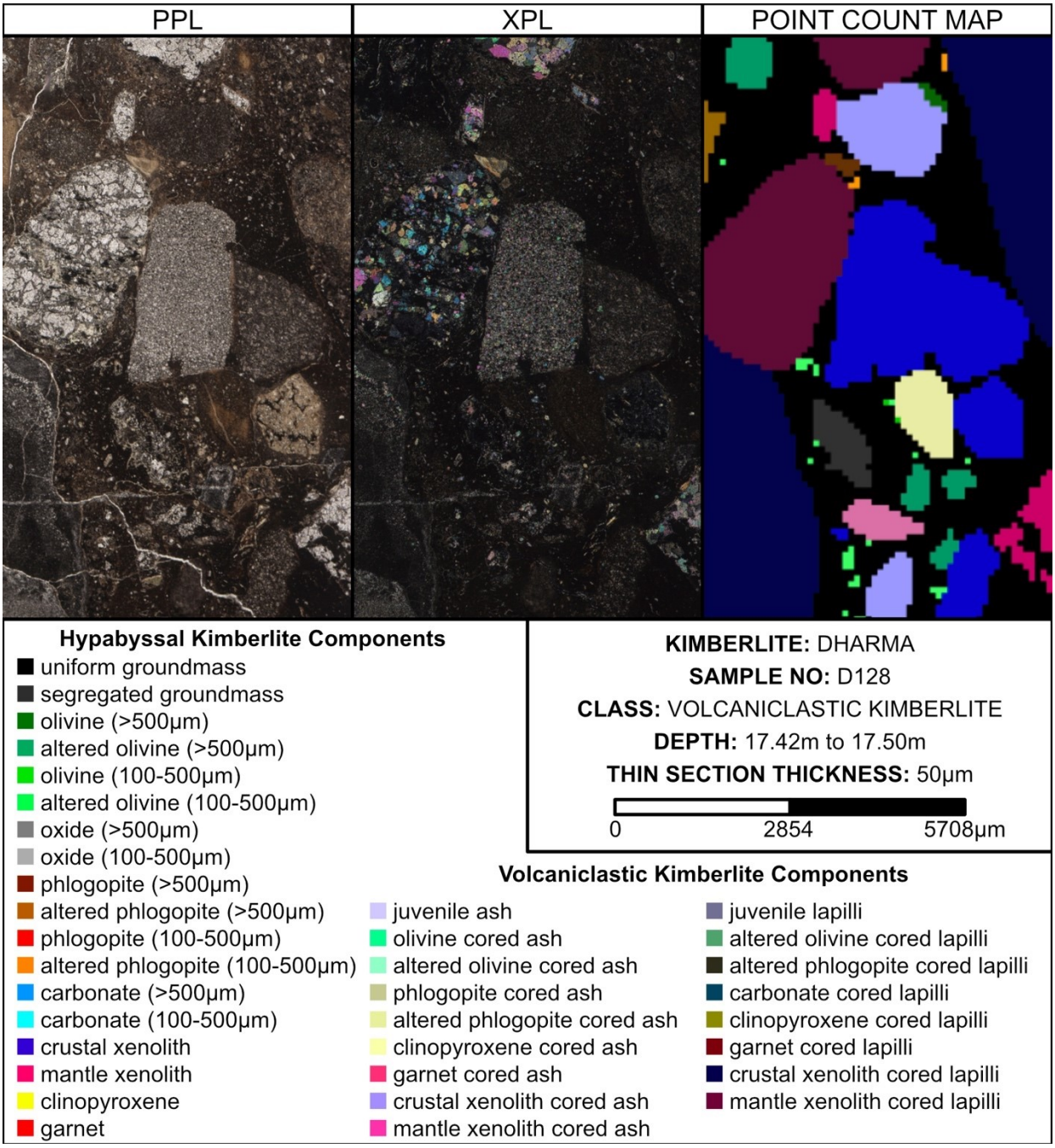

Appendix A: Rock.AR Point Count Figures

Appendix A.32: Rock.AR Point Count of Dharma kimberlite sample D129.

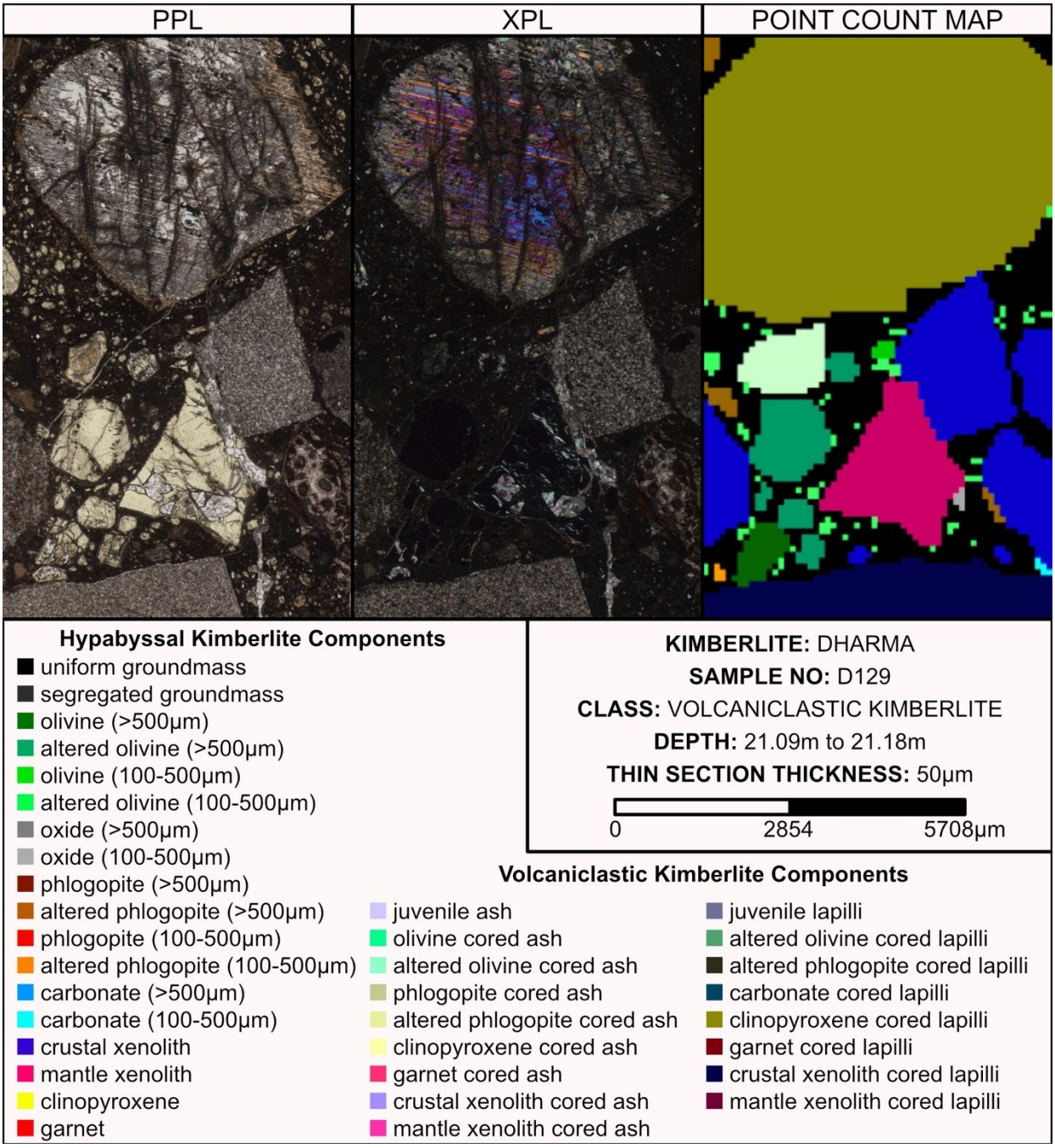

Appendix A: Rock.AR Point Count Figures

Appendix A.33: Rock.AR Point Count of Dharma kimberlite sample D132.

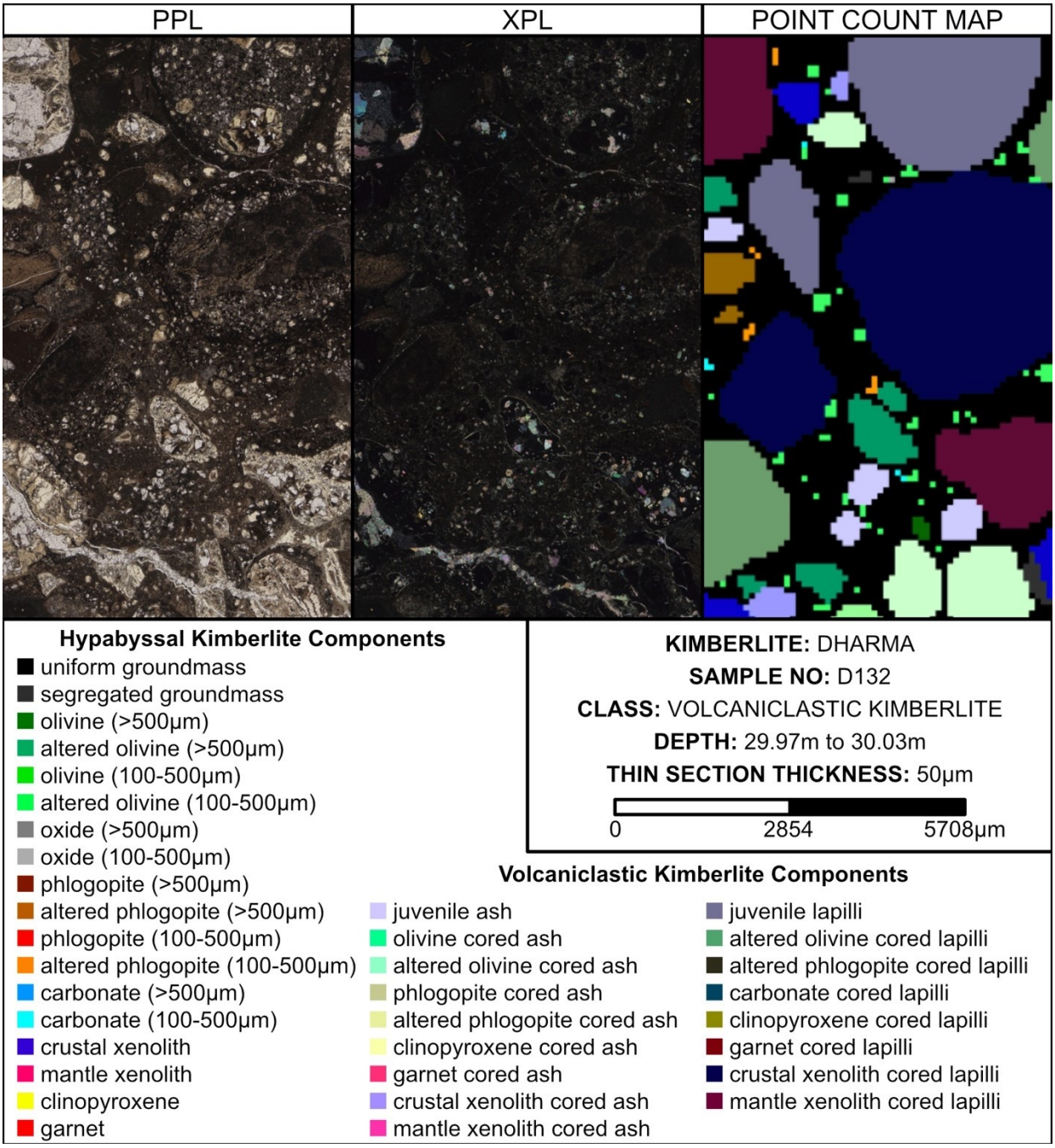

Appendix B – Mel Kimberlite EPMA Data Tables

Appendix B.01: Mel hypabyssal kimberlite mica EPMA analyses. Zones: C – core, M – middle, R – rim. Size: P - >500µm, MP – 100-500µm, GM - <100µm.

Kimberlite	*Sample*	*Zone*	*Size*	*Nb_2O_5*	*SiO_2*	*TiO_2*	*ZnO*	*Al_2O_3*	*V_2O_3*	*Cr_2O_3*	*FeO*	*NiO*	*MnO*	*MgO*	*CaO*	*BaO*	*Na_2O*	*K_2O*	*P_2O_5*	*Total*
ML8 Upper	16.01.003phl	R	MP	0	35.7	3.47	0	17.03	0	0.11	5.98	0.04	0.08	20.96	0.02	1.03	0.46	9.38	0	94.26
ML8 Upper	16.01.017phl	C	MP	0	41.82	0.15	0	12.6	0	0.42	3.04	0.16	0.02	26.49	0	0.17	0.41	10.17	0	95.45
ML8 Upper	16.01.017phl	M	MP	0	38.62	5.32	0	13.85	0	2.03	5.3	0.12	0	20.24	0.05	0.13	0.65	9.4	0	95.71
ML8 Upper	16.01.017phl	R	MP	0	38.32	5.1	0	14.63	0.04	1.65	5.17	0.16	0	20.53	0	0	0.56	9.42	0	95.58
ML8 Upper	16.01.019phl	C	MP	0	38.93	4.8	0	13.89	0	1.59	5.24	0.11	0.04	20.92	0	0	0.57	9.68	0	95.77
ML8 Upper	16.01.019phl	M	MP	0	37.53	4.51	0	15.41	0.04	0.75	5.69	0.06	0.03	21.18	0	0.36	0.65	9.46	0	95.67
ML8 Upper	16.01.019phl	M	MP	0	37.91	2.83	0	14.54	0.04	0.04	6.52	0.03	0.08	22.62	0.05	0.39	0.39	9.49	0	94.93
ML8 Upper	16.01.019phl	R	MP	0	36.26	4.56	0	15.51	0	0	6.71	0	0.06	21.87	0.09	0.67	0.39	9.04	0	95.16
ML8 Upper	16.01.020phl	C	MP	0	38.73	4.92	0	14.71	0.05	1.78	5.17	0.14	0.03	20.51	0	0.15	0.57	9.63	0	96.39
ML8 Upper	16.01.020phl	R	MP	0	38.58	4.93	0	14	0	1.77	5.35	0.14	0.03	20.59	0.01	0.17	0.58	9.44	0	95.59
ML8 Upper	16.03.001phl	C	MP	0	37.69	5.16	0.04	13.42	0	0	12.5	0.02	0.1	15.6	0	0.18	0.28	9.8	0	94.79
ML8 Upper	16.03.001phl	R	MP	0	36.28	3.92	0	16.71	0	0.09	5.91	0.03	0.06	21.05	0.01	0.73	0.64	9.33	0	94.76
ML8 Upper	16.03.005ox	C	MP	0	38.68	4.88	0	13.57	0.05	2.05	5.44	0.14	0.04	20.9	0	0	0.58	9.42	0	95.75
ML8 Upper	16.03.006ox	C	MP	0	38.13	5.11	0	14.26	0	1.41	5.58	0.12	0.03	20.73	0.02	0	0.62	9.44	0	95.45
ML8 Upper	16.03.006ox	M	MP	0	38.73	4.81	0	14.1	0	1.21	5.15	0.13	0.05	21.07	0.01	0	0.53	9.69	0	95.48
ML8 Upper	16.03.008phl	C	MP	0	37.82	4.72	0	12.45	0	1.29	6.99	0.08	0.04	22.16	0.03	0	0.45	8.07	0	94.1
ML8 Upper	16.03.009phl	C	GM	0	36.3	4.25	0	16.54	0	0.31	6	0.04	0.06	21.18	0.1	0.73	0.47	9.62	0	95.6
ML8 Upper	16.03.010phl	C	MP	0	35.49	2.71	0	17.43	0	0.05	5.86	0.03	0.08	21.91	0.07	1.14	0.48	9.02	0	94.27
ML8 Upper	16.03.016phl	C	GM	0	38.29	4.72	0	14.9	0	1.22	5.58	0.18	0.03	20.78	0	0	0.45	9.78	0	95.93
ML8 Upper	16.03.017phl	C	MP	0	38.5	4.5	0	15.34	0	1.28	5.36	0.15	0.04	21.04	0.02	0.15	0.48	9.76	0	96.62
ML8 Upper	16.03.017phl	R	MP	0.05	37.79	4.59	0	14.25	0.04	1.17	6.08	0.15	0.05	20.8	0.9	0	0.45	9.16	0	95.48
ML8 Upper	16.03.018phl	C	MP	0	39.89	3.15	0	12.41	0	0.76	5.77	0.15	0.02	23.92	0	0	0.47	8.58	0.05	95.17
ML8 Upper	16.05.001phl	C	P	0	39.35	4.42	0	14.05	0.06	0.76	4.8	0.16	0.03	21.79	0	0	0.5	9.91	0	95.83
ML8 Upper	16.05.001phl	M	P	0	39.73	4.32	0	14.25	0.03	0.82	4.75	0.16	0.02	22.09	0	0	0.52	9.89	0	96.58
ML8 Upper	16.05.001phl	R	P	0	35.76	3.31	0	17.44	0	0.05	6.4	0.04	0.08	22.33	0.07	1.04	0.48	8.71	0.03	95.74
ML8 Upper	16.05.003phl	R	MP	0	38.13	4.3	0	13.89	0	0.24	7.17	0.07	0.06	21.7	0.03	0.34	0.62	9.15	0	95.7
ML8 Upper	16.05.003phl	M	MP	0	36.06	3	0	18	0	0.04	5.69	0.06	0.07	21.69	0.03	1.37	0.63	9.13	0	95.77
ML8 Upper	16.05.003phl	M	MP	0	36.54	4.72	0	16.65	0	0.09	6.29	0.06	0.05	20.59	0	0.81	0.69	9.26	0	95.75
ML8 Upper	16.05.003phl	C	MP	0	36.73	3.99	0.03	15.74	0	0.1	6.53	0.03	0.06	21.28	0.01	0.57	0.63	8.89	0	94.59
ML8 Upper	16.05.003phl	C	MP	0	36.45	4.85	0	16.9	0	0.06	6.41	0.04	0.05	20.27	0.02	0.56	0.62	9.38	0	95.61
ML8 Upper	16.05.003phl	M	MP	0.05	36.59	4.82	0	16.61	0	0.08	6.24	0.07	0.06	20.5	0	0.84	0.69	9.22	0	95.77
ML8 Upper	16.05.003phl	M	MP	0	35.88	4.78	0	16.89	0.04	0.08	6.3	0.06	0.06	20.44	0.02	0.63	0.63	9.17	0	94.98
ML8 Upper	16.05.003phl	R	MP	0	36.16	4.45	0	14.18	0	0.26	7.93	0.06	0.06	21.25	0.12	0.29	0.54	8.36	0	93.66
ML8 Upper	16.05.004phl	R	MP	0	37.24	4.25	0	15.07	0	0	7.12	0.03	0.08	21.69	0.13	0.57	0.55	9.26	0	95.99
ML8 Upper	16.05.004phl	M	MP	0	36.79	4.6	0.04	14.89	0	0.13	7.74	0.09	0.07	21.25	0.02	0.36	0.51	8.97	0	95.46
ML8 Upper	16.05.004phl	C	MP	0	37.81	4.66	0	14.37	0	1.27	6.2	0.1	0.04	21.18	0.04	0.25	0.61	8.95	0	95.48
ML8 Upper	16.05.004phl	C	MP	0	38.26	4.91	0	14.54	0.03	1.41	5.51	0.11	0.04	20.79	0	0	0.58	9.54	0	95.72
ML8 Upper	16.05.004phl	M	MP	0	37.29	5.5	0	15.38	0	0.33	6.7	0.09	0.06	20.4	0	0.33	0.7	9.36	9.36	96.14

Appendix B – Mel Kimberlite EPMA Data Tables

Appendix B.01 (continued): Mel hypabyssal kimberlite mica EPMA analyses. Zones: C – core, M – middle, R – rim. Size: P - >500µm, MP – 100-500µm, GM - <100µm.

Kimberlite	*Sample*	*Zone*	*Size*	*Nb_2O_5*	*SiO_2*	*TiO_2*	*ZnO*	*Al_2O_3*	*V_2O_3*	*Cr_2O_3*	*FeO*	*NiO*	*MnO*	*MgO*	*CaO*	*BaO*	*Na_2O*	*K_2O*	*P_2O_5*	*Total*
ML8 Upper	16.05.010phl	C	GM	0	38.78	4.68	0	15.09	0	1.13	5.25	0.1	0.04	21.35	0.03	0	0.52	9.61	0	96.58
ML8 Upper	16.05.011phl	M	MP	0	35.56	4.71	0	15.36	0	0	7.05	0	0.25	22.48	0.03	0.78	0.39	8.56	0	95.17
ML8 Upper	16.05.012phl	C	MP	0	36.36	4.47	0	16.78	0	0.16	6.5	0.04	0.08	20.6	0.11	0.76	0.67	9.2	0	95.73
ML8 Upper	16.05.012phl	R	MP	0	37.66	2.98	0	15.31	0	0	6.52	0.04	0.1	22.41	0.07	0.35	0.54	9.43	0	95.41
ML8 Lower	20.01.005phl	C	MP	0	38.01	5.11	0	14.46	0.04	1.52	5.19	0.11	0.02	20.21	0	0	0.55	9.57	0	94.79
ML8 Lower	20.01.005phl	R	MP	0	35.37	3.55	0	17.4	0	0.06	5.66	0.03	0.04	21.67	0.06	0.9	0.63	8.85	0	94.22
ML8 Lower	20.01.009phl	C	MP	0	38.52	4.69	0	14.38	0.04	1.01	5.15	0.17	0.04	20.39	1.43	0	0.42	9.6	0	95.84
ML8 Lower	20.01.011phl	C	MP	0	38.4	5.01	0.03	13.84	0.04	1.54	5.93	0.09	0.04	20.62	0.03	0	0.52	9.45	0	95.54
ML8 Lower	20.01.012phl	C	MP	0	37.53	4.76	0	14.31	0.03	1.31	5.89	0.17	0.03	20.7	0.03	0.14	0.47	9.18	0	94.55
ML8 Lower	20.01.012phl	M	MP	0	36.33	5.14	0.03	14.97	0	0.31	7	0.04	0.05	20.65	0.04	0.46	0.63	8.76	0	94.41
ML8 Lower	21.02.001phl	C	GM	0	34.64	3.25	0	18.36	0	0.06	17.83	0	0.09	11.16	0.25	0.19	0.28	9.22	0	95.33
ML8 Lower	21.02.002phl	C	MP	0	36.57	3.96	0	15.25	0	0.71	6.16	0.08	0.05	21.76	0.06	0.33	0.55	9.08	0	94.56
ML8 Lower	21.02.011phl	R	MP	0	37.19	4.53	0	13.04	0.03	1.28	6.78	0.07	0.03	22.24	0.08	0	0.47	8.07	0	93.81
ML8 Lower	21.02.014phl	R	GM	0	38.29	4.46	0	12.99	0.05	1.26	5.84	0.11	0.03	21.62	0.08	0	0.47	8.89	0	94.09
ML8 Upper	22.01.008phl	C	GM	0	38.68	4.85	0	14.35	0	1.41	5.35	0.12	0.04	20.99	0.03	0	0.51	9.58	0	95.91
ML8 Upper	22.01.015ox	C	MP	0	36.77	4.2	0	15.89	0	0	8.83	0.03	0.07	18.85	0	0.43	0.84	9.14	0	95.05
ML8 Upper	22.01.015ox	M	MP	0	37.49	4.09	0	15.09	0	0.05	7.69	0.04	0.06	20.04	0.04	0.38	0.71	9.34	0	95.02
ML8 Upper	22.01.016phl	C	MP	0	38.1	4.09	0	14.16	0	0.23	7.29	0.04	0.07	21.25	0	0.23	0.66	9.36	0	95.48
ML8 Upper	22.01.016phl	M	MP	0	38.44	4.25	0	12.77	0	0.27	7.46	0.05	0.06	21.74	0.04	0.17	0.71	9.21	0	95.17
ML8 Upper	22.01.017phl	R	MP	0	36.84	4.53	0	14.87	0	0.09	7.17	0.03	0.07	21.62	0.06	0.53	0.63	8.7	0	95.14
ML8 Upper	22.03.005phl	C	MP	0	35.71	4.91	0	17.03	0	0.08	5.73	0.02	0.06	20.65	0.01	0.95	0.73	9.17	0	95.05
ML8 Upper	22.03.005phl	M	MP	0	36.38	4.75	0	16.71	0	0	5.49	0.04	0.05	21.23	0	0.74	0.72	9.24	0	95.35
ML8 Upper	22.03.005phl	M	MP	0	37.65	3.96	0	16.01	0	0.06	5.23	0.05	0.05	22.15	0.02	0.53	0.73	9.1	0	95.54
ML8 Upper	22.03.005phl	R	MP	0	37.28	3.96	0	16.01	0	0.05	5.41	0.07	0.03	22.14	0.02	0.55	0.75	9.11	0	95.38
ML8 Upper	22.03.006phl	C	MP	0	35.78	4.87	0	16.37	0	0.36	5.76	0.03	0.05	20.8	0.01	0.88	0.66	9.2	0	94.77
ML8 Upper	22.03.009phl	C	MP	0	37.76	4.14	0	14.84	0.03	0.5	6.72	0.06	0.05	21.52	0	0.14	0.82	8.16	0	94.74
ML8 Upper	22.03.010phl	C	MP	0	38.53	4.79	0	15.77	0	0.6	5.33	0.08	0.02	20.92	0	0.21	0.66	9.56	0	96.47
ML8 Upper	22.03.010phl	M	MP	0	38.21	4.27	0	15.1	0	0.51	6.02	0.07	0.05	21.09	0.02	0	0.6	8.62	0	94.56
ML8 Upper	22.03.014phl	C	MP	0	38	5	0	14.56	0	1.76	5.49	0.18	0.02	20.83	0.02	0.17	0.5	9.59	0	96.12
ML8 Upper	22.03.014phl	M	MP	0	37.51	4.74	0	14.14	0	0.66	6.39	0.08	0.04	21.7	0.03	0.38	0.59	8.5	0	94.76
ML8 Upper	22.03.015phl	C	MP	0	38.13	4.84	0	14.16	0	1.32	5.32	0.17	0.04	21.21	0	0	0.46	9.35	0	95
ML8 Upper	22.03.015phl	R	MP	0	38.58	4.85	0	13.51	0	1.4	5.43	0.12	0.03	21.26	0.04	0	0.54	9.42	0	95.18
ML345	23.02.001phl	C	MP	0	38.77	4.84	0	15.07	0	0.88	5.05	0.13	0.05	21.17	0.16	0	0.49	9.73	0	96.34
ML345	23.02.001phl	M	MP	0	37.08	5	0	15.02	0	0.2	6.82	0.06	0.06	20.62	0.06	0.45	0.62	9.24	0	95.23
ML345	23.02.001phl	R	MP	0	36.96	4.81	0	14.07	0	0.21	7.68	0.07	0.06	21.12	0.16	0.32	0.6	8.75	0	94.81
ML345	23.02.002phl	C	GM	0	38.53	4.97	0	14.75	0.04	1.62	5.3	0.13	0.03	20.78	0.01	0	0.47	9.39	0	96.02
ML345	23.02.003phl	C	MP	0	38.81	5	0	13.51	0	1.47	5.59	0.11	0.04	21.19	0.04	0	0.56	9.52	0	95.84
ML345	23.02.004phl	C	MP	0	38.73	5.17	0	14.11	0	1.52	5.23	0.09	0.03	20.56	0	0	0.56	9.74	0	95.74

Appendix B – Mel Kimberlite EPMA Data Tables

Appendix B.01 (continued): Mel hypayssal kimberlite mica EPMA analyses. Zones: C – core, M – middle, R – rim. Size: P - >500µm, MP – 100-500µm, GM - <100µm.

Kimberlite	***Sample***	***Zone***	***Size***	***Nb_2O_5***	***SiO_2***	***TiO_2***	***ZnO***	***Al_2O_3***	***V_2O_3***	***Cr_2O_3***	***FeO***	***NiO***	***MgO***	***MnO***	***CaO***	***BaO***	***Na_2O***	***K_2O***	***P_2O_5***	***Total***
ML345	23.02.004phl	R	MP	0	38.42	5.22	0	13.94	0.03	1.69	5.29	0.1	0	20.3	0.05	0	0.63	9.47	0	95.14
ML345	23.02.010phl	C	MP	0	38.73	5.18	0	14.09	0.09	1.53	5.45	0.08	0.03	20.79	0.06	0.14	0.61	9.56	0	96.34
ML345	23.02.010phl	M	MP	0	38.48	4.89	0	14.31	0.05	1.09	5.61	0.08	0.04	20.77	0.07	0.34	0.63	9.21	0	95.57
ML345	23.02.010phl	R	MP	0	38.34	4.49	0	13.93	0	0.12	6.87	0.03	0.06	21.83	0.13	0.32	0.64	9.29	0	96.05

Appendix B – Mel Kimberlite EPMA Data Tables

Appendix B.02: Mel hypabyssal kimberlite ilmenite EPMA analyses. n.m. – not measured. Zones: C – core, M – middle, R – rim. Size: P - >500µm, MP – 100-500µm, GM - <100µm. FeO and Fe_2O_3 calculated from FeOT.

Kimberlite	*Sample*	*Zone*	*Size*	*Nb_2O_5*	*SiO_2*	*TiO_2*	*ZnO*	*Al_2O_3*	*V_2O_3*	*Cr_2O_3*	*FeO*	*Fe_2O_3*	*NiO*	*MnO*	*MgO*	*CaO*	*BaO*	*Na_2O*	*K_2O*	*P_2O_5*	*Total*
ML8 Upper	16.01.001ox	C	GM	1.08	0	51.51	0.04	0	1.9	0.09	26.36	4.06	0	3.93	9.47	0.05	0	0.04	0	0	98.53
ML8 Upper	16.01.002ox	M	GM	0.44	0.02	53.16	0	0	1.02	0.05	25.19	3.57	0	3.73	10.4	0.39	0	0.06	0.01	0	98.04
ML8 Upper	16.01.002ox	R	GM	0.41	0.03	52.47	0	0	1.39	0.11	26.87	4.01	0	2.84	9.95	0.02	0	0.03	0.01	0	98.14
ML8 Upper	16.01.005ox	M	GM	0.71	0	52.03	0.06	0.02	1.5	0.07	27.02	4	0	3.76	9.22	0.02	0	0.05	0	0	98.46
ML8 Upper	16.01.006ox	R	GM	0.68	0.39	51.64	0.06	0.02	1.29	0.14	26.92	4.36	0	2.6	9.93	0.1	0	0.04	0.01	0	98.18
ML8 Upper	16.01.009ox	C	GM	0.55	0.02	52.99	0	0	1.12	0.05	27.17	3.88	0	2.45	10.24	0.12	0	0.05	0	0	98.64
ML8 Upper	16.01.010ox	C	MP	0.59	0.31	48.8	0	0.02	0	0	42.78	3.51	0	1.6	0.16	0.17	0	0	0	0.05	97.94
ML8 Upper	16.01.010ox	C	MP	0.45	0.11	50.71	0	0	0	0	43.24	0.76	0.03	1.7	0	0.97	0	0	0	0.04	97.97
ML8 Upper	16.01.010ox	R	MP	0.64	0.04	52.87	0	0	1.28	0.13	26.16	4.26	0	2.71	10.71	0.06	0	0.05	0	0	98.91
ML8 Upper	16.01.010ox	R	MP	0.56	0	52.19	0.04	0	1.47	0.14	25.68	4.76	0	3.28	10.11	0.24	0	0.04	0	0	98.51
ML8 Upper	16.01.011ox	C	GM	0.33	0.04	52.13	0.05	0	1.16	0.1	27.06	4.72	0	2.8	9.57	0.02	0	0.06	0	0	98.04
ML8 Upper	16.01.012ox	C	GM	1.09	0.02	50.95	0.05	0	1.57	0.09	25.45	5.13	0.02	4.55	9.27	0.05	0	0.07	0	0	98.31
ML8 Upper	16.01.015ox	C	MP	0.07	0	49.15	0	0.66	0.17	1.23	21.95	13.23	0.1	0.55	12.06	0.04	0	0.03	0	0	99.24
ML8 Upper	16.01.015ox	C	MP	0	0	49.82	0	0.46	0.11	3.64	21.2	10.32	0.09	0.62	12.75	0.06	0	0.02	0	0	99.09
ML8 Upper	16.01.015ox	R	MP	0.53	0.83	47.73	0	0	0	0.06	41.76	4.85	0	1.44	0.44	0.39	0	0	0	0	98.03
ML8 Upper	16.01.016ox	C	P	0.11	0	43.58	0	0.47	0.28	0.87	25.65	20.88	0.07	0.28	7.38	0.02	0	0.03	0	0	99.62
ML8 Upper	16.01.016ox	C	P	0.13	0	43.39	0.03	0.42	0.19	0.88	25.11	21	0.04	0.26	7.69	0.02	0	0	0	0	99.16
ML8 Upper	16.01.016ox	M	P	0.08	0.03	47.83	0	0.62	0.16	2.01	21.7	14.57	0.07	0.57	11.44	0.25	0	0.02	0	0	99.35
ML8 Upper	16.01.016ox	M	P	0	1.23	48.49	0	0.66	0.06	3.72	20.68	10.84	0.08	0.55	13.15	0.12	0	0.04	0	0	99.62
ML8 Upper	16.01.018ox	C	GM	0.49	0.02	52.22	0.05	0	1	0.16	25.94	4.92	0	2.97	10.14	0.23	0	0.03	0.01	0	98.18
ML8 Upper	16.03.004ox	C	GM	0	0	51.14	0	0.51	0	3.56	22.33	7.85	0.07	0.64	12.64	0.22	0	0.03	0	0	98.99
ML8 Upper	16.03.007ox	C	GM	0.8	0.03	51.96	0.03	0	0.7	0.1	24.51	5.33	0	4.24	10.15	0.37	0	0.04	0.02	0	98.28
ML8 Upper	16.03.011ox	C	GM	0	0	49.36	0	0.15	0	2.47	23.51	11.29	0.04	0.77	11.06	0.28	0	0	0	0	98.93
ML8 Upper	16.03.012ox	C	GM	0.34	0.05	50.61	0	0	0	0	43.6	1.6	0	1.96	0.05	0.11	0	0.03	0	0.05	98.35
ML8 Upper	16.03.012ox	R	GM	0.91	0.24	51.03	0.03	0	1.22	0.08	29.24	4.1	0	2.09	8	1.01	0	0.05	0	0	98
ML8 Upper	16.03.013ox	C	GM	0	0	50.6	0	0.28	0.03	4.11	22.68	8.55	0	0.94	12.11	0.16	0	0.02	0	0	99.48
ML8 Upper	16.03.013ox	C	GM	0	0	50.6	0	0.25	0	4	22.51	8.54	0.04	1.02	12.05	0.21	0	0.04	0	0	99.26
ML8 Upper	16.03.014ox	M	GM	0	0	51.27	0	0.3	0.04	3.28	22.33	8.22	0.07	0.78	12.66	0.14	0	0.04	0	0	99.13
ML8 Upper	16.05.006ox	C	MP	0.17	0	48.65	0	0.86	0.18	6.98	19.17	8.95	0.28	0.24	13.51	0	0	0.04	0	0	99.03
ML8 Upper	16.05.006ox	M	MP	0.18	0	48.39	0	0.85	0.21	6.94	19	9.34	0.3	0.21	13.51	0	0	0.03	0	0	98.96
ML8 Upper	16.05.006ox	R	MP	0.19	0	48.7	0	0.82	0.2	6.93	19.1	8.91	0.25	0.25	13.7	0	0	0	0	0	99.05
ML8 Upper	16.05.007ox	C	GM	1.31	0	52.94	0	0	0.52	0.12	24.05	2.88	0	5.34	10.57	0.14	0	0.12	0	0	97.99
ML8 Upper	16.05.008ox	C	GM	0.44	0.1	50.56	0	0.02	0	0	42.85	1.24	0	1.62	0	1.24	0	0	0	0	98.07
ML8 Upper	16.05.009ox	C	GM	0.55	0	53.79	0.05	0	0.86	0.09	23.16	4.37	0	3.72	12.32	0.04	0	0	0	0	98.95
ML8 Upper	16.05.009ox	M	GM	0.49	0.15	53.96	0.04	0	1.25	0	20.07	5.89	0	3.73	14.09	0.12	0	0.02	0	0	99.81
ML8 Lower	20.01.001ox	C	P	0.09	0	45.47	0	0.59	0.21	0.63	26.86	17.61	0.04	0.27	7.75	0.01	0	0	0	0	99.53
ML8 Lower	20.01.001ox	M	P	0.09	0	45.65	0	0.6	0.19	0.6	26.66	17.63	0.05	0.26	7.96	0	0	0	0	0	99.69
ML8 Lower	20.01.001ox	R	P	0.09	0.03	45.89	0.05	0.67	0.19	0.67	24.41	17.07	0.04	0.62	8.97	0.24	0	0	0	0	98.94

Appendix B – Mel Kimberlite EPMA Data Tables

Appendix B.02 (continued): Mel hypabyssal kimberlite ilmenite EPMA analyses. n.m. – not measured. Zones: C – core, M – middle, R – rim. Size: P - >500µm, MP – 100-500µm, GM - <100µm. FeO and Fe_2O_3 calculated from FeOT.

Kimberlite	*Sample*	*Zone*	*Size*	*Nb_2O_5*	*SiO_2*	*TiO_2*	*ZnO*	*Al_2O_3*	*V_2O_3*	*Cr_2O_3*	*FeO*	*Fe_2O_3*	*NiO*	*MnO*	*MgO*	*CaO*	*BaO*	*Na_2O*	*K_2O*	*P_2O_5*	*Total*
ML8 Lower	20.01.002ox	C	GM	0.45	0.06	50.98	0	0	0	0	43.56	0.9	0	2.53	0	0.23	0	0	0	0	98.71
ML8 Lower	20.01.003ox	C	GM	0.33	0.04	50.48	0	0	0	0	41.75	1.72	0	2.66	0	1.07	0	0	0	0	98.05
ML8 Lower	20.01.004ox	C	GM	0.98	7.65	41.42	0	0.03	0.86	0	17.89	13.34	0	2.67	14.71	0.2	0	0.06	0.04	0	99.85
ML8 Lower	20.01.006ox	R	MP	1.01	0.02	51.77	0.06	0	0.93	0	24.61	5.27	0	4.13	10.07	0.51	0	0.05	0	0	98.43
ML8 Lower	21.02.004ox	C	MP	0	0	52.41	0	1.04	0.16	0.18	25.2	7.52	0.08	0.52	11.86	0.05	0	0.03	0	0	99.05
ML8 Lower	21.02.004ox	C	MP	0	0.02	52.4	0	0.54	0.19	0.17	22.8	8.37	0.07	0.68	13.09	0.08	0	0.03	0.01	0	98.45
ML8 Lower	21.02.005ox	C	MP	0	0.05	52.15	0	0.92	0.09	0.18	25.4	7.65	0.05	0.64	11.67	0.06	0	0	0	0	98.86
ML8 Lower	21.02.005ox	C	MP	0	0.02	52.27	0	0.83	0.15	0.16	25.22	7.63	0.05	0.68	11.7	0.07	0	0.03	0	0	98.81
ML8 Lower	21.02.006ox	C	GM	0.66	0.02	53.56	0.03	0	0.37	0.05	24.35	4.33	0	2.6	11.93	0.13	0	0.09	0.02	0	98.14
ML8 Lower	21.02.009ox	C	GM	1.04	0.03	52.46	0	0	0.9	0.05	24.97	4.75	0	2.46	11.6	0.06	0	0.03	0	0	98.35
ML8 Lower	21.02.010ox	C	P	0	0.03	52.27	0	0.4	0	0.74	22.44	9.19	0.08	0.5	13.29	0.05	0	0.06	0	0	99.05
ML8 Lower	21.02.010ox	M	P	0	0.06	51.55	0	0.57	0.26	0.78	22.03	9.81	0.07	0.6	13.18	0.08	0	0.03	0	0	99.02
ML8 Lower	21.02.012ox	C	GM	1.26	0.03	51.05	0.05	0	0.69	0.12	25.08	6.45	0	2.53	10.19	0.97	0	0.05	0	0	98.47
ML8 Upper	22.01.011ox	C	MP	0	0	52.55	0	0.24	0.08	1.9	26.48	5.73	0.08	0.79	11.06	0.05	0	0.03	0	0	98.99
ML8 Upper	22.01.014ox	C	GM	0	0.82	45.36	0	0.03	0	0.3	38.81	10.56	0	1.6	0.5	0.36	0	0	0	0	98.34
ML8 Upper	22.03.001ox	R	P	0.12	0	44.69	0	0.74	0.26	1.1	21.83	20.07	0.08	0.34	10.09	0.07	0	0	0	0	99.39
ML8 Upper	22.03.001ox	R	P	0	0	51.45	0	0.45	0.04	3.05	21.87	8.49	0.08	0.58	12.99	0.28	0	0.05	0	0	99.33
ML8 Upper	22.03.001ox	M	P	0.12	0	42.76	0	0.47	0.28	0.91	26.35	21.32	0.04	0.22	6.71	0.02	0	0	0	0	99.2
ML8 Upper	22.03.001ox	C	P	0.07	0	42.89	0	0.46	0.21	0.86	26.39	21.32	0.04	0.2	6.74	0.01	0	0	0	0	99.19
ML8 Upper	22.03.001ox	C	P	0.14	0	42.84	0	0.48	0.25	0.87	26.6	20.96	0.05	0.24	6.62	0	0	0	0	0	99.05
ML8 Upper	22.03.002ox	C	GM	0.34	0.03	49.77	0	0	0	0	42.94	2.75	0	1.98	0.03	0.14	0	0	0	0	97.98
ML8 Upper	22.03.011ox	M	MP	0.07	0	52.08	0	0.35	0.11	3.11	21.11	7.39	0.06	0.79	13.8	0.17	0	0.03	0	0	99.07
ML8 Upper	22.03.012ox	C	MP	0	0.04	50.85	0	0.61	0.18	0.5	23.85	10.46	0.11	0.54	11.83	0.05	0	0.03	0	0	99.05
ML8 Upper	22.03.012ox	M	MP	0	0	51.25	0	0.4	0.18	1.21	24	9.42	0.05	0.64	11.88	0.07	0	0.03	0	0	99.13
ML8 Upper	22.03.013ox	C	P	0.08	0	42.51	0	0.41	0.25	1.01	23.54	22.76	0.05	0.27	8.1	0.02	0	0	0	0	99
ML8 Upper	22.03.013ox	C	P	0.11	0	42.7	0	0.51	0.27	1	21.85	23.28	0.07	0.41	9.05	0.05	0	0	0	0	99.3
ML8 Upper	22.03.013ox	R	P	0.35	0.07	50.48	0	0	0	0	42.27	1.76	0	1.47	0	1.54	0	0.03	0	0	97.97
ML345	23.02_001	C	GM	0.06	0.05	53.26	0	0.35	0	1.41	23.87	5.5	0.08	0.9	12.55	0.14	n.m.	0.05	0.13	n.m.	98.35
ML345	23.02_002	C	GM	0	0.1	52.12	0	0.36	0	2.25	0	33.03	0.03	0.8	11.25	0.48	n.m.	0	0.12	n.m.	100.54
ML345	23.02_004	C	MP	0.07	0	50.83	0	0.63	0.1	0.65	23.57	10.37	0.14	0.49	12.08	0.05	n.m.	0	0	n.m.	98.98
ML345	23.02_004	M	MP	0.07	0	50.7	0	0.6	0.07	0.7	23.78	10.36	0.13	0.43	11.94	0.05	n.m.	0	0	n.m.	98.83
ML345	23.02_004	R	MP	0	0	51.59	0	0.56	0.04	3.31	22.62	6.93	0.09	0.52	12.95	0.07	n.m.	0	0	n.m.	98.68
ML345	23.02_005	C	GM	0.11	0	48.6	0.03	0.77	0.28	3.6	22.43	10.71	0.13	0.4	11.55	0.06	n.m.	0.04	0	n.m.	98.71
ML345	23.02_005	M	GM	0	0	50.08	0	0.66	0.11	4.23	23.31	8.39	0.15	0.41	11.83	0.07	n.m.	0	0	n.m.	99.24
ML345	23.02_005	R	GM	0	0.09	51.57	0	0.45	0	3.77	23.64	5.66	0.1	0.64	12.31	0.13	n.m.	0	0	n.m.	98.36
ML345	23.02_007	C	MP	0	0	52.08	0	0.53	0.05	0.38	26.2	8.74	0.09	0.27	11.27	0.01	n.m.	0.04	0	n.m.	99.66
ML345	23.02_007	M	MP	0	0.05	51.77	0	0.54	0.1	0.38	26.13	8.32	0.09	0.28	11.14	0.03	n.m.	0.05	0	n.m.	98.88
ML345	23.02_007	R	MP	0	0.04	52.07	0	0.7	0.08	0.43	24.85	8.61	0.11	0.41	11.91	0.04	n.m.	0.05	0	n.m.	99.3

Appendix B – Mel Kimberlite EPMA Data Tables

Appendix B.02 (continued): Mel hypabyssal kimberlite ilmenite EPMA analyses. n.m. – not measured. Zones: C – core, M – middle, R – rim. Size: P - >500µm, MP – 100-500µm, GM - <100µm. FeO and Fe_2O_3 calculated from FeOT.

Kimberlite	*Sample*	*Zone*	*Size*	*Nb_2O_5*	*SiO_2*	*TiO_2*	*ZnO*	*Al_2O_3*	*V_2O_3*	*Cr_2O_3*	*FeO*	*Fe_2O_3*	*NiO*	*MnO*	*MgO*	*CaO*	*BaO*	*Na_2O*	*K_2O*	*P_2O_5*	*Total*
ML345	23.02 009	C	MP	0.08	0.05	52.07	0	0.6	0	0.7	23.83	8.2	0.12	0.47	12.41	0.09	n.m.	0.07	0	n.m.	98.69
ML345	23.02 009	M	MP	0	0	51.62	0	0.67	0.07	0.24	23.96	9.67	0.14	0.4	12.25	0.08	n.m.	0	0	n.m.	99.1
ML345	23.02 009	R	MP	0	0	52.12	0	0.4	0	2.95	23.13	6.7	0.11	0.42	12.84	0.24	n.m.	0	0.01	n.m.	98.92
ML345	23.02 012	C	GM	0.27	0	52.54	0	0	0.58	0.14	24.06	6.71	0	2.49	10.44	1.84	n.m.	0	0	n.m.	99.07
ML345	23.02 012	R	GM	0.29	0.06	53.74	0.04	0	0.49	0.17	25.32	4.2	0	2.39	10.25	2.09	n.m.	0	0	n.m.	99.04
ML345	23.02 013	C	GM	0.81	0.03	52.41	0	0	0.38	0.06	24.05	5.78	0	3.3	10.09	1.88	n.m.	0.06	0	n.m.	98.85
ML345	23.02 014	M	MP	0	0.04	52.27	0	0.64	0	0.57	24.21	8.54	0.15	0.39	12.36	0.04	n.m.	0.05	0	n.m.	99.26
ML345	23.02 014	R	MP	0.07	0.03	52.21	0	0.63	0.05	0.59	24.46	7.94	0.13	0.41	12.35	0.05	n.m.	0	0	n.m.	98.92
ML345	23.02 014	M	MP	0	0.02	51.9	0	0.46	0.04	3.71	23.63	5.57	0.12	0.48	12.54	0.1	n.m.	0	0	n.m.	98.57
ML345	23.02 015	R	MP	0.15	0	47.92	0	0.8	0.06	2.25	22.51	13.51	0.12	0.44	10.85	0.67	n.m.	0	0	n.m.	99.28
ML345	23.02 015	C	MP	0.06	0	47.04	0	0.96	0.14	1.53	22.04	15.55	0.1	0.42	10.57	0.76	n.m.	0	0	n.m.	99.17
ML345	23.02 015	C	MP	0.16	0	47.96	0	0.84	0.1	2.59	22.54	12.79	0.08	0.46	10.76	0.82	n.m.	0	0	n.m.	99.1
ML345	23.02 016	C	GM	0.11	0	47.02	0	0.97	0.12	1.79	21.6	15.48	0.1	0.42	10.69	0.97	n.m.	0	0	n.m.	99.27
ML345	23.02 017	R	GM	0.13	0	49.92	0	0.58	0.05	4.03	21.9	9.5	0.07	0.61	11.58	1.42	n.m.	0	0	n.m.	99.79

Appendix B – Mel Kimberlite EPMA Data Tables

Appendix B.03: Mel hypabyssal kimberlite spinel EPMA analyses. n.m. – not measured. Zones: C – core, M – middle, R – rim. Size: P - >500µm, MP – 100-500µm, GM - <100µm, I - inclusion. FeO and Fe_2O_3 calculated from FeOT.

Kimberlite	*Sample*	*Zone*	*Size*	*Nb_2O_5*	*SiO_2*	*TiO_2*	*ZnO*	*Al_2O_3*	*V_2O_3*	*Cr_2O_3*	*FeO*	*Fe_2O_3*	*NiO*	*MnO*	*MgO*	*CaO*	*BaO*	*Na_2O*	*K_2O*	*P_2O_5*	*Total*
ML8 Upper	16.01.003ox	C	I	0	0.08	14.86	0.06	5.56	0.04	3.72	29.77	34.05	0.11	0.83	9.19	0.17	0	0.04	0.09	0	98.57
ML8 Upper	16.01.008ox	C	GM	0	0	10.08	0.08	8.7	0.15	24.65	23.35	19.4	0.13	0.52	11.04	0.53	0	0.05	0	0	98.68
ML8 Upper	16.01.015ox	R	MP	0	0.03	7.1	0.06	1.02	0.17	1.62	27.7	54.91	0.04	1.05	5.15	0.71	0	0.03	0	0	99.59
ML8 Upper	16.01.016ox	R	P	0	0.07	20.72	0.05	3.2	0.04	2.03	34.7	27.72	0.11	0.9	9.67	0.12	0	0	0	0	99.33
ML8 Upper	16.03.011ox	R	GM	0	0.02	17.43	0.05	1.73	0.12	2.68	32.58	34.36	0.09	0.87	8.49	0.39	0	0.03	0	0	98.84
ML8 Upper	16.03.013ox	R	MP	0	0.78	17.54	0.07	4.91	0	1.68	32.71	29.53	0.08	1.14	8.95	0.65	0	0.03	0	0	98.07
ML8 Upper	16.03.013ox	R	MP	0	0.04	16.66	0.09	4.62	0.05	1.38	31.49	34.59	0.11	1.2	9.06	0.4	0	0	0	0	99.69
ML8 Upper	16.03.014ox	C	GM	0	0	12.21	0.09	6.65	0.22	33.91	26.43	8.05	0.12	0.74	10.58	0.13	0	0	0	0	99.13
ML8 Upper	16.05.002oxincl	C	I	0	0.26	7.42	0.04	8.77	0.1	28.32	21.78	19.69	0.11	0.49	10.7	0	0	0	0.25	0	97.93
ML8 Lower	21.02.008ox	C	GM	0	0.04	0.43	0	0.08	0.05	0.04	27.87	68.83	0.03	0.21	1.81	0.28	0	0.04	0	0	99.71
ML8 Upper	22.03.008ox	C	GM	0	0.06	14.57	0.05	2.14	0.14	0.8	30.51	40.51	0.07	0.83	7.66	1.1	0	0	0	0	98.44
ML8 Upper	22.03.013ox	R	P	0	0.13	16.67	0.09	5.69	0.06	2.64	31.47	31.88	0.07	0.81	9.59	0.17	0	0.03	0	0	99.3
ML345	23.02 008	C	GM	0.21	0	27.97	0.06	5.79	0.41	24.95	12.01	19.12	0.09	0.48	6.83	0.45	n.m.	0	0	n.m.	98.37
ML345	23.02 011	C	GM	0	0	4.06	0.06	13.33	0.3	44.45	19.4	5.53	0.16	0.27	11.4	0.11	n.m.	0	0	n.m.	99.07
ML345	23.02 011	M	GM	0	0	7.46	0.07	5.92	0.27	42.75	22.66	8.01	0.17	0.37	10.16	0.13	n.m.	0	0	n.m.	97.97

Appendix B – Mel Kimberlite EPMA Data Tables

Appendix B.04: Mel hypabyssal kimberlite rutile EPMA analyses. Zones: C – core, M – middle, R – rim. Size: P - >500µm, MP – 100-500µm, GM - <100µm.

Kimberlite	*Sample*	*Zone*	*Size*	*Nb_2O_5*	*SiO_2*	*TiO_2*	*ZnO*	*Al_2O_3*	*V_2O_3*	*Cr_2O_3*	*FeO*	*Fe_2O_3*	*NiO*	*MnO*	*MgO*	*CaO*	*BaO*	*Na_2O*	*K_2O*	*P_2O_5*	*Total*
ML345	23.02.005ox	C	GM	0.95	0.46	94.97	0	0	0.11	0.19	0	0.46	0	0	0.09	1.09	0	0.04	0.03	0	98.39
ML345	23.02.007ox	C	GM	1.6	1.06	93.53	0	0	0.18	0	0	0.26	0	0	0.53	1.8	0	0	0.02	0	98.98
ML345	23.02.008ox	C	GM	0.93	0.39	94.8	0	0.02	0.15	0.36	0	0.36	0	0	0.07	2.22	0	0	0.02	0	99.32
ML345	23.02.011ox	C	GM	1.26	5.91	80	0	0.05	0.18	0.05	0	1.84	0	0.03	6.47	2.35	0	0.05	0.02	0	98.21

Appendix C: Dharma Kimberlite EPMA Data Tables

Appendix C.01: Dharma hypabyssal kimberlite olivine EPMA analyses. n.m. – not measured. Zones: C – core, M – middle, R – rim. Size: P - >500µm, MP – 100-500µm, GM - <100µm. XN – xenolith.

Kimberlite	*Sample*	*Zone*	*Size*	*Nb_2O_5*	*SiO_2*	*TiO_2*	*ZnO*	*Al_2O_3*	*V_2O_3*	*Cr_2O_3*	*FeO*	*NiO*	*MnO*	*MgO*	*CaO*	*BaO*	*Na_2O*	*K_2O*	*P_2O_5*	*Total*
Dharma	D086001olv	C	P	0	40.63	0	0	0.02	0	0.04	9.76	0.29	0.12	48.9	0.04	0	0	0	0	99.8
Dharma	D086001olv	M	P	0	40.6	0	0	0	0	0.04	9.69	0.3	0.11	48.62	0.05	0	0.02	0	0	99.43
Dharma	D086001olv	R	P	0	40.78	0	0	0	0	0.06	9.61	0.29	0.11	49.29	0.06	0	0.06	0	0.03	100.29
Dharma	D086001olv	C	P	0	40.74	0	0	0.01	0	0	8.91	0.39	0.11	49.24	0.05	0	0.02	0	0	99.47
Dharma	D086001olv	M	P	0	40.56	0	0	0	0	0	8.92	0.39	0.1	49.27	0.06	0	0.04	0	0	99.34
Dharma	D086001olv	R	P	0	40.49	0	0	0.02	0	0.04	9	0.36	0.12	49	0.05	0	0.02	0	0	99.1
Dharma	D086003olv	C	P	0	40.82	0	0.03	0.02	0	0.05	8.34	0.41	0.11	49.66	0.04	0	0.04	0	0	99.52
Dharma	D086003olv	M	P	0	40.7	0	0	0.02	0	0.07	8.35	0.35	0.11	49.8	0.06	0	0.03	0	0	99.49
Dharma	D086003olv	R	P	0	40.94	0.03	0	0	0	0.11	9.58	0.17	0.12	49.51	0.04	0	0.02	0	0	100.52
Dharma	D086004olv	C	P	0	40.89	0	0	0	0	0	8.15	0.4	0.11	50.15	0.01	0	0	0	0	99.71
Dharma	D086004olv	R	P	0	41.11	0	0.03	0	0	0	8.14	0.39	0.09	50.32	0	0	0	0	0	100.08
Dharma	D086005olv	C	P	0	40.8	0	0	0	0	0	8.22	0.35	0.14	49.87	0.02	0	0.01	0	0	99.41
Dharma	D086005olv	M	P	0	40.72	0.06	0	0	0	0	8.3	0.35	0.12	49.74	0.03	0	0	0	0	99.32
Dharma	D086005olv	R	P	0	40.99	0	0	0	0	0.04	8.18	0.34	0.13	50.26	0.03	0	0.02	0	0	99.99
MX	D086006olv	C	P	0	40.47	0	0	0	0	0.04	8.67	0.38	0.13	49.13	0.06	0	0.01	0	0.03	98.92
MX	D086006olv	M	P	0	40.64	0	0	0	0	0	8.73	0.38	0.11	49.19	0.01	0	0.02	0	0	99.08
MX	D086006olv	R	P	0	40.64	0	0	0	0	0.05	8.83	0.37	0.14	49.26	0.03	0	0.01	0	0	99.33
MX	D086007olv	C	P	0	40.75	0	0	0	0	0.04	8.65	0.36	0.13	49.45	0.03	0	0.03	0	0	99.44
MX	D086007olv	M	P	0	40.74	0	0	0	0	0	8.71	0.37	0.12	49.41	0.02	0	0.02	0	0	99.39
MX	D086007olv	R	P	0	41.13	0	0.04	0	0	0	8.73	0.37	0.13	50.1	0.02	0	0.03	0	0	100.55
Dharma	D086008olv	C	P	0	40.88	0	0	0.02	0	0.07	8.22	0.4	0.1	49.98	0.05	0	0.02	0	0	99.74
Dharma	D086008olv	R	P	0	40.82	0	0	0	0	0.06	9.62	0.15	0.12	49.15	0.05	0	0	0	0	99.97
Dharma	D086009olv	C	MP	0	40.64	0	0	0.03	0	0	9.3	0.36	0.13	49.06	0.07	0	0.01	0	0	99.6
Dharma	D086009olv	C	MP	0	40.48	0	0	0.02	0	0	9.31	0.34	0.12	48.88	0.07	0	0.02	0	0	99.24
Dharma	D086009olv	R	MP	0	40.48	0	0	0.03	0	0.09	8.87	0.32	0.1	49.34	0.08	0	0.02	0	0	99.33
Dharma	D086009olv	R	MP	0	40.22	0	0	0	0	0.05	9.64	0.14	0.13	48.53	0.07	0	0.07	0.01	0	98.86
Dharma	D086010olv	C	MP	0	40.55	0	0	0.02	0	0.04	9.28	0.33	0.11	48.97	0.06	0	0.03	0	0	99.39
Dharma	D086010olv	M	MP	0	40.45	0.03	0	0.02	0	0	9.19	0.36	0.11	48.83	0.06	0	0.02	0	0	99.07
Dharma	D086010olv	R	MP	0	40.62	0.05	0	0	0	0.06	8.18	0.13	0.16	49.82	0.1	0	0	0	0	99.12
MX	D086018olv	R	P	0	41.09	0	0	0.02	0	0.06	8.31	0.35	0.11	50.37	0.05	0	0.01	0	0	100.37
MX	D086018olv	M	P	0	40.63	0	0	0	0	0.06	8.26	0.36	0.11	49.41	0.05	0	0.06	0	0	98.94
MX	D086018olv	C	P	0	40.72	0	0	0.01	0	0	8.27	0.39	0.1	49.77	0.05	0	0.02	0	0	99.33
MX	D086018olv	M	P	0	40.68	0	0	0	0	0	8.28	0.37	0.1	49.45	0.04	0	0.03	0	0	98.95
MX	D086018olv	R	P	0	39.92	0.03	0	0.02	0	0.05	8.35	0.36	0.1	48.81	0.09	0	0.03	0	0	97.76
Dharma	D086020olv	C	GM	0	40.24	0	0	0	0	0	7.97	0.37	0.11	49.52	0.07	0	0.01	0	0	98.29
Dharma	D086020olv	M	GM	0	39.94	0.03	0	0.01	0	0	10.09	0.11	0.27	47.68	0.17	0	0	0	0	98.3
Dharma	D086020olv	R	GM	0	40.96	0.05	0.03	0.02	0	0	5.8	0.08	0.16	51.92	0.14	0	0	0	0.07	99.23
Dharma	D086021olv	C	MP	0	39.65	0	0	0	0	0	11.73	0.16	0.15	46.39	0.06	0	0	0	0	98.14

Appendix C: Dharma Kimberlite EPMA Data Tables

Appendix C.01 (continued): Dharma hypabyssal kimberlite olivine EPMA analyses. n.m. – not measured. Zones: C – core, M – middle, R – rim. Size: P - >500µm, MP – 100-500µm, GM - <100µm. XN – xenolith.

Kimberlite	*Sample*	*Zone*	*Size*	*Nb_2O_5*	*SiO_2*	*TiO_2*	*ZnO*	*Al_2O_3*	*V_2O_3*	*Cr_2O_3*	*FeO*	*NiO*	*MnO*	*MgO*	*CaO*	*BaO*	*Na_2O*	*K_2O*	*P_2O_5*	*Total*
Dharma	D086023olv	R	MP	0	41.39	0.04	0	0	0	0.04	6.18	0.12	0.18	52.61	0.1	0	0	0	0	100.66
Dharma	D086024olv	C	MP	0	40.5	0.09	0	0.02	0	0.06	9.57	0.26	0.1	48.76	0.05	0	0.02	0	0	99.43
Dharma	D086024olv	R	MP	0	40.53	0.05	0.03	0	0	0	9.59	0.12	0.14	48.99	0.06	0	0.02	0	0	99.53
Dharma	D086026px	C	MP	0	40.49	0	0	0.02	0	0	8.55	0.36	0.11	49.16	0.08	0	0.07	0.01	0	98.85
Dharma	D086026px	M	MP	0	40.12	0.03	0	0.02	0	0	9.65	0.16	0.13	48.36	0.04	0	0	0	0	98.51
Dharma	D086026px	R	MP	0	40.25	0.03	0	0.02	0	0.05	9.33	0.11	0.15	48.36	0.05	0	0	0	0.03	98.38
Dharma	D086028olv	C	MP	0	40.3	0	0	0	0	0	9.56	0.17	0.1	48.47	0.07	0	0.01	0	0	98.68
Dharma	D086028olv	R	MP	0	40.52	0.05	0	0.02	0	0	8.7	0.17	0.15	49.53	0.12	0	0	0	0	99.26
Dharma	D086030olv	C	MP	0	40.31	0	0	0	0	0.06	9.83	0.26	0.13	48.29	0.05	0	0	0	0	98.93
Dharma	D086030olv	R	MP	0	40.31	0.04	0	0	0	0.05	9.36	0.16	0.16	48.53	0.12	0	0	0	0.04	98.77
Dharma	D086032olv	C	GM	0	40.33	0.05	0	0	0	0	9.62	0.25	0.14	48.63	0.06	0	0.02	0	0	99.1
Dharma	D086032olv	R	GM	0	40.48	0.05	0	0	0	0.04	9.6	0.12	0.14	49.15	0.12	0	0	0	0	99.7
Dharma	D086033olv	C	P	0	40.37	0	0	0	0	0.05	9.69	0.3	0.1	48.57	0.05	0	0.02	0	0	99.15
Dharma	D086033olv	M	P	0	40.13	0	0	0.01	0	0.04	9.57	0.29	0.11	48.35	0.05	0	0.05	0	0	98.6
Dharma	D086033olv	R	P	0	40.62	0	0	0.03	0	0.06	9.55	0.28	0.1	49.23	0.06	0	0.04	0	0	99.97
Dharma	D086034olv	C	P	0	40.31	0	0	0.03	0	0.05	8.43	0.39	0.12	49.32	0.06	0	0.02	0	0	98.73
Dharma	D086034olv	M	P	0	40.4	0	0	0.04	0	0.09	8.52	0.42	0.14	49.31	0.06	0	0.03	0	0	99.01
Dharma	D086034olv	R	P	0	40.32	0	0	0	0	0.07	8.66	0.4	0.12	49.05	0.08	0	0.01	0	0	98.71
Dharma	D086035olv	C	P	0	40.37	0	0	0	0	0	10.13	0.22	0.1	48.43	0.03	0	0	0	0	99.28
Dharma	D086035olv	M	P	0	40.2	0	0	0	0	0	10.03	0.21	0.11	48.22	0.03	0	0	0	0	98.8
Dharma	D086035olv	R	P	0	40.58	0	0	0	0	0.04	9.02	0.16	0.17	49.28	0.05	0	0	0	0	99.3
Dharma	D086036px	C	P	0	40.46	0	0	0	0	0.04	8.13	0.39	0.12	49.48	0.07	0	0	0	0	98.69
Dharma	D086036px	M	P	0	40.46	0	0	0.02	0	0	8.04	0.38	0.11	49.58	0.03	0	0	0	0	98.62
Dharma	D086036px	R	P	0	40.5	0.03	0	0.01	0	0	9.54	0.13	0.14	49.13	0.07	0	0.03	0	0	99.58
Dharma	D091002olv	C	P	0	40.66	0	0	0.02	0	0.04	8.51	0.37	0.11	49.37	0.05	0	0.01	0	0	99.14
Dharma	D091002olv	M	P	0	40.63	0	0	0	0	0	8.51	0.39	0.11	49.74	0.05	0	0	0	0	99.43
MX	D091003olv	R	P	0	40.53	0.03	0	0.02	0	0.07	9.38	0.33	0.11	48.79	0.05	0	0	0	0	99.31
MX	D091003olv	M	P	0	40.18	0	0	0.01	0	0	9.37	0.33	0.11	48.56	0.05	0	0.01	0	0	98.62
MX	D091003olv	C	P	0	40.48	0	0	0.03	0	0.06	9.44	0.33	0.11	48.72	0.05	0	0	0	0	99.22
MX	D091003olv	C	P	0	40.29	0.04	0	0	0	0.05	9.47	0.32	0.1	48.5	0.05	0	0	0	0	98.82
MX	D091003olv	M	P	0	40.27	0	0	0	0	0	9.33	0.3	0.11	48.46	0.05	0	0.02	0	0	98.54
MX	D091003olv	R	P	0	40.14	0	0	0.01	0	0	9.61	0.16	0.13	48.24	0.08	0	0	0	0	98.37
Dharma	D091004olv	C	MP	0	40.01	0.05	0	0.01	0	0	10.83	0.16	0.14	47.5	0.05	0	0	0	0	98.75
Dharma	D091004olv	R	MP	0	40.07	0.03	0	0.02	0	0	9.52	0.24	0.13	48.25	0.07	0	0	0	0	98.33
Dharma	D091005olv	C	MP	0	40.32	0	0	0.04	0	0	9.13	0.3	0.1	49.05	0.1	0	0.02	0	0	99.06
Dharma	D091005olv	R	MP	0	40.07	0.04	0	0	0	0.07	9.34	0.13	0.15	48.55	0.08	0	0	0	0	98.43
Dharma	D091006olv	C	MP	0	40.23	0	0	0.02	0	0	9.54	0.32	0.1	48.54	0.06	0	0	0	0	98.81

Appendix C: Dharma Kimberlite EPMA Data Tables

Appendix C.01 (continued): Dharma hypabyssal kimberlite olivine EPMA analyses. n.m. – not measured. Zones: C – core, M – middle, R – rim. Size: P - >500µm, MP – 100-500µm, GM - <100µm. XN – xenolith.

Kimberlite	*Sample*	*Zone*	*Size*	*Nb_2O_5*	*SiO_2*	*TiO_2*	*ZnO*	*Al_2O_3*	*V_2O_3*	*Cr_2O_3*	*FeO*	*NiO*	*MnO*	*MgO*	*CaO*	*BaO*	*Na_2O*	*K_2O*	*P_2O_5*	*Total*
Dharma	D091006olv	R	MP	0	40.31	0.04	0	0.02	0	0.06	9.52	0.3	0.11	48.75	0.05	0	0	0	0	99.16
Dharma	D091007olv	C	MP	0	40.41	0	0	0.03	0	0.07	8.48	0.35	0.1	49.25	0.1	0	0.01	0	0	98.8
Dharma	D091007olv	M	MP	0	40.27	0.04	0	0.01	0	0.05	8.8	0.31	0.13	48.98	0.09	0	0	0	0	98.68
Dharma	D091007olv	R	MP	0	40.21	0.05	0	0	0	0	9.18	0.15	0.13	48.85	0.12	0	0	0	0	98.69
Dharma	D091008olv	C	P	0	40.44	0	0	0.02	0	0	9.21	0.34	0.11	48.73	0.05	0	0.02	0	0	98.92
Dharma	D091008olv	M	P	0	40.35	0	0	0	0	0	8.81	0.28	0.11	49.27	0.06	0	0	0	0	98.88
Dharma	D091008olv	R	P	0	40.19	0.05	0	0	0	0.06	9.59	0.13	0.14	48.62	0.05	0	0	0	0	98.83
Dharma	D091009olv	C	P	0	40.16	0.04	0	0.02	0	0.06	8.85	0.37	0.12	49.03	0.06	0	0.02	0	0	98.73
Dharma	D091009olv	M	P	0	40.32	0	0	0.03	0	0	8.51	0.36	0.11	49.16	0.07	0	0	0	0	98.56
Dharma	D091009olv	R	P	0	40.22	0.04	0	0	0	0.07	9.46	0.18	0.13	48.8	0.06	0	0	0	0	98.96
Dharma	D091010olv	C	MP	0	40.12	0	0	0.03	0	0.04	9.31	0.31	0.12	48.52	0.07	0	0.03	0	0	98.55
Dharma	D091010olv	M	MP	0	40.26	0	0	0.02	0	0.05	9.21	0.32	0.11	48.76	0.08	0	0.02	0	0	98.83
Dharma	D091010olv	R	MP	0	40.46	0	0.04	0.01	0	0.04	9.55	0.11	0.13	48.41	0.13	0	0.01	0	0.03	98.92
Dharma	D091011olv	C	P	0	40.67	0	0	0	0	0.06	7.73	0.35	0.1	49.88	0.02	0	0.01	0	0	98.82
Dharma	D091011olv	M	P	0	40.46	0	0	0	0	0.09	9.55	0.25	0.13	48.7	0.07	0	0	0	0	99.25
Dharma	D091011olv	R	P	0	41.03	0.06	0	0.02	0	0	8.42	0.13	0.16	49.81	0.08	0	0	0	0	99.71
Dharma	D091012olv	C	MP	0	40.61	0	0	0.01	0	0	7.68	0.38	0.1	49.95	0.07	0	0	0.02	0	98.82
Dharma	D091012olv	R	MP	0	40.37	0.04	0	0.02	0	0.04	9.53	0.29	0.11	48.63	0.05	0	0	0	0	99.08
Dharma	D091014olv	C	P	0	40.36	0.03	0	0	0	0.07	9.53	0.12	0.17	48.53	0.04	0	0	0	0	98.85
Dharma	D091014olv	M	P	0	40.22	0.03	0	0	0	0.1	9.58	0.13	0.13	48.27	0.05	0	0	0	0	98.51
Dharma	D091014olv	R	P	0	40.19	0.05	0	0.02	0	0	8.5	0.15	0.15	48.98	0.13	0	0	0	0	98.17
Dharma	D092004gt	C	P	0	40.39	0.03	0	0	0	0	10.37	0.23	0.13	48.09	0.04	0	0	0	0	99.28
Dharma	D092004gt	M	P	0	40.4	0.03	0	0	0	0	10.32	0.22	0.11	48.28	0.04	0	0	0	0	99.4
Dharma	D092004gt	R	P	0	40.87	0.03	0	0	0	0.05	10.27	0.22	0.12	48.61	0.03	0	0	0	0.03	100.23
Dharma	D092005olv	C	P	0	41.17	0	0	0	0	0.04	7.45	0.35	0.1	50.67	0.03	0	0	0	0	99.81
Dharma	D092005olv	M	P	0	40.71	0.03	0	0.01	0	0	7.46	0.36	0.11	50.16	0.03	0	0	0	0	98.87
Dharma	D092005olv	R	P	0	40.49	0	0	0	0	0.1	9.63	0.19	0.11	48.77	0.03	0	0	0	0	99.32
Dharma	D092006olv	C	P	0	40.69	0	0	0.04	0	0.06	8.41	0.37	0.11	49.54	0.07	0	0.02	0	0	99.31
Dharma	D092006olv	M	P	0	40.43	0.05	0	0	0	0.07	9.7	0.14	0.13	48.71	0.04	0	0	0	0	99.27
Dharma	D092006olv	R	P	0	40.79	0	0	0.02	0	0	8.59	0.37	0.12	49.74	0.05	0	0	0	0.04	99.72
Dharma	D092007olv	C	P	0	40.65	0	0	0	0	0	8.23	0.38	0.11	49.51	0.04	0	0.02	0	0	98.94
Dharma	D092007olv	M	P	0	40.66	0	0	0.02	0	0.08	8.26	0.37	0.11	49.44	0.05	0	0.02	0	0	99.01
Dharma	D092007olv	R	P	0	40.37	0.05	0	0.02	0	0.12	9.7	0.14	0.14	48.46	0.05	0	0	0	0	99.05
Dharma	D092008olv	C	P	0	40.79	0	0	0.02	0	0.06	8.35	0.36	0.1	49.78	0.05	0	0.01	0	0	99.52
Dharma	D092008olv	M	P	0	40.74	0	0.03	0.02	0	0	8.38	0.37	0.11	49.69	0.04	0	0.02	0	0	99.4
Dharma	D092008olv	R	P	0	40.3	0.06	0	0.01	0	0.09	9.68	0.18	0.11	48.5	0.05	0	0	0	0	98.98
Dharma	D092009olv	C	P	0	40.86	0	0	0	0	0.06	8.37	0.38	0.12	49.7	0.04	0	0	0	0	99.53
Dharma	D092009olv	M	P	0	40.93	0.03	0.03	0.03	0	0.12	8.23	0.41	0.1	50.06	0.07	0	0.01	0	0	100.02

Appendix C: Dharma Kimberlite EPMA Data Tables

Appendix C.01 (continued): Dharma hypabyssal kimberlite olivine EPMA analyses. n.m. – not measured. Zones: C – core, M – middle, R – rim. Size: P - >500µm, MP – 100-500µm, GM - <100µm. XN – xenolith.

Kimberlite	*Sample*	*Zone*	*Size*	*Nb_2O_5*	*SiO_2*	*TiO_2*	*ZnO*	*Al_2O_3*	*V_2O_3*	*Cr_2O_3*	*FeO*	*NiO*	*MnO*	*MgO*	*CaO*	*BaO*	*Na_2O*	*K_2O*	*P_2O_5*	*Total*
Dharma	D092009olv	R	P	0	40.36	0.05	0	0	0	0.12	9.54	0.18	0.13	48.78	0.07	0	0	0	0	99.23
Dharma	D092010olv	C	MP	0	40.77	0	0	0	0	0	8.6	0.39	0.14	49.58	0.03	0	0	0	0	99.51
Dharma	D092010olv	R	MP	0	41.65	0.04	0	0.03	0	0	6.96	0.13	0.17	52.58	0.16	0	0	0	0	101.72
Dharma	D092011olv	C	MP	0	40.67	0	0	0	0	0	7.67	0.37	0.1	49.98	0.01	0	0	0	0	98.8
Dharma	D092011olv	M	MP	0	40.69	0	0	0	0	0	8.77	0.18	0.15	49.64	0.08	0	0	0	0	99.51
Dharma	D092011olv	R	MP	0	41.72	0	0	0.02	0	0	3.31	0.05	0.2	54.49	0.11	0	0	0	0	99.9
Dharma	D092012olv	C	MP	0	40.76	0	0	0	0	0.04	8.26	0.35	0.11	49.69	0.05	0	0	0	0	99.26
Dharma	D092012olv	R	MP	0	41.12	0	0	0	0	0.06	8.19	0.35	0.11	50.21	0.07	0	0.02	0	0	100.13
Dharma	D092013olv	C	P	0	40.59	0	0	0.03	0	0.06	9.16	0.31	0.14	49.17	0.06	0	0.02	0	0	99.54
Dharma	D092013olv	R	P	0	40.35	0	0	0.02	0	0	9.62	0.12	0.14	48.59	0.05	0	0	0	0	98.89
Dharma	D092014olv	C	MP	0	40.53	0	0	0.02	0	0.07	9.49	0.33	0.11	48.88	0.05	0	0.02	0	0	99.5
Dharma	D092014olv	R	MP	0	40.66	0	0	0.02	0	0.06	9.52	0.2	0.12	48.81	0.03	0	0.01	0	0	99.43
Dharma	D092016olv	C	P	0	40.49	0	0	0.03	0	0.05	8.76	0.38	0.12	49.23	0.06	0	0.01	0	0	99.13
Dharma	D092016olv	M	P	0	40.57	0	0	0.02	0	0.04	8.75	0.39	0.1	49.14	0.05	0	0.03	0	0	99.09
Dharma	D092016olv	R	P	0	40.72	0	0	0.02	0	0	8.88	0.35	0.08	49.33	0.05	0	0.02	0	0	99.45
Dharma	D092017olv	C	P	0	40.58	0.03	0	0.02	0	0.06	8.31	0.38	0.09	49.59	0.07	0	0.01	0	0	99.14
Dharma	D092017olv	M	P	0	40.61	0	0	0.02	0	0	8.24	0.38	0.11	49.49	0.05	0	0.01	0	0	98.91
Dharma	D092017olv	R	P	0	40.58	0.05	0	0.02	0	0	9.74	0.29	0.13	48.9	0.04	0	0	0	0	99.75
Dharma	D092019px	C	MP	0	40.8	0	0	0	0	0	7.7	0.36	0.09	50.22	0.02	0	0.02	0	0	99.21
Dharma	D092019px	R	MP	0	40.52	0.03	0	0.02	0	0.09	9.77	0.14	0.14	48.61	0.05	0	0	0	0	99.37
Dharma	D092020olv	R	MP	0	40.67	0.03	0	0	0	0.07	9.56	0.2	0.12	49	0.05	0	0	0	0	99.7
Dharma	D104007olv	C	P	0	40.32	0	0	0	0	0	9.81	0.21	0.13	48.4	0.04	0	0.02	0	0	98.93
Dharma	D104007olv	M	P	0	40.56	0	0	0	0	0	9.86	0.23	0.11	48.46	0.04	0	0.02	0	0	99.28
Dharma	D104007olv	R	P	0	40.42	0	0	0.02	0	0	9.86	0.24	0.12	48.66	0.03	0	0.02	0	0	99.37
Dharma	D104008olv	C	P	0	40.31	0	0	0	0	0	9.99	0.27	0.14	48.28	0.03	0	0.02	0	0	99.04
Dharma	D104011olv	C	P	0	40.21	0	0	0	0	0	10.28	0.32	0.15	48.18	0.03	0	0	0	0	99.17
Dharma	D104011olv	M	P	0	40.12	0.03	0	0	0	0	10.28	0.29	0.17	48.04	0.03	0	0.01	0	0	98.97
Dharma	D104011olv	R	P	0	41.09	0.05	0	0	0	0	9.71	0.18	0.11	49.63	0.03	0	0.01	0	0	100.81
Dharma	D104015olv	C	GM	0	40.2	0	0	0	0	0.04	9.51	0.35	0.13	48.57	0.05	0	0.01	0	0	98.86
Dharma	D104015olv	R	GM	0	40.88	0	0	0	0	0.05	9.5	0.17	0.12	49.31	0.05	0	0	0	0	100.08
Dharma	D104019olv	C	GM	0	40.33	0	0	0	0	0	10.19	0.23	0.12	48.29	0.09	0	0.01	0	0	99.26
Dharma	D104019olv	R	GM	0	41.1	0.05	0	0	0	0	7.85	0.11	0.13	51.08	0.1	0	0	0	0	100.42

Appendix C: Dharma Kimberlite EPMA Data Tables

Appendix C.02: Dharma hypabyssal kimberlite pyroxene EPMA analyses. Min. (mineral): cpx – clinopyroxene, opx – orthopyroxene. Zones: C – core, M – middle, R – rim. Size: P - >500µm, MP – 100-500µm, GM - <100µm. XN – xenolith.

Kimberlite	*Sample*	*Min.*	*Zone*	*Size*	*Nb_2O_5*	*SiO_2*	*TiO_2*	*ZnO*	*Al_2O_3*	*V_2O_3*	*Cr_2O_3*	*FeO*	*NiO*	*MnO*	*MgO*	*CaO*	*BaO*	*Na_2O*	*K_2O*	*P_2O_5*	*Total*
Dharma	D086011px	cpx	C	P	0	54.94	0.25	0	1.75	0	0.45	2.95	0	0.09	16.82	21.44	0	1.28	0.04	0	100.01
Dharma	D086011px	cpx	M	P	0	54.97	0.24	0	1.77	0.05	0.51	3.08	0.03	0.1	16.86	21.52	0	1.3	0.05	0	100.48
Dharma	D086011px	cpx	R	P	0	54.54	0.24	0	1.79	0.05	0.48	3.18	0.03	0.09	16.94	21.17	0	1.27	0.06	0	99.84
Dharma	D086012px	cpx	C	P	0	55.06	0.19	0	1.87	0	0.94	3.55	0.05	0.14	19.3	17.11	0	1.41	0.05	0	99.67
Dharma	D086012px	cpx	R	P	0	55.58	0.18	0	1.87	0	0.88	3.55	0.05	0.14	19.5	17.18	0	1.37	0.08	0	100.38
Dharma	D086013px	cpx	C	P	0	55.24	0.11	0	1.55	0	1.21	2.89	0.08	0.11	18.9	18.31	0	1.33	0.05	0	99.78
Dharma	D086013px	cpx	M	P	0	55.22	0.1	0	1.58	0	1.3	2.9	0.05	0.12	18.99	18.22	0	1.37	0.04	0	99.89
Dharma	D086013px	cpx	R	P	0	55.24	0.08	0	1.55	0	1.31	2.92	0.05	0.09	19.07	18.19	0	1.35	0.05	0	99.9
MX	D086014px	opx	C	P	0	57.81	0.04	0	0.65	0	0.33	4.87	0.12	0.1	34.7	0.93	0	0.17	0	0	99.72
MX	D086014px	opx	M	P	0	57.53	0.06	0	0.66	0	0.32	4.87	0.13	0.12	34.78	0.94	0	0.16	0	0	99.57
MX	D086014px	opx	R	P	0	57.81	0.06	0	0.64	0	0.38	4.85	0.11	0.13	34.87	0.95	0	0.18	0	0	99.98
Dharma	D086019olv	opx	C	P	0	57.19	0.13	0	0.55	0	0.35	4.48	0.11	0.1	35.12	0.62	0	0.15	0	0	98.8
Dharma	D086019olv	opx	M	P	0	57.03	0.13	0	0.55	0	0.27	4.46	0.11	0.11	34.91	0.61	0	0.14	0	0	98.32
Dharma	D086042px	opx	C	MP	0	56.39	0.22	0	0.75	0	0.8	6.33	0.04	0.2	32.89	1.24	0	0.1	0	0	98.96
Dharma	D086042px	cpx	C	MP	0	54.64	0.19	0	1.74	0.03	0.85	3.44	0.05	0.1	18.38	17.92	0	1.42	0.07	0	98.83
Dharma	D086042px	cpx	R	MP	0	55.07	0.19	0	1.77	0	0.84	3.47	0.05	0.11	18.67	17.89	0	1.37	0.06	0	99.49
Dharma	D091001px	cpx	R	P	0	54.49	0.27	0	1.84	0.05	0.46	3.14	0.03	0.08	16.75	21.17	0	1.35	0.04	0	99.67
Dharma	D091001px	cpx	M	P	0	54.22	0.27	0	1.84	0.05	0.42	3.07	0.04	0.1	16.71	21.09	0	1.37	0.04	0	99.22
Dharma	D091001px	cpx	C	P	0	54.33	0.26	0	1.83	0.08	0.41	3.12	0.02	0.06	16.77	21.22	0	1.4	0.04	0	99.54
Dharma	D091001px	cpx	C	P	0	54.11	0.25	0	1.83	0.05	0.43	3.08	0.03	0.09	16.66	21.18	0	1.36	0.04	0	99.11
Dharma	D091001px	cpx	M	P	0	54.17	0.24	0	1.83	0	0.42	3.1	0	0.12	16.73	21.01	0	1.37	0.04	0.03	99.06
Dharma	D091001px	cpx	R	P	0	54.26	0.22	0	1.82	0.06	0.42	3.12	0	0.08	16.61	21.15	0	1.36	0.04	0	99.14
Dharma	D091001px	cpx	R	P	0	54.22	0.24	0	1.84	0	0.42	3.1	0.03	0.08	16.77	21.08	0	1.35	0.04	0	99.17
Dharma	D092015px	cpx	C	P	0	54.94	0.25	0	1.78	0	0.59	3.26	0	0.09	17.1	20.45	0	1.36	0.03	0	99.85
Dharma	D092015px	cpx	M	P	0	54.62	0.31	0	1.77	0.05	0.59	3.32	0.04	0.1	17.04	20.59	0	1.38	0.03	0	99.84
Dharma	D092015px	cpx	R	P	0.06	54.66	0.26	0	1.78	0.04	0.6	3.28	0.03	0.09	17.06	20.5	0	1.41	0.04	0	99.81
Dharma	D094007gt	cpx	C	P	0	54.68	0.24	0	1.82	0.03	0.39	3.2	0	0.09	16.59	21.06	0	1.37	0.06	0	99.53
Dharma	D094007gt	cpx	M	P	0	54.61	0.24	0	1.83	0.04	0.37	3.2	0	0.1	16.59	20.93	0	1.34	0.04	0	99.29
Dharma	D094007gt	cpx	R	P	0	54.44	0.25	0	1.82	0	0.38	3.21	0	0.09	16.6	20.87	0	1.34	0.03	0	99.03

Appendix C: Dharma Kimberlite EPMA Data Tables

Appendix C.03: Dharma hypabyssal kimberlite mica EPMA analyses. n.m. – not measured. Min. (mineral): bt- biotite, phl - phlogopite. Zones: C – core, M – middle, R – rim. Size: P - >500µm, MP – 100-500µm, GM - <100µm.

Kimberlite	*Sample*	*Min.*	*Zone*	*Size*	*Nb_2O_5*	*SiO_2*	*TiO_2*	*ZnO*	*Al_2O_3*	*V_2O_3*	*Cr_2O_3*	*FeO*	*NiO*	*MnO*	*MgO*	*CaO*	*BaO*	*Na_2O*	*K_2O*	*P_2O_5*	*Total*
Dharma	D104001phl	phl	C	P	0	40.57	2.39	0	12.65	0	0.14	4.53	0.13	0.02	23.58	0	0	0.05	10.54	0	94.6
Dharma	D104001phl	phl	M	P	0	40.44	1.32	0	12.64	0.03	0.16	4.6	0.12	0.03	23.39	0	0	0.08	10.7	0	93.51
Dharma	D104001phl	phl	R	P	0	40.76	1.14	0	12.65	0	0.17	4.62	0.1	0.03	23.92	0	0	0.07	10.61	0	94.07
Dharma	D094004phl	phl	R	P	0.06	41.09	1.01	0	12.64	0	0	7.39	0	0.18	23.16	0.09	0.69	0.05	8.28	0.07	94.71
Dharma	D094005phl	phl	R	MP	0	43.69	0.92	0.03	11.72	0.07	0.23	4.29	0	0.05	23.46	0.11	0.32	0.07	9.11	0.16	94.23
Dharma	D108005phl	bt	C	MP	0	34.54	2.44	0.05	17.46	0.05	0	22.88	0	0.33	7.91	0	0	0.18	9.81	0	95.65
Dharma	D108005phl	bt	M	MP	0	34.54	2.39	0.05	17.59	0.04	0	22.89	0	0.29	8.22	0	0	0.2	9.73	0	95.94
Dharma	D108006phl	bt	C	P	0.06	34.97	2.46	0	17.22	0.05	0	22.3	0	0.3	8.12	0	0	0.22	9.81	0	95.51
Dharma	D108006phl	bt	M	P	0	34.27	2.48	0.04	16.95	0.03	0	22.94	0	0.32	7.86	0	0	0.2	9.59	0	94.68
Dharma	D108006phl	bt	R	P	0	34.12	2.28	0.03	16.72	0	0	22.92	0	0.28	8.75	0.02	0	0.12	9.3	0	94.54
Dharma	D108007phl	bt	C	MP	0	34.79	2.4	0.03	17.23	0	0	23.12	0	0.32	8.06	0	0	0.19	9.93	0	96.07
Dharma	D108007phl	bt	M	MP	0	34.52	2.45	0.03	16.98	0.06	0.05	23.06	0	0.3	8.13	0	0	0.19	9.76	0	95.53
Dharma	D108007phl	bt	R	MP	0	34.57	2.38	0	16.71	0.06	0	23.07	0	0.32	8.47	0	0	0.17	9.63	0	95.38
Dharma	D108008phl	bt	C	P	0	34.84	2.48	0.06	17.45	0	0	22.27	0.03	0.31	8.05	0	0	0.19	9.83	0	95.51
Dharma	D108008phl	bt	M	P	0	34.81	2.3	0	17.7	0.07	0	21.41	0	0.28	8.43	0	0	0.25	9.94	0	95.19
Dharma	D108008phl	bt	R	P	0	34.66	2.25	0.03	16.92	0.04	0	22.86	0	0.34	8.57	0	0	0.14	9.43	0	95.24
Dharma	D108009phl	bt	C	P	0	34.67	2.55	0.05	16.98	0.05	0	21.71	0	0.28	9	0	0	0.3	9.41	0	95
Dharma	D108009phl	bt	R	P	0	33.03	2.68	0	16.27	0.06	0	23.56	0	0.39	8.58	0.05	0.17	0.04	8.89	0	93.72
Dharma	D108010phl	bt	C	P	0	34.91	2.3	0.06	17.27	0.05	0	22.13	0	0.29	8.07	0	0	0.21	9.66	0	94.95
Dharma	D108010phl	bt	R	P	0	34.68	2.22	0	17.02	0	0	22.73	0	0.32	8.09	0	0	0.14	9.71	0	94.91
Dharma	D117_04	phl	M	P	0	40.2	3.98	0.04	11.57	0.06	1.02	4.03	0.07	0.05	22.97	0.03	0	0.22	10.73	n.m.	94.97
Dharma	D117_04	phl	R	P	0	43.49	2.27	0	7.43	0.04	0.48	4.57	0.03	0.05	24.83	0.04	0	0.08	9.57	n.m.	92.88
Dharma	D117_08	phl	M	MP	0	39.85	3.03	0	11.81	0	1.39	4.1	0.07	0.03	23.93	0.06	0	0.18	10.66	n.m.	95.11
Dharma	D117_08	phl	R	MP	0	39.9	3.19	0	12.08	0.05	1.09	4.12	0.05	0.05	23.63	0.09	0	0.14	11.03	n.m.	95.42
Dharma	D128_06	phl	C	P	0	38.54	3.36	0	12.82	0.03	1.72	3.99	0.15	0.04	21.95	0.12	0.18	0.14	10.48	n.m.	93.52

Appendix C: Dharma Kimberlite EPMA Data Tables

Appendix C.04: Dharma hypabyssal kimberlite ilmenite EPMA analyses. Zones: C – core, M – middle, R – rim. Size: P - >500µm, MP – 100-500µm, GM - <100µm, I - inclusion. FeO and Fe_2O_3 calculated from FeOT.

Kimberlite	*Sample*	*Zone*	*Size*	*Nb_2O_5*	*SiO_2*	*TiO_2*	*ZnO*	*Al_2O_3*	*V_2O_3*	*Cr_2O_3*	*FeO*	*Fe_2O_3*	*NiO*	*MnO*	*MgO*	*CaO*	*BaO*	*Na_2O*	*K_2O*	*P_2O_5*	*Total*
Dharma	D086041ox	M	GM	0.19	0	54.87	0	0.53	0.32	1.01	22.13	5.62	0.11	0.34	15.03	0.15	0	0	0	0	100.3
Dharma	D086049ox	C	GM	0.1	0.02	54.54	0	0.74	0.04	4.79	7.5	8.12	0.07	0.59	22.82	0.11	0	0.04	0.01	0	99.49
Dharma	D091013oxincl	C	I	0.15	0.06	55.98	0	0.3	0.07	3.86	15.21	3.16	0.11	0.4	19.48	0.11	0	0	0	0	98.89
Dharma	D091017ox	M	P	0.16	0	54.23	0	0.55	0.21	1.72	25.2	4.5	0.09	0.29	13.1	0.02	0.31	0	0	0	100.07
Dharma	D091017ox	C	P	0.18	0.03	54.13	0	0.57	0.16	1.67	25.28	4.3	0.12	0.26	12.95	0.03	0.28	0.03	0	0	99.71
Dharma	D091017ox	C	P	0.21	0	54.25	0	0.55	0.14	1.73	25.35	4.38	0.12	0.26	13.05	0.03	0	0	0	0	100.07
Dharma	D091017ox	M	P	0.16	0	54.25	0	0.53	0.21	1.77	25.18	4.61	0.1	0.28	13.04	0.02	0.18	0.03	0	0	100.18
Dharma	D091017ox	R	P	0.19	0	54.9	0	0.54	0.24	1.72	23.1	4.39	0.12	0.39	14.5	0.03	0.15	0.02	0	0	100.14
Dharma	D091018ox	M	P	0.19	0	55.46	0	0.65	0.25	2.04	18.4	4.96	0.1	0.37	17.47	0.06	0.27	0	0	0	99.95
Dharma	D091018ox	C	P	0.2	0.05	53.21	0	0.64	0.19	1.88	23.86	5.67	0.15	0.27	13.32	0.02	0	0.02	0	0	99.48
Dharma	D091018ox	C	P	0.15	0.34	53.05	0	0.5	0.22	1.8	22.76	6.13	0.13	0.28	14.02	0.1	0.26	0	0	0	99.48
Dharma	D091018ox	M	P	0.2	0.03	55.81	0	0.63	0.27	1.95	16.24	4.96	0.1	0.41	18.85	0.08	0.18	0	0	0	99.53
Dharma	D091019ox	C	GM	0.12	0.02	50.91	0	1.39	0.11	3.62	6.92	13.88	0.1	0.42	21.4	0.28	0.24	0	0	0	99.17
Dharma	D091020ox	C	GM	3.11	0.03	60.53	0	0.28	0	1.06	5.4	0	0.03	1.28	26.29	1.03	0.22	0.06	0	0	99.1
Dharma	D091021ox	C	GM	0.22	0	53.21	0	2.32	0	0.85	8.56	12.92	0.11	0.46	21.35	0.71	0.23	0	0	0	100.71
Dharma	D091025ox	R	GM	0.2	0.04	53.11	0	1.05	0.1	2.52	7.84	10.75	0.11	0.48	22.02	0.28	0.28	0	0	0	98.5
Dharma	D092025ox	C	P	0.23	0.02	53.23	0	0.53	0.16	1.08	25.92	5.9	0.09	0.32	12.23	0.02	0	0	0	0.04	99.73
Dharma	D092025ox	M	P	0.24	0.03	53.44	0	0.52	0.16	1.03	26.11	5.75	0.09	0.3	12.25	0.02	0	0	0	0	99.94
Dharma	D104008ox	C	P	0.2	0.03	54.48	0	0.48	0.18	1.69	25.07	4.05	0.15	0.31	13.22	0.02	0	0.03	0	0	99.91
Dharma	D104008ox	M	P	0.19	0.02	54.26	0.03	0.5	0	1.72	24.91	4.18	0.12	0.27	13.29	0.02	0	0	0	0	99.51
Dharma	D104009ox	C	P	0.37	0	50.73	0	0.24	0.2	6.02	23.98	5.9	0.2	0.3	12.04	0	0	0.02	0	0	100
Dharma	D104009ox	M	P	0.37	0	50.14	0	0.24	0.15	6.07	23.46	6.53	0.19	0.31	12.03	0.01	0	0.02	0	0	99.52
Dharma	D109003ox	M	P	0.11	0.02	54.89	0	0.59	0.16	3.78	14.35	6.41	0.1	0.41	19.39	0.07	0.21	0	0	0	100.28
Dharma	D109003ox	C	P	0.16	0.03	53.55	0	0.62	0.14	2	24.55	5.32	0.09	0.26	13.08	0.02	0.22	0.03	0	0	99.85
Dharma	D109003ox	C	P	0.14	0	53.81	0	0.58	0.21	1.95	24.82	4.86	0.11	0.26	13.06	0	0.15	0.02	0	0	99.82

Appendix C: Dharma Kimberlite EPMA Data Tables

Appendix C.05: Dharma hypabyssal kimberlite spinel EPMA analyses. Zones: C – core, M – middle, R – rim. Size: P - >500µm, MP – 100-500µm, GM - <100µm. FeO and Fe_2O_3 calculated from FeOT.

Kimberlite	*Sample*	*Zone*	*Size*	*Nb_2O_5*	*SiO_2*	*TiO_2*	*ZnO*	*Al_2O_3*	*V_2O_3*	*Cr_2O_3*	*FeO*	*Fe_2O_3*	*NiO*	*MnO*	*MgO*	*CaO*	*BaO*	*Na_2O*	*K_2O*	*P_2O_5*	*Total*
Dharma	D086037ox	C	GM	0	0.06	20.11	0.03	11.35	0.29	1.46	20.28	24.28	0.32	0.51	19.28	0.45	0	0	0	0	98.42
Dharma	D086039ox	C	GM	0	0.07	19.03	0	11.42	0.38	3.18	21.75	24.27	0.31	0.45	17.85	0.33	0	0.04	0.02	0	99.1
Dharma	D086040ox	C	GM	0	0.67	18.35	0	11.21	0.38	3.97	23.55	22.75	0.34	0.44	16.96	0.2	0	0	0	0	98.82
Dharma	D086040ox	R	GM	0	0.06	22.06	0.03	10.63	0.28	1.36	18.81	23.89	0.25	0.59	21.75	0.32	0	0	0	0	100.03
Dharma	D086041ox	C	GM	0.11	0.57	13.31	0	12.4	0.11	0.79	12.43	37.1	0.14	0.6	21.32	0.16	0	0	0	0	99.04
Dharma	D086041ox	R	GM	0.13	0.72	11.95	0.03	12.11	0.06	0.65	12.37	38.9	0.11	0.65	20.33	0.34	0	0	0	0	98.35
Dharma	D086043ox	C	GM	0	0.03	18.28	0.03	10.24	0.52	0.98	21.05	29.27	0.21	0.47	18.01	0.15	0	0	0	0	99.24
Dharma	D086043ox	R	GM	0	0.13	20.85	0	10.22	0.2	1.45	15.37	26.53	0.14	0.72	22.98	0.21	0	0.04	0.01	0	98.85
Dharma	D086044ox	C	GM	0	0.04	18.82	0	11.44	0.37	2.54	22.68	24.97	0.31	0.45	17.14	0.5	0	0	0	0	99.26
Dharma	D086045ox	C	GM	0	0.2	21.13	0.05	10.27	0.29	1.38	19.09	24.28	0.21	0.57	20.49	0.7	0	0.02	0	0	98.68
Dharma	D086046ox	C	GM	0	0.02	20.02	0.05	10.95	0.2	1.19	23.46	24.57	0.32	0.46	17.3	0.29	0	0	0	0	98.83
Dharma	D086046ox	R	GM	0	0.12	20.06	0.03	11.61	0.3	1.78	15.97	25.81	0.25	0.68	21.74	0.56	0	0.13	0	0	99.04
Dharma	D086047ox	C	GM	0	0.05	20.19	0	11.56	0.26	1.49	19.63	24.73	0.3	0.57	19.89	0.47	0	0	0	0	99.14
Dharma	D086047ox	R	GM	0	0.28	19.66	0	10.69	0.08	1.66	13.16	28.09	0.17	0.65	23.6	0.77	0	0	0	0	98.81
Dharma	D086048ox	C	GM	0	0.04	21.75	0.03	10.32	0.15	1.31	18.92	23.81	0.2	0.55	20.77	0.7	0	0.05	0	0	98.6
Dharma	D086048ox	R	GM	0	0.16	19.67	0	9.85	0.09	1.6	13.61	28.94	0.16	0.65	22.48	1.34	0	0.05	0.01	0	98.61
Dharma	D086049ox	C	GM	0	0.04	22.9	0.04	10.2	0.07	2.19	18.83	21.42	0.16	0.75	22.06	0.07	0	0	0	0	98.73
Dharma	D086049ox	C	GM	0	0.35	0.38	0	0	0	0.08	29.66	67.28	0	0.69	0.73	0.13	0	0	0	0	99.3
Dharma	D086050ox	C	GM	0	0.14	20.4	0.04	11.21	0.22	1.45	20.13	24.16	0.28	0.54	19.52	0.46	0	0.04	0	0	98.59
Dharma	D086050ox	M	GM	0	0.47	19	0	11.37	0.16	1.45	14.64	27.35	0.24	0.7	22.55	0.47	0	0	0	0	98.4
Dharma	D086050ox	R	GM	0.08	0.12	22.24	0.04	10.97	0.08	1.74	14.1	23.3	0.2	0.77	24.64	0.39	0	0	0	0	98.67
Dharma	D086050ox	R	GM	0	0.37	0.56	0	0.02	0	0.13	29.04	66.74	0	0.64	0.84	0.49	0	0.03	0	0	98.86
Dharma	D091017ox	R	P	0.11	0.03	33.64	0.03	2.19	0.1	1.25	29.82	10.7	0.2	1.02	20.55	0.07	0	0	0	0	99.71
Dharma	D091018ox	R	P	0	0	33.47	0	4.72	0	1.6	28.8	9.04	0.2	1.14	21.33	0.15	0.18	0	0	0	100.45
Dharma	D091018ox	R	P	0.1	0	26.09	0	7.23	0.09	1.78	19.91	19.82	0.19	0.63	23.14	0.03	0	0	0	0	99.01
Dharma	D091020ox	R	GM	0.24	0.22	15.57	0.03	8.89	0.1	2.14	9.66	36.66	0.12	0.9	22.84	0.89	0.18	0.03	0.02	0	98.31
Dharma	D091021ox	R	GM	0	0.11	22.29	0.04	11.11	0.13	2.27	15.97	21.76	0.2	0.65	23.31	0.56	0	0	0	0	98.4
Dharma	D091022ox	C	GM	0	0	4.3	0.07	10.06	0.34	47.34	16.45	6.17	0.1	0.25	12.79	0.38	0	0	0	0	98.25
Dharma	D091023ox	C	GM	0	0.07	20.51	0	11.24	0.26	1.47	16.91	25.16	0.26	0.61	21.82	0.35	0	0	0	0	98.66
Dharma	D091024ox	C	GM	0	0.03	19.7	0.04	11.25	0.27	1.75	20.62	24.88	0.3	0.5	18.76	0.55	0	0	0	0	98.65
Dharma	D091025ox	C	GM	0	0.02	34.82	0	7.51	0.15	3.72	27.74	0.93	0.19	0.67	23.15	0.29	0	0	0	0	99.19
Dharma	D091026ox	C	GM	0	0	4.01	0.06	11.03	0.36	47.02	16.49	6.01	0.13	0.25	12.85	0.21	0	0	0	0	98.42
Dharma	D092021ox	C	GM	0	0	4.07	0.08	12.19	0.34	46.09	16.77	5.22	0.16	0.2	12.88	0.04	0	0	0	0	98.04
Dharma	D092022ox	C	GM	0	0.13	19.67	0.03	11.52	0.29	1.6	19.74	25.04	0.26	0.47	19.83	0.11	0	0	0	0	98.69
Dharma	D092023ox	C	GM	0	0	4.04	0.06	12.1	0.33	46.32	16.54	5.28	0.16	0.23	13.01	0.04	0	0	0	0	98.11
Dharma	D092025ox	R	P	0	0.03	27.14	0	6.13	0.05	0.75	24.23	18.47	0.17	0.67	20.56	0.14	0	0	0	0	98.34
Dharma	D104008ox	R	P	0.06	0	27.83	0.03	6.66	0.09	2.09	19.95	17.58	0.17	0.8	23.92	0.18	0	0	0	0	99.36
Dharma	D104009ox	R	P	0.1	0	23.19	0	8.67	0.07	3.57	19.07	20.93	0.17	0.67	21.74	0.38	0	0	0	0	98.56

Appendix C: Dharma Kimberlite EPMA Data Tables

Appendix C.05 (continued): Dharma hypabyssal kimberlite spinel EPMA analyses. Zones: C – core, M – middle, R – rim. Size: P - >500µm, MP – 100-500µm, GM - <100µm. FeO and Fe_2O_3 calculated from FeOT.

Kimberlite	*Sample*	*Zone*	*Size*	*Nb_2O_5*	*SiO_2*	*TiO_2*	*ZnO*	*Al_2O_3*	*V_2O_3*	*Cr_2O_3*	*FeO*	*Fe_2O_3*	*NiO*	*MnO*	*MgO*	*CaO*	*BaO*	*Na_2O*	*K_2O*	*P_2O_5*	*Total*
Dharma	D104013ox	C	GM	0	0.04	13.6	0.05	17.37	0.29	11.75	22.16	18.78	0.37	0.39	15.59	0.16	0	0	0	0	100.55
Dharma	D104014ox	C	GM	0.08	0.04	20.12	0.04	9.53	0.24	1.15	19.56	27.01	0.15	0.49	19.56	0.68	0	0	0	0	98.65
Dharma	D104014ox	R	GM	0.11	0.87	20.48	0.03	9.05	0.15	2.02	13.54	26.05	0.11	0.59	24.07	0.85	0	0	0	0	97.92
Dharma	D104016ox	C	GM	0	0.04	20.19	0.03	11.27	0.26	1.67	15.63	26.09	0.23	0.57	22.33	0.59	0	0	0	0	98.9
Dharma	D104017ox	C	GM	0	0.04	20.18	0.04	10.87	0.26	1.62	17.02	25.28	0.29	0.63	21.12	0.55	0	0	0	0	97.9
Dharma	D104018ox	C	GM	0	0.07	18.59	0.03	13.34	0.28	3.27	23.59	21.88	0.35	0.57	16.66	0.24	0	0	0	0	98.87
Dharma	D108003ox	C	MP	0	0.29	0.03	0	0	0	0	29.87	68.31	0	0.1	0.85	0	0	0	0	0	99.45
Dharma	D108003ox	M	MP	0	0.39	0.09	0	0	0	0	30.19	67.87	0	0.29	0.64	0	0	0	0	0	99.47
Dharma	D108003ox	R	MP	0	1.38	0.11	0	0.16	0	0	30.91	65.4	0	0.09	1.14	0	0	0	0	0	99.19
Dharma	D108004ox	C	MP	0	0.74	0.12	0	0	0	0	30.56	67.19	0	0.2	0.8	0.02	0	0	0	0.04	99.63
Dharma	D108004ox	M	MP	0	0.48	0.06	0	0	0	0	29.98	67.54	0	0.11	0.6	0.24	0	0.03	0	0.2	99.04
Dharma	D108004ox	R	MP	0	1.16	0.07	0	0	0	0	32.07	65.61	0	0.03	0.18	0	0	0	0	0	99.12
Dharma	D109003ox	R	P	0.09	0	27.9	0	4.79	0.1	2.53	22.54	17.96	0.19	1.1	21.95	0.08	0	0	0	0	99.23
Dharma	D109005ox	C	GM	0	0.07	17.3	0	10.03	0.53	1.59	23.45	29.34	0.24	0.41	15.95	0.03	0	0	0	0	98.94
Dharma	D109005ox	R	GM	0	0.06	20.58	0	9.8	0.19	1.53	18.5	26.24	0.16	0.54	20.99	0.06	0	0	0	0	98.65
Dharma	D109006ox	C	GM	0	0.05	20.36	0	10.87	0.3	1.28	21	25.04	0.3	0.55	19.23	0.23	0	0	0	0	99.21

Appendix C: Dharma Kimberlite EPMA Data Tables

Appendix C.06: Dharma hypabyssal kimberlite rutile EPMA analyses. Zones: C – core, M – middle. Size: P-Rim – crystals on >500µm grain, I - inclusion. FeO and Fe_2O_3 calculated from FeOT.

Kimberlite	***Sample***	***Zone***	***Size***	***Nb_2O_5***	***SiO_2***	***TiO_2***	***Al_2O_3***	***V_2O_3***	***Cr_2O_3***	***Fe_2O_3***	***NiO***	***MnO***	***MgO***	***CaO***	***BaO***	***Na_2O***	***K_2O***	***Total***
Dharma	D086022oxideincl	C	*I*	2.96	0.33	91.42	0.03	0.21	2.79	1.2	0	0	0.89	0.04	0	0	0	99.87
Dharma	D086031oxincl	C	*I*	2.67	0.07	93.43	0	0.3	2.52	0.57	0.03	0.04	0.13	0.09	0	0.03	0	99.88
Dharma	D109003ox	C	*P-RIM*	0.49	0.02	97.88	0	0.16	1.39	0.43	0	0	0.03	0.01	0.55	0	0.04	100.45
Dharma	D109003oxzoned	C	*P-RIM*	0.58	0	98.12	0	0.05	1.26	0.28	0	0	0.08	0	0.44	0	0	100.37
Dharma	D109003oxzoned	M	*P-RIM*	0.51	0	97.67	0	0	1.27	0.38	0	0	0.07	0	0.43	0	0	99.9

Appendix D: Garnet Xenocryst EPMA Data Tables

Appendix D.01: Mel kimberlite garnet EPMA analyses. Zones: C – core, R – rim.

Sample	*Class*	*Zone*	*SiO_2*	*TiO_2*	*Al_2O_3*	*V_2O_3*	*Cr_2O_3*	*FeO*	*NiO*	*MnO*	*MgO*	*CaO*	*Na_2O*	*O*	*Total*
M1 47824_001	G9A_Ti	C	42.85	0.51	22.11	0.04	1.14	7.68	0.02	0.28	21.3	4.03	0.1	0	100.06
M1 47824_002	G9A_Ti	R	42.68	0.51	22.02	0	1.22	7.65	0	0.29	21.31	4.01	0.08	0	99.77
M1 47824_003	G9A_Ti	C	42.07	0.56	19.69	0.04	3.82	6.96	0.02	0.27	20.61	5.15	0.02	0	99.21
M1 47824_004	G9A_Ti	R	42.03	0.55	19.75	0.04	3.77	7.03	0	0.26	20.6	5.16	0.04	0.01	99.24
M1 47824_005	G1	C	41.64	0.8	21.82	0.05	0.26	11.01	0	0.37	18.8	4.26	0.13	0.05	99.19
M1 47824_006	G1	R	42.04	0.79	21.73	0.04	0.28	11.02	0	0.36	19.02	4.25	0.1	0.03	99.66
M1 47824_007	G1	C	41.76	0.61	22.15	0	0.21	10.47	0	0.37	18.47	5.11	0.12	0.05	99.32
M1 47824_008	G1	R	41.68	0.61	22.12	0	0.19	10.44	0	0.37	18.38	5.09	0.14	0.04	99.06
M1 47824_009	G1	C	41.67	0.7	22.09	0	0.21	10.46	0	0.38	18.53	5.21	0.15	0.09	99.49
M1 47824_010	G1	R	41.79	0.62	22.18	0	0.18	10.43	0	0.37	18.67	5.05	0.13	0.07	99.49
M1 47824_011	G9A_Ti	C	42.38	0.56	21.73	0.02	1.07	7.72	0	0.28	21.18	4.16	0.11	0.05	99.26
M1 47824_012	G9A_Ti	R	42.18	0.54	21.71	0	1.09	7.65	0.02	0.28	21.15	4.12	0.09	0.05	98.88
M1 47824_013	G1	C	41.6	0.68	21.95	0	0.2	10.53	0	0.37	18.42	5.15	0.13	0.06	99.09
M1 47824_014	G1	R	41.46	0.7	21.91	0.03	0.2	10.4	0	0.38	18.38	5.15	0.14	0.07	98.82
M1 47824_015	G1	C	42.17	0.73	21.65	0	0.76	9.21	0.02	0.3	20.19	4.17	0.08	0.02	99.3
M1 47824_016	G1	R	39.96	0.65	21.49	0.04	0.63	10.11	0	0.31	20.79	3.75	0.08	0.48	98.29
M1 47824_017	G9A	C	42.16	0.24	20.61	0.03	3.1	6.94	0	0.27	20.92	4.82	0.04	0.03	99.16
M1 47824_018	G9A	R	42.24	0.23	20.63	0.05	3.08	6.94	0.02	0.25	21.06	4.83	0.02	0.04	99.39
M1 47824_019	G9A_Ti	C	42.07	0.47	21.25	0	2.36	7.44	0	0.31	20.85	4.29	0.08	0.01	99.13
M1 47824_020	G9A_Ti	R	42.32	0.48	21.51	0.03	2.45	7.49	0	0.31	21.03	4.3	0.08	0.02	100.02
M1 47824_021	G1	C	41.9	0.64	22.22	0.02	0.19	10.49	0	0.38	18.63	4.98	0.13	0.04	99.62
M1 47824_022	G1	R	41.85	0.69	22.05	0	0.23	10.41	0.02	0.4	18.63	4.98	0.12	0.04	99.42
M1 47824_023	G9A_Ti	C	42.45	0.4	22.07	0	1.05	7.35	0	0.27	21.38	4.18	0.08	0.04	99.27
M1 47824_024	G9A_Ti	R	42.27	0.41	21.92	0.03	1.17	7.27	0	0.25	21.69	4.16	0.07	0.11	99.35
M1 47824_025	G1	C	42.22	0.6	22.12	0.03	0.55	8.08	0.02	0.28	20.93	4.38	0.09	0.08	99.38
M1 47824_026	G1	R	42.17	0.62	21.87	0	0.59	8.08	0.02	0.27	20.84	4.39	0.08	0.06	98.99
M1 47824_027	G1	C	41.31	0.64	22.24	0.03	0.2	10.45	0	0.39	18.75	4.97	0.11	0.13	99.22
M1 47824_028	G1	R	41.71	0.68	21.99	0	0.22	10.52	0	0.38	18.59	4.97	0.13	0.06	99.25
M1 47824_029	G9A_Ti	C	41.86	0.52	21.69	0	1.15	7.61	0.02	0.29	21.25	4.12	0.11	0.12	98.74
M1 47824_030	G9A_Ti	R	42.24	0.55	21.69	0.03	1.11	7.67	0	0.27	21.27	4.14	0.1	0.07	99.14
M1 47824_031	G9A_Ti	C	42.6	0.41	22.02	0.04	1.08	7.28	0	0.26	21.49	4.15	0.07	0.02	99.42
M1 47824_032	G9A_Ti	R	42.6	0.39	21.93	0.02	1.15	7.31	0	0.26	21.36	4.15	0.06	0	99.23
M1 47824_033	G1	C	41.89	0.63	22.2	0	0.21	10.48	0	0.38	18.81	4.94	0.12	0.07	99.73
M1 47824_034	G1	R	42.11	0.64	22.29	0.03	0.17	10.53	0	0.39	18.93	4.94	0.12	0.07	100.22
M1 47824_035	G9A_Ti	C	42.29	0.53	21.83	0.03	1.06	7.7	0.02	0.26	21.32	4.06	0.07	0.05	99.22
M1 47824_036	G9A_Ti	R	42.51	0.51	21.82	0.02	1.15	7.62	0	0.29	21.13	4.06	0.09	0	99.2
M1 47824_037	G9A	C	41.7	0.22	21.08	0	3.23	7.72	0	0.41	20.4	4.3	0.05	0.02	99.13
M1 47824_038	G9A	R	42	0.26	21.18	0	3.12	7.76	0	0.41	20.42	4.28	0.06	0	99.49
M1 47824_039	G9A	C	41.51	0.27	20.42	0	3.52	8.98	0	0.42	19.35	4.81	0.05	0.04	99.37

Appendix D: Garnet Xenocryst EPMA Data Tables

Appendix D.01 (continued): Mel kimberlite garnet EPMA analyses. Zones: C – core, R – rim.

Sample	*Class*	*Zone*	*SiO_2*	*TiO_2*	*Al_2O_3*	*V_2O_3*	*Cr_2O_3*	*FeO*	*NiO*	*MnO*	*MgO*	*CaO*	*Na_2O*	*O*	*Total*
M1 47824_040	G9A	R	41.69	0.27	20.78	0	3.2	8.98	0	0.42	19.67	4.72	0.05	0.07	99.85
M1 49724_001	G3_Na	C	41.68	0.48	22.37	0	0.54	11.43	0	0.46	18.25	4.56	0.11	0.06	99.94
M1 49724_002	G3_Na	R	41.74	0.45	22.31	0.03	0.52	11.44	0	0.44	18.2	4.6	0.11	0.05	99.89
M1 49724_003	G3_Na	C	41.39	0.57	22.14	0.03	0.18	11.98	0.03	0.25	16.86	6.22	0.09	0.08	99.82
M1 49724_004	G3_Na	R	41.55	0.61	22.14	0	0.21	12	0.02	0.24	16.93	6.21	0.1	0.07	100.08
M1 49724_005	G9A_Ti	C	42.51	0.75	21.08	0.03	1.18	8.11	0.03	0.24	21.27	4.4	0.06	0.08	99.74
M1 49724_006	G9A_Ti	R	42.63	0.72	21.24	0.03	1.18	8.07	0.02	0.24	21.3	4.41	0.07	0.07	99.98
M1 49724_007	G1	C	42.12	0.72	21.79	0.05	0.6	9.23	0	0.3	20.34	4.3	0.11	0.09	99.65
M1 49724_008	G1	R	42.24	0.72	21.98	0.02	0.6	9.2	0	0.28	20.31	4.29	0.1	0.05	99.79
M1 49724_009	G1	C	42.44	0.54	21.97	0	0.81	8.24	0.02	0.25	21.02	4.25	0.07	0.06	99.67
M1 49724_010	G1	R	42.21	0.53	21.89	0	0.84	8.26	0	0.24	20.95	4.25	0.07	0.08	99.32
M1 49724_011	G9A	C	42.51	0.31	21.2	0.04	2.1	7.24	0.03	0.25	21.36	4.45	0.08	0.06	99.63
M1 49724_012	G9A	R	42.61	0.29	21.23	0.03	2.17	7.21	0.02	0.25	21.3	4.44	0.07	0.03	99.65
M1 49724_013	G1	C	41.7	0.59	22.18	0.04	0.17	11.02	0.02	0.39	18.46	5.01	0.12	0.1	99.8
M1 49724_014	G1	R	41.66	0.61	22.23	0.03	0.22	11	0	0.4	18.61	5.02	0.11	0.13	100.02
M1 49724_015	G9A	C	42.4	0.35	20.8	0	2.6	7.33	0.02	0.27	21.2	4.72	0.06	0.08	99.83
M1 49724_016	G9A	R	42.56	0.36	21.04	0.04	2.58	7.24	0	0.27	21.25	4.7	0.07	0.06	100.17
M1 49724_017	G1	C	42.55	0.41	22.26	0.04	0.81	7.05	0.03	0.28	21.86	4.24	0.09	0.1	99.72
M1 49724_018	G1	R	42.9	0.4	22.44	0	0.77	7.05	0	0.25	21.93	4.19	0.1	0.06	100.09
M1 49724_019	G9A_Ti	C	42.23	0.69	21.61	0	1.18	8.27	0.02	0.29	20.95	4.26	0.11	0.09	99.7
M1 49724_020	G9A_Ti	R	42.35	0.64	21.69	0.02	1.16	8.26	0.02	0.26	20.73	4.27	0.12	0.04	99.56
M1 49724_021	G9A_Ti	C	42.33	0.69	21.56	0	1.22	8.33	0	0.29	20.9	4.29	0.11	0.07	99.79
M1 49724_022	G9A_Ti	R	42.38	0.7	21.59	0.02	1.24	8.32	0	0.27	20.99	4.29	0.11	0.08	99.99
M1 49724_023	G3_Na	C	41.32	0.62	22.08	0.03	0.22	12.02	0	0.25	16.94	6.16	0.1	0.1	99.84
M1 49724_024	G0	R	41.59	0.64	22.14	0	0.2	12.1	0.03	0.26	17	6.19	0.09	0.08	100.32
M1 49724_025	G1	C	41.75	0.75	22.04	0.04	0.35	10.69	0	0.38	19.45	4.21	0.12	0.12	99.9
M1 49724_026	G1	R	41.79	0.81	21.88	0.03	0.35	10.83	0	0.35	19.23	4.25	0.12	0.08	99.72
M1 49724_027	G0	C	41.4	0.74	21.84	0	0.23	12	0	0.24	16.84	6.52	0.13	0.12	100.06
M1 49724_028	G0	R	41.37	0.74	21.87	0	0.17	11.85	0	0.26	16.87	6.53	0.12	0.11	99.89
M1 49724_029	G9A_Ti	C	42.25	0.49	20.97	0.04	2.2	7.5	0	0.26	21.13	4.63	0.06	0.08	99.61
M1 49724_030	G9A_Ti	R	42.37	0.47	21.01	0	2.09	7.44	0	0.29	21.09	4.59	0.05	0.04	99.44
M1 49724_031	G1	C	41.82	0.66	22.06	0.03	0.3	10.52	0	0.36	19.33	4.37	0.12	0.1	99.67
M1 49724_032	G1	R	42.03	0.67	22.18	0.05	0.28	10.62	0	0.36	19.35	4.41	0.1	0.08	100.13
M1 49724_033	G9A_Ti	C	42.23	0.64	21.38	0	1.27	8.3	0	0.26	20.89	4.25	0.08	0.06	99.36
M1 49724_034	G9A_Ti	R	42.26	0.64	21.59	0	1.23	8.3	0	0.27	21	4.23	0.11	0.09	99.72
M1 49724_035	G9A_Ti	C	42.49	0.39	22.07	0	1.03	7	0.02	0.27	21.89	4.11	0.09	0.09	99.45
M1 49724_036	G9A_Ti	R	42.66	0.42	22.15	0.02	1.2	7.04	0.02	0.26	21.71	4.16	0.08	0.04	99.76
M1 49724_037	G1	C	42.39	0.56	22	0	0.82	8.22	0.02	0.25	21.1	4.25	0.06	0.07	99.74
M1 49724_038	G1	R	42.48	0.53	22.13	0.04	0.85	8.2	0	0.25	21.06	4.27	0.07	0.06	99.94

Appendix D: Garnet Xenocryst EPMA Data Tables

Appendix D.01 (continued): Mel kimberlite garnet EPMA analyses. Zones: C – core, R – rim.

Sample	*Class*	*Zone*	*SiO_2*	*TiO_2*	*Al_2O_3*	*V_2O_3*	*Cr_2O_3*	*FeO*	*NiO*	*MnO*	*MgO*	*CaO*	*Na_2O*	*O*	*Total*
M1 49724_039	G9B_Ti	C	42.08	0.43	21.64	0.04	1.56	7.03	0.02	0.29	21.31	4.73	0.08	0.12	99.33
M1 49724_040	G9B_Ti	R	42.6	0.45	21.97	0.03	1.49	6.96	0	0.29	21.34	4.76	0.07	0.04	100
M1 49724_041	G9A_Ti	C	42.18	0.67	21.55	0	1.13	8.35	0	0.27	20.95	4.26	0.1	0.1	99.56
M1 49724_042	G9A_Ti	R	42.32	0.68	21.55	0.04	1.17	8.31	0.02	0.28	20.89	4.25	0.1	0.06	99.67
M1 49725_001	G1	C	41.8	0.68	21.94	0.04	0.37	10.42	0	0.36	19.01	4.74	0.11	0.07	99.54
M1 49725_002	G1	R	42.04	0.65	22.09	0	0.34	10.46	0	0.36	19.1	4.79	0.13	0.08	100.04
M1 49725_003	G9A_Ti	C	42.12	0.62	21.52	0.03	1.12	7.89	0	0.24	21.08	4.29	0.08	0.07	99.06
M1 49725_004	G9A_Ti	R	42.51	0.6	21.8	0	1.11	7.98	0	0.27	21.03	4.31	0.1	0.04	99.75
M1 49725_005	G3	C	42.16	0.21	22.54	0	0.59	6.54	0	0.16	19.75	7.35	0.04	0.1	99.44
M1 49725_006	G3	R	42.26	0.2	22.77	0	0.54	6.48	0.02	0.15	19.83	7.4	0.05	0.11	99.81
M1 49725_007	G1	C	41.66	0.76	21.81	0.04	0.39	10.37	0	0.34	19.55	4.2	0.12	0.11	99.35
M1 49725_008	G1	R	41.88	0.79	21.95	0.03	0.34	10.28	0	0.34	19.62	4.22	0.12	0.09	99.66
M1 49725_009	G9A_Ti	C	42.36	0.5	20.7	0.04	2.43	7.16	0.02	0.24	21.41	4.3	0.07	0.03	99.26
M1 49725_010	G9A_Ti	R	42.31	0.49	20.79	0.02	2.47	7.2	0	0.24	21.53	4.27	0.08	0.07	99.47
M1 49725_011	G1	C	41.66	0.77	21.92	0.03	0.41	10.43	0	0.35	19.69	4.2	0.12	0.14	99.72
M1 49725_012	G1	R	41.75	0.77	21.84	0.03	0.35	10.29	0	0.35	19.64	4.19	0.13	0.11	99.45
M1 49725_013	G1	C	41.98	0.79	21.78	0	0.35	10.32	0	0.34	19.49	4.21	0.13	0.06	99.45
M1 49725_014	G1	R	41.63	0.78	21.77	0.03	0.37	10.3	0	0.36	19.46	4.2	0.13	0.1	99.13
M1 49725_015	G9A_Ti	C	42.19	0.58	21.68	0	1.12	7.98	0.02	0.28	21.12	4.29	0.08	0.09	99.43
M1 49725_016	G9A_Ti	R	42.1	0.59	21.65	0	1.16	7.96	0.02	0.26	21	4.29	0.08	0.07	99.18
M1 49725_017	G3	C	42.43	0.2	22.85	0.03	0.54	6.55	0.02	0.17	19.6	7.57	0.06	0.08	100.1
M1 49725_018	G3	R	42.02	0.2	22.65	0.03	0.49	6.47	0	0.15	19.48	7.58	0.06	0.1	99.23
M1 49725_019	G9A_Ti	C	42.13	0.59	21.6	0.04	1.15	7.9	0	0.26	21.05	4.28	0.09	0.08	99.17
M1 49725_020	G9A_Ti	R	42.14	0.6	21.67	0	1.11	7.94	0.03	0.26	21.1	4.28	0.06	0.08	99.27
M1 49725_021	G1	C	41.98	0.79	21.51	0.06	0.71	9.14	0	0.3	20.37	4.38	0.12	0.11	99.47
M1 49725_023	G9A_Ti	C	42.01	0.46	20.8	0.03	2.44	7.14	0	0.23	21.31	4.27	0.06	0.05	98.8
M1 49725_024	G9A_Ti	R	42.09	0.46	20.66	0.05	2.47	7.13	0.02	0.24	21.43	4.27	0.07	0.07	98.96
M1 49725_025	G9A_Ti	C	41.57	0.63	20.57	0.03	2.39	9.04	0	0.34	19.56	4.69	0.14	0.07	99.03
M1 49725_026	G9A_Ti	R	41.43	0.67	20.49	0.04	2.4	8.99	0	0.33	19.69	4.66	0.14	0.1	98.94
M1 49725_027	G9A_Ti	C	41.77	0.67	21.13	0	1.25	8.16	0	0.26	20.67	4.45	0.09	0.09	98.54
M1 49725_028	G9A_Ti	R	41.99	0.65	21.33	0.04	1.26	8.22	0	0.27	20.61	4.47	0.07	0.06	98.97
M1 49725_029	G1	C	41.82	0.58	21.6	0.03	0.85	8.24	0	0.28	20.81	4.3	0.08	0.11	98.7
M1 49725_030	G1	R	42.1	0.6	21.78	0	0.82	8.24	0	0.27	20.7	4.29	0.07	0.04	98.91
M1 49725_031	G9A_Ti	C	41.81	0.62	20.83	0	1.95	7.71	0.02	0.25	21	4.41	0.08	0.1	98.78
M1 49725_032	G9A_Ti	R	41.99	0.62	20.82	0.04	1.97	7.68	0	0.26	21.06	4.42	0.08	0.08	99.02
M1 49725_033	G9A_Ti	C	41.98	0.51	21.61	0.03	1.08	8.01	0.02	0.26	21.01	4.09	0.09	0.08	98.77
M1 49725_034	G9A_Ti	R	42.27	0.52	21.9	0.03	1.03	7.96	0.02	0.27	21.07	4.11	0.09	0.05	99.32
M1 49725_035	G1	C	41.66	0.57	21.81	0	0.71	9.06	0	0.32	19.96	4.39	0.1	0.08	98.66
M1 49725_037	G1	C	41.41	0.49	21.71	0	0.91	8.31	0	0.29	19.89	5.21	0.08	0.13	98.43

Appendix D: Garnet Xenocryst EPMA Data Tables

Appendix D.01 (continued): Mel kimberlite garnet EPMA analyses. Zones: C – core, R – rim.

Sample	*Class*	*Zone*	*SiO_2*	*TiO_2*	*Al_2O_3*	*V_2O_3*	*Cr_2O_3*	*FeO*	*NiO*	*MnO*	*MgO*	*CaO*	*Na_2O*	*O*	*Total*
M1 49725_038	G1	R	41.66	0.5	21.76	0	0.89	8.35	0.02	0.28	19.85	5.2	0.08	0.09	98.68
M1 49725_039	G9A_Ti	C	41.58	0.61	20.67	0.03	1.87	7.6	0	0.28	20.89	4.4	0.06	0.08	98.07
M1 49725_040	G9A_Ti	R	41.6	0.63	20.78	0.04	1.86	7.72	0	0.26	20.83	4.37	0.06	0.07	98.22
M1 49725_041	G9A_Ti	C	41.48	0.6	20.84	0	1.85	7.65	0.02	0.26	20.95	4.36	0.06	0.11	98.18
M1 49725_042	G9A_Ti	R	41.89	0.6	20.95	0.03	1.87	7.59	0.02	0.28	21.05	4.37	0.05	0.07	98.77
M1 49725_043	G9A_Ti	C	41.72	0.56	21.4	0.03	1.14	7.91	0	0.25	20.91	4.25	0.08	0.1	98.35
M1 49725_044	G9A_Ti	R	41.88	0.54	21.63	0.04	1.17	7.93	0	0.28	20.87	4.29	0.09	0.08	98.8
M1 49725_045	G9A_Ti	C	42.02	0.58	21.58	0	1.16	7.88	0.02	0.26	20.84	4.3	0.09	0.05	98.78
M1 49725_046	G9A_Ti	R	42.26	0.56	21.81	0	1.08	7.89	0.02	0.25	21	4.25	0.08	0.04	99.24
M1 49725_047	G9A_Ti	C	42.13	0.39	20.92	0.03	2.05	7.23	0.02	0.24	21.39	4.42	0.05	0.09	98.96
M1 49725_048	G9A_Ti	R	42.5	0.37	21.22	0.04	1.98	7.25	0	0.25	21.29	4.41	0.06	0.02	99.39
M1 49725_049	G9A_Ti	C	42.28	0.55	21.75	0.02	1.15	7.95	0	0.26	20.94	4.28	0.08	0.04	99.3
M1 49725_050	G9A_Ti	R	42.37	0.59	21.79	0	1.16	7.97	0.02	0.27	21.2	4.3	0.08	0.08	99.83
M1 49725_051	G9A_Ti	C	42.33	0.59	21.64	0	1.12	7.96	0.02	0.29	20.94	4.32	0.08	0.04	99.33
M1 49725_052	G9A_Ti	R	42.25	0.56	21.8	0.03	1.08	7.97	0	0.26	21.02	4.31	0.1	0.07	99.45
M1 49725_053	G9A_Ti	C	42.31	0.6	21.77	0.03	1.12	8.03	0	0.26	20.92	4.29	0.09	0.04	99.46
M1 49725_054	G9A_Ti	R	42.44	0.61	21.76	0	1.09	8.03	0	0.27	21.16	4.29	0.1	0.08	99.83
M1 49725_055	G1	C	42.3	0.58	21.85	0.04	0.86	8.24	0	0.25	20.86	4.28	0.08	0.05	99.39
M1 49725_056	G1	R	42.49	0.61	21.93	0.02	0.82	8.23	0	0.25	20.97	4.3	0.08	0.04	99.74
M1 49725_057	G9A_Ti	C	41.7	0.63	20.79	0	2.43	9.01	0	0.34	19.73	4.45	0.13	0.04	99.25
M1 49725_058	G9A_Ti	R	41.98	0.64	20.98	0.03	2.34	9.04	0	0.35	19.76	4.53	0.14	0.04	99.83
M1 49725_059	G1	C	41.45	0.9	21.65	0.04	0.24	11.43	0.02	0.37	18.77	4.07	0.12	0.08	99.14
M1 49725_060	G1	R	41.68	0.89	21.85	0	0.23	11.48	0	0.38	19.09	4.1	0.15	0.13	99.98
M1 49741_001	G9A	C	42.7	0.21	20.52	0.05	3.37	7.77	0.02	0.27	20.72	4.95	0.04	0.03	100.65
M1 49741_002	G9A	R	42.77	0.18	20.59	0.04	3.25	7.79	0.02	0.26	20.56	4.94	0.05	0	100.45
M1 49741_003	G1	C	42.45	0.53	22.29	0.03	0.52	9.53	0	0.33	19.98	4.49	0.11	0.06	100.32
M1 49741_004	G1	R	42.29	0.54	22.17	0	0.52	9.42	0	0.34	19.96	4.51	0.11	0.06	99.92
M1 49741_005	G9A_Ti	C	42.41	0.74	21.62	0	1.17	8.29	0	0.26	20.93	4.38	0.09	0.06	99.95
M1 49741_006	G9A_Ti	R	42.51	0.75	21.85	0	1.11	8.3	0	0.25	20.86	4.38	0.09	0.03	100.13
M1 49741_007	G9A_Ti	C	42.83	0.6	21.14	0.04	2	7.88	0.02	0.26	21.14	4.33	0.12	0.02	100.38
M1 49741_008	G9A_Ti	R	42.59	0.62	21.49	0.04	1.99	7.88	0	0.25	21.05	4.31	0.11	0.03	100.36
M1 49741_009	G1	C	42.51	0.51	22.3	0.05	0.59	9.41	0	0.34	19.97	4.6	0.11	0.05	100.44
M1 49741_010	G1	R	42.39	0.49	22.37	0	0.52	9.5	0	0.34	19.91	4.59	0.12	0.07	100.3
M1 49741_011	G1	C	41.98	0.57	22.52	0.03	0.22	10.23	0	0.39	18.95	5.06	0.13	0.09	100.17
M1 49741_012	G1	R	42.17	0.54	22.49	0	0.24	10.35	0	0.37	18.83	5.07	0.12	0.05	100.23
M1 49741_013	G1	C	42.38	0.56	22.23	0.04	0.53	9.55	0	0.33	19.71	4.74	0.1	0.04	100.21
M1 49741_014	G1	R	42.15	0.54	22.44	0.03	0.52	9.52	0	0.33	19.66	4.77	0.11	0.07	100.14
M1 49741_015	G9A	C	42.32	0.09	22.8	0	1.5	8.3	0	0.44	20.42	4.14	0.03	0	100.04
M1 49741_016	G9A	R	42.74	0.12	22.92	0	1.55	8.34	0	0.44	20.26	4.15	0.04	0	100.56

Appendix D: Garnet Xenocryst EPMA Data Tables

Appendix D.01 (continued): Mel kimberlite garnet EPMA analyses. Zones: C – core, R – rim.

Sample	*Class*	*Zone*	*SiO_2*	*TiO_2*	*Al_2O_3*	*V_2O_3*	*Cr_2O_3*	*FeO*	*NiO*	*MnO*	*MgO*	*CaO*	*Na_2O*	*O*	*Total*
M1 49741_017	G9A	C	42.09	0.25	20.3	0.05	3.47	7.1	0.02	0.27	20.81	4.97	0.03	0.05	99.41
M1 49741_018	G9A	R	42.38	0.24	20.47	0.05	3.37	7.09	0	0.25	20.87	4.98	0.03	0.02	99.75
M1 49741_019	G9A_Ti	C	42.21	0.7	21.5	0.02	1.07	8.23	0.03	0.25	20.72	4.34	0.09	0.04	99.2
M1 49741_020	G9A_Ti	R	42.49	0.76	21.73	0	1.1	8.26	0.02	0.27	20.88	4.35	0.1	0.04	100
M1 49741_021	G9A	C	41.86	0.12	22.58	0.03	1.62	8.27	0	0.44	20.16	4.13	0.04	0	99.25
M1 49741_022	G9A	R	42.22	0.11	22.64	0	1.64	8.32	0	0.44	20.14	4.14	0.03	0	99.68
M1 49741_023	G9A_Ti	C	41.88	0.59	21.32	0.02	1.67	7.69	0	0.26	21.14	4.35	0.07	0.1	99.09
M1 49741_024	G9A_Ti	R	42.23	0.63	21.24	0.03	1.72	7.65	0.03	0.26	21	4.34	0.07	0.02	99.22
M1 49741_025	G1	C	42	0.53	22.13	0.04	0.51	9.4	0.02	0.34	19.72	4.5	0.09	0.05	99.33
M1 49741_026	G1	R	42.29	0.55	22.3	0.05	0.5	9.43	0.03	0.34	19.81	4.41	0.11	0.03	99.85
M1 49741_027	G9A_Ti	C	42.16	0.67	21.12	0.03	1.61	7.8	0	0.25	20.99	4.16	0.1	0.03	98.92
M1 49741_028	G9A_Ti	R	42.03	0.67	20.98	0.02	1.57	7.83	0	0.26	21.05	4.13	0.12	0.07	98.73
M1 49741_029	G9A_Ti	C	42.27	0.72	21.63	0	1.08	8.22	0	0.27	20.7	4.33	0.09	0.02	99.33
M1 49741_030	G9A_Ti	R	42.19	0.68	21.57	0.03	1.06	8.22	0	0.26	20.8	4.32	0.09	0.05	99.27
M1 49741_031	G1	C	41.78	0.55	22.36	0.02	0.23	10.24	0	0.37	18.87	4.98	0.11	0.08	99.59
M1 49741_032	G3_Na	R	41.88	0.51	22.44	0	0.22	10.16	0	0.37	18.72	5.01	0.14	0.05	99.5
M1 49741_033	G9A_Ti	C	42.27	0.71	21.61	0.02	1.1	8.25	0.03	0.26	20.85	4.33	0.09	0.05	99.57
M1 49741_034	G9A_Ti	R	42.33	0.76	21.57	0	1.06	8.25	0	0.25	20.68	4.35	0.1	0.01	99.36
M1 49741_035	G1	C	42.23	0.52	22.17	0.02	0.49	9.64	0	0.33	19.38	4.81	0.1	0.02	99.71
M1 49741_036	G1	R	42.19	0.52	22.25	0	0.45	9.66	0	0.33	19.31	4.85	0.11	0.02	99.69
M1 49741_037	G9A_Ti	C	42.29	0.61	20.91	0.04	2.04	7.82	0.02	0.26	20.95	4.34	0.09	0.04	99.41
M1 49741_038	G9A_Ti	R	42.54	0.64	21.04	0.04	2	7.86	0	0.26	20.94	4.33	0.1	0.01	99.76
M1 49741_039	G9A_Ti	C	42.38	0.71	20.76	0.05	2.05	7.39	0	0.25	21.36	4.36	0.06	0.03	99.4
M1 49741_040	G9A_Ti	R	42.72	0.75	20.88	0	2.05	7.31	0	0.25	21.42	4.37	0.08	0	99.83
M1 49741_041	G9A_Ti	C	42.57	0.51	20.32	0.02	3.4	7.72	0.02	0.26	20.79	4.59	0.08	0	100.28
M1 49741_042	G9A_Ti	R	42.28	0.5	20.32	0	3.2	7.69	0	0.27	20.7	4.63	0.08	0.02	99.69
M1 49741_043	CRST	C	37.73	0	21.54	0	0	34.72	0	1.38	4.02	1.38	0	0	100.77
M1 49741_044	G3	R	37.82	0	21.53	0	0	34.97	0	1.8	3.65	1.38	0	0	101.15
M1 49741_045	G9A_Ti	C	42.53	0.63	21.18	0	1.88	7.88	0.02	0.27	21.13	4.28	0.1	0.04	99.94
M1 49741_046	G9A_Ti	R	42.4	0.62	21.09	0	1.93	7.9	0	0.26	21.03	4.21	0.11	0.03	99.58
M1 49741_047	G1	C	42.13	0.56	22.34	0	0.52	9.65	0	0.35	19.6	4.82	0.09	0.07	100.13
M1 49741_048	G1	R	42.25	0.61	22.12	0	0.52	9.63	0	0.35	19.51	4.8	0.11	0.04	99.94
M1 49741_049	G1	C	42.23	0.49	22.23	0.03	0.51	9.57	0	0.34	19.74	4.78	0.11	0.09	100.12
M1 49741_050	G1	R	42.26	0.5	22.22	0	0.45	9.52	0.02	0.34	19.59	4.76	0.11	0.05	99.82
M1 49741_051	G9A_Ti	C	42.69	0.37	20.76	0.03	2.67	7.2	0.02	0.24	21.35	4.6	0.05	0.03	100.01
M1 49741_052	G9A_Ti	R	42.81	0.38	20.8	0.02	2.61	7.11	0.02	0.23	21.19	4.62	0.05	0	99.84
M1 49741_053	G9A	C	42.29	0.31	20.14	0.04	3.98	6.96	0.03	0.26	20.93	5.03	0.02	0.03	100.02
M1 49741_054	G9A	R	42.48	0.31	20.2	0.04	4	6.96	0.03	0.27	20.7	5.01	0.04	0	100.04
M1 49741_055	G9A_Ti	C	42.7	0.71	21.8	0.03	1.14	8.24	0.02	0.26	20.81	4.36	0.11	0	100.18

Appendix D: Garnet Xenocryst EPMA Data Tables

Appendix D.01 (continued): Mel kimberlite garnet EPMA analyses. Zones: C – core, R – rim.

Sample	*Class*	*Zone*	*SiO_2*	*TiO_2*	*Al_2O_3*	*V_2O_3*	*Cr_2O_3*	*FeO*	*NiO*	*MnO*	*MgO*	*CaO*	*Na_2O*	*O*	*Total*
M1 49741_056	G9A_Ti	R	42.19	0.72	21.68	0.03	1.14	8.29	0.02	0.24	20.84	4.36	0.11	0.08	99.7
M1 49741_057	G1	C	42.18	0.53	22.37	0.02	0.42	9.57	0	0.34	19.39	4.84	0.11	0.03	99.8
M1 49741_058	G1	R	42.34	0.52	22.41	0	0.44	9.6	0.02	0.34	19.38	4.86	0.1	0.01	100.02
M1 49741_059	G9A_Ti	C	42.44	0.38	20.66	0.03	2.67	7.14	0.02	0.24	21.12	4.62	0.05	0.01	99.38
M1 49741_060	G9A_Ti	R	42.67	0.38	20.86	0.03	2.65	7.11	0	0.24	21.23	4.61	0.05	0	99.83
M2 47824_001	G1	C	41.83	0.71	21.57	0.03	0.76	9.23	0	0.3	20.46	4.13	0.1	0.12	99.24
M2 47824_002	G1	R	41.89	0.65	21.61	0.03	0.82	9.07	0.02	0.3	20.25	4.34	0.1	0.1	99.18
M2 47824_003	G9A_Ti	C	41.72	0.43	21.26	0	2.36	7.5	0	0.32	21.11	4.24	0.08	0.11	99.13
M2 47824_004	G9A_Ti	R	41.4	0.47	21.08	0	2.41	7.4	0	0.31	20.98	4.24	0.05	0.1	98.44
M2 47824_005	G1	C	41.71	0.55	21.78	0.04	0.8	8.82	0	0.31	20.33	4.39	0.12	0.13	98.98
M2 47824_006	G1	R	42	0.56	21.9	0.03	0.78	8.88	0	0.3	20.39	4.36	0.12	0.11	99.43
M2 47824_007	G9A_Ti	C	42.4	0.5	21.82	0.04	1.16	7.69	0.02	0.28	21.47	4.04	0.09	0.08	99.59
M2 47824_008	G9A_Ti	R	42.17	0.5	21.9	0	1.09	7.73	0.02	0.28	21.4	4.03	0.09	0.1	99.31
M2 47824_009	G1	C	41.64	0.65	22.19	0.05	0.19	10.46	0	0.39	18.91	4.95	0.13	0.12	99.68
M2 47824_010	G1	R	41.5	0.7	22.01	0	0.17	10.56	0	0.42	18.73	5.13	0.13	0.15	99.5
M2 47824_011	G1	C	42.03	0.55	21.95	0.03	0.77	8.84	0	0.31	20.34	4.49	0.11	0.1	99.52
M2 47824_013	G9A	C	41.64	0.32	20.35	0	3.95	7.42	0	0.37	20.98	4.27	0.06	0.09	99.45
M2 47824_014	G9A	R	41.8	0.33	20.37	0.03	3.94	7.42	0	0.37	20.8	4.29	0.07	0.04	99.46
M2 47824_015	G9A	C	41.92	0.24	20.39	0.04	3.21	7.02	0	0.26	21.1	4.78	0.04	0.1	99.1
M2 47824_016	G9A	R	41.86	0.24	20.21	0.04	3.27	7	0	0.28	21.25	4.79	0.04	0.13	99.11
M2 47824_017	G1	C	42.35	0.37	22.18	0	0.92	7.3	0.02	0.27	21.72	4.19	0.07	0.12	99.51
M2 47824_018	G1	R	42.34	0.37	22.23	0.02	0.9	7.26	0.02	0.28	21.7	4.17	0.08	0.11	99.48
M2 47824_019	G9A_Ti	C	42.12	0.39	22.04	0.03	1.05	7.34	0	0.28	21.67	4.14	0.05	0.12	99.23
M2 47824_020	G9A_Ti	R	42.12	0.39	22	0	1.08	7.31	0	0.27	21.82	4.14	0.07	0.16	99.36
M2 47824_021	G9A_Ti	C	41.7	0.77	20.56	0.04	2.09	7.91	0.02	0.26	20.96	4.62	0.07	0.14	99.14
M2 47824_022	G9A_Ti	R	41.6	0.77	20.42	0.04	2.27	7.88	0	0.26	20.96	4.64	0.07	0.15	99.06
M2 47824_023	G1	C	41.77	0.74	21.62	0	0.7	9.2	0	0.31	20.73	4.15	0.1	0.18	99.5
M2 47824_024	G1	R	41.59	0.72	21.54	0.03	0.77	9.23	0	0.3	20.46	4.16	0.09	0.15	99.04
M2 47824_025	G9A_Ti	C	41.85	0.53	20.95	0.04	1.96	7.69	0	0.29	21.19	4.4	0.05	0.13	99.08
M2 47824_026	G9A_Ti	R	41.89	0.56	20.98	0	1.88	7.7	0	0.26	21.1	4.4	0.05	0.1	98.92
M2 47824_027	G1	C	41.31	0.64	21.95	0.05	0.21	10.38	0	0.4	18.91	5.05	0.14	0.18	99.22
M2 47824_028	G1	R	41.19	0.65	21.87	0	0.22	10.48	0	0.4	18.85	5.04	0.14	0.2	99.04
M2 47824_029	G9A	C	41.8	0.23	20.34	0.05	3.16	6.96	0	0.28	21.24	4.74	0.04	0.13	98.97
M2 47824_030	G9A	R	41.77	0.24	20.42	0.06	3.05	6.96	0.02	0.27	21.09	4.72	0	0.09	98.69
M2 47824_031	G1	C	41.29	0.63	21.93	0.04	0.22	10.38	0	0.38	18.78	5.01	0.14	0.15	98.95
M2 47824_032	G1	R	41.37	0.64	22.05	0.03	0.18	10.42	0	0.38	18.59	5	0.12	0.1	98.88
M2 47824_033	G9A_Ti	C	41.64	0.5	21.5	0.03	1.11	7.63	0.02	0.29	21.3	4	0.09	0.13	98.24
M2 47824_034	G9A_Ti	R	41.88	0.54	21.7	0.03	1.08	7.71	0	0.27	21.36	4.04	0.09	0.12	98.82
M2 47824_035	G1	C	41.16	0.64	22	0.03	0.19	10.37	0	0.4	18.74	5.03	0.11	0.15	98.82

Appendix D: Garnet Xenocryst EPMA Data Tables

Appendix D.01 (continued): Mel kimberlite garnet EPMA analyses. Zones: C – core, R – rim.

Sample	*Class*	*Zone*	*SiO_2*	*TiO_2*	*Al_2O_3*	*V_2O_3*	*Cr_2O_3*	*FeO*	*NiO*	*MnO*	*MgO*	*CaO*	*Na_2O*	*O*	*Total*
M2 47824_036	G1	R	40.88	0.67	21.76	0.04	0.18	10.4	0	0.38	18.76	5.05	0.12	0.2	98.44
M2 47824_037	G9A_Ti	C	41.86	0.51	21.68	0	1.09	7.6	0.02	0.25	21.33	4	0.1	0.11	98.55
M2 47824_038	G9A_Ti	R	42.06	0.52	21.55	0	1.08	7.69	0	0.27	21.41	4.02	0.09	0.11	98.8
M2 47824_039	G9A_Ti	C	41.68	0.54	21.48	0	1.19	7.68	0.03	0.28	21.47	4.05	0.09	0.17	98.66
M2 47824_040	G9A_Ti	R	41.98	0.52	21.63	0	1.17	7.7	0.02	0.27	21.5	4.05	0.1	0.15	99.09
M2 49724_001	G9A_Ti	C	42.34	0.66	21.52	0.03	1.13	8.29	0	0.28	20.72	4.24	0.09	0.02	99.32
M2 49724_002	G9A_Ti	R	42.33	0.63	21.63	0	1.19	8.31	0.02	0.27	20.77	4.24	0.11	0.04	99.54
M2 49724_003	G9A_Ti	C	42.3	0.65	21.72	0.03	1.1	8.27	0.02	0.27	20.97	4.26	0.11	0.09	99.79
M2 49724_004	G9A_Ti	R	42.14	0.58	21.72	0.04	1.1	8.15	0	0.28	20.89	4.27	0.09	0.07	99.33
M2 49724_005	G1	C	41.54	0.58	22.31	0	0.36	10.53	0.03	0.23	17.99	5.84	0.08	0.06	99.55
M2 49724_006	G1	R	41.37	0.58	22.28	0	0.33	10.5	0.03	0.24	18.03	5.86	0.08	0.09	99.39
M2 49724_007	G9A_Ti	C	42.32	0.66	21.55	0.04	1.2	8.21	0.02	0.26	20.74	4.28	0.09	0.02	99.39
M2 49724_008	G9A_Ti	R	42.15	0.67	21.47	0	1.15	8.25	0.02	0.25	20.78	4.28	0.09	0.05	99.16
M2 49724_009	G3_Na	C	41.28	0.62	22.02	0	0.17	12.03	0.02	0.26	16.84	6.19	0.12	0.1	99.65
M2 49724_010	G0	R	41.32	0.66	22.02	0	0.24	12.1	0	0.26	16.76	6.2	0.09	0.07	99.72
M2 49724_011	G3_Na	C	41.31	0.45	22.2	0	0.53	11.33	0.02	0.43	18.35	4.5	0.1	0.1	99.32
M2 49724_012	G3_Na	R	41.72	0.48	22.42	0.02	0.44	11.24	0	0.43	18.43	4.51	0.1	0.05	99.84
M2 49724_013	G9A	C	42.14	0.35	20.89	0.04	2.51	7.25	0	0.27	21.07	4.71	0.06	0.08	99.37
M2 49724_014	G9A	R	42.28	0.34	20.96	0.05	2.49	7.25	0.02	0.27	20.99	4.7	0.04	0.03	99.42
M2 49724_015	G1	C	41.71	0.87	21.71	0.04	0.33	10.84	0	0.36	19.2	4.26	0.14	0.1	99.56
M2 49724_016	G1	R	41.85	0.83	21.8	0.02	0.33	10.74	0	0.36	19.24	4.29	0.12	0.07	99.65
M2 49724_018	G9A_Ti	R	41.94	0.67	21.57	0.03	1.27	8.18	0	0.26	20.93	4.26	0.11	0.11	99.33
M2 49724_019	G0	C	41.14	0.67	21.83	0.03	0.18	12.05	0	0.26	17.03	6.21	0.09	0.14	99.63
M2 49724_020	G0	R	41.03	0.65	21.76	0.02	0.21	12.06	0.02	0.26	16.57	6.2	0.11	0.07	98.96
M2 49724_021	G1	C	41.65	0.68	22.12	0	0.28	10.54	0	0.37	19.22	4.41	0.12	0.11	99.5
M2 49724_022	G1	R	42.02	0.68	22.12	0.03	0.27	10.58	0	0.37	19.2	4.43	0.12	0.06	99.88
M2 49724_023	G9A_Ti	C	42.26	0.67	21.62	0	1.12	8.2	0.02	0.28	21.01	4.2	0.08	0.06	99.52
M2 49724_024	G9A_Ti	R	42.13	0.68	21.68	0	1.13	8.17	0.02	0.27	21.07	4.24	0.11	0.11	99.61
M2 49724_025	G9A_Ti	C	42.02	0.57	21.7	0.05	1.05	8.23	0	0.28	21.11	4.2	0.12	0.15	99.48
M2 49724_026	G9A_Ti	R	42.28	0.58	21.68	0.04	1.05	8.18	0	0.27	20.94	4.21	0.1	0.06	99.39
M2 49724_027	G1	C	41.73	0.66	22.02	0	0.28	10.53	0	0.36	19.29	4.43	0.12	0.11	99.53
M2 49724_028	G1	R	41.88	0.64	22.11	0.04	0.28	10.49	0	0.35	19.14	4.39	0.09	0.04	99.45
M2 49724_029	G1	C	42.12	0.43	22.1	0	0.51	8.2	0.02	0.3	20.15	5.59	0.12	0.15	99.69
M2 49724_030	G3_Na	R	42.2	0.42	22.3	0	0.56	8.28	0.03	0.3	20.05	5.59	0.11	0.13	99.97
M2 49724_031	G9A_Ti	C	42.16	0.66	21.64	0	1.18	8.22	0.03	0.25	20.88	4.27	0.1	0.07	99.46
M2 49724_032	G9A_Ti	R	42.23	0.67	21.65	0	1.15	8.14	0.02	0.26	20.83	4.29	0.12	0.06	99.42
M2 49724_033	G9A_Ti	C	41.92	0.68	21.31	0	1.23	8.26	0	0.25	20.96	4.28	0.1	0.12	99.11
M2 49724_034	G9A_Ti	R	42.16	0.71	21.43	0	1.21	8.27	0.02	0.25	20.76	4.32	0.1	0.06	99.29
M2 49724_035	G1	C	42.09	0.55	22.06	0.03	0.69	8.83	0	0.32	20.14	4.52	0.13	0.07	99.43

Appendix D: Garnet Xenocryst EPMA Data Tables

Appendix D.01 (continued): Mel kimberlite garnet EPMA analyses. Zones: C – core, R – rim.

Sample	*Class*	*Zone*	*SiO_2*	*TiO_2*	*Al_2O_3*	*V_2O_3*	*Cr_2O_3*	*FeO*	*NiO*	*MnO*	*MgO*	*CaO*	*Na_2O*	*O*	*Total*
M2 49724_036	G1	R	41.68	0.52	21.79	0.03	0.7	8.93	0.02	0.32	20.11	4.55	0.1	0.12	98.87
M2 49724_037	G9A_Ti	C	42.11	0.7	21.55	0	1.23	8.23	0.02	0.27	20.95	4.29	0.12	0.1	99.57
M2 49724_038	G9A_Ti	R	42.42	0.67	21.62	0	1.2	8.26	0	0.26	20.89	4.3	0.11	0.05	99.78
M2 49724_039	G1	C	42.17	0.58	22	0.03	0.65	8.1	0.02	0.25	20.82	4.25	0.07	0.03	98.97
M2 49724_040	G1	R	42.54	0.57	22.29	0.03	0.57	8.14	0.03	0.26	21.05	4.21	0.06	0.03	99.78
M2 49724_041	G9A_Ti	C	42.16	0.65	21.7	0	1.09	8.25	0.02	0.28	21.05	4.25	0.1	0.11	99.66
M2 49724_042	G9A_Ti	R	42.32	0.63	21.83	0	1.09	8.24	0.02	0.26	21.03	4.24	0.09	0.08	99.83
M2 49724_043	G3_Na	C	41.5	0.5	22.27	0.02	0.5	11.4	0.02	0.46	18.44	4.49	0.11	0.11	99.82
M2 49724_044	G3_Na	R	41.64	0.46	22.38	0	0.6	11.08	0	0.43	18.55	4.41	0.1	0.06	99.71
M2 49724_045	G3_Na	C	41.28	0.43	22.17	0.03	0.64	11.18	0	0.43	18.4	4.51	0.1	0.1	99.27
M2 49724_046	G3_Na	R	41.55	0.47	22.21	0	0.68	11.16	0	0.46	18.47	4.45	0.08	0.06	99.59
M2 49724_047	G9A_Ti	C	42.33	0.5	21.33	0.02	2	7.56	0.02	0.28	21.39	4.52	0.06	0.11	100.12
M2 49724_048	G9A_Ti	R	42.12	0.47	21.23	0.03	1.91	7.53	0	0.28	21.13	4.49	0.09	0.09	99.37
M2 49724_049	G9A	C	42.16	0.35	20.99	0.05	2.52	7.19	0.02	0.26	21.1	4.67	0.07	0.08	99.46
M2 49724_050	G9A	R	42.3	0.34	20.88	0.05	2.5	7.33	0	0.27	20.9	4.72	0.04	0.02	99.35
M2 49724_051	G3_Na	C	41.5	0.49	22.04	0	0.66	11.27	0	0.45	18.35	4.54	0.08	0.07	99.45
M2 49724_052	G3_Na	R	41.47	0.47	22.11	0	0.69	11.37	0	0.44	18.39	4.53	0.09	0.09	99.65
M2 49724_053	G9A_Ti	C	41.85	0.62	21.58	0.04	1.13	8.61	0	0.26	20.78	4.3	0.08	0.14	99.39
M2 49724_054	G9A_Ti	R	42.28	0.63	21.73	0	1.15	8.6	0.02	0.29	20.55	4.42	0.09	0.06	99.82
M2 49724_055	G1	C	41.63	0.58	22.33	0.03	0.25	10.37	0	0.37	19.25	4.49	0.13	0.13	99.56
M2 49724_056	G1	R	41.9	0.61	22.22	0	0.24	10.48	0	0.37	19.44	4.58	0.13	0.15	100.12
M2 49724_057	G9A	C	42.46	0.31	21.29	0.04	2.15	7.24	0.02	0.25	21.34	4.45	0.07	0.06	99.68
M2 49724_058	G9A	R	42.45	0.33	21.27	0.04	2.11	7.23	0	0.24	21.51	4.41	0.07	0.08	99.74
M2 49724_059	G9A_Ti	C	42.01	0.57	20.82	0.03	2.26	7.5	0.03	0.26	21.12	4.49	0.06	0.08	99.23
M2 49724_060	G9A_Ti	R	42.36	0.57	20.91	0.04	2.24	7.52	0.02	0.26	20.93	4.5	0.05	0	99.4
M2 49724_061	G9A_Ti	C	42.2	0.6	21.51	0	1.16	8.3	0	0.29	20.93	4.22	0.1	0.09	99.4
M2 49724_062	G9A_Ti	R	42.26	0.68	21.58	0	1.23	8.24	0	0.27	20.82	4.24	0.09	0.04	99.45
M2 49724_063	G9A_Ti	C	42.16	0.69	21.53	0.03	1.11	8.18	0	0.25	20.89	4.26	0.09	0.06	99.25
M2 49724_064	G9A_Ti	R	42.07	0.64	21.54	0.04	1.11	8.19	0.02	0.26	21.15	4.26	0.1	0.13	99.51
M2 49724_065	G3_Na	C	41.65	0.45	22.15	0	0.69	11.21	0	0.44	18.51	4.5	0.09	0.07	99.76
M2 49724_066	G3_Na	R	41.69	0.44	22.46	0	0.58	11.06	0	0.42	18.46	4.35	0.1	0.02	99.58
M2 49724_067	G3_Na	C	41.6	0.47	22.26	0	0.45	11.41	0	0.44	18.2	4.51	0.1	0.05	99.49
M2 49724_068	G3_Na	R	41.25	0.48	22.25	0.05	0.5	11.5	0	0.45	18.22	4.56	0.1	0.11	99.47
M2 49724_069	G1	C	41.22	0.66	21.83	0.04	0.41	12.15	0	0.25	17.31	5.4	0.13	0.1	99.5
M2 49724_070	G1	R	41.24	0.69	21.94	0	0.41	12.16	0.03	0.23	17.29	5.41	0.11	0.08	99.59
M2 49724_071	G3_Na	C	40.85	0.37	22.23	0	0.27	13.27	0	0.57	16.38	5.5	0.09	0.15	99.68
M2 49724_072	G3_Na	R	40.82	0.36	22.07	0	0.32	13.1	0	0.58	16.4	5.43	0.08	0.12	99.28
M2 49724_073	G9A_Ti	C	41.81	0.69	20.8	0.03	1.68	8.02	0.03	0.25	20.78	4.47	0.13	0.12	98.81
M2 49724_074	G9A_Ti	R	42.42	0.71	21.1	0.03	1.72	7.99	0.03	0.24	21	4.49	0.07	0.05	99.85

Appendix D: Garnet Xenocryst EPMA Data Tables

Appendix D.01 (continued): Mel kimberlite garnet EPMA analyses. Zones: C – core, R – rim.

Sample	*Class*	*Zone*	*SiO_2*	*TiO_2*	*Al_2O_3*	*V_2O_3*	*Cr_2O_3*	*FeO*	*NiO*	*MnO*	*MgO*	*CaO*	*Na_2O*	*O*	*Total*
M2 49724_075	G9A_Ti	C	42.06	0.72	21	0	1.64	8.01	0.02	0.25	21.02	4.5	0.09	0.11	99.42
M2 49724_076	G9A_Ti	R	42.39	0.73	21.05	0.03	1.61	8	0.03	0.27	20.92	4.49	0.07	0.04	99.63
M2 49725_001	G9A_Ti	C	41.71	0.41	20.71	0.03	2.58	7.95	0.04	0.26	20.65	4.6	0.02	0.09	99.05
M2 49725_002	G9A_Ti	R	41.74	0.42	20.7	0.03	2.6	7.85	0.02	0.26	20.62	4.59	0.04	0.07	98.94
M2 49725_003	G9A	C	41.71	0.28	19.72	0	4.06	7.07	0.03	0.28	20.84	5.01	0.05	0.12	99.17
M2 49725_004	G9A	R	41.8	0.28	19.62	0.04	4.07	7.05	0.03	0.28	20.81	5	0.05	0.09	99.12
M2 49725_005	G9A_Ti	C	42.23	0.49	20.73	0	2.38	7.14	0	0.25	21.77	4.27	0.07	0.12	99.45
M2 49725_006	G9A_Ti	R	42.04	0.49	20.7	0.04	2.39	7.13	0.03	0.27	21.62	4.27	0.07	0.11	99.16
M2 49725_007	G9A_Ti	C	41.91	0.65	20.92	0.06	1.8	7.65	0	0.26	21.24	4.49	0.07	0.13	99.18
M2 49725_008	G9A_Ti	R	41.94	0.67	20.99	0.05	1.75	7.66	0.02	0.25	21.26	4.45	0.06	0.12	99.22
M2 49725_009	G9A_Ti	C	41.47	0.67	20.65	0.04	2.41	9.07	0	0.34	19.81	4.65	0.12	0.12	99.35
M2 49725_010	G9A_Ti	R	41.68	0.6	20.95	0.04	2.29	8.94	0.02	0.31	19.81	4.49	0.12	0.06	99.31
M2 49725_011	G9A_Ti	C	42.29	0.59	21.7	0.03	1.08	7.91	0.04	0.26	21.16	4.32	0.08	0.08	99.54
M2 49725_012	G9A_Ti	R	42.42	0.6	21.61	0	1.09	8.05	0.02	0.26	21.14	4.28	0.09	0.07	99.63
M2 49725_013	G1	C	41.69	0.78	21.79	0.05	0.35	10.3	0	0.34	19.71	4.18	0.12	0.13	99.44
M2 49725_014	G1	R	41.78	0.78	21.91	0.03	0.34	10.33	0	0.36	19.79	4.17	0.13	0.14	99.76
M2 49725_015	G1	C	41.99	0.48	22.22	0.03	0.81	8.67	0	0.3	20.25	4.64	0.08	0.08	99.55
M2 49725_016	G1	R	42.09	0.48	22.3	0.03	0.8	8.64	0.03	0.31	20.39	4.7	0.09	0.11	99.97
M2 49725_017	G1	C	41.81	0.75	21.99	0.04	0.37	10.29	0	0.36	19.72	4.2	0.13	0.13	99.79
M2 49725_018	G1	R	41.68	0.79	22.04	0.04	0.34	10.34	0	0.35	19.65	4.22	0.13	0.13	99.71
M2 49725_019	G1	C	41.77	0.66	21.97	0.04	0.34	10.48	0	0.36	19.37	4.49	0.12	0.13	99.73
M2 49725_020	G1	R	41.57	0.7	22.07	0.03	0.39	10.41	0	0.36	19.4	4.42	0.1	0.13	99.58
M2 49725_021	G9A_Ti	C	42.31	0.6	21.71	0.03	1.1	8.02	0.02	0.25	21.26	4.3	0.1	0.12	99.82
M2 49725_022	G9A_Ti	R	42.16	0.61	21.7	0.03	1.11	7.99	0	0.26	21.21	4.28	0.08	0.11	99.54
M2 49725_023	G1	C	41.35	0.74	21.67	0	0.39	10.25	0	0.35	19.61	4.16	0.13	0.15	98.8
M2 49725_024	G1	R	41.58	0.72	21.88	0.04	0.37	10.29	0	0.34	19.65	4.16	0.12	0.13	99.28
M2 49725_025	G0	C	40.72	0.83	21.79	0	0.15	12.24	0.02	0.25	14.87	8.46	0.15	0.13	99.61
M2 49725_026	G0	R	40.86	0.83	21.83	0	0.15	12.24	0.02	0.27	14.87	8.48	0.14	0.1	99.79
M2 49725_027	G0	C	40.88	0.83	21.99	0.04	0.18	12.22	0.02	0.27	15.07	8.45	0.15	0.14	100.24
M2 49725_028	G0	R	40.68	0.85	21.76	0.02	0.13	12.16	0.02	0.25	14.95	8.42	0.13	0.12	99.49
M2 49725_029	G11	C	41.63	0.6	18.99	0.04	4.97	6.94	0	0.27	20.85	4.95	0.07	0.08	99.39
M2 49725_030	G11	R	41.82	0.61	19.42	0.04	4.28	6.9	0	0.28	21.18	4.76	0.07	0.09	99.45
M2 49725_031	G1	C	41.38	0.62	22.04	0.04	0.21	11.58	0	0.25	17.7	5.45	0.1	0.09	99.46
M2 49725_032	G1	R	41.38	0.66	22.12	0	0.18	11.65	0.03	0.28	17.79	5.45	0.11	0.12	99.77
M2 49725_033	G9A_Ti	C	42.32	0.48	21.71	0	1.25	7.97	0	0.27	21.25	4.02	0.07	0.06	99.4
M2 49725_034	G9A_Ti	R	42.11	0.48	21.84	0	1.18	7.97	0	0.27	21.38	4.03	0.08	0.13	99.47
M2 49725_035	G1	C	41.55	0.68	21.87	0.03	0.39	10.44	0	0.35	19.19	4.73	0.1	0.14	99.47
M2 49725_036	G1	R	41.61	0.66	21.93	0.04	0.38	10.39	0	0.37	19.19	4.7	0.12	0.14	99.53
M2 49725_037	G1	C	41.49	0.71	21.9	0.03	0.36	10.43	0	0.34	19.45	4.51	0.11	0.17	99.5

Appendix D: Garnet Xenocryst EPMA Data Tables

Appendix D.01 (continued): Mel kimberlite garnet EPMA analyses. Zones: C – core, R – rim.

Sample	*Class*	*Zone*	*SiO_2*	*TiO_2*	*Al_2O_3*	*V_2O_3*	*Cr_2O_3*	*FeO*	*NiO*	*MnO*	*MgO*	*CaO*	*Na_2O*	*O*	*Total*
M2 49725_038	G1	R	41.41	0.73	21.85	0.03	0.34	10.4	0	0.35	19.57	4.4	0.13	0.19	99.4
M2 49725_039	G9A_Ti	C	41.98	0.59	21.68	0.02	1.12	7.93	0.03	0.26	21.12	4.33	0.1	0.13	99.29
M2 49725_040	G9A_Ti	R	42.14	0.59	21.68	0.03	1.12	7.93	0.03	0.28	21.29	4.32	0.09	0.14	99.64
M2 49725_041	G1	C	41.37	0.63	22.08	0	0.23	11.58	0	0.27	17.86	5.52	0.11	0.14	99.79
M2 49725_042	G1	R	41.55	0.63	22.18	0	0.21	11.61	0.03	0.26	17.59	5.5	0.1	0.06	99.72
M2 49725_043	G0	C	40.73	0.85	21.75	0.04	0.16	12.25	0.02	0.26	14.8	8.39	0.13	0.09	99.47
M2 49725_044	G0	R	40.83	0.81	21.73	0.04	0.15	12.2	0.02	0.25	14.76	8.41	0.16	0.09	99.45
M2 49725_045	G9A_Ti	C	41.98	0.48	20.6	0.04	2.44	7.16	0	0.25	21.46	4.27	0.08	0.1	98.86
M2 49725_046	G9A_Ti	R	42.16	0.5	20.89	0	2.42	7.11	0	0.25	21.41	4.29	0.08	0.06	99.17
M2 49725_047	G9A_Ti	C	41.94	0.61	21.15	0	1.78	7.62	0.02	0.26	21.2	4.42	0.06	0.11	99.17
M2 49725_048	G9A_Ti	R	41.96	0.69	21.07	0.03	1.83	7.71	0.02	0.25	21.23	4.42	0.08	0.12	99.41
M2 49725_049	G9A_Ti	C	42.22	0.59	21.55	0.04	1.15	7.95	0.02	0.26	20.99	4.31	0.09	0.06	99.23
M2 49725_050	G9A_Ti	R	42.2	0.58	21.72	0.03	1.16	7.95	0.02	0.27	21.15	4.31	0.09	0.1	99.58
M2 49725_051	G9A	C	41.93	0.32	19.77	0.05	3.95	7.09	0.02	0.27	20.9	4.97	0.05	0.09	99.41
M2 49725_052	G9A	R	42.02	0.35	19.74	0.04	3.95	7.09	0.02	0.28	20.66	4.92	0.03	0.01	99.11
M2 49725_053	G1	C	41.9	0.69	21.72	0.05	0.88	8.3	0.02	0.27	20.98	4.17	0.1	0.12	99.2
M2 49725_054	G1	R	42	0.69	21.9	0.03	0.88	8.35	0	0.27	20.89	4.18	0.1	0.09	99.38
M2 49725_055	G9A_Ti	C	42.13	0.62	21.63	0.04	1.21	8.13	0.02	0.26	20.98	4.4	0.08	0.1	99.6
M2 49725_056	G9A_Ti	R	42.17	0.59	21.76	0.05	1.16	8.1	0	0.26	20.92	4.37	0.08	0.08	99.54
M2 49725_057	G1	C	41.6	0.66	22.02	0	0.37	10.5	0	0.36	19.12	4.69	0.1	0.12	99.54
M2 49725_058	G1	R	41.56	0.64	21.93	0.03	0.35	10.48	0	0.35	19.06	4.67	0.12	0.12	99.31
M2 49725_059	G9A	C	41.78	0.28	19.65	0.05	4.04	7.06	0.02	0.26	20.86	5.07	0.04	0.11	99.22
M2 49725_060	G9A	R	41.7	0.31	19.77	0.03	4.03	7.06	0	0.26	20.8	5	0.04	0.1	99.1
M2 49725_061	G3	C	41.58	0.31	22.72	0.03	0.37	10.67	0	0.39	19.16	4.04	0.07	0.08	99.42
M2 49725_062	G3	R	41.52	0.32	22.66	0	0.38	10.7	0	0.41	19.06	4	0.07	0.07	99.19
M2 49725_063	G1	C	41.57	0.76	21.83	0	0.39	10.28	0	0.35	19.75	4.18	0.12	0.15	99.38
M2 49725_064	G1	R	41.88	0.76	21.94	0.04	0.38	10.26	0	0.36	19.65	4.21	0.13	0.1	99.71
M2 49725_065	G0	C	40.79	0.82	21.91	0	0.15	12.19	0.02	0.25	14.9	8.44	0.14	0.11	99.72
M2 49725_066	G0	R	41.05	0.84	22.04	0	0.18	12.25	0	0.26	14.89	8.47	0.14	0.08	100.2
M2 49741_001	G9A_Ti	C	41.86	0.74	21.41	0.04	1.2	8.31	0	0.25	21.08	4.35	0.12	0.17	99.53
M2 49741_002	G9A_Ti	R	41.88	0.74	21.44	0.04	1.15	8.29	0	0.25	21.03	4.33	0.08	0.13	99.36
M2 49741_003	G1	C	41.6	0.47	22	0	0.52	9.18	0	0.34	19.83	4.87	0.1	0.16	99.07
M2 49741_004	G1	R	41.8	0.49	22.08	0.03	0.5	9.25	0.02	0.33	19.93	4.91	0.13	0.18	99.65
M2 49741_005	G1	C	41.59	0.5	22.1	0	0.48	9.56	0	0.35	19.75	4.77	0.11	0.17	99.38
M2 49741_006	G1	R	41.68	0.5	22.07	0.03	0.47	9.57	0	0.33	19.73	4.76	0.12	0.16	99.42
M2 49741_007	G1	C	41.61	0.53	22	0.02	0.47	9.68	0	0.33	19.7	4.77	0.13	0.18	99.42
M2 49741_008	G1	R	41.58	0.53	21.95	0.03	0.48	9.6	0	0.33	19.79	4.74	0.11	0.18	99.32
M2 49741_009	G1	C	41.64	0.55	21.9	0	0.51	9.62	0	0.34	19.77	4.79	0.11	0.18	99.41
M2 49741_010	G1	R	41.51	0.55	21.89	0	0.45	9.68	0	0.33	19.62	4.8	0.11	0.17	99.11

Appendix D: Garnet Xenocryst EPMA Data Tables

Appendix D.01 (continued): Mel kimberlite garnet EPMA analyses. Zones: C – core, R – rim.

Sample	*Class*	*Zone*	*SiO_2*	*TiO_2*	*Al_2O_3*	*V_2O_3*	*Cr_2O_3*	*FeO*	*NiO*	*MnO*	*MgO*	*CaO*	*Na_2O*	*O*	*Total*
M2 49741_011	G1	C	41.77	0.51	21.93	0	0.58	9.36	0	0.33	19.96	4.56	0.11	0.14	99.25
M2 49741_012	G1	R	41.7	0.52	21.97	0.03	0.57	9.41	0	0.34	20	4.59	0.11	0.17	99.41
M2 49741_013	G1	C	41.58	0.53	22.2	0	0.24	10.26	0	0.38	19.07	5.06	0.12	0.16	99.6
M2 49741_014	G1	R	41.48	0.54	22.12	0.02	0.22	10.3	0	0.38	18.94	5.04	0.13	0.16	99.33
M2 49741_015	G9A_Ti	C	41.92	0.63	21.42	0.03	1.26	8.67	0	0.26	20.78	4.27	0.07	0.12	99.43
M2 49741_016	G9A_Ti	R	41.87	0.62	21.39	0	1.26	8.69	0	0.26	20.76	4.27	0.08	0.13	99.33
M2 49741_017	G9A_Ti	C	41.96	0.43	21.59	0	1.48	8.14	0.02	0.27	20.94	4.34	0.09	0.13	99.39
M2 49741_018	G9A_Ti	R	41.95	0.43	21.47	0.03	1.45	8.11	0	0.28	20.82	4.32	0.1	0.11	99.07
M2 49741_019	G1	C	41.85	0.51	22.22	0.04	0.52	9.25	0.02	0.32	20.2	4.31	0.12	0.13	99.49
M2 49741_020	G1	R	42.03	0.51	22.28	0	0.5	9.28	0	0.33	20.23	4.33	0.13	0.13	99.75
M2 49741_021	G1	C	41.72	0.57	22.06	0	0.52	9.68	0	0.33	19.61	4.77	0.12	0.14	99.52
M2 49741_022	G1	R	41.98	0.53	22.27	0	0.43	9.61	0	0.33	19.67	4.8	0.13	0.12	99.87
M2 49741_023	G1	C	41.96	0.52	22.15	0	0.49	9.61	0.02	0.33	19.84	4.76	0.12	0.15	99.95
M2 49741_024	G1	R	41.81	0.55	22.18	0	0.49	9.57	0	0.34	19.69	4.74	0.1	0.12	99.59
M2 49741_025	G9A_Ti	C	42.04	0.47	21.54	0	1.43	8.15	0	0.28	21.1	4.33	0.12	0.16	99.62
M2 49741_026	G9A_Ti	R	42.15	0.43	21.47	0	1.4	8.12	0.02	0.3	20.78	4.38	0.11	0.09	99.25
M2 49741_027	G1	C	41.77	0.53	22.15	0	0.46	9.62	0.02	0.36	19.65	4.8	0.1	0.14	99.6
M2 49741_028	G1	R	41.81	0.52	22.11	0.04	0.44	9.65	0	0.33	19.58	4.77	0.09	0.11	99.45
M2 49741_029	G1	C	41.81	0.66	22.03	0.02	0.54	9.78	0	0.34	19.88	4.6	0.12	0.16	99.94
M2 49741_030	G1	R	42.01	0.59	22.17	0	0.48	9.65	0	0.34	19.81	4.45	0.12	0.09	99.71
M2 49741_031	G1	C	41.55	0.61	22.12	0	0.27	10.3	0	0.37	19.12	4.77	0.12	0.13	99.36
M2 49741_032	G1	R	41.54	0.58	22.24	0	0.23	10.26	0	0.37	19.16	4.75	0.12	0.14	99.39
M2 49741_033	G9A_Ti	C	42.13	0.74	21.53	0	1.13	8.24	0.02	0.27	21.01	4.31	0.11	0.11	99.6
M2 49741_034	G9A_Ti	R	41.9	0.73	21.45	0	1.09	8.27	0	0.26	20.87	4.33	0.11	0.11	99.12
M2 49741_035	G1	C	41.81	0.51	22.08	0	0.45	9.61	0	0.34	19.69	4.79	0.1	0.13	99.51
M2 49741_036	G1	R	41.86	0.52	22.23	0	0.46	9.69	0	0.35	19.78	4.79	0.12	0.16	99.96
M2 49741_037	G1	C	41.94	0.49	22.21	0.03	0.49	9.49	0	0.34	19.78	4.66	0.11	0.11	99.65
M2 49741_038	G1	R	41.73	0.49	22.3	0	0.49	9.5	0	0.33	19.86	4.71	0.1	0.15	99.66
M2 49741_039	G9A_Ti	C	42.1	0.73	21.34	0.03	1.15	8.22	0.02	0.27	20.95	4.34	0.11	0.11	99.37
M2 49741_040	G9A_Ti	R	42.14	0.76	21.54	0.04	1.12	8.17	0	0.28	20.97	4.34	0.1	0.09	99.55
M2 49741_041	G1	C	41.96	0.55	22.17	0	0.54	9.14	0	0.32	19.9	4.81	0.12	0.11	99.62
M2 49741_042	G1	R	42.07	0.53	22.33	0	0.6	9.05	0	0.33	19.86	4.94	0.11	0.09	99.91
M2 49741_043	G1	C	41.86	0.49	22.23	0.03	0.43	9.46	0.02	0.33	19.78	4.72	0.1	0.12	99.57
M2 49741_044	G1	R	41.75	0.5	22.31	0	0.47	9.48	0	0.36	19.8	4.7	0.11	0.14	99.62
M2 49741_045	G1	C	41.88	0.53	22.15	0	0.52	9.66	0.02	0.35	19.77	4.76	0.11	0.15	99.9
M2 49741_046	G1	R	42.01	0.53	22.2	0.03	0.47	9.59	0	0.34	19.56	4.77	0.12	0.08	99.7
M2 49742_001	G1	C	41.85	0.56	22.06	0.02	0.61	9.11	0	0.31	20.56	4.4	0.1	0.18	99.76
M2 49742_002	G1	R	41.86	0.55	22.08	0.03	0.61	9.05	0	0.33	20.44	4.41	0.11	0.16	99.63
M2 49742_003	G3_Na	C	40.67	0.54	22.53	0.04	0.05	12.34	0.02	0.27	13.56	9.73	0.19	0.12	100.06

Appendix D: Garnet Xenocryst EPMA Data Tables

Appendix D.01 (continued): Mel kimberlite garnet EPMA analyses. Zones: C – core, R – rim.

Sample	*Class*	*Zone*	*SiO_2*	*TiO_2*	*Al_2O_3*	*V_2O_3*	*Cr_2O_3*	*FeO*	*NiO*	*MnO*	*MgO*	*CaO*	*Na_2O*	*O*	*Total*
M2 49742_004	G3_Na	R	40.92	0.53	22.69	0	0.06	12.34	0	0.25	13.52	9.79	0.18	0.07	100.35
M2 49742_005	G3_Na	C	40.63	0.5	22.46	0	0.04	12.2	0.02	0.28	13.46	9.84	0.17	0.09	99.69
M2 49742_006	G3_Na	R	40.78	0.51	22.64	0	0.04	12.24	0.02	0.24	13.48	9.82	0.17	0.08	100.02
M2 49742_007	G1	C	42.08	0.62	21.8	0.03	0.89	8.26	0	0.27	21.1	4.29	0.1	0.14	99.58
M2 49742_008	G1	R	42.15	0.61	21.89	0.03	0.9	8.23	0	0.27	21.05	4.27	0.07	0.1	99.57
M2 49742_009	G1	C	41.82	0.53	21.92	0	0.77	8.92	0.02	0.32	20.36	4.66	0.1	0.16	99.58
M2 49742_010	G1	R	42.05	0.5	22.03	0.03	0.76	8.88	0.02	0.31	20.26	4.66	0.09	0.11	99.7
M2 49742_011	G3_Na	C	40.26	0.57	21.53	0	0.06	12.06	0	0.27	15.52	7.65	0.15	0.21	98.28
M2 49742_012	G3_Na	R	40.96	0.62	22.17	0	0.07	11.41	0.02	0.25	15.65	7.94	0.17	0.11	99.37
M2 49742_013	G1	C	41.91	0.58	21.91	0	0.69	8.96	0.02	0.3	20.37	4.46	0.1	0.13	99.43
M2 49742_014	G1	R	41.75	0.6	21.67	0.03	0.79	8.97	0	0.3	20.3	4.41	0.12	0.14	99.08
M2 49742_015	G1	C	41.94	0.56	21.96	0	0.63	8.97	0.02	0.3	20.46	4.4	0.11	0.14	99.49
M2 49742_016	G1	R	42.02	0.55	22.13	0	0.6	9.06	0	0.3	20.3	4.4	0.11	0.1	99.57
M2 49742_017	G1	C	41.96	0.58	21.88	0	0.75	8.94	0	0.3	20.27	4.5	0.11	0.11	99.4
M2 49742_018	G1	R	42.06	0.54	21.98	0	0.61	8.92	0	0.3	20.37	4.48	0.12	0.12	99.5
M2 49742_019	G1	C	41.92	0.55	21.86	0	0.71	9.05	0.02	0.31	20.39	4.46	0.1	0.14	99.51
M2 49742_020	G1	R	42.07	0.57	22.16	0.05	0.62	9	0	0.31	20.36	4.41	0.09	0.1	99.74
M2 49742_021	G1	C	41.88	0.53	21.81	0.03	0.77	8.97	0	0.33	20.37	4.49	0.11	0.15	99.44
M2 49742_022	G1	R	41.7	0.57	21.9	0	0.69	9.01	0	0.3	20.26	4.54	0.11	0.15	99.23
M2 49742_023	G1	C	41.8	0.7	21.61	0	0.67	9.09	0	0.3	20.34	4.45	0.11	0.14	99.21
M2 49742_024	G1	R	41.87	0.7	21.57	0	0.68	9.05	0	0.29	20.38	4.34	0.15	0.14	99.17
M2 49742_025	G1	C	41.84	0.6	21.9	0	0.66	8.97	0.02	0.31	20.4	4.41	0.11	0.14	99.36
M2 49742_026	G1	R	42.23	0.57	22.06	0	0.64	9.02	0.02	0.3	20.38	4.42	0.12	0.1	99.86
M2 49742_027	G9B_Ti	C	41.81	0.85	20.99	0.02	1.25	8.33	0	0.26	20.91	4.59	0.08	0.15	99.24
M2 49742_028	G9B_Ti	R	42.09	0.88	21.22	0	1.24	8.32	0	0.26	21.01	4.61	0.1	0.14	99.87
M2 49742_029	G1	C	42.15	0.64	21.91	0	0.54	8.24	0.02	0.27	21.14	4.26	0.1	0.13	99.4
M2 49742_030	G1	R	41.97	0.63	22.03	0.03	0.48	8.21	0	0.26	21.02	4.25	0.08	0.11	99.07
M2 49742_031	G9A	C	41.88	0.28	20.43	0	3.12	7.31	0	0.26	21.02	4.71	0.05	0.11	99.17
M2 49742_032	G9A	R	42.2	0.3	20.4	0.03	3.09	7.33	0.02	0.27	20.89	4.72	0.04	0.04	99.33
M2 49742_033	G9A	C	41.83	0.14	19.37	0.05	4.86	6.62	0	0.26	20.79	5.36	0	0.08	99.36
M2 49742_034	G9A	R	41.8	0.12	19.21	0.05	5.04	6.69	0	0.27	20.68	5.43	0	0.08	99.37
M2 49742_035	G3_Na	C	40.67	0.51	22.47	0	0	12.19	0	0.25	13.46	9.82	0.16	0.08	99.61
M2 49742_036	G3_Na	R	40.89	0.5	22.72	0.03	0.07	12.25	0	0.27	13.47	9.85	0.18	0.07	100.3
M2 49742_037	G1	C	42.12	0.53	22.1	0.03	0.61	9.05	0	0.29	20.34	4.48	0.11	0.11	99.77
M2 49742_038	G1	R	42.43	0.54	22.14	0	0.62	9.11	0	0.29	20.25	4.51	0.11	0.06	100.06
M2 49742_039	G12	C	41.5	0.14	22.39	0	1.31	8.73	0	0.32	17.95	7.36	0.03	0.1	99.83
M2 49742_040	G12	R	41.59	0.14	22.27	0	1.34	8.65	0.02	0.31	18.02	7.36	0.05	0.1	99.85
M2 49742_041	G1	C	41.95	0.62	21.96	0	0.75	8.96	0	0.29	20.47	4.48	0.14	0.16	99.78
M2 49742_042	G1	R	42.26	0.59	22.06	0.03	0.84	9.06	0	0.31	20.34	4.43	0.1	0.08	100.1

Appendix D: Garnet Xenocryst EPMA Data Tables

Appendix D.01 (continued): Mel kimberlite garnet EPMA analyses. Zones: C – core, R – rim.

Sample	*Class*	*Zone*	*SiO_2*	*TiO_2*	*Al_2O_3*	*V_2O_3*	*Cr_2O_3*	*FeO*	*NiO*	*MnO*	*MgO*	*CaO*	*Na_2O*	*O*	*Total*
M2 49742_043	G9A_Ti	C	42.03	0.55	20.92	0.04	2.16	7.93	0	0.28	21.05	4.42	0.08	0.12	99.58
M2 49742_044	G9A_Ti	R	41.95	0.58	20.91	0.03	2.15	7.92	0	0.28	20.94	4.42	0.07	0.09	99.34
M2 49742_045	G3_Na	C	40.7	0.51	22.65	0	0.06	12.34	0	0.26	13.48	9.71	0.17	0.08	99.96
M2 49742_046	G3_Na	R	40.84	0.48	22.57	0	0.04	12.24	0	0.24	13.48	9.68	0.18	0.06	99.81
M2 49742_047	G1	C	42.17	0.53	22.04	0.02	0.61	9.05	0	0.3	20.21	4.46	0.12	0.08	99.59
M2 49742_048	G1	R	42.25	0.56	22.19	0.02	0.63	9.04	0	0.31	20.23	4.5	0.11	0.07	99.91
M2 49742_049	G1	C	42.45	0.55	22.16	0.04	0.88	8.21	0.02	0.25	21.19	4.28	0.08	0.1	100.21
M2 49742_050	G1	R	42.08	0.56	21.99	0.03	0.86	8.18	0	0.26	21.2	4.29	0.08	0.14	99.67
M2 49742_051	G1	C	42.39	0.65	21.81	0.03	0.9	8.27	0	0.25	21	4.34	0.07	0.06	99.77
M2 49742_052	G1	R	42.28	0.62	21.59	0	0.9	8.22	0	0.27	21.01	4.34	0.07	0.08	99.38
M2 49742_053	G1	C	42.24	0.65	21.77	0	0.9	8.26	0.02	0.27	21.13	4.35	0.09	0.12	99.8
M2 49742_054	G1	R	42.27	0.64	21.61	0.05	0.9	8.29	0.02	0.26	21.12	4.33	0.08	0.12	99.69
M2 49742_055	G1	C	42.19	0.58	21.84	0	0.92	8.19	0	0.24	20.99	4.3	0.07	0.08	99.4
M2 49742_056	G1	R	42.08	0.57	21.82	0	0.93	8.18	0	0.25	21.11	4.3	0.07	0.12	99.43
M2 49742_057	G9A	C	41.65	0.2	21.81	0.03	2.28	8.09	0	0.39	20.77	4.24	0.06	0.14	99.66
M2 49742_058	G9A	R	42.29	0.2	22.01	0	2.24	8.1	0	0.39	20.56	4.19	0.06	0	100.04
M2 49742_059	G1	C	41.74	0.55	21.83	0	0.77	8.86	0	0.27	20.41	4.57	0.12	0.17	99.29
M2 49742_060	G1	R	42.05	0.55	21.94	0.04	0.73	8.66	0	0.32	20.37	4.57	0.1	0.1	99.43
M2 49742_061	G1	C	41.67	0.55	21.85	0	0.77	8.85	0	0.3	20.16	4.68	0.11	0.14	99.08
M2 49742_062	G1	R	41.59	0.51	21.82	0	0.76	8.83	0.02	0.3	20.17	4.64	0.1	0.15	98.89
M2 49742_063	G1	C	41.77	0.53	21.83	0	0.77	8.85	0	0.32	20.29	4.52	0.1	0.13	99.11
M2 49742_064	G1	R	41.84	0.54	21.9	0.03	0.76	8.91	0.02	0.31	20.05	4.51	0.09	0.07	99.03
M2 49742_065	G9B_Ti	C	41.78	0.83	21.21	0	1.14	8.24	0.02	0.25	20.84	4.59	0.08	0.13	99.11
M2 49742_066	G9B_Ti	R	42.02	0.85	21.2	0	1.24	8.34	0	0.24	20.83	4.57	0.09	0.11	99.49
M2 49742_067	G1	C	42	0.62	21.85	0.03	0.9	8.2	0.02	0.27	21.17	4.26	0.07	0.14	99.53
M2 49742_068	G1	R	41.86	0.59	21.79	0.03	0.89	8.14	0.02	0.25	20.96	4.27	0.06	0.11	98.97
M2 49742_069	G9A_Ti	C	42.2	0.4	20.05	0.03	2.95	7.38	0	0.24	21.2	4.97	0.03	0.12	99.57
M2 49742_070	G9B	R	42.3	0.36	20.03	0.06	2.91	7.33	0.02	0.25	20.85	4.98	0.02	0.04	99.15
M2 49742_071	G12	C	41.46	0.16	22.18	0	1.56	8.64	0	0.3	17.87	7.45	0.04	0.09	99.75
M2 49742_072	G1	R	41.75	0.52	21.94	0	0.72	8.85	0.02	0.32	20.1	4.58	0.11	0.11	99.02
M2 49742_073	G1	C	41.95	0.53	21.86	0.04	0.77	8.88	0	0.29	20.23	4.57	0.11	0.11	99.34
M2 49742_074	G1	R	41.83	0.55	21.91	0	0.86	8.96	0	0.32	20.37	4.4	0.11	0.14	99.45
M2 49742_075	G1	C	41.74	0.64	21.65	0.02	0.69	9.06	0	0.31	20.32	4.45	0.13	0.16	99.17
M2 49742_076	G1	R	42.01	0.73	21.66	0	0.69	9.08	0	0.3	20.39	4.4	0.11	0.11	99.48
M2 49742_077	G9A_Ti	C	42.1	0.44	20.82	0.05	2.49	6.96	0	0.26	21.66	4.4	0.05	0.11	99.34
M2 49742_078	G9A_Ti	R	42.35	0.42	20.97	0.03	2.4	6.99	0.02	0.23	21.71	4.39	0.07	0.1	99.68
M2 49742_079	G9A_Ti	C	42.04	0.38	20.04	0.05	2.98	7.39	0	0.24	21.07	4.97	0.03	0.12	99.31
M2 49742_080	G9A_Ti	R	42.34	0.38	20.09	0.05	3.04	7.42	0.03	0.25	21.09	4.97	0	0.08	99.74
M2 49742_081	G9A_Ti	C	42.15	0.58	21.45	0	1.18	8.22	0.03	0.25	20.82	4.37	0.06	0.06	99.17

Appendix D: Garnet Xenocryst EPMA Data Tables

Appendix D.01 (continued): Mel kimberlite garnet EPMA analyses. Zones: C – core, R – rim.

Sample	*Class*	*Zone*	*SiO_2*	*TiO_2*	*Al_2O_3*	*V_2O_3*	*Cr_2O_3*	*FeO*	*NiO*	*MnO*	*MgO*	*CaO*	*Na_2O*	*O*	*Total*
M2 49742_082	G9A_Ti	R	42.14	0.59	21.6	0.03	1.2	8.23	0	0.26	20.95	4.36	0.09	0.1	99.55
M2 49742_083	G3_Na	C	40.75	0.53	22.31	0	0.11	11.91	0	0.25	14.71	8.73	0.13	0.11	99.54
M2 49742_084	G3_Na	R	40.97	0.53	22.35	0.04	0.1	11.88	0	0.27	14.66	8.76	0.16	0.09	99.81
M2 49742_085	G12	C	41.54	0.15	22.39	0	1.27	8.68	0	0.31	17.85	7.35	0.03	0.06	99.63
M2 49742_086	G12	R	41.75	0.17	22.52	0	1.25	8.68	0	0.3	17.99	7.41	0.04	0.07	100.18
M2 49742_087	G1	C	41.87	0.55	21.75	0.03	0.82	8.96	0.02	0.3	20.42	4.45	0.13	0.16	99.46
M2 49742_088	G1	R	42.17	0.54	22.04	0.03	0.84	8.97	0	0.31	20.25	4.42	0.09	0.06	99.72
M2 49742_089	G12	C	41.27	0.14	22.14	0	1.29	8.71	0	0.31	18.16	7.31	0.03	0.16	99.52
M2 49742_090	G12	R	41.65	0.14	22.48	0	1.3	8.65	0	0.32	18.07	7.31	0.02	0.08	100.02
M2 49742_091	G1	C	42.12	0.62	21.77	0.06	0.93	8.27	0.02	0.25	21.1	4.33	0.09	0.13	99.69
M2 49742_092	G1	R	42.31	0.62	21.75	0	0.91	8.27	0.02	0.25	21	4.34	0.07	0.08	99.62
M2 49742_093	G9A_Ti	C	42.07	0.62	21.66	0	1.15	8.23	0	0.27	21.03	4.33	0.09	0.12	99.57
M2 49742_094	G9A_Ti	R	41.9	0.58	21.52	0.03	1.17	8.22	0.03	0.25	20.98	4.37	0.08	0.13	99.26
M2 49742_095	G1	C	41.96	0.64	21.8	0.04	0.78	9.08	0.02	0.3	20.49	4.48	0.12	0.16	99.87
M2 49742_096	G1	R	42.15	0.65	21.96	0	0.75	8.96	0	0.29	20.32	4.48	0.12	0.09	99.77
M2 49742_097	G1	C	42.1	0.52	22.02	0.03	0.75	8.87	0	0.3	20.26	4.67	0.09	0.1	99.71
M2 49742_098	G1	R	42.12	0.53	22.11	0.03	0.76	8.92	0	0.3	20.15	4.66	0.1	0.08	99.76
M2 49742_099	G1	C	42.21	0.65	21.7	0	0.94	8.18	0.02	0.26	21.26	4.34	0.08	0.14	99.78
M2 49742_100	G1	R	42.16	0.64	21.73	0.04	0.92	8.23	0	0.26	21.08	4.32	0.09	0.11	99.58
M2 49742_101	G1	C	41.91	0.49	22.04	0	0.79	8.88	0	0.29	20.25	4.7	0.1	0.13	99.58
M2 49742_102	G1	R	41.77	0.55	21.97	0.02	0.77	8.89	0.02	0.29	20.27	4.64	0.11	0.15	99.45
M2 49742_103	G1	C	42.05	0.63	21.97	0.03	0.59	9.04	0	0.31	20.4	4.44	0.11	0.12	99.69
M2 49742_104	G1	R	41.94	0.61	21.94	0.04	0.75	9.05	0	0.32	20.24	4.31	0.1	0.08	99.38
M2 49742_105	G1	C	41.99	0.56	21.96	0.03	0.75	8.93	0	0.3	20.17	4.7	0.1	0.11	99.6
M2 49742_106	G1	R	42.15	0.53	22.07	0.02	0.74	8.94	0	0.32	20.09	4.73	0.1	0.08	99.77
M2 49742_107	G9A_Ti	C	42.19	0.59	21.65	0.03	1.18	8.14	0.02	0.26	20.97	4.36	0.08	0.09	99.56
M2 49742_108	G9A_Ti	R	42.45	0.57	21.87	0.02	1.08	8.16	0.02	0.27	21.08	4.37	0.07	0.08	100.04
M2 49742_109	G1	C	41.96	0.73	21.5	0.05	0.98	9.27	0	0.31	20.35	4.47	0.12	0.15	99.89
M2 49742_110	G1	R	41.97	0.77	21.45	0.05	0.95	9.19	0	0.32	20.3	4.48	0.11	0.12	99.71
M2 49742_111	G1	C	41.97	0.6	21.99	0	0.69	9	0	0.32	20.52	4.51	0.11	0.17	99.88
M2 49742_112	G1	R	42.09	0.57	22.2	0.03	0.71	8.97	0	0.3	20.43	4.52	0.12	0.13	100.07
M2 49742_113	G3_Na	C	40.8	0.53	22.71	0	0.04	12.31	0	0.27	13.65	9.72	0.19	0.11	100.33
M2 49742_114	G3_Na	R	40.58	0.5	22.65	0	0.05	12.31	0.02	0.26	13.49	9.73	0.19	0.12	99.9
M2 49742_115	G1	C	42.12	0.66	22	0.03	0.54	8.88	0	0.3	20.8	4.21	0.09	0.13	99.76
M2 49742_116	G1	R	42.21	0.67	21.9	0.02	0.55	8.84	0	0.29	20.56	4.2	0.11	0.07	99.42
M2 49742_117	G1	C	41.96	0.53	22.15	0.03	0.63	9	0.02	0.31	20.14	4.48	0.1	0.09	99.44
M2 49742_118	G1	R	42.19	0.55	22.09	0	0.65	8.95	0	0.31	20.16	4.52	0.1	0.06	99.58
M2 49742_119	G1	C	42.14	0.6	21.79	0.03	1	8.18	0.02	0.25	21.09	4.32	0.09	0.12	99.63
M2 49742_120	G9A_Ti	R	42.25	0.58	21.75	0.04	1.13	8.19	0.02	0.26	20.91	4.34	0.09	0.08	99.64

Appendix D: Garnet Xenocryst EPMA Data Tables

Appendix D.01 (continued): Mel kimberlite garnet EPMA analyses. Zones: C – core, R – rim.

Sample	*Class*	*Zone*	*SiO_2*	*TiO_2*	*Al_2O_3*	*V_2O_3*	*Cr_2O_3*	*FeO*	*NiO*	*MnO*	*MgO*	*CaO*	*Na_2O*	*O*	*Total*
P3 49725_001	G9A_Ti	C	41.86	0.59	20.73	0.04	1.84	7.97	0.02	0.25	20.7	4.44	0.09	0.07	98.6
P3 49725_002	G9A_Ti	R	41.78	0.59	21.05	0.03	1.84	7.71	0.02	0.27	21.58	4.42	0.05	0.21	99.55
P3 49725_003r	G9A_Ti	R	41.59	0.58	20.91	0.04	1.85	7.64	0	0.28	21.24	4.46	0.05	0.16	98.8
P3 49725_004	G9A_Ti	C	41.89	0.58	21.44	0	1.86	7.7	0	0.27	21.55	4.43	0.07	0.2	99.99
P3 49725_005	G9A_Ti	R	42	0.64	21.63	0	1.16	7.94	0	0.26	21.74	4.33	0.09	0.23	100.02
P3 49725_006	G9A_Ti	C	42.39	0.57	21.84	0.03	1.1	7.87	0	0.26	21.67	4.33	0.08	0.17	100.31
P3 49725_007	G0	R	40.76	0.8	21.91	0.03	0.15	12.15	0	0.26	15.27	8.52	0.14	0.19	100.18
P3 49725_008	G0	C	40.65	0.85	21.84	0.03	0.13	12.21	0	0.26	15.14	8.51	0.14	0.18	99.94
P3 49725_009	G9A_Ti	R	42.12	0.6	21.7	0.03	1.12	7.83	0	0.25	21.89	4.32	0.09	0.24	100.19
P3 49725_010	G9A_Ti	C	41.97	0.6	21.68	0.04	1.08	7.93	0	0.25	21.79	4.32	0.09	0.25	100
P3 49725_011	G1	R	41.15	0.99	21.78	0.05	0.22	11.54	0	0.39	19.33	4.14	0.14	0.25	99.98
P3 49725_012	G1	C	41.32	0.95	21.64	0	0.25	11.5	0	0.36	19.33	4.12	0.12	0.21	99.8
P3 49725_013	G0	R	40.71	0.81	21.78	0.03	0.15	12.21	0	0.26	15.27	8.53	0.13	0.21	100.09
P3 49725_014	G0	C	41.18	0.85	21.95	0.02	0.17	12.26	0.02	0.25	15.17	8.51	0.14	0.13	100.65
P3 49725_015	G1	R	41.9	0.68	21.98	0	0.58	8.29	0	0.3	21.17	4.78	0.1	0.25	100.03
P3 49725_016	G1	C	42.17	0.65	21.96	0	0.59	8.22	0	0.27	21.12	4.75	0.12	0.2	100.05
P3 49725_017	G9B_Ti	R	41.99	0.67	21.51	0.03	1.25	8.19	0	0.27	21.36	4.51	0.06	0.2	100.04
P3 49725_018	G9A_Ti	C	41.75	0.64	21.24	0.03	1.26	8.03	0	0.24	20.77	4.43	0.09	0.1	98.58
P3 49725_019	G1	R	41.41	0.77	21.88	0.03	0.4	10.4	0	0.33	20.12	4.22	0.12	0.26	99.94
P3 49725_020	G1	C	41.81	0.78	22.04	0	0.36	10.37	0	0.36	20.01	4.21	0.11	0.18	100.23
P3 49725_021	G1	R	42.26	0.64	22.14	0.03	0.43	8.3	0.03	0.26	21.68	4.32	0.09	0.23	100.41
P3 49725_022	G1	C	42.4	0.62	22.18	0.03	0.58	8.29	0.03	0.25	21.65	4.29	0.08	0.2	100.6
P3 49725_023	G9A_Ti	R	42.01	0.59	21.76	0	1.15	7.95	0.02	0.25	21.71	4.33	0.1	0.24	100.11
P3 49725_024	G9A_Ti	C	41.91	0.6	21.64	0.03	1.17	7.99	0.02	0.27	21.69	4.32	0.07	0.24	99.95
P3 49725_025	G3	R	41.82	0.18	22.64	0	0.53	6.5	0.02	0.15	20.31	7.45	0.04	0.27	99.91
P3 49725_026	G3	C	42.32	0.19	22.85	0.02	0.6	6.42	0.03	0.15	20.51	7.44	0.05	0.24	100.82
P3 49725_027	G9A_Ti	R	41.9	0.63	21.53	0	1.13	7.88	0.02	0.27	21.77	4.33	0.11	0.26	99.83
P3 49725_028	G9A_Ti	C	41.93	0.63	21.59	0	1.11	7.97	0.02	0.25	21.67	4.35	0.09	0.24	99.85
P3 49725_029	G9A_Ti	R	41.89	0.59	21.5	0.03	1.11	7.89	0	0.26	21.37	4.33	0.1	0.18	99.25
P3 49725_030	G9A_Ti	C	41.97	0.59	21.49	0	1.17	7.85	0.02	0.26	21.33	4.34	0.09	0.16	99.27
P3 49725_031	G9A_Ti	R	41.81	0.67	21.36	0	1.23	8.31	0	0.25	21.11	4.3	0.11	0.18	99.33
P3 49725_032	G9A_Ti	C	41.89	0.63	21.4	0	1.22	8.2	0	0.27	21.07	4.28	0.11	0.15	99.22
P3 49725_033	G1	R	41.49	0.77	21.79	0.05	0.37	10.37	0	0.34	19.77	4.19	0.11	0.17	99.42
P3 49725_034	G1	C	41.43	0.74	21.62	0.03	0.34	10.4	0	0.34	19.73	4.21	0.12	0.19	99.15
P3 49725_035	G1	R	41.67	0.61	21.64	0.03	0.65	8.65	0.02	0.27	21.18	4.17	0.09	0.23	99.21
P3 49725_036	G1	C	41.97	0.63	21.87	0	0.62	8.62	0	0.28	21.05	4.16	0.08	0.15	99.43
P3 49725_037	G9A_Ti	R	41.98	0.62	20.98	0.02	1.76	7.53	0.03	0.26	21.58	4.44	0.07	0.18	99.45
P3 49725_038	G9A_Ti	C	42.01	0.67	21.05	0.04	1.79	7.58	0	0.26	21.42	4.5	0.06	0.14	99.52
P3 49725_039r	G9B_Ti	C	41.94	0.65	21.22	0.03	1.25	8.15	0.02	0.26	21.21	4.52	0.09	0.19	99.53

Appendix D: Garnet Xenocryst EPMA Data Tables

Appendix D.01 (continued): Mel kimberlite garnet EPMA analyses. Zones: C – core, R – rim.

Sample	*Class*	*Zone*	*SiO_2*	*TiO_2*	*Al_2O_3*	*V_2O_3*	*Cr_2O_3*	*FeO*	*NiO*	*MnO*	*MgO*	*CaO*	*Na_2O*	*O*	*Total*
P3 49725_040	G9B_Ti	R	42.06	0.66	21.29	0.05	1.27	8.14	0	0.26	21.04	4.51	0.09	0.13	99.5
P3 49725_041	G9A_Ti	C	41.9	0.63	20.93	0	1.83	7.59	0	0.26	21.54	4.46	0.07	0.18	99.39
P3 49725_042	G9A_Ti	R	41.8	0.62	20.95	0.05	1.75	7.63	0.02	0.25	21.39	4.45	0.06	0.17	99.14
P3 49725_043	G1	C	41.87	0.61	21.62	0.02	0.68	8.64	0	0.25	20.97	4.19	0.08	0.16	99.09
P3 49725_044	G1	R	41.93	0.59	21.72	0.04	0.64	8.68	0	0.28	21.04	4.16	0.09	0.18	99.35
P3 49725_045	G0	C	40.74	0.84	21.65	0	0.15	12.1	0.03	0.27	14.95	8.5	0.13	0.12	99.48
P3 49725_046	G0	R	40.61	0.87	21.71	0	0.16	12.11	0.03	0.27	14.87	8.48	0.14	0.12	99.37
P3 49725_047	G1	C	41.75	0.61	21.63	0.03	0.86	8.15	0	0.27	21.26	4.3	0.1	0.2	99.16
P3 49725_048	G1	R	41.68	0.56	21.53	0.04	0.86	8.23	0.02	0.25	21.14	4.3	0.08	0.19	98.88
P3 49725_049	G9A_Ti	C	42.18	0.59	21.59	0.04	1.1	7.93	0	0.26	21.28	4.34	0.09	0.13	99.53
P3 49725_050	G9A_Ti	R	41.99	0.59	21.46	0	1.16	7.84	0.02	0.25	21.26	4.32	0.09	0.14	99.12
P3 49725_051	G9A_Ti	C	41.38	0.52	21.29	0.02	2.11	7.5	0	0.34	20.93	4.63	0.09	0.17	98.98
P3 49725_052	G9A_Ti	R	41.48	0.53	21.49	0	1.8	7.47	0	0.35	21.13	4.52	0.08	0.17	99.02
P3 49725_053	G9A_Ti	C	41.62	0.59	21.36	0.02	1.12	7.9	0	0.27	21.33	4.34	0.09	0.21	98.85
P3 49725_054	G9A_Ti	R	41.95	0.62	21.47	0	1.13	7.9	0.03	0.28	21.49	4.33	0.09	0.2	99.49
P3 49725_055	G9A_Ti	C	41.8	0.58	21.52	0	1.18	7.9	0.02	0.26	21.32	4.36	0.08	0.18	99.2
P3 49725_056	G9A_Ti	R	41.82	0.57	21.47	0	1.19	7.89	0.02	0.27	21.02	4.35	0.1	0.13	98.83
P3 49725_057	G9A_Ti	C	41.9	0.6	21.6	0	1.11	7.89	0	0.25	21.38	4.33	0.09	0.18	99.33
P3 49725_058	G9A_Ti	R	41.65	0.55	21.37	0	1.12	7.89	0.03	0.26	21.47	4.36	0.1	0.24	99.04
P3 49725_059	G9A_Ti	C	42.02	0.51	20.61	0.04	2.41	7.14	0.02	0.23	21.75	4.31	0.05	0.14	99.23
P3 49725_060	G9A_Ti	R	41.9	0.48	20.63	0	2.45	7.13	0.02	0.26	21.65	4.31	0.06	0.14	99.03
P3 49725_061	G9A_Ti	C	41.85	0.64	21.37	0	1.09	7.89	0	0.26	21.26	4.37	0.08	0.16	98.97
P3 49725_062	G9A_Ti	R	41.67	0.63	21.22	0	1.16	7.85	0.02	0.26	21.33	4.37	0.1	0.2	98.81
P3 49725_063	G9A_Ti	C	41.81	0.5	20.63	0.03	2.4	7.09	0.02	0.26	21.87	4.3	0.06	0.19	99.16
P3 49725_064	G9A_Ti	R	42.04	0.47	20.58	0.03	2.41	7.07	0.03	0.26	21.71	4.32	0.07	0.14	99.13
P3 49725_065	G9A_Ti	C	41.99	0.62	21	0.03	1.77	7.56	0.02	0.26	21.33	4.44	0.08	0.13	99.23
P3 49725_066	G9A_Ti	R	41.58	0.64	20.74	0	1.76	7.53	0	0.26	21.37	4.47	0.07	0.18	98.6
P3 49725_067	G1	C	41.83	0.66	21.68	0.04	0.42	8.28	0.04	0.24	21.22	4.32	0.09	0.19	99.01
P3 49725_068	G1	R	41.72	0.64	21.61	0	0.45	8.23	0.02	0.25	21.26	4.32	0.08	0.21	98.79
P3 49725_069	G1	C	41.61	0.74	21.36	0.03	0.69	9.1	0	0.29	20.63	4.37	0.11	0.21	99.14
P3 49725_070	G1	R	41.54	0.73	21.28	0.04	0.7	9.08	0	0.3	20.61	4.36	0.12	0.22	98.98
P3 49725_071	G1	C	41.29	0.72	21.59	0.04	0.37	10.26	0	0.34	19.94	4.19	0.12	0.23	99.09
P3 49725_072	G1	R	41.28	0.77	21.59	0	0.37	10.16	0	0.35	19.95	4.21	0.12	0.22	99.02
P3 49736_001	G9A_Ti	R	41.74	0.58	20.96	0	1.92	7.63	0	0.29	21.7	4.43	0.07	0.24	99.56
P3 49736_002	G9A_Ti	C	41.54	0.58	20.73	0.03	1.92	7.63	0.02	0.25	21.75	4.4	0.07	0.27	99.19
P3 49736_003	G1	R	41	0.85	21.44	0.04	0.35	11.83	0	0.42	19.1	3.9	0.15	0.25	99.33
P3 49736_004	G1	C	40.95	0.81	21.56	0.03	0.34	11.83	0	0.41	19.09	3.89	0.14	0.25	99.3
P3 49736_005	G3_Na	R	40.58	0.63	21.63	0.03	0.09	13.72	0.02	0.32	15.9	6.06	0.15	0.2	99.33
P3 49736_006	G3_Na	C	40.61	0.64	21.68	0.03	0.11	13.73	0	0.32	16.22	6.05	0.14	0.25	99.78

Appendix D: Garnet Xenocryst EPMA Data Tables

Appendix D.01 (continued): Mel kimberlite garnet EPMA analyses. Zones: C – core, R – rim.

Sample	*Class*	*Zone*	*SiO_2*	*TiO_2*	*Al_2O_3*	*V_2O_3*	*Cr_2O_3*	*FeO*	*NiO*	*MnO*	*MgO*	*CaO*	*Na_2O*	*O*	*Total*
P3 49736_007	G9A_Ti	R	41.71	0.44	21.01	0.03	2.04	7.49	0	0.26	21.84	4.47	0.03	0.26	99.58
P3 49736_008	G9A_Ti	C	42.05	0.48	20.96	0.04	2.08	7.41	0	0.26	21.7	4.49	0.04	0.18	99.69
P3 49736_009	G9A_Ti	R	41.67	0.54	20.83	0.05	2	7.45	0	0.26	21.7	4.51	0.06	0.24	99.31
P3 49736_010	G9A_Ti	C	41.92	0.57	21.06	0.03	1.97	7.45	0.02	0.25	21.7	4.52	0.05	0.2	99.74
P3 49736_011	G3_Na	R	40.8	0.54	21.98	0.02	0	13.29	0	0.33	16.28	6.16	0.14	0.22	99.76
P3 49736_012	G3_Na	C	40.9	0.53	22.08	0.03	0.06	13.26	0.02	0.34	16.3	6.19	0.13	0.2	100.04
P3 49736_013	G9A	R	41.79	0.36	20.98	0.04	2.49	7.5	0.02	0.27	21.66	4.37	0.08	0.23	99.79
P3 49736_014	G9A	C	41.71	0.35	20.75	0.03	2.6	7.49	0.02	0.27	21.27	4.45	0.06	0.17	99.17
P3 49736_015	G1	R	41.66	0.61	21.95	0	0.71	9.17	0	0.34	20.59	4.47	0.12	0.24	99.86
P3 49736_016	G1	C	41.43	0.62	21.88	0.03	0.69	9.16	0	0.33	20.43	4.5	0.14	0.25	99.46
P3 49736_017	G9A	R	41.73	0.31	20.77	0.03	2.73	7.29	0	0.28	21.56	4.73	0.04	0.23	99.7
P3 49736_018	G9A	C	41.83	0.31	20.73	0.03	2.68	7.12	0	0.27	21.74	4.71	0.04	0.23	99.69
P3 49736_019	G9A_Ti	R	41.79	0.63	20.79	0	2.17	8.15	0.02	0.27	21.33	4.4	0.08	0.22	99.85
P3 49736_020	G9A_Ti	C	41.87	0.63	20.9	0.03	2.18	8.23	0	0.28	21.41	4.42	0.08	0.23	100.26
P3 49736_021	G3_Na	R	40.61	0.62	21.86	0.04	0.12	13.77	0	0.31	16.14	6.03	0.15	0.24	99.89
P3 49736_022	G3_Na	C	40.65	0.64	21.8	0	0.07	13.68	0	0.32	16.25	6.04	0.15	0.25	99.85
P3 49736_023	G9A_Ti	R	42	0.6	21.73	0.03	1.02	8.91	0	0.29	21.19	4.21	0.09	0.23	100.3
P3 49736_024	G9A_Ti	C	41.92	0.65	21.53	0	1.01	8.88	0	0.31	21.1	4.2	0.1	0.22	99.92
P3 49736_025	G9A_Ti	R	41.83	0.65	21.24	0.03	1.74	7.75	0.02	0.26	21.71	4.37	0.07	0.23	99.9
P3 49736_026	G9A_Ti	C	41.74	0.66	21	0.03	1.74	7.77	0	0.26	21.53	4.38	0.07	0.21	99.39
P3 49736_027	G9B_Ti	R	41.65	0.6	21.44	0.06	1.22	8.35	0	0.29	21.12	4.52	0.1	0.25	99.6
P3 49736_028	G9B_Ti	C	41.93	0.59	21.53	0	1.23	8.32	0	0.29	21.11	4.54	0.13	0.22	99.89
P3 49736_029	G1	R	41.79	0.65	21.49	0	0.95	8.95	0	0.29	21.08	4.17	0.1	0.23	99.7
P3 49736_030	G9A_Ti	C	41.18	0.64	21.25	0.03	1.08	8.99	0.02	0.29	21	4.18	0.1	0.3	99.06
P3 49736_031	G1	R	41.23	0.7	21.83	0	0.27	10.69	0	0.36	19.55	4.57	0.12	0.26	99.58
P3 49736_032	G1	C	41.17	0.69	21.95	0	0.26	10.62	0	0.38	19.54	4.55	0.12	0.26	99.54
P3 49736_033	G9A_Ti	R	41.7	0.52	21.56	0.03	1.34	8.25	0.02	0.3	21.04	4.44	0.1	0.21	99.51
P3 49736_034	G9A_Ti	C	41.7	0.53	21.5	0	1.33	8.31	0	0.3	21.17	4.42	0.09	0.24	99.59
P3 49736_035	G9B_Ti	R	41.75	0.54	21.57	0	1.3	8.14	0	0.29	21.14	4.57	0.1	0.22	99.62
P3 49736_036	G9B_Ti	C	41.63	0.55	21.39	0.03	1.28	8.1	0.02	0.3	21.19	4.57	0.13	0.27	99.46
P3 49736_037	G9B_Ti	R	41.86	0.51	21.64	0	1.24	8.22	0	0.32	21.01	4.49	0.1	0.19	99.58
P3 49736_038	G9A_Ti	C	41.97	0.51	21.67	0.04	1.32	8.29	0	0.31	21.03	4.47	0.12	0.19	99.92
P3 49736_039	G9A_Ti	R	41.73	0.61	21.5	0.03	1.19	8.86	0	0.31	20.94	4.18	0.1	0.21	99.66
P3 49736_040	G9A_Ti	C	41.62	0.61	21.41	0.03	1.11	8.84	0	0.3	21.02	4.18	0.1	0.24	99.46
P3 49736_041	G1	R	41.66	0.65	21.73	0.03	0.91	8.77	0	0.28	21.08	4.23	0.11	0.24	99.69
P3 49736_042	G1	C	41.56	0.64	21.52	0.04	0.86	8.76	0.03	0.29	21.05	4.22	0.1	0.24	99.31
P3 49736_043	G1	R	42.09	0.66	21.6	0.03	0.67	7.9	0.03	0.23	21.85	4.11	0.06	0.19	99.42
P3 49736_044	G1	C	41.8	0.64	21.45	0.03	0.66	7.9	0.03	0.22	22.02	4.09	0.07	0.27	99.18
P3 49736_045	G1	R	41.63	0.6	21.82	0.04	0.66	8.19	0	0.25	21.51	4.31	0.09	0.27	99.37

Appendix D: Garnet Xenocryst EPMA Data Tables

Appendix D.01 (continued): Mel kimberlite garnet EPMA analyses. Zones: C – core, R – rim.

Sample	*Class*	*Zone*	*SiO_2*	*TiO_2*	*Al_2O_3*	*V_2O_3*	*Cr_2O_3*	*FeO*	*NiO*	*MnO*	*MgO*	*CaO*	*Na_2O*	*O*	*Total*
P3 49736_046	G1	C	41.76	0.63	21.59	0	0.72	8.16	0	0.26	21.4	4.35	0.07	0.22	99.16
P3 49736_047	G9A_Ti	R	41.63	0.58	20.66	0	2	7.43	0.03	0.25	21.63	4.47	0.07	0.22	98.97
P3 49736_048	G9A_Ti	C	41.75	0.53	20.86	0.03	1.95	7.48	0.02	0.26	21.45	4.4	0.05	0.16	98.94
P3 49736_049	G1	R	41.99	0.59	21.43	0	0.63	7.94	0.03	0.22	21.81	4.07	0.06	0.21	98.98
P3 49736_050	G1	C	41.98	0.57	21.46	0.03	0.66	7.84	0.02	0.21	21.94	4.04	0.07	0.22	99.04
P3 49736_051	G9A_Ti	R	41.47	0.68	20.46	0.05	2.09	8.33	0	0.29	20.94	4.42	0.11	0.22	99.06
P3 49736_052	G9A_Ti	C	41.36	0.72	20.42	0.03	2.12	8.38	0.02	0.28	20.87	4.41	0.1	0.21	98.92
P3 49736_053	G1	R	41.79	0.46	21.75	0	0.99	8.38	0.02	0.32	20.46	5.01	0.1	0.19	99.47
P3 49736_054	G9B_Ti	C	41.73	0.48	21.68	0	1.01	8.38	0	0.31	20.23	5	0.12	0.16	99.1
P3 49736_055	G1	R	41.48	0.42	21.69	0.02	0.87	8.07	0	0.29	20.32	5.18	0.12	0.2	98.66
P3 49736_056	G1	C	41.45	0.47	21.65	0	0.92	8.1	0.02	0.3	20.49	5.19	0.12	0.24	98.95
P3 49736_057	G9A_Ti	R	41.26	0.68	20.44	0	2.04	8.44	0	0.3	21.01	4.41	0.1	0.27	98.95
P3 49736_058	G9A_Ti	C	41.43	0.72	20.36	0.03	2.13	8.37	0	0.28	20.82	4.42	0.1	0.19	98.85
P3 49736_059	G9B_Ti	R	41.55	0.5	21.48	0	1.25	8.08	0	0.29	21.05	4.62	0.13	0.25	99.2
P3 49736_060	G9B_Ti	C	41.58	0.46	21.62	0.02	1.17	8.14	0	0.28	21.03	4.65	0.1	0.25	99.3
P3 49736_061	G9A_Ti	R	41.25	0.42	20.67	0.05	2.37	7.75	0	0.27	21.38	4.51	0.04	0.27	98.98
P3 49736_062	G9A_Ti	C	41.45	0.63	20.71	0	2.2	7.78	0	0.25	21.09	4.5	0.06	0.17	98.84
P3 49736_063	G1	R	41.28	0.66	21.78	0.03	0.42	9.59	0	0.33	20.33	4.3	0.13	0.26	99.11
P3 49736_064	G1	C	41.29	0.62	21.76	0.03	0.53	9.47	0	0.32	20.34	4.38	0.13	0.26	99.13
P3 49736_065	G9A_Ti	R	41.12	0.64	21.03	0	1.7	8.76	0	0.3	20.67	4.16	0.13	0.23	98.74
P3 49736_066	G9A_Ti	C	41.48	0.66	21.14	0.03	1.74	8.66	0	0.31	20.73	4.3	0.14	0.21	99.4
P3 49736_067	G9A_Ti	R	41.98	0.49	20.94	0.04	2.09	7.4	0.02	0.27	21.65	4.44	0.05	0.17	99.54
P3 49736_068	G9A_Ti	C	41.5	0.52	20.72	0	2.01	7.34	0	0.27	21.43	4.46	0.07	0.2	98.52
P3 49736_069	G1	R	41.48	0.64	21.72	0	0.71	8.03	0.02	0.26	21.5	4.3	0.08	0.26	99
P3 49736_070	G1	C	41.47	0.59	21.67	0	0.69	8.05	0	0.26	21.25	4.3	0.08	0.22	98.58
P3 49736_071	G9A_Ti	R	41.44	0.62	20.62	0	2	8.01	0	0.29	21.34	4.17	0.08	0.22	98.79
P3 49736_072	G9A_Ti	C	41.87	0.66	20.8	0	2	8.04	0	0.29	21.32	4.23	0.09	0.17	99.47
P3 49736_073	G1	R	41.29	0.45	21.8	0.03	0.6	8.42	0.02	0.32	20.68	5.11	0.12	0.33	99.17
P3 49736_074	G1	C	41.47	0.47	21.81	0	0.54	8.44	0	0.32	20.31	5.08	0.1	0.22	98.76
P3 49736_075	G1	R	41.29	0.47	21.64	0	0.64	9.12	0	0.34	19.59	5.62	0.11	0.26	99.08
P3 49736_076	G1	C	41.22	0.47	21.68	0.04	0.62	9.08	0	0.35	19.67	5.55	0.11	0.27	99.06
P3 49736_077	G9A_Ti	R	41.22	0.66	21.24	0	1.02	8.83	0.02	0.28	20.85	4.21	0.12	0.26	98.71
P3 49736_078	G9A_Ti	C	41.54	0.65	21.46	0	1.08	8.78	0	0.31	20.77	4.23	0.11	0.2	99.13
P3 49736_079	G1	R	40.87	0.67	21.51	0	0.26	10.54	0	0.37	19.38	4.57	0.13	0.27	98.57
P3 49736_080	G1	C	41	0.66	21.79	0	0.22	10.66	0	0.36	19.25	4.55	0.13	0.24	98.86
P3 49736_081	G9A_Ti	R	41.57	0.48	20.88	0	2.03	7.38	0.02	0.26	21.56	4.45	0.06	0.21	98.9
P3 49736_082	G9A_Ti	C	41.93	0.45	20.97	0.04	2.09	7.38	0	0.26	21.72	4.46	0.04	0.19	99.53
P3 49736_083	G1	R	41.27	0.52	21.73	0	0.65	9	0.01	0.36	19.61	5.62	0.11	0.25	99.13
P3 49736_084	G1	C	41.38	0.5	21.8	0.03	0.66	9.02	0	0.34	19.58	5.59	0.1	0.22	99.22

Appendix D: Garnet Xenocryst EPMA Data Tables

Appendix D.01 (continued): Mel kimberlite garnet EPMA analyses. Zones: C – core, R – rim.

Sample	*Class*	*Zone*	*SiO_2*	*TiO_2*	*Al_2O_3*	*V_2O_3*	*Cr_2O_3*	*FeO*	*NiO*	*MnO*	*MgO*	*CaO*	*Na_2O*	*O*	*Total*
P3 49736_085	G1	R	41.83	0.65	21.68	0	0.8	8.18	0.02	0.27	21.45	4.38	0.09	0.24	99.59
P3 49736_086	G1	C	41.43	0.64	21.6	0.04	0.74	8.15	0.02	0.25	21.26	4.4	0.07	0.24	98.84
P3 49736_087	G9A_Ti	R	41.47	0.52	21.5	0	1.04	8.54	0.02	0.3	20.91	4.29	0.08	0.22	98.89
P3 49736_088	G9A_Ti	C	41.36	0.52	21.37	0	1.04	8.57	0	0.29	20.82	4.28	0.1	0.22	98.57
P3 49736_089	G1	R	41.53	0.68	21.45	0.04	0.91	8.67	0.02	0.3	21.07	4.22	0.12	0.25	99.26
P3 49736_090	G1	C	41.28	0.69	21.34	0.03	0.89	8.79	0	0.3	21.25	4.22	0.11	0.33	99.23
P3 49736_091	G1	R	41.53	0.6	21.44	0.05	0.91	8.56	0	0.31	20.83	4.26	0.1	0.19	98.78
P3 49736_092	G1	C	41.33	0.69	21.24	0	0.89	8.64	0	0.29	20.95	4.22	0.09	0.23	98.57
P3 49736_093	G9A_Ti	R	41.57	0.7	21.2	0	1.29	8.18	0	0.25	21.22	4.34	0.12	0.23	99.1
P3 49736_094	G9A_Ti	C	41.61	0.7	21.14	0.03	1.3	8.2	0	0.28	21.12	4.35	0.11	0.2	99.04
P3 49736_095	G9A_Ti	R	41.31	0.47	20.85	0.04	2.45	8.33	0.02	0.32	20.64	4.37	0.1	0.19	99.09
P3 49736_096	G9A_Ti	C	41.48	0.44	20.95	0	2.45	8.5	0	0.32	20.62	4.39	0.11	0.19	99.45
P3 49736_097	G9B_Ti	R	41.44	0.59	21.29	0.03	1.26	8.25	0	0.29	20.77	4.54	0.11	0.2	98.77
P3 49736_098	G9B_Ti	C	41.3	0.58	21.19	0	1.3	8.22	0	0.29	20.82	4.52	0.11	0.23	98.56
P3 49736_099	G1	R	41.65	0.63	21.62	0.02	0.68	8.06	0	0.27	21.37	4.17	0.11	0.22	98.8
P3 49736_100	G1	C	41.57	0.51	21.51	0	0.98	7.94	0.02	0.28	21.1	4.22	0.09	0.17	98.39
P3 49736_101	G9A_Ti	R	41.53	0.52	20.66	0.03	2.18	7.43	0.02	0.27	21.41	4.49	0.07	0.2	98.81
P3 49736_102	G9A_Ti	C	41.48	0.49	20.68	0.03	2.15	7.4	0	0.26	21.22	4.5	0.06	0.17	98.44
P3 49736_103	G1	R	41.51	0.64	21.43	0.04	0.96	8.8	0.02	0.29	20.82	4.22	0.11	0.21	99.05
P3 49736_104	G1	C	41.43	0.63	21.37	0.04	0.99	8.78	0	0.29	20.69	4.21	0.1	0.19	98.72
P3 49736_105	G9A_Ti	R	41.7	0.67	21.02	0.04	1.79	7.75	0	0.25	21.39	4.4	0.07	0.18	99.26
P3 49736_106	G9A_Ti	C	41.66	0.65	20.87	0.03	1.78	7.69	0	0.26	21.49	4.4	0.08	0.21	99.12
P3 49736_107	G9B_Ti	R	41.58	0.51	21.51	0	1.31	8.09	0	0.3	20.85	4.58	0.11	0.2	99.04
P3 49736_108	G9B_Ti	C	41.66	0.55	21.42	0	1.24	8.11	0	0.3	20.89	4.59	0.09	0.18	99.03
P3 49736_109	G11	R	41.46	0.34	19.04	0.04	4.59	6.51	0	0.27	21.23	5.27	0.03	0.19	98.97
P3 49736_110	G11	C	41.37	0.38	19.1	0.03	4.64	6.46	0	0.29	21.09	5.28	0.04	0.17	98.85
P3 49736_111	G1	R	41.94	0.69	22.27	0	0.14	8.24	0	0.24	21.13	4.47	0.06	0.16	99.34
P3 49736_112	G1	C	41.69	0.69	22.08	0.03	0.16	8.27	0.03	0.27	21.11	4.47	0.06	0.19	99.05
P3 49736_113	G1	R	41.44	0.65	21.75	0.03	0.64	8.24	0	0.27	21	4.3	0.1	0.2	98.62
P3 49736_114	G1	C	41.21	0.67	21.48	0.05	0.64	8.16	0	0.26	20.98	4.33	0.08	0.21	98.07
P3 49736_115	G9A	R	41.31	0.28	20	0.03	3.64	6.7	0	0.27	21.01	5	0.04	0.15	98.43
P3 49736_116	G9A	C	41.4	0.26	20.15	0	3.51	6.76	0	0.26	21.24	5.01	0.02	0.18	98.79
P3 49736_117	G1	R	41.35	0.64	21.42	0.02	0.92	8.94	0	0.31	20.6	4.19	0.11	0.2	98.7
P3 49736_118	G1	C	41.68	0.62	21.5	0	0.98	8.89	0	0.29	20.66	4.23	0.11	0.17	99.13
P3 49736_119	G9A_Ti	R	42.05	0.45	21.18	0	1.84	7.31	0	0.26	21.9	4.1	0.06	0.17	99.32
P3 49736_120	G9A_Ti	C	42	0.45	21.15	0	1.86	7.25	0.02	0.24	21.88	4.11	0.06	0.16	99.18
P3 49746_001	G1	R	41.96	0.64	21.8	0	0.55	9.21	0.03	0.29	20.91	4.5	0.12	0.27	100.28
P3 49746_002	G1	C	42.09	0.64	21.87	0	0.51	9.24	0	0.31	20.79	4.49	0.13	0.23	100.3
P3 49746_003	G9A_Ti	R	41.86	0.62	21.33	0	1.31	8	0.02	0.25	21.6	4.37	0.09	0.25	99.7

Appendix D: Garnet Xenocryst EPMA Data Tables

Appendix D.01 (continued): Mel kimberlite garnet EPMA analyses. Zones: C – core, R – rim.

Sample	*Class*	*Zone*	*SiO_2*	*TiO_2*	*Al_2O_3*	*V_2O_3*	*Cr_2O_3*	*FeO*	*NiO*	*MnO*	*MgO*	*CaO*	*Na_2O*	*O*	*Total*
P3 49746_004	G9A_Ti	C	41.9	0.58	21.4	0	1.21	8.06	0.02	0.26	21.69	4.35	0.1	0.27	99.84
P3 49746_005	G9A_Ti	R	41.83	0.81	20.92	0	1.43	8.11	0.03	0.25	21.65	4.4	0.13	0.27	99.83
P3 49746_006	G9A_Ti	C	41.86	0.86	20.82	0.05	1.4	8.13	0.02	0.26	21.46	4.41	0.11	0.22	99.6
P3 49746_007	G3	R	36.98	0	21.29	0	0	34.12	0	3.02	3.91	0.94	0	0.13	100.39
P3 49746_008	CRST	C	35.94	0	20.63	0	0	33.65	0	4.56	2.93	0.96	0	0.2	98.87
P3 49746_009	G1	R	41.56	0.76	21.62	0	0.59	9.33	0	0.29	20.82	4.29	0.1	0.26	99.62
P3 49746_010	G1	C	41.54	0.78	21.53	0.03	0.6	9.39	0.02	0.3	20.73	4.28	0.11	0.25	99.56
P3 49746_011	G9B	R	40.87	0	20.36	0	4.44	8.64	0	0.54	18.72	6	0	0.16	99.73
P3 49746_012	G9B	C	40.96	0.02	20.31	0.03	4.36	8.94	0	0.55	18.58	5.91	0	0.14	99.8
P3 49746_013	G3	R	36.81	0	21.25	0	0	33.59	0	2.66	4.36	0.94	0	0.14	99.75
P3 49746_014	CRST	C	36.95	0	21.27	0	0	33.81	0	3.31	3.79	0.93	0	0.1	100.16
P3 49746_015	G9B	R	41.12	0.11	21.21	0	3.16	8.84	0	0.54	19.43	5.08	0	0.15	99.64
P3 49746_016	G9A	C	41.3	0.07	21.28	0	3.13	8.86	0	0.57	19.3	5	0	0.09	99.6
P3 49746_017	G9A	R	41.11	0.29	20.93	0.03	2.64	10.05	0	0.36	19.35	4.51	0.05	0.17	99.49
P3 49746_018	G9A	C	40.98	0.27	20.9	0.03	2.5	10.04	0.02	0.4	19.19	4.5	0.06	0.16	99.05
P3 49746_019	G1	R	41.44	0.76	21.56	0.03	0.56	9.3	0	0.31	20.75	4.2	0.11	0.25	99.27
P3 49746_020	G1	C	41.31	0.8	21.23	0.02	0.61	9.34	0.02	0.29	20.45	4.24	0.11	0.21	98.63
P3 49746_021	G9A_Ti	R	41.53	0.8	20.57	0.05	1.59	8.1	0	0.26	21.35	4.35	0.11	0.24	98.95
P3 49746_022	G9A_Ti	C	41.55	0.81	20.71	0.04	1.55	8.16	0.02	0.27	21.45	4.37	0.13	0.28	99.34
P3 49746_023	G0	R	40.54	0.66	21.87	0.03	0.06	11.15	0.02	0.26	16.35	7.73	0.17	0.25	99.09
P3 49746_024	G0	C	40.69	0.68	22.03	0	0.07	11.04	0.02	0.25	16.19	7.77	0.16	0.18	99.08
P3 49746_025	G9A_Ti	R	41.52	0.66	21.12	0.03	1.52	8.29	0	0.27	21.23	4.19	0.09	0.22	99.14
P3 49746_026	G9A_Ti	C	41.44	0.63	21.18	0.02	1.52	8.31	0.02	0.26	21.27	4.18	0.08	0.24	99.15
P3 49746_027	G3	R	36.84	0	21.13	0	0	33.23	0	2.49	4.48	1.01	0	0.11	99.29
P3 49746_028	CRST	C	36.44	0	20.86	0	0	33.66	0	4.06	3.31	0.91	0	0.14	99.38
P3 49746_029	G9B	R	40.98	0.06	21.2	0.03	3.1	8.43	0	0.44	19.52	5.11	0	0.13	99
P3 49746_030	G9B	C	41.15	0.07	21.11	0	3.14	8.38	0	0.43	19.47	5.14	0	0.1	98.99
P3 49746_031	G1	R	41.4	0.78	21.36	0.04	0.59	9.26	0	0.3	20.6	4.21	0.12	0.23	98.89
P3 49746_032	G1	C	41.43	0.73	21.68	0.04	0.55	9.25	0.02	0.29	20.48	4.17	0.09	0.18	98.91
P3 49746_033	G1	R	41.7	0.51	21.77	0.03	0.91	8.05	0	0.28	21.44	4.07	0.1	0.21	99.07
P3 49746_034	G1	C	41.76	0.55	21.66	0	0.95	8.09	0.02	0.28	21.32	4.07	0.1	0.18	98.98
P3 49746_035	G1	R	41.51	0.61	21.81	0.04	0.56	9.07	0.02	0.29	20.55	4.44	0.11	0.23	99.24
P3 49746_036	G1	C	41.56	0.67	21.68	0	0.57	9.17	0	0.31	20.44	4.44	0.08	0.19	99.11
P3 49746_037	G1	R	41.75	0.64	21.83	0.04	0.56	9.12	0.02	0.3	20.56	4.45	0.13	0.21	99.61
P3 49746_038	G1	C	41.51	0.64	21.67	0	0.51	9.1	0.02	0.3	20.41	4.44	0.11	0.2	98.91
P3 49746_039	G1	R	41.44	0.78	21.49	0.03	0.59	9.3	0	0.28	20.66	4.22	0.11	0.23	99.13
P3 49746_040	G1	C	41.57	0.8	21.45	0.04	0.59	9.31	0	0.3	20.57	4.24	0.1	0.2	99.17
P3 49746_041	G1	R	41.64	0.75	21.71	0.04	0.57	9.33	0	0.3	20.68	4.16	0.11	0.21	99.5
P3 49746_042	G1	C	41.56	0.74	21.45	0.05	0.55	9.32	0.03	0.3	20.64	4.16	0.1	0.21	99.11

Appendix D: Garnet Xenocryst EPMA Data Tables

Appendix D.01 (continued): Mel kimberlite garnet EPMA analyses. Zones: C – core, R – rim.

Sample	*Class*	*Zone*	*SiO_2*	*TiO_2*	*Al_2O_3*	*V_2O_3*	*Cr_2O_3*	*FeO*	*NiO*	*MnO*	*MgO*	*CaO*	*Na_2O*	*O*	*Total*
P3 49746_043	G1	R	41.37	0.71	21.84	0	0.29	10.06	0	0.35	20.02	4.43	0.11	0.24	99.42
P3 49746_044	G1	C	41.45	0.69	21.85	0.03	0.34	10.01	0	0.36	20.18	4.45	0.13	0.27	99.76
P3 49746_045	G1	R	41.75	0.61	21.78	0	0.55	9.18	0.02	0.32	20.55	4.47	0.11	0.22	99.56
P3 49746_046	G1	C	41.7	0.67	21.75	0	0.53	9.22	0.02	0.28	20.76	4.45	0.1	0.25	99.73
P3 49746_047	G1	R	41.67	0.67	21.75	0.03	0.54	9.17	0.02	0.31	20.69	4.47	0.12	0.25	99.69
P3 49746_048	G1	C	41.74	0.67	21.85	0	0.51	9.17	0	0.32	20.47	4.46	0.12	0.2	99.51
P3 49746_049	G11	R	41.29	0.38	18.35	0	6.68	6.39	0	0.34	21.19	4.83	0.08	0.15	99.68
P3 49746_050	G11	C	41.27	0.37	18.45	0.04	6.57	6.31	0	0.34	21.21	4.74	0.06	0.13	99.49
P3 49746_051	G1	R	41.52	0.64	22.13	0.04	0.28	10.3	0	0.37	19.5	4.86	0.11	0.22	99.97
P3 49746_052	G1	C	41.4	0.69	22.07	0.06	0.2	10.21	0	0.36	19.34	4.88	0.14	0.2	99.55
P3 49746_053	G1	R	41.78	0.8	21.72	0	0.6	9.33	0	0.29	20.81	4.22	0.1	0.21	99.86
P3 49746_054	G1	C	41.75	0.76	21.67	0.03	0.61	9.31	0.03	0.31	20.7	4.21	0.1	0.2	99.68
P3 49746_055	G9A_Ti	R	42.01	0.44	20.84	0.04	2.16	7.26	0	0.24	21.85	4.45	0.05	0.2	99.54
P3 49746_056	G9A_Ti	C	41.96	0.44	20.97	0.04	2.12	7.21	0.02	0.26	21.76	4.44	0.07	0.19	99.48
P3 49746_057	G1	R	41.58	0.72	21.72	0.04	0.57	9.31	0.02	0.29	20.98	4.18	0.08	0.27	99.76
P3 49746_058	G1	C	41.87	0.76	21.7	0	0.57	9.32	0	0.29	20.78	4.22	0.11	0.2	99.82
P3 49746_059	G9A	R	41.55	0.21	20.1	0.02	4.36	6.5	0	0.33	21.63	4.81	0.03	0.2	99.74
P3 49746_060	G9A	C	41.85	0.18	20.22	0.05	4.4	6.48	0.02	0.34	21.43	4.8	0.02	0.12	99.91
P3 49746_061	G9A_Ti	R	41.87	0.86	20.87	0.02	1.52	8.18	0.02	0.25	21.4	4.46	0.11	0.22	99.78
P3 49746_062	G9A_Ti	C	41.53	0.82	20.52	0.04	1.54	8.11	0.03	0.25	21.35	4.47	0.11	0.26	99.03
P3 49746_063	G9A_Ti	R	41.73	0.81	20.87	0.06	1.61	8.17	0.02	0.25	21.38	4.45	0.13	0.25	99.73
P3 49746_064	G9A_Ti	C	41.88	0.86	20.8	0.05	1.55	8.14	0.03	0.24	21.37	4.45	0.12	0.22	99.71
P3 49746_065	G9A_Ti	R	41.68	0.82	20.8	0.06	1.33	8.15	0.02	0.25	21.48	4.41	0.13	0.27	99.4
P3 49746_066	G9A_Ti	C	42.11	0.85	21.12	0.04	1.33	8.1	0.02	0.25	21.76	4.39	0.13	0.25	100.35
P3 49746_067	G1	R	41.69	0.76	21.68	0.04	0.59	9.4	0	0.29	20.73	4.19	0.11	0.22	99.7
P3 49746_068	G1	C	41.93	0.73	21.84	0.04	0.6	9.32	0	0.31	20.88	4.22	0.09	0.21	100.17
P3 49746_069	G9A_Ti	R	41.9	0.84	20.8	0.03	1.61	8.16	0	0.23	21.4	4.47	0.11	0.22	99.77
P3 49746_070	G9A_Ti	C	41.92	0.86	20.74	0.04	1.61	8.16	0.03	0.25	21.62	4.45	0.12	0.26	100.06
P3 49746_071	G1	R	41.63	0.66	21.69	0.02	0.53	9.1	0	0.31	20.69	4.45	0.13	0.25	99.46
P3 49746_072	G1	C	41.68	0.66	21.77	0.02	0.54	9.12	0.02	0.29	20.8	4.46	0.1	0.25	99.71
P3 49746_073	G9A_Ti	R	41.78	0.82	20.93	0.06	1.32	8.23	0	0.26	21.43	4.37	0.13	0.24	99.57
P3 49746_074	G9A_Ti	C	41.64	0.82	20.92	0.05	1.37	8.12	0.02	0.25	21.59	4.37	0.13	0.29	99.57
P3 49746_075	G9B	R	40.86	0	20.28	0	4.25	8.88	0	0.51	18.71	5.95	0	0.17	99.61
P3 49746_076	G9B	C	40.82	0.05	20.25	0	4.32	8.78	0	0.54	18.46	5.91	0	0.11	99.24
P3 49746_077	G1	R	41.48	0.72	21.57	0.04	0.61	9.36	0.02	0.3	20.8	4.24	0.11	0.28	99.53
P3 49746_078	G1	C	41.73	0.74	21.65	0.03	0.58	9.4	0.02	0.31	20.69	4.24	0.08	0.21	99.68
P3 49746_079	G9A_Ti	R	41.96	0.83	20.81	0.06	1.45	8.19	0	0.27	21.54	4.43	0.12	0.24	99.9
P3 49746_080	G9A_Ti	C	42.06	0.86	20.94	0	1.45	8.19	0.02	0.26	21.49	4.44	0.13	0.22	100.06
P3 49746_081	G9A	R	41.14	0.25	21.17	0.05	2.4	10.06	0	0.39	19.61	4.46	0.05	0.21	99.79

Appendix D: Garnet Xenocryst EPMA Data Tables

Appendix D.01 (continued): Mel kimberlite garnet EPMA analyses. Zones: C – core, R – rim.

Sample	*Class*	*Zone*	*SiO_2*	*TiO_2*	*Al_2O_3*	*V_2O_3*	*Cr_2O_3*	*FeO*	*NiO*	*MnO*	*MgO*	*CaO*	*Na_2O*	*O*	*Total*
P3 49746_082	G9A	C	41.21	0.27	21.32	0	2.26	10.02	0	0.38	19.67	4.44	0.04	0.2	99.81
P3 49746_083	G1	R	41.85	0.67	21.82	0	0.55	9.19	0	0.32	20.79	4.48	0.1	0.24	100.01
P3 49746_084	G1	C	42.12	0.65	21.95	0	0.55	9.19	0	0.29	20.78	4.48	0.11	0.2	100.32
P3 49746_085	G1	R	42.09	0.68	21.99	0.03	0.6	8.42	0.02	0.26	21.28	4.37	0.06	0.17	99.97
P3 49746_086	G1	C	41.95	0.66	21.91	0.04	0.68	8.46	0	0.25	21.33	4.39	0.06	0.21	99.94
P3 49746_087	G9A_Ti	R	41.96	0.83	20.97	0	1.33	8.12	0	0.24	21.59	4.42	0.13	0.25	99.84
P3 49746_088	G9A_Ti	C	41.98	0.82	20.95	0.03	1.29	8.13	0.02	0.25	21.56	4.41	0.11	0.23	99.78
P3 49746_089	G1	R	41.78	0.82	21.48	0.03	0.63	9.38	0.02	0.31	20.75	4.26	0.1	0.22	99.78
P3 49746_090	G1	C	41.57	0.76	21.53	0.03	0.55	9.36	0	0.29	20.96	4.23	0.12	0.29	99.69
P3 49746_091	G9A_Ti	R	41.78	0.83	20.66	0	1.48	8.15	0	0.26	21.46	4.44	0.11	0.24	99.41
P3 49746_092	G9A_Ti	C	41.97	0.81	20.89	0.06	1.53	8.24	0.03	0.25	21.52	4.44	0.12	0.24	100.1
P3 49746_093	G1	R	41.67	0.68	21.67	0	0.63	8.97	0	0.29	20.9	4.44	0.11	0.25	99.61
P3 49746_094	G1	C	41.93	0.66	22.05	0.04	0.52	8.99	0.02	0.31	20.83	4.46	0.09	0.21	100.11
P3 49746_095	G1	R	41.7	0.8	21.64	0.04	0.59	9.4	0	0.3	20.87	4.22	0.09	0.24	99.89
P3 49746_096	G1	C	41.7	0.77	21.62	0.04	0.61	9.39	0.02	0.29	20.85	4.24	0.1	0.24	99.87
P3 49746_097	G1	R	41.8	0.66	21.73	0	0.52	9.18	0	0.31	20.6	4.48	0.12	0.21	99.61
P3 49746_098	G1	C	41.9	0.66	21.81	0	0.51	9.18	0	0.3	20.69	4.48	0.12	0.22	99.87
P3 49746_099	G1	R	41.73	0.78	21.86	0	0.6	9.3	0	0.29	21	4.18	0.11	0.25	100.1
P3 49746_100	G1	C	41.89	0.76	21.86	0.03	0.58	9.35	0	0.3	21.04	4.17	0.11	0.25	100.34
P3 49746_101	G9A_Ti	R	41.94	0.62	20.99	0	1.53	8.22	0	0.27	21.05	4.18	0.07	0.11	98.98
P3 49746_102	G9A_Ti	C	42.01	0.64	21.32	0.03	1.52	8.31	0	0.27	21.29	4.22	0.07	0.16	99.84
P3 49746_103	G9B	R	41.02	0.03	20.31	0	4.45	9.08	0	0.61	18.27	6.2	0	0.13	100.1
P3 49746_104	G9B	C	41.14	0	20.44	0	4.17	9.26	0	0.67	18.06	5.95	0	0.06	99.75
P3 49746_105	G1	R	41.8	0.66	21.75	0.03	0.49	9.12	0	0.31	20.7	4.49	0.1	0.22	99.67
P3 49746_106	G1	C	41.75	0.67	21.72	0	0.55	9.09	0.02	0.28	20.49	4.49	0.1	0.18	99.34

Appendix D: Garnet Xenocryst EPMA Data Tables

Appendix D.02: Dharma kimberlite garnet EPMA analyses. Zones: C – core, R – rim.

Sample	*Class*	*Zone*	*SiO_2*	*TiO_2*	*Al_2O_3*	*V_2O_3*	*Cr_2O_3*	*FeO*	*NiO*	*MnO*	*MgO*	*CaO*	*Na_2O*	*O*	*Total*
D104 set1_67	G9A	C	41.27	0.23	21.91	0.02	1.71	9.57	0	0.37	19.75	4.52	0	0.16	99.51
D104 set1_68	G9A	R	41.35	0.23	22.09	0.03	1.69	9.44	0	0.37	19.64	4.52	0.02	0.12	99.5
D104 set1_69	G9A_Ti	C	41.96	0.35	21.72	0.02	1.48	6.72	0	0.28	21.96	4.5	0.03	0.17	99.19
D104 set1_70	G9A_Ti	R	41.98	0.35	21.85	0.03	1.5	6.77	0.02	0.29	22.02	4.51	0.05	0.21	99.58
D104 set1_71	G9A	C	41.23	0.23	21.81	0.04	1.6	9.37	0	0.38	19.8	4.52	0	0.15	99.13
D104 set1_72	G9A	R	41.4	0.26	22.07	0.04	1.71	9.3	0	0.36	19.81	4.5	0.04	0.13	99.62
D104 set1_73	G9A_Ti	C	41.45	0.41	20.03	0.04	3.57	7.59	0	0.31	20.99	4.73	0.06	0.19	99.37
D104 set1_74	G9A_Ti	R	41.38	0.4	20.15	0	3.62	7.52	0	0.32	21.07	4.72	0.03	0.2	99.41
D104 set1_75	G9A_Ti	C	41.64	0.63	20.22	0	2.81	7.5	0	0.3	21.13	4.89	0.05	0.18	99.35
D104 set1_76	G9A_Ti	R	41.69	0.62	20.29	0.03	2.9	7.53	0	0.3	21.14	4.91	0.06	0.19	99.66
D104 set1_77	G9A	C	41.4	0.25	22.07	0.03	1.76	9.44	0	0.37	19.83	4.56	0.03	0.16	99.9
D104 set1_78	G9A	R	41.29	0.24	22.15	0.04	1.76	9.4	0	0.39	19.67	4.57	0.03	0.14	99.68
D104 set1_79	G9A_Ti	C	41.66	0.6	20.16	0.04	3.29	7.53	0	0.3	20.98	4.93	0.06	0.16	99.71
D104 set1_80	G9A_Ti	R	41.69	0.57	20.08	0.04	3.28	7.47	0	0.28	20.76	4.91	0.07	0.11	99.26
D104 set1_81	G9A_Ti	C	42.05	0.37	21.83	0.03	1.48	6.72	0	0.29	21.97	4.5	0.06	0.18	99.48
D104 set1_82	G9A_Ti	R	42.17	0.38	21.75	0.04	1.52	6.69	0.02	0.27	22.02	4.51	0.04	0.16	99.57
D104 set1_83	G9A	C	41.23	0.19	22.32	0	1.4	9.54	0	0.32	20.01	3.93	0.04	0.14	99.12
D104 set1_84	G9A	R	41.32	0.21	22.32	0.05	1.41	9.55	0	0.31	20.22	3.96	0.05	0.18	99.58
D104 set1_85	G9A	C	41.41	0.23	22.28	0	1.52	9.35	0	0.37	19.94	4.49	0.03	0.16	99.78
D104 set1_86	G9A	R	41.47	0.22	22.53	0.03	1.59	9.38	0	0.35	19.89	4.54	0.04	0.16	100.2
D104 set1_87	G9A	C	41.43	0.23	22.22	0.03	1.67	9.4	0	0.39	19.84	4.54	0.03	0.15	99.93
D104 set1_88	G9A	R	41.41	0.21	22.36	0.03	1.64	9.41	0	0.37	19.86	4.52	0.04	0.16	100.01
D104 set1_89	G9B_Ti	C	41.59	0.62	20.91	0.03	2.57	8.16	0	0.32	20.74	4.88	0.07	0.2	100.09
D104 set1_90	G9B_Ti	R	41.7	0.6	20.93	0.05	2.51	8.22	0	0.34	20.78	4.87	0.07	0.2	100.27
D104 set1_91	G9A	C	41.35	0.25	22.06	0.03	1.83	9.43	0	0.39	19.71	4.6	0.03	0.14	99.82
D104 set1_92	G9A	R	41.52	0.24	22.26	0.04	1.69	9.44	0	0.38	19.68	4.56	0.03	0.11	99.95
D104 set1_93	G9A	C	41.18	0.24	21.91	0.05	1.8	9.51	0	0.38	19.72	4.59	0.05	0.19	99.62
D104 set1_94	G9A	R	41.25	0.25	21.9	0.04	1.88	9.5	0	0.38	19.58	4.59	0.04	0.14	99.55
D104 set1_95	G9A	C	41.18	0.25	22.14	0.04	1.79	9.43	0	0.38	19.74	4.56	0.04	0.17	99.72
D104 set1_96	G9A	R	41.43	0.26	21.99	0.03	1.79	9.42	0	0.38	19.61	4.55	0.03	0.11	99.6
D104 set1_97	G9A	C	41.31	0.23	22.3	0.03	1.75	9.4	0	0.39	19.89	4.56	0.03	0.18	100.07
D104 set1_98	G9A	R	41.35	0.22	22.02	0.04	1.78	9.46	0	0.38	19.73	4.56	0.04	0.16	99.74
D104 set1_99	G9A	C	41.47	0.21	22.38	0.06	1.42	9.65	0	0.3	20.16	3.98	0.05	0.16	99.84
D104 set1_100	G9A	R	41.44	0.2	22.32	0.05	1.41	9.74	0	0.3	19.99	3.98	0.05	0.14	99.62
D104 set1_101	G9A_Ti	C	41.64	0.55	19.49	0.04	4.35	6.99	0.02	0.26	21.12	5.12	0.07	0.17	99.82
D104 set1_102	G9A_Ti	R	41.75	0.54	19.54	0.03	4.27	6.95	0.02	0.29	21.25	5.11	0.05	0.17	99.97
D104 set1_103	G9A_Ti	C	41.69	0.67	20.06	0.03	3.47	7.58	0	0.31	20.96	5.05	0.03	0.16	100.01
D104 set1_104	G9A_Ti	R	41.56	0.59	20.3	0.02	3.34	7.53	0	0.29	21.02	5	0.06	0.19	99.9
D104 set1_105	G9A	C	41.49	0.24	22.34	0.05	1.83	9.4	0.02	0.38	19.79	4.57	0.03	0.14	100.28

Appendix D: Garnet Xenocryst EPMA Data Tables

Appendix D.02 (continued): Dharma kimberlite garnet EPMA analyses. Zones: C – core, R – rim.

Sample	*Class*	*Zone*	*SiO_2*	*TiO_2*	*Al_2O_3*	*V_2O_3*	*Cr_2O_3*	*FeO*	*NiO*	*MnO*	*MgO*	*CaO*	*Na_2O*	*O*	*Total*
D104 set1_106	G9A	R	41.47	0.24	22.07	0.03	1.78	9.45	0	0.38	19.77	4.57	0.04	0.15	99.95
D104 set1_107	G9A	C	41.64	0.21	22.32	0.04	1.68	9.44	0	0.36	19.78	4.55	0.02	0.11	100.15
D104 set1_108	G9A	R	41.47	0.23	22.24	0.03	1.62	9.42	0	0.37	19.86	4.54	0.02	0.15	99.95
D104 set1_109	G9A	C	41.53	0.24	22.37	0.03	1.63	9.33	0	0.38	19.95	4.54	0.02	0.15	100.17
D104 set1_110	G9A	R	41.56	0.22	22.41	0.03	1.72	9.38	0	0.39	19.73	4.54	0.03	0.12	100.13
D104 set2_111	G10A	C	40.73	0.09	15.24	0.05	11.05	6.2	0	0.34	20.87	4.86	0	0.14	99.57
D104 set2_112	G10A	R	40.71	0.08	15.36	0.04	11.03	6.12	0	0.32	20.76	4.85	0	0.1	99.37
D104 set2_114	G9A_Ti	R	41.55	0.58	20.58	0.03	3.16	7.54	0.02	0.31	20.83	4.91	0.05	0.15	99.71
D104 set2_115	G9A_Ti	C	41.15	0.47	18.22	0.05	6.17	6.86	0.02	0.3	20.56	5.56	0.07	0.18	99.61
D104 set2_116	G9A_Ti	R	41.35	0.47	18.54	0.05	6.11	6.85	0.03	0.32	20.52	5.55	0.03	0.13	99.95
D104 set2_117	G9A_Ti	C	41.6	0.57	20.48	0.04	3.27	7.5	0	0.31	21.08	4.9	0.05	0.18	99.98
D104 set2_118	G9A_Ti	R	41.43	0.6	20.32	0.02	3.27	7.46	0.02	0.31	21.09	4.94	0.05	0.21	99.72
D104 set2_119	G9A_Ti	C	41.33	0.64	20.58	0.05	2.88	7.87	0	0.31	20.77	4.95	0.06	0.2	99.64
D104 set2_120	G9A_Ti	R	41.53	0.59	20.86	0.05	3.18	7.76	0.02	0.31	20.73	4.99	0.04	0.16	100.22
D104 set2_121	G9A_Ti	C	41.96	0.55	21.76	0.02	1.87	7.24	0	0.29	21.54	4.55	0.04	0.14	99.96
D104 set2_122	G9A_Ti	R	42.03	0.53	22.04	0.03	1.88	7.27	0	0.28	21.6	4.53	0.04	0.15	100.38
D104 set2_123	G9A	C	41.43	0.1	19.57	0.03	6	6.5	0	0.33	20.57	5.54	0.02	0.12	100.21
D104 set2_124	G9A	R	41.43	0.1	19.42	0.04	5.99	6.53	0	0.34	20.58	5.57	0.02	0.13	100.15
D104 set2_125	G9A	C	41.7	0.21	22.82	0.04	1.4	9.54	0	0.31	20.27	3.94	0.05	0.14	100.42
D104 set2_126	G9A	R	41.51	0.19	22.79	0.04	1.36	9.54	0	0.31	20.24	3.95	0.05	0.16	100.14
D104 set2_127	G9A	C	41.44	0.25	22.55	0.02	1.6	9.41	0	0.37	19.86	4.51	0.03	0.15	100.19
D104 set2_128	G9A	R	41.45	0.24	22.46	0.03	1.59	9.32	0	0.38	19.83	4.53	0.04	0.14	100.01
D104 set2_129	G9A_Ti	C	41.78	0.63	20.71	0.04	2.84	7.72	0.03	0.3	20.95	4.93	0.06	0.16	100.15
D104 set2_130	G9A_Ti	R	41.66	0.63	20.79	0.03	2.72	7.58	0.02	0.3	21.03	4.84	0.03	0.15	99.78
D104 set2_131	G9A_Ti	C	42.18	0.38	22.42	0	1.47	6.79	0.02	0.29	22.07	4.51	0.05	0.19	100.37
D104 set2_132	G9A_Ti	R	42.1	0.39	22.39	0.03	1.5	6.75	0	0.3	22.06	4.5	0.04	0.18	100.24
D104 set2_133	G9A	C	41.51	0.23	22.31	0.03	1.77	9.37	0	0.38	19.76	4.54	0.03	0.12	100.05
D104 set2_134	G9A	R	41.26	0.21	22.28	0	1.69	9.36	0	0.4	19.8	4.55	0.02	0.16	99.73
D104 set2_135	G9A	C	41.38	0.23	22.58	0.04	1.68	9.38	0	0.36	19.61	4.55	0.03	0.11	99.95
D104 set2_136	G9A	R	41.4	0.22	22.47	0.04	1.75	9.42	0	0.36	19.7	4.57	0.03	0.13	100.09
D104 set2_137	G9A_Ti	C	41.19	0.7	20.08	0.04	3.37	8.57	0	0.36	20.14	4.96	0.05	0.17	99.63
D104 set2_138	G9A_Ti	R	41.29	0.7	20.28	0.05	3.38	8.53	0.02	0.34	20.14	4.97	0.06	0.16	99.92
D104 set2_139	G9B	C	40.76	0.26	19.15	0.08	5.48	9.06	0.02	0.37	18.46	5.97	0.02	0.12	99.75
D104 set2_140	G9B	R	40.8	0.25	19.05	0.1	5.53	8.96	0	0.39	18.56	6	0.03	0.14	99.81
D104 set2_141	G9A	C	41.49	0.23	22.37	0.03	1.84	9.48	0	0.39	19.84	4.6	0.03	0.16	100.46
D104 set2_142	G9A	R	41.55	0.22	22.15	0.03	1.84	9.38	0	0.36	19.84	4.6	0.03	0.14	100.14
D104 set2_143	G9A_Ti	C	41.44	0.67	18.11	0.04	6.51	6.53	0	0.32	20.63	5.78	0.06	0.13	100.22
D104 set2_144	G9A_Ti	R	41.32	0.64	18.02	0.06	6.63	6.58	0	0.3	20.68	5.82	0.06	0.17	100.28
D104 set2_145	G9A	C	41.66	0.24	22.59	0.02	1.67	9.45	0	0.38	19.9	4.51	0.05	0.14	100.61

Appendix D: Garnet Xenocryst EPMA Data Tables

Appendix D.02 (continued): Dharma kimberlite garnet EPMA analyses. Zones: C – core, R – rim.

Sample	*Class*	*Zone*	*SiO_2*	*TiO_2*	*Al_2O_3*	*V_2O_3*	*Cr_2O_3*	*FeO*	*NiO*	*MnO*	*MgO*	*CaO*	*Na_2O*	*O*	*Total*
D104 set2_146	G9A	R	41.44	0.22	22.24	0.04	1.67	9.38	0	0.4	19.77	4.52	0.03	0.14	99.85
D104 set2_147	G9A	C	41.31	0.09	19.55	0.03	5.97	6.45	0	0.34	20.53	5.55	0.02	0.13	99.97
D104 set2_148	G9A	R	41.46	0.09	19.36	0.03	6.02	6.47	0	0.35	20.64	5.54	0.03	0.14	100.13
D104 set2_149	G9A	C	41.37	0.22	22.41	0.03	1.78	9.44	0	0.36	19.76	4.59	0.03	0.16	100.15
D104 set2_150	G9A	R	41.56	0.25	22.37	0.03	1.78	9.36	0.02	0.37	19.64	4.6	0.04	0.1	100.12
D104 set2_151	G9A_Ti	C	41.65	0.58	20.58	0.04	3.42	7.48	0	0.29	21.06	4.97	0.05	0.18	100.3
D104 set2_152	G9A_Ti	R	41.6	0.58	20.27	0.03	3.35	7.58	0.03	0.31	20.86	4.96	0.06	0.17	99.8
D104 set2_153	G9B_Ti	C	41.62	0.63	20.95	0.04	2.44	8.11	0	0.32	20.65	4.86	0.05	0.15	99.82
D104 set2_154	G9B_Ti	R	41.85	0.6	21.1	0.04	2.48	8.19	0	0.35	20.8	4.86	0.04	0.16	100.47
D104 set2 rerun_367	G9A_Ti	C	41.48	0.59	20.05	0.04	3.25	7.67	0	0.31	21.05	4.99	0.06	0.23	99.72
D104 set3_155	G9A	C	41.28	0.22	22.14	0.04	1.76	9.45	0	0.4	19.89	4.53	0.03	0.19	99.93
D104 set3_156	G9A	R	41.35	0.24	22.18	0.03	1.72	9.47	0.02	0.37	19.81	4.54	0.02	0.16	99.91
D104 set3_157	G9A_Ti	C	41.61	0.63	20.57	0.05	2.77	7.81	0	0.31	21	4.9	0.04	0.19	99.88
D104 set3_158	G9A_Ti	R	41.59	0.63	20.76	0.04	2.7	7.73	0	0.32	21	4.88	0.05	0.19	99.89
D104 set3_159	G9A_Ti	C	41.2	0.61	20.33	0.04	3.02	7.52	0	0.3	20.93	4.94	0.07	0.22	99.18
D104 set3_160	G9A_Ti	R	41.55	0.62	20.46	0.02	3.04	7.52	0	0.3	20.84	4.91	0.05	0.14	99.45
D104 set3_161	G9A	C	41.3	0.24	22.27	0.04	1.74	9.35	0.02	0.37	19.75	4.56	0.03	0.15	99.82
D104 set3_162	G9A	R	41.4	0.25	22.28	0.04	1.74	9.32	0	0.37	19.89	4.53	0.04	0.16	100.02
D104 set3_163	G9A	C	41.4	0.22	22.54	0.02	1.58	9.49	0	0.36	19.84	4.49	0.04	0.16	100.14
D104 set3_164	G9A	R	41.31	0.23	22.38	0.04	1.58	9.38	0.02	0.38	19.81	4.5	0.03	0.16	99.82
D104 set3_165	G9A	C	41.19	0.06	21.03	0.04	3.91	7.97	0.02	0.42	20.01	5.07	0.02	0.15	99.89
D104 set3_166	G9A	R	40.93	0.07	20.88	0.04	3.89	7.94	0	0.41	19.93	5.06	0	0.16	99.31
D104 set3_167	G9A	C	41.27	0.24	22.27	0.02	1.8	9.47	0	0.4	19.62	4.56	0.03	0.15	99.83
D104 set3_168	G9A	R	41.28	0.25	22.31	0.04	1.76	9.39	0	0.36	19.63	4.57	0.04	0.13	99.76
D104 set3_169	G9A_Ti	C	40.76	0.71	18.69	0.05	5.16	8.04	0	0.32	19.82	5.6	0.07	0.21	99.43
D104 set3_170	G9A_Ti	R	40.67	0.69	18.7	0.04	5.1	8.08	0	0.34	19.7	5.55	0.06	0.19	99.12
D104 set3_171	G9A	C	41.28	0.23	22.22	0.02	1.83	9.44	0	0.37	19.6	4.56	0.04	0.14	99.73
D104 set3_172	G9A	R	41.22	0.25	22.49	0.05	1.76	9.3	0	0.38	19.63	4.57	0.03	0.13	99.81
D104 set3_173	G9A_Ti	C	41.91	0.43	21.09	0.02	2.35	7.02	0	0.27	21.61	4.48	0.05	0.14	99.37
D104 set3_174	G9A_Ti	R	41.76	0.43	21.12	0.02	2.33	6.95	0.02	0.28	21.84	4.46	0.05	0.2	99.46
D104 set3_175	G9A	C	41.25	0.23	22.2	0.02	1.57	9.37	0	0.36	19.78	4.52	0.03	0.15	99.48
D104 set3_176	G9A	R	41.65	0.21	22.45	0.03	1.56	9.31	0	0.36	19.84	4.53	0.03	0.11	100.08
D104 set3_177	G9A	C	41.34	0.23	22.48	0	1.59	9.43	0.02	0.39	19.7	4.5	0.03	0.13	99.84
D104 set3_178	G9A	R	41.37	0.23	22.46	0.02	1.63	9.27	0.02	0.36	19.78	4.5	0	0.12	99.76
D104 set3_179	G9A	C	41.29	0.23	22.21	0.04	1.79	9.42	0	0.38	19.59	4.59	0.02	0.13	99.69
D104 set3_180	G9A	R	41.08	0.25	21.94	0.02	1.82	9.42	0	0.36	19.56	4.59	0.03	0.15	99.22
D104 set3_181	G9A_Ti	C	41.46	0.59	20.78	0.04	2.89	7.96	0	0.33	20.76	4.88	0.05	0.19	99.93
D104 set3_182	G9A_Ti	R	41.41	0.63	20.61	0.05	3	7.86	0.02	0.3	20.65	4.95	0.04	0.16	99.68

Appendix D: Garnet Xenocryst EPMA Data Tables

Appendix D.02 (continued): Dharma kimberlite garnet EPMA analyses. Zones: C – core, R – rim.

Sample	*Class*	*Zone*	*SiO_2*	*TiO_2*	*Al_2O_3*	*V_2O_3*	*Cr_2O_3*	*FeO*	*NiO*	*MnO*	*MgO*	*CaO*	*Na_2O*	*O*	*Total*
D104 set3_183	G9A_Ti	C	41.32	0.6	20.3	0.05	3.28	7.57	0.02	0.3	20.95	4.98	0.05	0.21	99.63
D104 set3_184	G9A_Ti	R	41.32	0.63	20.25	0.05	3.33	7.49	0	0.27	20.96	4.99	0.06	0.21	99.56
D104 set3_185	G10A	C	40.57	0.07	15.38	0.04	11.02	6.13	0	0.32	20.89	4.83	0	0.16	99.41
D104 set3_186	G10A	R	40.78	0.08	15.55	0.06	11.05	6.15	0	0.33	20.8	4.83	0	0.1	99.73
D104 set3_187	G9A	C	41.49	0.23	22.38	0.04	1.6	9.39	0	0.36	19.62	4.54	0.03	0.1	99.78
D104 set3_188	G9A	R	41.05	0.23	22.06	0.04	1.64	9.36	0	0.37	19.61	4.53	0.03	0.15	99.07
D104 set3_189	G9A_Ti	C	41.28	0.69	20.76	0.06	2.72	8.71	0	0.36	20.21	4.86	0.06	0.18	99.89
D104 set3_190	G9A_Ti	R	41.22	0.68	20.67	0.04	2.82	8.62	0	0.34	20.32	4.86	0.06	0.2	99.83
D104 set3_191	G9A	C	41.44	0.22	22.18	0.02	1.84	9.36	0	0.4	19.7	4.56	0.05	0.14	99.91
D104 set3_192	G9A	R	41.47	0.23	22.18	0.02	1.8	9.43	0	0.39	19.62	4.58	0.04	0.12	99.88
D104 set3_193	G9A_Ti	C	41.21	0.61	20.1	0.04	3.25	7.63	0	0.3	20.97	4.94	0.05	0.23	99.33
D104 set3_194	G9A_Ti	R	41.57	0.6	20.44	0.06	3.1	7.54	0	0.3	20.98	4.94	0.05	0.18	99.76
D104 set3_195	G9A_Ti	C	41.3	0.7	20.5	0.05	2.75	8.7	0	0.36	20.22	4.89	0.07	0.19	99.73
D104 set3_196	G9A_Ti	R	41.33	0.68	20.7	0.04	2.81	8.67	0	0.36	20.14	4.88	0.06	0.16	99.83
D104 set3_197	G10A	C	40.58	0.09	15.27	0.03	11.07	6.08	0.02	0.33	20.67	4.91	0.03	0.12	99.2
D104 set3_198	G10A	R	40.59	0.06	15.11	0.03	11.03	6.03	0	0.32	20.84	4.89	0	0.14	99.04
D104 set3_199	G12_Ti	C	40.64	0.61	21.05	0.05	1.62	9.89	0	0.48	17.17	7.65	0.04	0.2	99.4
D104 set3_200	G12_Ti	R	40.7	0.6	21.08	0.05	1.6	9.91	0	0.46	17.12	7.73	0.07	0.21	99.53
D104 set3_201	G9A_Ti	C	41.7	0.6	20.99	0	2.5	7.44	0	0.28	21.23	4.72	0.07	0.17	99.7
D104 set3_202	G9A_Ti	R	41.68	0.58	20.79	0.05	2.52	7.34	0.02	0.29	21.18	4.72	0.06	0.15	99.38
D104 set3_203	G9A	C	41.31	0.22	22.1	0.03	1.76	9.45	0	0.36	19.78	4.55	0.02	0.16	99.74
D104 set3_204	G9A	R	41.24	0.23	22.08	0.03	1.72	9.33	0	0.36	19.71	4.56	0	0.13	99.39
D104 set4_205	G9A_Ti	C	41.78	0.37	21.99	0.04	1.51	6.7	0.02	0.3	21.87	4.48	0.03	0.18	99.27
D104 set4_206	G9A_Ti	R	41.73	0.37	21.71	0.02	1.5	6.72	0.02	0.28	22	4.53	0.03	0.22	99.13
D104 set4_207	G9A	C	41.17	0.24	22	0.03	1.69	9.44	0	0.39	19.66	4.53	0.03	0.15	99.33
D104 set4_208	G9A	R	41.3	0.22	22	0.04	1.66	9.43	0	0.39	19.68	4.52	0.03	0.14	99.41
D104 set4_209	G9A	C	41.9	0.3	21.13	0.03	2.64	6.69	0	0.23	21.92	4.52	0.04	0.18	99.58
D104 set4_210	G9A_Ti	R	42.1	0.34	21.35	0.04	2.57	6.72	0	0.26	21.97	4.59	0.04	0.17	100.15
D104 set4_211	G9A_Ti	C	41.34	0.71	20.53	0.06	2.77	8.78	0	0.35	20.11	4.88	0.07	0.17	99.77
D104 set4_212	G9A_Ti	R	41.33	0.7	20.45	0.04	2.78	8.65	0	0.35	20.19	4.89	0.07	0.17	99.62
D104 set4_213	G9A	C	41.17	0.24	22.16	0.05	1.72	9.4	0.02	0.37	19.75	4.55	0	0.16	99.59
D104 set4_214	G9A	R	41.07	0.23	21.9	0.04	1.77	9.41	0	0.37	19.72	4.54	0.02	0.17	99.24
D104 set4_215	G9A	C	41.32	0.27	22.18	0.04	1.61	9.41	0.02	0.38	19.91	4.51	0.03	0.18	99.86
D104 set4_216	G9A	R	41.38	0.25	22.3	0.03	1.54	9.29	0	0.37	19.71	4.51	0.02	0.11	99.51
D104 set4_217	G9A	C	41.12	0.22	22.01	0.04	1.61	9.4	0	0.38	19.73	4.53	0.03	0.17	99.24
D104 set4_218	G9A	R	41.07	0.22	21.89	0	1.61	9.29	0	0.39	19.8	4.52	0.03	0.18	99
D104 set4_219	G9A	C	41.07	0.27	21.74	0.04	1.83	9.45	0	0.39	19.61	4.61	0.02	0.16	99.19
D104 set4_220	G9A	R	41.15	0.26	21.8	0.03	1.84	9.49	0	0.39	19.58	4.62	0.04	0.16	99.36
D104 set4_221	G9A_Ti	C	41.83	0.36	21.9	0.04	1.5	6.74	0	0.3	21.96	4.49	0.03	0.19	99.34

Appendix D: Garnet Xenocryst EPMA Data Tables

Appendix D.02 (continued): Dharma kimberlite garnet EPMA analyses. Zones: C – core, R – rim.

Sample	*Class*	*Zone*	*SiO_2*	*TiO_2*	*Al_2O_3*	*V_2O_3*	*Cr_2O_3*	*FeO*	*NiO*	*MnO*	*MgO*	*CaO*	*Na_2O*	*O*	*Total*
D104 set4_222	G9A_Ti	R	41.84	0.38	22.28	0.03	1.48	6.68	0	0.3	22.2	4.51	0.04	0.24	99.98
D104 set4_223	G9A_Ti	C	41.31	0.59	20.07	0.05	3.28	7.59	0.02	0.29	20.82	4.92	0.04	0.18	99.16
D104 set4_224	G9A_Ti	R	41.61	0.61	20.41	0.04	3.17	7.59	0.02	0.28	20.85	4.91	0.04	0.14	99.67
D104 set4_225	G9A_Ti	C	41.37	0.63	20.53	0.04	2.73	8.16	0	0.33	20.46	4.9	0.06	0.17	99.38
D104 set4_226	G9A_Ti	R	41.24	0.62	20.93	0.04	2.57	8.11	0	0.32	20.6	4.83	0.05	0.19	99.5
D104 set4_227	G9A_Ti	C	41.63	0.39	19.79	0.04	4.48	6.53	0.02	0.28	21.29	5.07	0.03	0.14	99.69
D104 set4_228	G9A_Ti	R	41.54	0.41	19.54	0.05	4.76	6.46	0	0.29	21.19	5.13	0.03	0.13	99.53
D104 set4_229	G9A	C	41.32	0.24	21.84	0.03	1.76	9.5	0	0.39	19.73	4.57	0.04	0.16	99.58
D104 set4_230	G9A	R	41.26	0.24	21.88	0.03	1.79	9.4	0	0.37	19.59	4.58	0.02	0.13	99.29
D104 set4_231	G9A	C	41.13	0.08	19.1	0.03	5.99	6.52	0	0.36	20.59	5.53	0	0.16	99.49
D104 set4_232	G9A	R	41.19	0.09	19.22	0.04	5.97	6.44	0	0.34	20.47	5.56	0	0.12	99.44
D104 set4_233	G10A	C	40.6	0.07	15.32	0.05	11.17	6.12	0	0.31	20.92	4.88	0	0.16	99.6
D104 set4_234	G10B	R	40.41	0.08	15.17	0.04	10.96	6.1	0	0.33	20.55	5.26	0.02	0.17	99.09
D104 set4_235	G10A	C	40.55	0.09	15.11	0.03	11.01	6.12	0	0.32	20.7	4.81	0.02	0.12	98.88
D104 set4_236	G10A	R	40.33	0.08	15.2	0.04	11.22	6.14	0	0.32	20.69	4.79	0.03	0.14	98.98
D104 set4_237	G9A_Ti	C	40.78	0.71	20.02	0.04	3.38	8.6	0	0.37	20.12	4.94	0.05	0.22	99.23
D104 set4_238	G9A_Ti	R	40.9	0.71	19.92	0.04	3.35	8.45	0	0.36	20.18	4.96	0.07	0.21	99.15
D104 set4_239	G9A	C	41.19	0.23	22.19	0	1.69	9.36	0	0.37	19.61	4.54	0.02	0.13	99.33
D104 set4_240	G9A	R	41.28	0.21	21.99	0.03	1.78	9.45	0	0.37	19.52	4.54	0.04	0.12	99.33
D104 set4_241	G9A_Ti	C	41.32	0.59	20.5	0.04	2.77	7.87	0.02	0.32	20.63	4.89	0.05	0.17	99.17
D104 set4_242	G9A_Ti	R	41.45	0.66	20.55	0.03	2.97	7.9	0	0.32	20.62	4.94	0.05	0.15	99.64
D104 set4_243	G9B	C	40.53	0.24	18.84	0.09	5.5	9.09	0	0.39	18.52	5.97	0.03	0.18	99.38
D104 set4_244	G9B	R	40.65	0.23	19.03	0.1	5.44	8.93	0	0.4	18.43	5.95	0	0.12	99.28
D104 set4_245	G9A	C	41.26	0.24	22.3	0.02	1.58	9.34	0	0.37	19.77	4.5	0.04	0.15	99.57
D104 set4_246	G9A	R	41.37	0.22	22.31	0.04	1.58	9.37	0	0.38	19.89	4.5	0.03	0.16	99.85
D104 set4_247	G9A_Ti	C	41.3	0.37	19.4	0	4.81	6.78	0.03	0.3	21.01	5.15	0.04	0.18	99.37
D104 set4_248	G9A_Ti	R	41.44	0.4	19.67	0.02	4.76	6.84	0	0.29	20.93	5.13	0.03	0.14	99.65
D104 set4_249	G9A	C	41.32	0.22	21.93	0.03	1.7	9.39	0	0.34	19.79	4.56	0.03	0.15	99.46
D104 set4_250	G9A	R	41.28	0.24	22.31	0.05	1.65	9.37	0	0.38	19.7	4.52	0.03	0.14	99.67
D104 set4_251	G9A	C	41.16	0.09	18.95	0.04	6.06	6.54	0	0.34	20.52	5.53	0	0.15	99.38
D104 set4_252	G9A	R	41.38	0.08	19.16	0.05	6	6.51	0	0.34	20.5	5.55	0.02	0.12	99.71
D104 set4_253	G9A	C	41.17	0.24	22.01	0	1.8	9.52	0	0.38	19.83	4.55	0.05	0.21	99.76
D104 set4_254	G9A	R	41.33	0.24	22.13	0.04	1.8	9.42	0	0.39	19.72	4.55	0.03	0.15	99.8
D104 set4_255	G9A	C	41.25	0.23	22.02	0	1.54	9.42	0	0.36	19.77	4.53	0.03	0.16	99.31
D104 set4_256	G9A	R	41.29	0.22	22.01	0.04	1.62	9.38	0	0.37	19.79	4.52	0.02	0.15	99.41
D104 set5_257	G12_Ti	C	40.99	0.58	20.87	0.06	1.82	9.77	0	0.47	17.01	7.65	0.05	0.12	99.39
D104 set5_258	G12_Ti	R	41.19	0.6	21.29	0.04	1.8	9.83	0	0.47	17.37	7.65	0.07	0.18	100.49
D104 set5_259	G9A	C	41.52	0.23	21.94	0.02	1.79	9.35	0.02	0.38	19.84	4.54	0.04	0.14	99.81
D104 set5_260	G9A	R	41.67	0.24	22.23	0.03	1.7	9.4	0	0.35	19.7	4.54	0.04	0.09	99.99

Appendix D: Garnet Xenocryst EPMA Data Tables

Appendix D.02 (continued): Dharma kimberlite garnet EPMA analyses. Zones: C – core, R – rim.

Sample	*Class*	*Zone*	*SiO_2*	*TiO_2*	*Al_2O_3*	*V_2O_3*	*Cr_2O_3*	*FeO*	*NiO*	*MnO*	*MgO*	*CaO*	*Na_2O*	*O*	*Total*
D104 set5_261	G9A_Ti	C	41.31	0.71	20.17	0.04	2.93	8.67	0	0.35	20.1	4.9	0.05	0.15	99.38
D104 set5_262	G9A_Ti	R	41.54	0.73	20.31	0.05	2.9	8.66	0	0.36	20.11	4.92	0.06	0.12	99.76
D104 set5_263	G9A	C	41.51	0.22	22.11	0.03	1.75	9.4	0	0.37	19.68	4.56	0.04	0.12	99.79
D104 set5_264	G9A	R	41.24	0.24	21.73	0.03	1.75	9.44	0	0.38	19.7	4.55	0.03	0.15	99.24
D104 set5_265	G9A_Ti	C	41.76	0.65	19.97	0.04	3.42	7.61	0	0.32	20.89	5.05	0.05	0.15	99.91
D104 set5_266	G9A_Ti	R	41.44	0.62	19.86	0.05	3.52	7.53	0.02	0.28	20.95	5.02	0.06	0.2	99.55
D104 set5_267	G9A_Ti	C	41.59	0.6	20.12	0.05	3.26	7.55	0.02	0.3	20.99	4.97	0.04	0.18	99.67
D104 set5_268	G9A_Ti	R	41.5	0.57	20.12	0.05	3.35	7.48	0	0.31	21.02	4.93	0.06	0.19	99.58
D104 set5_269	G9A	C	41.35	0.24	21.8	0.03	1.71	9.44	0	0.36	19.94	4.55	0.03	0.18	99.63
D104 set5_270	G9A	R	41.37	0.24	21.8	0.03	1.68	9.32	0	0.37	19.94	4.56	0.02	0.17	99.5
D104 set5_271	G9A	C	41.48	0.25	22.04	0.04	1.71	9.47	0	0.38	19.85	4.53	0.04	0.16	99.95
D104 set5_272	G9A	R	41.61	0.23	21.93	0.04	1.79	9.37	0	0.36	19.81	4.59	0.03	0.13	99.89
D104 set5_273	G9A_Ti	C	41.36	0.69	20.24	0.04	2.79	8.75	0	0.32	20.31	4.88	0.04	0.18	99.6
D104 set5_274	G9A_Ti	R	41.23	0.73	20.27	0.05	2.73	8.73	0.02	0.35	20.33	4.87	0.05	0.21	99.57
D104 set5_275	G9A_Ti	C	41.57	0.61	20.53	0.03	2.84	8.09	0.02	0.33	20.59	4.91	0.04	0.15	99.71
D104 set5_276	G9A_Ti	R	41.47	0.6	20.41	0.05	2.74	8.07	0	0.31	20.52	4.89	0.05	0.15	99.26
D104 set5_277	G9A_Ti	C	41.7	0.6	20	0.05	3.31	7.62	0	0.3	20.88	4.97	0.05	0.15	99.63
D104 set5_278	G9A_Ti	R	41.75	0.61	20	0.05	3.15	7.56	0	0.29	21.02	4.95	0.05	0.16	99.59
D104 set5_279	G9A_Ti	C	41.69	0.6	20.6	0.03	2.54	8.11	0	0.34	20.72	4.84	0.06	0.16	99.69
D104 set5_280	G9A_Ti	R	41.46	0.59	20.42	0.04	2.71	8.19	0	0.33	20.52	4.87	0.04	0.16	99.33
D104 set5_281	G9A_Ti	C	41.67	0.59	20.47	0.04	3.04	7.65	0	0.32	20.9	4.9	0.05	0.15	99.78
D104 set5_282	G9A_Ti	R	41.43	0.53	20.64	0.03	2.68	7.62	0	0.3	20.86	4.82	0.06	0.17	99.14
D104 set5_283	G9A_Ti	C	41.58	0.52	20.2	0.04	3.66	7.14	0.02	0.3	21.29	4.91	0.06	0.2	99.92
D104 set5_284	G9A_Ti	R	41.53	0.51	20.02	0.04	3.52	7.14	0	0.29	21.18	4.88	0.05	0.17	99.33
D104 set5_285	G9A_Ti	C	41.8	0.52	20.53	0.03	2.64	6.85	0	0.26	21.61	4.71	0.05	0.16	99.16
D104 set5_286	G9A_Ti	R	41.95	0.53	20.48	0.02	2.54	6.87	0	0.25	21.75	4.72	0.05	0.17	99.33
D104 set5_288	G9A_Ti	R	41.66	0.59	20.08	0.04	3.31	7.54	0.02	0.29	20.9	4.96	0.06	0.15	99.6
D104 set5_289	G9A_Ti	C	41.61	0.5	20.11	0.04	3.03	7.06	0	0.28	21.42	4.83	0.05	0.19	99.12
D104 set5_290	G9A_Ti	R	40.78	0.48	20.36	0.04	3.05	7.1	0.02	0.28	21.66	4.78	0.04	0.35	98.94
D104 set5_291	G9A_Ti	C	41.65	0.6	20	0.03	3.34	7.58	0.02	0.31	21.04	5.01	0.06	0.2	99.84
D104 set5_292	G9A_Ti	R	41.6	0.61	20.2	0.05	3.19	7.52	0	0.32	20.92	4.95	0.07	0.17	99.6
D104 set5_293	G9A_Ti	C	41.58	0.53	19.93	0.04	3.69	7.39	0.02	0.29	21.08	4.98	0.04	0.18	99.75
D104 set5_294	G9A_Ti	R	41.76	0.54	19.99	0.03	3.73	7.37	0	0.29	20.91	4.96	0.06	0.13	99.77
D104 set5_295	G9A_Ti	C	41.65	0.64	20.35	0.02	2.75	7.65	0.02	0.3	21.03	4.87	0.05	0.18	99.51
D104 set5_296	G9A_Ti	R	41.52	0.58	20.38	0.04	2.64	7.62	0	0.32	21.16	4.83	0.05	0.22	99.36
D104 set5_297	G9A_Ti	C	41.89	0.38	21.74	0.03	1.51	6.79	0	0.29	21.92	4.49	0.04	0.19	99.27
D104 set5_298	G9A_Ti	R	42.04	0.37	21.69	0.03	1.47	6.75	0	0.28	21.97	4.49	0.04	0.17	99.3
D104 set5_299	G9A	C	41.66	0.17	19.98	0	3.86	6.79	0.02	0.27	21.48	4.88	0.02	0.19	99.32
D104 set5_300	G9A	R	41.52	0.16	20.01	0.04	3.88	6.69	0	0.28	21.57	4.89	0.03	0.23	99.3

Appendix D: Garnet Xenocryst EPMA Data Tables

Appendix D.02 (continued): Dharma kimberlite garnet EPMA analyses. Zones: C – core, R – rim.

Sample	*Class*	*Zone*	*SiO_2*	*TiO_2*	*Al_2O_3*	*V_2O_3*	*Cr_2O_3*	*FeO*	*NiO*	*MnO*	*MgO*	*CaO*	*Na_2O*	*O*	*Total*
D104 set5 rerun 368	G9A_Ti	C	41.37	0.59	19.91	0.06	3.33	7.53	0	0.29	21.15	4.91	0.06	0.24	99.44
D89_329	G9A	C	41.53	0.26	20.6	0.02	3.92	6.8	0	0.34	20.86	4.89	0.03	0.1	99.35
D89_330	G9A	R	41.43	0.25	20.7	0.02	3.89	6.82	0.02	0.34	20.86	4.87	0.04	0.12	99.36
D89_331	G9A_Ti	C	41.51	0.64	20.05	0.05	3.56	7.57	0	0.3	20.72	5.1	0.05	0.15	99.7
D89_332	G9A_Ti	R	41.47	0.62	20.21	0.03	3.53	7.49	0	0.32	20.84	5.11	0.04	0.17	99.83
D89_333	G9A_Ti	C	41.47	0.6	19.95	0.04	3.42	7.53	0	0.3	20.68	5	0.04	0.13	99.16
D89_334	G9A_Ti	R	41.39	0.58	20.1	0.03	3.44	7.49	0	0.3	21.59	4.98	0.05	0.32	100.27
D89_335	G9A	C	41.41	0.12	19.35	0.04	5.27	6.67	0	0.27	20.89	5.4	0	0.17	99.59
D89_336	G9A	R	41.47	0.12	19.52	0.04	4.94	6.63	0	0.28	20.86	5.36	0	0.15	99.37
D89_337	G9A	C	41.48	0.26	20.48	0	3.95	6.95	0	0.34	20.83	4.92	0.03	0.12	99.36
D89_338	G9A	R	41.39	0.27	20.43	0.02	3.97	6.84	0	0.35	20.86	4.87	0.04	0.12	99.16
D89_339	G9A_Ti	C	41.76	0.43	21	0	2.82	6.43	0	0.3	21.87	4.24	0.07	0.13	99.05
D89_340	G9A_Ti	R	41.69	0.42	21.02	0	2.83	6.26	0	0.3	21.86	4.26	0.06	0.12	98.82
D89_341	G9A_Ti	C	41.68	0.44	20.69	0.05	2.91	7.31	0	0.28	21.09	4.74	0.03	0.13	99.35
D89_342	G9A_Ti	R	41.74	0.43	20.91	0.03	2.89	7.26	0	0.29	21	4.74	0.03	0.1	99.42
D89_343	G9A_Ti	C	41.9	0.43	21.16	0	2.95	6.34	0	0.31	21.88	4.28	0.08	0.11	99.44
D89_344	G9A_Ti	R	41.7	0.4	21.27	0.04	2.98	6.35	0	0.3	21.77	4.28	0.05	0.11	99.25
D89_345	G9B	C	40.85	0.09	18.67	0.05	6.45	7.52	0	0.41	19	6.24	0.02	0.11	99.41
D89_346	G9B	R	40.77	0.1	18.66	0.04	6.46	7.35	0	0.41	19.02	6.23	0	0.09	99.13
D89_347	G9A_Ti	C	41.94	0.4	21.48	0.03	2.92	6.38	0	0.29	21.91	4.28	0.07	0.11	99.81
D89_348	G9A_Ti	R	41.92	0.41	21.49	0.03	2.97	6.35	0	0.31	22.03	4.26	0.07	0.14	99.98
D89_349	G9A_Ti	C	42.02	0.41	21.53	0.03	2.82	6.38	0.02	0.31	21.89	4.25	0.05	0.09	99.8
D89_350	G9A_Ti	R	42.12	0.41	21.51	0.04	2.79	6.32	0	0.32	21.84	4.27	0.07	0.07	99.76
D89_351	G9A_Ti	C	41.93	0.4	21.32	0.03	2.78	6.29	0	0.3	21.89	4.25	0.08	0.11	99.38
D89_352	G9A_Ti	R	42.03	0.41	21.47	0	2.78	6.34	0	0.32	21.82	4.26	0.05	0.07	99.55
D89_353	G9B	C	41.06	0.09	18.87	0.05	6.45	7.47	0	0.43	19.09	6.21	0	0.08	99.8
D89_354	G9B	R	40.93	0.07	18.69	0.04	6.51	7.5	0	0.44	19.05	6.23	0	0.11	99.57
D89_355	G9A_Ti	C	41.97	0.43	21.52	0.03	2.94	6.39	0	0.29	21.87	4.27	0.06	0.09	99.86
D89_356	G9A_Ti	R	42	0.42	21.4	0	2.94	6.29	0	0.31	21.86	4.31	0.08	0.1	99.71
D89_357	G10B_Ti	C	41.58	0.68	20.61	0.05	3.14	7.59	0	0.29	22.04	3.41	0.02	0.15	99.56
D89_358	G10B_Ti	R	41.7	0.63	21.01	0.04	2.98	7.52	0	0.27	22.16	3.18	0.04	0.13	99.66
D89_359	G9A_Ti	C	41.7	0.39	21.09	0.03	2.84	7.26	0	0.31	20.96	4.7	0.03	0.1	99.41
D89_360	G9A_Ti	R	41.94	0.39	21.16	0.02	2.86	7.18	0	0.28	20.99	4.72	0.05	0.07	99.66
D89_361	G9A	C	41.46	0.05	20.7	0.03	4.01	7.19	0	0.35	20.58	4.99	0.03	0.13	99.52
D89_362	G9A	R	41.66	0.08	21.07	0.04	3.98	7.22	0	0.33	20.81	4.95	0.02	0.13	100.29
D89_363	G9A_Ti	C	41.26	0.45	18.49	0.05	6.1	6.61	0	0.29	20.52	5.5	0.04	0.11	99.42
D89_364	G9A_Ti	R	41.38	0.47	18.37	0.04	6.07	6.58	0	0.31	20.71	5.5	0.04	0.13	99.6
D89_365	G9A	C	41.52	0.28	20.89	0.03	3.82	6.78	0	0.35	20.88	4.9	0.03	0.1	99.58

Appendix D: Garnet Xenocryst EPMA Data Tables

Appendix D.02 (continued): Dharma kimberlite garnet EPMA analyses. Zones: C – core, R – rim.

Sample	*Class*	*Zone*	*SiO_2*	*TiO_2*	*Al_2O_3*	*V_2O_3*	*Cr_2O_3*	*FeO*	*NiO*	*MnO*	*MgO*	*CaO*	*Na_2O*	*O*	*Total*
D89_366	G9A	R	41.64	0.26	20.86	0.02	3.86	6.86	0	0.32	20.85	4.87	0.03	0.08	99.65
D89_367	G9B	C	40.87	0.1	18.77	0.07	6.53	7.53	0	0.43	19.03	6.2	0	0.1	99.63
D89_368	G9B	R	40.84	0.09	18.72	0.05	6.41	7.54	0	0.44	18.86	6.24	0	0.08	99.27
D89_369	G9B	C	41.05	0.09	18.83	0.05	6.51	7.46	0.02	0.41	19	6.22	0	0.07	99.71
D89_370	G9B	R	40.99	0.08	18.89	0.05	6.46	7.45	0	0.41	18.9	6.21	0	0.05	99.49
D89_371	G9A	C	41.63	0.28	20.9	0.05	3.83	6.88	0	0.33	20.84	4.91	0.03	0.08	99.76
D89_372	G9A	R	41.78	0.27	20.86	0.03	3.86	6.84	0	0.36	20.85	4.9	0.05	0.07	99.87
D89_373	G10B_Ti	C	41.78	0.6	21.02	0.03	2.98	7.57	0	0.27	22.14	3.15	0.02	0.1	99.66
D89_374	G10B_Ti	R	41.79	0.67	20.74	0.04	3.16	7.6	0	0.29	22.13	3.31	0.04	0.13	99.9
D89_375	G9A_Ti	C	42.02	0.42	21.62	0.03	2.81	6.34	0	0.3	22.03	4.23	0.05	0.11	99.96
D89_376	G9A_Ti	R	41.9	0.44	21.68	0.03	2.81	6.37	0	0.31	21.97	4.2	0.06	0.11	99.88
D89_377	G9A_Ti	C	41.76	0.41	21.65	0.04	2.96	6.28	0	0.3	21.88	4.28	0.06	0.12	99.74
D89_378	G9A_Ti	R	42.11	0.39	21.32	0.03	2.87	6.3	0	0.29	21.68	4.3	0.05	0.04	99.38
D89_379	G9A	C	41.4	0.27	20.74	0.04	3.95	6.84	0	0.36	20.86	4.94	0.04	0.13	99.57
D89_380	G9A	R	41.71	0.25	20.59	0.03	3.96	6.79	0	0.35	20.91	4.95	0.03	0.09	99.66
D89_381	G9B_Ti	C	41.4	0.69	20.52	0.03	3.12	8.59	0.02	0.37	19.43	5.63	0.05	0.1	99.95
D89_382	G9B_Ti	R	41.27	0.68	20.8	0.06	3.05	8.54	0	0.37	19.42	5.65	0.06	0.12	100.02
D89_383	G9A	C	41.47	0.07	20.77	0.03	3.96	7.21	0	0.35	20.57	4.96	0.02	0.11	99.52
D89_384	G9A	R	41.53	0.06	20.75	0.03	4.03	7.18	0	0.34	20.6	4.96	0	0.1	99.58
D89_385	G9A_Ti	C	41.93	0.4	21.73	0.03	2.82	6.35	0.02	0.3	21.99	4.26	0.07	0.13	100.03
D89_386	G9A_Ti	R	41.83	0.38	21.32	0.03	2.8	6.35	0	0.29	21.82	4.26	0.06	0.1	99.24
D89_387	G10B_Ti	C	41.6	0.66	20.69	0.04	3.06	7.57	0	0.29	22.23	3.35	0.04	0.18	99.71
D89_388	G10B_Ti	R	41.72	0.63	20.76	0.04	3.04	7.53	0	0.25	22.23	3.26	0.03	0.14	99.63
D89_389	G9A	C	41.73	0.11	19.68	0.03	4.94	6.68	0.02	0.28	20.91	5.37	0.03	0.14	99.92
D89_390	G9A	R	41.79	0.13	19.75	0.04	4.94	6.54	0.02	0.25	20.9	5.38	0.03	0.11	99.88
D89_391	G9A_Ti	C	41.67	0.65	20.05	0.04	3.45	7.53	0	0.29	20.75	5.07	0.06	0.13	99.69
D89_392	G9A_Ti	R	41.65	0.64	20.04	0.04	3.5	7.56	0.02	0.3	20.77	5.12	0.05	0.15	99.84
D89_393	G10B_Ti	C	41.83	0.67	20.48	0.03	3.07	7.56	0.02	0.27	22.09	3.36	0.04	0.12	99.54
D89_394	G10B_Ti	R	41.8	0.69	20.6	0.05	3.07	7.59	0	0.27	22.23	3.29	0.06	0.15	99.8
D89_395	G9A_Ti	C	41.71	0.44	21.07	0.03	2.93	6.32	0	0.34	21.89	4.28	0.07	0.14	99.22
D89_396	G9A_Ti	R	41.76	0.39	21.38	0.04	2.32	6.4	0.03	0.3	21.71	4.29	0.06	0.1	98.78
D89_397	G9B_Ti	C	41.04	0.71	20.1	0.06	3.09	8.6	0	0.37	19.49	5.68	0.06	0.17	99.37
D89_398	G9B_Ti	R	40.96	0.69	20.22	0.05	3.11	8.48	0.02	0.39	19.28	5.65	0.07	0.14	99.06
D89_399	G9A_Ti	C	41.86	0.6	20.39	0.05	3.05	7.5	0	0.27	21.04	4.86	0.04	0.12	99.78
D89_400	G9A_Ti	R	41.6	0.6	20.44	0.05	2.96	7.49	0	0.3	21	4.84	0.06	0.16	99.5
D89_401	G9A_Ti	C	41.71	0.42	21.12	0	2.83	7.28	0.02	0.3	21.22	4.71	0.05	0.16	99.82
D89_402	G9A_Ti	R	41.93	0.42	20.91	0.03	2.89	7.27	0	0.29	21.13	4.75	0.06	0.12	99.8
D89_403	G9B	C	40.89	0.09	18.74	0.05	6.54	7.46	0	0.41	19.08	6.25	0	0.11	99.62
D89_404	G9B	R	40.77	0.08	18.6	0.04	6.6	7.35	0	0.38	19.01	6.28	0	0.09	99.2

Appendix D: Garnet Xenocryst EPMA Data Tables

Appendix D.02 (continued): Dharma kimberlite garnet EPMA analyses. Zones: C – core, R – rim.

Sample	*Class*	*Zone*	*SiO_2*	*TiO_2*	*Al_2O_3*	*V_2O_3*	*Cr_2O_3*	*FeO*	*NiO*	*MnO*	*MgO*	*CaO*	*Na_2O*	*O*	*Total*
D89_405	G9A_Ti	C	41.76	0.38	21.31	0.04	2.93	6.28	0	0.32	21.89	4.28	0.06	0.12	99.37
D89_406	G9A_Ti	R	41.84	0.4	21.36	0.04	2.94	6.28	0	0.3	21.95	4.3	0.06	0.12	99.59
D89_407	G9A	C	41.53	0.28	20.66	0.02	3.9	6.81	0.02	0.35	20.84	4.89	0.03	0.09	99.42
D89_408	G9A	R	41.48	0.29	20.59	0.03	3.91	6.81	0	0.35	20.98	4.89	0.04	0.13	99.5
D89_409	G9A	C	41.47	0.27	20.53	0.03	3.95	6.96	0	0.36	20.96	4.93	0.04	0.15	99.65
D89_410	G9A	R	41.62	0.28	20.66	0.03	4.06	6.86	0	0.35	20.89	4.95	0.05	0.11	99.86
D89_411	G9A	C	41.44	0.26	20.31	0.02	3.97	6.88	0	0.36	20.85	4.94	0.04	0.13	99.2
D89_412	G9A	R	41.56	0.26	20.62	0.04	3.92	6.91	0.02	0.37	20.97	4.94	0.03	0.14	99.78
D89_413	G9A_Ti	C	41.76	0.41	21.3	0	2.91	6.4	0	0.29	21.92	4.28	0.07	0.14	99.48
D89_414	G9A_Ti	R	41.89	0.38	21.44	0.04	2.88	6.36	0	0.3	22.01	4.28	0.08	0.15	99.81
D89_415	G9B	C	40.9	0.08	18.64	0.03	6.47	7.48	0	0.42	18.92	6.24	0	0.08	99.26
D89_416	G9B	R	40.86	0.07	19.01	0.04	6.53	7.47	0	0.4	19.14	6.21	0	0.12	99.85
D89_417	G9A	C	41.42	0.26	20.73	0.03	3.91	6.92	0	0.35	20.95	4.87	0.05	0.15	99.64
D89_418	G9A	R	41.35	0.26	20.54	0.03	3.83	6.95	0	0.34	20.84	4.88	0.03	0.13	99.18
D89_419	G9A_Ti	C	41.82	0.41	21.79	0.04	2.81	6.35	0	0.29	21.9	4.26	0.06	0.12	99.85
D89_420	G9A_Ti	R	41.98	0.41	21.66	0.03	2.91	6.29	0	0.31	21.92	4.27	0.06	0.1	99.94
D89_421	G10B_Ti	C	41.77	0.69	20.65	0.05	2.92	7.61	0	0.29	22.22	3.28	0.03	0.15	99.66
D89_422	G10B_Ti	R	41.52	0.72	20.4	0.04	3.15	7.55	0.02	0.28	22.02	3.45	0.04	0.16	99.35
D89_423	G9A_Ti	C	41.97	0.43	21.3	0.04	2.91	6.38	0.02	0.29	21.96	4.26	0.06	0.11	99.73
D89_424	G9A_Ti	R	41.64	0.4	21.2	0	2.9	6.25	0	0.3	21.88	4.28	0.07	0.14	99.06
D89_425	G9A_Ti	C	41.61	0.63	20.31	0	3.12	7.52	0	0.29	21	4.85	0.05	0.16	99.54
D89_426	G9A_Ti	R	41.14	0.59	20.36	0.04	2.99	7.48	0	0.31	20.83	4.81	0.05	0.18	98.78
D89_427	G10B_Ti	C	41.51	0.71	20.3	0.03	3.08	7.57	0	0.26	22.05	3.37	0.03	0.15	99.06
D89_428	G10B_Ti	R	41.3	0.76	20	0.03	3.07	7.53	0.02	0.27	21.92	3.52	0.03	0.17	98.62
D89_429	G9A	C	41.54	0.03	20.52	0.05	4.05	7.32	0	0.34	20.57	5	0.02	0.13	99.57
D89_430	G9A	R	41.3	0.09	20.52	0.04	3.97	7.15	0	0.34	20.71	4.93	0.02	0.15	99.22
D89_431	G9A	C	41.63	0.1	19.72	0.02	5.07	6.66	0.03	0.28	21.01	5.38	0	0.17	100.07
D89_432	G9A	R	41.71	0.13	19.45	0.04	4.95	6.64	0	0.26	20.9	5.37	0	0.12	99.57
D89_433	G9B	C	40.84	0.08	18.64	0.03	6.46	7.44	0	0.42	19.01	6.21	0	0.09	99.22
D89_434	G9B	R	40.81	0.08	18.65	0.04	6.52	7.52	0	0.41	19.08	6.26	0	0.12	99.49
D89_435	G9A_Ti	C	42	0.43	21.45	0.03	2.86	6.41	0	0.3	21.95	4.26	0.06	0.11	99.86
D89_436	G9A_Ti	R	41.79	0.39	21.23	0.04	2.79	6.32	0	0.3	21.9	4.26	0.06	0.12	99.2
D89_437	G9B_Ti	C	41.15	0.7	20.06	0.05	3.14	8.51	0	0.36	19.38	5.64	0.04	0.11	99.14
D89_438	G9B_Ti	R	41.24	0.69	20.05	0.04	3.15	8.54	0	0.37	19.47	5.64	0.06	0.13	99.38
D89_439	G9A_Ti	C	41.66	0.5	20.92	0.02	2.29	7.59	0.02	0.3	21.06	4.52	0.04	0.13	99.05
D89_440	G9A_Ti	R	41.85	0.53	20.94	0.03	2.4	7.72	0	0.32	21.05	4.55	0.06	0.13	99.58
D89_441	G9A	C	41.56	0.24	20.38	0.04	3.97	6.88	0	0.34	20.82	4.92	0.04	0.1	99.29
D89_442	G9A	R	41.47	0.26	20.27	0.04	3.98	6.82	0	0.34	20.83	4.96	0.04	0.11	99.12
D89_443	G9A_Ti	C	41.92	0.41	21.15	0	2.88	6.37	0	0.31	21.94	4.26	0.07	0.12	99.43

Appendix D: Garnet Xenocryst EPMA Data Tables

Appendix D.02 (continued): Dharma kimberlite garnet EPMA analyses. Zones: C – core, R – rim.

Sample	*Class*	*Zone*	*SiO_2*	*TiO_2*	*Al_2O_3*	*V_2O_3*	*Cr_2O_3*	*FeO*	*NiO*	*MnO*	*MgO*	*CaO*	*Na_2O*	*O*	*Total*
D89_444	G9A_Ti	R	42.12	0.41	21.27	0.03	2.93	6.35	0	0.32	21.95	4.29	0.07	0.1	99.84
D89_445	G9A_Ti	C	41.92	0.39	21.37	0.04	2.86	6.39	0	0.29	21.97	4.29	0.07	0.13	99.72
D89_446	G9A_Ti	R	41.85	0.39	21.26	0.02	2.88	6.24	0.02	0.32	21.9	4.28	0.07	0.11	99.34
D89_447	G9A_Ti	C	41.75	0.42	21.27	0.02	2.89	6.39	0	0.29	21.9	4.28	0.06	0.13	99.4
D89_448	G9A_Ti	R	41.82	0.39	21.23	0.04	2.87	6.31	0	0.3	21.72	4.26	0.07	0.08	99.09
D89_449	G9A_Ti	C	41.69	0.4	21.01	0.02	2.78	7.24	0.02	0.27	21.13	4.69	0.04	0.14	99.43
D89_450	G9A_Ti	R	41.85	0.43	20.85	0	2.84	7.26	0	0.3	21.14	4.73	0.04	0.12	99.56
D91_221	G9A	C	40.79	0.25	17.74	0.04	7.55	6.72	0	0.37	19.72	6.01	0.04	0.13	99.36
D91_222	G9A	R	40.9	0.26	17.93	0.05	7.58	6.66	0.02	0.37	19.84	5.98	0	0.11	99.7
D91_223	G9A	C	40.98	0.25	17.84	0.05	7.53	6.62	0	0.36	19.72	6.01	0.03	0.08	99.47
D91_224	G9A	R	40.97	0.26	17.77	0.04	7.51	6.65	0	0.35	19.77	6.02	0.02	0.09	99.45
D91_225	G9A_Ti	C	41.69	0.51	21.04	0	2.71	7.13	0	0.28	21.27	4.75	0.05	0.15	99.58
D91_226	G9A_Ti	R	41.88	0.52	20.86	0.02	2.77	7.15	0	0.27	21.23	4.82	0.04	0.12	99.68
D91_227	G9A	C	41.15	0.34	17.84	0.04	7.5	6.46	0	0.34	20.02	5.86	0.05	0.08	99.68
D91_228	G9A	R	41.05	0.33	17.83	0.04	7.46	6.43	0	0.3	20.15	5.88	0.04	0.11	99.62
D91_229	G9B	C	40.73	0.08	17.89	0.04	7.48	7.04	0	0.42	18.78	6.42	0.02	0.05	98.95
D91_230	G9B	R	40.88	0.09	18.01	0.05	7.48	7.15	0	0.4	19.04	6.41	0	0.09	99.6
D91_231	G9B	C	40.88	0.09	17.92	0.04	7.54	7.11	0	0.4	18.89	6.45	0	0.06	99.38
D91_232	G9B	R	40.87	0.09	17.72	0.05	7.83	7.06	0	0.42	18.96	6.56	0.03	0.1	99.69
D91_233	G9A_Ti	C	41.34	0.52	18.71	0.05	5.68	6.65	0	0.28	20.79	5.39	0.04	0.13	99.58
D91_234	G9A_Ti	R	41.55	0.52	18.79	0.04	5.7	6.63	0	0.28	20.71	5.43	0.05	0.09	99.79
D91_235	G9A	C	40.97	0.26	17.85	0.05	7.55	6.65	0	0.37	19.71	6.01	0.03	0.08	99.53
D91_236	G9A	R	40.88	0.27	17.69	0.04	7.57	6.64	0	0.38	19.64	6.02	0.03	0.08	99.24
D91_237	G9B	C	40.94	0.11	18.02	0.05	7.53	7.13	0	0.4	18.86	6.42	0	0.04	99.5
D91_238	G9B	R	41.01	0.11	17.97	0.04	7.46	7.17	0	0.44	18.86	6.42	0	0.04	99.52
D91_239	G9A_Ti	C	41.6	0.52	20.87	0.04	2.73	7.11	0	0.29	21.15	4.76	0.03	0.13	99.23
D91_240	G9A_Ti	R	42.05	0.53	20.92	0.02	2.75	7.18	0	0.28	21.18	4.74	0.02	0.07	99.74
D91_241	G9B	C	40.92	0.09	17.94	0.06	7.36	7.13	0.02	0.41	18.89	6.38	0	0.05	99.25
D91_242	G9B	R	40.88	0.1	18.06	0.04	7.42	7.12	0	0.41	19.06	6.39	0.02	0.09	99.59
D91_243	G9A	C	40.97	0.25	17.66	0	7.65	6.62	0	0.36	19.75	6.01	0.02	0.09	99.38
D91_244	G9A	R	41.06	0.26	17.64	0.04	7.46	6.64	0	0.35	19.68	6.01	0.04	0.07	99.25
D91_245	G9A	C	41.16	0.24	17.78	0.04	7.56	6.69	0	0.37	19.81	6.03	0	0.08	99.76
D91_246	G9A	R	40.95	0.27	17.68	0.04	7.52	6.66	0	0.37	19.63	6	0.04	0.08	99.24
D91_247	G9A_Ti	C	41.22	0.53	18.51	0.04	5.61	6.69	0.02	0.29	20.57	5.43	0.05	0.12	99.08
D91_248	G9A_Ti	R	41.43	0.54	18.64	0.03	5.67	6.67	0	0.3	20.81	5.43	0.05	0.14	99.71
D91_249	G9A	C	40.97	0.27	17.75	0.03	7.56	6.56	0.02	0.35	19.72	6.01	0.02	0.07	99.33
D91_250	G9A	R	40.95	0.26	17.72	0.03	7.6	6.65	0	0.35	19.68	6.01	0.03	0.08	99.36
D91_251	G9A	C	40.85	0.25	17.7	0.05	7.62	6.64	0	0.36	19.77	6.04	0.03	0.12	99.43
D91_252	G9A	R	40.7	0.27	17.73	0.06	7.61	6.64	0	0.37	19.78	6.04	0	0.13	99.33

Appendix D: Garnet Xenocryst EPMA Data Tables

Appendix D.02 (continued): Dharma kimberlite garnet EPMA analyses. Zones: C – core, R – rim.

Sample	*Class*	*Zone*	*SiO_2*	*TiO_2*	*Al_2O_3*	*V_2O_3*	*Cr_2O_3*	*FeO*	*NiO*	*MnO*	*MgO*	*CaO*	*Na_2O*	*O*	*Total*
D91_253	G9A_Ti	C	41.43	0.56	20.7	0.04	2.8	7.72	0	0.32	20.78	4.65	0.05	0.14	99.19
D91_254	G9A_Ti	R	41.74	0.56	20.96	0	2.74	7.82	0	0.3	20.91	4.66	0.06	0.14	99.89
D91_255	G9B	C	40.89	0.11	18.1	0.05	7.56	7.1	0.02	0.4	19.07	6.46	0.03	0.1	99.89
D91_256	G9B	R	40.88	0.08	18.06	0.07	7.45	7.11	0	0.4	18.81	6.44	0	0.04	99.34
D91_257	G9A_Ti	C	41.55	0.45	19.83	0.03	4.39	6.75	0	0.29	20.93	5.08	0.05	0.11	99.46
D91_258	G9A_Ti	R	41.54	0.45	19.66	0	4.41	6.78	0	0.29	20.91	5.08	0.03	0.1	99.25
D91_259	G9A_Ti	C	41.62	0.49	18.87	0.04	5.64	6.71	0.02	0.3	20.96	5.43	0.04	0.15	100.27
D91_260	G9A_Ti	R	41.21	0.5	18.81	0.05	5.36	6.64	0	0.3	20.58	5.31	0.04	0.1	98.9
D91_261	G9A	C	41.01	0.25	17.76	0.05	7.68	6.68	0	0.36	19.76	6.06	0.03	0.1	99.74
D91_262	G9A	R	40.81	0.26	17.65	0.04	7.61	6.65	0	0.38	19.74	6.01	0.04	0.12	99.31
D91_263	G9A_Ti	C	41.72	0.53	20.9	0.03	2.7	7.1	0.02	0.3	21.14	4.73	0.04	0.11	99.32
D91_264	G9A_Ti	R	41.74	0.5	20.95	0.03	2.77	7.14	0	0.28	21.22	4.73	0.05	0.13	99.54
D91_265	G9A	C	40.95	0.26	17.76	0.06	7.61	6.68	0	0.37	19.7	5.99	0.03	0.09	99.5
D91_266	G9A	R	40.87	0.27	17.71	0.03	7.62	6.69	0	0.37	19.79	6.04	0	0.12	99.51
D91_267	G9A	C	41.64	0.23	20.34	0.03	3.71	6.85	0	0.26	21.13	4.88	0.03	0.13	99.23
D91_268	G9A	R	41.94	0.25	20.61	0.05	3.65	6.88	0.03	0.29	21.18	4.89	0.04	0.11	99.92
D91_269	G9A_Ti	C	41.56	0.45	19.42	0.03	4.78	6.66	0	0.3	21	5.15	0.05	0.12	99.52
D91_270	G9A_Ti	R	41.45	0.47	19.44	0.03	4.8	6.66	0.02	0.29	20.92	5.14	0.02	0.11	99.35
D91_271	G9A	C	40.93	0.23	17.84	0.04	7.53	6.69	0	0.36	19.77	6.02	0.03	0.11	99.55
D91_272	G9A	R	41	0.25	17.77	0.04	7.65	6.63	0	0.37	19.8	6.03	0.03	0.1	99.67
D91_273	G9A	C	41.84	0.28	21.58	0.03	2.84	7.28	0	0.33	21.16	4.45	0	0.09	99.88
D91_274	G9A	R	41.6	0.31	21.34	0.03	2.81	7.2	0	0.36	21.19	4.45	0.04	0.14	99.47
D91_275	G9A_Ti	C	41.31	0.45	19.35	0.03	4.74	6.7	0.02	0.29	20.84	5.13	0.05	0.13	99.04
D91_276	G9A_Ti	R	41.61	0.47	19.51	0.03	4.73	6.7	0.02	0.28	20.96	5.14	0.05	0.11	99.61
D91_277	G9A_Ti	C	41.8	0.61	20.22	0.05	3.12	7.34	0	0.29	21.01	4.95	0.06	0.13	99.58
D91_278	G9A_Ti	R	41.65	0.61	20.21	0.04	3.24	7.43	0	0.3	21.03	4.95	0.05	0.16	99.67
D91_279	G9B_Ti	C	41.51	0.74	20.4	0.03	2.8	7.96	0	0.33	20.5	4.96	0.06	0.13	99.42
D91_280	G9B_Ti	R	41.5	0.71	20.39	0.04	2.78	7.98	0	0.33	20.61	4.99	0.05	0.16	99.54
D91_281	G9A	C	40.83	0.26	17.78	0.04	7.53	6.62	0	0.38	19.67	6	0.03	0.09	99.23
D91_282	G9A	R	40.9	0.24	17.86	0.05	7.44	6.68	0.02	0.36	19.74	6	0.04	0.11	99.44
D91_283	G9A	C	41.05	0.27	17.94	0.06	7.66	6.69	0	0.36	19.79	6.04	0	0.09	99.95
D91_284	G9A	R	41.22	0.26	17.76	0.05	7.53	6.64	0.02	0.38	19.82	6.02	0.06	0.09	99.85
D91_285	G9B	C	40.82	0.07	17.97	0.03	7.63	7.12	0.02	0.39	18.98	6.41	0	0.08	99.52
D91_286	G9B	R	40.84	0.11	18.08	0.05	7.5	7.17	0	0.41	18.94	6.41	0.02	0.08	99.61
D91_287	G9A_Ti	C	41.5	0.58	20.64	0.05	2.94	7.85	0.02	0.33	20.7	4.67	0.05	0.13	99.46
D91_288	G9A_Ti	R	41.38	0.57	20.6	0.04	2.74	7.69	0	0.31	20.92	4.66	0.03	0.16	99.1
D91_289	G9A_Ti	C	41.29	0.52	18.58	0.05	5.55	6.68	0	0.3	20.69	5.4	0.05	0.13	99.24
D91_290	G9A_Ti	R	41.47	0.49	18.79	0.04	5.65	6.65	0	0.28	20.87	5.38	0.04	0.14	99.8
D91_291	G9A_Ti	C	41.33	0.53	18.59	0.05	5.75	6.67	0	0.26	20.73	5.4	0.04	0.13	99.48

Appendix D: Garnet Xenocryst EPMA Data Tables

Appendix D.02 (continued): Dharma kimberlite garnet EPMA analyses. Zones: C – core, R – rim.

Sample	*Class*	*Zone*	*SiO_2*	*TiO_2*	*Al_2O_3*	*V_2O_3*	*Cr_2O_3*	*FeO*	*NiO*	*MnO*	*MgO*	*CaO*	*Na_2O*	*O*	*Total*
D91_292	G9A_Ti	R	41.24	0.53	18.54	0.03	5.72	6.61	0	0.29	20.72	5.41	0.03	0.13	99.25
D91_293	G9A_Ti	C	41.43	0.51	18.6	0.03	5.7	6.69	0.02	0.31	20.77	5.42	0.05	0.14	99.67
D91_294	G9A_Ti	R	41.43	0.51	18.66	0.04	5.7	6.7	0	0.29	20.82	5.42	0.05	0.14	99.76
D91_295	G9A_Ti	C	41.73	0.63	20.29	0.05	3.21	7.33	0	0.29	20.92	4.94	0.04	0.11	99.54
D91_296	G9A_Ti	R	41.57	0.61	20.11	0.04	3.28	7.34	0	0.28	21.08	4.93	0.06	0.17	99.47
D91_297	G9A_Ti	C	40.97	0.37	17.58	0.03	7.41	6.46	0	0.31	20.16	5.91	0.04	0.13	99.37
D91_298	G9A	R	40.8	0.33	17.78	0.03	7.59	6.41	0	0.32	20.16	5.91	0.05	0.16	99.54
D91_299	G9A_Ti	C	41.43	0.55	18.5	0.03	5.69	6.76	0.02	0.29	20.59	5.45	0.02	0.09	99.42
D91_300	G9A_Ti	R	41.22	0.5	18.77	0.05	5.68	6.68	0	0.31	20.76	5.43	0.03	0.15	99.58
D91_301	G9A	C	40.74	0.25	17.61	0.05	7.61	6.71	0	0.35	19.72	6.05	0.04	0.13	99.26
D91_302	G9A	R	40.85	0.27	17.6	0.04	7.56	6.64	0	0.35	19.62	6.03	0	0.08	99.04
D91_303	G9B	C	40.67	0.09	17.98	0.04	7.55	7.18	0	0.42	18.92	6.44	0	0.1	99.39
D91_304	G9B	R	40.33	0.1	17.97	0.04	7.48	7.11	0	0.4	18.76	6.39	0	0.1	98.68
D91_305	G9B	C	40.91	0.08	18.02	0.04	7.85	7.08	0	0.41	19.04	6.56	0	0.1	100.09
D91_306	G9B	R	40.86	0.08	17.97	0.06	7.61	7.02	0	0.41	19	6.47	0	0.08	99.56
D91_307	G9A	C	40.89	0.27	17.81	0.03	7.69	6.67	0.02	0.37	19.7	6.03	0.04	0.11	99.63
D91_308	G9A	R	40.97	0.28	17.7	0.04	7.6	6.69	0	0.36	19.72	6.02	0.04	0.1	99.52
D91_309	G9B	C	40.87	0.06	19.48	0.03	5.91	7.7	0	0.49	18.83	6.28	0	0.1	99.75
D91_310	G9B	R	41	0.05	19.45	0.05	5.81	7.7	0	0.46	18.64	6.32	0	0.05	99.53
D91_311	G9B	C	40.72	0.07	19.04	0.04	6.15	7.68	0	0.47	18.57	6.39	0	0.08	99.21
D91_312	G9B	R	40.91	0.05	19.05	0.03	6.38	7.66	0	0.47	18.55	6.45	0	0.06	99.61
D91_313	G9B	C	40.85	0.09	18.05	0.04	7.47	7.2	0	0.41	19.01	6.42	0	0.1	99.64
D91_314	G9B	R	40.78	0.1	17.96	0.07	7.52	7.16	0	0.45	18.89	6.43	0	0.08	99.44
D91_315	G9A	C	40.62	0.26	17.68	0.06	7.52	6.66	0	0.34	19.73	6	0.05	0.14	99.06
D91_316	G9A	R	40.86	0.27	17.8	0.03	7.54	6.6	0	0.35	19.71	6.01	0.03	0.1	99.3
D91_317	G9B	C	40.8	0.08	17.86	0.06	7.71	7.05	0	0.41	18.85	6.52	0	0.06	99.4
D91_318	G9B	R	40.94	0.08	17.59	0.05	7.71	7.1	0	0.41	18.86	6.49	0.02	0.06	99.31
D91_319	G9B	C	40.85	0.11	18.14	0.06	7.61	7.14	0	0.42	19.07	6.46	0	0.1	99.96
D91_320	G9B	R	40.85	0.13	17.94	0.04	7.55	7.17	0	0.41	18.99	6.42	0	0.08	99.58
D91_321	G9A	C	40.85	0.24	17.68	0.03	7.53	6.66	0.03	0.36	19.8	6.04	0.04	0.14	99.4
D91_322	G9A	R	40.98	0.26	17.77	0.04	7.57	6.66	0.02	0.36	19.67	6.03	0.03	0.08	99.47
D91_323	G9A	C	40.9	0.27	17.75	0.04	7.57	6.66	0	0.35	19.74	6.03	0.05	0.11	99.47
D91_324	G9A	R	40.98	0.29	17.8	0.03	7.53	6.64	0	0.36	19.76	6	0.03	0.09	99.51
D91_325	G9B	C	40.98	0.08	18.06	0.04	7.57	7.06	0	0.44	19.03	6.46	0.02	0.08	99.82
D91_326	G9B	R	40.83	0.09	17.94	0.06	7.63	7.06	0	0.44	18.87	6.45	0	0.05	99.42
D91_327	G9A	C	41.09	0.27	18.09	0.03	7.51	6.69	0	0.38	19.75	6.01	0.03	0.09	99.94
D91_328	G9A	R	41.14	0.27	17.96	0.06	7.54	6.62	0	0.35	19.76	6.02	0.03	0.07	99.82
D93_133	G9A	C	40.7	0.08	16.98	0.04	8.28	7.46	0	0.39	19.38	5.9	0.02	0.15	99.38
D93_134	G9A	R	40.79	0.09	16.99	0.04	8.26	7.22	0	0.41	19.25	5.87	0.02	0.08	99.02

Appendix D: Garnet Xenocryst EPMA Data Tables

Appendix D.02 (continued): Dharma kimberlite garnet EPMA analyses. Zones: C – core, R – rim.

Sample	*Class*	*Zone*	*SiO_2*	*TiO_2*	*Al_2O_3*	*V_2O_3*	*Cr_2O_3*	*FeO*	*NiO*	*MnO*	*MgO*	*CaO*	*Na_2O*	*O*	*Total*
D93_135	G9A_Ti	C	41.13	0.44	18.51	0.04	5.87	6.36	0	0.32	20.89	5.19	0.04	0.13	98.92
D93_136	G9A_Ti	R	41.3	0.41	18.75	0.05	5.92	6.4	0	0.3	20.91	5.19	0.03	0.11	99.37
D93_137	G9A	C	41.13	0.18	20.61	0.03	3.88	7.86	0	0.4	19.98	5	0.02	0.11	99.2
D93_138	G9A	R	41.18	0.17	20.47	0	3.83	7.8	0.03	0.42	19.97	5	0.04	0.11	99.02
D93_139	G9A_Ti	C	41.05	0.71	20.04	0.05	3.15	8.63	0.02	0.38	20	4.88	0.06	0.17	99.14
D93_140	G9A_Ti	R	41.25	0.69	19.94	0.06	3.13	8.66	0.02	0.35	20.01	4.91	0.06	0.15	99.23
D93_141	G9A_Ti	C	41.6	0.68	20.08	0.04	2.98	7.65	0.04	0.31	20.7	4.95	0.05	0.13	99.21
D93_142	G9A_Ti	R	41.39	0.74	19.95	0.02	3.02	7.67	0	0.29	20.85	4.97	0.05	0.18	99.13
D93_143	G9A	C	40.82	0.16	18.33	0.04	6.62	7.01	0	0.39	19.63	5.78	0	0.1	98.88
D93_144	G9A	R	40.9	0.15	18.32	0.03	6.69	7.02	0	0.34	19.62	5.79	0.02	0.09	98.97
D93_145	G9A_Ti	C	41.13	0.39	18.97	0.04	5.79	6.34	0	0.32	20.88	5.16	0.07	0.15	99.24
D93_146	G9A_Ti	R	41.19	0.37	19.12	0.06	5.62	6.35	0	0.33	20.89	5.12	0.04	0.12	99.21
D93_147	G9A_Ti	C	40.88	0.42	18.82	0.05	5.95	6.33	0.02	0.3	20.83	5.18	0.05	0.16	98.99
D93_148	G9A_Ti	R	41.13	0.42	18.74	0.07	5.95	6.33	0	0.3	20.83	5.18	0.05	0.12	99.12
D93_149	G9A_Ti	C	41.22	0.44	18.91	0.05	5.83	6.39	0	0.31	20.89	5.17	0.04	0.12	99.37
D93_150	G9A_Ti	R	41.32	0.42	18.94	0.04	5.95	6.35	0.02	0.3	20.76	5.2	0.04	0.08	99.42
D93_151	G9A	C	40.98	0.16	18.48	0	6.69	7.05	0	0.37	19.72	5.8	0	0.11	99.36
D93_152	G9A	R	40.87	0.17	18.31	0.05	6.71	7.02	0.02	0.39	19.64	5.79	0.02	0.11	99.1
D93_153	G9A	C	40.9	0.15	18.64	0.05	6.65	7.05	0	0.39	19.69	5.77	0.02	0.11	99.42
D93_154	G9A	R	40.91	0.17	18.42	0.05	6.6	6.99	0	0.39	19.66	5.77	0.03	0.1	99.09
D93_155	G9A	C	41.04	0.16	18.48	0.06	6.64	7.06	0	0.36	19.62	5.78	0	0.07	99.27
D93_156	G9A	R	40.88	0.16	18.42	0.05	6.55	7.07	0	0.37	19.61	5.78	0.04	0.11	99.04
D93_157	G9A_Ti	C	41.34	0.41	18.91	0.03	5.92	6.37	0	0.3	20.66	5.16	0.05	0.06	99.21
D93_158	G9A_Ti	R	41.18	0.42	19	0.04	5.77	6.34	0	0.29	20.88	5.14	0.04	0.11	99.21
D93_159	G9A_Ti	C	41.39	0.41	18.9	0.04	5.77	6.41	0	0.31	20.86	5.17	0.06	0.1	99.42
D93_160	G9A_Ti	R	41.53	0.41	18.98	0.06	5.73	6.32	0	0.29	20.81	5.17	0.05	0.06	99.41
D93_161	G9A	C	40.89	0.16	18.66	0.03	6.61	7	0	0.37	19.7	5.78	0.02	0.11	99.33
D93_162	G9A	R	41	0.18	18.56	0.04	6.54	7.14	0	0.4	19.61	5.81	0.03	0.1	99.41
D93_163	G9A_Ti	C	41.22	0.44	18.78	0.04	5.88	6.38	0	0.31	20.82	5.2	0.06	0.12	99.25
D93_164	G9A_Ti	R	41.6	0.43	19.15	0.04	5.97	6.4	0	0.31	20.84	5.19	0.04	0.06	100.03
D93_165	G9A	C	40.53	0.11	17.44	0.04	8.56	7.22	0	0.41	19.33	5.94	0	0.13	99.71
D93_166	G9A	R	40.86	0.09	17.32	0.02	8.51	7.24	0.02	0.39	19.17	5.95	0.03	0.07	99.67
D93_167	G9A	C	40.72	0.16	18.49	0.05	6.59	7	0.02	0.39	19.74	5.74	0.03	0.14	99.07
D93_168	G9A	R	41.03	0.16	18.48	0.03	6.67	7	0	0.38	19.47	5.81	0	0.04	99.07
D93_169	G9A_Ti	C	41.62	0.41	18.93	0.04	5.74	6.43	0	0.29	20.83	5.19	0.04	0.06	99.58
D93_170	G9A_Ti	R	41.45	0.41	19.1	0.06	5.69	6.35	0	0.31	21	5.16	0.05	0.11	99.69
D93_171	G9A	C	40.98	0.17	18.6	0.03	6.76	7.07	0	0.38	19.73	5.81	0.03	0.12	99.68
D93_172	G9A	R	41.17	0.18	18.74	0.03	6.64	7.09	0	0.37	19.79	5.81	0.02	0.1	99.94
D93_173	G9A	C	41.11	0.18	18.81	0.03	6.73	7.1	0	0.38	19.84	5.79	0.03	0.12	100.12

Appendix D: Garnet Xenocryst EPMA Data Tables

Appendix D.02 (continued): Dharma kimberlite garnet EPMA analyses. Zones: C – core, R – rim.

Sample	*Class*	*Zone*	*SiO_2*	*TiO_2*	*Al_2O_3*	*V_2O_3*	*Cr_2O_3*	*FeO*	*NiO*	*MnO*	*MgO*	*CaO*	*Na_2O*	*O*	*Total*
D93_174	G9A	R	40.98	0.16	18.6	0.03	6.63	7.11	0.02	0.36	19.79	5.77	0.03	0.13	99.61
D93_175	G9A	C	41.15	0.16	18.59	0.06	6.64	7.11	0.02	0.38	19.69	5.8	0.04	0.1	99.74
D93_176	G9A	R	41.11	0.17	18.66	0.03	6.72	7.05	0	0.38	19.64	5.82	0.03	0.08	99.69
D93_177	G9A_Ti	C	41.21	0.43	18.67	0.04	6.08	6.41	0	0.3	20.67	5.24	0.06	0.1	99.21
D93_178	G9A_Ti	R	41.39	0.44	19.05	0.05	5.91	6.35	0	0.3	20.8	5.23	0.06	0.09	99.67
D93_179	G9B_Ti	C	41.19	0.69	20.29	0.04	3.38	8.53	0	0.37	19.78	5.25	0.05	0.14	99.71
D93_180	G9B_Ti	R	41.22	0.71	20.1	0.05	3.39	8.43	0	0.33	19.82	5.29	0.05	0.13	99.52
D93_181	G9A_Ti	C	41.35	0.38	19.07	0.05	5.65	6.36	0	0.3	20.86	5.14	0.04	0.1	99.3
D93_182	G9A_Ti	R	41.46	0.4	19.23	0.03	5.68	6.36	0	0.33	20.8	5.16	0.04	0.07	99.56
D93_183	G9A	C	40.98	0.16	18.58	0.03	6.56	7.11	0	0.38	19.6	5.77	0.02	0.09	99.28
D93_184	G9A	R	41.11	0.18	18.54	0.04	6.69	7	0	0.37	19.75	5.81	0.04	0.1	99.63
D93_185	G9A_Ti	C	41.3	0.42	19.07	0.05	5.8	6.33	0.02	0.31	20.95	5.16	0.05	0.12	99.58
D93_186	G9A_Ti	R	41.38	0.42	18.97	0.05	5.82	6.27	0.02	0.31	20.87	5.14	0.05	0.08	99.38
D93_187	G9A_Ti	C	41.4	0.39	19.25	0.03	5.62	6.35	0	0.3	21.04	5.12	0.04	0.12	99.66
D93_188	G9A_Ti	R	41.43	0.4	19.13	0.05	5.71	6.36	0	0.3	20.8	5.14	0.03	0.07	99.42
D93_189	G9A	C	41.02	0.18	18.42	0.03	6.63	7.09	0	0.38	19.54	5.79	0.03	0.07	99.18
D93_190	G9A	R	41.02	0.14	18.71	0.05	6.68	7.03	0	0.37	19.76	5.78	0.02	0.11	99.67
D93_191	G9A	C	41.02	0.16	18.67	0.05	6.7	7.05	0	0.37	19.76	5.79	0.02	0.11	99.7
D93_192	G9A	R	41.25	0.17	18.6	0.03	6.71	7.04	0	0.4	19.65	5.82	0	0.05	99.72
D93_193	G9A_Ti	C	41.42	0.41	18.86	0.04	6.08	6.43	0	0.33	20.7	5.24	0.05	0.08	99.64
D93_194	G9A_Ti	R	41.29	0.42	18.76	0.05	5.98	6.34	0	0.31	20.72	5.22	0.05	0.08	99.22
D93_195	G9A_Ti	C	41.26	0.44	18.47	0.02	5.73	6.58	0.02	0.28	20.26	5.41	0.06	0.05	98.58
D93_196	G9A_Ti	R	41.47	0.47	18.62	0.04	5.68	6.63	0	0.29	20.5	5.42	0.04	0.06	99.22
D93_197	G9A_Ti	C	41.31	0.42	18.85	0.05	5.61	6.86	0	0.3	20.37	5.41	0.03	0.09	99.3
D93_198	G9A_Ti	R	41.43	0.44	18.78	0.03	5.65	6.77	0.02	0.3	20.54	5.42	0.02	0.09	99.49
D93_199	G9A_Ti	C	41.28	0.46	18.61	0.05	5.76	6.62	0	0.3	20.68	5.4	0.05	0.13	99.34
D93_200	G9A_Ti	R	41.43	0.46	18.67	0.05	5.68	6.64	0	0.28	20.7	5.45	0.02	0.11	99.49
D93_201	G9A	C	40.69	0.08	17.23	0.03	8.55	7.2	0	0.42	19.25	5.93	0.02	0.1	99.5
D93_202	G9A	R	40.69	0.08	17.17	0.04	8.64	7.21	0	0.41	19.03	5.96	0	0.06	99.29
D93_203	G9A	C	40.49	0.11	17.01	0.03	8.45	7.22	0	0.39	18.96	5.96	0.02	0.07	98.71
D93_204	G9A	R	40.82	0.08	17.12	0.05	8.53	7.25	0	0.39	19.15	5.93	0	0.06	99.38
D93_205	G9A_Ti	C	41.26	0.4	18.88	0.05	5.89	6.34	0	0.31	20.65	5.18	0.04	0.07	99.07
D93_206	G9A_Ti	R	41.43	0.45	19.1	0.04	5.78	6.32	0	0.32	20.83	5.16	0.06	0.08	99.57
D93_207	G9A_Ti	C	41.46	0.43	19.14	0.04	5.68	6.32	0	0.3	20.81	5.14	0.05	0.07	99.44
D93_208	G9A_Ti	R	41.62	0.43	19.09	0.04	5.71	6.33	0	0.3	20.72	5.16	0.05	0.03	99.48
D93_209	G9A	C	41.13	0.17	18.57	0.02	6.75	7.07	0	0.36	19.57	5.8	0.02	0.06	99.52
D93_210	G9A	R	41.25	0.18	18.8	0.05	6.59	7.04	0	0.39	19.74	5.8	0.03	0.08	99.95
D93_211	G9A_Ti	C	41.42	0.43	19.13	0.06	5.86	6.34	0	0.3	20.83	5.15	0.05	0.08	99.65
D93_212	G9A_Ti	R	41.88	0.41	19.05	0.04	5.92	6.41	0	0.32	20.84	5.24	0.05	0.04	100.2

Appendix D: Garnet Xenocryst EPMA Data Tables

Appendix D.02 (continued): Dharma kimberlite garnet EPMA analyses. Zones: C – core, R – rim.

Sample	***Class***	***Zone***	***SiO_2***	***TiO_2***	***Al_2O_3***	***V_2O_3***	***Cr_2O_3***	***FeO***	***NiO***	***MnO***	***MgO***	***CaO***	***Na_2O***	***O***	***Total***
D93_213	G9A	C	41.21	0.15	18.49	0.03	6.66	7.05	0	0.39	19.56	5.8	0.03	0.05	99.42
D93_214	G9A	R	41.2	0.17	18.59	0.05	6.67	7.08	0	0.38	19.62	5.79	0	0.06	99.61
D93_215	G9A_Ti	C	41.79	0.72	20.24	0.04	3	7.7	0	0.3	20.81	4.98	0.06	0.13	99.77
D93_216	G9A_Ti	R	41.72	0.72	20.14	0.03	2.96	7.68	0	0.27	20.59	4.97	0.05	0.08	99.21
D93_217	G9A_Ti	C	41.49	0.4	19.09	0.05	5.72	6.4	0	0.32	20.88	5.14	0.05	0.09	99.63
D93_218	G9A_Ti	R	41.32	0.41	18.92	0.03	5.77	6.35	0	0.33	20.56	5.17	0.05	0.05	98.96
D93_219	G9A	C	41.14	0.15	18.59	0.03	6.7	7.03	0	0.37	19.72	5.77	0.02	0.08	99.6
D93_220	G9A	R	41.15	0.16	18.71	0.05	6.64	7.05	0	0.36	19.86	5.8	0.03	0.12	99.93

Appendix E: Garnet Xenocryst LA-ICP-MS Data Tables

Appendix E.01: Mel kimberlite garnet trace element data measured by LA-ICPMS. 2SE – two times standard error. LOD – Limit of detection (Pettke et al., 2014). <LOD – bellow limit of detection.

Sample	*Class*	*Spot Size*	*Ca ppm*	*Ca 2SE*	*Ca LOD*	*Sc ppm*	*Sc 2SE*	*Sc LOD*	*Ti ppm*	*Ti 2SE*	*Ti LOD*	*V ppm*	*V 2SE*	*V LOD*
M1_47824_003_263	G9A_Ti	285	37370	240	3.25085	118.63	0.98	0.00572	3625	0.144954	0.14	319.6	2.1	0.00268
M1_47824_017_277	G9A	285	34590	190	3.52047	114.37	0.93	0.00589	1433.5	0.152711	0.15	281.8	1.5	0.00289
M1_47824_035_295	G9A_Ti	130	26360	200	15.7161	78.65	0.49	0.01987	2731	0.64777	0.65	181.3	1.2	0.00865
M1_47824_037_297	G9A	285	31150	140	3.56047	132.93	0.65	0.00578	1533	0.154573	0.15	163.7	0.7	0.00278
M1_47824_039_299	G9A	285	34560	150	3.48461	191.55	0.84	0.00584	1677.7	0.15307	0.15	213.5	1.1	0.00271
M1_49724_011_371	G9A	285	32110	160	3.66692	110.68	0.52	0.00625	1957.2	0.161654	0.16	257.3	1	0.00299
M1_49724_015_375	G9A	130	48300	1100	16.9376	84.3	1.1	0.02062	1873	0.697734	0.70	281.5	3.4	0.01082
M1_49724_019_379	G9A_Ti	285	31780	150	3.60870	101.7	0.35	0.00610	4223	0.158625	0.16	204.19	0.91	0.00285
M1_49724_021_381	G9A_Ti	130	27470	190	16.9382	76.5	0.55	0.02046	3582	0.689624	0.69	194.2	1.1	0.01007
M1_49724_035_395	G9A_Ti	285	29700	140	3.71963	94.11	0.44	0.00652	2603	0.164281	0.16	245.1	0.86	0.00297
M1_49724_039_399	G9B_Ti	285	43250	310	3.57802	108.98	0.57	0.00579	2850	0.155145	0.16	308.4	1.3	0.00281
M1_49724_041_401	G9A_Ti	285	30870	170	3.55204	100.48	0.48	0.00714	4544	0.163121	0.16	206.9	1.5	0.00232
M1_49725_015_417	G9A_Ti	285	30640	120	3.57843	97.22	0.42	0.00647	3946	0.156394	0.16	194.91	0.83	0.00246
M1_49725_019_421	G9A_Ti	285	30620	160	3.71547	98.31	0.5	0.00686	3949	0.164437	0.16	192.85	0.84	0.00256
M1_49725_023_425	G9A_Ti	285	40500	1400	3.56162	104.92	0.43	0.00624	3176	0.156673	0.16	219.3	0.86	0.00255
M1_49725_025_427	G9A_Ti	285	34570	130	3.26427	110.37	0.52	0.00554	4555	0.144552	0.14	223.6	1.1	0.00282
M1_49725_039_441	G9A_Ti	130	33370	320	16.9120	81.26	0.72	0.02029	2667	0.698907	0.70	158.4	2.6	0.01108
M1_49725_041_443	G9A_Ti	285	31610	140	3.44186	98.4	0.42	0.00585	4084	0.148692	0.15	257.5	1	0.00273
M1_49725_051_453	G9A_Ti	285	30650	120	3.54705	98.68	0.38	0.00619	3769	0.15318	0.15	200.12	0.84	0.00254
M1_49741_001_301	G9A	285	35720	190	3.27420	124.96	0.95	0.00522	1331.8	0.141687	0.14	347.3	2.1	0.00279
M1_49741_005_305	G9A_Ti	285	31260	130	3.68511	99.51	0.4	0.00572	4754	0.162151	0.16	221.27	0.71	0.00310
M1_49741_015_315	G9A	285	30740	120	3.49843	108.34	0.4	0.00543	755.4	0.153223	0.15	151.03	0.67	0.00274
M1_49741_017_317	G9A	285	36230	150	3.42702	132.62	0.51	0.00528	1704.7	0.151361	0.15	348	1.5	0.00307
M1_49741_021_321	G9A	285	29500	110	3.69298	102.51	0.48	0.00569	711.4	0.161524	0.16	147.11	0.51	0.00300
M1_49741_029_329	G9A_Ti	285	31300	150	3.31444	101.78	0.6	0.00654	4800	0.155045	0.16	212.4	1.1	0.00233
M1_49741_041_341	G9A_Ti	285	33790	180	3.46550	119.17	0.38	0.00625	3479	0.158786	0.16	246.2	1.2	0.00252
M1_49741_053_353	G9A	285	36840	150	3.54217	147.45	0.65	0.00612	2020.8	8.7	0.15	326.1	1.2	0.00284
M1_49741_059_359	G9A_Ti	285	33270	160	3.63507	111.06	0.37	0.00601	2507.4	8.8	0.16	275.1	1.1	0.00292
M2_47824_003_465	G9A_Ti	285	30620	140	3.69842	100.08	0.41	0.00581	3013	12	0.16	198.01	0.86	0.00287
M2_47824_013_475	G9A	285	30790	170	3.63070	122.61	0.51	0.00598	2224.6	9.4	0.15	188.91	0.97	0.00281
M2_47824_015_477	G9A	130	30920	230	3.94152	92.49	0.55	0.00674	1303.7	8.2	0.17	279.9	1.8	0.00278
M2_47824_029_491	G9A	285	34140	130	16.5813	116.15	0.49	0.01911	1564.5	6.4	0.67	292.8	1.1	0.01008
M2_47824_033_495	G9A_Ti	285	28470	150	3.78164	99.78	0.39	0.00696	3346	13	0.18	193.5	0.93	0.00260
M2_47824_037_499	G9A_Ti	130	25470	190	3.87056	78.48	0.46	0.00675	2674	16	0.17	176.3	1	0.00244
M2_49724_009_743	G3_Na	130	40130	320	16.8633	50.46	0.39	0.02000	3683	32	0.67	170.2	1.2	0.01142
M2_49724_013_747	G9A	285	33540	150	18.0089	114.67	0.42	0.02168	2372	9.3	0.72	295	1.3	0.00997
M2_49724_037_771	G9A_Ti	285	30240	130	3.93894	99.37	0.3	0.00687	4346	16	0.18	203.04	0.8	0.00275
M2_49724_045_779	G3_Na	130	29470	270	4.08208	84.22	0.73	0.00734	2734	25	0.18	156.6	1.2	0.00284

Appendix E: Garnet Xenocryst LA-ICP-MS Data Tables

Appendix E.01 (continued): Mel kimberlite garnet trace element data measured by LA-ICPMS. 2SE – two times standard error. LOD – Limit of detection (Pettke et al., 2014). <LOD – bellow limit of detection.

Sample	*Class*	*Spot Size*	*Ni ppm*	*Ni 2SE*	*Ni LOD*	*Rb ppm*	*Rb 2SE*	*Rb LOD*	*Sr ppm*	*Sr 2SE*	*Sr LOD*	*Y ppm*	*Y 2SE*	*Y LOD*
M1_47824_003_263	G9A_Ti	285	122.36	0.87	0.0239	0.0268	0.003	0.0057	0.3003	0.0049	0.00125	14.32	0.18	0.00047
M1_47824_017_277	G9A	285	119.1	0.84	0.0243	0.0078	0.0037	0.0056	0.3374	0.0079	0.00120	13.14	0.15	0.00051
M1_47824_035_295	G9A_Ti	130	105.73	0.8	0.1251	0.054	0.019	0.0316	0.312	0.013	0.00531	14.18	0.15	0.00195
M1_47824_037_297	G9A	285	44.15	0.28	0.0246	0.0173	0.0033	0.0056	0.3657	0.0079	0.00115	28.51	0.16	0.00052
M1_47824_039_299	G9A	285	38.28	0.24	0.0251	0.015	0.0031	0.0055	0.4582	0.0065	0.00117	14.346	0.078	0.00042
M1_49724_011_371	G9A	285	139.46	0.7	0.0258	0.0044	0.0026	0.0044	0.5029	0.0086	0.00104	20.28	0.11	0.00046
M1_49724_015_375	G9A	130	113.2	1.7	0.1346	0.044	0.018	0.0322	9.61	0.36	0.00670	12.84	0.2	0.00156
M1_49724_019_379	G9A_Ti	285	117.96	0.68	0.0248	0.0129	0.0023	0.0043	0.888	0.016	0.00102	26.12	0.15	0.00038
M1_49724_021_381	G9A_Ti	130	114.12	0.83	0.1359	0.038	0.018	0.0294	0.36	0.014	0.00601	18.79	0.17	0.00153
M1_49724_035_395	G9A_Ti	285	120.3	2.5	0.0263	0.065	0.022	0.0044	0.663	0.077	0.00105	19.92	0.13	0.00047
M1_49724_039_399	G9B_Ti	285	117.67	0.64	0.0253	0.0114	0.0022	0.0040	7.07	0.11	0.00090	17.88	0.1	0.00051
M1_49724_041_401	G9A_Ti	285	118.23	0.66	0.0257	0.0125	0.0022	0.0042	0.3989	0.0082	0.00104	25.72	0.17	0.00045
M1_49725_015_417	G9A_Ti	285	121.32	0.65	0.0254	0.0079	0.0031	0.0041	0.4132	0.009	0.00108	23.37	0.14	0.00045
M1_49725_019_421	G9A_Ti	285	124.75	0.77	0.0268	0.0075	0.0032	0.0042	0.408	0.0073	0.00097	25.91	0.19	0.00052
M1_49725_023_425	G9A_Ti	285	136.98	0.74	0.0248	0.0115	0.0025	0.0039	7.5	1	0.00091	21.1	0.15	0.00050
M1_49725_025_427	G9A_Ti	285	80.36	0.4	0.0225	0.0062	0.0023	0.0035	0.4837	0.0095	0.00092	24.23	0.13	0.00046
M1_49725_039_441	G9A_Ti	130	100	1.1	0.1385	0.038	0.016	0.0307	0.396	0.013	0.00603	19.04	0.21	0.00154
M1_49725_041_443	G9A_Ti	285	119.47	0.56	0.0243	0.0078	0.0031	0.0037	0.3857	0.0067	0.00097	23.63	0.11	0.00034
M1_49725_051_453	G9A_Ti	285	118.37	0.59	0.0253	0.0091	0.003	0.0038	0.4163	0.0081	0.00098	22.45	0.13	0.00050
M1_49741_001_301	G9A	285	132	1.1	0.0233	0.0081	0.0034	0.0050	0.5271	0.0085	0.00101	11.41	0.15	0.00049
M1_49741_005_305	G9A_Ti	285	134.51	0.64	0.0259	0.007	0.003	0.0054	0.4059	0.0092	0.00124	26.29	0.15	0.00051
M1_49741_015_315	G9A	285	23.27	0.17	0.0246	0.008	0.0026	0.0051	0.1026	0.0045	0.00111	17.59	0.11	0.00046
M1_49741_017_317	G9A	285	125.37	0.58	0.0245	0.0102	0.003	0.0050	0.4002	0.0063	0.00105	12.958	0.066	0.00047
M1_49741_021_321	G9A	285	22.69	0.14	0.0265	0.0024	0.003	0.0051	0.0982	0.0038	0.00118	16.57	0.12	0.00047
M1_49741_029_329	G9A_Ti	285	128.41	0.69	0.0240	0.0328	0.0034	0.0045	0.66	0.037	0.00115	26.82	0.19	0.00055
M1_49741_041_341	G9A_Ti	285	120.6	0.64	0.0253	0.0108	0.0031	0.0045	0.4269	0.0079	0.00111	17.18	0.1	0.00047
M1_49741_053_353	G9A	285	120.56	0.7	0.0240	0.0082	0.0022	0.0045	0.4421	0.0079	0.00102	7.798	0.05	0.00042
M1_49741_059_359	G9A_Ti	285	140.3	0.69	0.0249	0.0058	0.0021	0.0046	0.2232	0.005	0.00108	18.863	0.095	0.00048
M2_47824_003_465	G9A_Ti	285	70.86	0.34	0.0282	0.0082	0.0022	0.0037	0.2683	0.0053	0.00100	21.19	0.12	0.00029
M2_47824_013_475	G9A	285	48.15	0.31	0.0248	0.0052	0.0022	0.0039	0.5054	0.0079	0.00079	24.12	0.15	0.00049
M2_47824_015_477	G9A	130	113.75	0.82	0.0269	0.058	0.017	0.0041	0.255	0.012	0.00099	10.64	0.11	0.00049
M2_47824_029_491	G9A	285	119.56	0.54	0.1314	0.0173	0.0033	0.0278	0.3425	0.0069	0.00555	13.951	0.096	0.00154
M2_47824_033_495	G9A_Ti	285	112.55	0.63	0.0307	0.0073	0.0025	0.0048	0.3504	0.0099	0.00136	18.95	0.13	0.00051
M2_47824_037_499	G9A_Ti	130	107.26	0.81	0.0317	0.011	0.015	0.0046	0.332	0.015	0.00124	14.08	0.13	0.00039
M2_49724_009_743	G3_Na	130	123.69	0.87	0.1309	0.0042	0.0058	0.0279	0.541	0.016	0.00577	17.86	0.18	0.00148
M2_49724_013_747	G9A	285	116.16	0.76	0.2917	0.0064	0.0019	0.0088	0.3669	0.0067	0.00430	16.84	0.1	0.00160
M2_49724_037_771	G9A_Ti	285	118.36	0.62	0.0294	0.0061	0.0021	0.0037	0.4013	0.0051	0.00093	25.32	0.14	0.00033
M2_49724_045_779	G3_Na	130	19	0.36	0.0305	0.0145	0.007	0.0038	0.1983	0.0092	0.00099	21.36	0.23	0.00034

Appendix E: Garnet Xenocryst LA-ICP-MS Data Tables

Appendix E.01 (continued): Mel kimberlite garnet trace element data measured by LA-ICPMS. 2SE – two times standard error. LOD – Limit of detection (Pettke et al., 2014). <LOD – bellow limit of detection.

Sample	*Class*	*Spot Size*	*Zr ppm*	*Zr 2SE*	*Zr LOD*	*Nb ppm*	*Nb 2SE*	*Nb LOD*	*Ba ppm*	*Ba 2SE*	*Ba LOD*	*La ppm*	*La 2SE*	*La LOD*
M1_47824_003_263	G9A_Ti	285	47.92	0.59	0.00174	0.179	0.0045	0.00031	<LOD	<LOD	0.00229	0.02272	0.00078	0.00009
M1_47824_017_277	G9A	285	11.76	0.12	0.00161	0.2414	0.0055	0.00039	<LOD	<LOD	0.00207	0.02418	0.0007	0.00011
M1_47824_035_295	G9A_Ti	130	31.34	0.29	0.00436	0.0759	0.0057	0.00113	<LOD	<LOD	0.00924	0.00875	0.00094	0.00041
M1_47824_037_297	G9A	285	75.33	0.41	0.00156	0.2978	0.0052	0.00033	<LOD	<LOD	0.00245	0.01451	0.00058	0.00012
M1_47824_039_299	G9A	285	55.65	0.25	0.00159	0.2018	0.0046	0.00032	<LOD	<LOD	0.00221	0.01645	0.0007	0.00013
M1_49724_011_371	G9A	285	12.382	0.09	0.00145	0.1889	0.0047	0.00037	<LOD	<LOD	0.00208	0.02821	0.00085	0.00013
M1_49724_015_375	G9A	130	6.75	0.19	0.00493	0.0768	0.0058	0.00148	0.081	0.013	0.00795	3.77	0.1	0.00040
M1_49724_019_379	G9A_Ti	285	57.18	0.3	0.00126	0.0923	0.0032	0.00042	0.109	0.0099	0.00177	0.2826	0.0081	0.00011
M1_49724_021_381	G9A_Ti	130	43.72	0.34	0.00458	0.0649	0.0053	0.00137	<LOD	<LOD	0.00913	0.0081	0.001	0.00040
M1_49724_035_395	G9A_Ti	285	32.46	0.24	0.00143	0.198	0.027	0.00038	0.177	0.038	0.00192	0.069	0.018	0.00013
M1_49724_039_399	G9B_Ti	285	40.81	0.27	0.00111	0.165	0.023	0.00044	0.0657	0.0065	0.00202	3.008	0.046	0.00013
M1_49724_041_401	G9A_Ti	285	59.76	0.35	0.00121	0.0767	0.0032	0.00045	<LOD	<LOD	0.00164	0.01254	0.00067	0.00013
M1_49725_015_417	G9A_Ti	285	57.38	0.42	0.00101	0.0968	0.0047	0.00044	0.00111	0.00091	0.00195	0.0146	0.0011	0.00012
M1_49725_019_421	G9A_Ti	285	57.69	0.43	0.00133	0.1035	0.0042	0.00035	<LOD	<LOD	0.00188	0.0152	0.0012	0.00012
M1_49725_023_425	G9A_Ti	285	42.76	0.28	0.00098	0.2543	0.005	0.00035	0.616	0.077	0.00173	0.81	0.13	0.00011
M1_49725_025_427	G9A_Ti	285	59.52	0.34	0.00087	0.0739	0.0027	0.00030	0.00126	0.00096	0.00194	0.01078	0.00053	0.00010
M1_49725_039_441	G9A_Ti	130	31.63	0.38	0.00449	0.0896	0.0068	0.00139	0.0097	0.0051	0.00987	0.0174	0.0021	0.00043
M1_49725_041_443	G9A_Ti	285	49.57	0.28	0.00101	0.1263	0.0049	0.00042	0.0055	0.0038	0.00163	0.0229	0.0011	0.00010
M1_49725_051_453	G9A_Ti	285	53.18	0.32	0.00112	0.0822	0.0031	0.00036	0.0084	0.0037	0.00177	0.0152	0.0011	0.00012
M1_49741_001_301	G9A	285	2.354	0.035	0.00132	0.3029	0.0059	0.00032	<LOD	<LOD	0.00206	0.0432	0.0012	0.00009
M1_49741_005_305	G9A_Ti	285	64.23	0.36	0.00138	0.0841	0.0026	0.00027	<LOD	<LOD	0.00201	0.01309	0.00071	0.00012
M1_49741_015_315	G9A	285	12.188	0.09	0.00133	0.0446	0.0024	0.00033	0.003	0.0016	0.00208	0.02042	0.00068	0.00011
M1_49741_017_317	G9A	285	10.904	0.066	0.00122	0.401	0.0074	0.00040	<LOD	<LOD	0.00174	0.04537	0.00094	0.00011
M1_49741_021_321	G9A	285	11.622	0.085	0.00134	0.0492	0.0023	0.00042	0.0043	0.0016	0.00253	0.02097	0.00085	0.00011
M1_49741_029_329	G9A_Ti	285	66.09	0.44	0.00144	0.1336	0.0061	0.00035	0.255	0.031	0.00204	0.0449	0.0045	0.00012
M1_49741_041_341	G9A_Ti	285	37.78	0.26	0.00144	0.1318	0.0038	0.00043	<LOD	<LOD	0.00169	0.015	0.00049	0.00012
M1_49741_053_353	G9A	285	7.025	0.067	0.00137	0.1977	0.0049	0.00044	<LOD	<LOD	0.00187	0.02395	0.00076	0.00010
M1_49741_059_359	G9A_Ti	285	19.348	0.095	0.00143	0.4603	0.0086	0.00038	<LOD	<LOD	0.00182	0.04664	0.00095	0.00013
M2_47824_003_465	G9A_Ti	285	36.37	0.22	0.00090	0.0908	0.0035	0.00028	<LOD	<LOD	0.00150	0.00763	0.00037	0.00008
M2_47824_013_475	G9A	285	66.15	0.46	0.00117	0.3982	0.0054	0.00048	<LOD	<LOD	0.00193	0.02107	0.00066	0.00011
M2_47824_015_477	G9A	130	5.312	0.084	0.00120	0.211	0.01	0.00048	<LOD	<LOD	0.00187	0.0185	0.0013	0.00012
M2_47824_029_491	G9A	285	7.179	0.071	0.00459	0.2295	0.0057	0.00182	<LOD	<LOD	0.00745	0.02426	0.00092	0.00046
M2_47824_033_495	G9A_Ti	285	40.1	0.28	0.00115	0.0832	0.0038	0.00034	<LOD	<LOD	0.00165	0.01107	0.00057	0.00010
M2_47824_037_499	G9A_Ti	130	29.63	0.26	0.00099	0.0664	0.0054	0.00037	0.0305	0.0086	0.00205	0.0188	0.0017	0.00010
M2_49724_009_743	G3_Na	130	24.39	0.28	0.00456	0.1402	0.0087	0.00124	<LOD	<LOD	0.00843	0.0223	0.0016	0.00039
M2_49724_013_747	G9A	285	10.323	0.086	0.00667	0.0793	0.0031	0.00150	<LOD	<LOD	0.00847	0.00882	0.00045	0.00045
M2_49724_037_771	G9A_Ti	285	56.61	0.29	0.00098	0.0836	0.0029	0.00027	<LOD	<LOD	0.00191	0.0108	0.00044	0.00009
M2_49724_045_779	G3_Na	130	69.31	0.77	0.00077	0.0626	0.0042	0.00039	0.039	0.013	0.00131	0.00653	0.00078	0.00011

Appendix E: Garnet Xenocryst LA-ICP-MS Data Tables

Appendix E.01 (continued): Mel kimberlite garnet trace element data measured by LA-ICPMS. 2SE – two times standard error. LOD – Limit of detection (Pettke et al., 2014). <LOD – bellow limit of detection.

Sample	*Class*	*Spot Size*	*Ce ppm*	*Ce 2SE*	*Ce LOD*	*Pr ppm*	*Pr 2SE*	*Pr LOD*	*Nd ppm*	*Nd 2SE*	*Nd LOD*	*Sm ppm*	*Sm 2SE*	*Sm LOD*
M1_47824_003_263	G9A_Ti	285	0.2278	0.0037	0.00009	0.0871	0.0014	0.00009	0.933	0.016	0.00058	0.871	0.015	0.00083
M1_47824_017_277	G9A	285	0.2269	0.004	0.00012	0.0775	0.0019	0.00009	0.706	0.011	0.00051	0.492	0.01	0.00091
M1_47824_035_295	G9A_Ti	130	0.0917	0.0032	0.00043	0.0354	0.0015	0.00032	0.367	0.014	0.00213	0.394	0.017	0.00358
M1_47824_037_297	G9A	285	0.2568	0.0032	0.00009	0.137	0.0019	0.00009	1.707	0.018	0.00059	1.631	0.02	0.00075
M1_47824_039_299	G9A	285	0.237	0.0031	0.00014	0.1238	0.002	0.00009	1.582	0.019	0.00061	1.48	0.019	0.00099
M1_49724_011_371	G9A	285	0.2418	0.0025	0.00011	0.0762	0.0014	0.00010	0.605	0.011	0.00055	0.4263	0.0087	0.00089
M1_49724_015_375	G9A	130	8.36	0.23	0.00044	0.986	0.027	0.00031	4.03	0.11	0.00194	1.013	0.033	0.00408
M1_49724_019_379	G9A_Ti	285	0.571	0.015	0.00011	0.0918	0.0021	0.00009	0.684	0.012	0.00052	0.664	0.011	0.00100
M1_49724_021_381	G9A_Ti	130	0.0972	0.0033	0.00042	0.0417	0.0023	0.00036	0.52	0.018	0.00226	0.627	0.021	0.00368
M1_49724_035_395	G9A_Ti	285	0.21	0.035	0.00011	0.0489	0.0049	0.00010	0.435	0.019	0.00059	0.4094	0.0081	0.00091
M1_49724_039_399	G9B_Ti	285	6.228	0.091	0.00012	0.78	0.011	0.00010	3.44	0.049	0.00057	1.125	0.016	0.00091
M1_49724_041_401	G9A_Ti	285	0.1119	0.0026	0.00011	0.0446	0.001	0.00009	0.5708	0.0098	0.00059	0.762	0.014	0.00093
M1_49725_015_417	G9A_Ti	285	0.1598	0.0033	0.00011	0.076	0.0016	0.00008	0.874	0.013	0.00052	0.837	0.014	0.00090
M1_49725_019_421	G9A_Ti	285	0.1752	0.0029	0.00013	0.0821	0.0019	0.00009	0.94	0.015	0.00064	0.88	0.013	0.00084
M1_49725_023_425	G9A_Ti	285	1.76	0.24	0.00010	0.285	0.028	0.00009	1.83	0.11	0.00059	1.001	0.024	0.00091
M1_49725_025_427	G9A_Ti	285	0.1052	0.0016	0.00010	0.04314	0.00072	0.00009	0.516	0.01	0.00057	0.6436	0.0087	0.00082
M1_49725_039_441	G9A_Ti	130	0.1441	0.0054	0.00038	0.0488	0.0023	0.00040	0.478	0.018	0.00206	0.437	0.017	0.00367
M1_49725_041_443	G9A_Ti	285	0.208	0.003	0.00011	0.0851	0.0016	0.00009	0.944	0.01	0.00062	0.93	0.013	0.00071
M1_49725_051_453	G9A_Ti	285	0.1373	0.0025	0.00011	0.0609	0.0017	0.00009	0.6839	0.0093	0.00062	0.73	0.013	0.00081
M1_49741_001_301	G9A	285	0.3902	0.0061	0.00011	0.1091	0.0018	0.00010	0.62	0.013	0.00043	0.2206	0.0056	0.00080
M1_49741_005_305	G9A_Ti	285	0.1744	0.0023	0.00014	0.0819	0.0014	0.00009	0.955	0.011	0.00067	0.932	0.012	0.00094
M1_49741_015_315	G9A	285	0.1562	0.0021	0.00011	0.04937	0.00089	0.00009	0.4645	0.0088	0.00059	0.4523	0.0093	0.00083
M1_49741_017_317	G9A	285	0.3896	0.0036	0.00012	0.1046	0.0015	0.00008	0.797	0.0092	0.00055	0.4736	0.0094	0.00078
M1_49741_021_321	G9A	285	0.162	0.0021	0.00013	0.0499	0.001	0.00011	0.4623	0.0077	0.00057	0.4343	0.0075	0.00094
M1_49741_029_329	G9A_Ti	285	0.243	0.0068	0.00012	0.0896	0.0019	0.00009	0.976	0.014	0.00057	0.894	0.015	0.00093
M1_49741_041_341	G9A_Ti	285	0.1441	0.0019	0.00008	0.0563	0.0011	0.00008	0.6767	0.0098	0.00056	0.771	0.011	0.00098
M1_49741_053_353	G9A	285	0.2424	0.0028	0.00014	0.0961	0.0013	0.00009	0.988	0.013	0.00056	0.483	0.0087	0.00097
M1_49741_059_359	G9A_Ti	285	0.3932	0.0036	0.00011	0.1225	0.0018	0.00010	0.734	0.01	0.00057	0.3459	0.007	0.00089
M2_47824_003_465	G9A_Ti	285	0.1227	0.002	0.00009	0.0592	0.0011	0.00011	0.6841	0.0099	0.00045	0.69	0.012	0.00060
M2_47824_013_475	G9A	285	0.3115	0.0028	0.00012	0.1566	0.0022	0.00010	1.924	0.02	0.00058	1.798	0.021	0.00080
M2_47824_015_477	G9A	130	0.2002	0.0047	0.00010	0.0645	0.0023	0.00010	0.565	0.018	0.00060	0.391	0.016	0.00078
M2_47824_029_491	G9A	285	0.2179	0.0027	0.00042	0.0727	0.0011	0.00035	0.6699	0.0081	0.00210	0.453	0.0075	0.00354
M2_47824_033_495	G9A_Ti	285	0.1011	0.0017	0.00009	0.03895	0.00084	0.00007	0.4296	0.0095	0.00052	0.464	0.0091	0.00077
M2_47824_037_499	G9A_Ti	130	0.1141	0.0042	0.00009	0.0371	0.0018	0.00008	0.388	0.014	0.00052	0.38	0.016	0.00068
M2_49724_009_743	G3_Na	130	0.2386	0.0053	0.00038	0.0871	0.0033	0.00035	0.852	0.018	0.00242	0.707	0.016	0.00322
M2_49724_013_747	G9A	285	0.1176	0.0024	0.00051	0.0644	0.0011	0.00037	0.782	0.014	0.00199	0.551	0.011	0.00185
M2_49724_037_771	G9A_Ti	285	0.1067	0.0018	0.00007	0.042	0.0011	0.00008	0.495	0.01	0.00037	0.667	0.013	0.00081
M2_49724_045_779	G3_Na	130	0.0732	0.0026	0.00007	0.0342	0.0018	0.00007	0.453	0.014	0.00043	0.555	0.017	0.00066

Appendix E: Garnet Xenocryst LA-ICP-MS Data Tables

Appendix E.01 (continued): Mel kimberlite garnet trace element data measured by LA-ICPMS. 2SE – two times standard error. LOD – Limit of detection (Pettke et al., 2014). <LOD – bellow limit of detection.

Sample	*Class*	*Spot Size*	*Eu ppm*	*Eu 2SE*	*Eu LOD*	*Gd ppm*	*Gd 2SE*	*Gd LOD*	*Tb ppm*	*Tb 2SE*	*Tb LOD*	*Dy ppm*	*Dy 2SE*	*Dy LOD*
M1_47824_003_263	G9A_Ti	285	0.4214	0.0073	0.00017	1.785	0.034	0.00086	0.3477	0.0058	0.00010	2.455	0.04	0.00043
M1_47824_017_277	G9A	285	0.2222	0.0043	0.00020	1.049	0.022	0.00085	0.2344	0.0042	0.00011	1.926	0.035	0.00049
M1_47824_035_295	G9A_Ti	130	0.2342	0.0063	0.00068	1.096	0.027	0.00337	0.2726	0.0054	0.00035	2.215	0.031	0.00148
M1_47824_037_297	G9A	285	0.7841	0.0062	0.00019	3.417	0.033	0.00088	0.6986	0.0062	0.00011	5.011	0.037	0.00055
M1_47824_039_299	G9A	285	0.6632	0.006	0.00021	2.658	0.027	0.00079	0.4558	0.005	0.00010	2.822	0.022	0.00054
M1_49724_011_371	G9A	285	0.2263	0.0035	0.00018	1.284	0.016	0.00067	0.3258	0.0038	0.00013	2.83	0.031	0.00055
M1_49724_015_375	G9A	130	0.2677	0.0084	0.00075	1.385	0.043	0.00470	0.264	0.0069	0.00038	2.005	0.039	0.00193
M1_49724_019_379	G9A_Ti	285	0.3597	0.0045	0.00017	1.904	0.024	0.00071	0.4596	0.0053	0.00012	3.866	0.037	0.00053
M1_49724_021_381	G9A_Ti	130	0.351	0.0079	0.00072	1.56	0.038	0.00341	0.3674	0.0069	0.00037	2.984	0.052	0.00209
M1_49724_035_395	G9A_Ti	285	0.2214	0.004	0.00019	1.216	0.014	0.00096	0.3148	0.0038	0.00014	2.8	0.025	0.00050
M1_49724_039_399	G9B_Ti	285	0.3447	0.0044	0.00018	1.782	0.021	0.00083	0.3551	0.0041	0.00012	2.728	0.027	0.00057
M1_49724_041_401	G9A_Ti	285	0.4082	0.0053	0.00018	2.023	0.022	0.00082	0.488	0.005	0.00012	4.065	0.034	0.00049
M1_49725_015_417	G9A_Ti	285	0.4289	0.0061	0.00020	2	0.025	0.00081	0.454	0.0055	0.00012	3.692	0.044	0.00056
M1_49725_019_421	G9A_Ti	285	0.4313	0.0074	0.00020	2.065	0.025	0.00079	0.4809	0.0063	0.00013	4.008	0.045	0.00061
M1_49725_023_425	G9A_Ti	285	0.4424	0.007	0.00017	2.042	0.031	0.00074	0.4351	0.0054	0.00012	3.413	0.039	0.00057
M1_49725_025_427	G9A_Ti	285	0.3556	0.0042	0.00017	1.928	0.021	0.00069	0.475	0.005	0.00011	3.921	0.033	0.00053
M1_49725_039_441	G9A_Ti	130	0.2535	0.0066	0.00078	1.188	0.03	0.00349	0.312	0.0067	0.00038	2.712	0.042	0.00189
M1_49725_041_443	G9A_Ti	285	0.4577	0.0048	0.00020	2.183	0.02	0.00083	0.4871	0.0048	0.00010	3.84	0.03	0.00049
M1_49725_051_453	G9A_Ti	285	0.3829	0.005	0.00019	1.887	0.026	0.00082	0.4405	0.0052	0.00013	3.579	0.031	0.00052
M1_49741_001_301	G9A	285	0.1097	0.0027	0.00015	0.646	0.018	0.00065	0.172	0.0039	0.00009	1.566	0.028	0.00042
M1_49741_005_305	G9A_Ti	285	0.4662	0.0058	0.00022	2.21	0.022	0.00078	0.5094	0.0047	0.00011	4.14	0.036	0.00052
M1_49741_015_315	G9A	285	0.2583	0.0033	0.00020	1.263	0.015	0.00074	0.3166	0.0032	0.00011	2.714	0.026	0.00057
M1_49741_017_317	G9A	285	0.1975	0.0029	0.00019	0.989	0.013	0.00083	0.2238	0.0024	0.00010	1.873	0.018	0.00054
M1_49741_021_321	G9A	285	0.2493	0.0038	0.00021	1.214	0.016	0.00096	0.2995	0.0031	0.00013	2.558	0.027	0.00053
M1_49741_029_329	G9A_Ti	285	0.4541	0.0055	0.00020	2.149	0.026	0.00094	0.4924	0.0047	0.00012	4.03	0.04	0.00054
M1_49741_041_341	G9A_Ti	285	0.3945	0.0045	0.00019	1.777	0.021	0.00083	0.3672	0.0039	0.00012	2.716	0.027	0.00055
M1_49741_053_353	G9A	285	0.1521	0.0028	0.00023	0.5337	0.0099	0.00076	0.1126	0.0017	0.00012	0.997	0.013	0.00044
M1_49741_059_359	G9A_Ti	285	0.2064	0.0031	0.00018	1.267	0.015	0.00090	0.3219	0.0037	0.00011	2.724	0.029	0.00054
M2_47824_003_465	G9A_Ti	285	0.3512	0.0044	0.00014	1.795	0.021	0.00064	0.4126	0.0042	0.00008	3.366	0.03	0.00044
M2_47824_013_475	G9A	285	0.8233	0.0074	0.00021	3.43	0.033	0.00075	0.6362	0.0054	0.00011	4.371	0.042	0.00052
M2_47824_015_477	G9A	130	0.1825	0.0066	0.00019	0.822	0.026	0.00081	0.193	0.0045	0.00012	1.606	0.035	0.00057
M2_47824_029_491	G9A	285	0.2091	0.0029	0.00064	1.038	0.016	0.00324	0.241	0.0028	0.00031	2.031	0.023	0.00179
M2_47824_033_495	G9A_Ti	285	0.2556	0.0032	0.00014	1.354	0.021	0.00070	0.3405	0.0043	0.00009	2.908	0.03	0.00041
M2_47824_037_499	G9A_Ti	130	0.2201	0.0066	0.00019	1.03	0.029	0.00080	0.2631	0.0063	0.00008	2.175	0.042	0.00048
M2_49724_009_743	G3_Na	130	0.3623	0.0082	0.00070	1.552	0.03	0.00317	0.3643	0.0079	0.00037	2.891	0.043	0.00183
M2_49724_013_747	G9A	285	0.2612	0.0044	0.00070	1.307	0.021	0.00324	0.305	0.0041	0.00047	2.533	0.037	0.00149
M2_49724_037_771	G9A_Ti	285	0.3764	0.0045	0.00014	1.951	0.022	0.00073	0.4666	0.0043	0.00010	3.918	0.04	0.00045
M2_49724_045_779	G3_Na	130	0.3295	0.0087	0.00014	1.514	0.033	0.00059	0.383	0.0072	0.00009	3.322	0.054	0.00034

Appendix E: Garnet Xenocryst LA-ICP-MS Data Tables

Appendix E.01 (continued): Mel kimberlite garnet trace element data measured by LA-ICPMS. 2SE – two times standard error. LOD – Limit of detection (Pettke et al., 2014). <LOD – bellow limit of detection.

Sample	*Class*	*Spot Size*	*Ho ppm*	*Ho 2SE*	*Ho LOD*	*Er ppm*	*Er 2SE*	*Er LOD*	*Tm ppm*	*Tm 2SE*	*Tm LOD*	*Yb ppm*	*Yb 2SE*	*Yb LOD*
M1_47824_003_263	G9A_Ti	285	0.5406	0.009	0.00012	1.63	0.027	0.00041	0.2417	0.004	0.00018	1.743	0.034	0.00077
M1_47824_017_277	G9A	285	0.4898	0.0083	0.00013	1.642	0.034	0.00037	0.2604	0.0048	0.00019	1.91	0.037	0.00124
M1_47824_035_295	G9A_Ti	130	0.5472	0.0096	0.00039	1.758	0.024	0.00103	0.2623	0.0053	0.00041	1.919	0.035	0.00179
M1_47824_037_297	G9A	285	1.0961	0.0074	0.00013	3.227	0.023	0.00038	0.4581	0.0043	0.00018	3.121	0.026	0.00093
M1_47824_039_299	G9A	285	0.57	0.0061	0.00010	1.648	0.016	0.00038	0.2346	0.0031	0.00019	1.598	0.02	0.00117
M1_49724_011_371	G9A	285	0.7376	0.0071	0.00009	2.468	0.022	0.00040	0.3798	0.0043	0.00018	2.758	0.028	0.00130
M1_49724_015_375	G9A	130	0.473	0.011	0.00044	1.523	0.036	0.00112	0.2314	0.0064	0.00039	1.698	0.042	0.00391
M1_49724_019_379	G9A_Ti	285	0.979	0.012	0.00012	3.185	0.034	0.00042	0.4891	0.0061	0.00020	3.458	0.045	0.00110
M1_49724_021_381	G9A_Ti	130	0.744	0.012	0.00045	2.383	0.043	0.00123	0.3571	0.0065	0.00048	2.584	0.041	0.00344
M1_49724_035_395	G9A_Ti	285	0.7409	0.0078	0.00014	2.552	0.02	0.00039	0.4126	0.0044	0.00021	3.139	0.037	0.00112
M1_49724_039_399	G9B_Ti	285	0.6637	0.0063	0.00014	2.111	0.023	0.00036	0.3164	0.0039	0.00017	2.23	0.022	0.00108
M1_49724_041_401	G9A_Ti	285	1.0186	0.0079	0.00011	3.303	0.032	0.00037	0.4981	0.0057	0.00016	3.51	0.035	0.00115
M1_49725_015_417	G9A_Ti	285	0.917	0.011	0.00013	2.989	0.035	0.00030	0.4559	0.0058	0.00015	3.254	0.034	0.00114
M1_49725_019_421	G9A_Ti	285	1.018	0.011	0.00013	3.333	0.036	0.00037	0.5091	0.0057	0.00019	3.582	0.041	0.00123
M1_49725_023_425	G9A_Ti	285	0.819	0.011	0.00013	2.584	0.028	0.00035	0.3874	0.0061	0.00017	2.746	0.037	0.00082
M1_49725_025_427	G9A_Ti	285	0.9432	0.0077	0.00012	2.961	0.025	0.00037	0.4364	0.0038	0.00013	3.016	0.03	0.00110
M1_49725_039_441	G9A_Ti	130	0.733	0.014	0.00039	2.533	0.039	0.00128	0.4011	0.0069	0.00039	2.987	0.051	0.00276
M1_49725_041_443	G9A_Ti	285	0.9211	0.0075	0.00013	2.913	0.021	0.00039	0.4361	0.0051	0.00019	3.053	0.027	0.00136
M1_49725_051_453	G9A_Ti	285	0.8896	0.0078	0.00012	2.861	0.03	0.00038	0.4334	0.0045	0.00018	3.048	0.034	0.00117
M1_49741_001_301	G9A	285	0.423	0.0085	0.00012	1.486	0.03	0.00036	0.2409	0.0055	0.00014	1.84	0.033	0.00084
M1_49741_005_305	G9A_Ti	285	1.0297	0.0081	0.00013	3.305	0.028	0.00034	0.5025	0.0048	0.00016	3.544	0.04	0.00084
M1_49741_015_315	G9A	285	0.6811	0.0064	0.00011	2.185	0.019	0.00034	0.3282	0.0038	0.00019	2.313	0.022	0.00137
M1_49741_017_317	G9A	285	0.4861	0.0037	0.00013	1.646	0.016	0.00040	0.2649	0.0028	0.00023	1.995	0.022	0.00138
M1_49741_021_321	G9A	285	0.6457	0.0071	0.00012	2.066	0.022	0.00030	0.3089	0.0043	0.00019	2.171	0.026	0.00122
M1_49741_029_329	G9A_Ti	285	0.9992	0.0096	0.00011	3.234	0.028	0.00032	0.4927	0.0049	0.00014	3.514	0.033	0.00102
M1_49741_041_341	G9A_Ti	285	0.6288	0.0059	0.00013	1.976	0.02	0.00031	0.2994	0.0037	0.00013	2.143	0.022	0.00111
M1_49741_053_353	G9A	285	0.2769	0.0039	0.00012	1.008	0.012	0.00039	0.1732	0.003	0.00016	1.387	0.021	0.00096
M1_49741_059_359	G9A_Ti	285	0.6891	0.0056	0.00013	2.27	0.018	0.00034	0.3485	0.0042	0.00017	2.535	0.025	0.00131
M2_47824_003_465	G9A_Ti	285	0.8239	0.0066	0.00012	2.659	0.025	0.00022	0.405	0.0043	0.00011	2.85	0.025	0.00081
M2_47824_013_475	G9A	285	0.9575	0.0098	0.00012	2.84	0.027	0.00033	0.4114	0.0048	0.00023	2.861	0.034	0.00141
M2_47824_015_477	G9A	130	0.4048	0.0068	0.00011	1.325	0.027	0.00048	0.2093	0.0047	0.00018	1.545	0.03	0.00124
M2_47824_029_491	G9A	285	0.5216	0.0054	0.00038	1.741	0.019	0.00113	0.275	0.0038	0.00039	2.003	0.022	0.00290
M2_47824_033_495	G9A_Ti	285	0.7346	0.0069	0.00008	2.408	0.026	0.00032	0.3604	0.0047	0.00011	2.529	0.029	0.00083
M2_47824_037_499	G9A_Ti	130	0.547	0.01	0.00011	1.765	0.026	0.00028	0.266	0.005	0.00016	1.961	0.041	0.00113
M2_49724_009_743	G3_Na	130	0.678	0.011	0.00040	2.085	0.032	0.00130	0.298	0.0071	0.00043	2.074	0.034	0.00373
M2_49724_013_747	G9A	285	0.6332	0.0081	0.00041	2.053	0.025	0.00125	0.3193	0.005	0.00045	2.275	0.036	0.00204
M2_49724_037_771	G9A_Ti	285	0.9894	0.0083	0.00012	3.212	0.033	0.00027	0.4835	0.0064	0.00010	3.378	0.032	0.00071
M2_49724_045_779	G3_Na	130	0.853	0.014	0.00009	2.873	0.047	0.00028	0.4591	0.008	0.00011	3.326	0.051	0.00101

Appendix E: Garnet Xenocryst LA-ICP-MS Data Tables

Appendix E.01 (continued): Mel kimberlite garnet trace element data measured by LA-ICPMS. 2SE – two times standard error. LOD – Limit of detection (Pettke et al., 2014). <LOD – bellow limit of detection.

Sample	*Class*	*Spot Size*	*Lu ppm*	*Lu 2SE*	*Lu LOD*	*Hf ppm*	*Hf 2SE*	*Hf LOD*	*Ta ppm*	*Ta 2SE*	*Ta LOD*
M1_47824_003_263	G9A_Ti	285	0.2826	0.0058	0.00017	1.211	0.028	0.00146	0.0223	0.0012	0.00015
M1_47824_017_277	G9A	285	0.316	0.0065	0.00034	0.368	0.014	0.00192	0.0231	0.001	0.00019
M1_47824_035_295	G9A_Ti	130	0.2938	0.0063	0.00052	0.873	0.027	0.00298	0.0077	0.0013	0.00079
M1_47824_037_297	G9A	285	0.4879	0.0056	0.00029	1.13	0.019	0.00100	0.0274	0.0012	0.00020
M1_47824_039_299	G9A	285	0.245	0.0032	0.00025	0.911	0.019	0.00112	0.022	0.0011	0.00021
M1_49724_011_371	G9A	285	0.4486	0.0049	0.00023	0.496	0.015	0.00112	0.0229	0.0011	0.00026
M1_49724_015_375	G9A	130	0.2669	0.0079	0.00087	0.259	0.019	0.00470	0.0102	0.0015	0.00079
M1_49724_019_379	G9A_Ti	285	0.5491	0.0066	0.00031	1.671	0.027	0.00096	0.00817	0.0006	0.00019
M1_49724_021_381	G9A_Ti	130	0.403	0.0082	0.00110	1.265	0.049	0.00377	0.0058	0.0012	0.00084
M1_49724_035_395	G9A_Ti	285	0.5219	0.0056	0.00031	0.923	0.023	0.00142	0.0145	0.0016	0.00023
M1_49724_039_399	G9B_Ti	285	0.3485	0.0046	0.00030	1.177	0.024	0.00116	0.01144	0.00085	0.00023
M1_49724_041_401	G9A_Ti	285	0.5566	0.0069	0.00018	1.772	0.028	0.00106	0.00748	0.00058	0.00020
M1_49725_015_417	G9A_Ti	285	0.5272	0.0054	0.00024	1.629	0.024	0.00087	0.0143	0.0027	0.00020
M1_49725_019_421	G9A_Ti	285	0.5698	0.0091	0.00028	1.637	0.035	0.00135	0.0135	0.00096	0.00019
M1_49725_023_425	G9A_Ti	285	0.4426	0.0063	0.00027	1.26	0.021	0.00086	0.0254	0.0013	0.00019
M1_49725_025_427	G9A_Ti	285	0.4768	0.0064	0.00022	1.672	0.033	0.00104	0.00723	0.00061	0.00018
M1_49725_039_441	G9A_Ti	130	0.468	0.01	0.00109	0.904	0.031	0.00591	0.0083	0.0017	0.00058
M1_49725_041_443	G9A_Ti	285	0.4816	0.0045	0.00032	1.427	0.023	0.00119	0.0156	0.0013	0.00021
M1_49725_051_453	G9A_Ti	285	0.4899	0.0065	0.00021	1.575	0.027	0.00132	0.0104	0.0013	0.00024
M1_49741_001_301	G9A	285	0.3064	0.0071	0.00028	0.1511	0.0084	0.00094	0.0319	0.0014	0.00017
M1_49741_005_305	G9A_Ti	285	0.5594	0.0065	0.00022	1.87	0.032	0.00121	0.01311	0.00082	0.00024
M1_49741_015_315	G9A	285	0.3664	0.0045	0.00034	0.1939	0.0074	0.00126	0.00055	0.0002	0.00022
M1_49741_017_317	G9A	285	0.3417	0.0035	0.00040	0.301	0.011	0.00176	0.055	0.0016	0.00021
M1_49741_021_321	G9A	285	0.3437	0.0044	0.00032	0.165	0.0087	0.00192	0.0005	0.00019	0.00021
M1_49741_029_329	G9A_Ti	285	0.5595	0.0056	0.00026	1.847	0.027	0.00154	0.0172	0.001	0.00021
M1_49741_041_341	G9A_Ti	285	0.347	0.0034	0.00028	0.965	0.018	0.00126	0.01228	0.00086	0.00021
M1_49741_053_353	G9A	285	0.2454	0.004	0.00027	0.1349	0.0063	0.00134	0.0222	0.001	0.00022
M1_49741_059_359	G9A_Ti	285	0.4103	0.0046	0.00024	0.745	0.017	0.00090	0.046	0.0015	0.00024
M2_47824_003_465	G9A_Ti	285	0.458	0.0049	0.00019	0.885	0.023	0.00071	0.01536	0.00098	0.00018
M2_47824_013_475	G9A	285	0.4543	0.006	0.00025	1.195	0.023	0.00140	0.0461	0.0018	0.00022
M2_47824_015_477	G9A	130	0.2485	0.0062	0.00026	0.23	0.018	0.00115	0.0198	0.002	0.00026
M2_47824_029_491	G9A	285	0.3268	0.0047	0.00119	0.291	0.011	0.00378	0.0238	0.0013	0.00077
M2_47824_033_495	G9A_Ti	285	0.3998	0.0055	0.00024	1.143	0.02	0.00088	0.00887	0.00066	0.00017
M2_47824_037_499	G9A_Ti	130	0.2996	0.0075	0.00020	0.813	0.036	0.00183	0.0072	0.0011	0.00019
M2_49724_009_743	G3_Na	130	0.3002	0.0066	0.00122	0.646	0.027	0.00420	0.0147	0.0018	0.00084
M2_49724_013_747	G9A	285	0.3748	0.006	0.00050	0.373	0.01	0.00308	0.01111	0.00068	0.00060
M2_49724_037_771	G9A_Ti	285	0.5401	0.0055	0.00016	1.643	0.026	0.00055	0.00736	0.00056	0.00017
M2_49724_045_779	G3_Na	130	0.521	0.01	0.00018	1.602	0.043	0.00073	0.0065	0.0012	0.00019

Appendix E: Garnet Xenocryst LA-ICP-MS Data Tables

Appendix E.01 (continued): Mel kimberlite garnet trace element data measured by LA-ICPMS. 2SE – two times standard error. LOD – Limit of detection (Pettke et al., 2014). <LOD – bellow limit of detection.

Sample	*Class*	*Spot Size*	*Ca ppm*	*Ca 2SE*	*Ca LOD*	*Sc ppm*	*Sc 2SE*	*Sc LOD*	*Ti ppm*	*Ti 2SE*	*Ti LOD*	*V ppm*	*V 2SE*	*V LOD*
M2_49724_049_783	G9A	285	36320	790	18.9038	114.18	0.53	0.02164	2291.3	9.8	0.75	279	1.3	0.01109
M2_49724_051_785	G3_Na	130	31030	280	4.01792	83.28	0.63	0.00705	2731	26	0.18	157.9	1.4	0.00308
M2_49724_057_791	G9A	285	31190	130	18.8623	106.2	0.37	0.02186	1927.1	6.2	0.75	257.2	1.1	0.01125
M2_49724_063_797	G9A_Ti	285	29840	150	4.06439	97.91	0.49	0.00706	4307	16	0.18	202.31	0.81	0.00297
M2_49724_067_801	G3_Na	130	27550	230	4.15444	72.13	0.64	0.00718	3592	44	0.18	185.7	1.4	0.00287
M2_49724_073_807	G9A_Ti	285	31580	140	17.1168	99.39	0.46	0.02013	4570	18	0.68	223.09	0.9	0.00957
M2_49725_003_505	G9A	285	36350	150	3.75910	144.21	0.61	0.00648	1906.7	7.2	0.17	329.7	1.7	0.00279
M2_49725_007_509	G9A_Ti	285	57400	1200	3.52963	88.3	0.44	0.00589	4299	15	0.16	244.2	1	0.00254
M2_49725_009_511	G9A_Ti	285	33250	130	4.06772	102.43	0.35	0.00625	4290	20	0.18	222.2	1.1	0.00293
M2_49725_029_531	G11	285	35610	140	4.01638	137.68	0.52	0.00630	3844	13	0.17	283.6	1.2	0.00295
M2_49725_039_541	G9A_Ti	130	28050	210	3.85174	86.23	0.54	0.00584	3585	20	0.17	216	1.2	0.00299
M2_49725_051_553	G9A	285	30270	140	18.2414	94.39	0.56	0.02199	3819	20	0.73	202	1.1	0.01150
M2_49725_059_561	G9A	285	36640	140	3.87544	143.87	0.61	0.00621	1778.1	7.3	0.17	330	1.5	0.00275
M2_49725_061_563	G3	285	28190	250	3.48062	87.84	0.64	0.00652	2184	16	0.16	168.7	1.3	0.00274
M2_49741_039_607	G9A_Ti	285	31620	110	7.41153	100.35	0.36	0.00976	4834	18	0.30	220.7	0.96	0.00497
M2_49742_003_617	G3_Na	130	72000	1500	4.04452	47.6	1.1	0.00693	3570	170	0.18	139.1	3.3	0.00296
M2_49742_005_619	G3_Na	285	72110	540	41.1035	62.38	0.36	0.04922	3384	21	1.66	138.9	1	0.02592
M2_49742_011_625	G3_Na	285	57470	360	10.1571	53.02	0.38	0.01528	4167	31	0.42	141.4	1.3	0.00621
M2_49742_027_641	G9B_Ti	285	32590	180	8.67092	87.71	0.51	0.01304	5526	26	0.36	206.4	1.2	0.00530
M2_49742_031_645	G9A	285	33410	160	4.01472	121.61	0.43	0.00694	1897.6	8.3	0.18	284.1	1.2	0.00276
M2_49742_033_647	G9A	285	39040	150	3.84697	132.74	0.62	0.00660	983	3.6	0.17	310.1	1.2	0.00283
M2_49742_039_653	G12	285	51530	180	4.24537	69.24	0.33	0.00651	944.2	3.4	0.18	142.44	0.63	0.00298
M2_49742_057_671	G9A	285	29457	99	4.16878	104.81	0.35	0.00646	1260.5	4.5	0.18	149.17	0.54	0.00268
M2_49742_065_679	G9B_Ti	285	32660	160	3.89149	89.48	0.33	0.00613	5345	19	0.17	201.48	0.84	0.00266
M2_49742_069_683	G9A_Ti	130	31440	200	17.7838	101.46	0.66	0.02056	1820	11	0.70	323.3	1.6	0.01150
M2_49742_071_685	G12	285	51670	280	4.09617	66.73	0.48	0.00627	1066.4	7.1	0.17	156.3	1.4	0.00263
M2_49742_079_693	G9A_Ti	285	35530	180	3.69949	133.71	0.57	0.00743	2387.8	9.4	0.17	355.5	1.5	0.00268
M2_49742_085_699	G12	285	52920	240	3.97534	70.73	0.31	0.00724	970.3	4.3	0.18	144.36	0.56	0.00250
M2_49742_089_703	G12	130	45510	360	17.4580	51.61	0.35	0.02133	768.4	4.9	0.74	127.83	0.67	0.01047
M2_49742_113_727	G3_Na	130	63020	550	18.0065	47.76	0.44	0.02264	2789	20	0.75	124.31	0.84	0.00984
M2_49742_119_733	G1	285	31110	110	3.91623	94.89	0.36	0.00693	3855	12	0.18	213.94	0.82	0.00251
P3_49725_001_133	G9A_Ti	285	32340	110	3.57236	101.12	0.44	0.00748	4028	14	0.16	258.01	0.99	0.00244
P3_49725_003_135	G9A_Ti	285	31110	120	4.04018	97.55	0.31	0.00762	3825	12	0.18	247.96	0.9	0.00275
P3_49725_030_388	G9A_Ti	285	29800	140	4.07686	92.25	0.52	0.00761	3696	19	0.18	202.3	1.4	0.00289
P3_49725_049_407	G9A_Ti	285	30400	130	4.09414	96.98	0.35	0.00755	3956	16	0.18	195.31	0.78	0.00305
P3_49725_061_419	G9A_Ti	285	30310	130	4.00751	94.4	0.47	0.00883	4059	16	0.18	208.84	0.94	0.00251
P3_49725_39r_498	G9B_Ti	285	31130	170	3.96713	90.57	0.38	0.00856	4163	17	0.18	233.5	1.2	0.00269
P3_49736_008_274	G9A_Ti	285	32470	140	3.78533	102.53	0.44	0.00698	3091	10	0.17	248.28	0.91	0.00271

Appendix E: Garnet Xenocryst LA-ICP-MS Data Tables

Appendix E.01 (continued): Mel kimberlite garnet trace element data measured by LA-ICPMS. 2SE – two times standard error. LOD – Limit of detection (Pettke et al., 2014). <LOD – bellow limit of detection.

Sample	*Class*	*Spot Size*	*Ni ppm*	*Ni 2SE*	*Ni LOD*	*Rb ppm*	*Rb 2SE*	*Rb LOD*	*Sr ppm*	*Sr 2SE*	*Sr LOD*	*Y ppm*	*Y 2SE*	*Y LOD*
M2_49724_049_783	G9A	285	116.96	0.61	0.3266	0.0072	0.0023	0.0088	1.21	0.22	0.00359	16.52	0.11	0.00139
M2_49724_051_785	G3_Na	130	18.61	0.36	0.0304	0.012	0.0055	0.0038	1.026	0.087	0.00098	21.2	0.22	0.00044
M2_49724_057_791	G9A	285	139.74	0.75	0.3243	0.0039	0.0018	0.0087	0.4792	0.0069	0.00333	19.47	0.12	0.00150
M2_49724_063_797	G9A_Ti	285	118.01	0.63	0.0307	0.0036	0.0021	0.0039	0.39	0.0078	0.00107	24.52	0.16	0.00031
M2_49724_067_801	G3_Na	130	109.51	0.8	0.0304	0.0146	0.0061	0.0038	0.431	0.016	0.00090	17.71	0.17	0.00038
M2_49724_073_807	G9A_Ti	285	150.82	0.97	0.2746	0.0052	0.0017	0.0079	0.7116	0.0098	0.00360	25.73	0.18	0.00163
M2_49725_003_505	G9A	285	116.76	0.74	0.0287	0.0093	0.0026	0.0034	0.4349	0.0072	0.00082	7.146	0.065	0.00035
M2_49725_007_509	G9A_Ti	285	127.31	0.73	0.0280	0.0131	0.003	0.0041	12.85	0.53	0.00106	24.59	0.16	0.00034
M2_49725_009_511	G9A_Ti	285	81.28	0.59	0.0315	0.005	0.0025	0.0045	0.468	0.01	0.00137	22.92	0.15	0.00044
M2_49725_029_531	G11	285	123.59	0.62	0.0317	0.0124	0.0024	0.0042	0.89	0.018	0.00115	10.309	0.075	0.00041
M2_49725_039_541	G9A_Ti	130	44.82	0.41	0.0292	0.051	0.017	0.0041	0.597	0.048	0.00107	19.51	0.17	0.00040
M2_49725_051_553	G9A	285	119.12	0.9	0.1488	0.0051	0.0022	0.0289	0.4106	0.0077	0.00564	21.77	0.23	0.00196
M2_49725_059_561	G9A	285	114.37	0.67	0.0305	0.0131	0.0028	0.0041	0.4201	0.007	0.00106	6.632	0.05	0.00035
M2_49725_061_563	G3	285	31.96	0.27	0.0289	0.0024	0.002	0.0037	0.2026	0.0099	0.00113	14.33	0.13	0.00037
M2_49741_039_607	G9A_Ti	285	133.31	0.81	0.1180	0.243	0.011	0.0037	2.021	0.085	0.00121	26.44	0.16	0.00062
M2_49742_003_617	G3_Na	130	203	17	0.0310	2.88	0.29	0.0040	15	1.5	0.00115	15.15	0.36	0.00042
M2_49742_005_619	G3_Na	285	73.21	0.77	0.7206	0.0154	0.0036	0.0199	1.07	0.024	0.00821	19.51	0.17	0.00371
M2_49742_011_625	G3_Na	285	97.43	0.92	0.1622	0.0215	0.0052	0.0051	1.25	0.11	0.00220	17.15	0.17	0.00104
M2_49742_027_641	G9B_Ti	285	131.15	0.86	0.1385	0.0077	0.0019	0.0044	0.4399	0.0098	0.00188	38.09	0.38	0.00089
M2_49742_031_645	G9A	285	115.59	0.51	0.0310	0.0091	0.002	0.0039	0.3815	0.0076	0.00112	11.096	0.068	0.00040
M2_49742_033_647	G9A	285	117.24	0.62	0.0303	0.0074	0.0022	0.0038	0.3252	0.0068	0.00101	7.709	0.062	0.00044
M2_49742_039_653	G12	285	41.52	0.22	0.0319	0.0037	0.0017	0.0042	0.183	0.005	0.00108	5.409	0.032	0.00047
M2_49742_057_671	G9A	285	44.22	0.24	0.0307	0.002	0.0024	0.0040	0.2696	0.0066	0.00102	16.76	0.1	0.00041
M2_49742_065_679	G9B_Ti	285	129.47	0.73	0.0293	0.009	0.0023	0.0038	0.4244	0.0069	0.00093	38.8	0.25	0.00040
M2_49742_069_683	G9A_Ti	130	130.24	0.84	0.1389	0.044	0.017	0.0271	0.365	0.014	0.00604	12.29	0.11	0.00194
M2_49742_071_685	G12	285	40.42	0.43	0.0302	0.0052	0.0021	0.0038	0.1764	0.0046	0.00104	5.21	0.072	0.00039
M2_49742_079_693	G9A_Ti	285	133.12	0.58	0.0297	0.0072	0.0022	0.0037	0.3763	0.0061	0.00114	16.42	0.1	0.00035
M2_49742_085_699	G12	285	42.13	0.24	0.0301	0.0056	0.0022	0.0038	0.1943	0.0055	0.00102	5.591	0.044	0.00038
M2_49742_089_703	G12	130	39.05	0.46	0.1381	0.026	0.016	0.0264	0.191	0.013	0.00559	3.936	0.054	0.00178
M2_49742_113_727	G3_Na	130	71.92	0.67	0.2951	0.059	0.027	0.0090	0.919	0.034	0.00406	14.45	0.16	0.00171
M2_49742_119_733	G1	285	127.6	0.58	0.0299	0.0038	0.0018	0.0036	0.409	0.0065	0.00108	21.91	0.13	0.00034
P3_49725_001_133	G9A_Ti	285	121.33	0.59	0.0274	0.0166	0.0032	0.0032	0.3829	0.0058	0.00102	24.36	0.13	0.00038
P3_49725_003_135	G9A_Ti	285	119.46	0.56	0.0296	0.0059	0.0021	0.0035	0.3699	0.0055	0.00103	22.95	0.14	0.00033
P3_49725_030_388	G9A_Ti	285	116.3	1	0.0300	0.0019	0.0021	0.0035	0.3983	0.0089	0.00095	19.77	0.23	0.00040
P3_49725_049_407	G9A_Ti	285	125.12	0.67	0.0293	0.0116	0.0026	0.0034	0.4339	0.0081	0.00090	25.09	0.17	0.00040
P3_49725_061_419	G9A_Ti	285	119.43	0.56	0.0300	0.008	0.0022	0.0033	0.536	0.018	0.00110	21.45	0.16	0.00038
P3_49725_39r_498	G9B_Ti	285	126.4	0.63	0.0300	0.0062	0.0022	0.0033	0.4168	0.008	0.00106	25.73	0.17	0.00048
P3_49736_008_274	G9A_Ti	285	128.16	0.58	0.0282	0.0059	0.0018	0.0034	0.553	0.012	0.00094	20.94	0.11	0.00045

Appendix E: Garnet Xenocryst LA-ICP-MS Data Tables

Appendix E.01 (continued): Mel kimberlite garnet trace element data measured by LA-ICPMS. 2SE – two times standard error. LOD – Limit of detection (Pettke et al., 2014). <LOD – bellow limit of detection.

Sample	*Class*	*Spot Size*	*Zr ppm*	*Zr 2SE*	*Zr LOD*	*Nb ppm*	*Nb 2SE*	*Nb LOD*	*Ba ppm*	*Ba 2SE*	*Ba LOD*	*La ppm*	*La 2SE*	*La LOD*
M2_49724_049_783	G9A	285	12.24	0.1	0.00652	0.087	0.0038	0.00145	0.0107	0.0032	0.00787	0.86	0.2	0.00046
M2_49724_051_785	G3_Na	130	67.64	0.56	0.00083	0.0627	0.0051	0.00033	0.0056	0.0047	0.00131	0.399	0.039	0.00008
M2_49724_057_791	G9A	285	12.024	0.087	0.00664	0.1821	0.0041	0.00152	<LOD	<LOD	0.00768	0.0286	0.00098	0.00047
M2_49724_063_797	G9A_Ti	285	56.21	0.44	0.00111	0.0743	0.0032	0.00031	<LOD	<LOD	0.00142	0.01046	0.00054	0.00008
M2_49724_067_801	G3_Na	130	38.17	0.34	0.00084	0.0727	0.0053	0.00033	0.097	0.017	0.00152	0.0184	0.0018	0.00009
M2_49724_073_807	G9A_Ti	285	64.02	0.46	0.00627	0.187	0.0051	0.00143	<LOD	<LOD	0.00800	0.0422	0.0011	0.00044
M2_49725_003_505	G9A	285	6.095	0.064	0.00092	0.1867	0.0036	0.00029	<LOD	<LOD	0.00101	0.02459	0.00065	0.00007
M2_49725_007_509	G9A_Ti	285	53.31	0.39	0.00106	0.1641	0.005	0.00043	0.733	0.051	0.00139	0.0869	0.0051	0.00010
M2_49725_009_511	G9A_Ti	285	55.58	0.39	0.00114	0.0715	0.0029	0.00031	<LOD	<LOD	0.00210	0.01034	0.00052	0.00009
M2_49725_029_531	G11	285	44.38	0.26	0.00098	0.2059	0.0042	0.00035	0.0035	0.0012	0.00163	0.1991	0.0085	0.00009
M2_49725_039_541	G9A_Ti	130	40.55	0.35	0.00113	0.0907	0.0085	0.00039	0.433	0.083	0.00174	0.0207	0.0025	0.00009
M2_49725_051_553	G9A	285	55.06	0.58	0.00438	0.0877	0.0033	0.00173	<LOD	<LOD	0.00987	0.013	0.0005	0.00045
M2_49725_059_561	G9A	285	3.399	0.029	0.00101	0.1873	0.0047	0.00035	0.001	0.0011	0.00086	0.02402	0.00067	0.00008
M2_49725_061_563	G3	285	61.76	0.47	0.00086	0.0474	0.0027	0.00034	0.0053	0.0029	0.00187	0.0335	0.007	0.00008
M2_49741_039_607	G9A_Ti	285	64.3	0.46	0.00295	0.1754	0.007	0.00057	12.6	1.2	0.00266	0.1201	0.0039	0.00018
M2_49742_003_617	G3_Na	130	59.7	5.1	0.00120	3.71	0.74	0.00028	22.4	1.9	0.00106	3.33	0.28	0.00008
M2_49742_005_619	G3_Na	285	24.03	0.37	0.01544	0.36	0.011	0.00302	0.052	0.017	0.02084	0.0538	0.0038	0.00098
M2_49742_011_625	G3_Na	285	44.59	0.43	0.00433	0.143	0.0077	0.00079	0.126	0.039	0.00477	0.122	0.026	0.00026
M2_49742_027_641	G9B_Ti	285	72.85	0.67	0.00370	0.1657	0.0048	0.00068	0.0039	0.0018	0.00407	0.0272	0.0014	0.00022
M2_49742_031_645	G9A	285	14.17	0.11	0.00100	0.1434	0.0031	0.00042	<LOD	<LOD	0.00157	0.01701	0.00065	0.00009
M2_49742_033_647	G9A	285	7.557	0.07	0.00097	0.4751	0.0076	0.00039	<LOD	<LOD	0.00147	0.0453	0.0012	0.00008
M2_49742_039_653	G12	285	41.03	0.24	0.00120	0.2298	0.0057	0.00034	<LOD	<LOD	0.00119	0.03104	0.00087	0.00010
M2_49742_057_671	G9A	285	27.61	0.15	0.00076	0.1913	0.0051	0.00030	<LOD	<LOD	0.00188	0.01248	0.0005	0.00010
M2_49742_065_679	G9B_Ti	285	72.41	0.44	0.00093	0.141	0.0041	0.00040	<LOD	<LOD	0.00139	0.02211	0.00075	0.00008
M2_49742_069_683	G9A_Ti	130	8.38	0.12	0.00496	0.616	0.016	0.00142	<LOD	<LOD	0.00777	0.0764	0.0044	0.00042
M2_49742_071_685	G12	285	41.42	0.55	0.00087	0.2501	0.0061	0.00029	0.002	0.00099	0.00181	0.0371	0.0014	0.00007
M2_49742_079_693	G9A_Ti	285	11.316	0.086	0.00085	0.696	0.0082	0.00034	<LOD	<LOD	0.00123	0.0819	0.0015	0.00007
M2_49742_085_699	G12	285	42.3	0.2	0.00088	0.2357	0.0045	0.00032	<LOD	<LOD	0.00180	0.03066	0.00078	0.00010
M2_49742_089_703	G12	130	30.12	0.29	0.00460	0.2062	0.01	0.00201	<LOD	<LOD	0.00948	0.0271	0.003	0.00040
M2_49742_113_727	G3_Na	130	19.05	0.17	0.00675	0.306	0.015	0.00149	0.37	0.24	0.00874	0.0362	0.0025	0.00048
M2_49742_119_733	G1	285	53.81	0.28	0.00065	0.1247	0.0043	0.00027	<LOD	<LOD	0.00173	0.01791	0.0005	0.00009
P3_49725_001_133	G9A_Ti	285	49.48	0.26	0.00088	0.1199	0.0032	0.00029	<LOD	<LOD	0.00155	0.02008	0.00059	0.00007
P3_49725_003_135	G9A_Ti	285	46.4	0.32	0.00102	0.1145	0.0028	0.00030	<LOD	<LOD	0.00175	0.01928	0.00067	0.00009
P3_49725_030_388	G9A_Ti	285	49.65	0.62	0.00082	0.0835	0.0038	0.00029	<LOD	<LOD	0.00196	0.01206	0.00063	0.00008
P3_49725_049_407	G9A_Ti	285	55.66	0.42	0.00083	0.099	0.0038	0.00039	0.016	0.0058	0.00153	0.01548	0.0008	0.00010
P3_49725_061_419	G9A_Ti	285	57.29	0.43	0.00084	0.0995	0.0039	0.00033	0.128	0.026	0.00180	0.01699	0.00063	0.00010
P3_49725_39r_498	G9B_Ti	285	54.15	0.4	0.00079	0.1175	0.0043	0.00037	<LOD	<LOD	0.00152	0.01768	0.00072	0.00007
P3_49736_008_274	G9A_Ti	285	28.87	0.13	0.00106	0.1824	0.0048	0.00028	0.1426	0.0092	0.00103	0.0394	0.0012	0.00009

Appendix E: Garnet Xenocryst LA-ICP-MS Data Tables

Appendix E.01 (continued): Mel kimberlite garnet trace element data measured by LA-ICPMS. 2SE – two times standard error. LOD – Limit of detection (Pettke et al., 2014). <LOD – bellow limit of detection.

Sample	*Class*	*Spot Size*	*Ce ppm*	*Ce 2SE*	*Ce LOD*	*Pr ppm*	*Pr 2SE*	*Pr LOD*	*Nd ppm*	*Nd 2SE*	*Nd LOD*	*Sm ppm*	*Sm 2SE*	*Sm LOD*
M2_49724_049_783	G9A	285	1.7	0.38	0.00049	0.246	0.042	0.00036	1.46	0.15	0.00224	0.655	0.025	0.00235
M2_49724_051_785	G3_Na	130	0.959	0.085	0.00010	0.1376	0.0097	0.00009	0.839	0.04	0.00048	0.612	0.018	0.00075
M2_49724_057_791	G9A	285	0.2477	0.0033	0.00049	0.0759	0.0012	0.00041	0.6034	0.0087	0.00220	0.4213	0.0088	0.00230
M2_49724_063_797	G9A_Ti	285	0.1036	0.002	0.00011	0.0418	0.0012	0.00008	0.5098	0.0082	0.00046	0.674	0.011	0.00071
M2_49724_067_801	G3_Na	130	0.1122	0.0039	0.00009	0.0387	0.0018	0.00007	0.434	0.012	0.00042	0.499	0.016	0.00064
M2_49724_073_807	G9A_Ti	285	0.3651	0.0046	0.00048	0.1311	0.0022	0.00036	1.347	0.02	0.00209	1.12	0.018	0.00193
M2_49725_003_505	G9A	285	0.2554	0.0037	0.00008	0.1039	0.002	0.00006	1.099	0.015	0.00034	0.576	0.011	0.00061
M2_49725_007_509	G9A_Ti	285	0.3008	0.008	0.00008	0.0889	0.0017	0.00008	0.896	0.013	0.00045	0.865	0.011	0.00061
M2_49725_009_511	G9A_Ti	285	0.1061	0.0017	0.00009	0.04396	0.0009	0.00008	0.5064	0.007	0.00049	0.633	0.011	0.00067
M2_49725_029_531	G11	285	0.655	0.017	0.00010	0.1447	0.003	0.00008	1.218	0.016	0.00054	1.041	0.014	0.00074
M2_49725_039_541	G9A_Ti	130	0.1177	0.0066	0.00009	0.0371	0.002	0.00006	0.423	0.017	0.00039	0.466	0.017	0.00066
M2_49725_051_553	G9A	285	0.143	0.0026	0.00044	0.0644	0.0014	0.00039	0.772	0.014	0.00232	0.775	0.017	0.00372
M2_49725_059_561	G9A	285	0.2571	0.0027	0.00009	0.1054	0.0016	0.00007	1.074	0.013	0.00048	0.4708	0.0078	0.00061
M2_49725_061_563	G3	285	0.118	0.012	0.00010	0.0391	0.0021	0.00006	0.455	0.011	0.00045	0.629	0.013	0.00066
M2_49741_039_607	G9A_Ti	285	0.378	0.0075	0.00016	0.1053	0.0021	0.00013	1.04	0.014	0.00080	0.932	0.012	0.00093
M2_49742_003_617	G3_Na	130	7.4	1.1	0.00008	0.871	0.064	0.00006	3.57	0.19	0.00046	1.146	0.057	0.00064
M2_49742_005_619	G3_Na	285	0.395	0.011	0.00107	0.1301	0.003	0.00084	1.174	0.019	0.00457	0.783	0.022	0.00509
M2_49742_011_625	G3_Na	285	0.42	0.052	0.00024	0.1026	0.0066	0.00020	0.918	0.028	0.00118	0.898	0.021	0.00116
M2_49742_027_641	G9B_Ti	285	0.2555	0.0048	0.00020	0.0954	0.0019	0.00017	1.011	0.018	0.00101	1.042	0.02	0.00099
M2_49742_031_645	G9A	285	0.1783	0.0024	0.00010	0.0792	0.0013	0.00007	1.006	0.011	0.00037	0.748	0.012	0.00070
M2_49742_033_647	G9A	285	0.4461	0.0048	0.00009	0.1459	0.002	0.00006	1.055	0.015	0.00039	0.3265	0.0063	0.00059
M2_49742_039_653	G12	285	0.2344	0.0028	0.00011	0.075	0.0014	0.00007	0.7072	0.0095	0.00049	0.4321	0.009	0.00072
M2_49742_057_671	G9A	285	0.217	0.0026	0.00009	0.1038	0.0014	0.00008	1.099	0.015	0.00045	0.79	0.011	0.00064
M2_49742_065_679	G9B_Ti	285	0.2216	0.0031	0.00009	0.0867	0.0017	0.00005	0.939	0.014	0.00049	0.988	0.014	0.00059
M2_49742_069_683	G9A_Ti	130	0.419	0.012	0.00043	0.0873	0.0033	0.00038	0.654	0.018	0.00235	0.499	0.015	0.00386
M2_49742_071_685	G12	285	0.2436	0.0048	0.00010	0.0743	0.002	0.00007	0.717	0.017	0.00045	0.452	0.013	0.00076
M2_49742_079_693	G9A_Ti	285	0.4311	0.0038	0.00009	0.0963	0.0015	0.00010	0.749	0.0096	0.00048	0.5798	0.0089	0.00069
M2_49742_085_699	G12	285	0.2346	0.0026	0.00008	0.0779	0.0013	0.00007	0.727	0.01	0.00040	0.45	0.0093	0.00067
M2_49742_089_703	G12	130	0.2194	0.009	0.00044	0.0699	0.0024	0.00038	0.624	0.017	0.00192	0.358	0.015	0.00381
M2_49742_113_727	G3_Na	130	0.344	0.01	0.00050	0.1116	0.0032	0.00038	1.032	0.023	0.00228	0.688	0.022	0.00256
M2_49742_119_733	G1	285	0.1841	0.0024	0.00008	0.0737	0.0013	0.00007	0.823	0.012	0.00044	0.776	0.013	0.00073
P3_49725_001_133	G9A_Ti	285	0.2056	0.0024	0.00007	0.08	0.0013	0.00007	0.891	0.012	0.00036	0.873	0.011	0.00056
P3_49725_003_135	G9A_Ti	285	0.1951	0.0023	0.00010	0.0759	0.0013	0.00008	0.839	0.013	0.00048	0.823	0.013	0.00074
P3_49725_030_388	G9A_Ti	285	0.1362	0.0028	0.00010	0.0566	0.0013	0.00007	0.671	0.017	0.00048	0.709	0.014	0.00067
P3_49725_049_407	G9A_Ti	285	0.1791	0.0027	0.00010	0.0807	0.0015	0.00007	0.921	0.014	0.00048	0.843	0.018	0.00065
P3_49725_061_419	G9A_Ti	285	0.179	0.0031	0.00008	0.0775	0.0015	0.00010	0.895	0.014	0.00054	0.81	0.015	0.00065
P3_49725_39r_498	G9B_Ti	285	0.1835	0.0022	0.00011	0.0735	0.0017	0.00007	0.824	0.015	0.00042	0.785	0.012	0.00069
P3_49736_008_274	G9A_Ti	285	0.2937	0.004	0.00009	0.0981	0.0017	0.00008	0.96	0.013	0.00045	0.787	0.012	0.00059

Appendix E: Garnet Xenocryst LA-ICP-MS Data Tables

Appendix E.01 (continued): Mel kimberlite garnet trace element data measured by LA-ICPMS. 2SE – two times standard error. LOD – Limit of detection (Pettke et al., 2014). <LOD – bellow limit of detection.

Sample	*Class*	*Spot Size*	*Eu ppm*	*Eu 2SE*	*Eu LOD*	*Gd ppm*	*Gd 2SE*	*Gd LOD*	*Tb ppm*	*Tb 2SE*	*Tb LOD*	*Dy ppm*	*Dy 2SE*	*Dy LOD*
M2_49724_049_783	G9A	285	0.2664	0.0044	0.00072	1.347	0.026	0.00304	0.3041	0.0047	0.00042	2.498	0.035	0.00172
M2_49724_051_785	G3_Na	130	0.3331	0.0084	0.00017	1.549	0.03	0.00071	0.3915	0.0071	0.00010	3.299	0.046	0.00042
M2_49724_057_791	G9A	285	0.2293	0.0036	0.00070	1.295	0.017	0.00276	0.3238	0.004	0.00046	2.824	0.031	0.00173
M2_49724_063_797	G9A_Ti	285	0.3716	0.0045	0.00018	1.901	0.028	0.00058	0.455	0.0063	0.00009	3.816	0.048	0.00047
M2_49724_067_801	G3_Na	130	0.2808	0.0073	0.00015	1.354	0.03	0.00069	0.3276	0.0069	0.00010	2.684	0.037	0.00043
M2_49724_073_807	G9A_Ti	285	0.5084	0.0077	0.00067	2.397	0.031	0.00289	0.5243	0.0073	0.00044	4.122	0.05	0.00145
M2_49725_003_505	G9A	285	0.1902	0.0034	0.00014	0.621	0.013	0.00046	0.1135	0.0021	0.00008	0.937	0.016	0.00043
M2_49725_007_509	G9A_Ti	285	0.4635	0.0058	0.00016	2.259	0.029	0.00054	0.5125	0.0061	0.00009	4.005	0.041	0.00042
M2_49725_009_511	G9A_Ti	285	0.3429	0.0049	0.00021	1.814	0.025	0.00068	0.4439	0.0048	0.00010	3.697	0.038	0.00048
M2_49725_029_531	G11	285	0.4988	0.0058	0.00017	1.82	0.021	0.00070	0.2919	0.0037	0.00009	1.802	0.02	0.00034
M2_49725_039_541	G9A_Ti	130	0.266	0.0076	0.00015	1.277	0.03	0.00053	0.3275	0.0077	0.00007	2.935	0.047	0.00043
M2_49725_051_553	G9A	285	0.3994	0.0075	0.00096	1.906	0.037	0.00403	0.4312	0.0085	0.00041	3.487	0.068	0.00210
M2_49725_059_561	G9A	285	0.142	0.0024	0.00016	0.462	0.0094	0.00064	0.092	0.0015	0.00009	0.816	0.011	0.00037
M2_49725_061_563	G3	285	0.3684	0.0062	0.00016	1.782	0.024	0.00068	0.4011	0.0046	0.00010	2.886	0.037	0.00038
M2_49741_039_607	G9A_Ti	285	0.4896	0.0063	0.00033	2.203	0.026	0.00119	0.5026	0.0043	0.00020	4.103	0.032	0.00085
M2_49742_003_617	G3_Na	130	0.475	0.019	0.00014	1.686	0.06	0.00072	0.341	0.01	0.00009	2.585	0.077	0.00046
M2_49742_005_619	G3_Na	285	0.4016	0.007	0.00159	1.692	0.027	0.00676	0.3993	0.0068	0.00100	3.185	0.046	0.00369
M2_49742_011_625	G3_Na	285	0.4785	0.008	0.00037	2.127	0.039	0.00180	0.431	0.0075	0.00028	3.053	0.042	0.00118
M2_49742_027_641	G9B_Ti	285	0.5571	0.0091	0.00032	2.936	0.048	0.00154	0.714	0.011	0.00024	5.899	0.092	0.00101
M2_49742_031_645	G9A	285	0.296	0.0043	0.00015	1.26	0.016	0.00060	0.2313	0.0034	0.00008	1.703	0.023	0.00045
M2_49742_033_647	G9A	285	0.1218	0.0027	0.00013	0.55	0.011	0.00060	0.1276	0.0023	0.00010	1.094	0.014	0.00039
M2_49742_039_653	G12	285	0.194	0.0031	0.00016	0.688	0.012	0.00079	0.1267	0.0021	0.00010	0.925	0.011	0.00046
M2_49742_057_671	G9A	285	0.3496	0.0047	0.00013	1.53	0.023	0.00057	0.3298	0.0046	0.00010	2.571	0.033	0.00036
M2_49742_065_679	G9B_Ti	285	0.5379	0.0067	0.00016	2.936	0.033	0.00056	0.7309	0.0084	0.00007	6.131	0.066	0.00043
M2_49742_069_683	G9A_Ti	130	0.2577	0.0075	0.00073	1.112	0.034	0.00342	0.2459	0.0058	0.00045	1.936	0.032	0.00181
M2_49742_071_685	G12	285	0.2043	0.0055	0.00011	0.681	0.02	0.00059	0.1271	0.0036	0.00010	0.923	0.025	0.00042
M2_49742_079_693	G9A_Ti	285	0.2984	0.0043	0.00015	1.427	0.015	0.00057	0.3192	0.0033	0.00010	2.581	0.028	0.00038
M2_49742_085_699	G12	285	0.1969	0.0031	0.00015	0.704	0.011	0.00065	0.1274	0.0021	0.00009	0.947	0.012	0.00047
M2_49742_089_703	G12	130	0.1577	0.005	0.00077	0.525	0.021	0.00282	0.0965	0.0029	0.00040	0.668	0.016	0.00188
M2_49742_113_727	G3_Na	130	0.3649	0.0097	0.00081	1.357	0.037	0.00300	0.3111	0.0069	0.00046	2.41	0.04	0.00174
M2_49742_119_733	G1	285	0.3854	0.0046	0.00014	1.886	0.022	0.00072	0.4271	0.0047	0.00011	3.469	0.027	0.00032
P3_49725_001_133	G9A_Ti	285	0.4371	0.0049	0.00015	2.14	0.022	0.00059	0.4798	0.0053	0.00009	3.83	0.039	0.00041
P3_49725_003_135	G9A_Ti	285	0.4184	0.0054	0.00017	2.062	0.025	0.00071	0.4579	0.0048	0.00011	3.648	0.033	0.00041
P3_49725_030_388	G9A_Ti	285	0.3645	0.0085	0.00015	1.727	0.038	0.00064	0.3962	0.0084	0.00006	3.177	0.064	0.00041
P3_49725_049_407	G9A_Ti	285	0.4103	0.0067	0.00015	1.941	0.026	0.00067	0.4514	0.0068	0.00011	3.713	0.049	0.00046
P3_49725_061_419	G9A_Ti	285	0.3986	0.0065	0.00013	1.89	0.024	0.00061	0.4228	0.0057	0.00010	3.365	0.043	0.00038
P3_49725_39r_498	G9B_Ti	285	0.4009	0.0055	0.00018	1.977	0.025	0.00062	0.4706	0.0063	0.00009	3.99	0.043	0.00037
P3_49736_008_274	G9A_Ti	285	0.369	0.0048	0.00017	1.757	0.021	0.00052	0.3985	0.0046	0.00008	3.189	0.028	0.00041

Appendix E: Garnet Xenocryst LA-ICP-MS Data Tables

Appendix E.01 (continued): Mel kimberlite garnet trace element data measured by LA-ICPMS. 2SE – two times standard error. LOD – Limit of detection (Pettke et al., 2014). <LOD – bellow limit of detection.

Sample	*Class*	*Spot Size*	*Ho ppm*	*Ho 2SE*	*Ho LOD*	*Er ppm*	*Er 2SE*	*Er LOD*	*Tm ppm*	*Tm 2SE*	*Tm LOD*	*Yb ppm*	*Yb 2SE*	*Yb LOD*
M2_49724_049_783	G9A	285	0.6192	0.0089	0.00036	2.026	0.029	0.00123	0.3108	0.0048	0.00039	2.207	0.031	0.00183
M2_49724_051_785	G3_Na	130	0.839	0.015	0.00011	2.832	0.044	0.00030	0.4424	0.0074	0.00010	3.295	0.05	0.00051
M2_49724_057_791	G9A	285	0.7357	0.0077	0.00041	2.421	0.028	0.00131	0.3755	0.0048	0.00046	2.688	0.032	0.00201
M2_49724_063_797	G9A_Ti	285	0.956	0.013	0.00011	3.105	0.042	0.00031	0.4719	0.0074	0.00011	3.319	0.046	0.00100
M2_49724_067_801	G3_Na	130	0.674	0.012	0.00011	2.205	0.034	0.00030	0.3381	0.007	0.00009	2.476	0.043	0.00093
M2_49724_073_807	G9A_Ti	285	0.994	0.012	0.00038	3.133	0.04	0.00131	0.4651	0.0062	0.00044	3.183	0.036	0.00206
M2_49725_003_505	G9A	285	0.2566	0.0042	0.00008	0.955	0.015	0.00022	0.1687	0.0033	0.00010	1.349	0.022	0.00070
M2_49725_007_509	G9A_Ti	285	0.9545	0.0097	0.00010	2.895	0.028	0.00031	0.4247	0.0056	0.00013	2.911	0.036	0.00110
M2_49725_009_511	G9A_Ti	285	0.8874	0.009	0.00010	2.777	0.026	0.00036	0.4113	0.0057	0.00012	2.878	0.032	0.00122
M2_49725_029_531	G11	285	0.3821	0.0047	0.00011	1.174	0.015	0.00029	0.1825	0.0031	0.00012	1.386	0.018	0.00104
M2_49725_039_541	G9A_Ti	130	0.769	0.013	0.00008	2.651	0.036	0.00030	0.4191	0.0085	0.00010	3.136	0.054	0.00060
M2_49725_051_553	G9A	285	0.853	0.018	0.00043	2.726	0.057	0.00099	0.4143	0.0088	0.00048	2.945	0.06	0.00326
M2_49725_059_561	G9A	285	0.2327	0.0033	0.00009	0.881	0.015	0.00029	0.1573	0.0027	0.00011	1.258	0.017	0.00098
M2_49725_061_563	G3	285	0.6158	0.0083	0.00009	1.718	0.025	0.00025	0.2264	0.004	0.00011	1.457	0.023	0.00101
M2_49741_039_607	G9A_Ti	285	1.0107	0.0099	0.00018	3.254	0.027	0.00063	0.4936	0.0049	0.00021	3.505	0.029	0.00089
M2_49742_003_617	G3_Na	130	0.592	0.016	0.00008	1.787	0.041	0.00024	0.2542	0.0096	0.00011	1.761	0.043	0.00076
M2_49742_005_619	G3_Na	285	0.759	0.013	0.00085	2.34	0.037	0.00262	0.3422	0.0069	0.00089	2.358	0.04	0.00436
M2_49742_011_625	G3_Na	285	0.668	0.011	0.00024	1.94	0.033	0.00082	0.2696	0.0057	0.00024	1.804	0.031	0.00126
M2_49742_027_641	G9B_Ti	285	1.455	0.023	0.00021	4.593	0.075	0.00070	0.66	0.011	0.00020	4.531	0.074	0.00107
M2_49742_031_645	G9A	285	0.409	0.0046	0.00009	1.375	0.016	0.00027	0.2224	0.003	0.00009	1.711	0.022	0.00072
M2_49742_033_647	G9A	285	0.2834	0.0036	0.00009	0.981	0.014	0.00029	0.1595	0.0026	0.00011	1.241	0.018	0.00120
M2_49742_039_653	G12	285	0.2085	0.0023	0.00011	0.6394	0.008	0.00030	0.094	0.0018	0.00011	0.647	0.011	0.00094
M2_49742_057_671	G9A	285	0.6221	0.0079	0.00009	2.012	0.023	0.00048	0.3126	0.0049	0.00061	2.273	0.034	0.00066
M2_49742_065_679	G9B_Ti	285	1.523	0.015	0.00008	4.789	0.051	0.00024	0.6952	0.0099	0.00009	4.731	0.062	0.00068
M2_49742_069_683	G9A_Ti	130	0.4722	0.0084	0.00043	1.521	0.022	0.00120	0.2238	0.0053	0.00048	1.622	0.033	0.00357
M2_49742_071_685	G12	285	0.2087	0.0049	0.00010	0.637	0.017	0.00028	0.091	0.0028	0.00009	0.645	0.019	0.00097
M2_49742_079_693	G9A_Ti	285	0.6298	0.0064	0.00009	2.001	0.022	0.00030	0.2989	0.0043	0.00010	2.111	0.025	0.00079
M2_49742_085_699	G12	285	0.218	0.0027	0.00009	0.6624	0.009	0.00028	0.0954	0.0015	0.00011	0.655	0.011	0.00103
M2_49742_089_703	G12	130	0.1516	0.0047	0.00038	0.457	0.013	0.00109	0.0699	0.0035	0.00049	0.475	0.016	0.00388
M2_49742_113_727	G3_Na	130	0.568	0.01	0.00040	1.736	0.028	0.00146	0.2461	0.0065	0.00046	1.697	0.029	0.00224
M2_49742_119_733	G1	285	0.8454	0.0082	0.00010	2.705	0.028	0.00032	0.3962	0.0043	0.00009	2.741	0.027	0.00073
P3_49725_001_133	G9A_Ti	285	0.9282	0.0091	0.00011	2.937	0.029	0.00026	0.4384	0.0055	0.00008	3.067	0.034	0.00097
P3_49725_003_135	G9A_Ti	285	0.8808	0.0079	0.00010	2.779	0.025	0.00035	0.4155	0.0047	0.00010	2.916	0.034	0.00095
P3_49725_030_388	G9A_Ti	285	0.785	0.014	0.00010	2.508	0.051	0.00027	0.3771	0.0078	0.00010	2.703	0.052	0.00054
P3_49725_049_407	G9A_Ti	285	0.953	0.015	0.00010	3.119	0.042	0.00031	0.4766	0.0068	0.00012	3.388	0.048	0.00041
P3_49725_061_419	G9A_Ti	285	0.82	0.013	0.00010	2.606	0.039	0.00028	0.3861	0.0055	0.00009	2.702	0.037	0.00035
P3_49725_39r_498	G9B_Ti	285	1	0.011	0.00008	3.182	0.032	0.00026	0.4674	0.0068	0.00011	3.179	0.037	0.00054
P3_49736_008_274	G9A_Ti	285	0.7843	0.0079	0.00008	2.523	0.023	0.00025	0.3828	0.0043	0.00012	2.714	0.031	0.00072

Appendix E: Garnet Xenocryst LA-ICP-MS Data Tables

Appendix E.01 (continued): Mel kimberlite garnet trace element data measured by LA-ICPMS. 2SE – two times standard error. LOD – Limit of detection (Pettke et al., 2014). <LOD – bellow limit of detection.

Sample	*Class*	*Spot Size*	*Lu ppm*	*Lu 2SE*	*Lu LOD*	*Hf ppm*	*Hf 2SE*	*Hf LOD*	*Ta ppm*	*Ta 2SE*	*Ta LOD*
M2_49724_049_783	G9A	285	0.3617	0.0054	0.00057	0.43	0.012	0.00298	0.01259	0.0009	0.00076
M2_49724_051_785	G3_Na	130	0.5054	0.0086	0.00011	1.527	0.047	0.00080	0.0069	0.0014	0.00024
M2_49724_057_791	G9A	285	0.4407	0.0054	0.00045	0.482	0.015	0.00352	0.0229	0.0012	0.00081
M2_49724_063_797	G9A_Ti	285	0.5285	0.0078	0.00020	1.66	0.025	0.00102	0.00756	0.00071	0.00020
M2_49724_067_801	G3_Na	130	0.3792	0.0061	0.00020	1.125	0.034	0.00081	0.0056	0.0013	0.00013
M2_49724_073_807	G9A_Ti	285	0.5132	0.0064	0.00050	1.888	0.031	0.00422	0.01792	0.00095	0.00080
M2_49725_003_505	G9A	285	0.241	0.0043	0.00020	0.1326	0.0072	0.00054	0.021	0.0011	0.00012
M2_49725_007_509	G9A_Ti	285	0.4517	0.0062	0.00021	1.528	0.03	0.00135	0.0174	0.0011	0.00013
M2_49725_009_511	G9A_Ti	285	0.4452	0.0064	0.00024	1.541	0.03	0.00079	0.0064	0.00065	0.00020
M2_49725_029_531	G11	285	0.2391	0.0041	0.00019	0.972	0.022	0.00128	0.0209	0.001	0.00018
M2_49725_039_541	G9A_Ti	130	0.4908	0.0091	0.00015	1.119	0.042	0.00148	0.0085	0.0019	0.00017
M2_49725_051_553	G9A	285	0.469	0.01	0.00113	1.614	0.04	0.00372	0.00982	0.00079	0.00078
M2_49725_059_561	G9A	285	0.2263	0.0034	0.00022	0.0658	0.0037	0.00077	0.0211	0.0013	0.00020
M2_49725_061_563	G3	285	0.2178	0.0031	0.00019	1.246	0.029	0.00089	0.00613	0.00069	0.00016
M2_49741_039_607	G9A_Ti	285	0.5539	0.0057	0.00022	1.84	0.033	0.00141	0.0171	0.0012	0.00031
M2_49742_003_617	G3_Na	130	0.2623	0.0094	0.00022	0.909	0.073	0.00098	0.234	0.035	0.00016
M2_49742_005_619	G3_Na	285	0.3558	0.0059	0.00107	0.574	0.018	0.00561	0.0449	0.0022	0.00195
M2_49742_011_625	G3_Na	285	0.2687	0.004	0.00032	1.069	0.025	0.00173	0.0181	0.0018	0.00056
M2_49742_027_641	G9B_Ti	285	0.681	0.012	0.00028	2.195	0.044	0.00148	0.0221	0.0011	0.00047
M2_49742_031_645	G9A	285	0.2931	0.0033	0.00022	0.369	0.012	0.00088	0.0156	0.001	0.00019
M2_49742_033_647	G9A	285	0.2194	0.0038	0.00024	0.259	0.01	0.00076	0.0536	0.0017	0.00017
M2_49742_039_653	G12	285	0.1024	0.002	0.00025	0.905	0.02	0.00111	0.0193	0.0013	0.00017
M2_49742_057_671	G9A	285	0.3732	0.0061	0.00015	0.412	0.013	0.00057	0.0186	0.0011	0.00022
M2_49742_065_679	G9B_Ti	285	0.7183	0.0099	0.00021	2.296	0.036	0.00063	0.0166	0.0011	0.00016
M2_49742_069_683	G9A_Ti	130	0.2497	0.0064	0.00106	0.342	0.022	0.00407	0.0577	0.0036	0.00080
M2_49742_071_685	G12	285	0.0999	0.0028	0.00020	0.952	0.034	0.00117	0.0194	0.0014	0.00010
M2_49742_079_693	G9A_Ti	285	0.334	0.0043	0.00021	0.471	0.014	0.00111	0.073	0.0023	0.00022
M2_49742_085_699	G12	285	0.1031	0.0023	0.00021	0.901	0.018	0.00083	0.0197	0.0011	0.00021
M2_49742_089_703	G12	130	0.0745	0.0026	0.00108	0.632	0.026	0.00417	0.0167	0.0023	0.00101
M2_49742_113_727	G3_Na	130	0.2525	0.0062	0.00049	0.455	0.022	0.00356	0.0378	0.0035	0.00089
M2_49742_119_733	G1	285	0.438	0.0049	0.00017	1.556	0.026	0.00113	0.0135	0.00087	0.00018
P3_49725_001_133	G9A_Ti	285	0.4899	0.0057	0.00017	1.374	0.026	0.00059	0.01405	0.00079	0.00012
P3_49725_003_135	G9A_Ti	285	0.4646	0.005	0.00014	1.302	0.027	0.00078	0.0133	0.0011	0.00019
P3_49725_030_388	G9A_Ti	285	0.425	0.009	0.00010	1.467	0.038	0.00077	0.00839	0.00072	0.00020
P3_49725_049_407	G9A_Ti	285	0.5364	0.0075	0.00011	1.548	0.03	0.00099	0.01244	0.0009	0.00022
P3_49725_061_419	G9A_Ti	285	0.4268	0.0061	0.00011	1.609	0.034	0.00062	0.01301	0.00078	0.00018
P3_49725_39r_498	G9B_Ti	285	0.4903	0.0064	0.00013	1.545	0.024	0.00043	0.01288	0.00077	0.00024
P3_49736_008_274	G9A_Ti	285	0.4369	0.0055	0.00016	0.916	0.019	0.00089	0.0194	0.0011	0.00020

Appendix E: Garnet Xenocryst LA-ICP-MS Data Tables

Appendix E.01 (continued): Mel kimberlite garnet trace element data measured by LA-ICPMS. 2SE – two times standard error. LOD – Limit of detection (Pettke et al., 2014). <LOD – bellow limit of detection.

Sample	*Class*	*Spot Size*	*Ca ppm*	*Ca 2SE*	*Ca LOD*	*Sc ppm*	*Sc 2SE*	*Sc LOD*	*Ti ppm*	*Ti 2SE*	*Ti LOD*	*V ppm*	*V 2SE*	*V LOD*
P3_49736_018_284	G9A	285	33870	140	3.98876	120.04	0.4	0.00716	1987.7	7	0.18	300.8	1.1	0.00306
P3_49736_028_294	G9B_Ti	285	32350	210	4.05906	115.9	0.85	0.00734	3956	28	0.18	194.4	1.8	0.00277
P3_49736_030_296	G9A_Ti	285	29300	130	4.00138	108.59	0.63	0.00698	4096	16	0.18	219.3	1.1	0.00275
P3_49736_040_306	G9A_Ti	285	29330	120	4.04516	111.2	0.48	0.00760	4009	15	0.19	214.33	0.96	0.00291
P3_49736_054_320	G9B_Ti	285	34020	130	4.09660	113.04	0.52	0.00860	3002	8.3	0.19	165.93	0.66	0.00256
P3_49736_060_326	G9B_Ti	285	31670	130	4.03160	112.72	0.5	0.00808	3214	11	0.18	164.09	0.59	0.00256
P3_49736_082_348	G9A_Ti	285	30540	160	5.36981	95.04	0.53	0.01075	2953	14	0.24	239.7	1.3	0.00368
P3_49736_098_364	G9B_Ti	285	30520	140	4.24799	109.83	0.48	0.00782	3577	15	0.18	180.37	0.79	0.00303
P3_49736_110_376	G11	285	36800	190	3.95618	121.3	0.54	0.00706	2356	11	0.17	304.8	1.7	0.00303
P3_49746_012_172	G9B	285	42660	190	4.00421	271.96	0.88	0.00713	198.7	1.2	0.18	176.68	0.52	0.00267
P3_49746_016_176	G9A	285	37510	120	3.76762	112.25	0.41	0.00648	976	13	0.16	159.84	0.7	0.00247
P3_49746_018_178	G9A	285	32340	110	4.01228	164.95	0.67	0.00706	1834.9	6.7	0.17	211.13	0.94	0.00287
P3_49746_050_210	G11	285	35090	170	3.74392	151.28	0.63	0.00622	2614	11	0.16	215.9	1.1	0.00273
P3_49746_060_220	G9A	285	34140	190	3.99972	134.67	0.56	0.00707	1329.2	4.3	0.18	249.7	1.2	0.00309
P3_49746_070_230	G9A_Ti	285	31430	140	4.13812	101.72	0.39	0.00712	5426	16	0.19	278.49	0.95	0.00322
P3_49746_076_236	G9B	285	41290	190	3.99321	260.7	1.3	0.00660	196.8	1.3	0.17	174.7	1.2	0.00287
P3_49746_082_242	G9A	285	31660	210	3.93382	158.3	1.2	0.00795	1770	12	0.18	197.8	1.6	0.00253
P3_49746_092_252	G9A_Ti	285	32020	120	3.89360	103.74	0.51	0.00769	5492	22	0.18	283.5	1.4	0.00281
P3_49746_104_264	G9B	285	45000	190	4.07812	278	1	0.00742	238.1	1.7	0.18	204.04	0.75	0.00287

Appendix E: Garnet Xenocryst LA-ICP-MS Data Tables

Appendix E.01 (continued): Mel kimberlite garnet trace element data measured by LA-ICPMS. 2SE – two times standard error. LOD – Limit of detection (Pettke et al., 2014). <LOD – bellow limit of detection.

Sample	*Class*	*Spot Size*	*Ni ppm*	*Ni 2SE*	*Ni LOD*	*Rb ppm*	*Rb 2SE*	*Rb LOD*	*Sr ppm*	*Sr 2SE*	*Sr LOD*	*Y ppm*	*Y 2SE*	*Y LOD*
P3_49736_018_284	G9A	285	124.77	0.61	0.0294	0.0044	0.0022	0.0036	0.4788	0.0075	0.00094	14.18	0.1	0.00047
P3_49736_028_294	G9B_Ti	285	103.9	1.2	0.0297	0.0101	0.0025	0.0036	0.474	0.011	0.00088	27.71	0.47	0.00038
P3_49736_030_296	G9A_Ti	285	98.65	0.64	0.0287	0.0037	0.002	0.0035	0.42	0.0084	0.00089	23.62	0.18	0.00039
P3_49736_040_306	G9A_Ti	285	100.55	0.44	0.0308	0.0054	0.0021	0.0036	0.462	0.0085	0.00089	22.92	0.15	0.00042
P3_49736_054_320	G9B_Ti	285	99.98	0.63	0.0303	0.0083	0.0022	0.0033	0.43	0.0092	0.00113	24.2	0.2	0.00040
P3_49736_060_326	G9B_Ti	285	101.52	0.56	0.0298	0.0053	0.0018	0.0035	0.4327	0.0078	0.00100	20.91	0.1	0.00043
P3_49736_082_348	G9A_Ti	285	122.9	0.84	0.0405	0.0045	0.0016	0.0046	0.3521	0.0058	0.00146	19.02	0.18	0.00043
P3_49736_098_364	G9B_Ti	285	100.15	0.57	0.0294	0.012	0.0026	0.0037	0.4164	0.0089	0.00096	25.43	0.14	0.00038
P3_49736_110_376	G11	285	115.19	0.77	0.0279	0.0065	0.0017	0.0035	0.4732	0.0092	0.00090	13.14	0.13	0.00031
P3_49746_012_172	G9B	285	10.953	0.087	0.0296	0.0072	0.0024	0.0036	0.0379	0.0028	0.00103	6.555	0.041	0.00032
P3_49746_016_176	G9A	285	9.926	0.093	0.0274	0.0063	0.0017	0.0032	1.79	0.17	0.00091	22.1	0.14	0.00041
P3_49746_018_178	G9A	285	38.06	0.23	0.0291	0.0073	0.0018	0.0034	0.3429	0.0079	0.00089	18.88	0.11	0.00043
P3_49746_050_210	G11	285	65.39	0.37	0.0275	0.0083	0.0022	0.0034	0.317	0.0057	0.00076	10.553	0.09	0.00033
P3_49746_060_220	G9A	285	67.31	0.41	0.0297	0.0055	0.0024	0.0038	0.4852	0.0084	0.00088	14.257	0.084	0.00047
P3_49746_070_230	G9A_Ti	285	148.64	0.77	0.0307	0.0034	0.0022	0.0037	0.739	0.011	0.00094	29.7	0.17	0.00045
P3_49746_076_236	G9B	285	10.91	0.12	0.0293	0.0072	0.0022	0.0035	0.0473	0.003	0.00087	6.115	0.063	0.00042
P3_49746_082_242	G9A	285	38.73	0.43	0.0297	0.0069	0.0022	0.0035	0.637	0.086	0.00104	17.44	0.32	0.00045
P3_49746_092_252	G9A_Ti	285	149.4	0.69	0.0301	0.0064	0.002	0.0034	0.757	0.01	0.00098	30.71	0.18	0.00035
P3_49746_104_264	G9B	285	10.832	0.078	0.0304	0.0052	0.0021	0.0035	0.0395	0.0022	0.00102	6.972	0.046	0.00028

Appendix E: Garnet Xenocryst LA-ICP-MS Data Tables

Appendix E.01 (continued): Mel kimberlite garnet trace element data measured by LA-ICPMS. 2SE – two times standard error. LOD – Limit of detection (Pettke et al., 2014). <LOD – bellow limit of detection.

Sample	*Class*	*Spot Size*	*Zr ppm*	*Zr 2SE*	*Zr LOD*	*Nb ppm*	*Nb 2SE*	*Nb LOD*	*Ba ppm*	*Ba 2SE*	*Ba LOD*	*La ppm*	*La 2SE*	*La LOD*
P3_49736_018_284	G9A	285	2.473	0.03	0.00083	0.3042	0.0057	0.00033	<LOD	<LOD	0.00164	0.03527	0.00099	0.00008
P3_49736_028_294	G9B_Ti	285	53.35	0.92	0.00101	0.0941	0.004	0.00016	0.096	0.029	0.00164	0.0359	0.0028	0.00008
P3_49736_030_296	G9A_Ti	285	52.79	0.49	0.00102	0.0994	0.0034	0.00026	<LOD	<LOD	0.00147	0.0138	0.00069	0.00008
P3_49736_040_306	G9A_Ti	285	51.79	0.37	0.00098	0.099	0.0035	0.00032	0.0671	0.006	0.00135	0.0738	0.0044	0.00009
P3_49736_054_320	G9B_Ti	285	28.48	0.24	0.00090	0.0689	0.0028	0.00037	0.014	0.0032	0.00160	0.0239	0.0026	0.00011
P3_49736_060_326	G9B_Ti	285	41.62	0.2	0.00100	0.0876	0.0038	0.00045	<LOD	<LOD	0.00143	0.01208	0.00061	0.00010
P3_49736_082_348	G9A_Ti	285	26.34	0.21	0.00153	0.1777	0.0053	0.00037	<LOD	<LOD	0.00168	0.02418	0.00086	0.00014
P3_49736_098_364	G9B_Ti	285	45.62	0.24	0.00115	0.0808	0.0035	0.00036	0.0017	0.001	0.00169	0.01365	0.00063	0.00012
P3_49736_110_376	G11	285	39.11	0.34	0.00083	0.2048	0.0048	0.00030	<LOD	<LOD	0.00104	0.0263	0.00093	0.00008
P3_49746_012_172	G9B	285	5.529	0.045	0.00093	0.0213	0.0014	0.00035	<LOD	<LOD	0.00161	0.00204	0.00022	0.00010
P3_49746_016_176	G9A	285	23.77	0.44	0.00085	0.0283	0.0024	0.00019	0.81	0.11	0.00119	1.19	0.15	0.00010
P3_49746_018_178	G9A	285	62.61	0.36	0.00077	0.1426	0.004	0.00033	<LOD	<LOD	0.00135	0.01198	0.00053	0.00008
P3_49746_050_210	G11	285	26.41	0.22	0.00087	0.1222	0.004	0.00029	<LOD	<LOD	0.00140	0.00715	0.00046	0.00008
P3_49746_060_220	G9A	285	20.87	0.14	0.00102	0.2487	0.0058	0.00034	<LOD	<LOD	0.00179	0.01702	0.00074	0.00008
P3_49746_070_230	G9A_Ti	285	73.13	0.4	0.00105	0.1393	0.0051	0.00043	<LOD	<LOD	0.00154	0.0352	0.001	0.00007
P3_49746_076_236	G9B	285	5.336	0.075	0.00097	0.022	0.0014	0.00023	0.0226	0.0051	0.00127	0.00312	0.00036	0.00008
P3_49746_082_242	G9A	285	57.7	1	0.00112	0.1641	0.0091	0.00037	0.063	0.022	0.00188	0.0485	0.0097	0.00009
P3_49746_092_252	G9A_Ti	285	73.95	0.47	0.00106	0.1323	0.0041	0.00030	<LOD	<LOD	0.00144	0.03482	0.00092	0.00007
P3_49746_104_264	G9B	285	6.188	0.05	0.00080	0.023	0.0018	0.00026	<LOD	<LOD	0.00177	0.00153	0.00017	0.00008

Appendix E: Garnet Xenocryst LA-ICP-MS Data Tables

Appendix E.01 (continued): Mel kimberlite garnet trace element data measured by LA-ICPMS. 2SE – two times standard error. LOD – Limit of detection (Pettke et al., 2014). <LOD – bellow limit of detection.

Sample	*Class*	*Spot Size*	*Ce ppm*	*Ce 2SE*	*Ce LOD*	*Pr ppm*	*Pr 2SE*	*Pr LOD*	*Nd ppm*	*Nd 2SE*	*Nd LOD*	*Sm ppm*	*Sm 2SE*	*Sm LOD*
P3_49736_018_284	G9A	285	0.3329	0.0038	0.00009	0.1143	0.002	0.00006	0.913	0.012	0.00044	0.3765	0.0058	0.00069
P3_49736_028_294	G9B_Ti	285	0.1747	0.0052	0.00011	0.0574	0.0017	0.00007	0.611	0.018	0.00043	0.636	0.018	0.00058
P3_49736_030_296	G9A_Ti	285	0.1359	0.0025	0.00008	0.0518	0.0012	0.00007	0.573	0.012	0.00045	0.591	0.013	0.00066
P3_49736_040_306	G9A_Ti	285	0.2307	0.0051	0.00008	0.0624	0.0012	0.00007	0.611	0.0093	0.00042	0.609	0.01	0.00067
P3_49736_054_320	G9B_Ti	285	0.146	0.0065	0.00010	0.0453	0.0014	0.00009	0.4522	0.01	0.00050	0.4501	0.0098	0.00059
P3_49736_060_326	G9B_Ti	285	0.1136	0.0015	0.00008	0.0427	0.001	0.00008	0.4606	0.0084	0.00049	0.48	0.011	0.00073
P3_49736_082_348	G9A_Ti	285	0.2453	0.0034	0.00012	0.0875	0.0016	0.00010	0.898	0.014	0.00080	0.717	0.014	0.00089
P3_49736_098_364	G9B_Ti	285	0.1215	0.0017	0.00010	0.0456	0.0011	0.00007	0.4986	0.0085	0.00038	0.544	0.011	0.00075
P3_49736_110_376	G11	285	0.2827	0.0047	0.00010	0.1177	0.002	0.00007	1.311	0.018	0.00046	0.874	0.016	0.00066
P3_49746_012_172	G9B	285	0.0219	0.00079	0.00009	0.01332	0.00058	0.00006	0.2612	0.005	0.00045	0.4075	0.0079	0.00070
P3_49746_016_176	G9A	285	1.85	0.16	0.00009	0.103	0.0068	0.00006	0.643	0.016	0.00048	0.83	0.012	0.00066
P3_49746_018_178	G9A	285	0.159	0.0022	0.00009	0.0838	0.0016	0.00006	1.148	0.014	0.00045	1.349	0.017	0.00066
P3_49746_050_210	G11	285	0.111	0.0018	0.00009	0.062	0.0013	0.00005	0.831	0.013	0.00049	0.901	0.016	0.00059
P3_49746_060_220	G9A	285	0.2211	0.0032	0.00009	0.1089	0.0015	0.00005	1.159	0.018	0.00029	0.688	0.012	0.00061
P3_49746_070_230	G9A_Ti	285	0.331	0.003	0.00009	0.1248	0.0018	0.00007	1.313	0.014	0.00047	1.187	0.018	0.00072
P3_49746_076_236	G9B	285	0.02174	0.00085	0.00010	0.01246	0.00053	0.00006	0.2438	0.0078	0.00045	0.387	0.011	0.00070
P3_49746_082_242	G9A	285	0.206	0.014	0.00009	0.0866	0.0026	0.00007	1.149	0.029	0.00048	1.258	0.034	0.00064
P3_49746_092_252	G9A_Ti	285	0.3002	0.003	0.00009	0.1147	0.0017	0.00006	1.264	0.018	0.00048	1.168	0.017	0.00064
P3_49746_104_264	G9B	285	0.0227	0.0026	0.00010	0.01445	0.00049	0.00007	0.2725	0.0069	0.00052	0.4509	0.009	0.00076

Appendix E: Garnet Xenocryst LA-ICP-MS Data Tables

Appendix E.01 (continued): Mel kimberlite garnet trace element data measured by LA-ICPMS. 2SE – two times standard error. LOD – Limit of detection (Pettke et al., 2014). <LOD – bellow limit of detection.

Sample	*Class*	*Spot Size*	*Eu ppm*	*Eu 2SE*	*Eu LOD*	*Gd ppm*	*Gd 2SE*	*Gd LOD*	*Tb ppm*	*Tb 2SE*	*Tb LOD*	*Dy ppm*	*Dy 2SE*	*Dy LOD*
P3_49736_018_284	G9A	285	0.1613	0.003	0.00014	0.878	0.012	0.00052	0.2234	0.0028	0.00007	1.986	0.025	0.00036
P3_49736_028_294	G9B_Ti	285	0.342	0.01	0.00014	1.8	0.06	0.00054	0.458	0.014	0.00009	4.04	0.12	0.00041
P3_49736_030_296	G9A_Ti	285	0.3115	0.0065	0.00016	1.629	0.03	0.00063	0.4014	0.0063	0.00008	3.523	0.05	0.00041
P3_49736_040_306	G9A_Ti	285	0.3136	0.0039	0.00017	1.596	0.019	0.00064	0.3942	0.004	0.00011	3.412	0.032	0.00046
P3_49736_054_320	G9B_Ti	285	0.2509	0.004	0.00018	1.33	0.019	0.00058	0.3582	0.0052	0.00010	3.319	0.042	0.00039
P3_49736_060_326	G9B_Ti	285	0.25	0.0034	0.00017	1.332	0.013	0.00073	0.3372	0.0037	0.00011	3.041	0.028	0.00047
P3_49736_082_348	G9A_Ti	285	0.3501	0.0046	0.00014	1.645	0.025	0.00083	0.3698	0.0056	0.00012	2.968	0.046	0.00040
P3_49736_098_364	G9B_Ti	285	0.2996	0.0037	0.00018	1.609	0.023	0.00053	0.4174	0.0048	0.00009	3.757	0.038	0.00035
P3_49736_110_376	G11	285	0.3854	0.0073	0.00017	1.69	0.028	0.00057	0.3399	0.0054	0.00007	2.382	0.04	0.00038
P3_49746_012_172	G9B	285	0.1795	0.0033	0.00015	0.738	0.013	0.00052	0.1323	0.0021	0.00011	0.983	0.012	0.00045
P3_49746_016_176	G9A	285	0.429	0.0064	0.00014	2.2	0.024	0.00058	0.4654	0.0049	0.00007	3.58	0.035	0.00034
P3_49746_018_178	G9A	285	0.65	0.0082	0.00013	2.862	0.026	0.00055	0.5281	0.0047	0.00009	3.592	0.036	0.00044
P3_49746_050_210	G11	285	0.4093	0.007	0.00014	1.705	0.031	0.00059	0.2985	0.0041	0.00009	1.926	0.027	0.00037
P3_49746_060_220	G9A	285	0.2642	0.0039	0.00011	1.158	0.019	0.00053	0.244	0.0033	0.00009	2.044	0.022	0.00043
P3_49746_070_230	G9A_Ti	285	0.5614	0.0066	0.00016	2.773	0.03	0.00075	0.6169	0.0056	0.00010	4.865	0.046	0.00050
P3_49746_076_236	G9B	285	0.1733	0.0044	0.00018	0.695	0.013	0.00043	0.126	0.0025	0.00011	0.938	0.016	0.00043
P3_49746_082_242	G9A	285	0.592	0.014	0.00014	2.461	0.066	0.00057	0.466	0.011	0.00008	3.149	0.079	0.00042
P3_49746_092_252	G9A_Ti	285	0.555	0.0061	0.00013	2.715	0.032	0.00058	0.6136	0.0059	0.00007	4.87	0.051	0.00031
P3_49746_104_264	G9B	285	0.2012	0.003	0.00014	0.816	0.012	0.00065	0.1436	0.002	0.00009	1.035	0.015	0.00033

Appendix E: Garnet Xenocryst LA-ICP-MS Data Tables

Appendix E.01 (continued): Mel kimberlite garnet trace element data measured by LA-ICPMS. 2SE – two times standard error. LOD – Limit of detection (Pettke et al., 2014). <LOD – bellow limit of detection.

Sample	*Class*	*Spot Size*	*Ho ppm*	*Ho 2SE*	*Ho LOD*	*Er ppm*	*Er 2SE*	*Er LOD*	*Tm ppm*	*Tm 2SE*	*Tm LOD*	*Yb ppm*	*Yb 2SE*	*Yb LOD*
P3_49736_018_284	G9A	285	0.518	0.0053	0.00009	1.756	0.017	0.00028	0.2783	0.0032	0.00008	2.056	0.022	0.00079
P3_49736_028_294	G9B_Ti	285	1.073	0.033	0.00010	3.65	0.12	0.00032	0.572	0.019	0.00011	4.18	0.13	0.00050
P3_49736_030_296	G9A_Ti	285	0.919	0.013	0.00010	3.115	0.049	0.00026	0.492	0.0078	0.00010	3.612	0.063	0.00102
P3_49736_040_306	G9A_Ti	285	0.8866	0.0088	0.00010	2.991	0.027	0.00023	0.47	0.0051	0.00011	3.455	0.036	0.00058
P3_49736_054_320	G9B_Ti	285	0.937	0.013	0.00010	3.378	0.042	0.00024	0.557	0.0071	0.00010	4.254	0.056	0.00048
P3_49736_060_326	G9B_Ti	285	0.8148	0.0083	0.00010	2.833	0.026	0.00024	0.4565	0.005	0.00010	3.456	0.039	0.00045
P3_49736_082_348	G9A_Ti	285	0.7308	0.0095	0.00015	2.346	0.035	0.00035	0.3562	0.0059	0.00012	2.538	0.036	0.00065
P3_49736_098_364	G9B_Ti	285	1.0149	0.0098	0.00010	3.517	0.034	0.00022	0.5569	0.0053	0.00011	4.102	0.039	0.00046
P3_49736_110_376	G11	285	0.5131	0.0072	0.00011	1.5	0.018	0.00024	0.2174	0.0033	0.00010	1.555	0.025	0.00043
P3_49746_012_172	G9B	285	0.2416	0.0033	0.00010	0.857	0.012	0.00028	0.1553	0.0024	0.00011	1.45	0.014	0.00072
P3_49746_016_176	G9A	285	0.8427	0.0084	0.00009	2.626	0.024	0.00022	0.3953	0.0046	0.00010	2.812	0.033	0.00043
P3_49746_018_178	G9A	285	0.7575	0.0075	0.00010	2.141	0.021	0.00028	0.2908	0.0032	0.00009	1.872	0.026	0.00072
P3_49746_050_210	G11	285	0.4021	0.0062	0.00009	1.157	0.018	0.00032	0.1685	0.003	0.00009	1.205	0.02	0.00052
P3_49746_060_220	G9A	285	0.534	0.0064	0.00009	1.842	0.022	0.00023	0.2958	0.0031	0.00010	2.233	0.023	0.00077
P3_49746_070_230	G9A_Ti	285	1.166	0.01	0.00010	3.625	0.033	0.00023	0.5303	0.0051	0.00012	3.625	0.033	0.00082
P3_49746_076_236	G9B	285	0.2259	0.0045	0.00008	0.799	0.016	0.00029	0.1455	0.003	0.00009	1.359	0.028	0.00073
P3_49746_082_242	G9A	285	0.669	0.017	0.00010	1.886	0.05	0.00029	0.257	0.0065	0.00010	1.699	0.046	0.00088
P3_49746_092_252	G9A_Ti	285	1.166	0.011	0.00009	3.654	0.037	0.00021	0.5312	0.0057	0.00010	3.658	0.038	0.00071
P3_49746_104_264	G9B	285	0.2507	0.0031	0.00009	0.8714	0.0097	0.00029	0.1573	0.0026	0.00009	1.458	0.021	0.00089

Appendix E: Garnet Xenocryst LA-ICP-MS Data Tables

Appendix E.01 (continued): Mel kimberlite garnet trace element data measured by LA-ICPMS. 2SE – two times standard error. LOD – Limit of detection (Pettke et al., 2014). <LOD – bellow limit of detection.

Sample	*Class*	*Spot Size*	*Lu ppm*	*Lu 2SE*	*Lu LOD*	*Hf ppm*	*Hf 2SE*	*Hf LOD*	*Ta ppm*	*Ta 2SE*	*Ta LOD*
P3_49736_018_284	G9A	285	0.3404	0.0039	0.00012	0.1712	0.0071	0.00063	0.0339	0.0016	0.00015
P3_49736_028_294	G9B_Ti	285	0.675	0.021	0.00015	1.512	0.057	0.00088	0.01017	0.00067	0.00017
P3_49736_030_296	G9A_Ti	285	0.586	0.01	0.00020	1.553	0.033	0.00076	0.01043	0.00084	0.00020
P3_49736_040_306	G9A_Ti	285	0.5656	0.0059	0.00018	1.499	0.023	0.00073	0.01129	0.00094	0.00021
P3_49736_054_320	G9B_Ti	285	0.7126	0.0098	0.00012	0.83	0.022	0.00064	0.00634	0.00073	0.00017
P3_49736_060_326	G9B_Ti	285	0.5754	0.0062	0.00014	1.184	0.023	0.00071	0.00935	0.00086	0.00019
P3_49736_082_348	G9A_Ti	285	0.4021	0.0068	0.00016	0.838	0.02	0.00116	0.0181	0.001	0.00032
P3_49736_098_364	G9B_Ti	285	0.6742	0.0072	0.00011	1.321	0.024	0.00084	0.00858	0.00071	0.00019
P3_49736_110_376	G11	285	0.2576	0.005	0.00010	1.127	0.022	0.00079	0.0245	0.0013	0.00023
P3_49746_012_172	G9B	285	0.3099	0.0034	0.00015	0.1429	0.0065	0.00094	0.000064	0.000076	0.00022
P3_49746_016_176	G9A	285	0.4612	0.0061	0.00010	0.372	0.013	0.00083	0.00096	0.0003	0.00013
P3_49746_018_178	G9A	285	0.283	0.0036	0.00021	1.083	0.019	0.00098	0.01465	0.00095	0.00016
P3_49746_050_210	G11	285	0.2068	0.0037	0.00010	0.685	0.019	0.00077	0.0146	0.001	0.00014
P3_49746_060_220	G9A	285	0.3787	0.0054	0.00019	0.594	0.016	0.00091	0.0438	0.0019	0.00021
P3_49746_070_230	G9A_Ti	285	0.5593	0.0055	0.00022	2.172	0.029	0.00083	0.01472	0.00093	0.00019
P3_49746_076_236	G9B	285	0.2882	0.0057	0.00022	0.1351	0.0069	0.00129	0.00038	0.00019	0.00018
P3_49746_082_242	G9A	285	0.2533	0.0065	0.00019	0.958	0.025	0.00062	0.0138	0.0011	0.00016
P3_49746_092_252	G9A_Ti	285	0.5654	0.0062	0.00016	2.156	0.032	0.00068	0.01381	0.00088	0.00012
P3_49746_104_264	G9B	285	0.3127	0.0036	0.00015	0.1523	0.007	0.00076	0.00038	0.00019	0.00020

Appendix E: Garnet Xenocryst LA-ICP-MS Data Tables

Appendix E.02: Dharma kimberlite garnet trace element data measured by LA-ICPMS. 2SE – two times standard error. LOD – Limit of detection (Pettke et al., 2014). <LOD – bellow limit of detection.

Sample	*Class*	*Spot Size*	*Ca ppm*	*Ca 2SE*	*Ca LOD*	*Sc ppm*	*Sc 2SE*	*Sc LOD*	*Ti ppm*	*Ti 2SE*	*Ti LOD*	*V ppm*	*V 2SE*	*V LOD*
D104_1_67	G9A	285	31260	320	7.15627	133.4	1.10	0.01048	1506	13	0.31347	263.2	3.1	0.00434
D104_1_81	G9A_Ti	285	31030	300	7.11217	77.48	0.60	0.00949	2435	25	0.29790	224.8	2.2	0.00426
D104_1_89	G9B_Ti	130	31570	300	18.6535	97.55	0.82	0.02117	3423	25	0.73103	308.2	2.4	0.01062
D104_1_93	G9A	285	31340	350	7.27900	133.9	1.20	0.00909	1619	16	0.30618	278.9	2.6	0.00455
D104_1_97	G9A	285	31350	240	7.47993	134.1	1.40	0.00904	1550	13	0.31063	272.1	2.4	0.00467
D104_1_99	G9A	285	27330	280	7.77764	108.2	1.40	0.00921	1415	13	0.31515	359.5	2.9	0.00513
D104_2_111	G10A	130	32750	290	17.3729	145.5	1.30	0.01836	471.8	4.8	0.65332	358.3	3.2	0.00996
D104_2_123	G9A	130	36300	330	18.9676	113.2	0.84	0.02019	537.1	4.2	0.71276	303	2.6	0.01143
D104_2_139	G9B	130	38770	310	18.5873	108.14	0.82	0.01986	1448	12	0.69917	633	5.3	0.01175
D104_2_143	G9A_Ti	130	38460	370	18.4951	115.72	0.99	0.01948	3955	38	0.68987	305.8	2.4	0.01152
D104_2_153	G9B_Ti	130	31490	270	19.0338	98.21	0.68	0.02056	3463	20	0.72249	308.7	2.1	0.01187
D104_3_155	G9A	285	31390	330	7.63791	134.1	1.20	0.00893	1529	13	0.31456	269.8	2.6	0.00495
D104_3_161	G9A	285	31480	290	8.01057	134.1	1.10	0.00929	1581	15	0.32815	277.3	2.6	0.00536
D104_3_179	G9A	285	31800	310	7.76455	136.9	1.30	0.00898	1664	15	0.31285	287.5	2.5	0.00528
D104_3_185	G10A	285	35130	370	7.25877	187.3	2.00	0.00822	520.7	5.5	0.28204	366.9	4.1	0.00524
D104_3_199	G12_Ti	130	49510	520	18.4782	128.8	1.10	0.02066	3375	25	0.71946	356.8	2.8	0.01175
D104_4_209	G9A	130	29310	280	18.6587	87.53	0.79	0.02071	1717	14	0.72405	231.3	1.9	0.01134
D104_4_223	G9A_Ti	130	31710	230	18.7042	95.36	0.79	0.02060	3412	23	0.71321	289	2.7	0.01163
D104_4_227	G9A_Ti	130	33590	350	18.7107	101.26	0.81	0.02009	2289	19	0.70465	267.5	2.2	0.01172
D104_4_233	G10A	130	32330	340	17.1065	147.9	1.30	0.01763	475.7	4.2	0.63913	356.9	3.2	0.01081
D104_4_235	G10A	130	32330	350	16.7214	145.3	1.40	0.01725	475.5	4.3	0.61494	361.5	3.4	0.01036
D104_4_239	G9A	285	31590	350	7.76317	134.5	1.30	0.00919	1528	16	0.32168	269.1	2.8	0.00552
D104_4_243	G9B	130	38210	460	17.8009	106.2	1.10	0.01910	1450	16	0.66506	632.8	7.9	0.01195
D104_4_247	G9A_Ti	285	35790	360	6.98994	129	1.20	0.00992	2558	28	0.29243	269.2	2.5	0.00420
D104_4_249	G9A	130	28900	200	19.3689	104.91	0.79	0.02101	1309	10	0.73110	247.7	1.8	0.01240
D104_4_251	G9A	130	35980	340	18.5801	112.72	0.97	0.01973	539.5	4.3	0.68707	304.4	2.7	0.01178
D104_5_257	G12_Ti	130	49460	400	18.9118	128.14	0.98	0.02026	3316	19	0.71557	349	2.3	0.01236
D104_5_267	G9A_Ti	130	32090	310	18.8587	96.45	0.63	0.02006	3364	25	0.71788	287.1	2.2	0.01222
D104_5_275	G9A_Ti	130	31800	320	18.6521	99.19	0.81	0.02023	3379	30	0.70906	310	3	0.01217
D104_5_293	G9A_Ti	130	32240	350	18.7559	96.15	0.89	0.02036	2939	32	0.71202	257	2.8	0.01237
D104_5_297	G9A_Ti	285	30900	310	7.36867	79.95	0.66	0.00980	2440	26	0.30652	225.4	2.3	0.00451
D104_5_299	G9A_Ti	285	33810	340	7.42212	130.5	1.40	0.00945	1152	12	0.29773	256.6	2.8	0.00465
D89_329	G9A	285	33700	250	7.22890	124.58	0.91	0.00934	1756	13	0.29366	256.5	1.9	0.00520
D89_331	G9A_Ti	285	35140	310	7.23152	125.7	1.00	0.00952	4125	33	0.29277	318.2	2.6	0.00534
D89_335	G9A	285	37170	300	7.37757	140.2	1.20	0.00928	795.6	6.4	0.28861	310.5	3.1	0.00533
D89_337	G9A	130	31790	330	17.6068	96.51	0.76	0.02011	1569	13	0.68159	236.6	2.6	0.01120
D89_349	G9A_Ti	285	29270	230	7.70234	102.98	0.89	0.01010	2686	21	0.30731	270.1	1.9	0.00539
D89_353	G9B	285	43890	340	7.33126	156.5	1.30	0.00902	600.7	5.6	0.28568	402.3	3.4	0.00557

Appendix E: Garnet Xenocryst LA-ICP-MS Data Tables

Appendix E.02 (continued): Dharma kimberlite garnet trace element data measured by LA-ICPMS. 2SE – two times standard error. LOD – Limit of detection (Pettke et al., 2014). <LOD – bellow limit of detection.

Sample	*Class*	*Spot Size*	*Ni ppm*	*Ni 2SE*	*Ni LOD*	*Rb ppm*	*Rb 2SE*	*Rb LOD*	*Sr ppm*	*Sr 2SE*	*Sr LOD*	*Y ppm*	*Y 2SE*	*Y LOD*
D104_1_67	G9A	285	46.23	0.54	0.16559	0.0121	0.003	0.00432	0.0985	0.0042	0.00241	15.66	0.17	0.00094
D104_1_81	G9A_Ti	285	100.98	0.98	0.15875	0.0046	0.003	0.00401	0.2689	0.0078	0.00220	14.19	0.18	0.00103
D104_1_89	G9B_Ti	130	63.67	0.68	0.29961	0.0125	0.0056	0.00840	0.2613	0.0099	0.00374	10.97	0.12	0.00156
D104_1_93	G9A	285	46.15	0.41	0.16050	0.0061	0.0027	0.00410	0.0868	0.0041	0.00224	16.84	0.15	0.00093
D104_1_97	G9A	285	46.25	0.5	0.16022	0.0068	0.0026	0.00410	0.0905	0.0038	0.00213	16.07	0.17	0.00100
D104_1_99	G9A	285	23.94	0.3	0.16612	0.0103	0.0028	0.00428	0.1136	0.0046	0.00204	12.92	0.12	0.00103
D104_2_111	G10A	130	68.81	0.52	0.26007	0.0201	0.0056	0.00860	0.808	0.017	0.00368	2.218	0.033	0.00135
D104_2_123	G9A	130	56.15	0.62	0.28499	0.0029	0.0055	0.00930	0.421	0.013	0.00377	2.537	0.034	0.00155
D104_2_139	G9B	130	37.02	0.45	0.27961	0.0066	0.0055	0.00910	0.1208	0.0068	0.00352	9.79	0.1	0.00150
D104_2_143	G9A_Ti	130	96.94	0.78	0.27934	0.0123	0.006	0.00931	0.395	0.011	0.00330	13.21	0.15	0.00149
D104_2_153	G9B_Ti	130	64.14	0.6	0.29731	0.0022	0.0062	0.00883	0.274	0.01	0.00358	11.42	0.13	0.00139
D104_3_155	G9A	285	46.78	0.54	0.16420	0.0082	0.0029	0.00411	0.0973	0.0045	0.00196	16.19	0.19	0.00092
D104_3_161	G9A	285	46.51	0.51	0.16898	0.0192	0.0031	0.00441	0.0973	0.004	0.00202	16.32	0.16	0.00093
D104_3_179	G9A	285	46.69	0.45	0.16364	0.0072	0.0027	0.00418	0.0888	0.0052	0.00186	16.99	0.21	0.00091
D104_3_185	G10A	285	66.8	0.7	0.13892	0.0153	0.0026	0.00464	0.749	0.015	0.00169	2.959	0.032	0.00069
D104_3_199	G12_Ti	130	28.57	0.37	0.29632	0.0147	0.0058	0.00888	0.398	0.04	0.00342	19.85	0.21	0.00160
D104_4_209	G9A	130	124.26	1	0.29833	0.0101	0.0063	0.00891	0.351	0.013	0.00391	12.54	0.13	0.00135
D104_4_223	G9A_Ti	130	89.53	0.78	0.29584	0.0113	0.0059	0.00878	0.399	0.014	0.00371	11.86	0.13	0.00134
D104_4_227	G9A_Ti	130	101.93	0.74	0.29368	0.008	0.0052	0.00868	0.36	0.014	0.00324	9.68	0.12	0.00164
D104_4_233	G10A	130	66.47	0.54	0.26478	0.0198	0.0047	0.00840	0.761	0.019	0.00293	2.182	0.034	0.00142
D104_4_235	G10A	130	67.17	0.79	0.24903	0.0071	0.0052	0.00811	1.13	0.28	0.00284	2.067	0.032	0.00110
D104_4_239	G9A	285	46.9	0.46	0.15867	0.0006	0.0039	0.00458	0.1042	0.0044	0.00201	16.11	0.16	0.00090
D104_4_243	G9B	130	36.19	0.49	0.27392	0.0075	0.0053	0.00875	0.1088	0.0068	0.00303	9.56	0.13	0.00129
D104_4_247	G9A_Ti	285	95.51	0.85	0.14234	0.0118	0.003	0.00417	0.3698	0.0085	0.00189	9.183	0.09	0.00092
D104_4_249	G9A	130	47.87	0.52	0.30761	0.0092	0.0074	0.00917	0.0992	0.0058	0.00356	12.77	0.11	0.00165
D104_4_251	G9A	130	56.12	0.59	0.28623	0.004	0.0048	0.00882	0.429	0.013	0.00326	2.546	0.037	0.00145
D104_5_257	G12_Ti	130	35.7	0.44	0.30144	0.0056	0.0053	0.00886	0.268	0.01	0.00345	19.77	0.21	0.00145
D104_5_267	G9A_Ti	130	89.7	0.84	0.29644	0.0126	0.0057	0.00883	0.378	0.012	0.00309	12.07	0.12	0.00168
D104_5_275	G9A_Ti	130	64.71	0.77	0.29694	0.0023	0.0048	0.00878	0.277	0.011	0.00340	10.82	0.1	0.00130
D104_5_293	G9A_Ti	130	92.15	0.79	0.30206	0.0082	0.0055	0.00902	0.392	0.016	0.00314	11.42	0.16	0.00143
D104_5_297	G9A_Ti	285	99.2	1	0.15313	0.0014	0.0026	0.00398	0.2427	0.0069	0.00192	13.73	0.15	0.00073
D104_5_299	G9A_Ti	285	97.7	1.1	0.14860	0.0083	0.0027	0.00411	0.2963	0.0075	0.00184	9.22	0.1	0.00078
D89_329	G9A	285	57.07	0.55	0.12274	0.0069	0.0032	0.00418	0.2905	0.0061	0.00138	12.27	0.12	0.00072
D89_331	G9A_Ti	285	88.1	0.79	0.12255	0.0075	0.003	0.00418	0.399	0.01	0.00124	16.01	0.17	0.00068
D89_335	G9A	285	104.9	1.1	0.12006	0.0064	0.003	0.00415	0.2782	0.0072	0.00132	6.132	0.064	0.00067
D89_337	G9A	130	56.49	0.63	0.28834	0.0081	0.004	0.00898	0.304	0.011	0.00321	9.92	0.11	0.00119
D89_349	G9A_Ti	285	62.45	0.62	0.12855	0.0076	0.0029	0.00428	0.2199	0.0065	0.00148	25.16	0.22	0.00072
D89_353	G9B	285	43.12	0.44	0.11729	0.0105	0.0027	0.00421	0.3136	0.007	0.00130	4.298	0.048	0.00070

Appendix E: Garnet Xenocryst LA-ICP-MS Data Tables

Appendix E.02 (continued): Dharma kimberlite garnet trace element data measured by LA-ICPMS. 2SE – two times standard error. LOD – Limit of detection (Pettke et al., 2014). <LOD – bellow limit of detection.

Sample	*Class*	*Spot Size*	*Zr ppm*	*Zr 2SE*	*Zr LOD*	*Nb ppm*	*Nb 2SE*	*Nb LOD*	*Ba ppm*	*Ba 2SE*	*Ba LOD*	*La ppm*	*La 2SE*	*La LOD*
D104_1_67	G9A	285	9.47	0.11	0.00562	1.041	0.017	0.00063	0.0067	0.0037	0.00454	0.0629	0.0019	0.00027
D104_1_81	G9A_Ti	285	24.19	0.35	0.00536	0.357	0.0094	0.00060	0.0086	0.0034	0.00425	0.02243	0.00096	0.00026
D104_1_89	G9B_Ti	130	35.18	0.33	0.00648	0.265	0.01	0.00113	<LOD	<LOD	0.00895	0.0217	0.0013	0.00045
D104_1_93	G9A	285	9.7	0.11	0.00538	0.712	0.012	0.00057	<LOD	<LOD	0.00435	0.0522	0.0014	0.00025
D104_1_97	G9A	285	9.53	0.12	0.00525	0.923	0.017	0.00059	<LOD	<LOD	0.00411	0.0558	0.0016	0.00024
D104_1_99	G9A	285	8.17	0.1	0.00533	0.4733	0.009	0.00054	0.0419	0.0072	0.00497	0.02089	0.00078	0.00026
D104_2_111	G10A	130	20.36	0.27	0.00602	0.707	0.016	0.00117	<LOD	<LOD	0.00769	0.0877	0.0029	0.00044
D104_2_123	G9A	130	6.921	0.095	0.00643	0.761	0.019	0.00143	<LOD	<LOD	0.00885	0.0569	0.0029	0.00050
D104_2_139	G9B	130	5.239	0.075	0.00626	0.945	0.023	0.00120	<LOD	<LOD	0.00764	0.085	0.0033	0.00042
D104_2_143	G9A_Ti	130	36.81	0.37	0.00622	0.478	0.015	0.00140	<LOD	<LOD	0.00773	0.0411	0.0021	0.00042
D104_2_153	G9B_Ti	130	35.01	0.31	0.00667	0.275	0.01	0.00128	<LOD	<LOD	0.00868	0.0228	0.0012	0.00036
D104_3_155	G9A	285	9.54	0.12	0.00523	0.992	0.016	0.00061	<LOD	<LOD	0.00444	0.0583	0.002	0.00026
D104_3_161	G9A	285	9.7	0.1	0.00543	0.858	0.013	0.00068	0.167	0.016	0.00488	0.0587	0.0019	0.00025
D104_3_179	G9A	285	9.794	0.1	0.00515	0.532	0.012	0.00054	0.0051	0.0031	0.00400	0.0441	0.0016	0.00026
D104_3_185	G10A	285	29.88	0.33	0.00437	0.774	0.013	0.00062	<LOD	<LOD	0.00399	0.0773	0.0018	0.00019
D104_3_199	G12_Ti	130	60	0.58	0.00655	0.299	0.013	0.00127	0.102	0.057	0.00873	0.0384	0.0048	0.00044
D104_4_209	G9A	130	11.6	0.13	0.00670	0.358	0.012	0.00122	<LOD	<LOD	0.00659	0.0488	0.0025	0.00043
D104_4_223	G9A_Ti	130	38.89	0.35	0.00653	0.329	0.012	0.00138	0.0388	0.0084	0.00838	0.0375	0.0021	0.00049
D104_4_227	G9A_Ti	130	24.16	0.23	0.00659	0.453	0.014	0.00163	<LOD	<LOD	0.00773	0.0323	0.0019	0.00044
D104_4_233	G10A	130	20.48	0.24	0.00555	0.686	0.018	0.00111	<LOD	<LOD	0.00670	0.0838	0.0027	0.00037
D104_4_235	G10A	130	19.4	0.19	0.00567	0.734	0.029	0.00117	2.8	2.8	0.00775	0.0926	0.0079	0.00034
D104_4_239	G9A	285	9.67	0.11	0.00464	1.073	0.017	0.00057	<LOD	<LOD	0.00466	0.0621	0.0018	0.00025
D104_4_243	G9B	130	5.21	0.11	0.00597	0.862	0.021	0.00144	<LOD	<LOD	0.00669	0.0744	0.0025	0.00040
D104_4_247	G9A_Ti	285	20.66	0.21	0.00443	0.4623	0.0091	0.00059	<LOD	<LOD	0.00365	0.0344	0.0012	0.00020
D104_4_249	G9A	130	7.61	0.1	0.00661	0.938	0.022	0.00137	0.0168	0.0078	0.00815	0.0553	0.0023	0.00043
D104_4_251	G9A	130	7.12	0.1	0.00655	0.769	0.019	0.00136	0.0077	0.0056	0.00679	0.0544	0.0023	0.00038
D104_5_257	G12_Ti	130	57.45	0.51	0.00660	0.298	0.01	0.00138	0.0095	0.0047	0.00888	0.0246	0.0015	0.00047
D104_5_267	G9A_Ti	130	39.22	0.37	0.00647	0.329	0.012	0.00140	0.0198	0.0064	0.00837	0.0367	0.0021	0.00043
D104_5_275	G9A_Ti	130	35.97	0.36	0.00654	0.282	0.01	0.00156	<LOD	<LOD	0.00810	0.0239	0.0016	0.00044
D104_5_293	G9A_Ti	130	32.3	0.51	0.00618	0.337	0.012	0.00164	<LOD	<LOD	0.00605	0.038	0.002	0.00048
D104_5_297	G9A_Ti	285	24.49	0.3	0.00490	0.3516	0.0086	0.00053	<LOD	<LOD	0.00317	0.02153	0.00089	0.00021
D104_5_299	G9A_Ti	285	15.07	0.19	0.00479	0.5237	0.0099	0.00064	0.0345	0.0066	0.00370	0.0351	0.0012	0.00020
D89_329	G9A	285	32.15	0.27	0.00344	0.2908	0.0071	0.00055	<LOD	<LOD	0.00261	0.0179	0.00076	0.00019
D89_331	G9A_Ti	285	52.56	0.46	0.00317	0.3704	0.0084	0.00049	<LOD	<LOD	0.00268	0.039	0.0013	0.00017
D89_335	G9A	285	12.15	0.12	0.00344	0.592	0.013	0.00045	<LOD	<LOD	0.00253	0.0514	0.0014	0.00016
D89_337	G9A	130	27.36	0.33	0.00567	0.2703	0.0093	0.00157	0.042	0.0091	0.00791	0.0187	0.0012	0.00039
D89_349	G9A_Ti	285	37.06	0.35	0.00353	0.2778	0.0085	0.00062	<LOD	<LOD	0.00338	0.01896	0.00084	0.00018
D89_353	G9B	285	6.136	0.078	0.00307	1.178	0.018	0.00058	<LOD	<LOD	0.00305	0.1682	0.0027	0.00018

Appendix E: Garnet Xenocryst LA-ICP-MS Data Tables

Appendix E.02 (continued): Dharma kimberlite garnet trace element data measured by LA-ICPMS. 2SE – two times standard error. LOD – Limit of detection (Pettke et al., 2014). <LOD – bellow limit of detection.

Sample	*Class*	*Spot Size*	*Ce ppm*	*Ce 2SE*	*Ce LOD*	*Pr ppm*	*Pr 2SE*	*Pr LOD*	*Nd ppm*	*Nd 2SE*	*Nd LOD*	*Sm ppm*	*Sm 2SE*	*Sm LOD*
D104_1_67	G9A	285	0.3224	0.0051	0.00026	0.0621	0.0016	0.00024	0.419	0.012	0.00135	0.3034	0.0087	0.00123
D104_1_81	G9A_Ti	285	0.2085	0.0036	0.00026	0.0709	0.0018	0.00022	0.688	0.014	0.00114	0.529	0.013	0.00124
D104_1_89	G9B_Ti	130	0.2308	0.0059	0.00047	0.0785	0.0031	0.00039	0.752	0.023	0.00217	0.549	0.021	0.00233
D104_1_93	G9A	285	0.2635	0.0047	0.00024	0.0542	0.001	0.00021	0.391	0.012	0.00110	0.3154	0.0092	0.00108
D104_1_97	G9A	285	0.28	0.0062	0.00026	0.0568	0.0015	0.00021	0.393	0.01	0.00109	0.3012	0.0084	0.00117
D104_1_99	G9A	285	0.1264	0.0028	0.00024	0.0321	0.0011	0.00021	0.2672	0.0096	0.00118	0.2115	0.0074	0.00117
D104_2_111	G10A	130	0.966	0.014	0.00038	0.3291	0.0053	0.00038	2.909	0.056	0.00202	1.13	0.029	0.00217
D104_2_123	G9A	130	0.675	0.011	0.00052	0.2496	0.0059	0.00042	2.071	0.043	0.00209	0.582	0.017	0.00267
D104_2_139	G9B	130	0.478	0.0097	0.00051	0.1248	0.0037	0.00039	0.935	0.023	0.00218	0.391	0.016	0.00223
D104_2_143	G9A_Ti	130	0.3748	0.0077	0.00051	0.1196	0.0034	0.00038	1.096	0.025	0.00219	0.773	0.022	0.00252
D104_2_153	G9B_Ti	130	0.2307	0.0051	0.00054	0.0798	0.0026	0.00035	0.733	0.02	0.00202	0.552	0.022	0.00231
D104_3_155	G9A	285	0.2916	0.0047	0.00025	0.0579	0.0016	0.00020	0.413	0.012	0.00112	0.312	0.01	0.00117
D104_3_161	G9A	285	0.2983	0.006	0.00026	0.0594	0.0015	0.00021	0.417	0.011	0.00134	0.298	0.011	0.00139
D104_3_179	G9A	285	0.2368	0.0049	0.00022	0.051	0.0015	0.00025	0.388	0.012	0.00119	0.315	0.011	0.00160
D104_3_185	G10A	285	0.822	0.012	0.00022	0.3081	0.005	0.00017	3.028	0.043	0.00112	1.523	0.029	0.00086
D104_3_199	G12_Ti	130	0.2756	0.0081	0.00049	0.0966	0.0032	0.00036	1.01	0.029	0.00209	0.89	0.024	0.00247
D104_4_209	G9A	130	0.4149	0.0073	0.00046	0.1147	0.0031	0.00035	0.919	0.025	0.00205	0.467	0.019	0.00222
D104_4_223	G9A_Ti	130	0.3427	0.0069	0.00046	0.1069	0.0028	0.00038	0.957	0.022	0.00200	0.664	0.021	0.00228
D104_4_227	G9A_Ti	130	0.316	0.0077	0.00041	0.1006	0.0026	0.00035	0.936	0.025	0.00192	0.651	0.022	0.00266
D104_4_233	G10A	130	0.943	0.018	0.00046	0.3182	0.0075	0.00033	2.822	0.052	0.00181	1.106	0.031	0.00213
D104_4_235	G10A	130	0.918	0.025	0.00045	0.3138	0.0068	0.00034	2.805	0.049	0.00169	1.113	0.027	0.00219
D104_4_239	G9A	285	0.3253	0.0062	0.00027	0.0637	0.0017	0.00022	0.4192	0.009	0.00119	0.316	0.01	0.00118
D104_4_243	G9B	130	0.435	0.01	0.00047	0.1175	0.0037	0.00036	0.902	0.025	0.00210	0.371	0.014	0.00200
D104_4_247	G9A_Ti	285	0.3001	0.0051	0.00022	0.101	0.0022	0.00018	0.94	0.015	0.00087	0.62	0.015	0.00101
D104_4_249	G9A	130	0.3108	0.0062	0.00042	0.0597	0.0022	0.00036	0.39	0.016	0.00222	0.269	0.013	0.00240
D104_4_251	G9A	130	0.689	0.011	0.00048	0.2613	0.0054	0.00032	2.168	0.043	0.00203	0.614	0.016	0.00221
D104_5_257	G12_Ti	130	0.2437	0.0045	0.00048	0.0966	0.003	0.00039	0.987	0.026	0.00213	0.856	0.023	0.00247
D104_5_267	G9A_Ti	130	0.3389	0.0075	0.00049	0.112	0.0034	0.00035	0.979	0.019	0.00223	0.654	0.022	0.00235
D104_5_275	G9A_Ti	130	0.235	0.0055	0.00051	0.0807	0.0024	0.00032	0.774	0.018	0.00231	0.571	0.018	0.00218
D104_5_293	G9A_Ti	130	0.3628	0.008	0.00049	0.117	0.0034	0.00034	0.997	0.024	0.00212	0.682	0.024	0.00234
D104_5_297	G9A_Ti	285	0.1935	0.0036	0.00022	0.0656	0.0018	0.00019	0.636	0.015	0.00101	0.479	0.013	0.00115
D104_5_299	G9A_Ti	285	0.2979	0.0054	0.00023	0.0994	0.0024	0.00015	0.892	0.021	0.00089	0.592	0.017	0.00101
D89_329	G9A	285	0.204	0.0039	0.00019	0.0845	0.0018	0.00013	0.952	0.018	0.00093	0.777	0.015	0.00092
D89_331	G9A_Ti	285	0.3622	0.0054	0.00018	0.1214	0.0022	0.00015	1.159	0.022	0.00073	0.818	0.019	0.00091
D89_335	G9A	285	0.3889	0.0055	0.00016	0.1067	0.0021	0.00012	0.748	0.012	0.00075	0.2669	0.0083	0.00081
D89_337	G9A	130	0.2034	0.0049	0.00045	0.0785	0.0027	0.00034	0.801	0.02	0.00205	0.692	0.02	0.00207
D89_349	G9A_Ti	285	0.2073	0.003	0.00020	0.0846	0.002	0.00015	0.979	0.019	0.00094	0.882	0.015	0.00108
D89_353	G9B	285	1.596	0.022	0.00020	0.3802	0.0057	0.00014	1.794	0.028	0.00092	0.359	0.011	0.00092

Appendix E: Garnet Xenocryst LA-ICP-MS Data Tables

Appendix E.02 (continued): Dharma kimberlite garnet trace element data measured by LA-ICPMS. 2SE – two times standard error. LOD – Limit of detection (Pettke et al., 2014). <LOD – bellow limit of detection.

Sample	*Class*	*Spot Size*	*Eu ppm*	*Eu 2SE*	*Eu LOD*	*Gd ppm*	*Gd 2SE*	*Gd LOD*	*Tb ppm*	*Tb 2SE*	*Tb LOD*	*Dy ppm*	*Dy 2SE*	*Dy LOD*
D104_1_67	G9A	285	0.1677	0.005	0.00047	0.908	0.019	0.00245	0.2516	0.0044	0.00035	2.247	0.036	0.00108
D104_1_81	G9A_Ti	285	0.2604	0.0054	0.00041	1.166	0.024	0.00222	0.2725	0.0057	0.00031	2.288	0.041	0.00109
D104_1_89	G9B_Ti	130	0.268	0.0071	0.00078	1.088	0.021	0.00276	0.2394	0.005	0.00040	1.778	0.033	0.00165
D104_1_93	G9A	285	0.1753	0.0045	0.00041	0.969	0.022	0.00210	0.2738	0.004	0.00031	2.454	0.036	0.00116
D104_1_97	G9A	285	0.1691	0.0041	0.00041	0.921	0.016	0.00218	0.2555	0.0048	0.00029	2.344	0.032	0.00108
D104_1_99	G9A	285	0.1932	0.0043	0.00043	0.764	0.019	0.00233	0.2159	0.0044	0.00034	1.955	0.03	0.00120
D104_2_111	G10A	130	0.3241	0.0087	0.00071	0.852	0.025	0.00289	0.105	0.0037	0.00040	0.52	0.014	0.00160
D104_2_123	G9A	130	0.163	0.0049	0.00066	0.432	0.018	0.00313	0.0613	0.0024	0.00045	0.393	0.014	0.00175
D104_2_139	G9B	130	0.1694	0.0057	0.00067	0.769	0.021	0.00313	0.1765	0.0043	0.00043	1.467	0.028	0.00177
D104_2_143	G9A_Ti	130	0.3799	0.0088	0.00068	1.537	0.031	0.00306	0.3226	0.0069	0.00046	2.308	0.039	0.00161
D104_2_153	G9B_Ti	130	0.2724	0.0072	0.00071	1.12	0.028	0.00314	0.2384	0.0054	0.00042	1.844	0.034	0.00173
D104_3_155	G9A	285	0.1673	0.004	0.00038	0.926	0.02	0.00214	0.2551	0.0044	0.00033	2.381	0.032	0.00112
D104_3_161	G9A	285	0.1687	0.0046	0.00045	0.92	0.024	0.00236	0.2549	0.0049	0.00031	2.36	0.031	0.00109
D104_3_179	G9A	285	0.1779	0.0044	0.00032	0.996	0.023	0.00195	0.272	0.0051	0.00026	2.507	0.039	0.00106
D104_3_185	G10A	285	0.4559	0.0091	0.00031	1.288	0.027	0.00185	0.1563	0.0035	0.00024	0.747	0.018	0.00087
D104_3_199	G12_Ti	130	0.4634	0.0095	0.00077	1.89	0.044	0.00279	0.4173	0.0071	0.00041	3.305	0.053	0.00169
D104_4_209	G9A	130	0.1919	0.0067	0.00071	0.814	0.026	0.00298	0.2005	0.0044	0.00040	1.683	0.033	0.00168
D104_4_223	G9A_Ti	130	0.3053	0.0091	0.00077	1.214	0.03	0.00326	0.2581	0.0058	0.00036	1.939	0.036	0.00175
D104_4_227	G9A_Ti	130	0.3062	0.0071	0.00061	1.164	0.031	0.00291	0.2293	0.0045	0.00043	1.639	0.032	0.00174
D104_4_233	G10A	130	0.3175	0.0064	0.00064	0.814	0.022	0.00275	0.1045	0.0036	0.00038	0.514	0.013	0.00172
D104_4_235	G10A	130	0.3068	0.0066	0.00063	0.783	0.02	0.00263	0.0998	0.003	0.00038	0.485	0.012	0.00133
D104_4_239	G9A	285	0.1738	0.0042	0.00039	0.932	0.024	0.00231	0.2592	0.0048	0.00032	2.376	0.03	0.00098
D104_4_243	G9B	130	0.1686	0.0057	0.00070	0.749	0.026	0.00273	0.1756	0.0051	0.00043	1.473	0.036	0.00167
D104_4_247	G9A_Ti	285	0.2681	0.0049	0.00031	1.104	0.025	0.00170	0.2181	0.0038	0.00022	1.55	0.026	0.00100
D104_4_249	G9A	130	0.1476	0.0049	0.00068	0.754	0.023	0.00271	0.2001	0.0049	0.00036	1.747	0.033	0.00146
D104_4_251	G9A	130	0.1672	0.0054	0.00069	0.444	0.017	0.00271	0.0614	0.0026	0.00038	0.3969	0.0092	0.00179
D104_5_257	G12_Ti	130	0.4522	0.0087	0.00069	1.88	0.041	0.00306	0.423	0.008	0.00048	3.343	0.048	0.00164
D104_5_267	G9A_Ti	130	0.3148	0.0077	0.00067	1.249	0.029	0.00343	0.264	0.0049	0.00039	1.995	0.038	0.00172
D104_5_275	G9A_Ti	130	0.2784	0.0064	0.00072	1.126	0.03	0.00257	0.2403	0.005	0.00043	1.812	0.034	0.00180
D104_5_293	G9A_Ti	130	0.3081	0.0097	0.00062	1.212	0.033	0.00286	0.2478	0.0054	0.00044	1.9	0.037	0.00142
D104_5_297	G9A_Ti	285	0.2296	0.0054	0.00033	1.066	0.026	0.00180	0.2415	0.0044	0.00023	2.026	0.035	0.00092
D104_5_299	G9A_Ti	285	0.244	0.006	0.00033	0.979	0.021	0.00163	0.1782	0.0035	0.00023	1.311	0.024	0.00081
D89_329	G9A	285	0.3431	0.0056	0.00026	1.361	0.026	0.00123	0.2591	0.0035	0.00020	1.942	0.031	0.00082
D89_331	G9A_Ti	285	0.3766	0.0079	0.00027	1.664	0.028	0.00149	0.3539	0.0042	0.00021	2.657	0.032	0.00075
D89_335	G9A	285	0.0996	0.0032	0.00025	0.426	0.011	0.00120	0.0965	0.0022	0.00017	0.871	0.013	0.00065
D89_337	G9A	130	0.3177	0.0072	0.00056	1.175	0.031	0.00276	0.2264	0.0047	0.00038	1.571	0.033	0.00167
D89_349	G9A_Ti	285	0.3792	0.0054	0.00030	1.795	0.03	0.00148	0.416	0.0066	0.00021	3.611	0.048	0.00088
D89_353	G9B	285	0.1137	0.0028	0.00029	0.429	0.013	0.00123	0.0847	0.002	0.00021	0.637	0.013	0.00078

Appendix E: Garnet Xenocryst LA-ICP-MS Data Tables

Appendix E.02 (continued): Dharma kimberlite garnet trace element data measured by LA-ICPMS. 2SE – two times standard error. LOD – Limit of detection (Pettke et al., 2014). <LOD – bellow limit of detection.

Sample	*Class*	*Spot Size*	*Ho ppm*	*Ho 2SE*	*Ho LOD*	*Er ppm*	*Er 2SE*	*Er LOD*	*Tm ppm*	*Tm 2SE*	*Tm LOD*	*Yb ppm*	*Yb 2SE*	*Yb LOD*
D104_1_67	G9A	285	0.6102	0.0094	0.00031	2.146	0.037	0.00088	0.3577	0.0067	0.00031	2.754	0.047	0.00120
D104_1_81	G9A_Ti	285	0.579	0.01	0.00028	1.934	0.034	0.00080	0.2945	0.0054	0.00030	2.109	0.035	0.00128
D104_1_89	G9B_Ti	130	0.4146	0.0072	0.00038	1.351	0.028	0.00132	0.2056	0.0045	0.00043	1.484	0.028	0.00180
D104_1_93	G9A	285	0.69	0.01	0.00025	2.415	0.035	0.00079	0.4104	0.007	0.00028	3.11	0.044	0.00120
D104_1_97	G9A	285	0.6472	0.0098	0.00025	2.297	0.041	0.00077	0.3807	0.0071	0.00030	2.952	0.055	0.00135
D104_1_99	G9A	285	0.5143	0.0076	0.00026	1.734	0.027	0.00090	0.2733	0.0053	0.00028	2.037	0.036	0.00116
D104_2_111	G10A	130	0.0851	0.0028	0.00041	0.2019	0.0055	0.00116	0.0254	0.0016	0.00038	0.1723	0.0078	0.00184
D104_2_123	G9A	130	0.0858	0.0031	0.00043	0.3117	0.0098	0.00121	0.0555	0.0026	0.00047	0.501	0.018	0.00203
D104_2_139	G9B	130	0.3743	0.0092	0.00043	1.197	0.026	0.00120	0.1804	0.0047	0.00044	1.389	0.034	0.00197
D104_2_143	G9A_Ti	130	0.506	0.01	0.00037	1.426	0.021	0.00134	0.1909	0.0041	0.00044	1.296	0.028	0.00208
D104_2_153	G9B_Ti	130	0.4432	0.0081	0.00034	1.397	0.026	0.00116	0.2135	0.0066	0.00044	1.55	0.033	0.00205
D104_3_155	G9A	285	0.6486	0.0096	0.00028	2.283	0.034	0.00076	0.3798	0.0074	0.00026	2.911	0.045	0.00137
D104_3_161	G9A	285	0.644	0.011	0.00027	2.301	0.035	0.00077	0.3831	0.0062	0.00027	2.932	0.052	0.00136
D104_3_179	G9A	285	0.682	0.01	0.00021	2.433	0.035	0.00074	0.4082	0.0061	0.00026	3.163	0.049	0.00088
D104_3_185	G10A	285	0.1225	0.003	0.00020	0.2894	0.0068	0.00061	0.0351	0.0017	0.00025	0.2597	0.0089	0.00100
D104_3_199	G12_Ti	130	0.797	0.015	0.00042	2.517	0.047	0.00119	0.3854	0.0084	0.00043	2.76	0.05	0.00217
D104_4_209	G9A	130	0.458	0.01	0.00040	1.551	0.026	0.00115	0.2545	0.0062	0.00047	1.871	0.038	0.00205
D104_4_223	G9A_Ti	130	0.4591	0.0082	0.00040	1.455	0.027	0.00112	0.2144	0.0047	0.00042	1.598	0.04	0.00188
D104_4_227	G9A_Ti	130	0.3687	0.0062	0.00041	1.134	0.025	0.00129	0.1718	0.0049	0.00041	1.282	0.028	0.00186
D104_4_233	G10A	130	0.0865	0.0028	0.00034	0.198	0.0076	0.00105	0.0249	0.0016	0.00037	0.1849	0.0075	0.00205
D104_4_235	G10A	130	0.0777	0.0026	0.00033	0.1895	0.0071	0.00109	0.0247	0.0017	0.00034	0.1694	0.0084	0.00176
D104_4_239	G9A	285	0.648	0.011	0.00029	2.295	0.03	0.00084	0.381	0.0059	0.00029	2.91	0.048	0.00128
D104_4_243	G9B	130	0.3727	0.0082	0.00039	1.184	0.028	0.00123	0.185	0.0047	0.00036	1.371	0.034	0.00215
D104_4_247	G9A_Ti	285	0.3302	0.0066	0.00022	0.922	0.016	0.00067	0.1225	0.0028	0.00025	0.785	0.016	0.00106
D104_4_249	G9A	130	0.4816	0.0075	0.00038	1.663	0.03	0.00115	0.2743	0.0055	0.00044	2.143	0.035	0.00180
D104_4_251	G9A	130	0.0936	0.0033	0.00037	0.325	0.01	0.00115	0.0575	0.0023	0.00040	0.512	0.014	0.00187
D104_5_257	G12_Ti	130	0.806	0.011	0.00045	2.556	0.033	0.00132	0.3864	0.0068	0.00046	2.84	0.047	0.00226
D104_5_267	G9A_Ti	130	0.4689	0.0081	0.00045	1.489	0.024	0.00132	0.2252	0.005	0.00048	1.624	0.029	0.00225
D104_5_275	G9A_Ti	130	0.4305	0.0077	0.00045	1.367	0.027	0.00122	0.2002	0.0042	0.00049	1.494	0.035	0.00207
D104_5_293	G9A_Ti	130	0.4442	0.0097	0.00041	1.425	0.03	0.00126	0.2139	0.0054	0.00045	1.581	0.036	0.00197
D104_5_297	G9A_Ti	285	0.5199	0.0078	0.00024	1.714	0.034	0.00068	0.2601	0.0043	0.00025	1.929	0.032	0.00120
D104_5_299	G9A_Ti	285	0.3276	0.0059	0.00020	1.134	0.021	0.00070	0.1925	0.0047	0.00025	1.511	0.027	0.00103
D89_329	G9A	285	0.4714	0.0064	0.00018	1.572	0.022	0.00052	0.2445	0.0044	0.00021	1.866	0.036	0.00096
D89_331	G9A_Ti	285	0.6189	0.0085	0.00018	1.916	0.024	0.00059	0.2905	0.0039	0.00019	2.07	0.033	0.00086
D89_335	G9A	285	0.2284	0.0037	0.00014	0.822	0.013	0.00051	0.1387	0.0031	0.00021	1.119	0.021	0.00080
D89_337	G9A	130	0.3833	0.0079	0.00035	1.242	0.023	0.00098	0.2019	0.0041	0.00040	1.496	0.034	0.00196
D89_349	G9A_Ti	285	0.946	0.012	0.00021	3.297	0.04	0.00070	0.5275	0.0081	0.00021	4.014	0.057	0.00111
D89_353	G9B	285	0.1583	0.0034	0.00020	0.561	0.011	0.00055	0.0969	0.0027	0.00022	0.794	0.015	0.00099

Appendix E: Garnet Xenocryst LA-ICP-MS Data Tables

Appendix E.02 (continued): Dharma kimberlite garnet trace element data measured by LA-ICPMS. 2SE – two times standard error. LOD – Limit of detection (Pettke et al., 2014). <LOD – bellow limit of detection.

Sample	*Class*	*Spot Size*	*Lu ppm*	*Lu 2SE*	*Lu LOD*	*Hf ppm*	*Hf 2SE*	*Hf LOD*	*Ta ppm*	*Ta 2SE*	*Ta LOD*
D104_1_67	G9A	285	0.4753	0.0085	0.00030	0.244	0.012	0.00254	0.0569	0.0031	0.00043
D104_1_81	G9A_Ti	285	0.3343	0.0063	0.00036	0.788	0.026	0.00195	0.0394	0.002	0.00052
D104_1_89	G9B_Ti	130	0.2372	0.0051	0.00055	0.948	0.034	0.00392	0.0292	0.0026	0.00065
D104_1_93	G9A	285	0.5319	0.009	0.00034	0.268	0.015	0.00208	0.0273	0.0019	0.00044
D104_1_97	G9A	285	0.4993	0.008	0.00030	0.248	0.012	0.00220	0.036	0.0021	0.00049
D104_1_99	G9A	285	0.3257	0.0063	0.00032	0.216	0.012	0.00208	0.0348	0.0022	0.00057
D104_2_111	G10A	130	0.0323	0.0019	0.00045	0.518	0.025	0.00300	0.0805	0.0039	0.00066
D104_2_123	G9A	130	0.1027	0.0031	0.00053	0.148	0.011	0.00338	0.0537	0.0035	0.00084
D104_2_139	G9B	130	0.2172	0.0059	0.00050	0.203	0.015	0.00324	0.0334	0.0024	0.00076
D104_2_143	G9A_Ti	130	0.1907	0.0042	0.00049	0.971	0.031	0.00356	0.0457	0.0034	0.00081
D104_2_153	G9B_Ti	130	0.2439	0.005	0.00053	0.918	0.04	0.00289	0.027	0.0029	0.00087
D104_3_155	G9A	285	0.4941	0.0081	0.00033	0.248	0.015	0.00188	0.0427	0.0022	0.00046
D104_3_161	G9A	285	0.5067	0.009	0.00031	0.25	0.014	0.00207	0.0322	0.0021	0.00036
D104_3_179	G9A	285	0.5304	0.0094	0.00030	0.26	0.013	0.00135	0.0234	0.0016	0.00047
D104_3_185	G10A	285	0.0457	0.0015	0.00024	0.807	0.026	0.00153	0.0847	0.0031	0.00044
D104_3_199	G12_Ti	130	0.4329	0.009	0.00057	1.517	0.05	0.00373	0.0323	0.0027	0.00082
D104_4_209	G9A	130	0.3045	0.0071	0.00047	0.261	0.018	0.00273	0.0324	0.003	0.00067
D104_4_223	G9A_Ti	130	0.2538	0.0056	0.00046	1.076	0.046	0.00305	0.0313	0.0023	0.00088
D104_4_227	G9A_Ti	130	0.2089	0.0053	0.00047	0.672	0.022	0.00259	0.0407	0.0032	0.00091
D104_4_233	G10A	130	0.0331	0.0019	0.00044	0.556	0.026	0.00287	0.0782	0.0042	0.00065
D104_4_235	G10A	130	0.031	0.0019	0.00041	0.546	0.023	0.00268	0.0767	0.0046	0.00074
D104_4_239	G9A	285	0.489	0.0068	0.00033	0.26	0.013	0.00145	0.0523	0.0028	0.00042
D104_4_243	G9B	130	0.2201	0.0064	0.00044	0.211	0.015	0.00286	0.0315	0.0025	0.00060
D104_4_247	G9A_Ti	285	0.1234	0.0033	0.00028	0.538	0.018	0.00184	0.0439	0.0025	0.00041
D104_4_249	G9A	130	0.3622	0.0064	0.00044	0.162	0.014	0.00279	0.0478	0.0036	0.00067
D104_4_251	G9A	130	0.1061	0.0035	0.00048	0.168	0.012	0.00330	0.053	0.0035	0.00067
D104_5_257	G12_Ti	130	0.4429	0.0085	0.00052	1.481	0.036	0.00284	0.0304	0.0028	0.00088
D104_5_267	G9A_Ti	130	0.2626	0.0062	0.00052	1.105	0.043	0.00291	0.0317	0.0028	0.00070
D104_5_275	G9A_Ti	130	0.2396	0.0057	0.00054	1.009	0.039	0.00342	0.0293	0.0023	0.00078
D104_5_293	G9A_Ti	130	0.2504	0.0058	0.00050	0.878	0.039	0.00351	0.0307	0.0026	0.00088
D104_5_297	G9A_Ti	285	0.3111	0.006	0.00027	0.773	0.029	0.00148	0.0362	0.0023	0.00050
D104_5_299	G9A_Ti	285	0.2688	0.005	0.00026	0.399	0.016	0.00178	0.054	0.0024	0.00049
D89_329	G9A	285	0.3086	0.0055	0.00019	0.817	0.023	0.00168	0.0272	0.0016	0.00031
D89_331	G9A_Ti	285	0.3368	0.006	0.00024	1.514	0.035	0.00122	0.0402	0.0017	0.00035
D89_335	G9A	285	0.1955	0.0035	0.00020	0.409	0.015	0.00145	0.0628	0.0032	0.00034
D89_337	G9A	130	0.2416	0.0052	0.00044	0.683	0.027	0.00282	0.0224	0.0023	0.00073
D89_349	G9A_Ti	285	0.6751	0.0091	0.00025	1.023	0.03	0.00200	0.0254	0.0017	0.00039
D89_353	G9B	285	0.1469	0.0031	0.00024	0.182	0.012	0.00170	0.0837	0.0033	0.00036

Appendix E: Garnet Xenocryst LA-ICP-MS Data Tables

Appendix E.02 (continued): Dharma kimberlite garnet trace element data measured by LA-ICPMS. 2SE – two times standard error. LOD – Limit of detection (Pettke et al., 2014). <LOD – bellow limit of detection.

Sample	*Class*	*Spot Size*	*Ca ppm*	*Ca 2SE*	*Ca LOD*	*Sc ppm*	*Sc 2SE*	*Sc LOD*	*Ti ppm*	*Ti 2SE*	*Ti LOD*	*V ppm*	*V 2SE*	*V LOD*
D89_357	G10B_Ti	130	21250	220	17.4924	90.08	0.81	0.01977	3678	47	0.67781	298.6	4.3	0.01113
D89_361	G9A	285	34110	300	7.25292	133.72	0.96	0.00922	431.3	3.2	0.28633	283.1	2	0.00540
D89_365	G9A	285	33880	270	7.40378	124.7	1.10	0.00931	1782	16	0.29515	260.2	2	0.00537
D89_367	G9B	285	44220	350	7.00195	157.2	1.40	0.00981	578.7	5.2	0.27977	391.4	3.9	0.00470
D89_369	G9B	285	43970	370	7.20977	156.4	1.40	0.00967	583.2	4.8	0.28587	392.3	3	0.00512
D89_371	G9A	285	34210	280	7.30047	126.64	0.81	0.00959	1787	14	0.28648	256.8	1.9	0.00512
D89_373	G10B_Ti	285	23680	190	7.27643	122.3	1.30	0.00968	4376	35	0.28681	325.1	2.4	0.00508
D89_375	G9A_Ti	285	29530	190	7.36377	104.19	0.74	0.00993	2769	19	0.29302	273.7	2	0.00514
D89_377	G9A_Ti	285	29980	230	7.44211	103.07	0.77	0.00985	2697	22	0.29013	270.1	2	0.00493
D89_381	G9B_Ti	130	36570	310	17.7885	110.71	0.91	0.02012	4008	43	0.69818	375.7	3.3	0.01174
D89_387	G10B_Ti	285	23310	190	7.49043	112.1	1.30	0.00972	4254	42	0.29406	316.4	2.7	0.00521
D89_391	G9A_Ti	285	35690	270	7.42684	127.7	1.10	0.00970	4155	32	0.27853	321.4	3	0.00528
D89_393	G10B_Ti	130	21850	170	17.3808	90.14	0.68	0.02023	4001	51	0.67613	306	3.1	0.01115
D89_395	G9A_Ti	285	29820	260	6.94174	106.3	1.20	0.00887	2786	21	0.27369	275.4	2.4	0.00494
D89_397	G9B_Ti	130	36600	340	17.4776	109.45	0.91	0.02024	4028	51	0.68782	371	3	0.01133
D89_399	G9A_Ti	285	34090	240	7.09848	120.38	0.86	0.00917	3949	31	0.28307	291.1	2.6	0.00488
D89_403	G9B	285	43750	310	6.66799	154.4	1.20	0.00946	577.9	4	0.26933	389.6	2.8	0.00450
D89_411	G9A	285	34400	250	7.09503	125	1.10	0.00954	1726	16	0.28172	257.2	2	0.00463
D89_415	G9B	285	43930	380	7.12128	154.5	1.30	0.00920	578.1	4.4	0.27667	388	3.5	0.00502
D89_417	G9A	130	31470	290	18.3526	95.48	0.72	0.02068	1557	13	0.72962	225.8	1.8	0.01178
D89_421	G10B_Ti	285	23420	200	7.05791	120.8	1.00	0.00936	4727	39	0.28112	330.5	2.5	0.00491
D89_423	G9A_Ti	285	29780	260	7.30981	103.21	0.68	0.00962	2672	21	0.28963	269.9	2.3	0.00502
D89_425	G9A_Ti	285	33800	260	6.94607	119.9	1.10	0.00897	4007	31	0.27402	296.5	2.5	0.00491
D89_427	G10B_Ti	285	24180	180	6.58149	123.27	0.87	0.00860	4887	34	0.26084	343.4	2.4	0.00455
D89_429	G9A	285	34690	290	7.19526	132.9	1.10	0.00912	274.4	2.4	0.27891	295.4	2.5	0.00497
D89_433	G9B	130	40690	360	17.7466	118.25	0.97	0.01952	499.1	3.9	0.69840	367.4	2.5	0.01157
D89_437	G9B_Ti	130	37320	440	17.0111	109.08	0.95	0.02030	4010	52	0.69071	372.9	2.6	0.01053
D89_441	G9A	285	34250	270	7.12958	124.8	1.00	0.00918	1734	13	0.28196	259	2	0.00487
D91_221	G9A	285	42700	350	7.45478	163.2	1.30	0.00893	1754	13	0.28287	337.9	2.6	0.00532
D91_227	G9A	130	39030	330	17.5688	121.74	0.93	0.01917	1944	19	0.66411	269.9	2.8	0.01102
D91_229	G9B	285	45690	420	7.25328	175.2	1.60	0.00869	628.1	6.2	0.28090	374.9	3.6	0.00550
D91_235	G9A	285	42700	390	7.67261	164.7	1.50	0.00893	1763	15	0.30169	334.5	3.4	0.00582
D91_239	G9A_Ti	285	33230	330	7.62415	109.3	1.40	0.00941	3460	27	0.30278	258.3	2.3	0.00564
D91_241	G9B	130	42210	360	17.2260	128.3	1.10	0.01885	542.8	4.4	0.65253	351	2.7	0.01122
D91_243	G9A	285	43120	420	7.42901	165.1	1.70	0.00875	1764	19	0.28947	343.5	3.4	0.00566
D91_245	G9A	285	43340	470	7.43255	166.5	1.70	0.00885	1763	18	0.29252	344.8	3.6	0.00564
D91_247	G9A_Ti	285	39000	350	7.21720	142.3	1.20	0.01009	3534	29	0.29523	321.2	2.7	0.00465
D91_255	G9B	130	42580	580	17.0984	126.6	1.30	0.01876	537.4	8.2	0.64783	355.1	4.9	0.01092

Appendix E: Garnet Xenocryst LA-ICP-MS Data Tables

Appendix E.02 (continued): Dharma kimberlite garnet trace element data measured by LA-ICPMS. 2SE – two times standard error. LOD – Limit of detection (Pettke et al., 2014). <LOD – bellow limit of detection.

Sample	*Class*	*Spot Size*	*Ni ppm*	*Ni 2SE*	*Ni LOD*	*Rb ppm*	*Rb 2SE*	*Rb LOD*	*Sr ppm*	*Sr 2SE*	*Sr LOD*	*Y ppm*	*Y 2SE*	*Y LOD*
D89_357	G10B_Ti	130	68.07	0.86	0.29362	0.0035	0.0059	0.00842	0.1774	0.0082	0.00349	10.07	0.13	0.00145
D89_361	G9A	285	66.02	0.6	0.11848	0.0053	0.0025	0.00418	0.2296	0.0051	0.00124	3.943	0.04	0.00062
D89_365	G9A	285	56.65	0.48	0.12120	0.0079	0.0025	0.00411	0.2844	0.0081	0.00129	12.4	0.13	0.00068
D89_367	G9B	285	43.67	0.42	0.11374	0.0128	0.0026	0.00400	0.3313	0.0074	0.00149	4.278	0.049	0.00069
D89_369	G9B	285	43.52	0.46	0.11459	0.008	0.0027	0.00414	0.3088	0.0076	0.00155	4.233	0.043	0.00067
D89_371	G9A	285	55.96	0.48	0.11656	0.0069	0.0027	0.00409	0.2812	0.0064	0.00143	12.47	0.11	0.00067
D89_373	G10B_Ti	285	65.92	0.57	0.11577	0.0046	0.002	0.00396	0.2157	0.0068	0.00140	13.48	0.14	0.00065
D89_375	G9A_Ti	285	62.02	0.5	0.11984	0.008	0.0022	0.00406	0.2343	0.0068	0.00134	25.4	0.24	0.00064
D89_377	G9A_Ti	285	62.01	0.61	0.12014	0.0063	0.0023	0.00393	0.2225	0.0061	0.00134	25.31	0.18	0.00059
D89_381	G9B_Ti	130	41.69	0.53	0.30153	0.0084	0.0056	0.00878	0.2536	0.01	0.00310	12.27	0.15	0.00122
D89_387	G10B_Ti	285	66.88	0.76	0.11883	0.007	0.0031	0.00393	0.2143	0.0063	0.00123	12.72	0.16	0.00064
D89_391	G9A_Ti	285	89.02	0.69	0.11655	0.007	0.0024	0.00377	0.4162	0.0086	0.00130	16.29	0.19	0.00065
D89_393	G10B_Ti	130	69.85	0.63	0.29314	0.0063	0.0044	0.00844	0.2021	0.008	0.00327	10.79	0.12	0.00136
D89_395	G9A_Ti	285	61.8	0.58	0.11048	0.0126	0.0024	0.00374	0.2306	0.0064	0.00118	25.74	0.25	0.00063
D89_397	G9B_Ti	130	41.05	0.5	0.29848	0.0129	0.0045	0.00851	0.256	0.011	0.00288	12.02	0.11	0.00144
D89_399	G9A_Ti	285	99.65	0.94	0.11397	0.0049	0.0028	0.00376	0.459	0.01	0.00128	15.76	0.14	0.00064
D89_403	G9B	285	44.64	0.3	0.10560	0.0129	0.0029	0.00378	0.3151	0.0082	0.00146	4.176	0.043	0.00055
D89_411	G9A	285	56.57	0.54	0.11086	0.0047	0.0027	0.00375	0.3003	0.0072	0.00133	12.3	0.13	0.00073
D89_415	G9B	285	44	0.42	0.10710	0.0125	0.0027	0.00389	0.3153	0.0075	0.00132	4.188	0.04	0.00062
D89_417	G9A	130	56.62	0.49	0.31240	0.0068	0.0055	0.00919	0.2732	0.0096	0.00288	10.002	0.093	0.00163
D89_421	G10B_Ti	285	68.54	0.58	0.11163	0.007	0.0025	0.00379	0.2229	0.0064	0.00127	13.94	0.13	0.00060
D89_423	G9A_Ti	285	62.08	0.6	0.11495	0.0091	0.002	0.00394	0.2248	0.0063	0.00123	25.31	0.24	0.00068
D89_425	G9A_Ti	285	99.92	0.82	0.10801	0.0053	0.0023	0.00363	0.444	0.01	0.00120	16.73	0.19	0.00069
D89_427	G10B_Ti	285	69.12	0.62	0.10299	0.0072	0.0027	0.00353	0.2374	0.0066	0.00104	14.5	0.14	0.00062
D89_429	G9A	285	66.68	0.57	0.10980	0.0061	0.0021	0.00384	0.2259	0.007	0.00119	3.884	0.047	0.00066
D89_433	G9B	130	44.51	0.46	0.29358	0.0116	0.0065	0.00880	0.291	0.013	0.00308	3.376	0.044	0.00134
D89_437	G9B_Ti	130	41.7	0.48	0.29336	0.014	0.0055	0.00869	0.2588	0.0084	0.00366	11.99	0.14	0.00133
D89_441	G9A	285	57.43	0.55	0.11109	0.0055	0.0029	0.00382	0.3012	0.007	0.00112	12.476	0.084	0.00069
D91_221	G9A	285	55.43	0.45	0.13491	0.009	0.0031	0.00450	0.564	0.013	0.00154	8.476	0.096	0.00082
D91_227	G9A	130	64.62	0.68	0.27622	0.0135	0.0061	0.00870	0.368	0.012	0.00311	5.899	0.066	0.00126
D91_229	G9B	285	40.16	0.39	0.13240	0.0085	0.0026	0.00454	0.1335	0.0046	0.00146	2.996	0.034	0.00076
D91_235	G9A	285	55.68	0.59	0.13593	0.0098	0.0034	0.00478	0.56	0.012	0.00158	8.46	0.1	0.00067
D91_239	G9A_Ti	285	102.06	0.99	0.14159	0.0018	0.0027	0.00464	0.3589	0.0086	0.00162	15.41	0.15	0.00070
D91_241	G9B	130	39.23	0.45	0.27384	0.0082	0.0052	0.00865	0.1155	0.0077	0.00300	2.334	0.035	0.00140
D91_243	G9A	285	55.91	0.58	0.13310	0.012	0.0029	0.00454	0.568	0.012	0.00154	8.423	0.094	0.00079
D91_245	G9A	285	55.96	0.63	0.13188	0.0104	0.0028	0.00465	0.558	0.01	0.00146	8.585	0.078	0.00079
D91_247	G9A_Ti	285	100.27	0.96	0.12947	0.0151	0.0025	0.00430	0.453	0.01	0.00179	14.77	0.16	0.00080
D91_255	G9B	130	40.84	0.61	0.26765	0.0088	0.005	0.00849	0.1126	0.006	0.00297	2.247	0.04	0.00140

Appendix E: Garnet Xenocryst LA-ICP-MS Data Tables

Appendix E.02 (continued): Dharma kimberlite garnet trace element data measured by LA-ICPMS. 2SE – two times standard error. LOD – Limit of detection (Pettke et al., 2014). <LOD – bellow limit of detection.

Sample	*Class*	*Spot Size*	*Zr ppm*	*Zr 2SE*	*Zr LOD*	*Nb ppm*	*Nb 2SE*	*Nb LOD*	*Ba ppm*	*Ba 2SE*	*Ba LOD*	*La ppm*	*La 2SE*	*La LOD*
D89_357	G10B_Ti	130	58.58	0.74	0.00593	0.317	0.011	0.00123	<LOD	<LOD	0.00806	0.0191	0.0013	0.00043
D89_361	G9A	285	5.107	0.051	0.00317	0.3565	0.0081	0.00061	<LOD	<LOD	0.00266	0.02235	0.00088	0.00015
D89_365	G9A	285	32.87	0.27	0.00322	0.2926	0.009	0.00049	0.0036	0.002	0.00266	0.02398	0.00089	0.00017
D89_367	G9B	285	6.308	0.068	0.00302	1.132	0.015	0.00053	<LOD	<LOD	0.00321	0.1894	0.0032	0.00019
D89_369	G9B	285	6.151	0.063	0.00307	1.217	0.016	0.00065	<LOD	<LOD	0.00318	0.1688	0.0032	0.00017
D89_371	G9A	285	33.39	0.3	0.00315	0.2887	0.0071	0.00047	<LOD	<LOD	0.00259	0.01954	0.00093	0.00020
D89_373	G10B_Ti	285	80.22	0.77	0.00311	0.3784	0.0084	0.00056	0.0096	0.003	0.00263	0.02391	0.00094	0.00018
D89_375	G9A_Ti	285	37.92	0.39	0.00316	0.2817	0.0076	0.00059	<LOD	<LOD	0.00280	0.01901	0.00074	0.00017
D89_377	G9A_Ti	285	37.66	0.32	0.00299	0.2794	0.0075	0.00044	<LOD	<LOD	0.00287	0.02015	0.00095	0.00017
D89_381	G9B_Ti	130	41.04	0.39	0.00579	0.263	0.0097	0.00139	<LOD	<LOD	0.00752	0.0185	0.0014	0.00040
D89_387	G10B_Ti	285	71.1	0.76	0.00311	0.3548	0.0076	0.00044	<LOD	<LOD	0.00271	0.0218	0.001	0.00015
D89_391	G9A_Ti	285	52.72	0.51	0.00310	0.381	0.0085	0.00051	<LOD	<LOD	0.00248	0.0415	0.0013	0.00018
D89_393	G10B_Ti	130	62.22	0.64	0.00615	0.341	0.01	0.00127	<LOD	<LOD	0.00715	0.0209	0.001	0.00040
D89_395	G9A_Ti	285	38.35	0.34	0.00280	0.2895	0.0061	0.00043	<LOD	<LOD	0.00258	0.0201	0.001	0.00018
D89_397	G9B_Ti	130	40.05	0.38	0.00630	0.2747	0.0084	0.00151	<LOD	<LOD	0.00542	0.0174	0.0014	0.00043
D89_399	G9A_Ti	285	50.28	0.49	0.00313	0.4057	0.0087	0.00049	0.0036	0.002	0.00222	0.0502	0.0018	0.00017
D89_403	G9B	285	6.207	0.062	0.00281	1.222	0.016	0.00046	<LOD	<LOD	0.00273	0.1767	0.0031	0.00016
D89_411	G9A	285	32.05	0.3	0.00288	0.2956	0.0063	0.00055	0.004	0.0023	0.00298	0.02561	0.00086	0.00017
D89_415	G9B	285	6.04	0.061	0.00301	1.212	0.018	0.00050	<LOD	<LOD	0.00285	0.1665	0.0029	0.00018
D89_417	G9A	130	26.41	0.26	0.00624	0.258	0.011	0.00148	<LOD	<LOD	0.00758	0.018	0.0011	0.00047
D89_421	G10B_Ti	285	88.64	0.67	0.00290	0.4251	0.0081	0.00045	<LOD	<LOD	0.00222	0.02779	0.00097	0.00015
D89_423	G9A_Ti	285	37.45	0.33	0.00306	0.282	0.0067	0.00057	0.0075	0.0063	0.00277	0.0209	0.001	0.00015
D89_425	G9A_Ti	285	51.74	0.53	0.00286	0.3888	0.0074	0.00061	<LOD	<LOD	0.00290	0.0501	0.0015	0.00017
D89_427	G10B_Ti	285	89.48	0.69	0.00283	0.439	0.01	0.00051	0.003	0.003	0.00246	0.03032	0.00094	0.00016
D89_429	G9A	285	3.151	0.045	0.00306	0.3857	0.0089	0.00046	<LOD	<LOD	0.00255	0.02529	0.00086	0.00018
D89_433	G9B	130	4.953	0.069	0.00585	1.079	0.022	0.00139	<LOD	<LOD	0.00628	0.1476	0.0038	0.00044
D89_437	G9B_Ti	130	40.03	0.4	0.00580	0.266	0.0088	0.00164	<LOD	<LOD	0.00754	0.0203	0.0015	0.00046
D89_441	G9A	285	32.62	0.23	0.00288	0.2921	0.0071	0.00058	<LOD	<LOD	0.00267	0.02045	0.0008	0.00015
D91_221	G9A	285	21.19	0.23	0.00402	0.51	0.01	0.00071	<LOD	<LOD	0.00350	0.0367	0.0012	0.00019
D91_227	G9A	130	24.5	0.27	0.00546	0.402	0.014	0.00144	<LOD	<LOD	0.00691	0.0286	0.0016	0.00036
D91_229	G9B	285	2.96	0.043	0.00417	0.5493	0.0095	0.00059	<LOD	<LOD	0.00347	0.127	0.0025	0.00020
D91_235	G9A	285	20.05	0.24	0.00430	0.543	0.013	0.00057	<LOD	<LOD	0.00335	0.0392	0.0014	0.00021
D91_239	G9A_Ti	285	41.2	0.44	0.00431	0.3432	0.0088	0.00068	0.0047	0.0027	0.00340	0.0455	0.0014	0.00021
D91_241	G9B	130	2.133	0.044	0.00572	0.415	0.013	0.00153	<LOD	<LOD	0.00722	0.0981	0.0025	0.00037
D91_243	G9A	285	19.13	0.2	0.00418	0.538	0.011	0.00063	<LOD	<LOD	0.00345	0.0406	0.0013	0.00022
D91_245	G9A	285	22.16	0.27	0.00387	0.4997	0.0088	0.00058	<LOD	<LOD	0.00342	0.0369	0.0011	0.00021
D91_247	G9A_Ti	285	38.46	0.38	0.00387	0.614	0.01	0.00066	<LOD	<LOD	0.00401	0.049	0.0014	0.00020
D91_255	G9B	130	2.151	0.055	0.00604	0.4	0.013	0.00105	<LOD	<LOD	0.00678	0.0908	0.0031	0.00042

Appendix E: Garnet Xenocryst LA-ICP-MS Data Tables

Appendix E.02 (continued): Dharma kimberlite garnet trace element data measured by LA-ICPMS. 2SE – two times standard error. LOD – Limit of detection (Pettke et al., 2014). <LOD – bellow limit of detection.

Sample	*Class*	*Spot Size*	*Ce ppm*	*Ce 2SE*	*Ce LOD*	*Pr ppm*	*Pr 2SE*	*Pr LOD*	*Nd ppm*	*Nd 2SE*	*Nd LOD*	*Sm ppm*	*Sm 2SE*	*Sm LOD*
D89_357	G10B_Ti	130	0.2161	0.0054	0.00051	0.074	0.0023	0.00032	0.692	0.019	0.00185	0.524	0.014	0.00218
D89_361	G9A	285	0.2508	0.0037	0.00022	0.0939	0.0017	0.00014	0.811	0.016	0.00078	0.2917	0.0081	0.00095
D89_365	G9A	285	0.2166	0.0033	0.00019	0.0857	0.0017	0.00015	0.951	0.014	0.00084	0.804	0.016	0.00096
D89_367	G9B	285	1.662	0.023	0.00020	0.3867	0.0056	0.00014	2.083	0.031	0.00079	0.441	0.011	0.00089
D89_369	G9B	285	1.567	0.021	0.00022	0.3751	0.005	0.00015	1.991	0.029	0.00080	0.4012	0.0097	0.00091
D89_371	G9A	285	0.2054	0.0042	0.00020	0.0833	0.0018	0.00016	0.904	0.013	0.00089	0.759	0.017	0.00093
D89_373	G10B_Ti	285	0.2378	0.0041	0.00020	0.0832	0.0014	0.00014	0.82	0.014	0.00079	0.648	0.013	0.00096
D89_375	G9A_Ti	285	0.2129	0.0033	0.00019	0.0873	0.0019	0.00015	0.972	0.016	0.00086	0.872	0.016	0.00096
D89_377	G9A_Ti	285	0.2117	0.0042	0.00021	0.0861	0.0016	0.00014	0.986	0.02	0.00082	0.878	0.017	0.00085
D89_381	G9B_Ti	130	0.216	0.0055	0.00050	0.0738	0.0025	0.00035	0.756	0.022	0.00194	0.623	0.022	0.00256
D89_387	G10B_Ti	285	0.2304	0.0045	0.00019	0.0804	0.0017	0.00012	0.799	0.014	0.00076	0.618	0.014	0.00096
D89_391	G9A_Ti	285	0.3788	0.0057	0.00018	0.1258	0.0028	0.00014	1.16	0.021	0.00069	0.823	0.016	0.00081
D89_393	G10B_Ti	130	0.2428	0.0059	0.00046	0.0838	0.0026	0.00035	0.805	0.023	0.00200	0.589	0.018	0.00230
D89_395	G9A_Ti	285	0.2223	0.0037	0.00018	0.0894	0.0021	0.00013	1.009	0.018	0.00071	0.895	0.017	0.00091
D89_397	G9B_Ti	130	0.2102	0.0056	0.00048	0.0773	0.0022	0.00041	0.734	0.016	0.00234	0.58	0.017	0.00240
D89_399	G9A_Ti	285	0.428	0.0064	0.00017	0.1336	0.0026	0.00013	1.173	0.02	0.00085	0.809	0.015	0.00101
D89_403	G9B	285	1.651	0.02	0.00020	0.3927	0.0056	0.00014	2.127	0.029	0.00075	0.448	0.01	0.00081
D89_411	G9A	285	0.2268	0.004	0.00018	0.0926	0.0017	0.00013	1.017	0.02	0.00074	0.83	0.019	0.00092
D89_415	G9B	285	1.597	0.017	0.00019	0.3893	0.0057	0.00012	2.056	0.031	0.00075	0.381	0.01	0.00094
D89_417	G9A	130	0.2073	0.0056	0.00053	0.0819	0.0022	0.00038	0.882	0.024	0.00235	0.713	0.025	0.00215
D89_421	G10B_Ti	285	0.279	0.0038	0.00016	0.0956	0.0023	0.00011	0.954	0.016	0.00081	0.715	0.013	0.00078
D89_423	G9A_Ti	285	0.2227	0.0034	0.00019	0.0896	0.0023	0.00012	1.016	0.016	0.00079	0.886	0.015	0.00093
D89_425	G9A_Ti	285	0.4302	0.0066	0.00018	0.1362	0.0024	0.00012	1.236	0.019	0.00083	0.865	0.019	0.00087
D89_427	G10B_Ti	285	0.3038	0.0045	0.00016	0.1069	0.002	0.00013	1.043	0.016	0.00072	0.78	0.014	0.00097
D89_429	G9A	285	0.2848	0.0044	0.00018	0.1024	0.0019	0.00012	0.824	0.015	0.00076	0.2649	0.0081	0.00079
D89_433	G9B	130	1.493	0.018	0.00049	0.3542	0.0067	0.00041	1.936	0.041	0.00196	0.373	0.013	0.00232
D89_437	G9B_Ti	130	0.2122	0.0054	0.00045	0.0763	0.0029	0.00037	0.745	0.023	0.00184	0.603	0.02	0.00222
D89_441	G9A	285	0.23	0.0036	0.00019	0.097	0.002	0.00013	1.047	0.016	0.00063	0.856	0.014	0.00094
D91_221	G9A	285	0.4801	0.0072	0.00023	0.2173	0.0041	0.00016	2.279	0.029	0.00105	1.231	0.026	0.00104
D91_227	G9A	130	0.3353	0.008	0.00048	0.1246	0.003	0.00034	1.148	0.031	0.00196	0.81	0.021	0.00193
D91_229	G9B	285	0.7279	0.0097	0.00024	0.1741	0.0028	0.00016	1.058	0.016	0.00093	0.2587	0.008	0.00107
D91_235	G9A	285	0.5107	0.0089	0.00024	0.2206	0.0042	0.00016	2.241	0.034	0.00110	1.2	0.021	0.00107
D91_239	G9A_Ti	285	0.3184	0.0056	0.00023	0.1014	0.0018	0.00018	0.936	0.018	0.00096	0.676	0.015	0.00111
D91_241	G9B	130	0.642	0.014	0.00043	0.1446	0.0041	0.00032	0.794	0.021	0.00177	0.197	0.011	0.00205
D91_243	G9A	285	0.5374	0.009	0.00024	0.2292	0.0036	0.00018	2.33	0.036	0.00090	1.217	0.024	0.00109
D91_245	G9A	285	0.4627	0.0082	0.00024	0.2145	0.0039	0.00017	2.318	0.038	0.00096	1.292	0.027	0.00110
D91_247	G9A_Ti	285	0.4064	0.0065	0.00022	0.1342	0.0024	0.00015	1.236	0.022	0.00097	0.882	0.019	0.00108
D91_255	G9B	130	0.632	0.012	0.00044	0.1401	0.0041	0.00031	0.817	0.025	0.00191	0.221	0.011	0.00204

Appendix E: Garnet Xenocryst LA-ICP-MS Data Tables

Appendix E.02 (continued): Dharma kimberlite garnet trace element data measured by LA-ICPMS. 2SE – two times standard error. LOD – Limit of detection (Pettke et al., 2014). <LOD – bellow limit of detection.

Sample	*Class*	*Spot Size*	*Eu ppm*	*Eu 2SE*	*Eu LOD*	*Gd ppm*	*Gd 2SE*	*Gd LOD*	*Tb ppm*	*Tb 2SE*	*Tb LOD*	*Dy ppm*	*Dy 2SE*	*Dy LOD*
D89_357	G10B_Ti	130	0.2546	0.0069	0.00062	1.064	0.029	0.00259	0.2243	0.0056	0.00040	1.689	0.035	0.00168
D89_361	G9A	285	0.088	0.0028	0.00027	0.2587	0.009	0.00121	0.0452	0.0012	0.00020	0.4355	0.0084	0.00089
D89_365	G9A	285	0.3558	0.0048	0.00028	1.396	0.022	0.00133	0.2682	0.0039	0.00018	1.998	0.027	0.00078
D89_367	G9B	285	0.1305	0.003	0.00029	0.448	0.011	0.00124	0.0786	0.0023	0.00017	0.6	0.012	0.00075
D89_369	G9B	285	0.1179	0.0034	0.00031	0.41	0.012	0.00141	0.0769	0.0016	0.00017	0.584	0.012	0.00076
D89_371	G9A	285	0.3343	0.0049	0.00030	1.358	0.021	0.00122	0.2589	0.0038	0.00022	1.927	0.026	0.00081
D89_373	G10B_Ti	285	0.2995	0.005	0.00029	1.353	0.026	0.00132	0.2934	0.0047	0.00019	2.263	0.031	0.00077
D89_375	G9A_Ti	285	0.3652	0.0062	0.00029	1.788	0.029	0.00125	0.4129	0.0061	0.00020	3.54	0.048	0.00079
D89_377	G9A_Ti	285	0.3692	0.0054	0.00028	1.814	0.031	0.00132	0.4119	0.0061	0.00018	3.539	0.049	0.00067
D89_381	G9B_Ti	130	0.3019	0.008	0.00062	1.219	0.032	0.00261	0.2714	0.0065	0.00037	2.024	0.042	0.00186
D89_387	G10B_Ti	285	0.289	0.0051	0.00028	1.313	0.026	0.00127	0.2866	0.0055	0.00018	2.165	0.035	0.00079
D89_391	G9A_Ti	285	0.3758	0.0068	0.00020	1.644	0.03	0.00116	0.349	0.0059	0.00017	2.687	0.041	0.00062
D89_393	G10B_Ti	130	0.2845	0.0076	0.00061	1.184	0.028	0.00250	0.25	0.005	0.00045	1.846	0.028	0.00145
D89_395	G9A_Ti	285	0.3816	0.0061	0.00025	1.877	0.032	0.00115	0.4355	0.0055	0.00015	3.681	0.048	0.00064
D89_397	G9B_Ti	130	0.2993	0.0091	0.00065	1.214	0.027	0.00264	0.2688	0.0057	0.00040	2.046	0.035	0.00156
D89_399	G9A_Ti	285	0.3653	0.0072	0.00028	1.593	0.026	0.00128	0.339	0.0051	0.00018	2.593	0.034	0.00085
D89_403	G9B	285	0.1342	0.003	0.00025	0.473	0.01	0.00109	0.0846	0.0019	0.00017	0.646	0.012	0.00066
D89_411	G9A	285	0.3567	0.0063	0.00029	1.402	0.027	0.00126	0.2705	0.0045	0.00018	2.039	0.028	0.00080
D89_415	G9B	285	0.1185	0.0033	0.00027	0.433	0.013	0.00103	0.0811	0.0021	0.00018	0.623	0.012	0.00073
D89_417	G9A	130	0.3139	0.0086	0.00075	1.152	0.03	0.00284	0.2222	0.0061	0.00045	1.576	0.026	0.00155
D89_421	G10B_Ti	285	0.339	0.0051	0.00027	1.518	0.029	0.00111	0.3293	0.0045	0.00020	2.514	0.029	0.00065
D89_423	G9A_Ti	285	0.3884	0.0072	0.00027	1.892	0.03	0.00099	0.4399	0.0063	0.00019	3.772	0.057	0.00071
D89_425	G9A_Ti	285	0.3941	0.0078	0.00026	1.742	0.026	0.00121	0.3775	0.0067	0.00021	2.929	0.046	0.00074
D89_427	G10B_Ti	285	0.3596	0.0061	0.00028	1.612	0.026	0.00117	0.3506	0.0052	0.00018	2.656	0.038	0.00071
D89_429	G9A	285	0.0748	0.0026	0.00026	0.2177	0.0083	0.00117	0.0424	0.0014	0.00019	0.4311	0.009	0.00075
D89_433	G9B	130	0.1181	0.0052	0.00069	0.373	0.015	0.00274	0.0671	0.0028	0.00045	0.498	0.014	0.00175
D89_437	G9B_Ti	130	0.294	0.0073	0.00067	1.188	0.023	0.00294	0.2657	0.0068	0.00038	2.024	0.034	0.00168
D89_441	G9A	285	0.3633	0.0056	0.00025	1.456	0.024	0.00110	0.2834	0.0044	0.00019	2.098	0.026	0.00066
D91_221	G9A	285	0.4111	0.0069	0.00033	1.3	0.022	0.00157	0.2123	0.0036	0.00025	1.406	0.022	0.00086
D91_227	G9A	130	0.3532	0.0089	0.00059	1.268	0.036	0.00288	0.1955	0.0051	0.00042	1.127	0.021	0.00156
D91_229	G9B	285	0.0816	0.0027	0.00030	0.2841	0.0089	0.00153	0.052	0.0016	0.00023	0.3933	0.0094	0.00084
D91_235	G9A	285	0.396	0.0084	0.00034	1.273	0.028	0.00161	0.2089	0.0042	0.00023	1.396	0.027	0.00099
D91_239	G9A_Ti	285	0.3116	0.0058	0.00035	1.353	0.029	0.00166	0.3014	0.0052	0.00025	2.353	0.035	0.00097
D91_241	G9B	130	0.0671	0.0031	0.00060	0.233	0.012	0.00271	0.0426	0.002	0.00038	0.318	0.0087	0.00160
D91_243	G9A	285	0.3995	0.0086	0.00034	1.265	0.029	0.00156	0.2084	0.0037	0.00023	1.386	0.022	0.00096
D91_245	G9A	285	0.4244	0.0075	0.00032	1.344	0.026	0.00161	0.2167	0.0036	0.00022	1.417	0.024	0.00092
D91_247	G9A_Ti	285	0.3906	0.0072	0.00032	1.741	0.031	0.00169	0.349	0.0061	0.00022	2.53	0.042	0.00089
D91_255	G9B	130	0.0733	0.0034	0.00063	0.229	0.011	0.00276	0.0415	0.0018	0.00040	0.311	0.012	0.00146

Appendix E: Garnet Xenocryst LA-ICP-MS Data Tables

Appendix E.02 (continued): Dharma kimberlite garnet trace element data measured by LA-ICPMS. 2SE – two times standard error. LOD – Limit of detection (Pettke et al., 2014). <LOD – bellow limit of detection.

Sample	*Class*	*Spot Size*	*Ho ppm*	*Ho 2SE*	*Ho LOD*	*Er ppm*	*Er 2SE*	*Er LOD*	*Tm ppm*	*Tm 2SE*	*Tm LOD*	*Yb ppm*	*Yb 2SE*	*Yb LOD*
D89_357	G10B_Ti	130	0.4008	0.007	0.00041	1.262	0.024	0.00119	0.1895	0.005	0.00043	1.393	0.027	0.00184
D89_361	G9A	285	0.1387	0.0025	0.00022	0.568	0.01	0.00060	0.1079	0.0026	0.00021	0.931	0.019	0.00080
D89_365	G9A	285	0.4824	0.0075	0.00018	1.602	0.025	0.00052	0.2545	0.0051	0.00020	1.912	0.036	0.00092
D89_367	G9B	285	0.1502	0.0031	0.00018	0.5221	0.0092	0.00059	0.0918	0.002	0.00018	0.755	0.012	0.00091
D89_369	G9B	285	0.1506	0.0032	0.00019	0.516	0.011	0.00057	0.09	0.0025	0.00022	0.753	0.016	0.00095
D89_371	G9A	285	0.4728	0.0071	0.00020	1.564	0.021	0.00058	0.2487	0.0046	0.00021	1.887	0.031	0.00093
D89_373	G10B_Ti	285	0.5292	0.0074	0.00019	1.692	0.025	0.00062	0.2555	0.0041	0.00020	1.825	0.026	0.00094
D89_375	G9A_Ti	285	0.942	0.011	0.00020	3.268	0.034	0.00054	0.5302	0.0073	0.00019	4.006	0.056	0.00083
D89_377	G9A_Ti	285	0.951	0.014	0.00020	3.31	0.045	0.00056	0.535	0.0082	0.00018	4.023	0.064	0.00092
D89_381	G9B_Ti	130	0.4872	0.0096	0.00039	1.532	0.032	0.00110	0.2307	0.0051	0.00040	1.658	0.037	0.00164
D89_387	G10B_Ti	285	0.5127	0.0086	0.00019	1.606	0.028	0.00049	0.2414	0.0052	0.00021	1.747	0.038	0.00092
D89_391	G9A_Ti	285	0.637	0.01	0.00013	2.001	0.034	0.00051	0.2996	0.0054	0.00016	2.188	0.04	0.00077
D89_393	G10B_Ti	130	0.4286	0.0074	0.00032	1.32	0.024	0.00115	0.2018	0.0052	0.00040	1.435	0.025	0.00195
D89_395	G9A_Ti	285	0.992	0.012	0.00017	3.403	0.039	0.00049	0.5514	0.0079	0.00017	4.129	0.053	0.00079
D89_397	G9B_Ti	130	0.4818	0.0091	0.00036	1.506	0.027	0.00118	0.2269	0.0051	0.00039	1.623	0.03	0.00193
D89_399	G9A_Ti	285	0.6239	0.0094	0.00017	1.982	0.028	0.00051	0.302	0.0053	0.00017	2.178	0.038	0.00097
D89_403	G9B	285	0.1585	0.0025	0.00019	0.554	0.011	0.00059	0.0953	0.0022	0.00018	0.756	0.014	0.00087
D89_411	G9A	285	0.4974	0.0085	0.00018	1.671	0.026	0.00055	0.2628	0.0046	0.00020	1.911	0.025	0.00070
D89_415	G9B	285	0.1569	0.0034	0.00018	0.5613	0.0095	0.00056	0.0952	0.0024	0.00018	0.751	0.014	0.00067
D89_417	G9A	130	0.3872	0.0082	0.00045	1.263	0.022	0.00127	0.2048	0.0058	0.00046	1.502	0.03	0.00216
D89_421	G10B_Ti	285	0.5843	0.009	0.00015	1.839	0.024	0.00050	0.2718	0.0054	0.00018	1.937	0.024	0.00080
D89_423	G9A_Ti	285	0.996	0.014	0.00016	3.489	0.051	0.00057	0.5571	0.0091	0.00018	4.099	0.055	0.00083
D89_425	G9A_Ti	285	0.6981	0.0095	0.00018	2.221	0.04	0.00056	0.3343	0.0053	0.00020	2.326	0.035	0.00082
D89_427	G10B_Ti	285	0.6135	0.0086	0.00017	1.939	0.024	0.00056	0.2865	0.0048	0.00018	1.975	0.026	0.00086
D89_429	G9A	285	0.1431	0.003	0.00017	0.5931	0.0099	0.00057	0.1124	0.0023	0.00020	0.948	0.017	0.00090
D89_433	G9B	130	0.1244	0.0043	0.00041	0.426	0.015	0.00134	0.0734	0.0026	0.00043	0.605	0.017	0.00170
D89_437	G9B_Ti	130	0.4749	0.0094	0.00040	1.479	0.032	0.00112	0.2217	0.005	0.00040	1.638	0.031	0.00211
D89_441	G9A	285	0.5124	0.0072	0.00016	1.715	0.027	0.00053	0.2704	0.0045	0.00020	1.985	0.032	0.00080
D91_221	G9A	285	0.3045	0.0054	0.00047	0.89	0.016	0.00059	0.1332	0.0031	0.00022	0.958	0.019	0.00103
D91_227	G9A	130	0.2246	0.0046	0.00039	0.628	0.014	0.00111	0.0935	0.0032	0.00040	0.685	0.018	0.00164
D91_229	G9B	285	0.1052	0.0024	0.00021	0.3909	0.0089	0.00061	0.0724	0.0023	0.00025	0.648	0.014	0.00097
D91_235	G9A	285	0.3043	0.0049	0.00021	0.894	0.019	0.00066	0.1307	0.003	0.00025	0.971	0.021	0.00102
D91_239	G9A_Ti	285	0.5923	0.0095	0.00023	1.944	0.032	0.00070	0.3057	0.0056	0.00026	2.203	0.033	0.00108
D91_241	G9B	130	0.0822	0.0025	0.00039	0.3117	0.009	0.00116	0.0606	0.0029	0.00031	0.519	0.017	0.00179
D91_243	G9A	285	0.3079	0.0055	0.00020	0.899	0.016	0.00075	0.1337	0.0032	0.00023	0.969	0.022	0.00109
D91_245	G9A	285	0.3075	0.006	0.00024	0.905	0.013	0.00062	0.1348	0.0036	0.00023	0.971	0.02	0.00097
D91_247	G9A_Ti	285	0.5632	0.0084	0.00021	1.712	0.031	0.00068	0.2458	0.0039	0.00024	1.722	0.028	0.00104
D91_255	G9B	130	0.0817	0.0027	0.00040	0.2909	0.0097	0.00100	0.0576	0.003	0.00036	0.498	0.016	0.00187

Appendix E: Garnet Xenocryst LA-ICP-MS Data Tables

Appendix E.02 (continued): Dharma kimberlite garnet trace element data measured by LA-ICPMS. 2SE – two times standard error. LOD – Limit of detection (Pettke et al., 2014). <LOD – bellow limit of detection.

Sample	*Class*	*Spot Size*	*Lu ppm*	*Lu 2SE*	*Lu LOD*	*Hf ppm*	*Hf 2SE*	*Hf LOD*	*Ta ppm*	*Ta 2SE*	*Ta LOD*
D89_357	G10B_Ti	130	0.214	0.0049	0.00045	1.713	0.053	0.00261	0.0362	0.0033	0.00078
D89_361	G9A	285	0.1744	0.0034	0.00024	0.1054	0.0067	0.00172	0.0372	0.0019	0.00032
D89_365	G9A	285	0.3229	0.0066	0.00022	0.888	0.029	0.00145	0.0294	0.0019	0.00032
D89_367	G9B	285	0.1376	0.0029	0.00021	0.1725	0.0092	0.00163	0.082	0.0031	0.00032
D89_369	G9B	285	0.1352	0.0034	0.00023	0.17	0.01	0.00163	0.0816	0.0032	0.00038
D89_371	G9A	285	0.3146	0.0049	0.00025	0.847	0.02	0.00162	0.0295	0.0017	0.00041
D89_373	G10B_Ti	285	0.2986	0.0047	0.00026	2.469	0.041	0.00165	0.0474	0.0023	0.00037
D89_375	G9A_Ti	285	0.6671	0.0083	0.00024	1.064	0.02	0.00175	0.0254	0.0017	0.00036
D89_377	G9A_Ti	285	0.679	0.011	0.00024	1.055	0.029	0.00162	0.0263	0.0018	0.00033
D89_381	G9B_Ti	130	0.2594	0.0065	0.00051	1.141	0.033	0.00324	0.0291	0.0023	0.00076
D89_387	G10B_Ti	285	0.2853	0.0055	0.00023	2.193	0.051	0.00163	0.0412	0.0017	0.00039
D89_391	G9A_Ti	285	0.3495	0.0066	0.00018	1.544	0.032	0.00128	0.0423	0.0021	0.00035
D89_393	G10B_Ti	130	0.2231	0.005	0.00044	1.812	0.048	0.00297	0.0395	0.0031	0.00075
D89_395	G9A_Ti	285	0.6964	0.0097	0.00020	1.106	0.028	0.00101	0.028	0.0014	0.00031
D89_397	G9B_Ti	130	0.2587	0.0058	0.00049	1.058	0.04	0.00261	0.0301	0.0026	0.00067
D89_399	G9A_Ti	285	0.3534	0.0048	0.00021	1.462	0.03	0.00157	0.0423	0.0023	0.00035
D89_403	G9B	285	0.1385	0.0029	0.00021	0.1791	0.0085	0.00128	0.0843	0.0029	0.00035
D89_411	G9A	285	0.3198	0.0051	0.00020	0.81	0.022	0.00131	0.0286	0.0016	0.00039
D89_415	G9B	285	0.1387	0.0029	0.00022	0.1681	0.0089	0.00147	0.0774	0.0028	0.00030
D89_417	G9A	130	0.2449	0.006	0.00047	0.666	0.032	0.00342	0.026	0.0025	0.00084
D89_421	G10B_Ti	285	0.3111	0.005	0.00021	2.703	0.051	0.00131	0.0513	0.0024	0.00029
D89_423	G9A_Ti	285	0.6893	0.0085	0.00021	1.009	0.031	0.00113	0.0247	0.0016	0.00031
D89_425	G9A_Ti	285	0.378	0.0062	0.00022	1.489	0.03	0.00141	0.039	0.002	0.00032
D89_427	G10B_Ti	285	0.3245	0.0038	0.00022	2.744	0.043	0.00157	0.0548	0.0023	0.00038
D89_429	G9A	285	0.1755	0.003	0.00020	0.0583	0.0061	0.00148	0.0397	0.002	0.00034
D89_433	G9B	130	0.1099	0.0037	0.00048	0.133	0.012	0.00322	0.0687	0.0049	0.00073
D89_437	G9B_Ti	130	0.2595	0.0065	0.00043	1.093	0.036	0.00274	0.028	0.0026	0.00074
D89_441	G9A	285	0.3312	0.0051	0.00018	0.844	0.02	0.00142	0.0285	0.0017	0.00035
D91_221	G9A	285	0.163	0.0038	0.00027	0.487	0.019	0.00165	0.0651	0.0029	0.00036
D91_227	G9A	130	0.1186	0.0029	0.00038	0.551	0.02	0.00260	0.0353	0.0035	0.00073
D91_229	G9B	285	0.1315	0.0027	0.00024	0.0815	0.0062	0.00162	0.0224	0.0016	0.00044
D91_235	G9A	285	0.1622	0.004	0.00028	0.475	0.019	0.00179	0.0684	0.003	0.00040
D91_239	G9A_Ti	285	0.3619	0.0061	0.00026	1.066	0.028	0.00174	0.0323	0.0024	0.00040
D91_241	G9B	130	0.1029	0.0032	0.00040	0.0678	0.0077	0.00221	0.016	0.0017	0.00068
D91_243	G9A	285	0.1685	0.0039	0.00029	0.461	0.018	0.00161	0.0695	0.0027	0.00035
D91_245	G9A	285	0.1686	0.0037	0.00027	0.506	0.021	0.00129	0.0617	0.0028	0.00044
D91_247	G9A_Ti	285	0.2753	0.0049	0.00028	1.105	0.026	0.00178	0.0612	0.0027	0.00041
D91_255	G9B	130	0.099	0.0028	0.00036	0.0663	0.008	0.00326	0.0156	0.0018	0.00081

Appendix E: Garnet Xenocryst LA-ICP-MS Data Tables

Appendix E.02 (continued): Dharma kimberlite garnet trace element data measured by LA-ICPMS. 2SE – two times standard error. LOD – Limit of detection (Pettke et al., 2014). <LOD – bellow limit of detection.

Sample	*Class*	*Spot Size*	*Ca ppm*	*Ca 2SE*	*Ca LOD*	*Sc ppm*	*Sc 2SE*	*Sc LOD*	*Ti ppm*	*Ti 2SE*	*Ti LOD*	*V ppm*	*V 2SE*	*V LOD*
D91_279	G9B_Ti	130	32340	240	18.0312	95.33	0.67	0.01991	4107	46	0.70343	307	2.7	0.01161
D91_283	G9A	285	43290	430	7.29427	166	1.70	0.00945	1776	16	0.29074	346.7	3.3	0.00499
D91_285	G9B	285	46070	430	7.47155	175.3	1.70	0.00932	645.8	5.7	0.29494	376.4	3.6	0.00534
D91_289	G9A_Ti	285	38460	400	7.31772	141.3	1.30	0.00920	3513	27	0.29421	319.8	2.5	0.00534
D91_291	G9A_Ti	285	38410	320	7.50545	141.11	0.89	0.00934	3501	28	0.29924	318.8	3.3	0.00555
D91_297	G9A_Ti	285	42480	430	7.28175	166	1.50	0.00897	2299	21	0.29115	294.6	3	0.00538
D91_303	G9B	130	42400	380	17.6537	127.3	1.10	0.01917	544.6	4.1	0.66945	351.1	3	0.01170
D91_305	G9B	130	43590	440	17.1034	129.65	1.00	0.01808	542	4.9	0.63766	362.3	3.2	0.01116
D91_307	G9A	130	40030	390	16.4446	122.3	1.00	0.01969	1483	12	0.66158	312.2	2.6	0.01012
D91_309	G9B	285	44690	390	7.66858	163.5	1.50	0.00940	354.3	3.1	0.30503	303.5	2.9	0.00556
D91_311	G9B	285	46020	450	7.75438	162.9	1.50	0.00942	336.4	3.3	0.30630	298.9	2.6	0.00561
D91_313	G9B	130	42010	370	16.9209	126.9	1.10	0.01948	568.1	4.9	0.66250	355.7	2.3	0.01063
D91_317	G9B	285	46750	410	7.59433	175	1.60	0.00900	637.5	6.4	0.30187	385.1	3	0.00592
D91_319	G9B	285	46210	500	10.2820	173	1.80	0.01212	659.4	6.5	0.41973	381.3	3.7	0.00790
D91_321	G9A	285	42070	360	7.18657	159.6	1.20	0.00991	1728	15	0.28757	341.3	2.8	0.00488
D91_323	G9A	130	39670	400	17.0309	122.1	1.00	0.01905	1505	11	0.65368	325.7	2.4	0.01031
D91_325	G9B	285	45290	370	7.04039	168.5	1.20	0.00929	634.1	5.3	0.28796	372	2.8	0.00511
D91_327	G9A	285	41950	320	7.25847	159.5	1.30	0.00920	1726	15	0.28991	334.8	2.8	0.00530
D93_139	G9A_Ti	130	31730	310	18.5270	98.27	0.82	0.02011	4044	39	0.70223	346.1	2.1	0.01220
D93_141	G9A_Ti	285	34600	380	7.19107	122.3	1.00	0.00901	4817	42	0.29579	309.1	2.9	0.00464
D93_145	G9A_Ti	285	35540	290	7.44762	132.6	1.10	0.00882	2716	19	0.28758	334.2	2.7	0.00507
D93_151	G9A	285	40450	320	7.24063	191	1.70	0.00865	1091.2	9.9	0.28835	308	2.7	0.00497
D93_153	G9A	285	40650	430	7.41103	193.9	2.10	0.00890	1094.6	9.9	0.29896	308.7	3.1	0.00519
D93_155	G9A	285	40330	390	7.13045	193.8	1.90	0.00865	1091	10	0.28954	314.9	2.7	0.00520
D93_173	G9A	285	40630	400	7.35512	193.8	2.00	0.00876	1094	11	0.29390	309.4	3.1	0.00549
D93_175	G9A	130	38360	350	16.6706	145.3	1.50	0.01985	937.1	7.8	0.66692	289.2	2.9	0.01051
D93_177	G9A_Ti	285	36600	330	7.28147	136.3	1.10	0.00860	2933	26	0.29160	358.5	2.9	0.00555
D93_179	G9B_Ti	285	37400	380	7.31845	139.8	1.30	0.01027	4754	51	0.29781	388.2	3.7	0.00490
D93_181	G9A_Ti	130	33310	400	16.5914	99.04	0.94	0.01881	2289	27	0.64041	320	3.5	0.01024
D93_183	G9A	285	40970	390	7.47117	192.9	1.80	0.00957	1087.8	9.5	0.29484	311.2	3	0.00491
D93_195	G9A_Ti	285	38480	380	7.35010	141.6	1.10	0.00940	3079	25	0.28968	323.3	3.2	0.00501
D93_205	G9A_Ti	285	36820	290	7.17171	136.1	1.30	0.00876	2822	23	0.28284	350.1	3.1	0.00513
D93_209	G9A	130	38020	340	17.4709	143.61	0.89	0.01960	940.1	7.5	0.66631	286.1	2.8	0.01096
D93_217	G9A_Ti	130	34050	350	17.6589	101.1	0.83	0.01963	2290	21	0.67597	318	2.2	0.01112

Appendix E: Garnet Xenocryst LA-ICP-MS Data Tables

Appendix E.02 (continued): Dharma kimberlite garnet trace element data measured by LA-ICPMS. 2SE – two times standard error. LOD – Limit of detection (Pettke et al., 2014). <LOD – bellow limit of detection.

Sample	*Class*	*Spot Size*	*Ni ppm*	*Ni 2SE*	*Ni LOD*	*Rb ppm*	*Rb 2SE*	*Rb LOD*	*Sr ppm*	*Sr 2SE*	*Sr LOD*	*Y ppm*	*Y 2SE*	*Y LOD*
D91_279	G9B_Ti	130	79.47	0.83	0.29353	0.0058	0.0058	0.00875	0.382	0.015	0.00315	14.89	0.14	0.00141
D91_283	G9A	285	55.52	0.49	0.12659	0.0104	0.0026	0.00442	0.562	0.012	0.00168	8.542	0.084	0.00066
D91_285	G9B	285	39.34	0.37	0.12973	0.0075	0.0028	0.00451	0.1299	0.0044	0.00159	3.132	0.046	0.00077
D91_289	G9A_Ti	285	99.44	0.99	0.12723	0.0102	0.003	0.00432	0.618	0.023	0.00154	14.36	0.12	0.00073
D91_291	G9A_Ti	285	99.18	0.98	0.12838	0.0113	0.003	0.00451	0.4609	0.0092	0.00157	14.46	0.14	0.00086
D91_297	G9A_Ti	285	65.04	0.64	0.12404	0.0105	0.0028	0.00438	0.4044	0.0099	0.00142	8.079	0.077	0.00066
D91_303	G9B	130	38.95	0.52	0.27817	0.0127	0.0058	0.00903	0.1234	0.0069	0.00304	2.328	0.029	0.00152
D91_305	G9B	130	41.03	0.52	0.26492	0.0077	0.005	0.00840	0.1436	0.0074	0.00293	2.325	0.037	0.00142
D91_307	G9A	130	57.47	0.59	0.27267	0.0208	0.0057	0.00873	0.478	0.017	0.00366	6.722	0.078	0.00139
D91_309	G9B	285	26.5	0.27	0.13051	0.0065	0.0028	0.00467	0.0167	0.0017	0.00140	2.092	0.027	0.00075
D91_311	G9B	285	26.17	0.25	0.13171	0.0058	0.0028	0.00475	0.0155	0.0018	0.00140	1.928	0.025	0.00073
D91_313	G9B	130	38.58	0.45	0.27535	0.009	0.0062	0.00868	0.1138	0.0076	0.00322	2.43	0.034	0.00138
D91_317	G9B	285	40.65	0.39	0.12715	0.0082	0.0031	0.00471	0.1396	0.0039	0.00135	3.017	0.038	0.00069
D91_319	G9B	285	39.17	0.43	0.17282	0.0061	0.0028	0.00666	0.1266	0.0053	0.00179	3.154	0.036	0.00093
D91_321	G9A	285	55.14	0.47	0.12208	0.0136	0.0026	0.00422	0.514	0.01	0.00162	8.001	0.091	0.00062
D91_323	G9A	130	57.4	0.71	0.27277	0.0105	0.0056	0.00844	0.505	0.017	0.00331	6.368	0.078	0.00118
D91_325	G9B	285	39.24	0.38	0.11850	0.0101	0.003	0.00428	0.1278	0.0043	0.00152	2.905	0.025	0.00072
D91_327	G9A	285	55.19	0.47	0.11946	0.0077	0.0026	0.00440	0.5232	0.0098	0.00139	7.946	0.067	0.00078
D93_139	G9A_Ti	130	53.21	0.5	0.29863	0.0062	0.0045	0.00871	0.2422	0.01	0.00316	10.66	0.1	0.00137
D93_141	G9A_Ti	285	99.8	1	0.14425	0.0086	0.0027	0.00412	0.484	0.01	0.00165	20.64	0.2	0.00089
D93_145	G9A_Ti	285	59.21	0.5	0.14292	0.0075	0.0028	0.00422	0.3354	0.0075	0.00171	16.72	0.16	0.00088
D93_151	G9A	285	51.18	0.5	0.13727	0.0077	0.0028	0.00415	0.399	0.0082	0.00163	7.849	0.09	0.00073
D93_153	G9A	285	51.23	0.63	0.14055	0.0106	0.0028	0.00434	0.4224	0.0083	0.00162	7.838	0.08	0.00084
D93_155	G9A	285	50.63	0.52	0.13603	0.0106	0.0026	0.00429	0.4154	0.009	0.00161	7.793	0.073	0.00075
D93_173	G9A	285	50.93	0.51	0.13853	0.0077	0.0034	0.00448	0.42	0.0097	0.00157	7.81	0.1	0.00075
D93_175	G9A	130	52.83	0.63	0.27344	0.0248	0.0057	0.00850	0.431	0.015	0.00325	6.251	0.069	0.00147
D93_177	G9A_Ti	285	60.01	0.6	0.13662	0.0092	0.0025	0.00444	0.3758	0.0098	0.00161	17.53	0.18	0.00073
D93_179	G9B_Ti	285	49.01	0.53	0.14348	0.0118	0.0031	0.00432	0.2929	0.0069	0.00181	13.48	0.16	0.00075
D93_181	G9A_Ti	130	62.66	0.73	0.26555	0.0125	0.0054	0.00827	0.307	0.011	0.00309	13.14	0.19	0.00152
D93_183	G9A	285	52.51	0.53	0.13931	0.0109	0.0028	0.00450	0.4335	0.0099	0.00170	8.11	0.1	0.00084
D93_195	G9A_Ti	285	97.2	0.99	0.13780	0.006	0.0028	0.00443	0.446	0.01	0.00170	13.75	0.13	0.00076
D93_205	G9A_Ti	285	61.46	0.59	0.13431	0.0072	0.0028	0.00438	0.3667	0.0092	0.00160	18.01	0.17	0.00078
D93_209	G9A	130	53.08	0.53	0.27875	0.0092	0.0057	0.00889	0.393	0.014	0.00315	6.205	0.071	0.00145
D93_217	G9A_Ti	130	63.24	0.6	0.28125	0	0.0059	0.00888	0.311	0.012	0.00316	13.41	0.12	0.00150

Appendix E: Garnet Xenocryst LA-ICP-MS Data Tables

Appendix E.02 (continued): Dharma kimberlite garnet trace element data measured by LA-ICPMS. 2SE – two times standard error. LOD – Limit of detection (Pettke et al., 2014). <LOD – bellow limit of detection.

Sample	*Class*	*Spot Size*	*Zr ppm*	*Zr 2SE*	*Zr LOD*	*Nb ppm*	*Nb 2SE*	*Nb LOD*	*Ba ppm*	*Ba 2SE*	*Ba LOD*	*La ppm*	*La 2SE*	*La LOD*
D91_279	G9B_Ti	130	49.1	0.48	0.00602	0.331	0.012	0.00126	<LOD	<LOD	0.00910	0.0383	0.0017	0.00043
D91_283	G9A	285	20.92	0.21	0.00369	0.494	0.012	0.00053	<LOD	<LOD	0.00294	0.0349	0.0012	0.00020
D91_285	G9B	285	2.862	0.052	0.00387	0.4436	0.0099	0.00067	0.0042	0.0024	0.00308	0.1106	0.0025	0.00020
D91_289	G9A_Ti	285	37.71	0.35	0.00375	0.606	0.011	0.00059	6.73	0.71	0.00314	0.0479	0.0016	0.00021
D91_291	G9A_Ti	285	37.58	0.35	0.00388	0.605	0.011	0.00063	<LOD	<LOD	0.00313	0.0469	0.0015	0.00020
D91_297	G9A_Ti	285	33.41	0.3	0.00363	0.455	0.01	0.00067	<LOD	<LOD	0.00319	0.0366	0.0011	0.00020
D91_303	G9B	130	2.09	0.035	0.00592	0.37	0.013	0.00126	<LOD	<LOD	0.00671	0.0915	0.003	0.00039
D91_305	G9B	130	2.418	0.047	0.00566	0.582	0.015	0.00093	<LOD	<LOD	0.00694	0.1438	0.0057	0.00041
D91_307	G9A	130	18.34	0.2	0.00567	0.412	0.013	0.00121	<LOD	<LOD	0.00675	0.0302	0.0016	0.00040
D91_309	G9B	285	2.057	0.034	0.00385	0.0387	0.0026	0.00060	<LOD	<LOD	0.00383	0.00094	0.00021	0.00022
D91_311	G9B	285	1.837	0.032	0.00383	0.0432	0.0023	0.00054	<LOD	<LOD	0.00304	0.00145	0.00025	0.00017
D91_313	G9B	130	2.125	0.046	0.00587	0.341	0.014	0.00136	<LOD	<LOD	0.00616	0.0943	0.0027	0.00041
D91_317	G9B	285	3.091	0.035	0.00379	0.581	0.011	0.00070	<LOD	<LOD	0.00267	0.1367	0.0023	0.00019
D91_319	G9B	285	2.886	0.041	0.00478	0.4364	0.0085	0.00058	<LOD	<LOD	0.00469	0.1101	0.0029	0.00028
D91_321	G9A	285	20.7	0.22	0.00315	0.4521	0.0087	0.00063	<LOD	<LOD	0.00284	0.0339	0.0013	0.00017
D91_323	G9A	130	14.96	0.17	0.00598	0.433	0.014	0.00147	<LOD	<LOD	0.00686	0.0323	0.0017	0.00041
D91_325	G9B	285	2.633	0.038	0.00319	0.4371	0.0081	0.00051	<LOD	<LOD	0.00287	0.1042	0.002	0.00017
D91_327	G9A	285	19.87	0.21	0.00343	0.472	0.01	0.00063	<LOD	<LOD	0.00299	0.033	0.0011	0.00017
D93_139	G9A_Ti	130	37.47	0.41	0.00605	0.273	0.011	0.00121	<LOD	<LOD	0.00665	0.0175	0.0011	0.00040
D93_141	G9A_Ti	285	65.75	0.64	0.00456	0.3773	0.0089	0.00052	<LOD	<LOD	0.00372	0.0554	0.0015	0.00020
D93_145	G9A_Ti	285	34.16	0.38	0.00435	0.5055	0.0094	0.00062	<LOD	<LOD	0.00314	0.0359	0.0012	0.00021
D93_151	G9A	285	25.62	0.29	0.00434	0.4468	0.0097	0.00067	<LOD	<LOD	0.00314	0.0388	0.0011	0.00020
D93_153	G9A	285	26.03	0.27	0.00422	0.4689	0.009	0.00063	0.0193	0.006	0.00370	0.0395	0.0014	0.00021
D93_155	G9A	285	25.64	0.27	0.00423	0.4664	0.0098	0.00065	<LOD	<LOD	0.00351	0.0357	0.0012	0.00018
D93_173	G9A	285	25.8	0.22	0.00427	0.461	0.011	0.00064	<LOD	<LOD	0.00378	0.0369	0.0014	0.00021
D93_175	G9A	130	20.12	0.22	0.00597	0.412	0.014	0.00113	0.072	0.011	0.00699	0.0394	0.002	0.00038
D93_177	G9A_Ti	285	36.54	0.36	0.00420	0.5451	0.009	0.00054	0.0195	0.0046	0.00375	0.048	0.0016	0.00021
D93_179	G9B_Ti	285	55.29	0.69	0.00443	0.3384	0.0076	0.00058	<LOD	<LOD	0.00446	0.0241	0.0011	0.00022
D93_181	G9A_Ti	130	26.44	0.37	0.00596	0.438	0.013	0.00121	<LOD	<LOD	0.00676	0.0318	0.0016	0.00037
D93_183	G9A	285	26.6	0.3	0.00425	0.464	0.01	0.00064	<LOD	<LOD	0.00329	0.0405	0.0013	0.00020
D93_195	G9A_Ti	285	36.74	0.34	0.00411	0.591	0.013	0.00065	<LOD	<LOD	0.00365	0.046	0.0012	0.00023
D93_205	G9A_Ti	285	37.07	0.35	0.00388	0.5387	0.009	0.00059	<LOD	<LOD	0.00265	0.0397	0.0013	0.00021
D93_209	G9A	130	20.14	0.2	0.00617	0.425	0.012	0.00136	<LOD	<LOD	0.00658	0.0342	0.0015	0.00038
D93_217	G9A_Ti	130	27.03	0.32	0.00600	0.44	0.014	0.00131	<LOD	<LOD	0.00855	0.0324	0.0017	0.00041

Appendix E: Garnet Xenocryst LA-ICP-MS Data Tables

Appendix E.02 (continued): Dharma kimberlite garnet trace element data measured by LA-ICPMS. 2SE – two times standard error. LOD – Limit of detection (Pettke et al., 2014). <LOD – bellow limit of detection.

Sample	*Class*	*Spot Size*	*Ce ppm*	*Ce 2SE*	*Ce LOD*	*Pr ppm*	*Pr 2SE*	*Pr LOD*	*Nd ppm*	*Nd 2SE*	*Nd LOD*	*Sm ppm*	*Sm 2SE*	*Sm LOD*
D91_279	G9B_Ti	130	0.3742	0.0078	0.00048	0.1234	0.0034	0.00042	1.121	0.024	0.00209	0.803	0.025	0.00241
D91_283	G9A	285	0.4894	0.0071	0.00021	0.2237	0.004	0.00017	2.37	0.034	0.00086	1.278	0.02	0.00088
D91_285	G9B	285	0.677	0.012	0.00024	0.1466	0.0029	0.00017	0.797	0.016	0.00093	0.2272	0.0083	0.00100
D91_289	G9A_Ti	285	0.3984	0.0062	0.00021	0.1313	0.0024	0.00016	1.206	0.019	0.00092	0.857	0.015	0.00096
D91_291	G9A_Ti	285	0.3944	0.0056	0.00021	0.1295	0.0024	0.00017	1.189	0.019	0.00088	0.855	0.017	0.00109
D91_297	G9A_Ti	285	0.347	0.0052	0.00021	0.1303	0.0024	0.00015	1.274	0.023	0.00088	0.937	0.019	0.00091
D91_303	G9B	130	0.633	0.012	0.00048	0.1379	0.0039	0.00040	0.697	0.021	0.00196	0.1953	0.0083	0.00217
D91_305	G9B	130	0.828	0.02	0.00041	0.1756	0.0052	0.00031	1.015	0.029	0.00192	0.256	0.011	0.00213
D91_307	G9A	130	0.4049	0.0082	0.00047	0.1823	0.0036	0.00036	1.962	0.033	0.00199	1.139	0.029	0.00196
D91_309	G9B	285	0.01488	0.00072	0.00024	0.00743	0.00047	0.00032	0.0917	0.0048	0.00103	0.0891	0.0054	0.00097
D91_311	G9B	285	0.01614	0.00076	0.00023	0.00709	0.00052	0.00017	0.0854	0.0037	0.00101	0.0768	0.0045	0.00098
D91_313	G9B	130	0.607	0.011	0.00049	0.1009	0.0033	0.00032	0.51	0.016	0.00212	0.1825	0.008	0.00228
D91_317	G9B	285	0.7948	0.009	0.00024	0.1843	0.0037	0.00017	1.103	0.019	0.00094	0.2797	0.0098	0.00112
D91_319	G9B	285	0.663	0.011	0.00030	0.1305	0.0027	0.00020	0.649	0.014	0.00104	0.2199	0.0084	0.00132
D91_321	G9A	285	0.4266	0.0077	0.00020	0.203	0.0033	0.00014	2.262	0.037	0.00081	1.268	0.023	0.00093
D91_323	G9A	130	0.4713	0.0068	0.00043	0.2035	0.005	0.00035	2.039	0.044	0.00189	1.033	0.026	0.00232
D91_325	G9B	285	0.658	0.0091	0.00021	0.1432	0.0028	0.00014	0.774	0.011	0.00084	0.2181	0.0066	0.00090
D91_327	G9A	285	0.4374	0.0053	0.00020	0.2002	0.0034	0.00013	2.187	0.031	0.00086	1.202	0.023	0.00086
D93_139	G9A_Ti	130	0.2016	0.0052	0.00043	0.0699	0.0026	0.00036	0.691	0.021	0.00203	0.538	0.02	0.00220
D93_141	G9A_Ti	285	0.4675	0.0071	0.00022	0.1498	0.0027	0.00017	1.377	0.023	0.00091	0.989	0.02	0.00106
D93_145	G9A_Ti	285	0.3471	0.0052	0.00022	0.1243	0.0023	0.00017	1.28	0.02	0.00094	0.978	0.015	0.00097
D93_151	G9A	285	0.3949	0.0069	0.00021	0.1598	0.0027	0.00017	1.617	0.022	0.00097	1.043	0.02	0.00092
D93_153	G9A	285	0.3899	0.0061	0.00023	0.1527	0.0026	0.00017	1.615	0.025	0.00107	1.035	0.02	0.00092
D93_155	G9A	285	0.3796	0.005	0.00023	0.1542	0.0028	0.00016	1.625	0.028	0.00093	1.047	0.02	0.00083
D93_173	G9A	285	0.3856	0.0064	0.00021	0.1551	0.003	0.00016	1.613	0.027	0.00105	1.039	0.022	0.00103
D93_175	G9A	130	0.401	0.0072	0.00048	0.1582	0.0037	0.00034	1.581	0.033	0.00193	0.983	0.028	0.00217
D93_177	G9A_Ti	285	0.393	0.0061	0.00021	0.1392	0.0028	0.00016	1.36	0.02	0.00094	1.034	0.018	0.00097
D93_179	G9B_Ti	285	0.247	0.0047	0.00023	0.0901	0.0023	0.00022	0.902	0.018	0.00110	0.7	0.015	0.00112
D93_181	G9A_Ti	130	0.3376	0.0073	0.00045	0.1184	0.0035	0.00037	1.19	0.028	0.00186	0.894	0.025	0.00209
D93_183	G9A	285	0.4088	0.0067	0.00021	0.1673	0.0027	0.00017	1.752	0.027	0.00104	1.124	0.021	0.00108
D93_195	G9A_Ti	285	0.3866	0.005	0.00024	0.1271	0.0026	0.00015	1.205	0.021	0.00098	0.855	0.015	0.00120
D93_205	G9A_Ti	285	0.3773	0.0055	0.00023	0.1383	0.0021	0.00019	1.429	0.021	0.00097	1.083	0.02	0.00107
D93_209	G9A	130	0.3833	0.0068	0.00042	0.1527	0.0041	0.00031	1.528	0.033	0.00212	0.994	0.028	0.00205
D93_217	G9A_Ti	130	0.3461	0.0071	0.00044	0.1203	0.0037	0.00036	1.219	0.029	0.00225	0.917	0.028	0.00212

Appendix E: Garnet Xenocryst LA-ICP-MS Data Tables

Appendix E.02 (continued): Dharma kimberlite garnet trace element data measured by LA-ICPMS. 2SE – two times standard error. LOD – Limit of detection (Pettke et al., 2014). <LOD – bellow limit of detection.

Sample	*Class*	*Spot Size*	*Eu ppm*	*Eu 2SE*	*Eu LOD*	*Gd ppm*	*Gd 2SE*	*Gd LOD*	*Tb ppm*	*Tb 2SE*	*Tb LOD*	*Dy ppm*	*Dy 2SE*	*Dy LOD*
D91_279	G9B_Ti	130	0.388	0.011	0.00070	1.554	0.041	0.00290	0.3339	0.0078	0.00045	2.479	0.037	0.00178
D91_283	G9A	285	0.4099	0.0067	0.00033	1.317	0.023	0.00152	0.2098	0.0035	0.00021	1.405	0.026	0.00082
D91_285	G9B	285	0.0758	0.0026	0.00032	0.2889	0.0085	0.00159	0.0548	0.0015	0.00023	0.409	0.011	0.00086
D91_289	G9A_Ti	285	0.3789	0.0061	0.00033	1.649	0.029	0.00143	0.3289	0.0054	0.00023	2.424	0.033	0.00084
D91_291	G9A_Ti	285	0.3829	0.0077	0.00036	1.651	0.029	0.00142	0.3372	0.0059	0.00022	2.434	0.031	0.00086
D91_297	G9A_Ti	285	0.3954	0.0065	0.00033	1.545	0.025	0.00151	0.2558	0.0044	0.00022	1.555	0.026	0.00078
D91_303	G9B	130	0.0688	0.0033	0.00066	0.24	0.013	0.00290	0.0404	0.0017	0.00041	0.313	0.012	0.00183
D91_305	G9B	130	0.0806	0.0037	0.00063	0.253	0.013	0.00261	0.0438	0.0019	0.00038	0.314	0.011	0.00138
D91_307	G9A	130	0.3935	0.0089	0.00062	1.189	0.028	0.00281	0.1832	0.0043	0.00037	1.153	0.025	0.00148
D91_309	G9B	285	0.0392	0.0019	0.00034	0.1812	0.0078	0.00159	0.0353	0.0013	0.00023	0.2722	0.0067	0.00097
D91_311	G9B	285	0.0359	0.0015	0.00031	0.1611	0.0068	0.00133	0.0336	0.001	0.00019	0.2493	0.0062	0.00086
D91_313	G9B	130	0.07	0.0027	0.00062	0.235	0.012	0.00262	0.0449	0.0019	0.00035	0.321	0.011	0.00146
D91_317	G9B	285	0.0857	0.0025	0.00030	0.3015	0.0098	0.00145	0.0533	0.0019	0.00023	0.3941	0.0082	0.00083
D91_319	G9B	285	0.0776	0.0026	0.00041	0.302	0.012	0.00189	0.0529	0.0017	0.00031	0.428	0.01	0.00123
D91_321	G9A	285	0.4168	0.0072	0.00030	1.316	0.018	0.00160	0.2051	0.0035	0.00018	1.38	0.019	0.00076
D91_323	G9A	130	0.3496	0.0085	0.00064	1.039	0.023	0.00266	0.1633	0.0039	0.00041	1.076	0.021	0.00142
D91_325	G9B	285	0.074	0.0024	0.00029	0.2717	0.0094	0.00139	0.0526	0.0015	0.00019	0.3886	0.0082	0.00077
D91_327	G9A	285	0.3996	0.0069	0.00026	1.248	0.023	0.00128	0.198	0.0035	0.00019	1.321	0.023	0.00067
D93_139	G9A_Ti	130	0.2611	0.0072	0.00068	1.054	0.031	0.00258	0.2356	0.0061	0.00041	1.813	0.028	0.00167
D93_141	G9A_Ti	285	0.4578	0.0082	0.00031	2.079	0.035	0.00189	0.4354	0.0076	0.00023	3.389	0.043	0.00087
D93_145	G9A_Ti	285	0.4116	0.0062	0.00032	1.868	0.028	0.00157	0.3712	0.0064	0.00023	2.727	0.034	0.00082
D93_151	G9A	285	0.3898	0.0072	0.00030	1.36	0.027	0.00171	0.2169	0.0044	0.00024	1.366	0.024	0.00086
D93_153	G9A	285	0.3856	0.0073	0.00037	1.351	0.025	0.00186	0.211	0.0038	0.00027	1.346	0.025	0.00084
D93_155	G9A	285	0.3828	0.007	0.00030	1.373	0.021	0.00148	0.2132	0.0043	0.00021	1.339	0.024	0.00087
D93_173	G9A	285	0.3869	0.0058	0.00033	1.346	0.023	0.00142	0.2121	0.0044	0.00023	1.34	0.021	0.00085
D93_175	G9A	130	0.3683	0.0085	0.00064	1.176	0.032	0.00274	0.1815	0.0042	0.00039	1.12	0.023	0.00156
D93_177	G9A_Ti	285	0.4275	0.0072	0.00030	1.932	0.028	0.00165	0.3898	0.006	0.00023	2.855	0.031	0.00101
D93_179	G9B_Ti	285	0.3286	0.0062	0.00032	1.421	0.026	0.00178	0.3091	0.0057	0.00026	2.29	0.04	0.00095
D93_181	G9A_Ti	130	0.3815	0.0075	0.00070	1.533	0.035	0.00269	0.3112	0.0066	0.00036	2.19	0.037	0.00155
D93_183	G9A	285	0.4145	0.0084	0.00034	1.421	0.026	0.00167	0.2228	0.0041	0.00023	1.429	0.025	0.00093
D93_195	G9A_Ti	285	0.3811	0.0077	0.00032	1.608	0.028	0.00148	0.3247	0.0047	0.00020	2.32	0.036	0.00095
D93_205	G9A_Ti	285	0.4497	0.0075	0.00034	2.041	0.035	0.00164	0.4139	0.0074	0.00023	3.045	0.034	0.00091
D93_209	G9A	130	0.3733	0.0083	0.00064	1.172	0.028	0.00264	0.1825	0.0044	0.00039	1.12	0.022	0.00167
D93_217	G9A_Ti	130	0.394	0.011	0.00068	1.658	0.037	0.00259	0.3223	0.0061	0.00042	2.269	0.037	0.00175

Appendix E: Garnet Xenocryst LA-ICP-MS Data Tables

Appendix E.02 (continued): Dharma kimberlite garnet trace element data measured by LA-ICPMS. 2SE – two times standard error. LOD – Limit of detection (Pettke et al., 2014). <LOD – bellow limit of detection.

Sample	*Class*	*Spot Size*	*Ho ppm*	*Ho 2SE*	*Ho LOD*	*Er ppm*	*Er 2SE*	*Er LOD*	*Tm ppm*	*Tm 2SE*	*Tm LOD*	*Yb ppm*	*Yb 2SE*	*Yb LOD*
D91_279	G9B_Ti	130	0.5822	0.0099	0.00041	1.795	0.029	0.00114	0.27	0.0072	0.00050	1.912	0.029	0.00218
D91_283	G9A	285	0.2984	0.007	0.00021	0.899	0.016	0.00067	0.132	0.0035	0.00023	0.956	0.018	0.00099
D91_285	G9B	285	0.1082	0.0027	0.00019	0.4082	0.0098	0.00072	0.0762	0.0023	0.00026	0.677	0.013	0.00111
D91_289	G9A_Ti	285	0.5388	0.0094	0.00021	1.609	0.028	0.00070	0.2327	0.004	0.00023	1.646	0.027	0.00108
D91_291	G9A_Ti	285	0.5389	0.0088	0.00021	1.632	0.029	0.00070	0.2353	0.0045	0.00024	1.653	0.027	0.00107
D91_297	G9A_Ti	285	0.3052	0.0051	0.00019	0.863	0.015	0.00072	0.1249	0.0021	0.00021	0.921	0.02	0.00092
D91_303	G9B	130	0.0815	0.0029	0.00040	0.2985	0.0089	0.00111	0.0561	0.0023	0.00042	0.514	0.014	0.00228
D91_305	G9B	130	0.0795	0.0027	0.00033	0.2969	0.0099	0.00102	0.0558	0.0021	0.00038	0.509	0.019	0.00157
D91_307	G9A	130	0.24	0.0052	0.00039	0.691	0.017	0.00102	0.1029	0.0034	0.00039	0.746	0.021	0.00171
D91_309	G9B	285	0.0723	0.0022	0.00022	0.2908	0.0069	0.00064	0.06	0.0019	0.00020	0.603	0.014	0.00104
D91_311	G9B	285	0.065	0.002	0.00019	0.2576	0.0059	0.00071	0.0525	0.0016	0.00025	0.543	0.012	0.00096
D91_313	G9B	130	0.0861	0.0025	0.00038	0.321	0.011	0.00109	0.0605	0.0028	0.00035	0.543	0.015	0.00159
D91_317	G9B	285	0.1027	0.0027	0.00020	0.3842	0.0087	0.00070	0.0715	0.0023	0.00022	0.629	0.014	0.00101
D91_319	G9B	285	0.1092	0.0028	0.00029	0.413	0.0095	0.00088	0.0791	0.0021	0.00028	0.7	0.016	0.00155
D91_321	G9A	285	0.2929	0.0043	0.00019	0.867	0.015	0.00058	0.1286	0.0024	0.00022	0.966	0.02	0.00088
D91_323	G9A	130	0.2305	0.0053	0.00037	0.676	0.016	0.00119	0.0994	0.003	0.00036	0.752	0.017	0.00170
D91_325	G9B	285	0.101	0.0024	0.00019	0.3834	0.0084	0.00055	0.0721	0.0021	0.00023	0.639	0.013	0.00075
D91_327	G9A	285	0.2849	0.0048	0.00019	0.834	0.013	0.00068	0.1228	0.0025	0.00023	0.915	0.018	0.00092
D93_139	G9A_Ti	130	0.4302	0.0091	0.00040	1.355	0.024	0.00126	0.2031	0.0047	0.00045	1.5	0.03	0.00193
D93_141	G9A_Ti	285	0.806	0.013	0.00021	2.536	0.037	0.00067	0.374	0.0071	0.00023	2.632	0.045	0.00112
D93_145	G9A_Ti	285	0.6193	0.0085	0.00018	1.884	0.027	0.00066	0.2711	0.005	0.00025	1.884	0.037	0.00105
D93_151	G9A	285	0.2875	0.0051	0.00023	0.883	0.017	0.00070	0.137	0.0031	0.00023	1.075	0.021	0.00112
D93_153	G9A	285	0.2855	0.0054	0.00022	0.884	0.015	0.00074	0.1363	0.003	0.00024	1.029	0.021	0.00108
D93_155	G9A	285	0.2929	0.0045	0.00021	0.882	0.018	0.00064	0.1344	0.0028	0.00025	1.06	0.02	0.00091
D93_173	G9A	285	0.2888	0.0049	0.00019	0.874	0.018	0.00067	0.1365	0.0033	0.00026	1.054	0.02	0.00098
D93_175	G9A	130	0.2393	0.0048	0.00039	0.713	0.016	0.00110	0.1081	0.0028	0.00043	0.844	0.019	0.00205
D93_177	G9A_Ti	285	0.646	0.01	0.00023	1.932	0.028	0.00066	0.2774	0.0055	0.00024	1.916	0.038	0.00102
D93_179	G9B_Ti	285	0.5437	0.009	0.00024	1.656	0.032	0.00075	0.2476	0.0054	0.00026	1.744	0.035	0.00102
D93_181	G9A_Ti	130	0.492	0.0092	0.00034	1.439	0.022	0.00108	0.2105	0.0055	0.00039	1.45	0.033	0.00150
D93_183	G9A	285	0.309	0.0058	0.00023	0.926	0.019	0.00064	0.1408	0.0027	0.00023	1.081	0.022	0.00112
D93_195	G9A_Ti	285	0.5191	0.0075	0.00022	1.559	0.025	0.00070	0.226	0.0041	0.00025	1.607	0.03	0.00103
D93_205	G9A_Ti	285	0.6888	0.009	0.00020	2.057	0.032	0.00067	0.2896	0.0051	0.00024	1.988	0.034	0.00107
D93_209	G9A	130	0.237	0.0056	0.00032	0.702	0.017	0.00117	0.1052	0.003	0.00041	0.849	0.02	0.00162
D93_217	G9A_Ti	130	0.5077	0.0073	0.00035	1.514	0.022	0.00113	0.2217	0.0052	0.00039	1.501	0.029	0.00201

Appendix E: Garnet Xenocryst LA-ICP-MS Data Tables

Appendix E.02 (continued): Dharma kimberlite garnet trace element data measured by LA-ICPMS. 2SE – two times standard error. LOD – Limit of detection (Pettke et al., 2014). <LOD – bellow limit of detection.

Sample	*Class*	*Spot Size*	*Lu ppm*	*Lu 2SE*	*Lu LOD*	*Hf ppm*	*Hf 2SE*	*Hf LOD*	*Ta ppm*	*Ta 2SE*	*Ta LOD*
D91_279	G9B_Ti	130	0.3009	0.0064	0.00047	1.317	0.041	0.00303	0.0313	0.0022	0.00088
D91_283	G9A	285	0.1682	0.0035	0.00026	0.457	0.019	0.00163	0.0664	0.003	0.00038
D91_285	G9B	285	0.1351	0.0029	0.00026	0.0894	0.007	0.00167	0.0194	0.0013	0.00037
D91_289	G9A_Ti	285	0.2626	0.0052	0.00024	1.024	0.027	0.00152	0.0609	0.0026	0.00039
D91_291	G9A_Ti	285	0.2612	0.0046	0.00025	1.07	0.03	0.00208	0.0575	0.0023	0.00045
D91_297	G9A_Ti	285	0.1583	0.0035	0.00027	0.76	0.029	0.00159	0.0437	0.002	0.00039
D91_303	G9B	130	0.0998	0.0033	0.00049	0.0628	0.0081	0.00289	0.0173	0.0018	0.00075
D91_305	G9B	130	0.0954	0.0033	0.00040	0.066	0.0066	0.00278	0.0212	0.0018	0.00075
D91_307	G9A	130	0.1262	0.0028	0.00047	0.38	0.024	0.00315	0.0461	0.0031	0.00058
D91_309	G9B	285	0.1307	0.0026	0.00025	0.0857	0.0062	0.00182	0.0002	0.00025	0.00041
D91_311	G9B	285	0.117	0.0025	0.00024	0.0654	0.0063	0.00183	0.00021	0.00026	0.00039
D91_313	G9B	130	0.1088	0.0034	0.00044	0.072	0.011	0.00279	0.0172	0.0022	0.00077
D91_317	G9B	285	0.124	0.0033	0.00026	0.0839	0.0069	0.00165	0.0239	0.0015	0.00045
D91_319	G9B	285	0.1405	0.0033	0.00043	0.0838	0.007	0.00209	0.0208	0.0017	0.00042
D91_321	G9A	285	0.1673	0.0038	0.00024	0.485	0.019	0.00148	0.0559	0.0024	0.00032
D91_323	G9A	130	0.1265	0.0037	0.00044	0.349	0.019	0.00315	0.0548	0.0031	0.00068
D91_325	G9B	285	0.1273	0.0024	0.00025	0.0885	0.0075	0.00138	0.0185	0.0012	0.00032
D91_327	G9A	285	0.1597	0.0035	0.00024	0.462	0.016	0.00162	0.0615	0.0029	0.00033
D93_139	G9A_Ti	130	0.2378	0.0057	0.00052	1.066	0.042	0.00410	0.0296	0.0027	0.00076
D93_141	G9A_Ti	285	0.4261	0.0068	0.00027	1.977	0.042	0.00146	0.0392	0.0019	0.00041
D93_145	G9A_Ti	285	0.2996	0.0061	0.00028	0.925	0.03	0.00182	0.0566	0.0032	0.00039
D93_151	G9A	285	0.1917	0.0044	0.00026	0.626	0.02	0.00190	0.0401	0.0021	0.00046
D93_153	G9A	285	0.1847	0.004	0.00027	0.581	0.021	0.00175	0.0439	0.0022	0.00043
D93_155	G9A	285	0.1858	0.0043	0.00026	0.601	0.022	0.00182	0.0406	0.0017	0.00041
D93_173	G9A	285	0.1876	0.0043	0.00026	0.59	0.023	0.00157	0.0431	0.0026	0.00040
D93_175	G9A	130	0.1459	0.004	0.00054	0.455	0.023	0.00326	0.0354	0.0029	0.00063
D93_177	G9A_Ti	285	0.3018	0.0052	0.00030	0.974	0.024	0.00133	0.0591	0.0026	0.00050
D93_179	G9B_Ti	285	0.2813	0.0052	0.00029	1.571	0.037	0.00165	0.0382	0.002	0.00045
D93_181	G9A_Ti	130	0.2217	0.0051	0.00041	0.666	0.024	0.00279	0.0454	0.0033	0.00066
D93_183	G9A	285	0.1885	0.0043	0.00026	0.587	0.024	0.00162	0.0409	0.0023	0.00042
D93_195	G9A_Ti	285	0.258	0.0041	0.00024	0.99	0.03	0.00141	0.0552	0.0026	0.00046
D93_205	G9A_Ti	285	0.3119	0.0053	0.00025	0.965	0.025	0.00158	0.061	0.0024	0.00041
D93_209	G9A	130	0.1414	0.0045	0.00048	0.443	0.02	0.00288	0.0381	0.0026	0.00065
D93_217	G9A_Ti	130	0.2369	0.005	0.00041	0.695	0.031	0.00248	0.0458	0.0035	0.00073

Appendix F: Garnet Xenocryst Ni Geothermometry Calculation Data Tables

Appendix F.01: Mel kimberlite garnet Ni temperature calculations. Note: non-peridotite garnet included.

Sample	***Class***	***Al apfu***	***Ca apfu***	***Cr apfu***	***Fe apfu***	***Mg apfu***	***Ni ppm***	T_{Canil}	T_{Ryan}	$T_{Shubrey}$	$T_{Sudholz}$
M1_47824_003_263	G9A_Ti	1.671	0.397	0.217	0.419	2.213	122.36	1267	1401	1383	1321
M1_47824_017_277	G9A	1.742	0.37	0.176	0.416	2.236	119.1	1260	1387	1371	1289
M1_47824_035_295	G9A_Ti	1.834	0.31	0.06	0.459	2.265	105.73	1229	1327	1322	1200
M1_47824_037_297	G9A	1.788	0.331	0.183	0.465	2.188	44.15	1033	993	1041	1036
M1_47824_039_299	G9A	1.742	0.373	0.201	0.544	2.088	38.28	1006	951	1004	1019
M1_49724_011_371	G9A	1.777	0.339	0.118	0.431	2.265	139.46	1303	1473	1442	1306
M1_49724_015_375	G9A	1.745	0.36	0.146	0.436	2.249	113.2	1246	1360	1350	1261
M1_49724_019_379	G9A_Ti	1.813	0.325	0.066	0.492	2.224	117.96	1257	1382	1367	1236
M1_49724_021_381	G9A_Ti	1.808	0.327	0.069	0.496	2.217	114.12	1249	1365	1353	1228
M1_49724_035_395	G9A_Ti	1.843	0.312	0.058	0.415	2.312	120.3	1263	1392	1376	1235
M1_49724_039_399	G9B_Ti	1.817	0.361	0.088	0.419	2.264	117.67	1257	1380	1366	1252
M1_49724_041_401	G9A_Ti	1.811	0.326	0.064	0.498	2.227	118.23	1258	1383	1368	1236
M1_49725_015_417	G9A_Ti	1.822	0.328	0.063	0.476	2.244	121.32	1265	1396	1379	1243
M1_49725_019_421	G9A_Ti	1.819	0.328	0.065	0.472	2.242	124.75	1272	1411	1391	1252
M1_49725_023_425	G9A_Ti	1.76	0.328	0.138	0.429	2.28	136.98	1298	1463	1433	1305
M1_49725_025_427	G9A_Ti	1.755	0.364	0.137	0.547	2.111	80.36	1161	1204	1221	1168
M1_49725_039_441	G9A_Ti	1.764	0.341	0.107	0.46	2.255	100	1214	1300	1301	1209
M1_49725_041_443	G9A_Ti	1.776	0.338	0.106	0.463	2.259	119.47	1261	1388	1373	1256
M1_49725_051_453	G9A_Ti	1.82	0.33	0.063	0.475	2.229	118.37	1258	1383	1369	1237
M1_49741_001_301	G9A	1.716	0.376	0.189	0.461	2.191	132	1288	1442	1416	1327
M1_49741_005_305	G9A_Ti	1.81	0.333	0.066	0.492	2.217	134.51	1293	1452	1425	1275
M1_49741_015_315	G9A	1.907	0.315	0.084	0.492	2.161	23.27	920	824	893	893
M1_49741_017_317	G9A	1.716	0.382	0.197	0.426	2.224	125.37	1274	1414	1394	1316
M1_49741_021_321	G9A	1.906	0.317	0.092	0.495	2.152	22.69	916	819	888	891
M1_49741_029_329	G9A_Ti	1.822	0.331	0.061	0.491	2.206	128.41	1280	1427	1404	1260
M1_49741_041_341	G9A_Ti	1.705	0.35	0.192	0.46	2.206	120.6	1263	1393	1377	1294
M1_49741_053_353	G9A	1.693	0.385	0.225	0.415	2.226	120.56	1263	1393	1377	1315
M1_49741_059_359	G9A_Ti	1.741	0.354	0.151	0.427	2.251	140.3	1305	1476	1444	1325
M2_47824_003_465	G9A_Ti	1.795	0.325	0.134	0.449	2.253	70.86	1132	1154	1179	1126
M2_47824_013_475	G9A	1.721	0.328	0.224	0.445	2.244	48.15	1050	1019	1064	1063
M2_47824_015_477	G9A	1.725	0.368	0.182	0.421	2.258	113.75	1248	1363	1352	1277
M2_47824_029_491	G9A	1.722	0.365	0.18	0.418	2.274	119.56	1261	1389	1373	1290
M2_47824_033_495	G9A_Ti	1.825	0.308	0.063	0.46	2.286	112.55	1245	1358	1348	1217
M2_47824_037_499	G9A_Ti	1.832	0.307	0.062	0.456	2.281	107.26	1232	1334	1328	1204
M2_49724_009_743	G3_Na	1.885	0.482	0.01	0.731	1.824	123.69	1270	1406	1388	1274
M2_49724_013_747	G9A	1.76	0.361	0.142	0.433	2.245	116.16	1253	1374	1361	1267
M2_49724_037_771	G9A_Ti	1.811	0.328	0.069	0.491	2.227	118.36	1258	1383	1369	1238
M2_49724_045_779	G3_Na	1.893	0.35	0.037	0.677	1.987	19	888	780	853	857
M2_49724_049_783	G9A	1.767	0.358	0.142	0.429	2.246	116.96	1255	1377	1364	1268

Appendix F: Garnet Xenocryst Ni Geothermometry Calculation Data Tables

Appendix F.01 (continued): Mel kimberlite garnet Ni temperature calculations. Note: non-peridotite garnet included.

Sample	*Class*	*Al apfu*	*Ca apfu*	*Cr apfu*	*Fe apfu*	*Mg apfu*	*Ni ppm*	T_{Canil}	T_{Ryan}	$T_{Shubrey}$	$T_{Sudholz}$
M2_49724_051_785	G3_Na	1.88	0.352	0.038	0.682	1.979	18.61	884	776	849	854
M2_49724_057_791	G9A	1.784	0.339	0.121	0.431	2.262	139.74	1304	1474	1443	1308
M2_49724_063_797	G9A_Ti	1.814	0.326	0.063	0.489	2.226	118.01	1257	1382	1367	1235
M2_49724_067_801	G3_Na	1.897	0.35	0.026	0.69	1.962	109.51	1238	1344	1337	1210
M2_49724_073_807	G9A_Ti	1.764	0.345	0.096	0.482	2.23	150.82	1326	1519	1479	1324
M2_49725_003_505	G9A	1.674	0.386	0.231	0.426	2.238	116.76	1255	1376	1363	1307
M2_49725_007_509	G9A_Ti	1.765	0.344	0.102	0.458	2.266	127.31	1278	1422	1400	1275
M2_49725_009_511	G9A_Ti	1.756	0.36	0.137	0.547	2.131	81.28	1164	1209	1225	1170
M2_49725_029_531	G11	1.614	0.382	0.283	0.418	2.24	123.59	1270	1406	1387	1344
M2_49725_039_541	G9A_Ti	1.824	0.331	0.063	0.473	2.248	44.82	1036	997	1045	1009
M2_49725_051_553	G9A	1.674	0.382	0.224	0.426	2.238	119.12	1260	1387	1371	1310
M2_49725_059_561	G9A	1.667	0.391	0.23	0.425	2.239	114.37	1249	1366	1354	1303
M2_49725_061_563	G3	1.926	0.312	0.021	0.642	2.055	31.96	973	902	961	933
M2_49741_039_607	G9A_Ti	1.797	0.332	0.065	0.492	2.232	133.31	1291	1447	1421	1272
M2_49742_003_617	G3_Na	1.944	0.763	0.003	0.755	1.48	203	1417	1720	1639	1538
M2_49742_005_619	G3_Na	1.944	0.774	0.003	0.749	1.474	73.21	1140	1167	1189	1210
M2_49742_011_625	G3_Na	1.878	0.607	0.004	0.746	1.713	97.43	1208	1288	1291	1238
M2_49742_027_641	G9B_Ti	1.773	0.353	0.071	0.499	2.234	131.15	1286	1438	1413	1274
M2_49742_031_645	G9A	1.728	0.362	0.177	0.439	2.249	115.59	1252	1371	1359	1278
M2_49742_033_647	G9A	1.643	0.414	0.276	0.398	2.231	117.24	1256	1378	1365	1334
M2_49742_039_653	G12	1.897	0.567	0.074	0.525	1.924	41.52	1022	974	1025	1045
M2_49742_057_671	G9A	1.835	0.324	0.129	0.483	2.211	44.22	1034	993	1041	1021
M2_49742_065_679	G9B_Ti	1.793	0.353	0.065	0.494	2.228	129.47	1283	1431	1408	1269
M2_49742_069_683	G9A_Ti	1.69	0.381	0.167	0.441	2.26	130.24	1284	1434	1410	1316
M2_49742_071_685	G12	1.882	0.574	0.089	0.52	1.917	40.42	1016	966	1018	1044
M2_49742_079_693	G9A_Ti	1.694	0.382	0.169	0.444	2.253	133.12	1290	1447	1420	1324
M2_49742_085_699	G12	1.9	0.567	0.072	0.523	1.916	42.13	1024	979	1029	1048
M2_49742_089_703	G12	1.88	0.564	0.073	0.525	1.951	39.05	1010	956	1009	1030
M2_49742_113_727	G3_Na	1.953	0.76	0.002	0.751	1.484	71.92	1136	1160	1183	1201
M2_49742_119_733	G1	1.828	0.329	0.057	0.487	2.237	127.6	1279	1423	1401	1255
P3_49725_001_133	G9A_Ti	1.763	0.343	0.105	0.481	2.227	121.33	1265	1396	1379	1262
P3_49725_003_135	G9A_Ti	1.818	0.352	0.108	0.478	2.113	119.46	1261	1388	1373	1264
P3_49725_030_388	G9A_Ti	1.807	0.332	0.066	0.468	2.269	116.3	1254	1374	1361	1233
P3_49725_049_407	G9A_Ti	1.812	0.331	0.062	0.472	2.259	125.12	1273	1413	1393	1252
P3_49725_061_419	G9A_Ti	1.803	0.335	0.061	0.472	2.269	119.43	1261	1388	1373	1239
P3_49725_39r_498	G9B_Ti	1.784	0.345	0.071	0.486	2.255	126.4	1276	1418	1397	1261
P3_49736_008_274	G9A_Ti	1.758	0.342	0.117	0.441	2.302	128.16	1280	1426	1403	1281
P3_49736_018_284	G9A	1.739	0.359	0.151	0.424	2.308	124.77	1272	1411	1391	1289

Appendix F: Garnet Xenocryst Ni Geothermometry Calculation Data Tables

Appendix F.01 (continued): Mel kimberlite garnet Ni temperature calculations.

Sample	***Class***	***Al apfu***	***Ca apfu***	***Cr apfu***	***Fe apfu***	***Mg apfu***	***Ni ppm***	T_{Canil}	T_{Ryan}	$T_{Shubrey}$	$T_{Sudholz}$
P3_49736_028_294	G9B_Ti	1.804	0.346	0.069	0.495	2.237	103.9	1224	1318	1315	1207
P3_49736_030_296	G9A_Ti	1.8	0.322	0.061	0.54	2.249	98.65	1211	1294	1295	1184
P3_49736_040_306	G9A_Ti	1.804	0.321	0.063	0.529	2.24	100.55	1216	1303	1303	1190
P3_49736_054_320	G9B_Ti	1.834	0.385	0.057	0.503	2.164	99.98	1214	1300	1300	1204
P3_49736_060_326	G9B_Ti	1.821	0.356	0.066	0.486	2.24	101.52	1218	1307	1306	1202
P3_49736_082_348	G9A_Ti	1.761	0.341	0.118	0.439	2.307	122.9	1268	1403	1385	1268
P3_49736_098_364	G9B_Ti	1.801	0.349	0.074	0.495	2.238	100.15	1215	1301	1301	1200
P3_49736_110_376	G11	1.627	0.409	0.265	0.391	2.272	115.19	1251	1369	1357	1323
P3_49746_012_172	G9B	1.735	0.459	0.25	0.542	2.008	10.953	809	676	758	828
P3_49746_016_176	G9A	1.808	0.386	0.179	0.534	2.075	9.926	796	660	743	792
P3_49746_018_178	G9A	1.79	0.35	0.144	0.61	2.078	38.06	1005	949	1003	1000
P3_49746_050_210	G11	1.569	0.366	0.375	0.38	2.281	65.39	1115	1124	1153	1187
P3_49746_060_220	G9A	1.699	0.366	0.248	0.386	2.278	67.31	1121	1135	1162	1156
P3_49746_070_230	G9A_Ti	1.736	0.339	0.091	0.485	2.29	148.64	1322	1510	1472	1314
P3_49746_076_236	G9B	1.739	0.462	0.249	0.535	2.005	10.91	808	675	757	827
P3_49746_082_242	G9A	1.808	0.342	0.129	0.603	2.11	38.73	1008	954	1007	998
P3_49746_092_252	G9A_Ti	1.748	0.338	0.086	0.49	2.278	149.4	1323	1514	1474	1314
P3_49746_104_264	G9B	1.749	0.463	0.239	0.563	1.955	10.832	807	674	756	825

Appendix F: Garnet Xenocryst Ni Geothermometry Calculation Data Tables

Appendix F.02: Dharma kimberlite garnet Ni temperature calculations.

Sample	***Class***	***Al apfu***	***Ca apfu***	***Cr apfu***	***Fe apfu***	***Mg apfu***	***Ni ppm***	T_{Canil}	T_{Ryan}	$T_{Shubrey}$	$T_{Sudholz}$
D104_1_67	G9A	1.856	0.348	0.097	0.575	2.117	46.23	1042	1007	1053	1027
D104_1_81	G9A_Ti	1.825	0.342	0.083	0.398	2.323	100.98	1217	1305	1304	1203
D104_1_89	G9B_Ti	1.758	0.373	0.145	0.487	2.206	63.67	1109	1114	1145	1115
D104_1_93	G9A	1.856	0.354	0.102	0.571	2.112	46.15	1042	1006	1052	1029
D104_1_97	G9A	1.878	0.349	0.099	0.562	2.118	46.25	1042	1007	1053	1027
D104_1_99	G9A	1.885	0.305	0.08	0.577	2.148	23.94	924	831	899	894
D104_2_111	G10A	1.314	0.381	0.639	0.379	2.276	68.81	1126	1143	1169	1290
D104_2_123	G9A	1.652	0.425	0.34	0.389	2.196	56.15	1082	1070	1107	1151
D104_2_139	G9B	1.645	0.466	0.315	0.552	2.005	37.02	1000	941	996	1059
D104_2_143	G9A_Ti	1.535	0.445	0.37	0.393	2.211	96.94	1207	1286	1289	1320
D104_2_153	G9B_Ti	1.765	0.372	0.138	0.485	2.201	64.14	1110	1117	1147	1114
D104_3_155	G9A	1.868	0.347	0.099	0.566	2.123	46.78	1045	1010	1056	1029
D104_3_161	G9A	1.881	0.35	0.099	0.56	2.109	46.51	1044	1009	1054	1029
D104_3_179	G9A	1.879	0.353	0.101	0.565	2.097	46.69	1044	1010	1056	1031
D104_3_185	G10A	1.327	0.379	0.638	0.375	2.28	66.8	1119	1132	1160	1279
D104_3_197	G10A	1.322	0.386	0.643	0.373	2.263	83	1169	1218	1232	1350
D104_3_199	G12_Ti	1.808	0.597	0.093	0.603	1.865	28.57	954	873	936	979
D104_4_209	G9A	1.77	0.345	0.148	0.398	2.323	124.26	1271	1409	1390	1283
D104_4_223	G9A_Ti	1.704	0.38	0.187	0.457	2.237	89.53	1187	1250	1259	1215
D104_4_227	G9A_Ti	1.67	0.389	0.254	0.391	2.271	101.93	1219	1309	1308	1275
D104_4_233	G10A	1.32	0.382	0.646	0.374	2.281	66.47	1118	1130	1158	1281
D104_4_235	G10A	1.312	0.379	0.641	0.377	2.273	67.17	1120	1134	1161	1284
D104_4_239	G9A	1.883	0.35	0.096	0.563	2.104	46.9	1045	1011	1057	1030
D104_4_243	G9B	1.625	0.468	0.318	0.556	2.02	36.19	996	935	991	1055
D104_4_247	G9A_Ti	1.646	0.397	0.274	0.408	2.255	95.51	1203	1279	1283	1266
D104_4_249	G9A	1.858	0.351	0.096	0.564	2.12	47.87	1049	1018	1062	1034
D104_4_251	G9A	1.614	0.428	0.346	0.395	2.21	56.12	1082	1070	1107	1154
D104_5_257	G12_Ti	1.793	0.597	0.105	0.596	1.849	35.7	993	931	987	1027
D104_5_267	G9A_Ti	1.699	0.382	0.185	0.453	2.242	89.7	1188	1251	1260	1215
D104_5_275	G9A_Ti	1.734	0.377	0.161	0.485	2.2	64.71	1112	1120	1150	1124
D104_5_293	G9A_Ti	1.683	0.382	0.209	0.443	2.251	92.15	1194	1263	1270	1230
D104_5_297	G9A_Ti	1.822	0.342	0.085	0.404	2.324	99.2	1212	1297	1297	1199
D104_5_299	G9A	1.688	0.375	0.219	0.407	2.295	97.7	1209	1289	1292	1247
D89_329	G9A	1.742	0.376	0.222	0.408	2.231	57.07	1085	1075	1112	1111
D89_331	G9A_Ti	1.695	0.392	0.202	0.454	2.215	88.1	1183	1243	1253	1219
D89_335	G9A	1.639	0.416	0.299	0.401	2.239	104.9	1227	1323	1319	1307
D89_337	G9A	1.733	0.378	0.224	0.417	2.23	56.49	1083	1072	1109	1110
D89_349	G9A_Ti	1.799	0.323	0.158	0.378	2.313	62.45	1104	1107	1139	1103
D89_353	G9B	1.614	0.483	0.37	0.453	2.065	43.12	1029	985	1035	1111

Appendix F: Garnet Xenocryst Ni Geothermometry Calculation Data Tables

Appendix F.02 (continued): Dharma kimberlite garnet Ni temperature calculations.

Sample	*Class*	*Al apfu*	*Ca apfu*	*Cr apfu*	*Fe apfu*	*Mg apfu*	*Ni ppm*	T_{Canil}	T_{Ryan}	$T_{Shubrey}$	$T_{Sudholz}$
D89_357	G10B_Ti	1.734	0.261	0.177	0.453	2.345	68.07	1123	1139	1166	1114
D89_361	G9A	1.75	0.384	0.228	0.431	2.201	66.02	1117	1127	1156	1149
D89_365	G9A	1.762	0.376	0.216	0.406	2.227	56.65	1084	1073	1110	1108
D89_367	G9B	1.61	0.483	0.375	0.458	2.064	43.67	1031	989	1038	1115
D89_369	G9B	1.612	0.485	0.374	0.453	2.058	43.52	1031	988	1037	1115
D89_371	G9A	1.76	0.376	0.217	0.411	2.22	55.96	1081	1069	1106	1105
D89_373	G10B_Ti	1.764	0.24	0.167	0.451	2.35	65.92	1116	1127	1156	1098
D89_375	G9A_Ti	1.803	0.32	0.157	0.375	2.323	62.02	1103	1105	1137	1100
D89_377	G9A_Ti	1.81	0.325	0.166	0.372	2.313	62.01	1103	1105	1137	1103
D89_381	G9B_Ti	1.74	0.434	0.178	0.517	2.084	41.69	1022	975	1026	1044
D89_387	G10B_Ti	1.737	0.256	0.172	0.451	2.36	66.88	1119	1132	1160	1107
D89_391	G9A_Ti	1.694	0.389	0.196	0.451	2.219	89.02	1186	1248	1257	1219
D89_393	G10B_Ti	1.722	0.257	0.173	0.451	2.35	69.85	1129	1149	1174	1118
D89_395	G9A_Ti	1.771	0.327	0.165	0.377	2.328	61.8	1102	1103	1136	1103
D89_397	G9B_Ti	1.715	0.44	0.177	0.521	2.103	41.05	1019	971	1022	1041
D89_399	G9A_Ti	1.717	0.372	0.173	0.448	2.242	99.65	1214	1299	1299	1237
D89_403	G9B	1.606	0.487	0.376	0.454	2.069	44.64	1036	996	1044	1121
D89_411	G9A	1.721	0.381	0.226	0.414	2.235	56.57	1083	1072	1109	1112
D89_415	G9B	1.603	0.488	0.374	0.457	2.059	44	1033	992	1040	1118
D89_417	G9A	1.748	0.373	0.221	0.414	2.234	56.62	1084	1073	1110	1108
D89_421	G10B_Ti	1.734	0.25	0.164	0.453	2.36	68.54	1125	1141	1168	1109
D89_423	G9A_Ti	1.781	0.323	0.163	0.379	2.323	62.08	1103	1105	1137	1103
D89_425	G9A_Ti	1.715	0.373	0.177	0.451	2.243	99.92	1214	1300	1300	1240
D89_427	G10B_Ti	1.716	0.259	0.175	0.454	2.358	69.12	1127	1145	1171	1116
D89_429	G9A	1.736	0.385	0.23	0.44	2.201	66.68	1119	1131	1159	1152
D89_433	G9B	1.604	0.486	0.373	0.454	2.069	44.51	1035	995	1043	1120
D89_437	G9B_Ti	1.715	0.438	0.18	0.517	2.096	41.7	1022	976	1026	1045
D89_441	G9A	1.726	0.379	0.225	0.413	2.23	57.43	1087	1078	1114	1114
D91_221	G9A	1.524	0.47	0.435	0.41	2.143	55.43	1079	1065	1103	1189
D91_227	G9A	1.525	0.456	0.43	0.392	2.164	64.62	1112	1119	1149	1225
D91_229	G9B	1.548	0.505	0.434	0.432	2.055	40.16	1015	965	1016	1117
D91_235	G9A	1.53	0.469	0.434	0.405	2.137	55.68	1080	1067	1105	1189
D91_239	G9A_Ti	1.762	0.365	0.154	0.426	2.259	102.06	1220	1310	1308	1235
D91_241	G9B	1.547	0.5	0.425	0.436	2.061	39.23	1011	958	1010	1109
D91_243	G9A	1.516	0.469	0.441	0.403	2.145	55.91	1081	1068	1106	1193
D91_245	G9A	1.52	0.469	0.434	0.406	2.143	55.96	1081	1069	1106	1191
D91_247	G9A_Ti	1.581	0.422	0.322	0.406	2.224	100.27	1215	1302	1302	1306
D91_255	G9B	1.551	0.503	0.435	0.432	2.068	40.84	1018	969	1021	1120
D91_279	G9B_Ti	1.728	0.382	0.159	0.478	2.197	79.47	1159	1200	1217	1176

Appendix F: Garnet Xenocryst Ni Geothermometry Calculation Data Tables

Appendix F.02 (continued): Dharma kimberlite garnet Ni temperature calculations.

Sample	*Class*	*Al apfu*	*Ca apfu*	*Cr apfu*	*Fe apfu*	*Mg apfu*	*Ni ppm*	T_{Canil}	T_{Ryan}	$T_{Shubrey}$	$T_{Sudholz}$
D91_283	G9A	1.532	0.469	0.439	0.405	2.138	55.52	1080	1066	1104	1190
D91_285	G9B	1.546	0.502	0.44	0.435	2.065	39.34	1011	959	1011	1113
D91_289	G9A_Ti	1.584	0.419	0.318	0.404	2.231	99.44	1213	1298	1298	1301
D91_291	G9A_Ti	1.582	0.418	0.328	0.402	2.232	99.18	1212	1296	1297	1303
D91_297	G9A_Ti	1.508	0.46	0.426	0.393	2.186	65.04	1113	1122	1151	1227
D91_303	G9B	1.549	0.505	0.436	0.439	2.062	38.95	1009	956	1009	1110
D91_305	G9B	1.543	0.51	0.451	0.43	2.062	41.03	1019	971	1022	1127
D91_307	G9A	1.527	0.47	0.442	0.406	2.136	57.47	1087	1078	1114	1200
D91_309	G9B	1.666	0.489	0.339	0.467	2.037	26.5	941	855	920	1000
D91_311	G9B	1.64	0.5	0.356	0.469	2.024	26.17	939	852	917	1004
D91_313	G9B	1.551	0.502	0.43	0.439	2.066	38.58	1008	953	1006	1106
D91_317	G9B	1.54	0.511	0.446	0.431	2.055	40.65	1017	968	1019	1124
D91_319	G9B	1.554	0.503	0.438	0.434	2.067	39.17	1010	957	1010	1111
D91_321	G9A	1.518	0.472	0.434	0.406	2.15	55.14	1078	1064	1102	1188
D91_323	G9A	1.523	0.47	0.436	0.405	2.143	57.4	1086	1077	1114	1198
D91_325	G9B	1.548	0.504	0.436	0.43	2.064	39.24	1011	958	1011	1112
D91_327	G9A	1.544	0.467	0.43	0.405	2.133	55.19	1078	1064	1102	1185
D93_139	G9A_Ti	1.711	0.379	0.18	0.523	2.16	53.21	1071	1052	1092	1085
D93_141	G9A_Ti	1.703	0.382	0.17	0.461	2.222	99.8	1214	1299	1300	1240
D93_145	G9A_Ti	1.615	0.399	0.331	0.383	2.248	59.21	1093	1088	1123	1157
D93_151	G9A	1.583	0.452	0.384	0.429	2.137	51.18	1063	1039	1081	1149
D93_153	G9A	1.596	0.449	0.382	0.428	2.133	51.23	1063	1039	1081	1147
D93_155	G9A	1.586	0.451	0.382	0.43	2.129	50.63	1061	1035	1078	1145
D93_173	G9A	1.599	0.448	0.384	0.428	2.134	50.93	1062	1037	1079	1146
D93_175	G9A	1.588	0.45	0.38	0.431	2.127	52.83	1069	1049	1090	1155
D93_177	G9A_Ti	1.593	0.406	0.348	0.388	2.23	60.01	1096	1093	1127	1167
D93_179	G9B_Ti	1.724	0.406	0.192	0.514	2.126	49.01	1054	1025	1069	1076
D93_181	G9A_Ti	1.621	0.397	0.322	0.384	2.244	62.66	1105	1108	1140	1168
D93_183	G9A	1.594	0.45	0.377	0.433	2.127	52.51	1068	1047	1088	1152
D93_195	G9A_Ti	1.586	0.422	0.33	0.401	2.201	97.2	1207	1287	1290	1299
D93_205	G9A_Ti	1.611	0.402	0.337	0.384	2.229	61.46	1101	1101	1134	1169
D93_209	G9A	1.589	0.452	0.388	0.429	2.119	53.08	1070	1051	1091	1159
D93_217	G9A_Ti	1.618	0.396	0.325	0.385	2.24	63.24	1107	1112	1143	1171